NTNU

Norwegian University of
Science and Technology

Experimental Investigation of Porous Structures in Splash Zone

Prateek Gupta

Marine Technology
Submission date: June 2018
Supervisor: Trygve Kristiansen, IMT
Co-supervisor: Fredrik Mentzoni, IMT

Norwegian University of Science and Technology
Department of Marine Technology

Acknowledgement

The success and final outcome of this thesis required a lot of support and assistance from many people and I am extremely privileged to have got this all along the completion of this work. All that I have done is only due to such supervision and assistance and I would not forget to thank them.

I respect and thank my supervisor Prof. Trygve Kristiansen and co-supervisor Fredrik Mentzoni, for providing me an opportunity to work on this extremely interesting topic and giving me all support and guidance which allowed me to obtain some really meaningful and useful results. I am extremely thankful to them for providing me their guidance.

I would like to extend my sincere esteems to all staff in laboratory, Torgeir Wahl, Marcus Almehagen, Ole Erik, Tor Magnus and Trond Innset who helped me during my experiments by providing all the necessary information and timely assistance for conducting lab test successfully.

I am thankful to and fortunate enough to get constant encouragement, support and guidance from my family, friends and the faculty of Marine Technology department, NTNU which helped me in successfully completing my thesis work.

Prateek Gupta

Abstract

The design of a structure is based on the strength requirements to sustain the operational as well as installation loads. An accurate estimation of such loads is also necessary for resource and mission planning of marine operations involving the deployment or installation of these structures. The hydrodynamic loads on a structure are often expressed as a summation of added mass and damping force components (as in Morison's equation) which can in-turn be calculated from analytically, experimentally or numerically determined added mass and drag coefficients. The purpose of this work is to experimentally determine hydrodynamic loads on porous structural components such as perforated plates and rod screens in different cases of fluid flow.

It is observed that the hydrodynamic loads, for a porous plate placed in a uniformly oscillating flow in infinite fluid (such as forced oscillations in deep water), are damping dominated due to high damping to added mass ratio. The objective of the current work is to investigate the damping or drag dominance, in different conditions of fluid flow, for two different type of porous plates: perforated plate with sharp edged circular openings, and rod screen with equally spaced circular rods. First, the KC number (or porous KC number) varying hydrodynamic coefficients for porous plates are determined from forced oscillations in deep water. Then water-entry drag coefficient is determined from the force impulse observed during constant velocity water-entry for both types of plates. Finally, the rod screen type porous plate is subjected to incident waves, while it is held fixed and fully submerged at a small water depth.

Results indicate that damping can be as high as 1.5 to 3.0 times the added mass for a porous structure in forced oscillation case whereas it can be, surprisingly, 10 to 100 times when subjected to incident waves. In case of constant velocity water-entry, it is observed that the slamming impact peak has negligible contribution to the force impulse and thus, the total force is drag dominated. This indicates that a strong emphasis should be placed on estimation of damping or drag loads on such structures.

Further, the empirical method suggested by DNV-GL to estimate zero amplitude (KC = 0) added mass and the added mass reduction factor curve to obtain conservative estimates of added mass for a porous structure were compared with the results from current work. In case of first a validity range, in terms of KC number, is defined where it can be applicable to obtain conservative estimates of added mass. Additionally, linearized damping model was discussed for deep water forced oscillation tests. The water-entry drag was found to be significantly influenced by free surface phenomenon like attachment of air bubbles and delayed wetting of top surface. Negative added mass was observed in some cases of wave tests.

Contents

Chapter 1
Introduction

The need for design and analysis of a structure originates from various important factors. For a structure located offshore or subsea, the process becomes critical and often more complicated due to the involved cost and risk factors. One of the most crucial task within the oil and gas industry is to estimate the hydrodynamic forces acting on structures due to excitation loads.

Splash zone hydrodynamics refers to the hydrodynamic forces acting on structures in splash zone, i.e., near the free surface, due to the action of waves. Such forces are highly dynamic in nature and may not be estimated accurately using simple calculations, specially for an irregular geometry. They are important for structures permanently installed in splash zone (i.e., near the free surface) as well as during the installation of subsea equipment like a subsea module.

According to DNV-GL's recommended practice for 'Modelling and Analysis of Marine Operations' [1], the subsea lift operation for installation of subsea equipment can be discretized into following 4 steps:

- Lift off from deck and maneuvering object clear of transportation vessel
- Lowering through the wave zone → *Splash-zone hydrodynamic loads*
- Further lowering down to sea bed → *Infinite fluid hydrodynamic loads*
- Positioning and landing

The infinite fluid hydrodynamic loads are estimated as a summation of 2 main force components which are proportional to accelerations and relative velocity between the structure and fluid, known as inertia[1] and damping force components, respectively. This was initially postulated by Morison, O'Brien, Johnson, and Schaaf in 1950 [3] and was presented as a formulation, now known as Morison's equation.

On the other hand, to estimate the splash zone hydrodynamic loads, the problem is modeled as a complex water-entry force (or water-exit for lifting up through the wave zone). As presented in DNV-GL's recommended practice [1], the water-entry force can be estimated as a summation of 4 main force components: Buoyancy force, Hydrodynamic mass force, Slamming impact force, and Hydrodynamic drag force. This is further discussed in detail in section 2.2.

[1]The inertia term consists of a body mass term (also known as Froude-Kriloff force), proportional only to fluid acceleration, and an added mass term, proportional to relative acceleration between structure and fluid (Faltinsen 1993 [2]).

Additionally, in many known cases like top plate of a suction anchor, protection cover for a subsea module, etc., the structure or a component is not completely solid but instead a porous geometry. For the efficient design of such structures the forces acting on the structure during installation as well as operational phase needs to be estimated. As a general practice now, the installation crew has to wait for the sea condition to become extremely calm (for example, significant wave height $(H_S) \leq 3m$) to carry-out the installation of any structure. Moreover, in some cases the structure is over-designed due to the uncertainty in estimated hydrodynamic loads. This leads to inefficient use to capital and resources. The motivation for this topic is based on the fact that if we can better estimate these hydrodynamic loads for porous structures these inefficiencies can be controlled to a better extent.

The current thesis presents the results from the experiments conducted to determine the above mentioned hydrodynamic loads for a porous plate by subjecting it to 3 different types of tests: deep water forced oscillations, constant velocity water-entry and fully submerged fixed plate in waves. The main structure of this report is as follows: the current chapter covers the introduction, motivation and literature review; chapter 2 contains the required theory; chapter 3 presents the experimental setup, model details, test parameters and post-processing procedure; and chapter 4 covers the obtained results and relevant discussion; chapter 5 presents the conclusions from obtained results and discusses the possible scope of further work on the current subject.

1.1 Estimation of Hydrodynamic Force

As mentioned above, according to Morison's equation, the total hydrodynamic force on a static or moving body in a flow field is calculated as an addition of added mass (or inertia force in case of an accelerating flow field like waves) and damping force components. These force components are further expressed in terms of added mass and damping (or drag) coefficients, as shown in section 2.7. Here, it should be duly noted that Morison's model is a simplified formulation for a much complex problem. It suffers from various deficiencies as discussed in detail by Sarpkaya, 1981 [4]. Additionally, it is only applicable in case of a uniform flow field or within the limits of long wave approximation, i.e, body dimension are small compared to wavelength ($\frac{\lambda}{D} \geq 5$, refer Faltinsen 1993 [2]).

There are many different ways to estimate the hydrodynamic coefficients, i.e., added mass, damping and drag coefficients, for a structure. Usually, a complex structure is approximated as a combination of many simple geometries. For these geometries, the hydrodynamic coefficients can be further determined using well established analytical, experimental or numerical methods.

Newman, 1977 [5], analytically calculated the added mass for some of these simple geometries, for example, a solid flat plate. He also presented the experimentally determined viscous drag coefficients for a sphere, a flat plate and other general

bodies. Blevins, 1984 [6], presented a method to analytically or empirically calculate the drag force for screens, grillages and perforated plates using the principles of fluid dynamics. He calculated the drag force in terms of the total static pressure drop across the plate. This method is further discussed in section 2.4. Based on some of the above developments and many other sources, DNV-GL, 2017 [1], has also presented a compiled list of these coefficients in its recommended practice.

The above method of discretizing a complex structure like a porous plate into simple geometries does not provide very accurate results as it does not take into account the interaction effects between the discretized members. DNV-GL [1] recommends that for porous structures with porosity ratio (or perforation area ratio) less than 50%, these interaction effects must not be neglected. So, to obtain accurate results, it is recommended to employ numerical or experimental methods for the whole structure. Some of the most popular numerical methods include CFD (Computational Fluid Dynamics) and BEM (Boundary Element Method). BEM, based on potential flow theory, is relatively simple and requires less resources but it is not feasible in some complex cases whereas CFD requires large computational power. An additional challenge with numerical methods is to establish the validity of results. On the other hand, experimental methods, if translated correctly from test to work environment, are more reliable but they can be expensive and time consuming.

There are two well established methods to experimentally determine the added mass and damping of a body as mentioned in DNV-GL's recommended practice [1]:

- Free decay tests
- Forced oscillations tests

Both the above methods yield quite reliable results. In the current work, the hydrodynamic coefficients for the porous plates are determined using the forced oscillations tests.

1.2 Case of a Porous Plate

As indicated above, the results for the added mass of a solid flat plate obtained by Newman, 1977 [5], cannot be directly used in case of a porous plate. According to DNV-GL's recommended practice [1], ventilated (or porous) structures comprises of structures where a plane normal to the oscillation direction is either arranged with holes or slots or consists of parallel slender elements. Examples are horizontal top plate of a suction anchor with ventilation holes and top area of a protection structure.

Molin, 2001 [8], started in the late eighties with the hydrodynamic analysis of the stabilizer of the Roseau (reed) compliant tower. This stabilizer is a sparsely

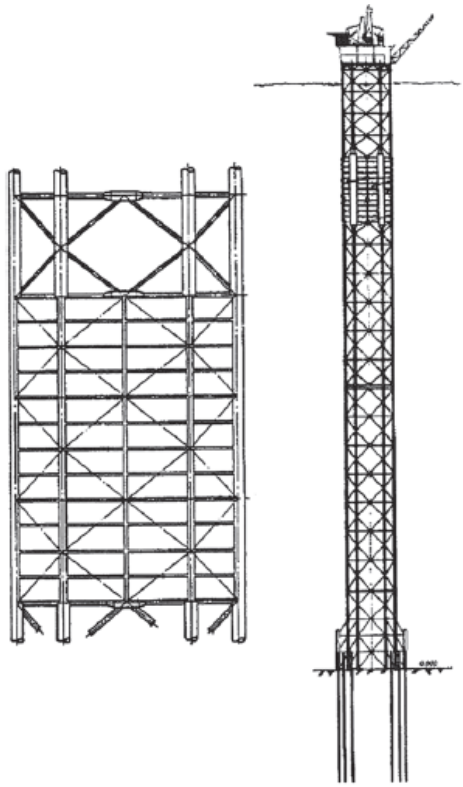

Figure 1.1: *The Roseau (reed) complaint tower and its stabilizer. Source: [7].*

Figure 1.2: *Example of porous structure, a protection cover for subsea modules. Source: [7].*

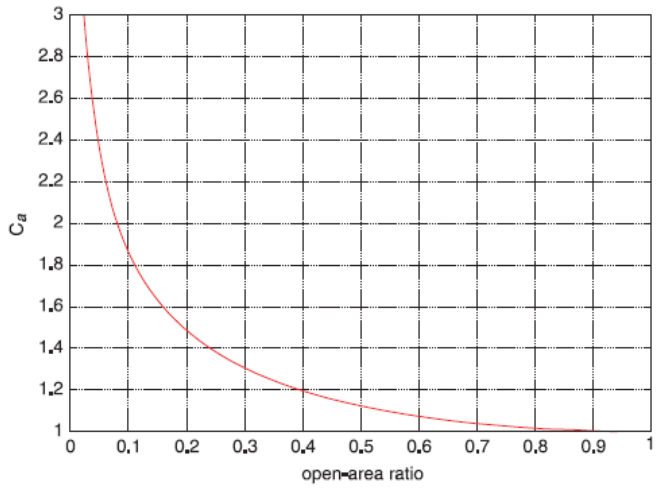

Figure 1.3: *Added mass coefficient vs. open-area ratio. Source: [7].*

porous flat structure as shown in Figure 1.1. Another example of porous structure is the tubular frame shown in Figure 1.2, used as a protection cover for subsea modules on the seabed. Molin [8] suggested a method to calculate the added mass and damping of periodic arrays of fully or partially porous discs using potential flow theory. This method includes the effect of pressure drop across the porous disc which is quadratic with respect to the normal relative velocity.

Molin, 2011 [7], presented the two-dimensional case of a channel flow through a slit or diaphragm. The width of the channel is d and the diaphragm width is $(d-2b)$. The added mass for the obstruction can be: $a = C_a(\tau)\rho\pi b^2$ (from Morse, 1971 [9]). Here, $C_a(\tau)$ is the porosity (τ) dependent added mass coefficient expressed as (also shown in Figure 1.3):

$$C_a(\tau) = \frac{8}{(1-\tau)^2\pi^2} \ln\left[\frac{1}{2}\tan\frac{\pi\tau}{4} + \frac{1}{2}\cot\frac{\pi\tau}{4}\right] \tag{1.1}$$

Based on above, Molin, 2011 [7], in order to extend the results to porous plates, considered a channel of width D with a series of N identical slots and solid parts of widths $(1-\tau)D/N$. The total added mass of channel obstruction (or porous plate) was formulated as:

$$a = N\rho\pi\frac{(1-\tau)^2 D^2}{4N^2} C_a(\tau) \tag{1.2}$$

It should be noted that a goes to zero as N goes to infinity, invariable of the value of τ. Thus, according to the potential flow theory, inertia loads (due to the added mass) are nil in the limiting case when the openings are infinitely small and numerous. So, the pressure drop is only proportional to the velocity square even in the case of an accelerated flow but the inertia load on the whole structure cannot be

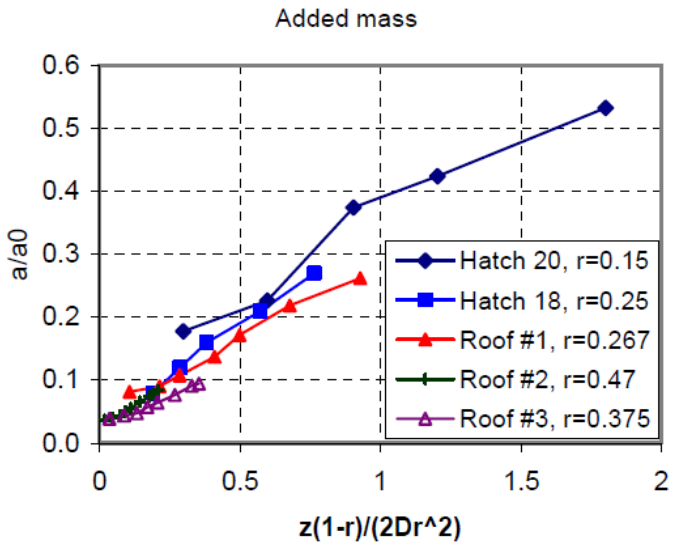

Figure 1.4: *Added mass ratios of 5 perforated objects vs μKC_{por}. Source: [10].*

neglected, due to the non-zero phase difference between the local flow and the outer flow. The above method always assumes flow separation even for small amplitudes of motion and it does not take into account the influence of flow separation along the disc edge. Thus, it has to be accounted separately.

Sandvik, 2006 [10], conducted experiments to determine the hydrodynamic added mass and damping for porous structures by using 5 different models representing typical protection structures, with perforation area ratio (r) varying from 0.15 to 0.47. The added mass (a) is normalized by the added mass of the solid plate (a_0) of the same dimensions. The variation of added mass with amplitude of oscillation (z or X_A) was found considerable as shown in Figure 1.4.

Sandvik [10] also compared the results for a hatch cover (Hatch 18) with the above discussed numerical method (shown in Figure 1.5). He also included the edge effect due to flow separation by using the drag coefficient for a solid plate suggested by Faltinsen, 1993 [2]. He used the $1/4^{th}$ of the suggested value for drag coefficient (i.e., $C_D = 2KC^{-1/3}$) to account for the rounding of the edges. As observed in Figure 1.5, including the edge effect reduced the added mass and increased the linearized damping and it becomes more prominent as the KC number increases.

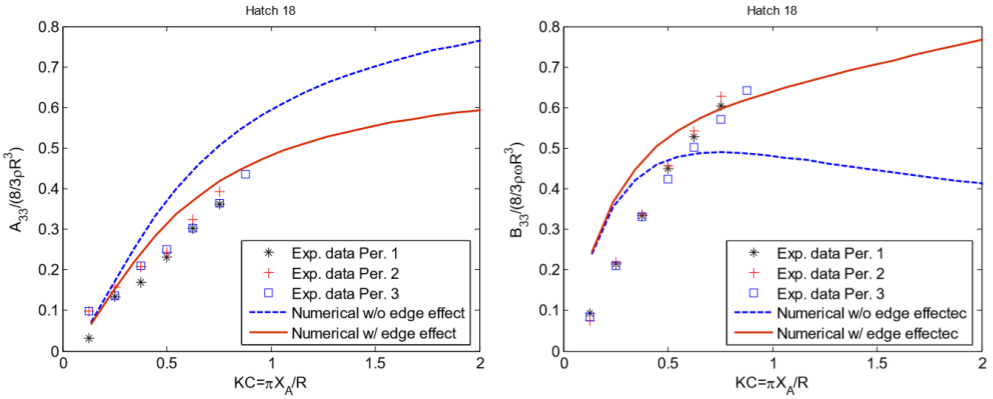

(a) Added mass **(b)** Damping

Figure 1.5: *Estimated and measured added mass and damping vs KC number for a hatch cover. Source: [10]*

1.3 Industry Standards & DNV-GL's Recommended Practices

As can be surmised from the above discussion, the majority of work done till now regarding the marine applications of porous structures is mostly focused on calculating or estimating the added mass of these type of structures. There seems to be a wide and significantly important gap when we look towards the damping or drag aspect of the total hydrodynamic loads. The same is also reflected in DNV-GL's recommended practice [1]. It is recommended to conduct model tests to accurately determine the hydrodynamic coefficients for complex 3D subsea structures. In case of added mass for porous (or ventilated) structures, it refers to the results obtained by Sandvik, 2006 [10], for 5 ventilated structures (shown in Figure 1.4), and the following method to estimate the asymptotic value of zero amplitude added mass.

The asymptotic value of zero amplitude (KC = 0) added mass for a porous structure can be found by BEM, i.e., within the limits of potential flow theory by using a source-sink panel method. Derived from this, DNV-GL, 2017 [1], recommends the following empirical relation:

$$\frac{A_{33}}{A_{33,0}} = e^{-r/0.28} \tag{1.3}$$

Where A_{33} is the zero amplitude limit ($KC \to 0$) added mass for a porous plate, and $A_{33,0}$ is the added mass for the equivalent solid plate. The above equation is established by curve fitting through the results for plates with circular holes, but it has also been found applicable for plates with ventilation openings (as shown for model in Figure 1.2). As can be seen and also clearly pointed-out in DNV-GL's

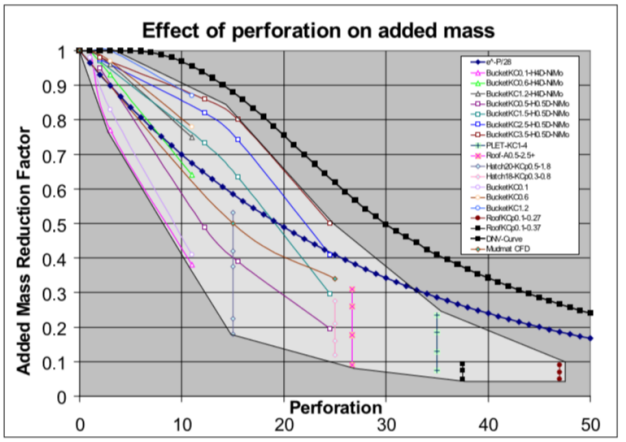

Figure 1.6: *Added mass reduction factor as a function of perforation area ratio. Source: [1].*

recommended practice [1], this relation do not agree with the results from oscillatory fluid flow case (as presented in Figure 1.4). In the current work, the zero amplitude added mass obtained from this empirical relation is compared to the experimental results and a validity range, in terms of KC number, is defined where it can be applicable to obtain conservative estimates of added mass. This is further discussed in section 4.2.

In addition to above, DNV-GL [1] suggests an added mass reduction factor curve (shown in Figure 1.6) solely based on the perforation area ratio to obtain conservative estimates of added mass irrespective of the range of KC number. For perforation area ratio greater that 50%, it is recommended to neglect interaction effects and calculate the added mass as a sum of added mass for individual components.

Here, it should be noted that no such methods are suggested for estimation of the damping or drag loads on porous structures due to lack of any significant work in this regard as well as complexity of the problem. The primary aim of the current work is to emphasize on the fact that hydrodynamic loads on porous (or ventilated) structures are damping or drag dominated and much work needs to be done in this field.

Chapter 2
Theory

This chapter covers the theory behind the work done in this thesis. It should give a clear incite to the reader about the derivations and calculations used in order to get to the results presented later in chapter 4.

2.1 Hydrodynamic Force: Harmonically Forced Oscillations

The steady-state hydrodynamic force acting on a body due to forced harmonic rigid body motions in vertical direction can be expressed as [2]:

$$F_{3,hyd} = -A_{33}\ddot{\eta_3} - B_{33}\dot{\eta_3} - C_{33}\eta_3 \tag{2.1}$$

Where A_{33} is the frequency dependent added mass in heave, B_{33} is the damping and C_{33} is the restoring force coefficient. η_3 is the displacement in vertical direction and a dot over it represents a time derivative.

The force measured during experiments would also include the inertia contributions due to the body mass. So the above equation can be re-written as:

$$F_{meas} = -(M + A_{33})\ddot{\eta_3} - B_{33}\dot{\eta_3} - C_{33}\eta_3 \tag{2.2}$$

Where M is the mass of the body and F_{meas} is the total measured force.

In case of a harmonic sinusoidal motion, acceleration and displacement are 90° out of phase with velocity and 180° out of phase with each other. It is also known that integral of harmonic orthogonal vectors over a cycle or period (T) is zero, for example, $\int_0^T \cos\omega t \sin\omega t dt = 0$. Thus, the force coefficients from equation 2.2 can be further calculated as:

$$A_{33} = -\frac{\int_t^{t+nT} F_{meas}\ddot{\eta_3}dt + \int_t^{t+nT} C_{33}\eta_3\ddot{\eta_3}dt}{\int_t^{t+nT} \ddot{\eta_3}\ddot{\eta_3}dt} - M \tag{2.3}$$

and

$$B_{33} = -\frac{\int_t^{t+nT} F_{meas}\dot{\eta_3}dt}{\int_t^{t+nT} \dot{\eta_3}\dot{\eta_3}dt} \tag{2.4}$$

2.2 Water-Entry Force

The total vertical water-entry force acting on a body can be expressed as a summation of different hydrodynamic force components (from DNV-GL [1]):

$$F_{WE} = F_\rho + F_m + F_s + F_d \tag{2.5}$$

Where F_ρ is the varying buoyancy force, F_m is the hydrodynamic mass force, F_s is the slamming impact force, and F_d is the hydrodynamic drag force.

The water-entry problem can be further simplified by assuming still horizontal water surface and constant vertical water-entry velocity of the moving body. With these assumptions the above hydrodynamic force components can be expressed as follows:

i. **Buoyancy Force (F_ρ):** For a surface piercing body, buoyancy force can be calculated as the mass of water displaced by the body:

$$F_\rho = \rho g A_{WP} h \tag{2.6}$$

Where A_{WP} is the horizontal water-plane area of body, ρ is the density of water, g is the acceleration due to gravity, and h is the submergence depth. For constant water-entry velocity (V), the submergence at time t can be calculated as $h = Vt$ (assuming $t = 0$ when body touches the still water surface).

ii. **Hydrodynamic Mass Force (F_m):** The hydrodynamic mass force is the inertial force due to the mass as well as added mass of the body:

$$F_m = -(A_{33} + M)\ddot{\eta}_3 \tag{2.7}$$

Thus, in case of constant vertical velocity this force component will be zero.

iii. **Slamming Impact Force (F_s):** The slamming impact force can be calculated as the rate of change of fluid momentum [1]:

$$F_s = \frac{d(A_{33}^\infty V_s)}{dt} \tag{2.8}$$

Where A_{33}^∞ is the infinite frequency added mass in heave of body, and V_s is the slamming impact velocity. The slamming impact force can also be calculated using experimentally determined slamming coefficient (C_s) as:

$$F_s = \frac{1}{2}\rho C_s A_s V_s^2 \tag{2.9}$$

Where A_s is the slamming area projected on the horizontal plane.

Additionally, it should be noted that slamming is characterized by very small time scales and initial impact loads. But for water-entry problems related to marine operations, integrated loads or force impulse are more important.

iv. **Hydrodynamic Drag Force (F_d):** The hydrodynamic drag force can be calculated using the drag coefficient:

$$F_d = \frac{1}{2}\rho C_D A_p \dot{\eta}_3 |\dot{\eta}_3| \tag{2.10}$$

Where A_p is the projected area of body on horizontal plane and C_D is the drag coefficient of the body.

Alternatively, the drag force can be calculated as the sum of linear and quadratic damping further explained in section 2.5.

2.3 Wave Excitation Force

A fixed plate fully submerged in waves experiences wave excitation loads due to the incident wave. The wave excitation loads can be calculated as (from Faltinsen, 1993 [2]):

$$F_{exc} = F_{FK} + F_{Diff} \tag{2.11}$$

where F_{FK} is the Froude-Kriloff force and F_{Diff} is the wave diffraction force. The Froude-Kriloff force can be interpreted as the force acting on the body due to the incident wave or moving fluid whereas the diffraction force can be interpreted as the body's reaction to the fluid while keeping itself static. These can be further expressed in terms of displaced fluid mass, added mass and damping components as follows:

$$F_{exc,3} = \rho V \overline{a}_{0,3} + A_{33}\overline{a}_{0,3} + B_{33}\overline{v}_{0,3} \tag{2.12}$$

where V is the body volume, $\overline{a}_{0,3}$ and $\overline{v}_{0,3}$ is the mean vertical acceleration and velocity, respectively, of fluid particles at body volume center. The above equation presents the excitation force in heave (z-direction) only and assumes the following:

- **Long Wave Approximation:** Body dimensions are small as compared to the wavelength, i.e., $\frac{\lambda}{D} \geq 5$, where D is the body dimension along the wave propagation direction. Thus, the variation of velocity and acceleration over the body volume is neglected.
- **Symmetry:** Body symmetry about vertical center plane. Thus, A_{31} and B_{31} are zero.

In case of a large volume body, discretization methods like strip theory can be used.

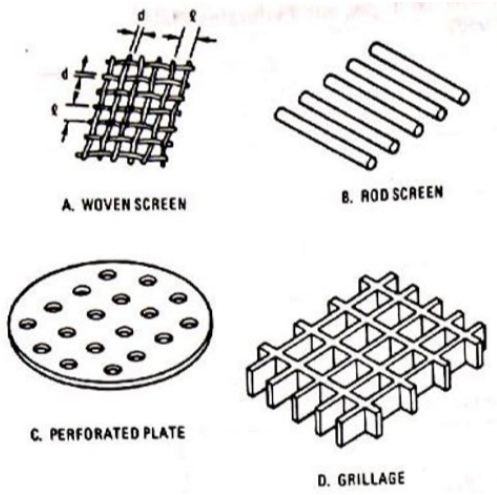

Figure 2.1: *Screens, Grillages and Perforated Plates. Source: [6].*

2.4 Drag Force estimation for Screens, Grillages and Perforated Plates

The drag force on a screen or perforated plate can be observed as a result of static pressure drop across the plate as the fluid flows through the screen [6]. The drag force, measured perpendicular to the plate, can be calculated as:

$$F_D = (p_2 - p_1)A \tag{2.13}$$

Where $(p_2 - p_1)$ is the static pressure drop across the plate and A is the total plate area.

Blevins, 2003 [6], has presented the experimentally or empirically obtained values of pressure loss coefficients for different types of screens and plates assuming in-compressible flow in a pipe or duct. The pressure loss coefficient is defined as:

$$K = \frac{(p_2 - p_1)}{\frac{1}{2}\rho U^2} \tag{2.14}$$

The pressure loss coefficient is dependent on following parameters:

- Perforation or open area ratio (r) of the plate
- Reynolds number (Re) based on gap or rod diameter

At low Reynolds number ($Re < 500$), the flow is laminar and the pressure loss coefficient (K) increases as Re decreases. In case of a turbulent flow, K becomes largely independent of Re.

Additionally, the presence of sharp corners or edges at the entrance and exit of the perforation openings increases the static pressure loss due to flow separation at the edge [6].

2.5 Linear and Quadratic Damping

In reality, the damping force experienced by a body, generally, is non-linear in nature. In order to account for these non-linearities damping force component ($B_{33}\dot{\eta_3}$) is replaced by a linear and quadratic term in the equation of motion, 2.2. The linear damping is contributed by linear phenomenon like skin friction due to laminar boundary layers and wave radiation whereas the quadratic term includes non-linear phenomenon like skin friction due to turbulent boundary layers and vortex shedding. Thus, the damping term in equation 2.2 is substituted as:

$$B_{33}\dot{\eta_3} = B_{33}^{(1)}\dot{\eta_3} + B_{33}^{(2)}\dot{\eta_3}|\dot{\eta_3}| \tag{2.15}$$

The above equation can be re-written by linearizing the second term as shown by Keulegan and Carpenter, 1958 [11]:

$$B_{33}\dot{\eta_3} = B_{33}^{(1)}\dot{\eta_3} + \frac{8\dot{\eta}_{3_a}}{3\pi}B_{33}^{(2)}\dot{\eta_3} \tag{2.16}$$

Here, it should be noted that the above linearization is a mathematical approximation and is obtained by neglecting higher order terms proportional to third order harmonics (3ω) and above [11]. The error in the above equation can be calculated as the difference between the measured force and the force recalculated using the obtained force coefficients, also known as first-order force (right hand side of equation 2.2). In current engineering practices, this error is generally neglected.

Linear damping coefficient, $B_{33}^{(1)}$, can be calculated as the y intercept of B_{33} (calculated from equation 2.4) vs heave velocity amplitude, $\dot{\eta}_{3_a}$, (or KC number as $KC \propto \dot{\eta}_{3_a}$) and the quadratic damping coefficient, $B_{33}^{(2)}$, can be calculated as the slope of B_{33} vs $\dot{\eta}_{3_a}$ curve or rewriting the equation 2.16 as:

$$B_{33}^{(2)} = \frac{3\pi}{8\dot{\eta}_{3_a}}(B_{33} - B_{33}^{(1)}) \tag{2.17}$$

Alternatively, $B_{33}^{(1)}$ can be estimated from the waves created by the body (assuming nil contributions from other factors like skin friction due to laminar boundary layers) as:

$$B_{33}^{(1)} = \rho L\left(\frac{\zeta_a}{\eta_{3_a}}\right)^2\frac{g^2}{\omega^3} \tag{2.18}$$

where ζ_a is the outgoing wave amplitude, η_{3_a} is the body heave amplitude, ω is the outgoing wave frequency, g is acceleration due to gravity, ρ is the fluid density

and L is the length of the body normal and horizontal to wave propagation direction.

At this point, it should be duly noted that this model, known as linearized damping model, is only one of the many damping models used for engineering purpose. Another well known damping model is Morison's load model. Morison's load model assumes that damping force is completely quadratic in nature, i.e., $B_{33}\dot{\eta}_3 = B_{33}^{(2)}\dot{\eta}_3|\dot{\eta}_3|$, thus, it completely neglects the linear damping component (i.e., $B_{33}^{(1)} = 0$). So the equation 2.17 can be simply written as:

$$B_{33}^{(2)} = \frac{3\pi}{8\dot{\eta}_{3_a}} B_{33} \tag{2.19}$$

The duty lies with the user to decide which model to adopt. The applicability of linearized damping model for porous plates is further discussed in section 4.2.

2.6 Parameter dependence of Added mass and Damping

2.6.1 Oscillating Flow Field

Sarpkaya, 1981 [4], suggested the following main non-dimensional parameters influencing the hydrodynamic force on a body in an *oscillating flow field*:

1. **Keulegan Carpenter Number (KC):** Defined as the ratio of drag force to the inertia force, i.e.,
$$KC = \frac{U_m T}{D} = \frac{2\pi A}{D} \tag{2.20}$$
where U_m is the velocity amplitude of oscillating flow, T is the oscillation period, D is the body length scale (diameter for a cylinder) and A is the wave amplitude (or displacement amplitude of a harmonically oscillating body).

2. **Reynolds Number (Re):** Defined as the ratio of inertial forces to viscous forces, i.e.,
$$Re = \frac{U_m D}{\nu} \tag{2.21}$$
where ν is the kinematic viscosity of the fluid.

3. **Relative Roughness:** Defined as the ratio of surface roughness (k) to the length scale (D) of the body, i.e., k/D.

4. **Time History:** Defined as the ratio of time instant (t) to the oscillation period (T), i.e., t/T.

Thus, the non-dimensional hydrodynamic force can be written as:

$$\frac{F}{\frac{1}{2}\rho D U_m^2} = f\Big(KC, Re, \frac{k}{D}, \frac{t}{T}\Big) \tag{2.22}$$

Assuming that Morison's equation holds valid, the added mass and drag coefficients for a body in an *oscillating flow field* would also depend on the above parameters:

$$C_{A,OF} = f_1\Big(KC, Re, \frac{k}{D}, \frac{t}{T}\Big) \tag{2.23}$$

and

$$C_{D,OF} = f_2\Big(KC, Re, \frac{k}{D}, \frac{t}{T}\Big) \tag{2.24}$$

It should be noted that above relation does not account for some additional case specific effects like 3D effects (coherence), end effects, wall boundary layers, free surface effects, etc.

As discussed by Sarpkaya, 1981 [4], the effect of time history cannot be included without introducing atleast 1 additional term in Morison's equation. But due to cited complications, it is unavoidable to approximate C_A and C_D as time-invariant averages over an oscillation cycle, thereby eliminating time as an independent parameter. The time-invariant averages can be calculated using many different mathematical techniques like Fourier averaging, least square method, two-point values, etc. These are broadly discussed by Sarpkaya and Isaacson, 1981 [12]. In the current work, Fourier averaging technique is adopted.

Additionally, Sarpkaya [4] suggested that Reynolds number (Re) may not be a suitable parameter in case of harmonically oscillating flows due to the fact that both KC and Re contains U_m. Keulegan and Carpenter, 1958 [11], could not demonstrate Re dependence of C_A and C_D but later Sarpkaya, 1976 [13], introduced a new parameter $\beta = Re/KC = D^2/\nu T$ (known as 'Frequency parameter') to clearly demonstrate this effect. Thus, the above equations for oscillating flow case can be rewritten as:

$$C_{A,OF} = f_1\Big(KC, Re, \frac{k}{D}\Big) = f_1'\Big(KC, \beta, \frac{k}{D}\Big) \tag{2.25}$$

and

$$C_{D,OF} = f_2\Big(KC, Re, \frac{k}{D}\Big) = f_2'\Big(KC, \beta, \frac{k}{D}\Big) \tag{2.26}$$

2.6.2 Non-Oscillating or Steady Flow Field

As obvious, KC is only defined in case of an oscillating flow such as deep water forced oscillations and wave excitation loads. For a steady or unsteady *non-oscillating flow* like in case of a body placed in a current, Strouhals number (St) is an important parameter, defined as:

$$St = \frac{f_v D}{\overline{V}} \tag{2.27}$$

where f_v is the vortex shedding frequency, D is the body length scale and $\overline{V}$ is the mean flow velocity. For a 2D flat plate section with flow normal to its length, Strouhals number represents the ratio between the plate length and the distance covered by the flow current during a shedding period. The value of St depends on the flow regime and boundary layer which in-turn depends on Re and surface roughness (k).

Thus, the drag coefficient ($C_{D,Steady}$) for steady *non-oscillatory flow* depends primarily on the following parameters:

1. Reynolds number, Re.
2. Relative roughness, k/D.

Here, it should be noted that C_D for steady non-oscillatory flow fluctuates with twice the vortex shedding frequency (i.e., $2f_v$) and non-symmetric vortex shedding phenomena gives rise to a transverse lift force [4].

Thus, the time averaged drag coefficient for steady non-oscillatory flow can be expressed as:

$$C_{D,Steady} = f_3\Big(Re, \frac{k}{D}\Big) \tag{2.28}$$

2.6.3 Water-Entry Drag

As discussed in section 2.2, the total water-entry force has a drag component. This drag component, after the body has travelled a substantial distance in water, will be same as the steady drag. But in initial phase of water-entry, this drag is not exactly same as the steady drag because during the water-entry we observe following 2 important free surface phenomenon:

- Attachment of air bubbles to the body.
- Delayed wetting of the top surface, i.e., top surface of the body remains dry for some time even after the whole body has translated past the still water level.

It should be noted that both these effects are diminished as the body travels some distance in water and disappear completely after certain depth limit. After this depth limit, the drag becomes steady and the free surface effects are negligible. This implies that during the initial phase of water-entry (until we reach this depth limit) the drag coefficient also depends on the instantaneous submergence below still water level, h. Ideally, the instantaneous submergence or, simply, submergence (h) should be non-dimensionalized using the above mentioned depth limit but since

this limit is not known here, we can use an arbitrary length scale like plate length instead. Thus, the parametric formulation for water-entry drag can be written as:

$$C_{D,WE} = f_4\Big(Re, \frac{k}{D}, \frac{h}{L}\Big) \tag{2.29}$$

It should be noted that the submergence (h) is later mentioned as $V_Z t$ where V_Z is the water-entry velocity and t is time with $t = 0$ at the instant when the plate touches the still water level.

2.6.4 Porous Plates

For a transversely moving thin plate, the dependence on surface roughness (k) disappears due to negligible transversely projected area. The added mass of porous plates is highly dependent on the amplitude of motion (z or X_a), and it is usually associated with strong damping [7]. This is surely due to the viscous effects, i.e., flow separation at the porous openings. Moreover, with the limit that we have very small but infinite number of openings, perforated plates are characterized by the following 2 additional parameters [14]:

1. Perforation area ratio (r) defined as the open area divided by the total area.
2. Discharge coefficient (μ) which depends on the shape of the openings and Reynolds number. Typical values of μ are usually between 0.5 to 1.0 for steady flow conditions.

Based on above, Molin, 2001 [8], introduced porous KC number, defined as:

$$KC_{por} = \frac{z}{D}\frac{(1-r)}{2\mu r^2} \tag{2.30}$$

Thus, the parameter dependency relations for transversely moving thin porous plates can be written as (modified from Equations 2.25, 2.26 and 2.29):

$$C_{A,OF} = f_1''(KC_{por}, Re) = f_1'''(KC_{por}, \beta) \tag{2.31}$$

$$C_{D,OF} = f_2''(KC_{por}, Re) = f_2'''(KC_{por}, \beta) \tag{2.32}$$

$$C_{D,WE} = f_4'\Big(Re, \frac{h}{D}, r, \mu\Big) \tag{2.33}$$

2.7 Hydrodynamic Coefficients

The force coefficients derived above can be non-dimensionalized in the form of hydrodynamic coefficients, i.e., added mass (C_A) and drag coefficients (C_D), used in Morison's equation. Morison's equation for a 1D flat plate section (or line) of width D extended in 2D by length L is:

$$F_3 = \rho\frac{\pi D^2}{4}LC_M\ddot{\eta_3} + \frac{\rho}{2}DLC_D|\dot{\eta_3}|\dot{\eta_3} \tag{2.34}$$

where C_M is the mass coefficient which is related to C_A as $C_M = 1 + C_A$.

Added Mass:

Comparing the above equation with equation 2.2 and equation 2.16, the force coefficients A_{33} can be non-dimensionalized as:

$$C_A = \frac{A_{33}}{\rho\frac{\pi D^2}{4}L} \tag{2.35}$$

A conventional way to non-dimensionalize added mass for a porous plate is to use the analytically calculated added mass of an equivalent solid plate. The added mass of a solid plate of dimensions DxL ($D < L$) is:

$$A_{33,0} = k\rho\frac{\pi D^2}{4}L \tag{2.36}$$

where k is a coefficient depending on the aspect ratio of the plate. But in our case, the flat plate is idealized as a 1D line of length D stretched in 2D over length L, therefore, $k = 1$. Thus, equation 2.35 can also be written as:

$$C_A = \frac{A_{33}}{A_{33,0}} \tag{2.37}$$

Linearized Damping:

The linearized damping (B_{33}) can be non-dimensionalized in a similar to added mass as:

$$B_{33,Non-dim} = \frac{B_{33}}{\omega A_{33,0}} = \frac{B_{33}}{\omega\rho\frac{\pi D^2}{4}L} \tag{2.38}$$

Drag Coefficient:

The drag coefficient (C_D) used in Morison's equation is quadratic in nature and is non-dimensionalized by comparing equation 2.34 with damping term in equation 2.2 resulting as follows:

$$C_D = \frac{3\pi}{8\dot{\eta}_{3a}}\frac{B_{33}}{\frac{\rho}{2}DL} \tag{2.39}$$

In above expression for C_D, the factor of $3\pi/8$ appears from the mathematical approximation discussed in section 2.5. Additionally, as mentioned earlier, Morison's equation neglects linear damping term ($B_{33}^{(1)}$). So, in case of linearized damping model explained in section 2.5, the quadratic damping component ($B^{(2)}$) can be non-dimensionalized as follows:

$$C_D = \frac{B_{33}^{(2)}}{\frac{\rho}{2}DL} = \frac{3\pi}{4\dot{\eta}_{3a}} \frac{B_{33} - B_{33}^{(1)}}{\rho DL} \tag{2.40}$$

2.8 Wave Modelling: Linear Wave Theory

Long-crested regular waves, propagating in a direction, can be modelled using linear wave theory (also known as Airy theory) [2]. For finite water depth, the velocity potential for a regular wave propagating in positive x-direction is expressed as:

$$\phi(t, x, z) = \frac{g\zeta_a}{\omega} \frac{\cosh k(z + h)}{\cosh kh} \cos(\omega t - kx) \tag{2.41}$$

Where ζ_a is the wave amplitude, $\omega = \frac{2\pi}{T}$ is the wave angular frequency, $k = \frac{2\pi}{\lambda}$ is the wave number, h is the water depth, g is the acceleration due to gravity and (t, x, z) refers to time, x- and z-position coordinates. Here, it should be noted that the origin is assumed to be located at Mean Water Level (MWL). So, z is negative below MWL.

The wave particle velocity in x- and z-directions can be derived by differentiating $\phi(t, x, z)$ with respect to x and z, respectively, as follows:

$$u(t, x, z) = \omega\zeta_a \frac{\cosh k(z + h)}{\sinh kh} \sin(\omega t - kx) \tag{2.42}$$

$$w(t, x, z) = \omega\zeta_a \frac{\sinh k(z + h)}{\sinh kh} \cos(\omega t - kx) \tag{2.43}$$

The respective accelerations can be further defined by differentiating the velocities with respect to time. Additionally, it should be noted that according to the linear wave theory the velocity potential and fluid particle velocities are assumed to be constant with respect to z from MWL to the actual free surface under the crest. Figure 2.2 shows the horizontal velocity distribution under a wave crest and a wave trough according to linear wave theory. The acceleration profiles will also be similar.

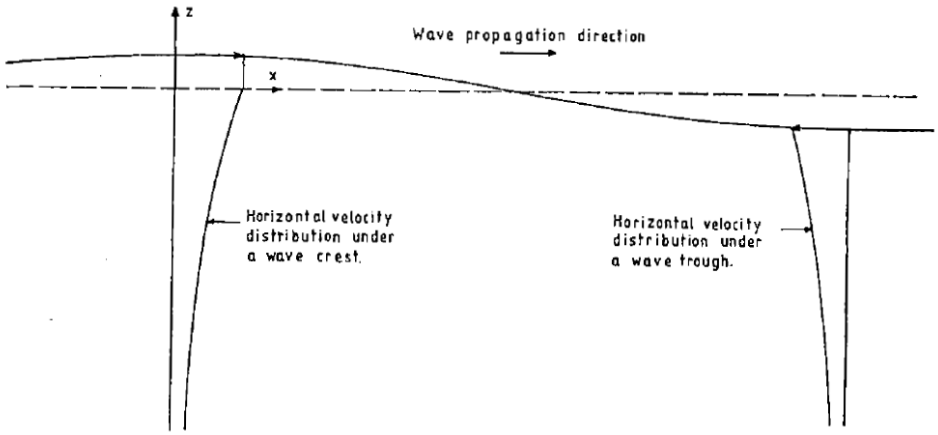

Figure 2.2: *Horizontal velocity distribution under a crest and a trough according to linear wave theory. Source: [2].*

Dispersion relation defines the relation between the wavelength (λ) and wave period (T). For finite water depth, this relation is defined as:

$$\omega^2 = gk \tanh kh \tag{2.44}$$

The velocity of the wave crest or trough for a regular wave, i.e., the phase velocity is defined as follows:

$$C_p = \frac{\omega}{k} = \sqrt{\frac{g}{k} \tanh kh} \tag{2.45}$$

The corresponding equations for infinite water depth can be derived from finite water depth equation by applying a limit for $h \to \infty$.

Chapter 3
Experimental Setup & Procedure

The current work is extensively based on experimental results and findings. Three main types of experiments were conducted during the course of this thesis:

- Deep water forced oscillations
- Constant velocity Water-entry
- Fully submerged fixed plate in waves

Deep water forced oscillations tests were conducted to determine the added mass and damping coefficients of the test models with varying KC_{por}. *Water-entry* tests were conducted to determine water-entry drag coefficient with varying water-entry velocity and the third type of tests were conducted to analyze the hydrodynamic loads on a static and fully submerged porous plate in waves.

This chapter will describe the experimental setup, test parameters and post-processing procedure for all these types of experiments.

3.1 Test Environment

The experiments were carried-out in an enclosed laboratory, Ladertanken, at NTNU's Tyholt campus. Ladertanken consists of a 2D wave flume tank with dimensions 13m x 0.6m x 1.3m. The tank is provided with a single flap type wave generator at one end and parabolic wave damping beach on the other to facilitate the breaking of created waves. During the course of deep water forced oscillations and water-entry tests beaches were installed at both the ends of the tank.

The mean water level in the tank was maintained at around $100 \sim 104cm$ and the wave beaches were installed such that they are always about $2 \sim 3mm$ submerged below the mean water level. Prior to running each test the mean water level as well as the position of beaches were duly noted.

The temperature of water in the tank was recorded on an every day basis and it was observed to be around $21°C \sim 23°C$.

Additional care was taken to limit any type of disturbances and structural vibrations while running the tests, specially during the pluck tests.

3.2 Test Rig

The wave flume tank is provided with a rails and carriage arrangement on the top. The test rig was installed on the carriage and tied down on all 4 corners to prevent any movement in horizontal plane. The carriage is provided with an electric motor to facilitate the vertical motion of the test rig. The rotational motion of the motor is converted into the vertical motion of the test rig using a ball-screw arrangement.

In further discussion, the plane containing carriage rails is defined as the horizontal plane with x-axis along the rails and the vertical or z direction is defined as along the water depth and upward positive.

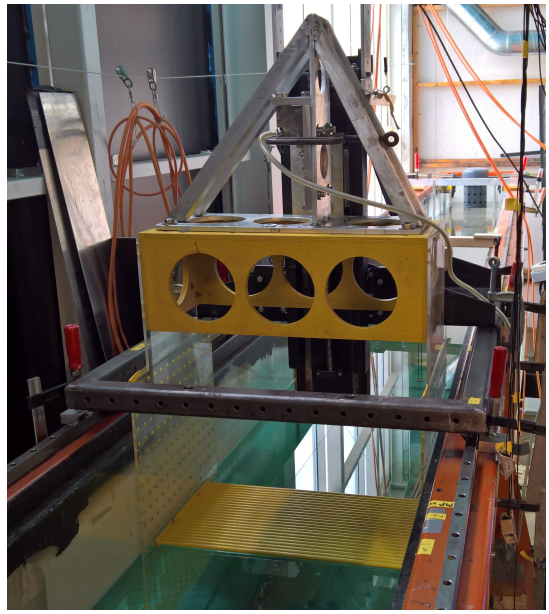

Figure 3.1: *Test rig.*

The rig top frame (triangular aluminium frame as shown in Figure 3.1) was bolted to the yellow wooden box which was provided with thin plexi-glass plates ($6.5mm$ thick) on either side. The plexi-glass plates were provided with a grid of holes to facilitate the installation of test models. Test models were installed between these plexi-glass plates at required depths. All the unused grid holes on plexi-glass plates were plugged using wax. The yellow box and plexi-glass plates is further on-wards referred to as lower rig.

Following points were always checked and ensured while installing or changing the lower rig:

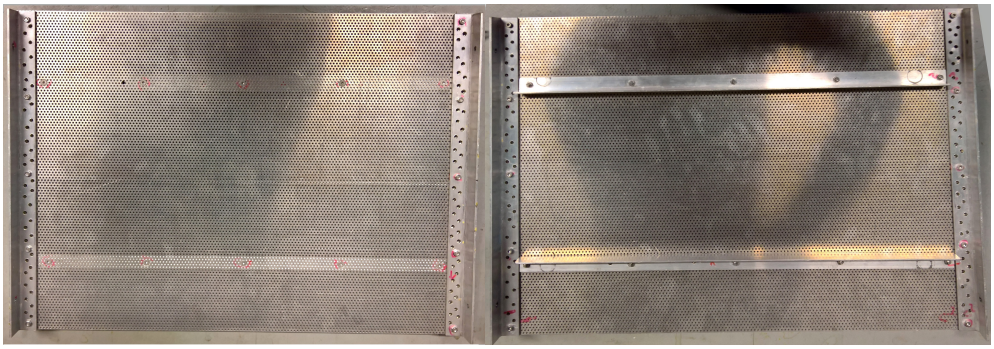

(a) Bottom View **(b)** Top View

Figure 3.2: *P19 Test Model.*

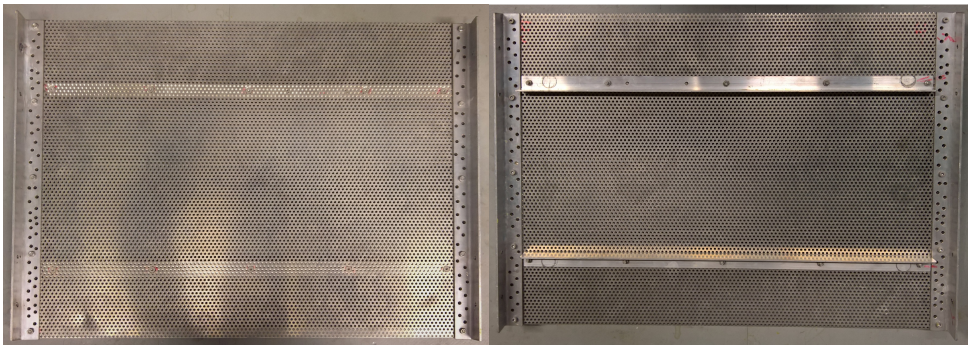

(a) Bottom View **(b)** Top View

Figure 3.3: *P28 Test Model.*

- The yellow box as well as the model plate is horizontally leveled within the practical limits of ~ 0.2°.
- The distance between plexi-glass plates and tank walls is almost equal on either side.
- All the unused grid holes on plexi-glass plates are plugged properly and the surface is flattened evenly.

3.3 Test Models & Configuration

Following two types of test models (depicted in Figure 2.1) were used:

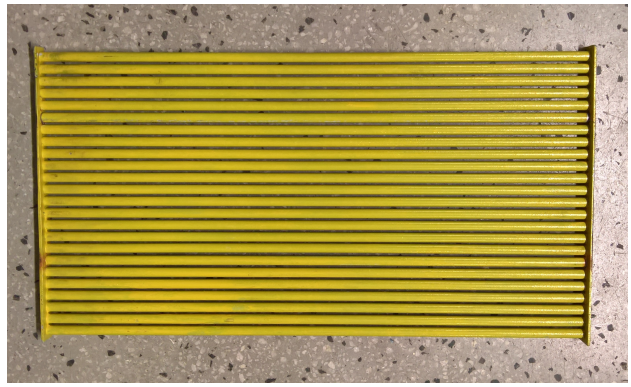

Figure 3.4: *FING Test Model.*

Table 3.1: *Test models.*

Model	**Type**	**Mass (kg)**	**Dimensions (DxLxt) (mm)**	**Perforation / rod diameter (mm)**	**Open area ratio (r)**
P19	Perforated Plate	2.31	420x570x3	2	0.186
P28		2.13		3	0.278
FING	Rod Screen (24 rods)	3.02	297x570x10	10	0.189

- **Perforated plates:** Flat aluminium plates provided with a grid of equal diameter circular perforations arranged in staggered fashion.
- **Rod screen:** A metallic rod screen containing a sequence of 24 equally spaced cylinders.

Total 3 test models of the above two types were used. The dimensions and properties of these models are presented in Table 3.1. The perforated aluminium plates were provided with 2 L-bar type transverse stiffeners to provide extra stiffening to the thin plates. The test models *P19*, *P28* and *FING* are shown in Figures 3.2, 3.3 and 3.4, respectively. The width (D) of the model plates was oriented along the length of the tank. The distance between the plexi-glass plates was equal to the plate length (L), i.e., $570mm$. The test models were installed between the plexi-glass plates using countersunk screws.

During deep water tests, the plates were installed at a mean position of about $49cm$ below the still water level. For water-entry tests, the plates were installed such that at mean position the plate mid horizontal plane is matching the still water level. For wave tests, only FING (rod screen) test model was used and it was positioned stationary and horizontal with plate mid plane (i.e., plane containing center-line of all the rods) $55mm$ below mean water level.

Table 3.2: *Sampling frequency & hardware filter.*

Test Type	Sampling frequency (Hz)	Hardware filter (Type & Hz)
Deep water oscillations	200	BU[1] 20
Water-entry	2400	BU 500
Fully submerged plate in waves	2400	BU 500

3.4 Instrumentation

3.4.1 Measurements

The data collection system consists of transducers/sensors sending analogue signal via a 10V amplifier and a hardware filter to an analog to digital converter. The digital signal is then sent to a computer where it is interpreted, converted (as per the sensor calibration data) and recorded.

The data was recorded through a HBM Data Acquisition System (DAQ). The analogue signals from different sensors were recorded on different channels and gathered or saved using HBM's Catman Easy application. As mentioned in the beginning of this chapter that three main types of experiments were conducted as part of this thesis. Table 3.2 presents the sampling frequency and the hardware filter settings used during the data recording for these experiments.

Water-entry tests were recorded at very high sampling frequency because slamming, as well known, is a very short duration phenomenon and this would be helpful to observe slamming peak loads more accurately. Zero readings were taken for all the sensors in Catman Easy before starting each test to set a zero reference for data values.

3.4.2 Sensors

Following sensors were used to acquire required data during the experiments:

i **Force transducer:** A force transducer was used to measure force in z direction. The force transducer contains strain gauges in wheat stone bridge configuration. A wheat stone bridge type transducer measures the elongation (or strain) in gauge wires, due to force application, in terms of the output voltage. The output voltage is then converted to the force measurement by the software using the calibration factor. Thus, the calibration factor is critical to ensure the reliability of force measurements.

[1] BU stands for Butterworth filter

The force transducer used here has the maximum capacity of $6.6kN$ which is about 15 times the maximum force measurement taken during the experiments. The advantage of using such a force transducer is that it has a high natural frequency as it is very stiff but at the same time it was ensured that it behaved linearly around the actual force measurement values.

During the course of these experiments it was expected to measure the hydrodynamic loads in terms of measured force. There are 2 following ways, depending on the natural frequency of the system, to estimate the hydrodynamic force from experiments:

a. If natural frequency (ω_n) >> excitation frequency (ω_e) $\implies$ Stiff system $\implies$ measured force = hydrodynamic force.
b. If natural frequency (ω_n) ≤ excitation frequency (ω_e) $\implies$ Flexible system $\implies$ measured force ~ response $\implies$ hydrodynamic force to be estimated from the analysis of response.

In this case, the first option was the obvious choice, so we need to ensure that the test setup is sufficiently stiff. But as further discussed in section 3.7.2 and results obtained from pluck test (presented in section 4.1), this could not be achieved here.

ii **Accelerometers:** In total 6 inertia based accelerometers were used to measure accelerations and observe rig vibrations. These accelerometers were installed in the following configuration:

- 3 accelerometers were placed on the rig top frame at mid and either corners along a diagonal to measure accelerations in z direction.
- 2 accelerometers were placed on the plexi-glass plates to observe vibrations or accelerations in y direction (along the width of the tank). During wave tests these accelerometers were installed on top of the force transducer. This was done to observe the vibrations in the force transducer.
- 1 accelerometer was placed at the carriage base on the other side of the force transducer to observe rig vibrations.

iii **Potentiometer:** A mechanical string type potentiometer was used to measure the changes in vertical position of the test rig. The fixed end of the potentiometer was mounted on the top fixed part of the rig. In case of wave tests, an additional potentiometer was used to record the wave generator flap position.

iv **Wave Probes:** Total 8 wave probes were placed in 2 different configuration. The wave probe configuration for deep water oscillations and water-entry tests is shown in Figure 3.5 and for wave tests is shown in Figure 3.6. These 8 wave probes are annotated as WP1 to WP8 for further reference.

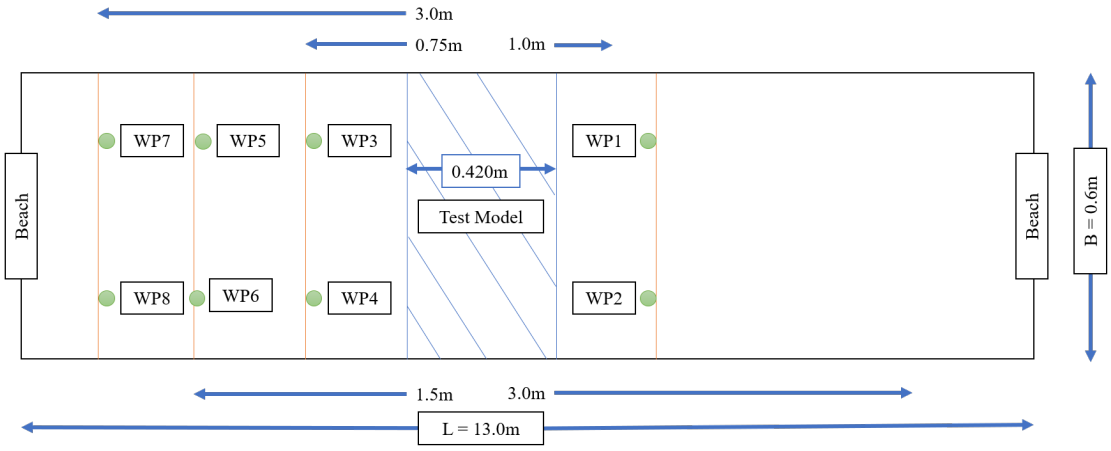

Figure 3.5: *Wave probe layout for deep water oscillations and water-entry tests.*

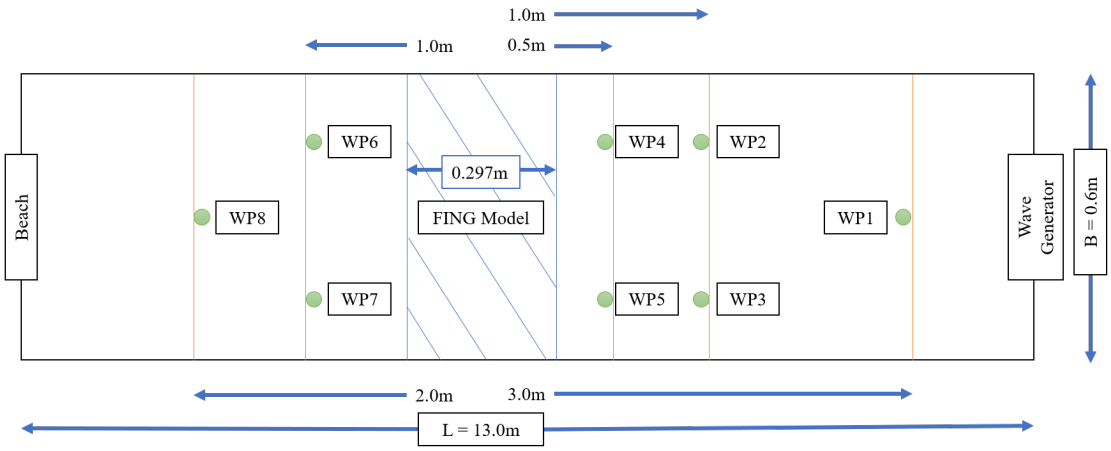

Figure 3.6: *Wave probe layout for fully submerged plate in waves tests.*

3.4.3 Calibration

Calibration is necessary to take reliable measurements from sensors. This fact raises a very fundamental question 'how often should we re-calibrate these sensors?'. To answer this question, we need to understand the sensitivity of each of these sensors to external factors. The following can be said about the current set of sensors:

- The type of force transducer used here is quite robust and do not get much affected by small changes in the environment and its calibration does not deteriorate much over time. The same applies for the potentiometers.
- The accelerometers and wave probes are quite sensitive to the changes. Thus, they needs to be re-calibrated more frequently.
- Additionally, whenever a sensor is newly installed or physically displaced it is best to re-calibrate it.

Keeping all these points in mind, all the 6 accelerometers, and 8 wave probes were calibrated before initial installation according to the standard calibration procedures. For remaining sensors, force transducer and potentiometers, proper calibration checks were performed to ensure the validity of old calibration factors. It should be noted that since the test model was changed many times during the experiments, 2 of the accelerometers (installed on plexi-glass plates) had to be removed, re-calibrated and re-installed every time. Additionally, during the course of these experiments accelerometers and wave probes were re-calibrated roughly after every 10 days.

3.5 Wave Characteristics

Waves were generated in the tank using a single flap type wave generator. This type of wave generator creates waves by the oscillatory motion of a large single flap extended and hinged to the tank bottom. It requires the following 2 parameters to create a specific wave of given period and steepness:

- Flap amplitude
- Oscillation period

The oscillation period corresponds to the wave period and the steepness of the wave is determined by flap amplitude. Thus, the steepness of the wave is limited by the maximum allowed flap amplitude ($\leq 30cm$) as well as the wave breaking limit ($H/\lambda \approx 1/8$ for deep water).

In order to create a desired wave, the wave generator needs to be calibrated for the given water depth. The calibration results in a transfer function which is required to calculate the flap amplitude for the input wave. An approximate transfer function was created by conducting a series of tests in the tank in the absence of

Table 3.3: *Test matrix for deep water oscillations tests.*

Period (s)	Minimum Amplitude (mm)	Maximum Amplitude (mm)	Amplitude Increment (mm)	Total Runs
1.00	16	48	1.7	20
1.25	16	80	1.7	38
1.50	16	116	1.7	59
1.75	16	156	1.7	83
2.00	16	166	1.7	91

the test model. The created transfer function was later verified. The procedure for creating the wave generator transfer function is not in the scope of the project and shall not be discussed any further in this report.

3.6 Test Matrix

Deep Water Forced Oscillations: The oscillation period was varied from $1.0s$ to $2.0s$ in steps of $0.25s$ and the range of oscillation amplitudes is shown in Table 3.3. Each combination of period and amplitude corresponds to a test which consisted of 20 oscillation cycles including 5 ramp-up and 5 ramp-down. Thus, each test was run for 10 full amplitude oscillation cycles.

Constant Velocity Water-Entry: The water-entry velocity was varied from $0.05m/s$ to $0.40m/s$ for $P19$ and $P28$ with an increment of $0.01m/s$. For FING, tests were carried-out to the maximum water-entry velocity of $0.60m/s$, with the same increment. Additionally, 5 repetition was carried-out for each water-entry velocity. The test matrix for water-entry tests is shown in Table 3.4. For each test, the model was started from a position of $20cm$ above the still water level and stopped at $20cm$ below and constant velocity was maintained around the still water level. The acceleration and deceleration at the beginning and the end were limited by the capacity of the rig motor and so the duration of constant velocity was reduced gradually as the velocity was increased.

Fully Submerged Plate in Waves: The wave periods were varied from $0.6s$ to $1.3s$ in steps of $0.05s$ and 1/steepness (i.e., λ/H) was varied from 10 to 60 in steps of 2 but only the waves with amplitude between $20mm$ and $45mm$ were included in the test matrix. So the model was always in fully submerged condition during the tests. The test matrix is shown in Table 3.5. For each run or test, 20 full waves lengths were created including 5 ramp-up, 5 ramp-down and 10 full amplitude waves .

Table 3.4: *Test matrix for water-entry tests.*

Model	Water-entry Velocity (m/s)	Velocity Increment (m/s)	Total Runs
P19	0.05 to 0.40	0.01	36 x 5
P28	0.05 to 0.40	0.01	36 x 5
FING	0.05 to 0.60	0.01	56 x 5

Table 3.5: *Test matrix for wave tests.*

Wave Period (s)	1/Steepness (λ/H)	Increment (λ/H)	Total Runs
1.30	30 to 60	2	16
1.25	28 to 60	2	17
1.20	26 to 54	2	15
1.15	24 to 50	2	14
1.10	22 to 46	2	13
1.05	20 to 42	2	12
1.00	18 to 38	2	11
0.95	16 to 36	2	10
0.90	14 to 30	2	9
0.85	14 to 28	2	8
0.80	12 to 24	2	7
0.75	10 to 22	2	7
0.70	10 to 18	2	5
0.65	10 to 16	2	4
0.60	10 to 14	2	3

3.7 Post Processing

Following section shall present an overview of the work done for post-processing the experimental data. The raw data recorded by DAQ system (as explained in section 3.4.1) was processed using numerous *python* scripts. The main post-processing scripts for all 3 types of experiments were completely different but various functions, like data filtering, were shared among these scripts. The work flow of these main scripts is explained in the following sub-sections.

3.7.1 Deep Water Oscillation

As the sampling frequency for these tests was not very high ($200Hz$), all the runs for a model were conducted at once and recorded in the same output file. Other than tests with models, a test (for all runs listed in table 3.3) with empty rig (i.e., no model installed) was also conducted which was later deducted from main tests (with models) to remove inertia and hydrodynamic forces acting on the rig and plexi-glass plates. This test is further referred to as *empty rig test*. The basic work flow for post-processing deep water oscillation tests is as follows:

I. **Splitting data:** The raw data file, containing all the runs (listed in Table 3.3) for a test model or empty rig, was slip into individual runs.

II. **Extracting full amplitude oscillations:** Further, full amplitude oscillations were extracted from the time series using position signal z-crossing. Corresponding to that time series for all the other required channels were also extracted.

III. **Data filtering:** The extracted data was filtered using frequency domain band pass filtering, after converting data from time domain to frequency domain using Fast Fourier Transform (FFT). The filtering frequency band was defined as ±10%[2] around the harmonic frequency. The first harmonic frequency is the oscillation frequency.

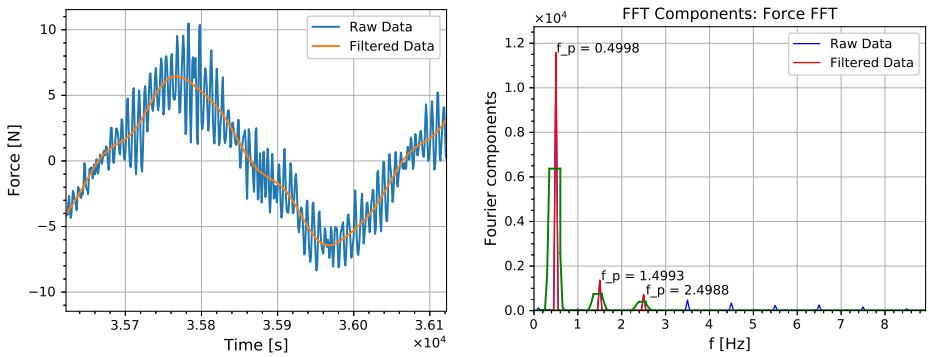

(a) Filtered Force **(b)** FFT

Figure 3.7: *Force signal band pass filtering upto 5^{th} order harmonics (5ω).*

The position and acceleration readings were filtered around only the first harmonic frequency while the force signal was filtered upto 5^{th} order harmonic [3]

[2]The band was reduced to ±5% and ±2% for higher order harmonics while filtering force to avoid overlapping of these bands.

[3]As observed from the force FFT 2^{nd} and 4^{th} order harmonics are nil as there are no 2ω and 4ω loads.

(5ω) as shown in Figure 3.7. This was done due to the well known fact that a body in an oscillating flow experiences additional higher order loads (due to higher order damping force components as shown by KC, 1958 [11]).

Additionally, while filtering a signal in frequency domain, it is important to confirm that data and noise are far away from each other, i.e., frequency of data and noise are different and they lie wide apart. The frequency of noise depends on its origin and the most common source of noise is the oscillations of the experimental setup components. The noise from this source can be located in frequency domain by determining the natural frequency of these components using pluck tests. In the current case, the frequency of data was very low as compared to the natural frequency of the rig components. Thus, it was possible to filter data from noise using frequency domain filtering technique.

IV. **Velocity and position calculation:** The acceleration signal was converted to velocity and position by frequency domain integration. For frequency domain integration, the time series data is first converted into frequency domain using FFT, then divided by $i\omega$ and finally converted back to time domain using inverse FFT.

V. **Run parameters calculation:** All the required run parameters like porous KC, oscillation amplitude, oscillation period, etc. were calculated using acceleration, velocity and position time series. It should be noted that the position time series used here and further is the one which was calculated from acceleration time series and not the recorded one. This was done keeping in mind that since potentiometer is a mechanical type sensor, it may not have a very good accuracy due to known issues like overshoot because of inertial momentum.

VI. **Hydrodynamic force:** The total hydrodynamic force, obtained after subtracting empty rig test force time series from the model run force time series, was separated into inertia and damping force components using the method explained in section 2.1. Since we have subtracted the empty rig test force, the restoring force and rig mass inertia components would be eliminated automatically. But the model mass inertia had to be subtracted from the calculated inertia force component to obtain the added mass force coefficient. The integration for calculating the force coefficients was carried-out over all the extracted full amplitude oscillation cycles at once.

VII. **Hydrodynamic coefficients:** Further, non-dimensional hydrodynamic force coefficients were calculated from added mass and damping force coefficients obtained in the above step as explained in section 2.7. Both linearized damping and Morison's load model were used. The calculated coefficients are presented in results chapter, section 4.2.

VIII. **Rig mass estimation:** The mass of empty rig was estimated from the empty

rig test as it is not practically possible to measure the rig mass physically[4]. This was done using equation 2.3, assuming nil added mass of the empty rig, as follows:

$$M_{Rig} = -\frac{\int_t^{t+nT}(F_{empty-rig} + C_{33}\eta_3)\ddot{\eta}_3 dt}{\int_t^{t+nT}\ddot{\eta}_3\ddot{\eta}_3 dt} \tag{3.1}$$

The restoring force in the above equation was calculated using the cross-section area of plexi-glass plates and the position signal calculated from acceleration time series. The mass of the empty rig was found to be about $16.15kg$.

IX. **Wave radiation damping:** The wave probe time series was filtered around the first harmonic as explained above in step III. The average height of the radiated wave, recorded at WP3 $0.75m$ away from the model (as shown in Figure 3.5), was determined and the wave radiation damping was calculated according to equation 2.18. The results for the same are presented in section 4.2.

X. **Misc.:** In addition to above steps, numerous intermediate checks were done to ensure the consistency of run parameters across the extracted full amplitude oscillation cycles. The 3 main parameters which were checked included: oscillation period, oscillation amplitude and calculated velocity amplitude. In all the cases, these parameters were found within the acceptable consistency limits.

3.7.2 Water-Entry

The post-processing of water-entry tests was significantly different from the previous case due to the following 2 reasons:

- **Sampling frequency:** The data, here, was recorded at very high sampling frequency ($2400Hz$). Due to that the recorded data files were relatively large in size and it was necessary to use some efficient scripting techniques to handle this issue.

  All of the current data was processed on a normal personal computer with only $8GB$ of RAM and some of the data files were as large as $7.1GB$. To solve this problem, a CPU intensive code (avoiding memory intensive steps like loading the complete data file in memory) was written in python and further, python's pickling technique was used for faster data fetching and execution.

[4]The actual physical mass of the rig would not be same as the rig mass felt by the force transducer as the transducer itself is part of the rig.

- **FFT techniques:** Since the time series for water-entry tests were not cyclic like in the case of deep water oscillations, it was, at first, challenging to use FFT techniques for filtering and integrating (or differentiating) data. It should be noted here that FFT techniques works best for closed loop cyclic data like a sinusoidal curve starting and ending at $y = 0$. This is due to the fact that while performing the FFT of a signal, the signal is treated as a closed cycle, i.e., the first and last point of the signal is joined to make a closed loop cycle. So if both the ends of the signal have large difference of values, the closed loop cyclic signal, created to perform FFT, will have a discontinuity at the joining point. Thus, leading to large error in the mathematical calculations. Figure 3.8 presents an example of cyclic and non-cyclic signals. One way to avoid this issue, is to filter a longer time series and then clipping it to some length after and before the starting and end of the signal, respectively.

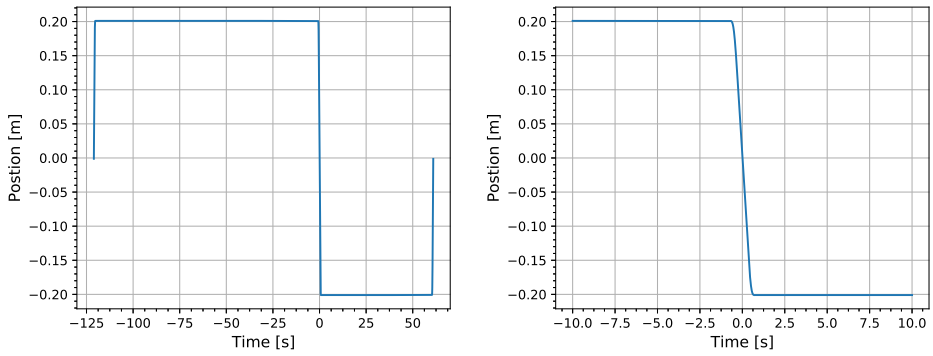

(a) Cyclic Signal **(b)** Non-cyclic Signal

Figure 3.8: *Example of cyclic and non-cyclic signals.*

Further to this, for non-zero mean signals, the FFT technique fails to carry-over the mean of the signal while doing frequency domain integration or differentiation. This is due to the fact that mean of the signal is converted to an equivalent zero frequency value (in frequency domain) which would be divided[5] or multiplied by zero in frequency domain and so it will be lost before the signal is converted back to time domain. Moreover, if the resulting signal from the integration or differentiation of a signal is bound to have a non-zero mean, then this resulting signal would also be produced with a zero mean. Thus, the mean has to be manually adjusted to obtain the correct integration or differentiation of a non-zero mean signal.

[5]In case of division by zero, for integration, the zero frequency value is simply replaced by zero.

Work Flow:

Keeping these points in mind, the raw data from water-entry tests was post-processed according to the following work flow:

I. **Splitting data:** All the raw data files were split according to position time series, i.e., potentiometer readings. The splitting points were selected as starting, ending or water-exit time instants to ensure that all the split position time signals are closed loop cyclic as shown in Figure 3.8.

II. **Water-entry instant:** The above obtained position time signal was low pass filtered at $4Hz$[6] and its mean was adjusted to remove any error due to fluctuations in zero reference. This filtered and corrected position signal was used to find the water-entry instant. All the plates were installed at zero position with still water level approximately matching the plate mid plane. So, the water-entry instant was then corrected for the thickness of the plate such that time t = 0, i.e., water-entry instant, is defined as the time when the plate first touches the water surface. Additionally, even with such high sampling frequency, the exact water-entry instant cannot be recorded, i.e., it will occur between 2 sampled time instants. So a time correction was applied by interpolating for the exact water-entry instant.

III. **Data filtering:** The acceleration time series was filtered using a low pass filter at $4Hz$ to remove noise from the data. As mentioned earlier that the filtering frequency is decided such that it would not cause any loss of data and helps remove all the noise. In case of force time series, it was not possible to do this. As we know that slamming impact peak is a very short duration phenomenon so the data in this case was spread over a wider range of frequency. So the force time series data was instead low pass filtered at $45Hz$[7] and therefore, even the filtered force time series has noise due to rig oscillations. Figure 3.9 show a water-entry force time series filtered at both $4Hz$ and $45Hz$. It should be noted that the $4Hz$ filtered signal looses the slamming peak all together.

[6] This filtering frequency was decided after observing the natural frequencies of the noise from pluck tests and determining the data frequency from the FFT of the signal.

[7] One of the main reasons for choosing $45Hz$ was due to the fact that electrical noise due to alternate current (AC) frequency is at $50Hz$.

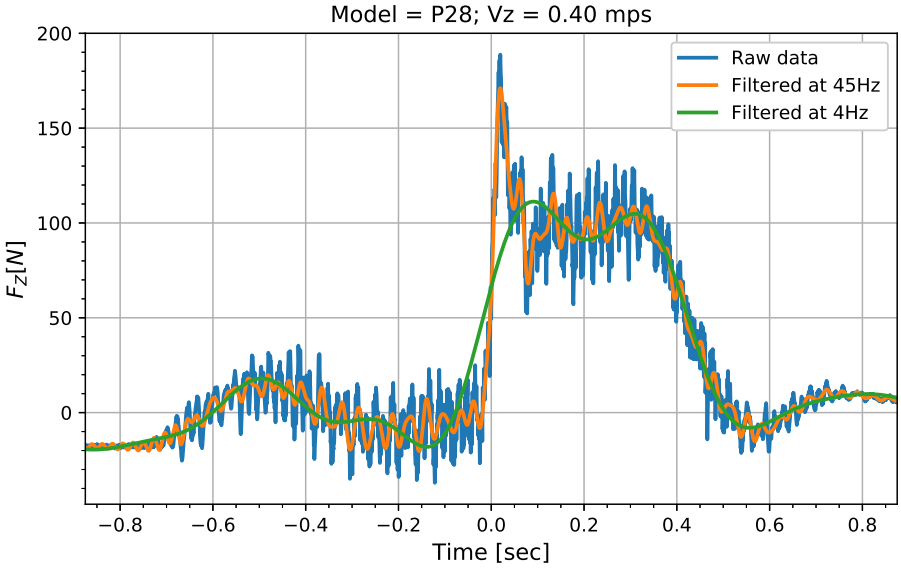

Figure 3.9: *Water-entry force signal low pass filtered at $4Hz$ and $45Hz$.*

At this point some would argue that the rig oscillations in the force signal would introduce some error in the results and moreover, all the data, i.e., position, acceleration and force, should be filtered at the same frequency. But it should be duly noted here that the aim of our data analysis is to calculate the impulse or time integral of the force signal. The rig oscillations would surely introduce significant error in the slamming peak load but since the error would be oscillating about a mean position, it will not contribute to any significant error for the impulse. Additionally, since the filtered acceleration and position time series does not really have a direct involvement in impulse calculation, it will also not pose as a problem.

IV. **Force corrections:** As discussed in section 2.2, the total water-entry force has 4 main components. In order to mainly extract the drag component, following corrections were applied to the measured force:

- **Buoyancy (or hydrostatic) force:** The buoyancy force acting on the plexi-glass plates and the test model was deducted from the measured force using the filtered position signal. The submerged plexi-glass plate volume at an instant was calculated using its cross-section area and filtered position signal. And for simplicity, the total test model volume was assumed to be linearly distributed over the model plate thickness.
- **Inertia (or mass) force correction:** The inertia force acting on the rig and test model due to non-zero accelerations was deducted from the measured force using the filtered acceleration signal. Here, it should be

noted that this force will be zero in the constant velocity duration and thus, would not effect the impulse calculations.

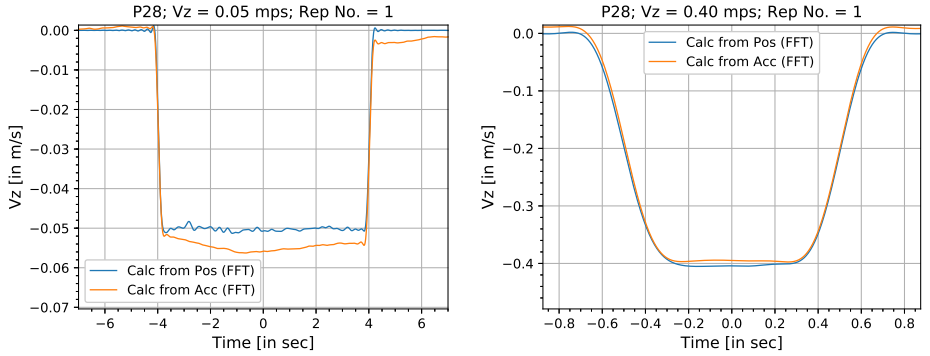

(a) $V_Z = 0.05m/s$ **(b)** $V_Z = 0.40m/s$

Figure 3.10: *Velocity signal calculated from position and acceleration signal using frequency domain differentiation and integration, respectively.*

V. **Velocity calculation:** As mentioned earlier in step V of deep water oscillation post-processing work-flow, it is generally desired to calculate velocity and position time series from accelerometer readings rather than using potentiometer readings. But in this case as pointed out above (in the point citing problems with FFT techniques), the frequency domain integral of acceleration signal resulted in large error probably due to the non-zero mean of the output (velocity) time series, specially for small water-entry velocities. Thus, instead, the potentiometer signal was differentiated in frequency domain to obtain the velocity time series. Further, it was also noticed that the velocity time series calculated from accelerometer and potentiometer signals were in quite good agreement for higher water-entry velocities. Figure 3.10 shows the comparison of velocity time series calculated from position and acceleration signals at $0.05m/s$ and $0.40m/s$ water-entry velocity.

VI. **Impulse calculation:** The force impulse was calculated using simpsons numerical integration rule only over the constant velocity duration. Two values or bounds of impulse were calculated here, this is later explained in section 4.3.1. The constant velocity duration was determined from the filtered acceleration signal but the mean velocity in this duration was calculated using the velocity signal calculated from the position signal (due to reasons cited above).

VII. **Drag coefficient calculation:** The drag coefficient was calculated by using the impulse, calculated over duration T, in equation 2.39 as follows:

$$C_D = \frac{3\pi}{8\dot{\eta}_{3_a}} \frac{B_{33}}{\frac{\rho}{2}DL} = \frac{3\pi \int_0^T F.dt}{4(V_{mean})^2 T\rho DL} = \frac{3\pi.Imp}{4(V_{mean})^2 T\rho DL} \tag{3.2}$$

VIII. **Plate volume calculation**: The plate volume was estimated from the difference between the mean force readings for when model was stationary outside and inside the water. This difference was calculated after applying the buoyancy force correction for plexi-glass plates. Additionally, the volume of the test models was also calculated from geometry and was found to be in satisfactory agreement with the estimated value.

3.7.3 Wave Tests

This section describes the post-processing of raw data for experiments with fully submerged fixed plate in waves. As mentioned before, these tests were carried-out only for FING test model (shown in Figure 3.4). This case is similar to deep water oscillations but with the following 2 major challenges:

- **Incident Wave phase estimation:** Model is stationary and the fluid is oscillating. The first biggest challenge here would be to estimate the incident wave phase accurately at the model center (or any other point on the model).
- **Decomposing hydrodynamic force:** The phase of acceleration and velocity at different points on the model will be different. Even if we can estimate this phase accurately, it is not possible to separate acceleration and velocity proportional components, i.e., added mass and damping, from the total hydrodynamic force using conventional methods. The rule of integral of harmonically orthogonal vectors (as discussed in section 2.1), i.e., $\int_0^{2\pi} \cos\theta \sin\theta d\theta = 0$, cannot be applied here straight forward. But it is possible to apply this rule if we assume long wave approximation and thereby assuming that the phase of wave is almost the same at all the points on the model. The results for these experiments are processed with this assumption. It is obvious that longer waves will give better results while the shorter ones will have large errors due to higher variability of wave phase across the plate.

Work Flow:

Due to the similarity with deep water oscillations case, the first basic steps like splitting, extracting full amplitude wave cycles and data filtering were done in a similar manner as describe in section 3.7.1. The splitting was done using the wave flap position signal and only 5 full amplitude wave cycles were extracted here using the translated wave phase signal at the plate center. The remaining work flow is described as follows:

I. **Wave parameter calculation:** The wave period was determined from the FFT of the signal recorded at WP1. The phase velocity of the wave was calculated using equation 2.45 and it was further cross checked with the velocity

of wave phase from the readings at individual wave probe (using the time difference between zero crossings and wave length calculated using dispersion relation from equation 2.44).

II. **Incident wave at plate center:** The wave phase was translated to the plate center in 2 steps to ensure better accuracy of results. Referring to Figure 3.6, first, the undisturbed wave signal at WP1 was translated to WP4 and matched to be exactly in phase with the readings from WP4. Then it was further translated to plate center using the calculated phase velocity of the wave and the known distance between WP4 and plate center. Special care was taken while installing WP4 exactly at $0.5m$ in front of the plate edge.

III. **Run parameter calculation:** Unlike deep water oscillation tests, the run parameters like wave amplitude, wave period, water particles' velocity and acceleration, etc. were calculated cycle wise within each run. This was done because the wave amplitudes were found to be inconsistent, even across the full amplitude wave cycles, in a run and following this, further calculations were also done on cycle by cycle basis. Thus, instead of getting a single point data for each porous KC number, we will get 5 points (corresponding to 5 full amplitude wave cycles) spread around the input incident wave porous KC number.

Unfortunately, the reason for this inconsistency could not be determined during the course of these experiments. But since the same inconsistency was reflected in the force time series, it is quite clear that it is not due to the wave diffraction from the test model.

IV. **Hydrodynamic force:** The total measured and filtered force was first split into cycles as per the calculated wave signal at the plate center. Further, total Froude-Kriloff force acting on the plate was calculated accurately using the wave particle acceleration at each rod center on FING. The Froude-Kriloff force was then subtracted from the filtered force time series, as discussed in section 2.3, thus, leaving only the added mass and damping force components. To separate these components, as discussed before, we assumed long wave approximation, i.e., assuming that velocity and acceleration do not vary over the whole plate and can be assumed to be equal to that calculated at plate center. Finally, Fourier averaged added mass and damping force coefficients were calculated.

V. **Hydrodynamic coefficients:** The hydrodynamic coefficients were calculated in a similar way as for deep water oscillations case. The results are presented in section 4.4.

3.8 Sources of Error

There are 2 main sources of error in an experimental investigation: *precision* and *bias*. This section will briefly discuss both these sources.

3.8.1 Precision Error

Precision error is defined as a random error and it is known to effect the precision of the data. This error can be removed by taking repeated data readings and averaging over them. By taking the repeated measurements, it is also possible to calculate the mean and bound for precision error using simple statistical methods.

The current set of experiments were, in fact, conducted with repetitions like deep water oscillations and wave tests both were conducted with 10 full amplitude repeated oscillations or cycles and water-entry tests were repeated 5 times for each entry velocity but the mean and precision bounds were not calculated here.

Another way to observe the precision of a data set is to observe the spread in the data values of the repeated tests. Larger the spread more will be the precision error. From the results of water-entry tests we can observe that the precision error is not very significant. Additionally, as mentioned earlier in section 3.7.1 for deep water oscillation tests, the consistency of oscillation parameters was ensured across the repeated oscillation cycles, so there is no reason to believe that there will be any significant precision error. Lastly, in the case of wave tests, the wave parameters were found to be inconsistent across the repeated cycles, this might indicate large precision error but it can also be due to a bias error. Thus, no clear conclusion can be drawn about the wave tests with any further in-depth analysis.

3.8.2 Bias Error

Bias errors are also known as systematic errors. They can be more difficult to detect and estimate. But once detected, they can be eliminated or estimated using various methods depending on the type of error. In the following section, some of these possible bias errors relevant for the current set of experiments are discussed briefly.

Measurement Errors:

There can be a bias error in the measurement readings related to the calibration or Data Acquisition System (DAQ). One such error was observed during the first phase of experiments conducted in January (2018). It was found that most of the accelerometer readings were twice the expected values. It was further confirmed after cross checking the accelerometer readings with the accelerations calculated using the potentiometer readings.

This was initially attributed to faulty calibrations but after a complete analysis during the second phase of experiments during April (2018), it was found that the error was due to a bug in the data recording application Catman Easy. A temporary work around was found during the second phase of experiments to avoid this error. But all the experiments had to be repeated and this error was successfully eliminated.

Change in Water Temperature:

As mentioned earlier, during the course of these experiments the water temperature was found to be varying between 21° to 23°C. For the data process, it was assumed that the water temperature was fixed as 22°C. As a result of this, a bias error will be introduced due to an error in the values of water density and viscosity used for calculating the results.

Change in Water Level:

The mean water level was recorded on every day basis while conducting these experiments. It was observed that the water level reduces or increases by about 1 to 1.5mm in 24 hours due to leakage of the water inlet and outlet valves. Although it will be very difficult to estimate this error but since the duration of a single test was much smaller than 24 hours and the water-level was carefully checked and adjusted (if required) before starting a new test, the bias error due to this factor will be insignificant.

Transverse Waves:

Formation of transverse sloshing waves in the tank can be a source of bias error in wave probe readings. The period of these transverse sloshing waves can be estimated as (refer Faltinsen, 1993 [2]):

$$T = \frac{2\pi}{\sqrt{\frac{g\pi}{b}\tanh\frac{\pi h}{b}}} = 0.877s \tag{3.3}$$

Where b is the breadth of the tank and h is the water depth. This period corresponds to 1.14Hz frequency. No such frequency or its multiple was observed on the FFT plots for the wave probe data for the current set of experiments. Thus, the contributions from this error is negligible.

Chapter 4
Results & Discussion

This chapter presents the final results of this work and the qualitative as well as quantitative discussion based on it.

4.1 Pluck Tests

Numerous pluck tests were conducted during the course of these experiments to identify the natural frequencies associated with experimental setup components. Each pluck test included plucking the rig at 5 different points (marked as 1 to 5 in Figure 4.1). But after processing the results, it was observed that all these plucks gave almost the same results so only one plot is presented here per pluck test. Additionally, each pluck in a pluck test was conducted twice as:

- **Pluck 1:** Soft pluck with a finger knuckle.
- **Pluck 2:** Hard pluck with a stiff object like a scale.

Following section will present the results from these tests.

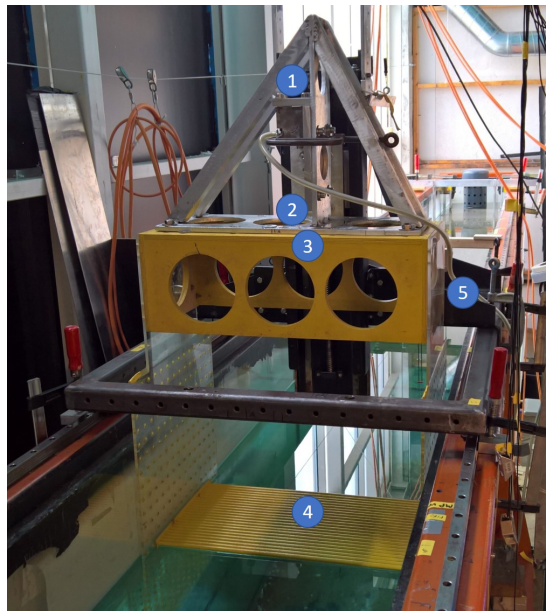

Figure 4.1: *Test rig with marked pluck points (1 to 5).*

4.1.1 Natural Frequencies

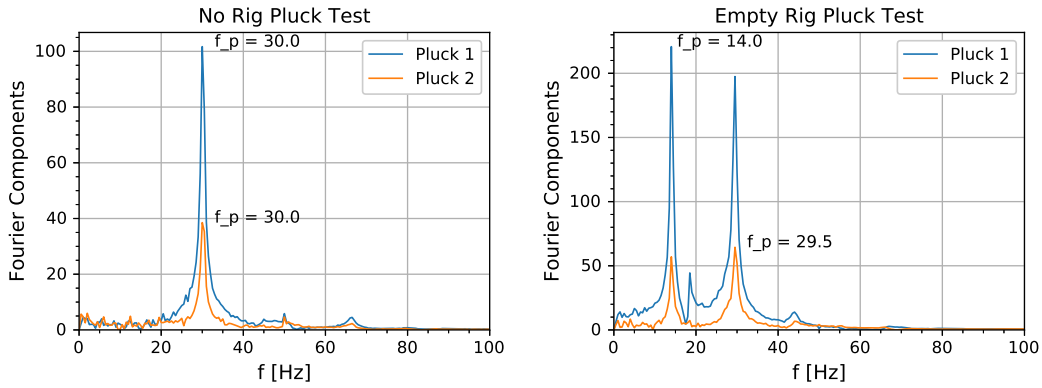

(a) No Rig Pluck Test

(b) Empty rig Pluck Test.

Figure 4.2: *No rig and empty rig pluck tests.*

Figure 4.2 shows the results from the pluck tests for no rig and empty rig case. No rig means that the lower rig (yellow box and below in Figure 4.1) was completely removed. Thus, the only main vibrating component left was the force transducer. Empty rig means that only the plate model was not installed in the Figure 4.1. Comparing the two figures, it is quite clear that the natural frequency of force transducer is about $30Hz$ and $14Hz$ frequency is associated with lower rig (yellow box and plexi-glass plates). Additionally, we observe small peaks at about $18Hz$, $44Hz$, $50Hz$ and $66Hz$. Out of this $50Hz$ is probably associated with electrical noise due to Alternating Current (AC) supply frequency.

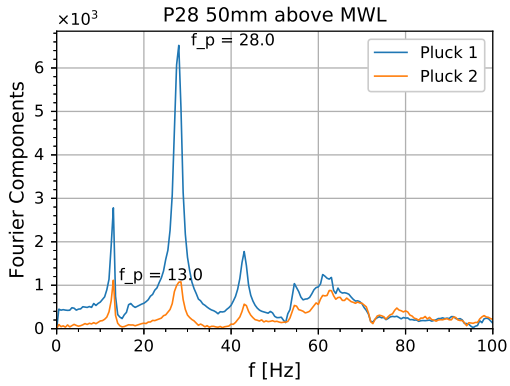

(a) Dry plate pluck

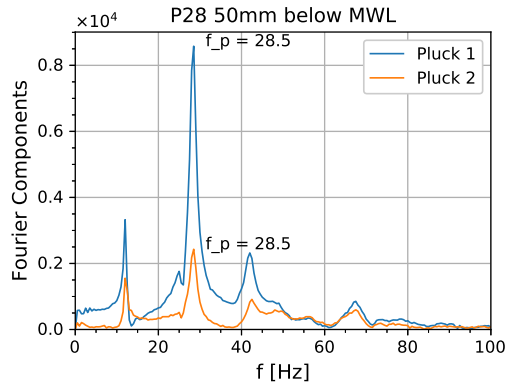

(b) Wet plate pluck

Figure 4.3: *P28 pluck tests.*

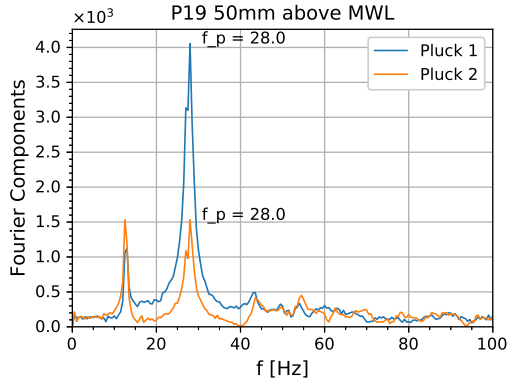

(a) Dry plate pluck

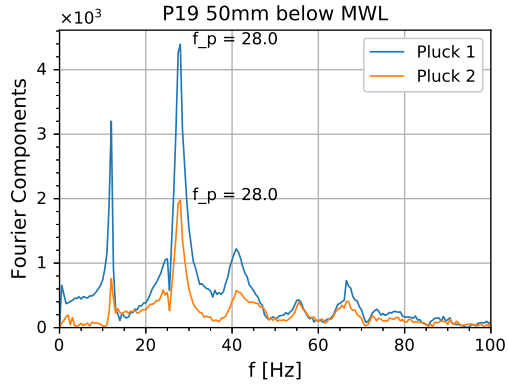

(b) Wet plate pluck

Figure 4.4: *P19 pluck tests.*

Figures 4.3, 4.4 and 4.5 show the results from pluck test conducted with P28, P19 and FING models installed. These tests were conducted for both dry (plate 50mm above Mean Water Level) and wet (plate 50mm below MWL) plate conditions. The main purpose for these 3 tests was to determine the natural frequency of plates but since no additional peaks are visible on these plot. The results here are inconclusive.

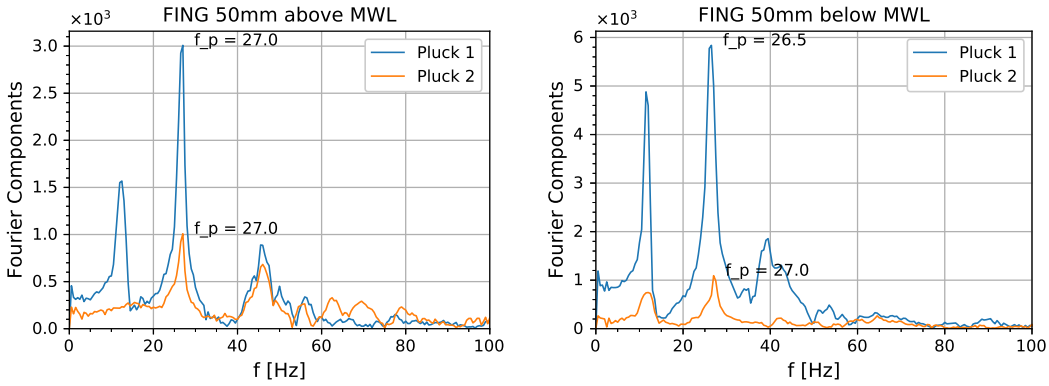

(a) Dry plate pluck

(b) Wet plate pluck

Figure 4.5: *FING pluck tests.*

As we know that the natural frequency (ω_n) of an undamped system is related to its mass (M) and stiffness (K) as follows:

$$\omega_n = \sqrt{\frac{K}{M}} \tag{4.1}$$

So when the mass of the system is increased, its natural frequency reduces. This is clearly visible in these results, if we just observe the natural frequency of force transducer with increasing mass of the system as: M (No rig) < M (Empty rig) < M (Rig + P28) ≈ M (Rig + P19) < M (Rig + FING). This proves the consistency and validity of these results. The observed natural frequencies are listed in Table 4.1.

Table 4.1: *Pluck test results: Natural frequencies.*

Component	**Natural frequency (Hz)**
Force Transducer	30.0
Lower Rig	14.0
Alternating Current	50.0
Other frequencies of interest	18, 44 & 66

4.2 Deep Water Forced Oscillations

4.2.1 Added-mass

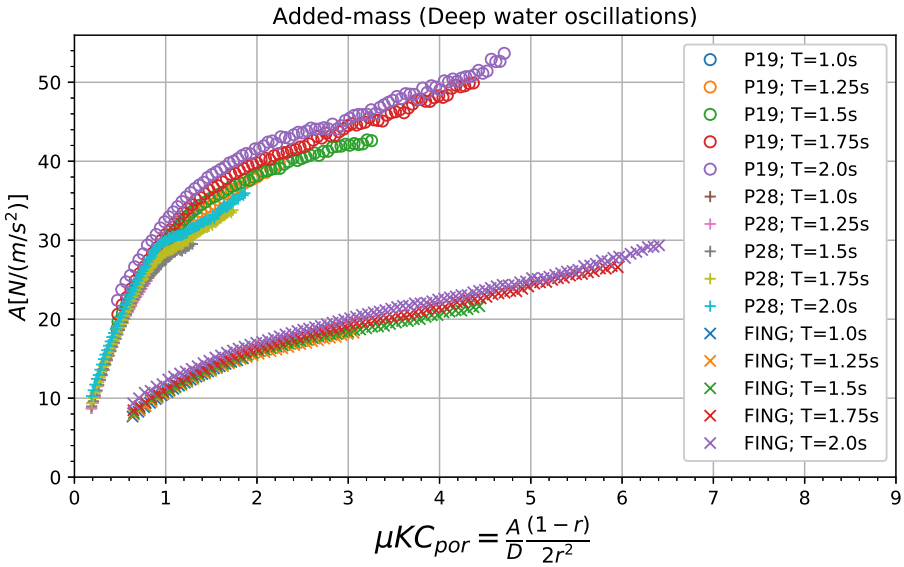

Figure 4.6: *Added mass for P19 (r = 0.186), P28 (r = 0.278) and FING (r = 0.189).*

Figure 4.6 presents the added mass for all three test models, i.e., P19 (r = 0.186), P28 (r = 0.278) and FING (r = 0.189). Table 3.1 contains the physical properties of these model like dimensions, mass, etc. The added mass of FING is smaller as compared to P19 and P28 as it is smaller in width (D). The added mass of P19 and P28 is almost overlapping due to the use of μKC_{por} which reduces the spread between similar plates of different perforation area ratio. The P28 curve lies on the lower side as compared to P19. This is in agreement with results from Sandvik, 2006 [10]. Here, it should be noted that the experiments done by Sandvik [10] were done in a 3D environment while the results presented here are 2D. Sandvik [10] used the appropriate 3D correction factor (or aspect ratio correction, k, referred to in section 2.7), while calculating the analytical added mass of the equivalent solid plate, and here we are using k = 1 (due to 2D setup). This should make the 2 cases similar but it should be duly noted Sandvik's results would also have the influence of vortex shedding from 2 additional edges which is absent in our case.

Further, as expected added mass does not show much dependence on oscillation period (or frequency) but lower frequency added mass lies on the higher side. The frequency dependence of added mass and damping is generally observed near the free surface and it diminishes as we go deeper in water. Thus, this slight variation

with oscillation frequency is due to some remaining free surface effects and it is increasing with oscillation amplitude as higher amplitude will cause more disturbance at the free surface. This can be verified from the increased free surface deformation at higher oscillation amplitudes and therefore, from the theoretical estimates of wave radiation damping (calculated using the free surface deformation and shown in Figure 4.9). Sandvik [10] also observed that added mass for porous plates is independent of oscillation period but only depends on the oscillation amplitude (proportional to KC_{por}).

4.2.2 Linearized Damping

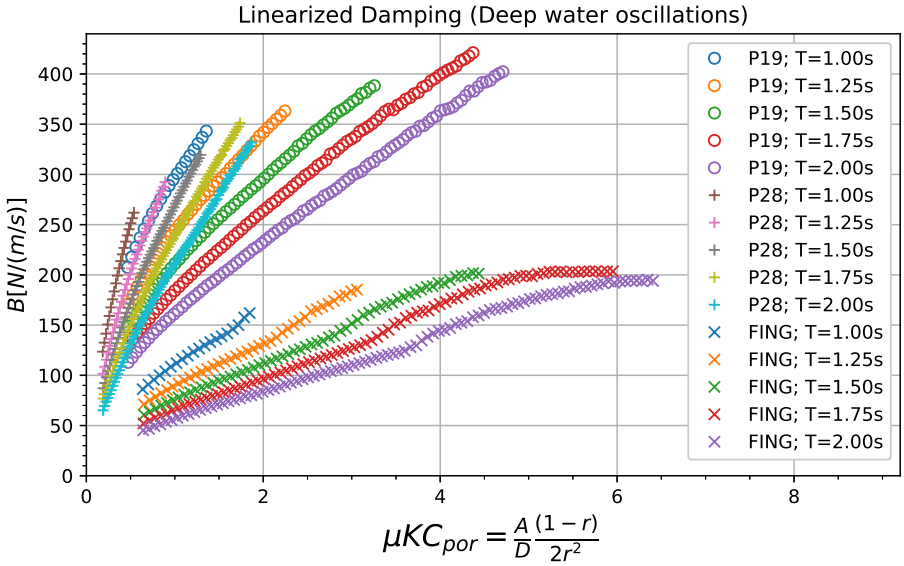

Figure 4.7: *Linearized damping for P19 (r = 0.186), P28 (r = 0.278) and FING (r = 0.189).*

Figure 4.7 shows the variation of linearized damping (B_{33}) with discharge coefficient (μ) times porous KC number (KC_{por}). Again, FING experiences smaller total damping force due to smaller plate dimensions. The linearized damping force coefficient shows variation with oscillation period as well as amplitude. Higher period gives lower linearized damping but it is expected that non-dimensionalized linear damping would be independent of oscillation frequency (as seen in Sandvik [10]).

Here, it should be duly noted that this damping model assumes that the damping force coefficient (B) varies linearly with instantaneous relative velocity between

body and fluid, so it is called linearized damping force coefficient. Further to this, as described in section 2.5, we can fit a straight line to the obtained values to calculate the slope[1] and y-intercept (as shown in Figure 4.8) thereby decomposing the total linearized damping into pure linear and quadratic components (as shown in equation 2.15). Figure 4.8 shows the values of y-intercept, i.e., $B_{33}^{(1)}$, obtained after fitting the straight lines to B_{33} vs oscillation velocity amplitude ($\dot{\eta_{3a}}$) curve.

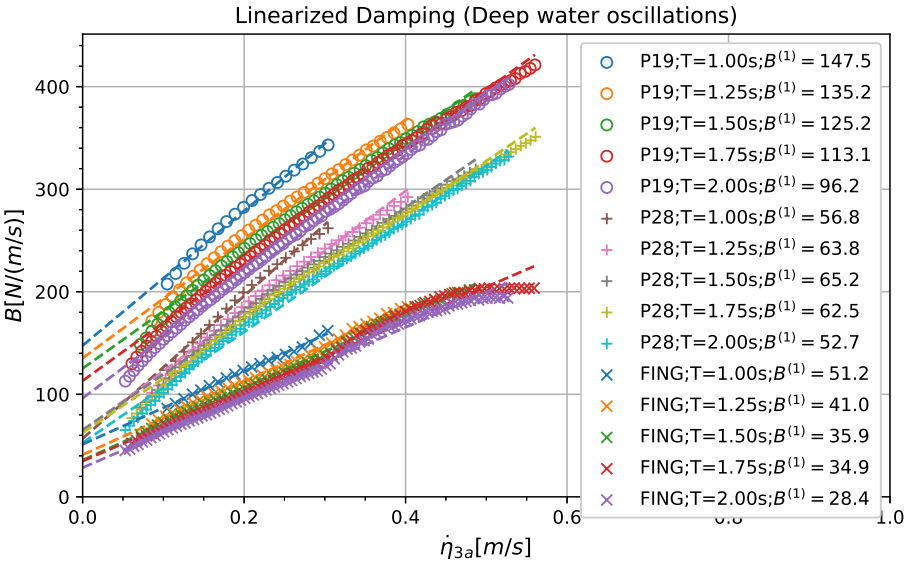

Figure 4.8: *Linearized damping vs velocity amplitude with straight lines fitted for P19 (r = 0.186), P28 (r = 0.278) and FING (r = 0.189).*

This decomposition of damping into pure linear and quadratic component can be physically interpreted as decomposing total damping into following:

- **Linear damping** → Skin friction due to laminar boundary layers, wave radiation, and other linear phenomenon.
- **Non-linear damping** → Skin friction due to turbulent boundary layers, vortex shedding, and other non-linear phenomenon.

Due to almost linear form of the curves obtained (in Figure 4.8), it is tempting to accept the above hypothesis but one must always think about the physical justification for the formulated method. For example, in the present case, it is un-physical to calculate pure linear damping coefficient ($B^{(1)}$) as there is no significant source of linear damping. Figure 4.9 shows the wave radiation damping

[1] As discussed in section 2.5, $B^{(2)}$ is the slope of linearized damping (B) vs oscillation velocity amplitude (η_a) curve.

calculated from the amplitude of radiated waves using equation 2.18. Clearly, $B^{(1)}$ values from y-intercept (in Figure 4.8) are not physically justifiable. But still this method can be used to estimate damping for engineering purpose atleast in the current range of μKC_{por}.

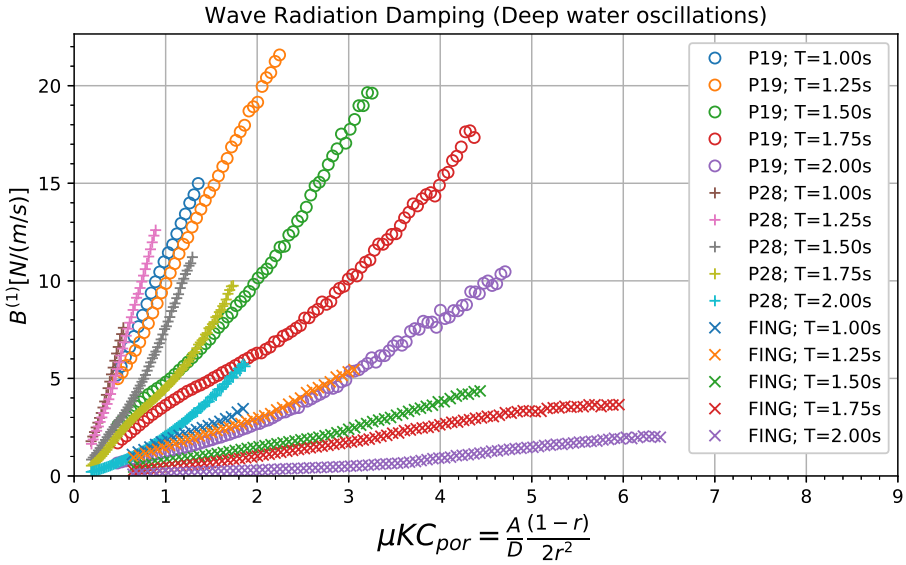

Figure 4.9: *Wave radiation damping for P19 (r = 0.186), P28 (r = 0.278) and FING (r = 0.189).*

A possible explanation for the linear nature of the obtained curve can be that the curve is only linear piece-wise in some range of μKC_{por} but since we do not have results for the entire range of μKC_{por}, this linear range cannot be defined here. This point seems further realistic when we observe the B values for low μKC_{por} for P19 and P28 (shown in Figure 4.8). It can be said that the curves are converging faster towards origin (0,0), i.e., B is not linear for small oscillation amplitudes (or μKC_{por}) and seems to follow a diminishing trend to intercept y-axis near origin, thereby diminishing linear damping component and thus, satisfying the physical phenomena. A consequence of this is that the linearized damping model will result in over-estimation of damping force for small μKC_{por}.

As shown by Graham, 1980 [15], the drag coefficient for a flat plate at very small KC follows: $C_D \propto KC^{-1/3} \implies B \propto KC^{2/3}$. A similar trend may be observed in the case of porous plates but due to the lack of data at low μKC_{por} it cannot be confirmed.

It is also worth noticing that the linearized damping curve for FING (Figure

4.7) at higher μKC_{por} does not follow linear trend and seems to be plateauing to a constant value. This is surprisingly observed for all the oscillation periods for $\dot{\eta}_{3a}$ greater than about $0.3m/s$ (shown in Figure 4.8). This is further discussed in next section.

Non-dimensionalized Linearized Damping:

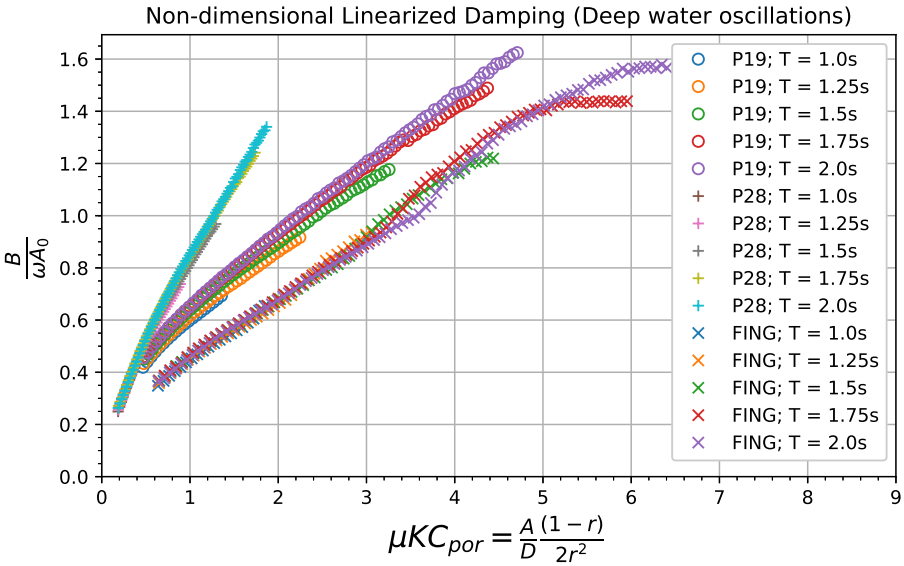

Figure 4.10: *Non-dimensional linearized damping for P19 (r = 0.186), P28 (r = 0.278) and FING (r = 0.189).*

Figure 4.10 presents the non-dimensional linearized damping for 3 test models. Here, it should be noted that the linearized damping is non-dimensionalized using the added mass of an equivalent solid plate and since these tests were carried-out in a 2D wave flume tank this added mass is calculated with no aspect ratio correction, i.e., k = 1, as discussed in section 2.7. As expected the non-dimensionalized linearized damping is independent of oscillation frequency but strongly dependent on oscillation amplitude (similar to results from Sandvik [10]). And similar to added mass, the higher oscillation period values are on the higher side due to some remaining free surface effect.

Comparing the values for 3 models, Figure 4.10 can mislead a reader into thinking that P28 has the highest damping for a given oscillation amplitude. But it should be noted that here the x-axis is also a function of perforation area ratio (r) which causes the P28 curve to shrink to left and it seems to have a higher slope

and values. But the correct way to observe or compare the magnitude of damping is to plot non-dimensional linearized damping vs oscillation velocity amplitude (or an equivalent parameter as done by Mentzoni, 2018 [16]) as shown in Figure 4.11.

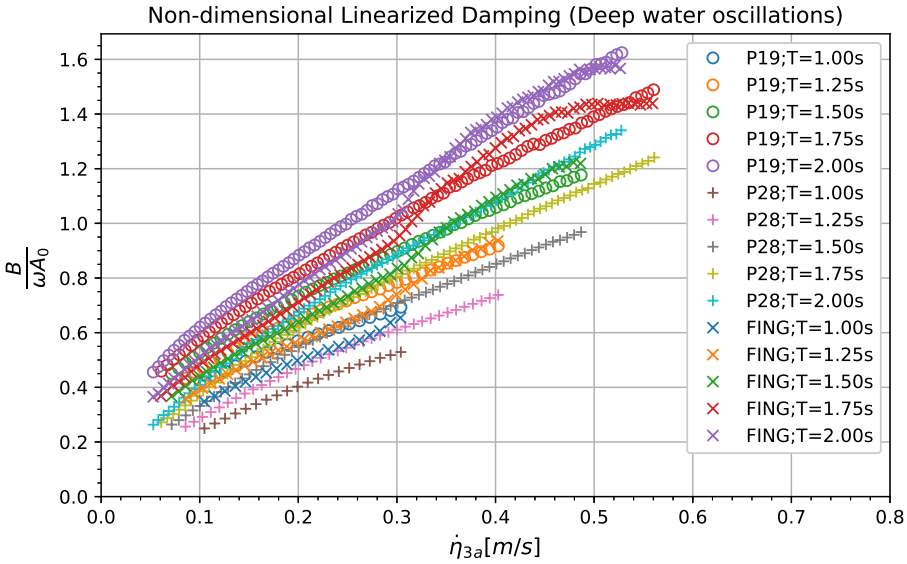

Figure 4.11: *Non-dimensional Linearized damping vs velocity amplitude for P19 (r = 0.186), P28 (r = 0.278) and FING (r = 0.189).*

The linearized damping shows significant dependence on oscillation frequency when plotted against velocity amplitude. This is inline with observations by Mentzoni, 2018 [16]. Comparing non-dimensional linearized damping for P19 and P28 (from Figure 4.11) indicates that P19 has a higher damping which is due to the following known reasons:

- **Blockage effect:** Higher blockage effect on lower perforation area ratio (r) plate.
- **Edge effect:** P19 has more number of perforations ($\sim$ 15.000) as compared to P28 ($\sim$ 10.000) $\rightarrow$ more sites for separation and vortex shedding.

FING (r = 0.189) has slightly higher perforation ratio than P19 (r = 0.186) but a lower damping for $\dot{\eta}_{3a} < 0.3m/s$. It is also interesting to note that for $\dot{\eta}_{3a} > 0.3m/s$ (corresponding to $\mu KC_{por} = 3 \sim 4$) damping for FING gradually increases and becomes more than P19 but at about $\dot{\eta}_{3a} = 0.5m/s$ it seems to be reaching a constant value. A similar trend was observed in Figure 4.8. Since these transitions occur at almost the same velocity amplitude for all the oscillation periods, it is tempting to say that this might be due to Reynolds number effect.

Reynolds number can be calculated as $\dot{\eta}_{3a}.D/\nu$, but here 2 points must be noted:

- **Local & Global Re:** The fluid-structure interaction for a porous plate like FING will be characterized by 2 different Reynolds number. The local Re is related to the local flow at each rod on FING, calculated using the diameter of individual rod (d). The global Re is related to global flow around the plate and it is calculated using the plate width (D).
- **Relative Velocity:** Firstly, the velocity amplitude only represents the velocity of the model relative to the ground when the plate reaches the mean position during an oscillation and thus, the velocity will be smaller at any other instant. Secondly, due to blockage effect this velocity would increase depending on the pressure difference across the plate. This increase in velocity can be accounted for in Reynolds number by dividing it by perforation area ratio (r) of the plate.

Table 4.2: *Local and Global Reynolds number for FING (r = 0.189).*

Velocity Amplitude (m/s)	**Re(local) (d=0.01m)**	**Re(local)/r**	**Re(global) (D=0.297m)**	**Re(global)/r**
0.30	3,140	16,614	93,259	$4.9\text{x}10^5$
0.50	5,233	27,688	155,432	$8.2\text{x}10^5$

Table 4.2 presents the local and global Reynolds number for FING at 0.3 and 0.5m/s velocity amplitude. At this point no clear conclusions can be drawn here but this indicates that the influence of Reynolds number on hydrodynamic loads for porous plates need to be studied further.

Linearized Damping to Added-mass Ratio:

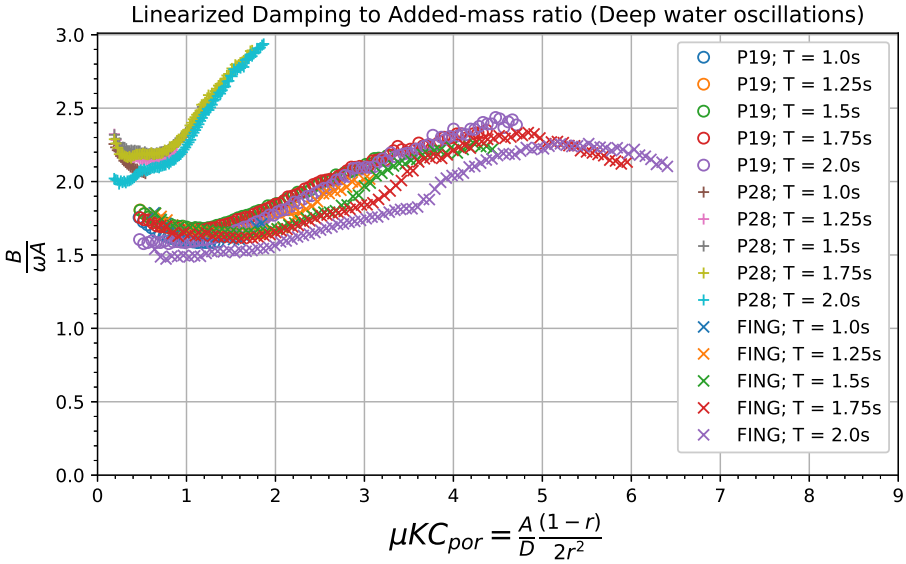

Figure 4.12: *Linearized damping to added mass ratio for P19 (r = 0.186), P28 (r = 0.278) and FING (r = 0.189).*

The non-dimensional linearized damping (shown in Figure 4.10) presents the relative magnitude of damping with respect to added mass of the equivalent solid plate. Figure 4.12 presents the linearized damping, non-dimensionalized using the added mass of the same porous plate and at the same oscillation amplitude (or μKC_{por}). Thus, it presents the comparison of the magnitude of damping and added mass for the porous plate. Higher ratio would mean that the hydrodynamic force acting on the plate is more damping dominated.

Following must be noted from Figure 4.12:

- Damping force on a porous plate can be as high as 1.5 to 3.0 times the added mass force for the given range of μKC_{por}.
- Higher perforation ratio → more damping dominated loads as P28 has substantially higher damping to added mass ratio as compared to P19.
- Type of porous plate (circular holes or rod screen) has small influence on damping to added mass ratio as the ratio is almost in the same range for P19 and FING.

4.2.3 Hydrodynamic Coefficients

Added-mass Coefficient (C_A):

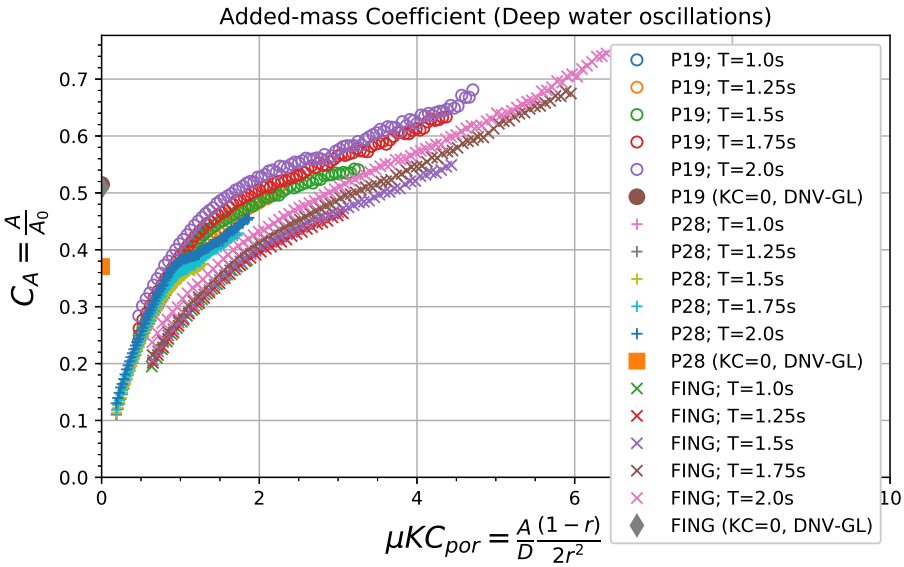

Figure 4.13: *Added mass coefficient for P19 (r = 0.186), P28 (r = 0.278) and FING (r = 0.189).*

Figure 4.13 presents the variation of non-dimensional added mass or added mass coefficient with μKC_{por}. Comparing P19 and P28, we can say that similar to the results from Sandvik, 2006 [10], the spread in added mass due to varying perforation area ratio is reduced by using μKC_{por} on the x-axis and the added mass tends to be on the lower side with increasing perforation area ratio.

Comparing P19 (r = 0.186) and FING (r = 0.189) in Figure 4.13, we observe that rod screen (FING) has smaller added mass as compared to perforated plate (P19), but they have almost the same perforation area ratio (r). Thus, it can be concluded that rod screen type porous plates have smaller added mass as compared to perforated plates with sharp edged circular openings.

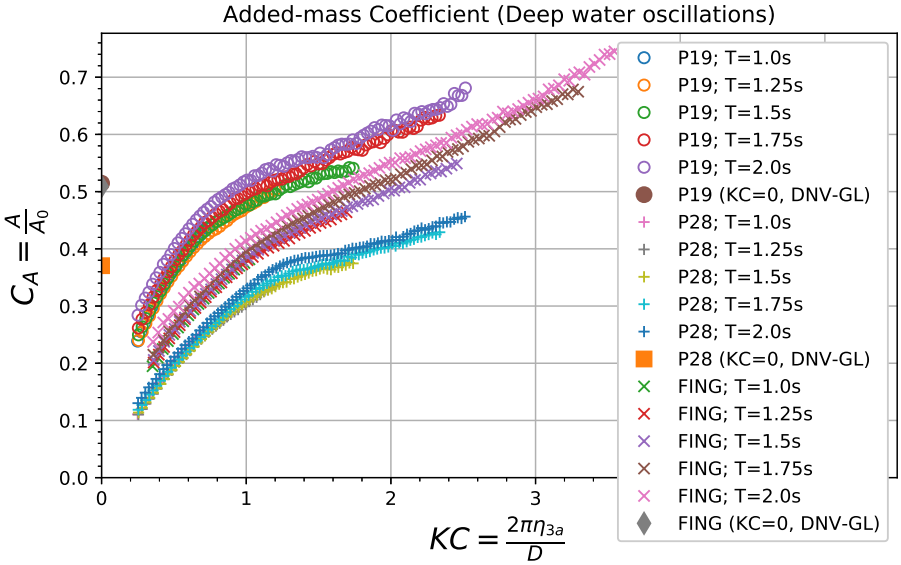

Figure 4.14: *Added mass coefficient vs KC for P19 (r = 0.186), P28 (r = 0.278) and FING (r = 0.189).*

Figure 4.14 presents the added mass coefficient for all 3 test model plotted against the KC number. It shows the same trend as discussed above.

Figures 4.13 and 4.14 also shows the empirically calculated values for C_A at KC = 0 (or zero amplitude) presented in DNV-GL's recommended practice [1]. These values are calculated using an empirically derived relation (equation 1.3) based on the values obtained using potential flow theory for plates with circular openings. The results from this empirical method are quite conservative and it appears that these results can even be used for a conservative estimate in range of small KC number ($KC < 1$ for P19 and P28, and $KC < 1.5$ for FING) but for a higher range a correction for increased KC must be applied.

Additionally, it should be noted that the empirical method gives the same value irrespective of the type of plate (perforated or rod screen). From the experimental results nothing can be concluded about this, but it is clearly observable that P19 curve is converging faster towards origin as compared to FING. According to Molin, 2011 [7], the zero amplitude added mass of a perforated plate (like P19) goes to zero as the number of porous openings goes to infinity but according to potential flow theory a rod screen type plate (considered as a sequence of cylinders) has a finite zero amplitude added mass. Thus, it is highly likely that P19 will cross the FING curve and will have a smaller zero amplitude added mass.

Further, as mentioned in section 1.3, DNV-GL [1] suggests a reduction factor

with respect to the added mass of the equivalent solid plate, corresponding to the perforation area ratio of a porous plate (shown in Figure 1.6), to obtain a conservative estimate of added mass, irrespective of KC number. For P19 and FING, this reduction factor is about 0.8 and for P28 it is about 0.55 (from Figure 1.6). Comparing with the current results it is observed that this reduction factor is still conservative (in current range of KC number) but may not remain so for a higher range of μKC_{por}.

Drag Coefficient (C_D):

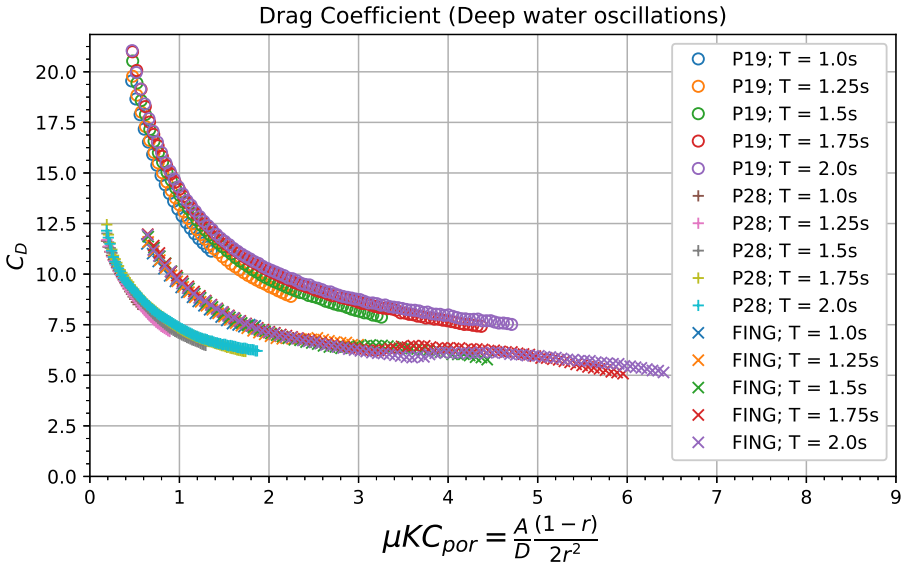

Figure 4.15: *Drag coefficient for P19 (r = 0.186), P28 (r = 0.278) and FING (r = 0.189).*

Figure 4.15 presents the drag coefficient for test models. This drag coefficient is calculated according to Morison's load model (using equation 2.39), i.e., quadratic damping with no linear component ($B^{(1)}$ = 0). Comparing the C_D for P19 and P28, we observe that P19 has a much higher drag. This can be explained using Molin's [8] theory about drag on porous plates and principles of fluid dynamics (explained by Blevins [6]).

According to Molin [8], the drag force on a transversely moving porous plate is proportional to the square of its velocity. The principles of fluid dynamics uses the same hypothesis for the steady flow across a porous plate or disc installed in the cross-section of a pipe or duct and the total drag force is calculated in terms of the total static pressure loss across the plate, which is found to be directly proportional

to the square of the relative velocity between the plate and fluid[2]. Also, we know that P19 will experience higher blockage effect due to smaller perforation ratio. Thus, it has higher static pressure difference across the plate and therefore, higher drag force.

The difference between P19 and FING is due to the higher edge effects and therefore, more vortex shedding and higher drag force on P19.

[2]This can be simply understood by Bernoulli's principle.

4.3 Water-Entry

4.3.1 Force Time Series

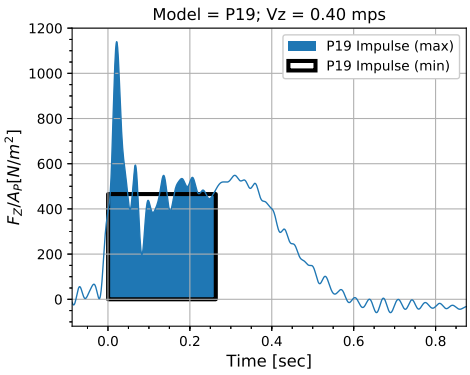

(a) P19

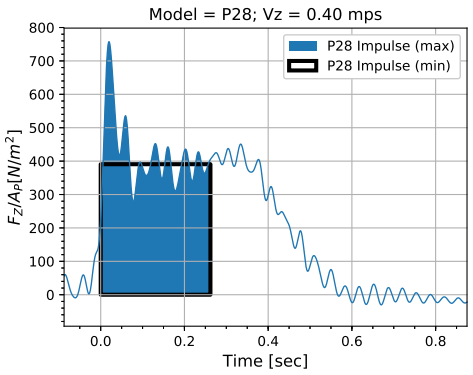

(b) P28

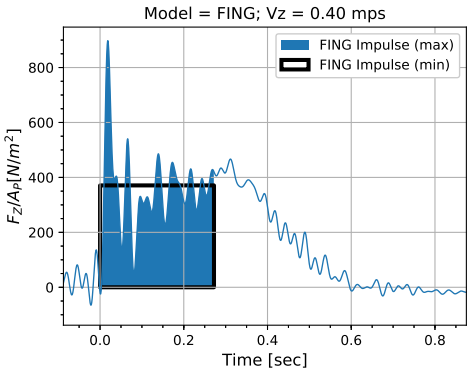

(c) FING

Figure 4.16: *Water-Entry force time series for P19 (r = 0.186), P28 (r = 0.278) and FING (r = 0.189).*

Figure 4.16 presents the water-entry force time series for all 3 test models for entry velocity of $0.4m/s$. These time series are obtained after post-processing the experimental raw data as explained in section 3.7.2. Time t = 0 is the instant when the plate bottom surface reaches the still water level. It should be noted that the time series presented here shows the force per unit plate area and the hydrostatic (or buoyancy) force due to submergence of plexi-glass plates as well as model plate and inertia force due to body mass has already been deducted from it. Thus, the remaining force has contributions from following (as discussed in section

2.2): Hydrodynamic mass force (due to added mass), Slamming impact force, and Hydrodynamic drag force. Further, the hydrodynamic added mass force becomes zero for constant velocity duration as it is proportional to acceleration. The blue shaded region in Figure 4.16 marks this constant velocity duration.

It is quite clearly observed (from Figure 4.16) that even after filtering the data, there is still some noise (or fluctuations) in the force readings. This is mainly due to rig oscillations which cannot be separated from slamming impact peak, using the conventional frequency domain filtering as discussed in section 3.7.2, as they are spread over the same frequency range. But since our aim is to calculate impulse by integrating the force, these rig oscillations would not contribute to any significant error in integration as they oscillate with same positive and negative amplitude about a mean position.

To estimate drag from the force time series, following 2 methods were used to calculate impulse:

- **Max:** Force time series is integrated including the slamming impact peak. Thus, it presents the maximum bound for the drag impulse. This is marked by the blue shaded region in Figure 4.16.
- **Min:** As well known and observed that slamming impact peak is of a very short duration. Thus, integrating force over the flat plateau followed by slamming impact peak would give a somewhat lower bound for the drag impulse. This is marked by the black box in Figure 4.16. Here, *min* should not be mis-interpreted as minimum impulse.

As shown in Figure 4.16, the *min* impulse is calculated by extrapolating the flat plateau upto $t = 0$. This is merely done so that impulse from *max* and *min* are integrated over the same time duration and has comparable magnitudes.

4.3.2 Free Surface Effects

As discussed in section 2.6.3, the water-entry drag is influenced by 2 main free surface effects: attachment of air bubbles and delayed wetting of top surface. Also, these free surface effects disappear after a certain depth of submergence. This free surface influenced depth will increase with increasing water-entry velocity. Beyond this depth the drag will converge to Reynolds number dependent steady drag. In order to observe this transition from free-surface influenced water-entry drag to Reynolds number dependent steady drag the water-entry force was plotted against non-dimensionalized submergence (defined in section 2.6.3).

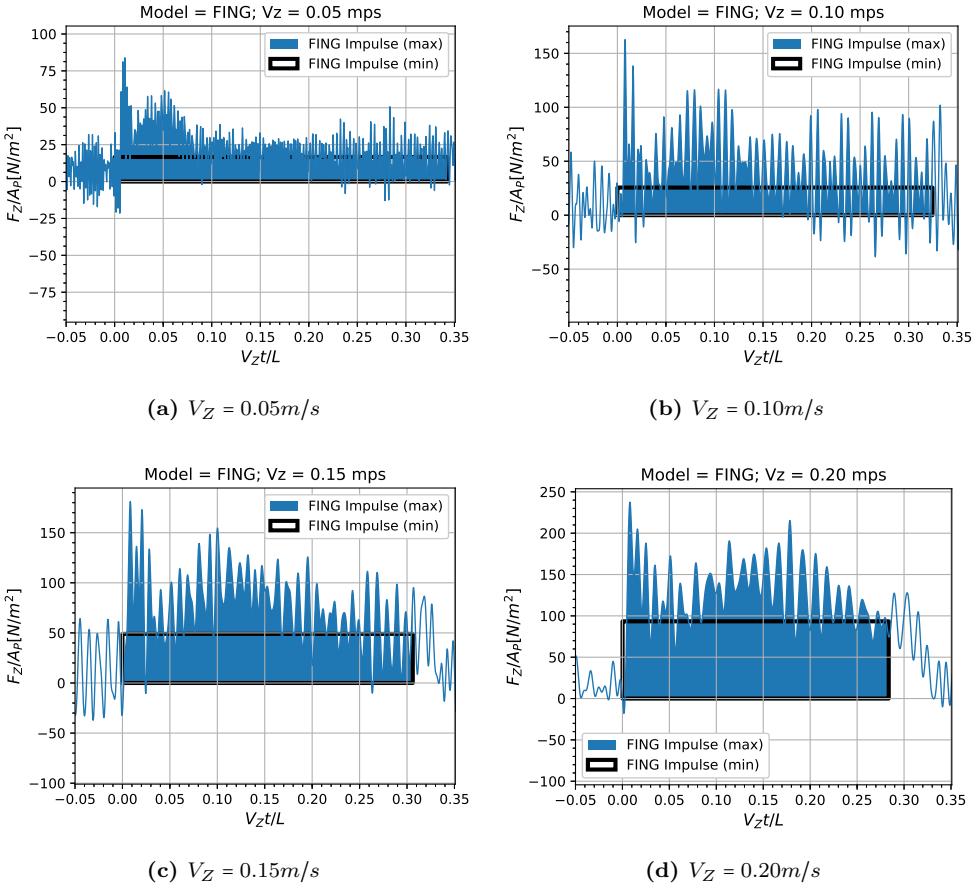

(a) $V_Z = 0.05m/s$ **(b)** $V_Z = 0.10m/s$

(c) $V_Z = 0.15m/s$ **(d)** $V_Z = 0.20m/s$

Figure 4.17: *Water-Entry force vs non-dimensional submergence for FING (r =* 0.189*).*

Figure 4.17 shows the water-entry force plotted against non-dimensionalized submergence for FING test model for 4 different test velocities (from $0.05m/s$ to $0.20m/s$). Comparing the 4 plots, we observe a bump over the upper line of *min* impulse box, which is growing as the water-entry velocity is increased. For $V_Z = 0.05m/s$, this bump is only upto about $45mm$ below the still water level whereas it became as large as the total impulse duration in case of $V_Z = 0.20m/s$. It is quite clear that the end of this bump is the point of transition of free surface influenced water-entry drag to Reynolds depend steady drag. But to further get the an accurate proof, a side-by-side comparison of force time series with recorded videos showing the influence of free surface needs to be done. Due to limited availability to time, this could not be achieved here.

Further as a consequence of this phenomena, we can say that the values of drag

coefficient estimated, for small water-entry velocities ($< 0.20m/s$), by *min* method, would coincide with Reynolds dependent drag coefficient. On the other hand, the drag coefficient calculated for higher velocities will be more closer to the, so called, water-entry drag which is characterized by free surface effects (as discussed above).

4.3.3 Force Impulse

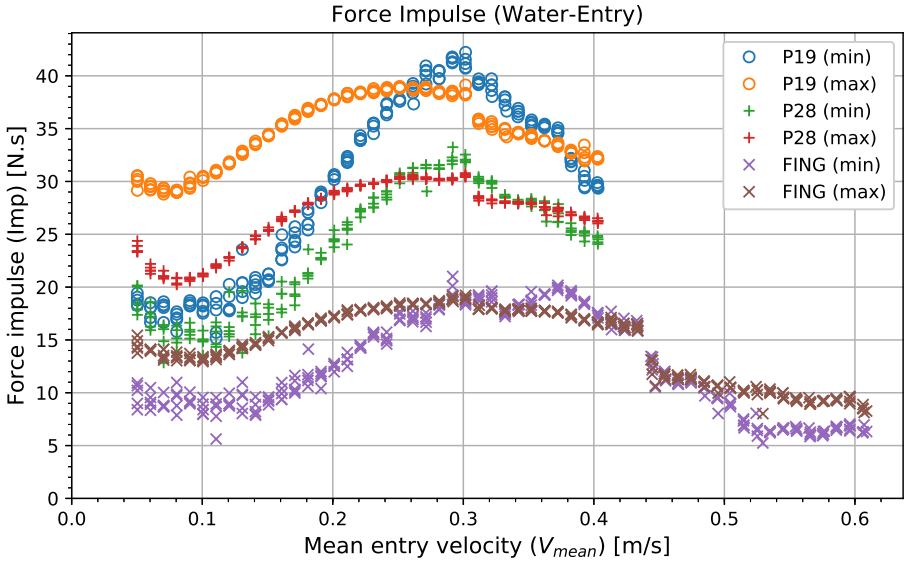

Figure 4.18: *Water-entry force impulse vs mean water-entry velocity for P19 ($r = 0.186$), P28 ($r = 0.278$) and FING ($r = 0.189$).*

Figure 4.18 shows the impulse calculated using the 2 methods (*max* and *min*), explained in section 4.3.1, for all 3 test models. As mentioned earlier that 5 repetition tests were carried-out for each water-entry velocity for validation of results and as can be seen from Figure 4.18, the repetitions present quite a good agreement. Appendix A and B contains force vs time (t) and force vs non-dimensionalized submergence ($V_z t/L$) plots, respectively, for all the water-entry velocities along with repetitions.

The impulse calculated from the 2 methods seems to converge for water-entry velocities of $0.25 \sim 0.50m/s$. Comparing the difference between the 2 methods, *max* impulse is as high as 51%, 40% and 47% as compared to *min* impulse for P19, P28 and FING, respectively, in the lower range of water-entry velocity ($< 0.25m/s$). For the range of $0.25 \sim 0.5m/s$, this difference reduces to 11%, 8% and 13%, respectively. For higher water-entry velocities ($V_{mean} > 0.5m/s$), it is observed from force

vs time plots that the duration of constant velocity is very short (due to high velocity and limited travel distance) and contains prominently the water-entry peak. So the *min* impulse does not give a correct measure of intended minimum bound drag impulse. Unfortunately, it was not possible to increase this duration due to the limitation of maximum vertical reach or travel distance for the rig setup.

Further, by disregarding the data for $V_{mean} > 0.5m/s$, we can say that for high range of water-entry velocities ($V_{mean} > 0.25m/s$), we can neglect the water-entry impact force peak while calculating the impulse required to analyze the splash zone hydrodynamics for impulse calculated over such short submergence limit[3]. Moreover, it should be noted that according to the discussion in the previous section, this drag calculated over short submergence limit is the actual water-entry drag influenced by free surface effects. Thus, it can be concluded that the slamming impact peak can be neglected while estimating water-entry drag from impulse calculated within the characteristic depth limit (h), as defined in section 2.6.3, within which the free surface effects are prominent.

FING has a smaller total impulse as the plate width (D) is about 29.3% smaller than P19 and P28. Additionally, we observe sudden jump in impulse at V_{mean} = 0.31 & $0.45m/s$. This jump is due to sudden reduction in impulse duration. To investigate further, we calculated the average force over this impulse per unit plate width (as shown in Figure 4.19).

[3]The maximum submergence for model plate after touching the still water level was $20cm$ but the constant velocity span would be even shorter depending upon the time required to decelerate the mode to zero velocity.

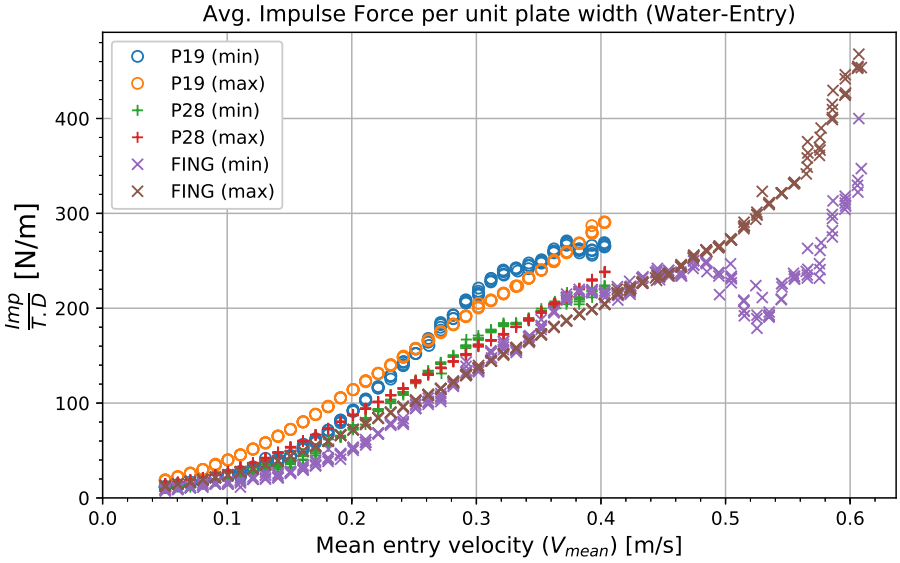

Figure 4.19: *Water-Entry average impulse force per unit plate width (D) vs mean water-entry velocity for P19 (r = 0.186), P28 (r = 0.278) and FING (r = 0.189); T is the impulse duration in seconds.*

Here, the jumps due to sudden change in impulse duration are eliminated. Comparing FING and P19, we observe that P19 has a higher average force indicating higher drag due to edge effects[4]. Also, P19 has a higher average force and impulse as compared to P28 due to higher blockage effect, i.e., higher pressure on the pressure side of the plate.

[4]Here, edge effects includes both edge effect due to plate ends and perforation openings' edge.

4.3.4 Drag Coefficient

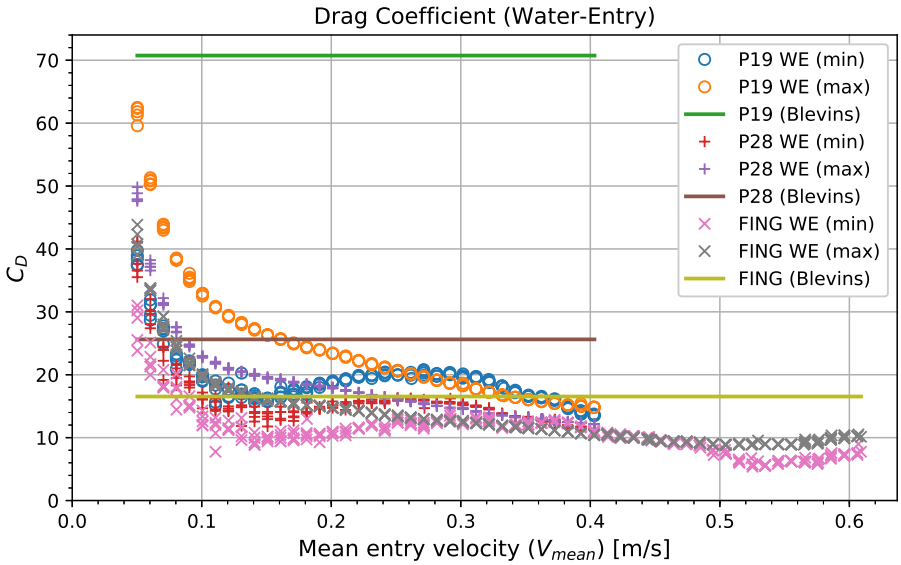

Figure 4.20: *Water-Entry drag coefficient vs mean water-entry velocity for P19 (r = 0.186), P28 (r = 0.278) and FING (r = 0.189).*

Figure 4.20 shows the drag coefficient calculated from the water-entry impulse as shown in equation 3.2. The results are also being compared with empirical estimates of drag force using principles of fluid dynamics (Blevins [6]). But before we compare the results, it should be duly noted that the current experiments and the empirical method has the following 2 major differences:

- **Plate edge effect:** Empirical method does not account for plate edge effect, i.e., separation and vortex shedding at plate edges.
- **Restricted flow:** Empirical method is established for the fluid flow in a closed conduit (pipe or duct) assuming the water-entry velocity times cross section area (or plate area), i.e., V_{mean}xLxD, as the volume flow rate through the conduit.

The first would cause under-estimation from empirical method whereas the second would cause over-estimation. And as clearly evident from Figure 4.20, the later has stronger influence for higher entry velocities. Results from Belvins [6] are about 65% higher for FING in high velocity range while it is about 2 and 7 times the experimental drag coefficient for P28 and P19, respectively. It should also be noted that the empirical method predicts constant value of drag coefficient in the current range of Reynolds number but the experimental values do not agree with

that, even the results from *min* impulse for small water-entry velocities (which are suspected to be same a steady drag) are not constant. But this variation or discrepancy may be purely due by plate edge effects.

With the above cited differences between Blevins [6] method and current experiments, it is not completely wise to compare them as they are quite different cases. It would be more practical to compare these experimental values with steady drag for transversely placed porous plates in unrestricted steady flow. It is also possible to apply some corrections to the empirical or experimental results to reduce the discrepancies due to the above mentioned differences so that they can become more comparable. Alternatively, a possible way to estimate steady drag is by extrapolating the deep water oscillations' drag vs KC to obtain drag coefficient for infinite KC. As pointed out by Keulegan and Carpenter, 1958 [11], C_D reaches the steady flow value at infinite KC and it is also the smallest value in the steady flow case, i.e., C_D reduces as KC increases from finite to infinite. Further, the steady value of C_D would depend on the Reynolds number.

As discussed in section 2.6, the water-entry drag is not exactly same as the steady drag. It is characterized by several other complex phenomenon like attachment of air bubbles, delayed wetting of top surface, etc. These free surface effects are reduced as the body goes deep in water. Keeping these points in mind, we can compare the above results with drag coefficient from deep water oscillations case. But also it should be noted here that the deep water oscillations' drag coefficient has clearly not reached the steady value (i.e., KC$\rightarrow \infty$). The water-entry drag coefficient for FING reached a stable value of around 10 at high water-entry velocity ($\sim 0.5m/s$) whereas $C_D \approx 5$ for high oscillation amplitude (corresponding to $\sim 0.5m/s$ oscillation velocity amplitude, thus in the same range of Reynolds number), as shown in Figure 4.15. This indicates that the free surface effects have increased the drag coefficient by atleast 100% in this range of water-entry velocity. Thus, these free surface effects must be taken into account while estimating the drag coefficient for water-entry case.

4.3.5 Snapshots: Blockage Effect

From the discussion until this point, it is quite clear that blockage effect is an important factor to determine the drag force acting on a porous plate. It is commented earlier that blockage effect increases with decreasing perforation area ratio, i.e., P19 has the highest blockage effect. In this section, we will try to prove this fact using snapshots from slow motion videos taken during the water-entry tests. In the later part of this section, we will present the variation of this effect with increasing water-entry velocity for FING. The slow motion videos were recorded using one of the best camera phones (Microsoft Lumia 950 XL fitted with Carl Zeiss lens) at 120 frames per second. And these videos were recorded approximately from the same position and with no zoom.

Blockage effect, for water-entry of a porous plate, is characterized by the following 2 main features:

- Static pressure build-up on the pressure side of the plate.
- Water rush-up through perforations or openings at a very high speed due to large static pressure difference across the plate.

According to Bernoulli's equation, the static pressure difference between two sides of the plate is converted into kinetic energy as the water rushes up through an opening and further into the gravitational potential energy when the rushed-up water reaches the highest point (assuming nil head losses). Thus, the distance of this highest point from the plate can be a measure of the blockage effect. Longer distance would mean higher static pressure difference and higher blockage effect. Additionally, the mass of the rushed-up fluid must also be considered while calculating this gravitational potential energy.

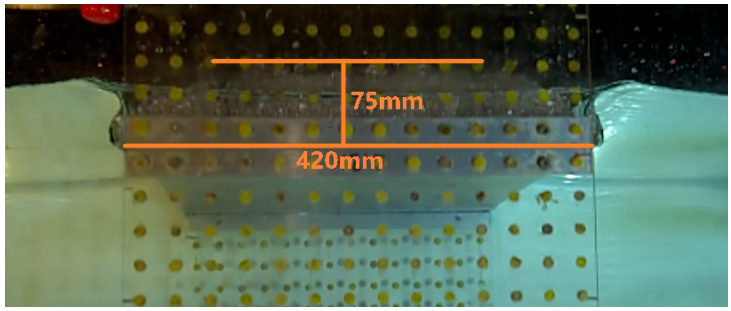

Figure 4.21: *Snapshot of water rush up for P19 (r = 0.186) at water-entry velocity of* $0.40m/s$.

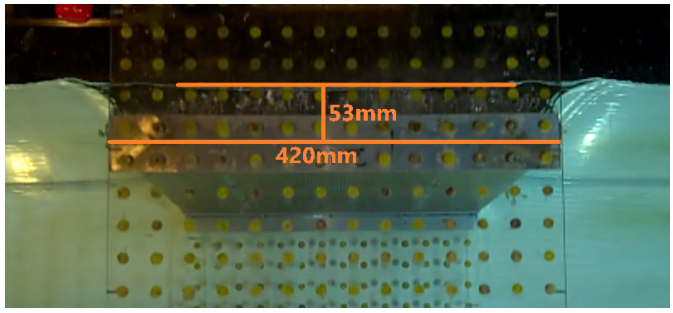

Figure 4.22: *Snapshot of water rush up for P28 (r = 0.278) at water-entry velocity of* $0.40m/s$.

Figure 4.21 and 4.22 presents the maximum reach of the rushed-up water for P19 and P28 at water-entry velocity of $0.40m/s$. Here the maximum reach is

measured from the plate mid plane and upto the highest observed water shoot-up. The distances are scaled according to the plate width. As observed, the maximum reach is about 29.3% higher for P19 as compare to P28 but P28 has larger pore or hole diameter[5], thus, rushed-up fluid would have about 11% more potential energy[6]. Contrary to the expectations, this indicates that P28 has higher blockage effect but this estimate is based on the assumption that we have no head loss. In reality, there will be head losses due to friction along the opening length (i.e., plate thickness) and vortex shedding at opening edge. The losses due to first will not be significant as the plates are quite thin but P28 will have significantly higher head loss (specially at high velocity) due vortex shedding at its opening circumference, which is about 33% longer as compared to P19. Thus, no definite conclusion can be drawn here. Unfortunately, a similar video for FING was not recorded at the same water-entry velocity but since FING has a smaller width as compared to P19 and P28, it would not be wise to compare them.

[5]The pore diameter for P28 is $3mm$ while it is $2mm$ for P19.

[6]Calculated by integrating the potential energy over the rush-up maximum reach.

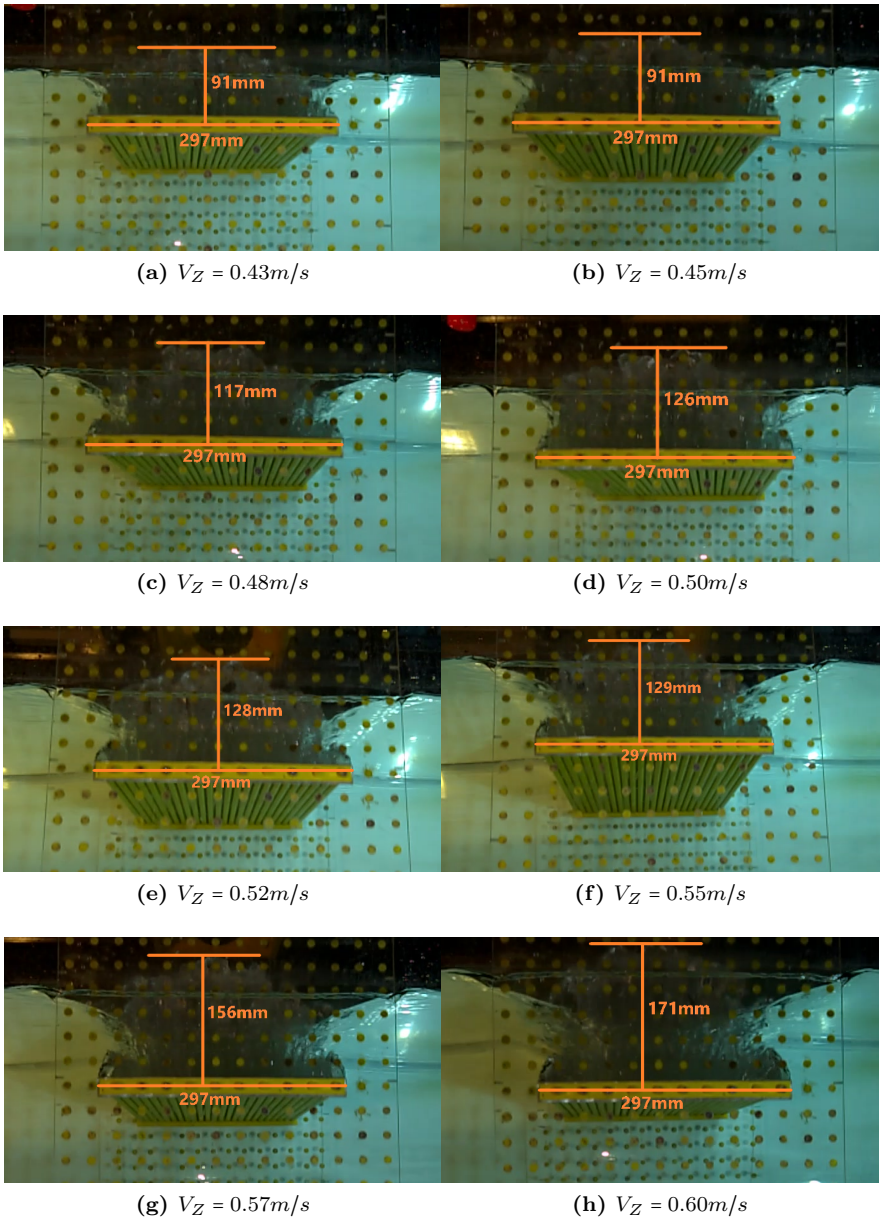

(a) $V_Z = 0.43m/s$ **(b)** $V_Z = 0.45m/s$

(c) $V_Z = 0.48m/s$ **(d)** $V_Z = 0.50m/s$

(e) $V_Z = 0.52m/s$ **(f)** $V_Z = 0.55m/s$

(g) $V_Z = 0.57m/s$ **(h)** $V_Z = 0.60m/s$

Figure 4.23: *Snapshot of water rush up for FING ($r = 0.189$) at different water-entry velocities (V_Z).*

Figure 4.23 shows the snapshots for water rush-up at varying water-entry velocity for FING. As expected, the maximum reach of rushed-up water is increasing with increasing water-entry velocity. Just to observe the trend of this increase, the

maximum reach was plotted against water-entry velocity (shown in Figure 4.24). As observed the values show almost a linear trend in this range of velocity. Clearly, this fitted straight line does not pass through origin, but the actual curve will pass through origin due to that fact the maximum reach would be zero as the water-entry velocity goes to zero.

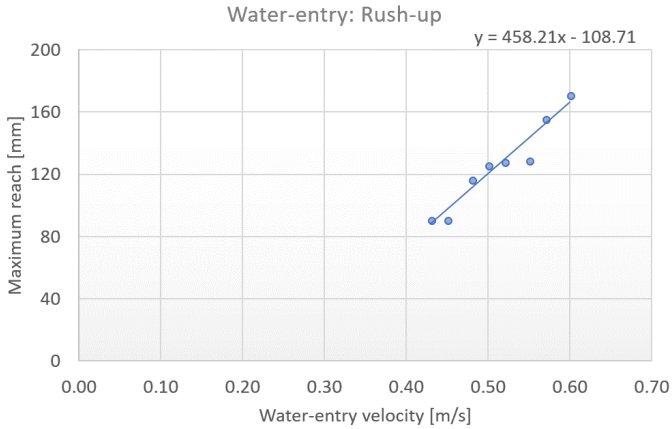

Figure 4.24: *Water-entry maximum water rush-up distance with increasing water-entry velocity for FING (r = 0.189).*

4.4 Fully Submerged Plate in Waves

The results presented in this section serves 2 main purpose:

- Studying the difference between the hydrodynamic loads acting on a porous plate in a uniformly oscillating flow (as in deep water oscillations) and a spatially varying oscillating flow, simulated by regular waves in this case.
- Further investigate the drag dominance of hydrodynamic loads on a porous plate in a more realistic near sea condition.

As discussed in section 3.7.3, two main challenges were faced during the post processing of these results: translating recorded wave (at a wave probe) to incident wave (at the plate center), and resolving total hydrodynamic force into added mass and damping components. Further sections will try to explain these challenges and present the obtained results.

4.4.1 Incident Wave

A regular wave travels with its phase velocity which can be calculated using the linear wave theory (given by the equation 2.45). The undisturbed generated wave

(recorded 3m in front on the model) was translated using this phase velocity. This translation was done in 2 steps, as mentioned is section 3.7.3, to increase the accuracy of results. The first step involved calculating the exact phase difference between the wave probes in terms of time taken by the wave to travel from first wave probe (WP1, as shown in Figure 3.6) to the remaining ones.

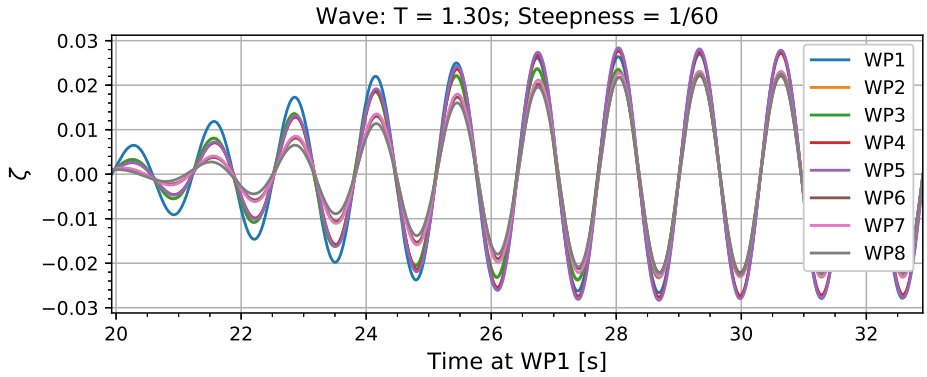

Figure 4.25: *Free surface elevation and phase matching for wave:* $T = 1.3s$ *and* $H/\lambda = 1/60$.

Figure 4.25 presents the result of phase matching after first step for the longest test wave. Here all the wave probe readings (except for WP1) are phase shifted back to WP1, according to the calculated phase velocity, and then re-matched at a zero crossing to get the exact time difference between an individual wave probe and WP1. Using this time difference the phase velocity was recalculated and it was found that in all the cases it was within the tolerance limit of $0.03m/s$. But this process did not work very well for smaller waves.

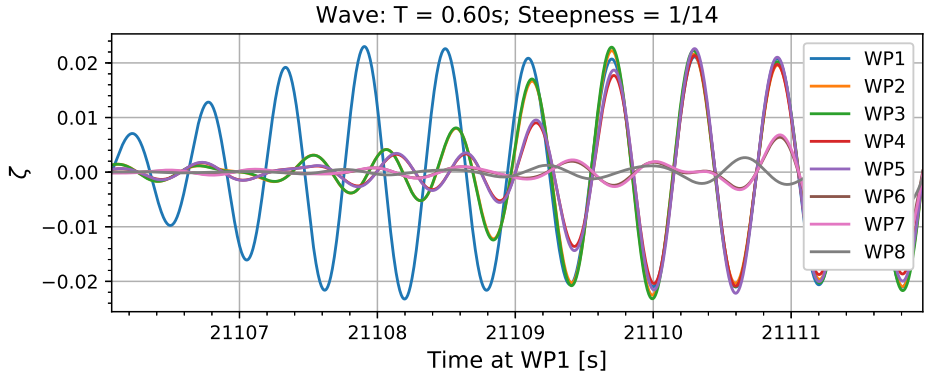

Figure 4.26: *Free surface elevation and phase matching for wave:* $T = 0.6s$ *and* $H/\lambda = 1/14$.

Figure 4.26 shows the phase matching result for the smallest test wave. It seems like the smaller waves are travelling at much smaller velocity than the calculated phase velocity. But due to limited availability of time no further analysis was done in this regard, and in view of this the results for very small waves ($T = 0.65s$ and $0.60s$) were discarded.

4.4.2 Excitation Force

As mentioned before, the wave tests were conducted only for FING test model. As discussed in section 2.3, the recorded wave excitation force has 2 main components: Froude-Kriloff, and wave diffraction. The wave diffraction force is further decomposed into added mass and damping.

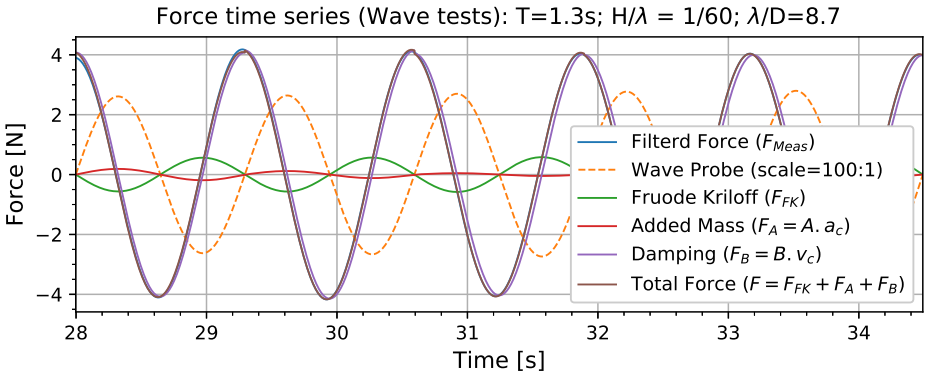

Figure 4.27: *Wave test force time series for wave:* $T = 1.3s$ *and* $H/\lambda = 1/60$.

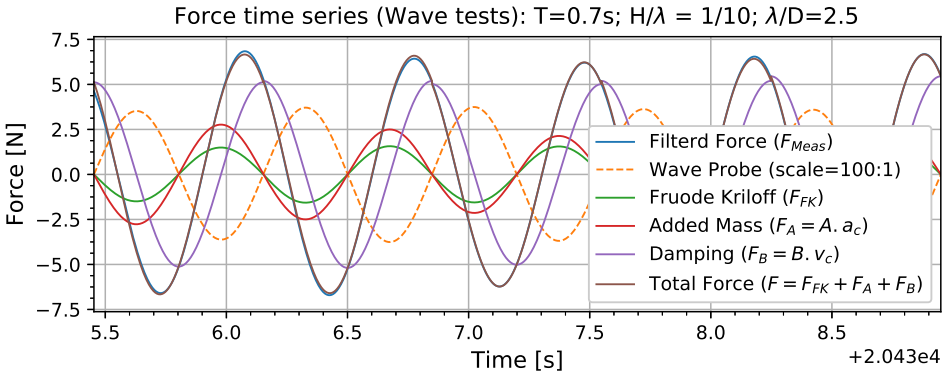

Figure 4.28: *Wave test force time series for wave:* $T = 0.7s$ *and* $H/\lambda = 1/10$.

Figures 4.27 and 4.28 presents the force time series for one of the longest and smallest test waves, respectively. λ/D is the ratio of wave length to the plate width (dimension along the wave propagation direction). It should be noted that the filtered force presented here is filtered around only the first order harmonic of the measured force in order to present a better comparison with re-calculated total force. The figure also show the wave probe time series translated to the plate center (in meters and scaled by 100 times), the Froude-Kriloff force calculated using the acceleration at each rod center (as discussed in section 3.7.3), the added mass and damping force re-calculated using the Fourier averaged added mass and damping coefficients, and the total first order force calculated as the summation of Froude-Kriloff, added mass and damping force components. As discussed in section 3.7.3, the added mass and damping coefficients are calculated cycle-wise (for 5 full amplitude cycles) due to variation of wave amplitude within a run. This will result in 5 added mass and damping coefficients per run (or wave period) for a value of μKC_{por} (as shown in results present in next section). The good agreement between the re-calculated total force and the filtered force shows that the calculated added mass and damping coefficients can be used to calculate total first order hydrodynamic loads on the test model in the present conditions.

4.4.3 Hydrodynamic Coefficients

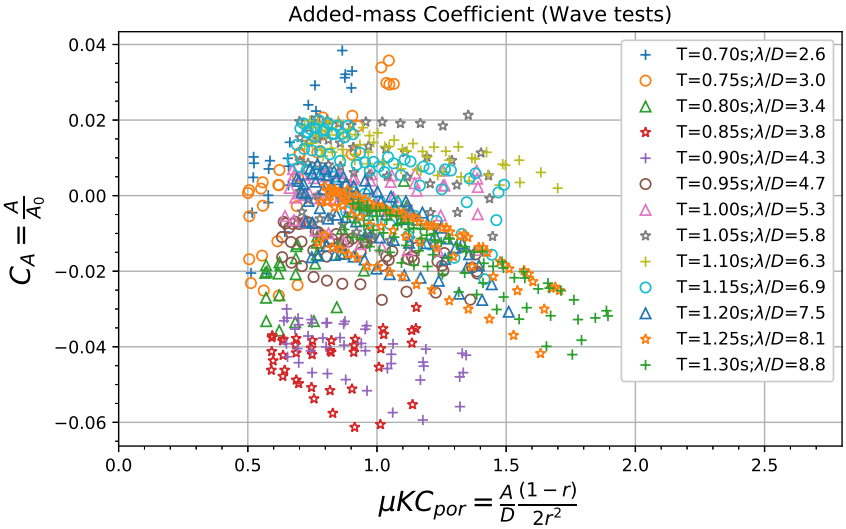

Figure 4.29: *Added mass coefficient (C_A).*

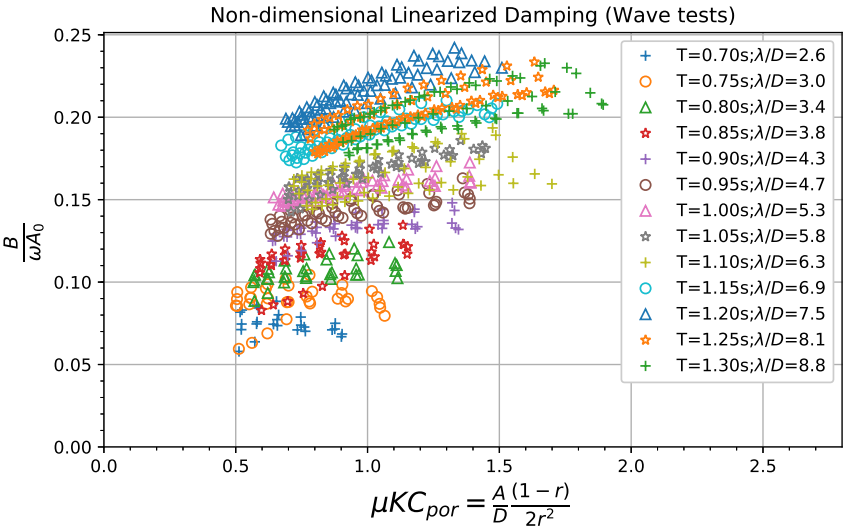

Figure 4.30: *Non-dimensional linearized damping.*

Figures 4.29 and 4.30 presents the added mass coefficient and non-dimensional linearized damping, respectively, calculated for all the test cases with varying μKC_{por}. As mentioned in section 3.7.3, the added mass and damping force coefficients are calculated here assuming that the acceleration and velocity do not vary spatially over the plate area at any instant of time. In other word, the waves are assumed to be very long as compared to model dimensions, even in the case of shortest waves. This assumption is also known as long-wave approximation or small-volume structure approximation. In case of a vertical pile of diameter D experiencing an incident wave of wave length λ, this approximation is considered valid for $\lambda/D > 5$. But in the current case no such validity range is established. Further, the calculated added mass and damping coefficients for $\lambda/D > 5$ does not give the same values for a unique value of μKC_{por} for different waves of similar length scale, which would be expected if the long wave approximation is valid. But since in this case the model is very near to the free surface, this may be due to the frequency dependence of added mass and damping.

Further, it should be noted that the added mass is negative in some cases. In case of a deeply submerged body, added mass is interpreted as the mass of the fluid accelerated by the body[7] and thus, it is always positive. Mciver, 1984 [17], mentioned various cases when added mass (i.e., the force coefficient proportional to acceleration) was found negative and all these cases were associated to problems strongly influenced by free-surface effects. He claimed that the definition of added mass, as in case of a deeply submerged body, is not exactly true in cases when free-surface effects are important. Ogilvie, 1963 [18], calculated negative added mass in case of a horizontal cylinder over a range of frequencies, when the depth of submergence was sufficiently small as compared to the diameter of the cylinder.

Ogilvie [18] presented the case of a submerged oscillating cylinder. He calculated negative added mass for a few cases when the cylinder was very close to the free surface. In our case the test model can be interpreted as a sequence of 24 cylinders fixed $55mm$ below the mean water level in an oscillating wave field. In this case, in addition to free-surface and frequency effects, the interaction between these 24 cylinders will also be important. Thus, due to lack of any such precedence no clear conclusion can be drawn here.

In comparison to deep water oscillations, for long waves, the absolute values of added mass coefficients are significantly small (less than $1/10^{th}$ of the corresponding values) but the linearized damping values are just about half the corresponding values. This shows that in a realistic sea condition, the damping dominance of hydrodynamic loads for a porous plate can be substantially more prominent.

[7]The added mass, as per the direct interpretation of equation of motion, is accelerated to the same acceleration as the body but in reality all the fluid around the body is not accelerated to the same extent. Thus, this definition is not 100% accurate.

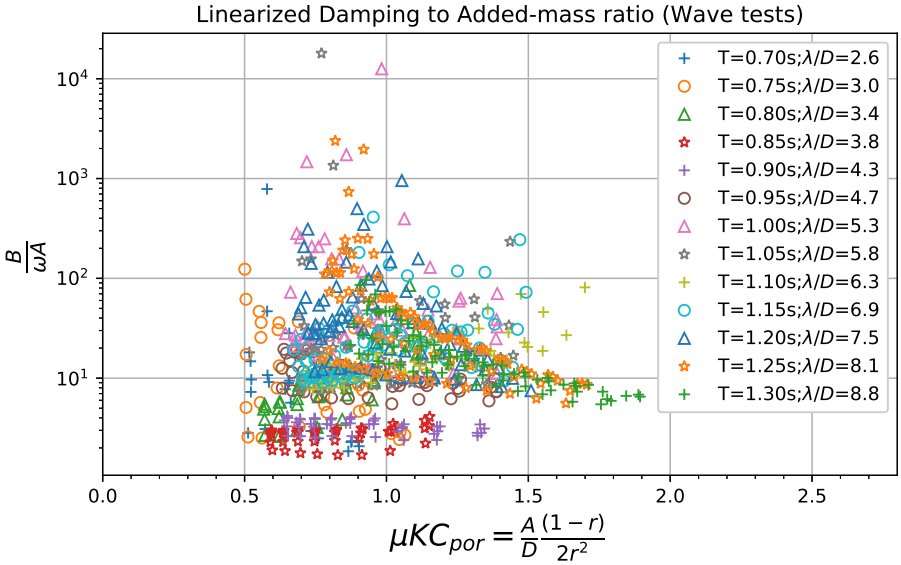

Figure 4.31: *Linearized damping to Added mass ratio.*

Figure 4.31 shows the relative magnitude of linearized damping to the absolute value of added mass. It should be noted here that the y-axis is plotted in logarithmic scale. For long waves the damping is of the order of 10 to 100 times the added mass. Thus, the hydrodynamic loads are strongly damping dominated for a porous plate in the presence of waves.

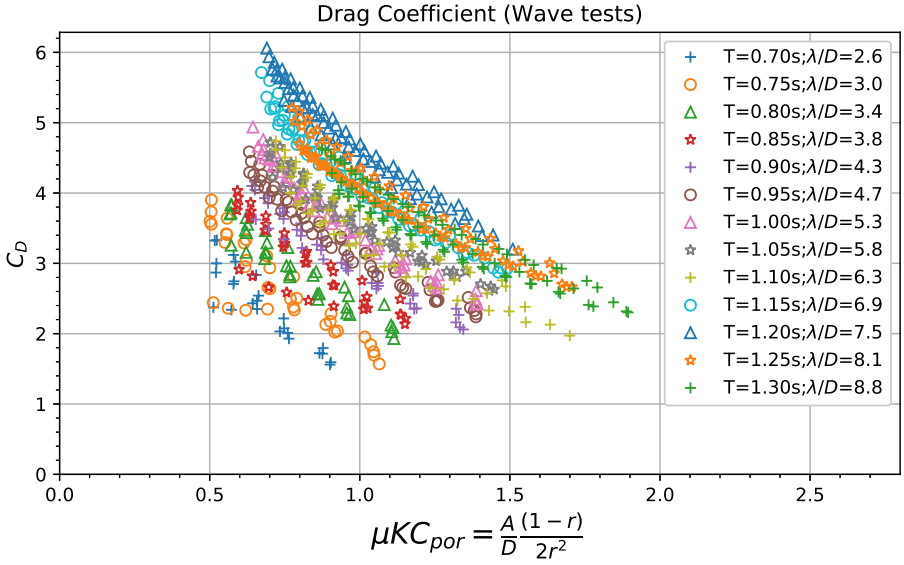

Figure 4.32: *Drag coefficient (C_D).*

Figure 4.32 shows the drag coefficient calculated according to the Morison's load model (discussed in section 2.6). The drag coefficient shows similar trend as linearized damping. The values obtained for long waves are about half the corresponding values for deep water oscillations case. The variation over wave periods may be due to frequency dependence of drag coefficient.

Chapter 5
Conclusion

5.1 Deep Water Oscillations

- Non-dimensionalized added mass and damping in infinite fluid for a porous plate strongly depends on the amplitude of oscillations but are independent of frequency.
- Higher perforation area ratio plates have smaller added mass and damping and thus, lesser hydrodynamic loads. It is suggested to use oscillation velocity amplitude (or an equivalent parameter) instead of μKC_{por} for the comparison of damping, as the later may be misleading. Additionally, results indicate that a rod screen type porous plate has smaller added mass and damping compared to a perforated plate (plate with circular holes and sharp edges).
- Linearized damping model should be used with care as it may result in over-estimation of damping force for small oscillation amplitudes in case of porous plates.
- For rod screen type porous plate, damping shows non-linear trend for higher oscillation velocity amplitudes ($> 0.3m/s$, corresponding to porous Re = 4.9x10^5). This may be due to Reynolds number dependence and needs to be further investigated.
- Damping can be as high as 1.5 to 3.0 times the added mass in case of a porous structure for the current range of μKC_{por}. Thus, the total hydrodynamic force is damping dominated. Moreover, the damping dominance increases with increasing perforation area ratio and seems to be independent of type of porous plate.
- The results from DNV-GL's [1] empirical formulation, for zero amplitude added mass for a porous plate, are quite conservative and it appears that these results can even be used to get a conservative estimate in range of small KC number ($KC < 1$ for perforated plate, and $KC < 1.5$ for rod screen type plate) but for a higher range of KC a correction must be applied. Additionally, the reduction factor curve suggested by DNV-GL [1] (shown in Figure 1.6) to obtain conservative estimate of added mass (based on perforation area ratio and irrespective of KC number) may not remain conservative for higher range of KC number.
- Drag coefficient for a porous plate in infinite fluid shows a consistently reducing trend with increasing oscillation amplitude. Increasing perforation area ratio reduces drag and rod screen type porous plates have a smaller drag.

5.2 Water-Entry

- The water-entry force shows fluctuations due to rig oscillation. This could not be filtered by using the frequency domain filtering as the slamming impact peak lies in the same frequency range as the natural frequency of rig components. But this would not contribute to any significant error in impulse calculations.
- A simple method to estimate the water-entry drag was demonstrated by calculating the force impulse using 2 different methods.
- Drag coefficients, calculated from water-entry force impulse, should not be compared with the theoretical estimates for restricted flow in a conduit (as presented by Blevins [6]), specially in the case of a perforated plates. It may be acceptable for a rod screen type plate for certain range of water-entry velocity.
- Slamming impact force peak can be neglected while calculating the force impulse within the characteristic depth limit, over which free surface phenomenon are prominent. Thus, the water-entry force is drag dominated but this drag is strongly influenced by free surface phenomenon like attachment of air bubbles and delayed wetting of top surface, and it is significantly higher than the Reynolds dependent steady drag.

5.3 Wave Tests

- Fourier averaged added mass and damping force coefficients, calculated assuming long-wave approximation, can be used to estimate first order hydrodynamic loads on a rod screen type porous plate. But these added mass and damping coefficients are much smaller than the corresponding coefficients from deep water forced oscillations, even for the longest wave (λ/D = 8.8). The added mass coefficient was observed to be about $1/10^{th}$ and non-dimensional linearized damping as well as drag coefficient were about half the corresponding values.
- Negative added mass was observed for some of the test cases. This is suspected to be due to the small submergence of test model and thus, the free surface effects.
- The obtained hydrodynamic coefficients are found to be dependent on wave frequency, which is also expected due to free surface effects.
- Due to significant reduction in added mass in wave tests, the damping to added mass ratio is observed to be in the range of 10 to 100 for long waves. Thus, the hydrodynamic loads on a rod screen type porous plate in waves is strongly damping dominated.

5.4 Further Work

As mentioned at many instances in this report that not much data is available regarding hydrodynamic loads on porous plates. Thus, much work needs to be done in this field. Based on the results and observations from the current work, following further work can be suggested:

- Investigation of Reynolds number dependence of added mass and damping in uniformly oscillating flow field as well as in steady flow for porous plates. The first would help us understand the non-linearity observed, at higher KC, in the case of rod screen type porous plate. And the later would help us understand and perform a quantitative comparison between steady drag and water-entry drag.
- Further study the influence of free surface phenomenon like attachment of air bubbles and delayed wetting of top surface in case of constant velocity water-entry using experimental as well as numerical methods. Establishing an empirical or numerical method to determine the free surface influenced submergence depth limit (h) for constant velocity water-entry. This is necessary to accurately estimate splash zone water-entry loads.
- A more realistic case of water-entry in presence of waves should be studied to understand the difference between real and idealized laboratory conditions.
- The case of a fully submerged porous plate in waves needs to be studied further to investigate and understand the physical interpretation of negative added mass.

Bibliography

[1] DNVGL-RP-N103. Modelling and Analysis of Marine Operations. DNVGL, 2017.

[2] O. Faltinsen. Sea Loads on Ships and Offshore Structures. Cambridge Ocean Technology Series. Cambridge University Press, 1993.

[3] J R. Morison, J W. Johnson, and S A. Schaaf. The force exerted by surface waves on piles. Journal of Petroleum Technology - J PETROL TECHNOL, 2:149–154, 05 1950.

[4] T Sarpkaya. Morison's equation and the wave forces on offshore structures. page 270, 12 1981.

[5] J.N. Newman and Knovel (Firm). Marine Hydrodynamics. Mit Press. MIT Press, 1977.

[6] R.D. Blevins. Applied Fluid Dynamics Handbook. Krieger Pub., 2003.

[7] Bernard Molin. Hydrodynamic modeling of perforated structures. Applied Ocean Research, 33(1):1–11, 2011.

[8] B Molin. On the added mass and damping of periodic arrays of fully or partially porous disks. Journal of fluids and structures, 15(2):275–290, 2001.

[9] P.M. Morse and K.U. Ingard. Theoretical Acoustics. International series in pure and applied physics. McGraw-Hill, 1971.

[10] Peter Chr Sandvik, Frøydis Solaas, Finn G Nielsen, et al. Hydrodynamic forces on ventilated structures. In The Sixteenth International Offshore and Polar Engineering Conference. International Society of Offshore and Polar Engineers, 2006.

[11] G. H. KEULEGAN and L. H. CARPENTER. Forces on cylinders and plates in an oscillating fluid. J. Research of the National Bureau of Standards Research Paper, 2857:423–440, 1958.

[12] T Sarpkaya, M Isaacson, and J V. Wehausen. The mechanics of ware forces on offshore structures. Journal of Applied Mechanics-transactions of The Asme - J APPL MECH, 49, 01 1981.

[13] Turgut Sarpkaya et al. In-line and transverse forces, on cylinders in oscillatory flow at high reynolds numbers. In Offshore Technology Conference. Offshore Technology Conference, 1976.

[14] B Molin, FG Nielsen, et al. Heave added mass and damping of a perforated disk below the free surface. In Proceedings of the 19th International Workshop on Water Waves and Floating Bodies, Cortona, Italy, 2004.

[15] J. M. R. Graham. The forces on sharp-edged cylinders in oscillatory flow at low keulegan–carpenter numbers. Journal of Fluid Mechanics, 97(2):331–346, 1980.

[16] F Mentzoni, M Abrahamsen-Prsic, and T Kristiansen. Hydrodynamic coefficients of simplified subsea structures. In Proceedings of the ASME 2018 37th International Conference on Ocean, Offshore and Arctic Engineering, 06 2018.

[17] P. Mciver and D. V. Evans. The occurrence of negative added mass in free-surface problems involving submerged oscillating bodies. Journal of Engineering Mathematics, 18(1):7–22, Mar 1984.

[18] T. Francis Ogilvie. First- and second-order forces on a cylinder submerged under a free surface. Journal of Fluid Mechanics, 16(3):451–472, 1963.

Appendix A: Water-Entry Force (F_z) vs Time (t)

Model: P19

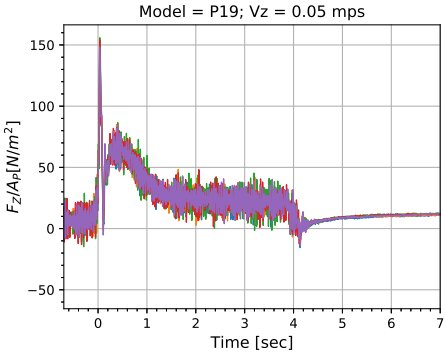

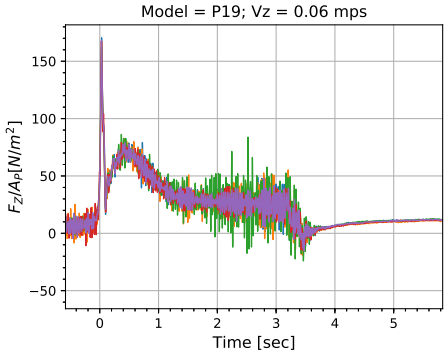

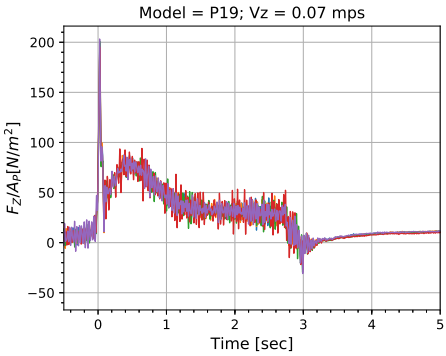

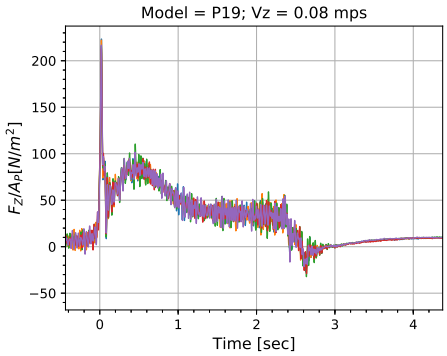

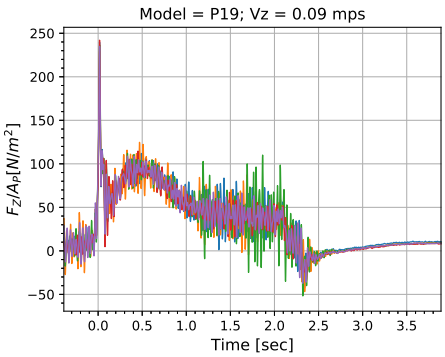

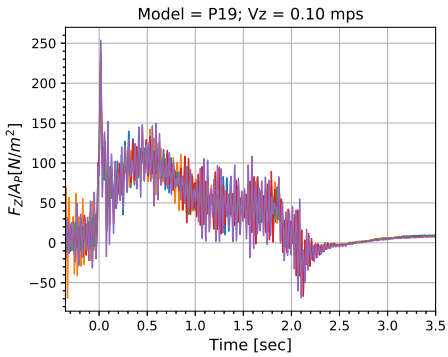

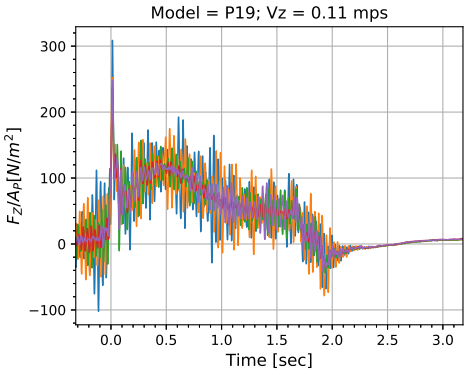
Model = P19; Vz = 0.11 mps
$F_Z/A_P[N/m^2]$
Time [sec]

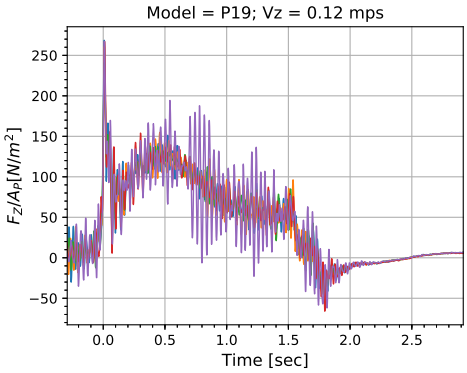
Model = P19; Vz = 0.12 mps
$F_Z/A_P[N/m^2]$
Time [sec]

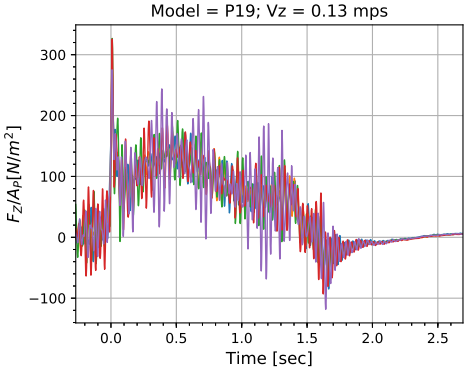
Model = P19; Vz = 0.13 mps
$F_Z/A_P[N/m^2]$
Time [sec]

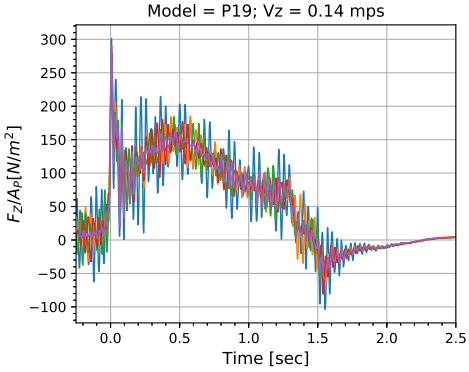
Model = P19; Vz = 0.14 mps
$F_Z/A_P[N/m^2]$
Time [sec]

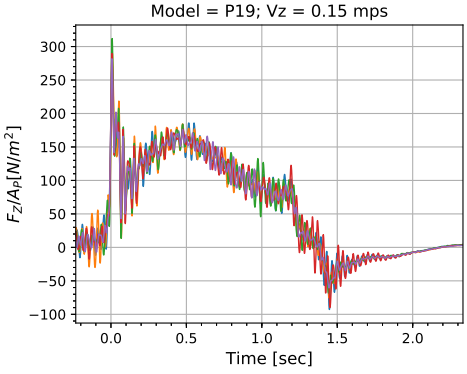
Model = P19; Vz = 0.15 mps
$F_Z/A_P[N/m^2]$
Time [sec]

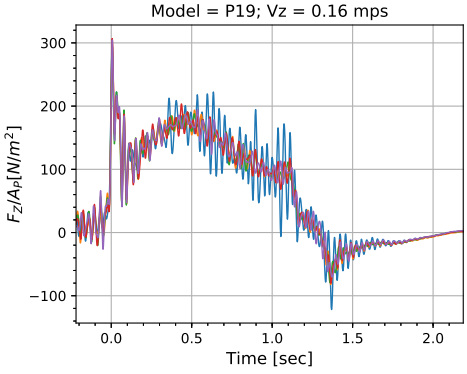
Model = P19; Vz = 0.16 mps
$F_Z/A_P[N/m^2]$
Time [sec]

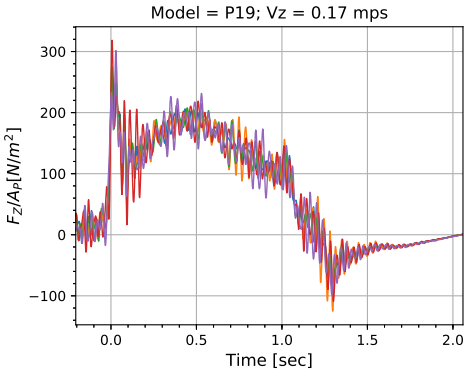
Model = P19; Vz = 0.17 mps
$F_Z/A_P[N/m^2]$
Time [sec]

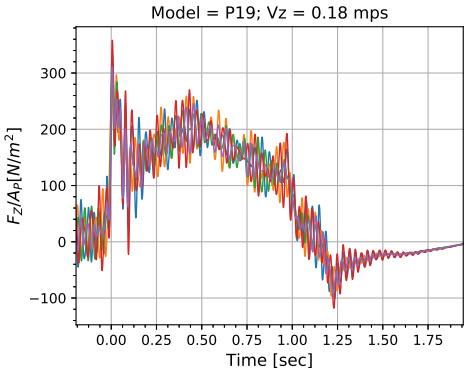
Model = P19; Vz = 0.18 mps
$F_Z/A_P[N/m^2]$
Time [sec]

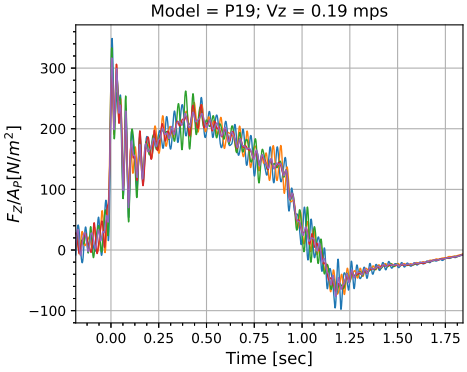
Model = P19; Vz = 0.19 mps
$F_Z/A_P[N/m^2]$
Time [sec]

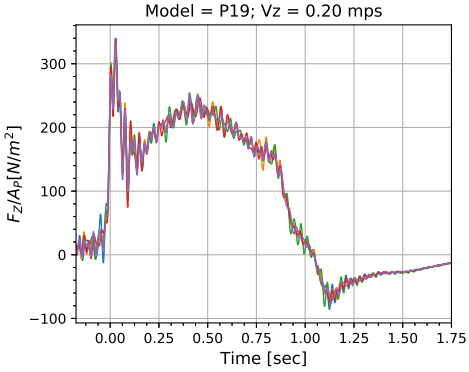
Model = P19; Vz = 0.20 mps
$F_Z/A_P[N/m^2]$
Time [sec]

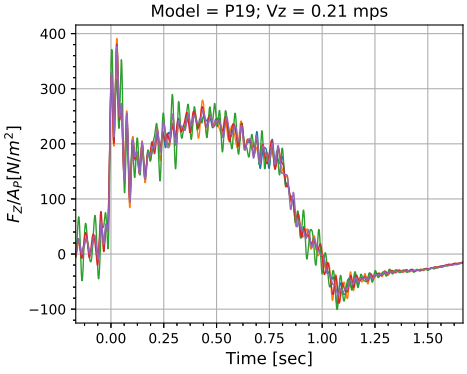
Model = P19; Vz = 0.21 mps
$F_Z/A_P[N/m^2]$
Time [sec]

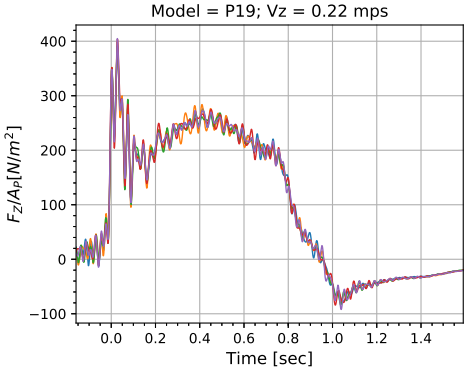
Model = P19; Vz = 0.22 mps
$F_Z/A_P[N/m^2]$
Time [sec]

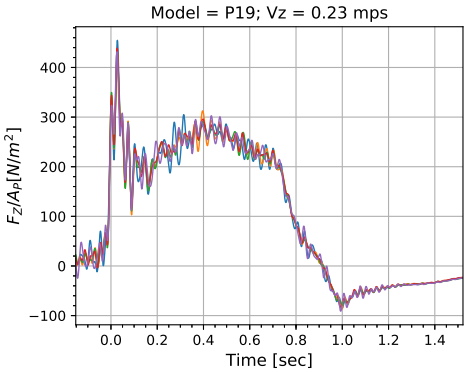
Model = P19; Vz = 0.23 mps
$F_Z/A_P[N/m^2]$
Time [sec]

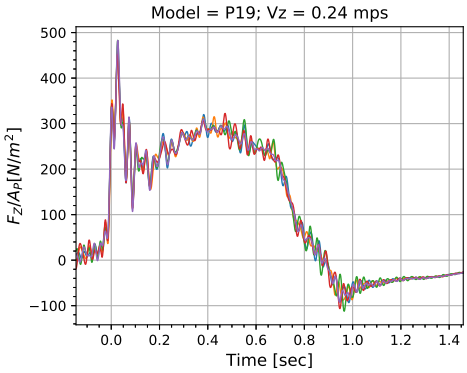
Model = P19; Vz = 0.24 mps
$F_Z/A_P[N/m^2]$
Time [sec]

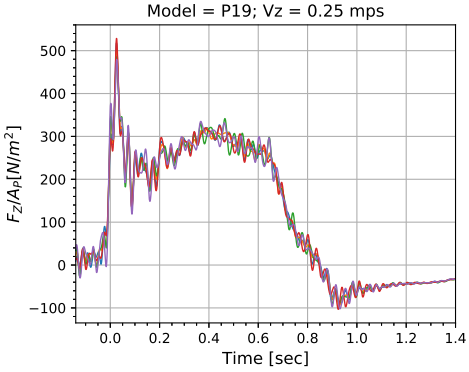
Model = P19; Vz = 0.25 mps
$F_Z/A_P[N/m^2]$
Time [sec]

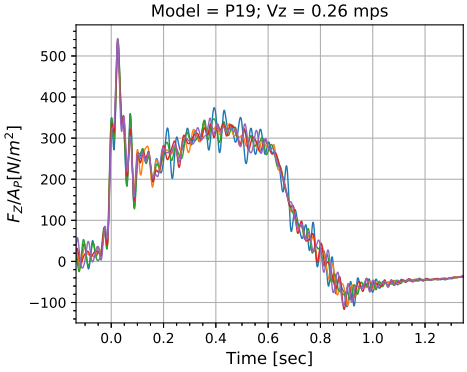
Model = P19; Vz = 0.26 mps
$F_Z/A_P[N/m^2]$
Time [sec]

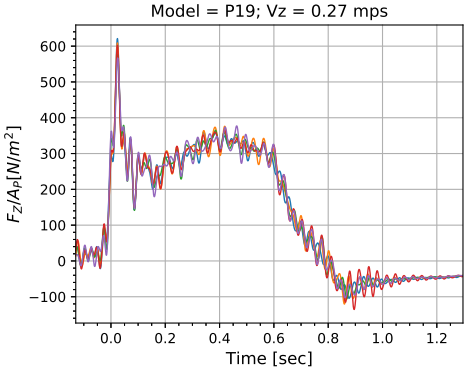
Model = P19; Vz = 0.27 mps
$F_Z/A_P[N/m^2]$
Time [sec]

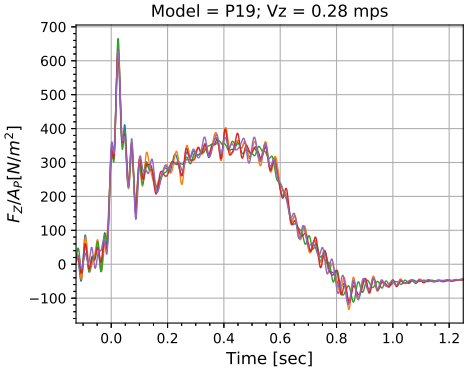
Model = P19; Vz = 0.28 mps
$F_Z/A_P[N/m^2]$
Time [sec]

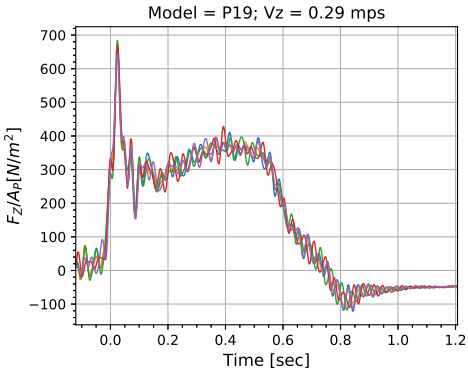
Model = P19; Vz = 0.29 mps
$F_Z/A_P[N/m^2]$
Time [sec]

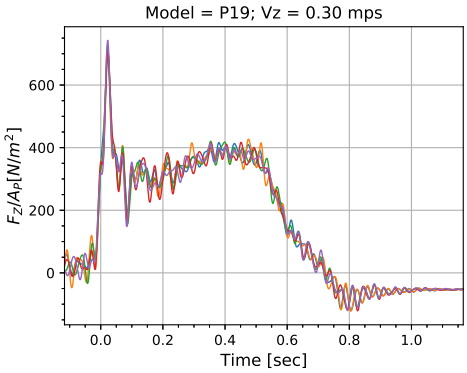
Model = P19; Vz = 0.30 mps
$F_Z/A_P[N/m^2]$
Time [sec]

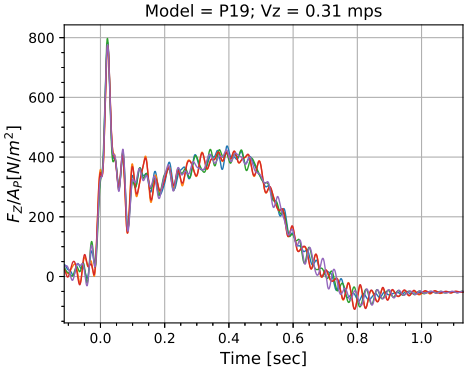
Model = P19; Vz = 0.31 mps
$F_Z/A_P[N/m^2]$
Time [sec]

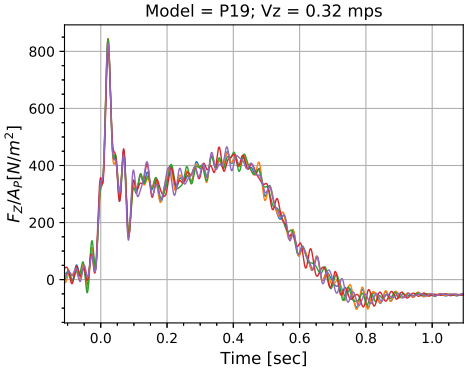
Model = P19; Vz = 0.32 mps
$F_Z/A_P[N/m^2]$
Time [sec]

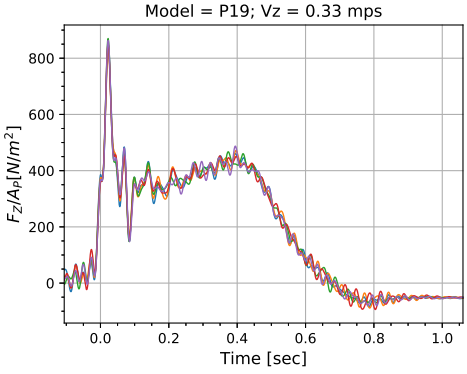
Model = P19; Vz = 0.33 mps
$F_Z/A_P[N/m^2]$
Time [sec]

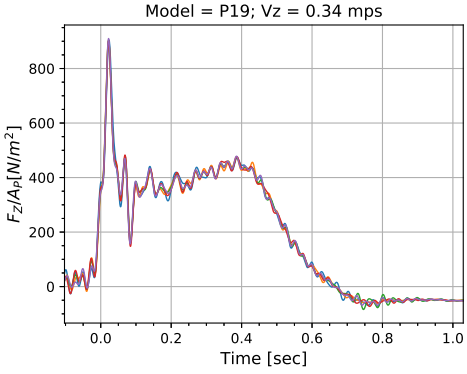
Model = P19; Vz = 0.34 mps
$F_Z/A_P[N/m^2]$
Time [sec]

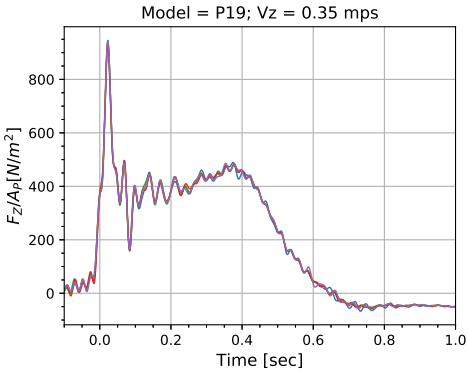
Model = P19; Vz = 0.35 mps
$F_Z/A_P[N/m^2]$
Time [sec]

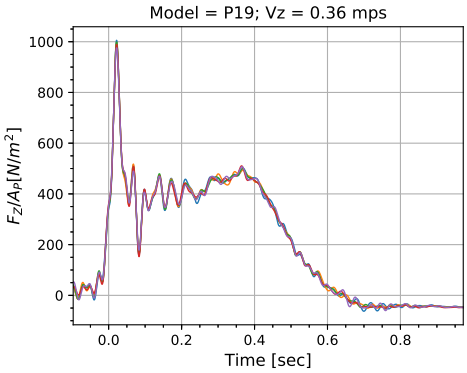
Model = P19; Vz = 0.36 mps
$F_Z/A_P[N/m^2]$
Time [sec]

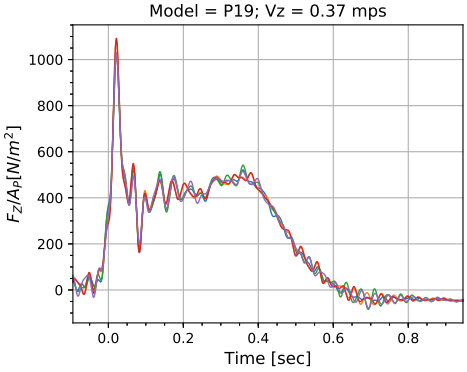
Model = P19; Vz = 0.37 mps
$F_Z/A_P[N/m^2]$
Time [sec]

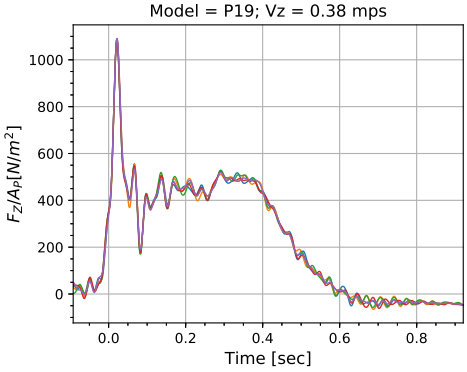
Model = P19; Vz = 0.38 mps
$F_Z/A_P[N/m^2]$
Time [sec]

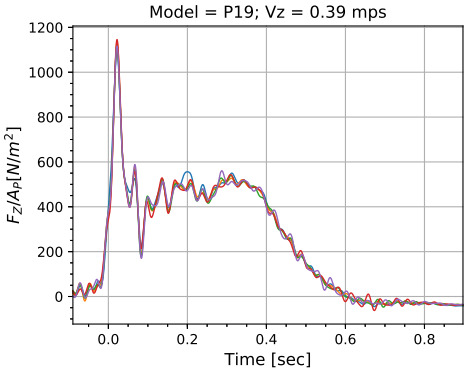
Model = P19; Vz = 0.39 mps
$F_Z/A_P[N/m^2]$
Time [sec]

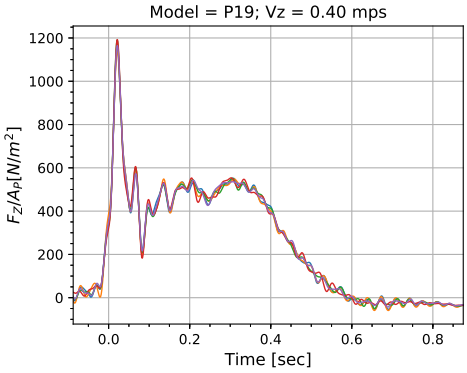
Model = P19; Vz = 0.40 mps
$F_Z/A_P[N/m^2]$
Time [sec]

Model: P28

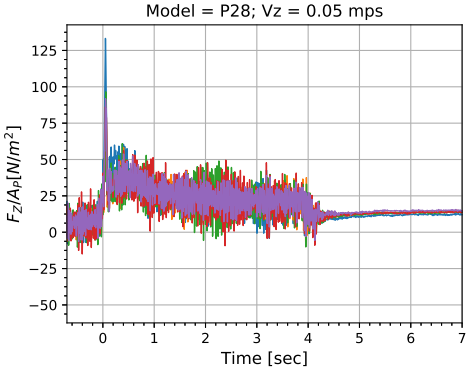
Model = P28; Vz = 0.05 mps
$F_Z/A_P[N/m^2]$
Time [sec]

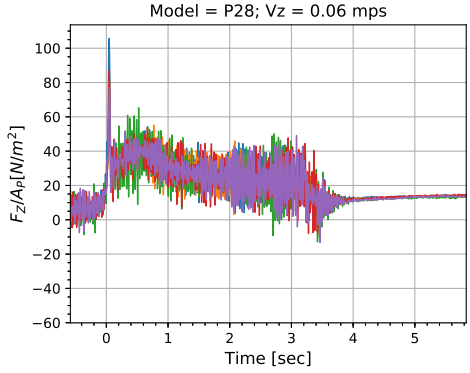
Model = P28; Vz = 0.06 mps
$F_Z/A_P[N/m^2]$
Time [sec]

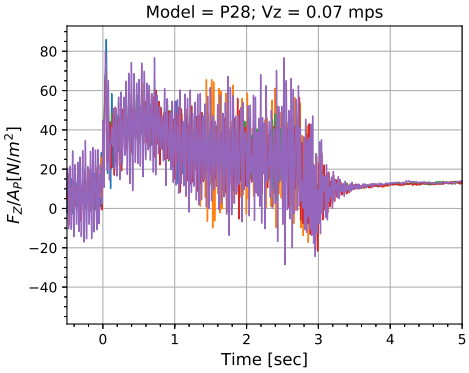
Model = P28; Vz = 0.07 mps
$F_Z/A_P[N/m^2]$
Time [sec]

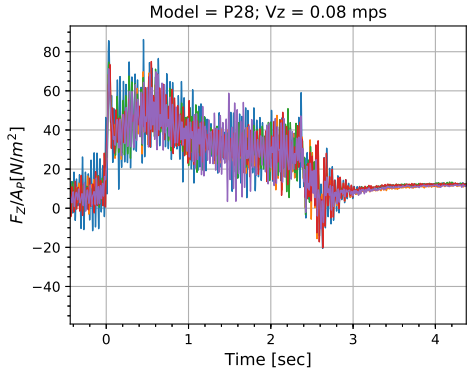
Model = P28; Vz = 0.08 mps
$F_Z/A_P[N/m^2]$
Time [sec]

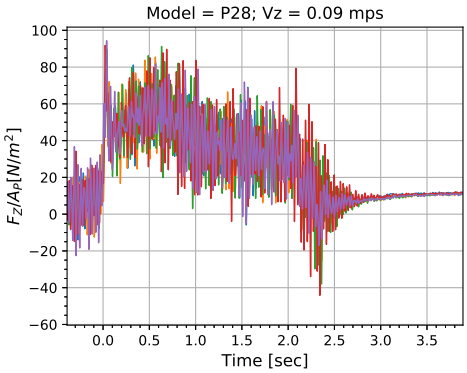
Model = P28; Vz = 0.09 mps
$F_Z/A_P[N/m^2]$
Time [sec]

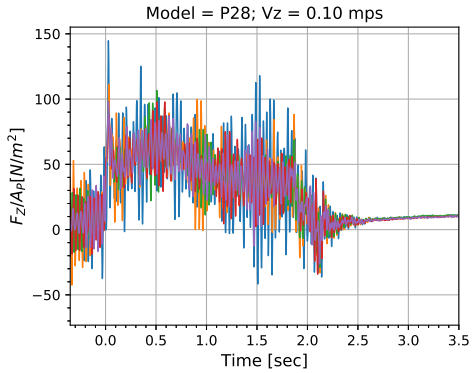
Model = P28; Vz = 0.10 mps
$F_Z/A_P[N/m^2]$
Time [sec]

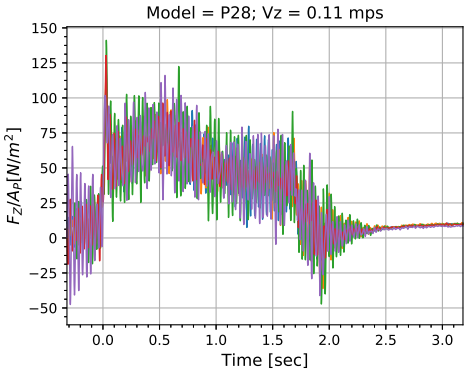
Model = P28; Vz = 0.11 mps
$F_Z/A_P[N/m^2]$
Time [sec]

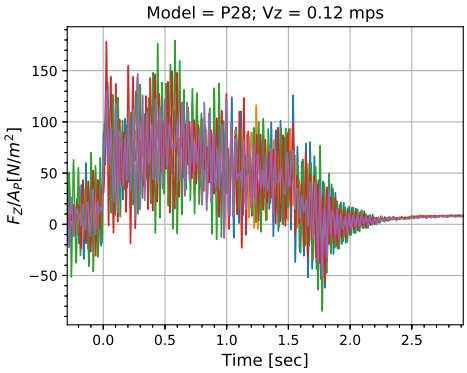
Model = P28; Vz = 0.12 mps
$F_Z/A_P[N/m^2]$
Time [sec]

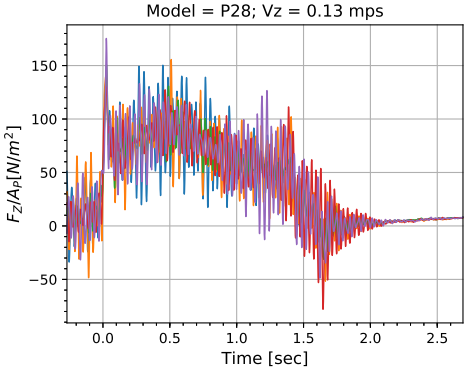
Model = P28; Vz = 0.13 mps
$F_Z/A_P[N/m^2]$
Time [sec]

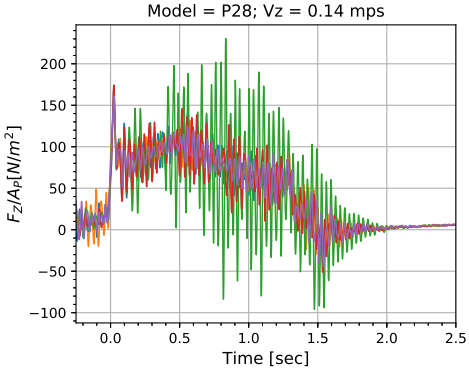
Model = P28; Vz = 0.14 mps
$F_Z/A_P[N/m^2]$
Time [sec]

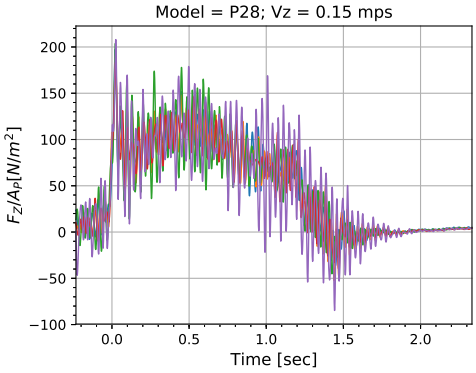
Model = P28; Vz = 0.15 mps
$F_Z/A_P[N/m^2]$
Time [sec]

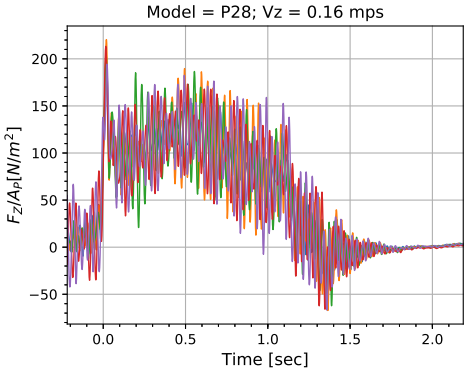
Model = P28; Vz = 0.16 mps
$F_Z/A_P[N/m^2]$
Time [sec]

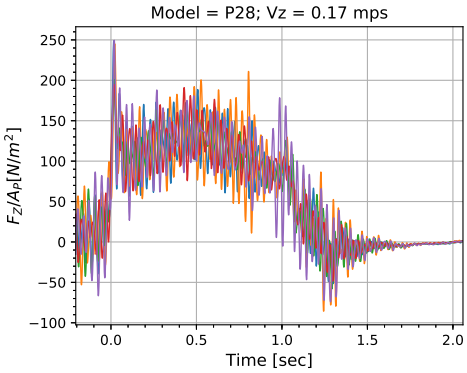
Model = P28; Vz = 0.17 mps
$F_Z/A_P[N/m^2]$
Time [sec]

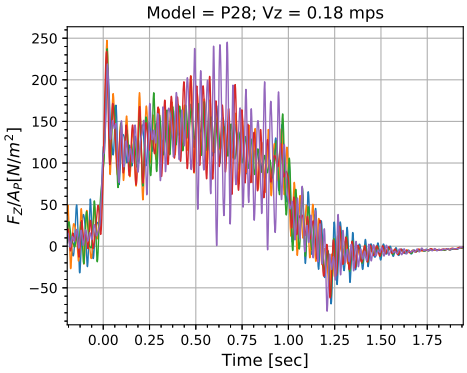
Model = P28; Vz = 0.18 mps
$F_Z/A_P[N/m^2]$
Time [sec]

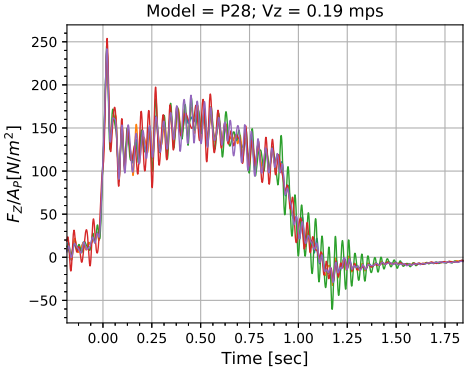
Model = P28; Vz = 0.19 mps
$F_Z/A_P[N/m^2]$
Time [sec]

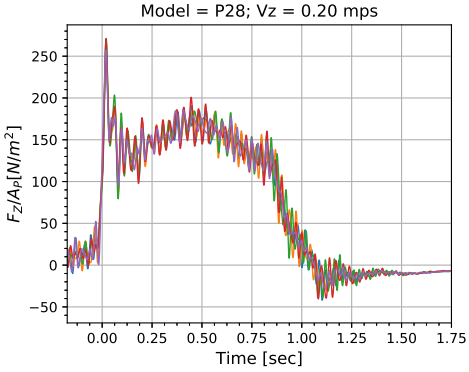
Model = P28; Vz = 0.20 mps
$F_Z/A_P[N/m^2]$
Time [sec]

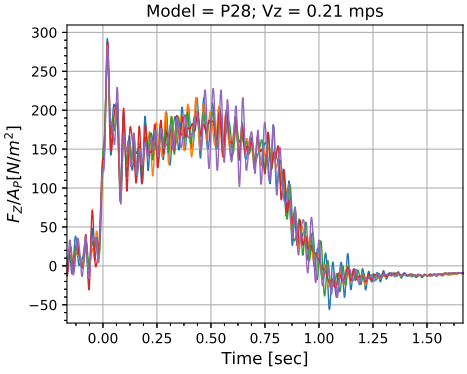
Model = P28; Vz = 0.21 mps
$F_Z/A_P[N/m^2]$
Time [sec]

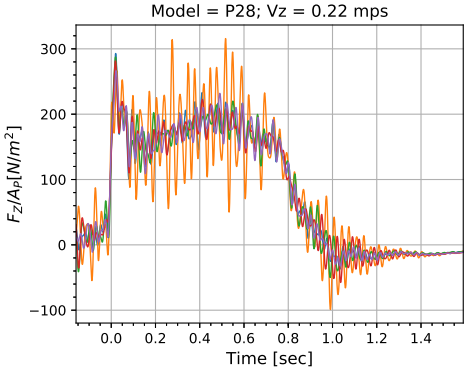
Model = P28; Vz = 0.22 mps
$F_Z/A_P[N/m^2]$
Time [sec]

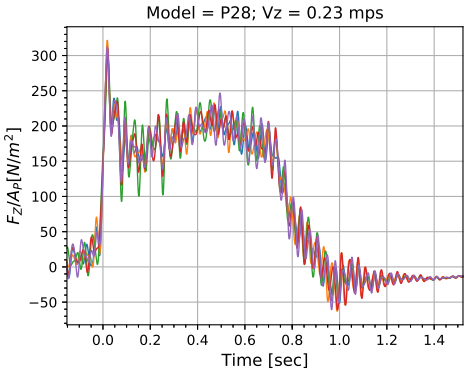
Model = P28; Vz = 0.23 mps
$F_Z/A_P[N/m^2]$
Time [sec]

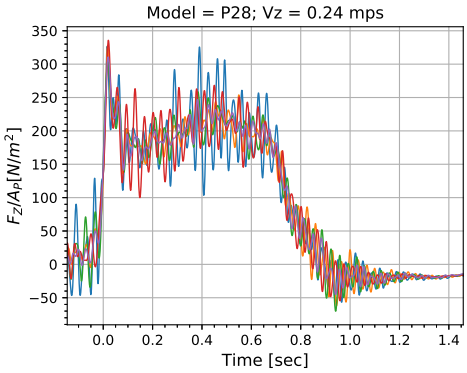
Model = P28; Vz = 0.24 mps
$F_Z/A_P[N/m^2]$
Time [sec]

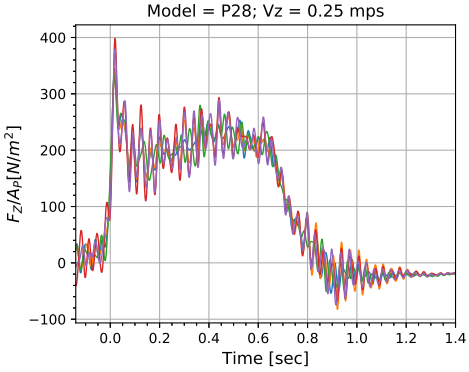
Model = P28; Vz = 0.25 mps
$F_Z/A_P[N/m^2]$
Time [sec]

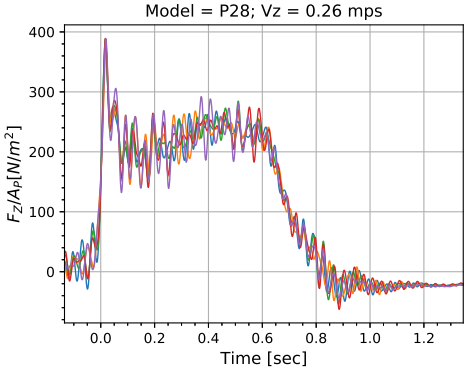
Model = P28; Vz = 0.26 mps
$F_Z/A_P[N/m^2]$
Time [sec]

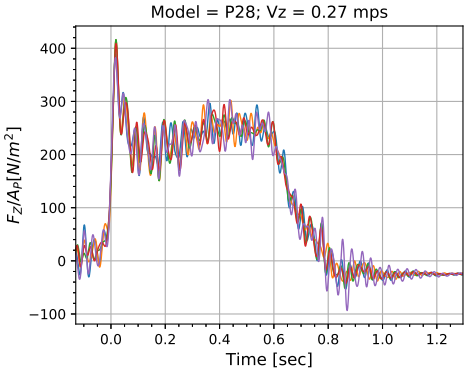
Model = P28; Vz = 0.27 mps
$F_Z/A_P[N/m^2]$
Time [sec]

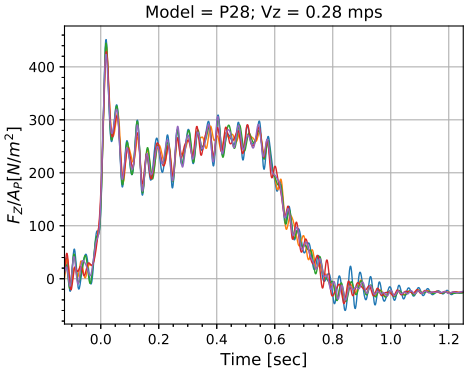
Model = P28; Vz = 0.28 mps
$F_Z/A_P[N/m^2]$
Time [sec]

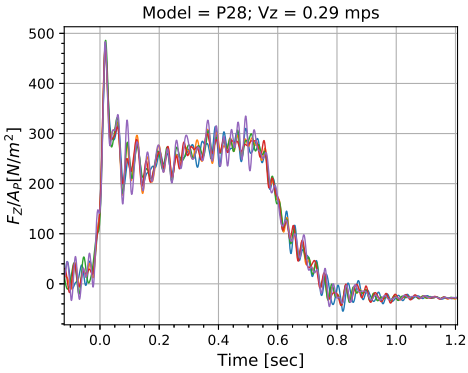
Model = P28; Vz = 0.29 mps
$F_Z/A_P[N/m^2]$
Time [sec]

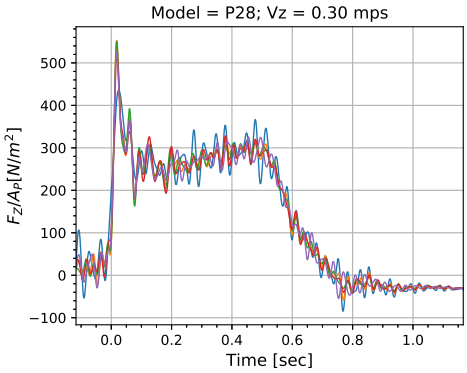
Model = P28; Vz = 0.30 mps
$F_Z/A_P[N/m^2]$
Time [sec]

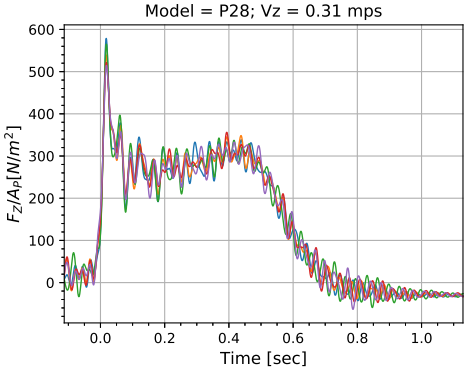
Model = P28; Vz = 0.31 mps
$F_Z/A_P[N/m^2]$
Time [sec]

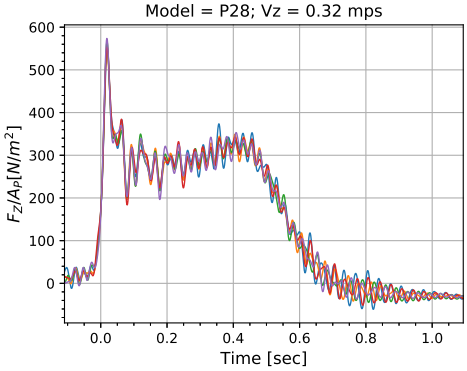
Model = P28; Vz = 0.32 mps
$F_Z/A_P[N/m^2]$
Time [sec]

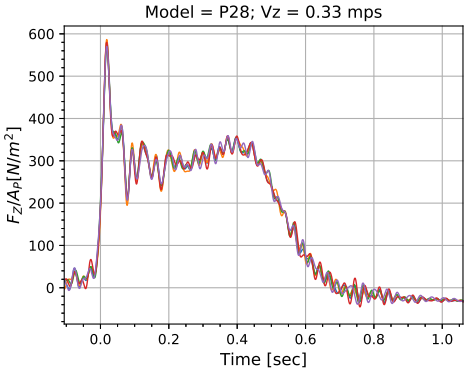
Model = P28; Vz = 0.33 mps
$F_Z/A_P[N/m^2]$
Time [sec]

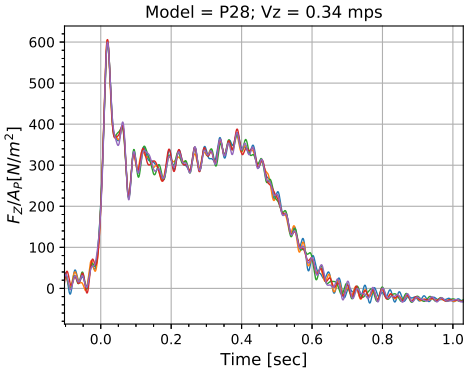
Model = P28; Vz = 0.34 mps
$F_Z/A_P[N/m^2]$
Time [sec]

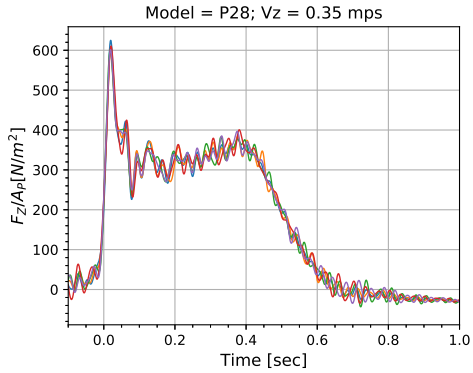
Model = P28; Vz = 0.35 mps
$F_Z/A_P[N/m^2]$
Time [sec]

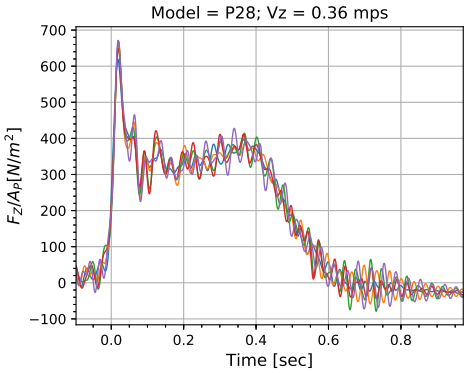
Model = P28; Vz = 0.36 mps
$F_Z/A_P[N/m^2]$
Time [sec]

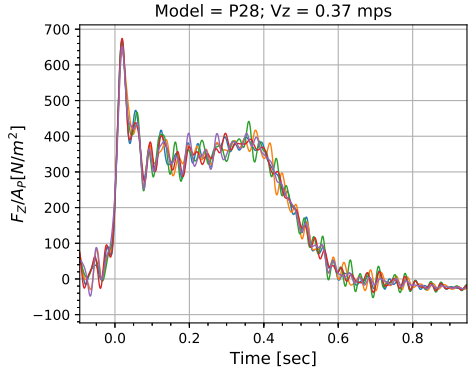
Model = P28; Vz = 0.37 mps
$F_Z/A_P[N/m^2]$
Time [sec]

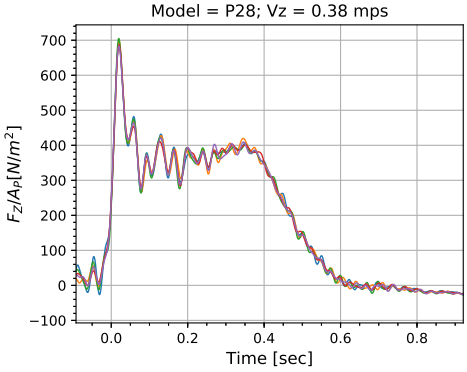
Model = P28; Vz = 0.38 mps
$F_Z/A_P[N/m^2]$
Time [sec]

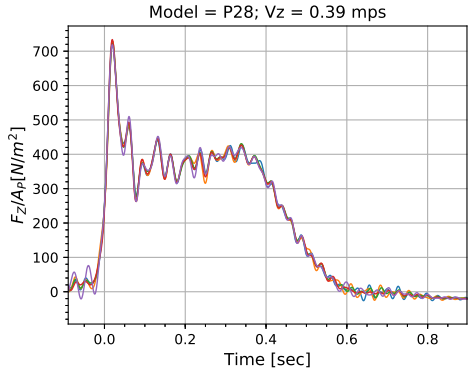
Model = P28; Vz = 0.39 mps
$F_Z/A_P[N/m^2]$
Time [sec]

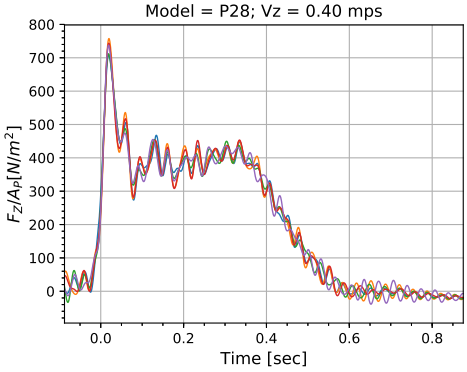
Model = P28; Vz = 0.40 mps
$F_Z/A_P[N/m^2]$
Time [sec]

Model: FING

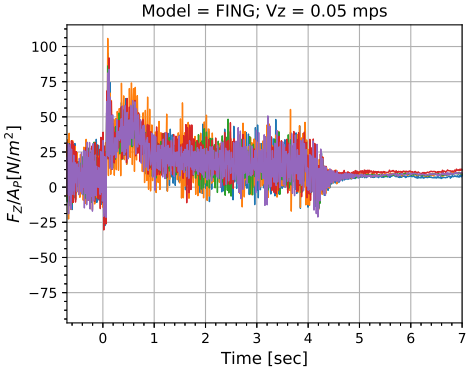
Model = FING; Vz = 0.05 mps
$F_Z/A_P[N/m^2]$
Time [sec]

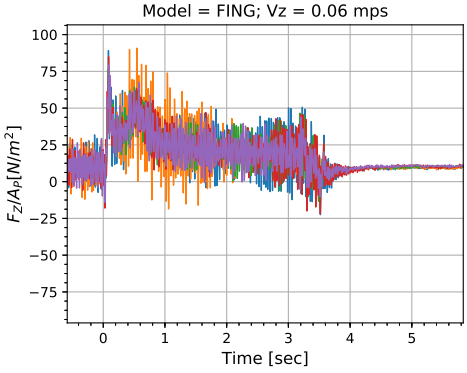
Model = FING; Vz = 0.06 mps
$F_Z/A_P[N/m^2]$
Time [sec]

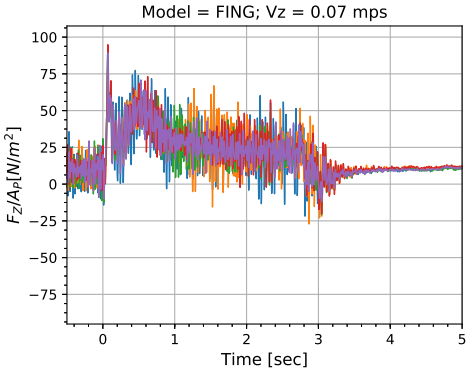
Model = FING; Vz = 0.07 mps
$F_Z/A_P[N/m^2]$
Time [sec]

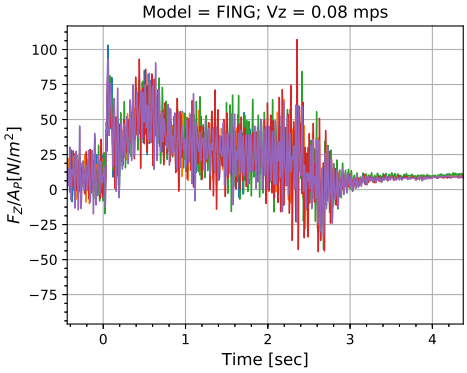
Model = FING; Vz = 0.08 mps
$F_Z/A_P[N/m^2]$
Time [sec]

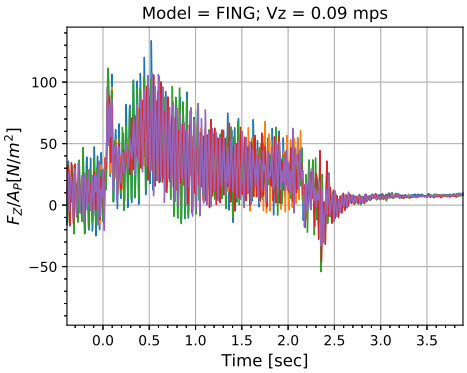
Model = FING; Vz = 0.09 mps
$F_Z/A_P[N/m^2]$
Time [sec]

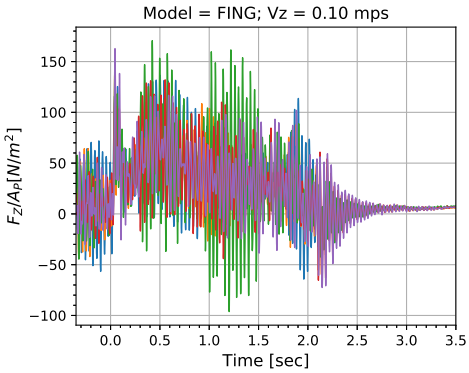
Model = FING; Vz = 0.10 mps
$F_Z/A_P[N/m^2]$
Time [sec]

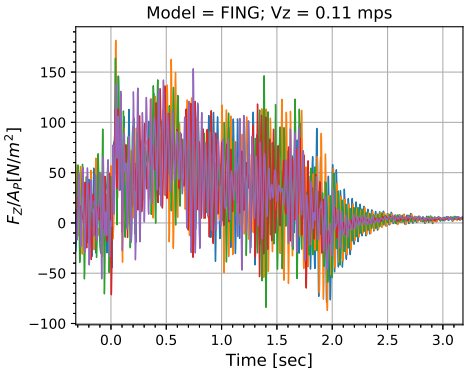
Model = FING; Vz = 0.11 mps
$F_Z/A_P[N/m^2]$
Time [sec]

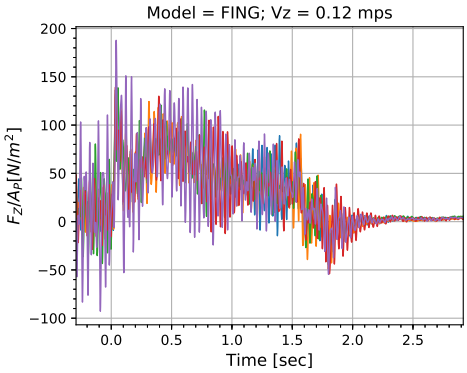
Model = FING; Vz = 0.12 mps
$F_Z/A_P[N/m^2]$
Time [sec]

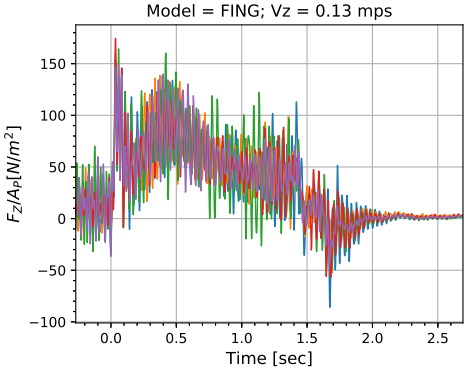
Model = FING; Vz = 0.13 mps
$F_Z/A_P[N/m^2]$
Time [sec]

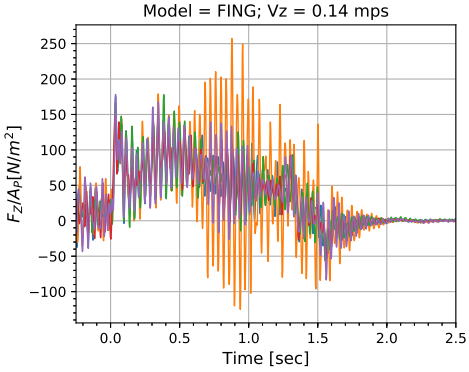
Model = FING; Vz = 0.14 mps
$F_Z/A_P[N/m^2]$
Time [sec]

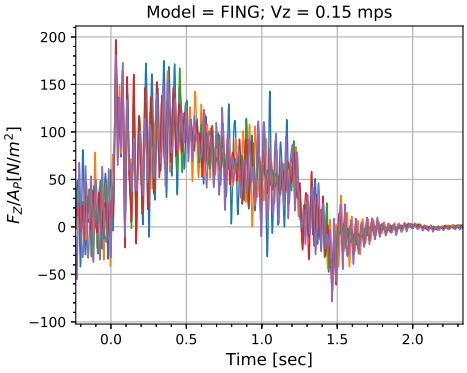
Model = FING; Vz = 0.15 mps
$F_Z/A_P[N/m^2]$
Time [sec]

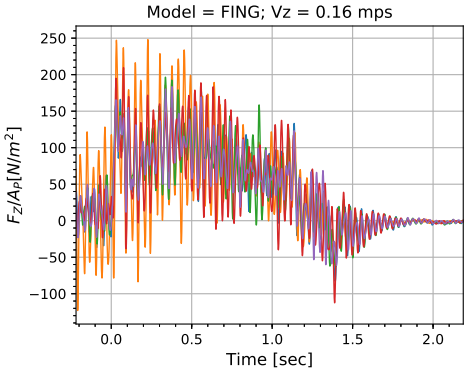
Model = FING; Vz = 0.16 mps
$F_Z/A_P[N/m^2]$
Time [sec]

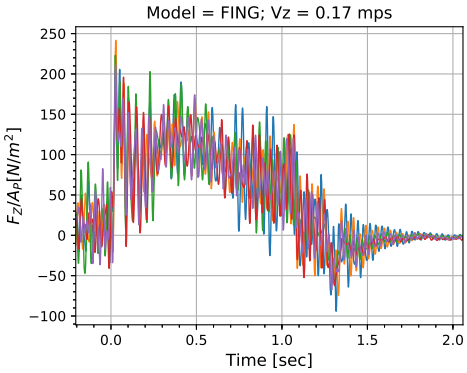
Model = FING; Vz = 0.17 mps
$F_Z/A_P[N/m^2]$
Time [sec]

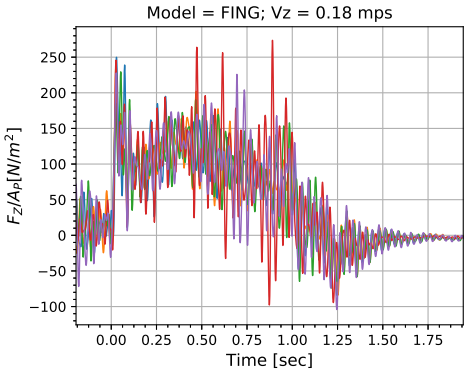
Model = FING; Vz = 0.18 mps
$F_Z/A_P[N/m^2]$
Time [sec]

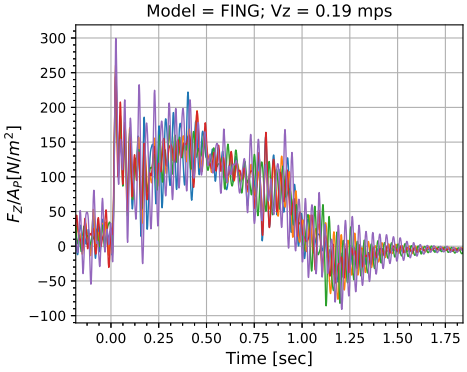
Model = FING; Vz = 0.19 mps
$F_Z/A_P[N/m^2]$
Time [sec]

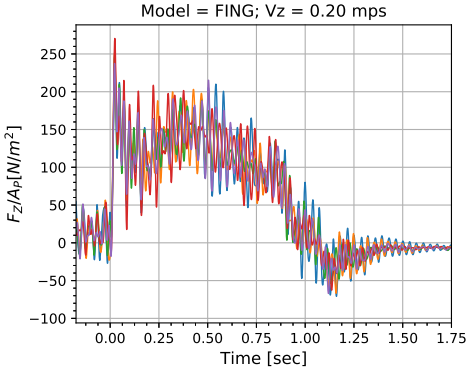
Model = FING; Vz = 0.20 mps
$F_Z/A_P[N/m^2]$
Time [sec]

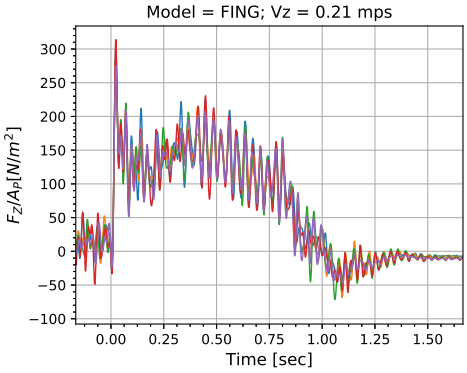
Model = FING; Vz = 0.21 mps
$F_Z/A_P[N/m^2]$
Time [sec]

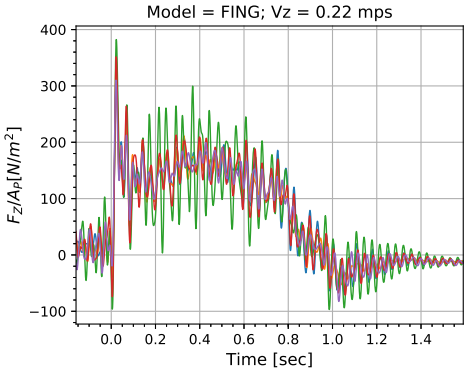
Model = FING; Vz = 0.22 mps
$F_Z/A_P[N/m^2]$
Time [sec]

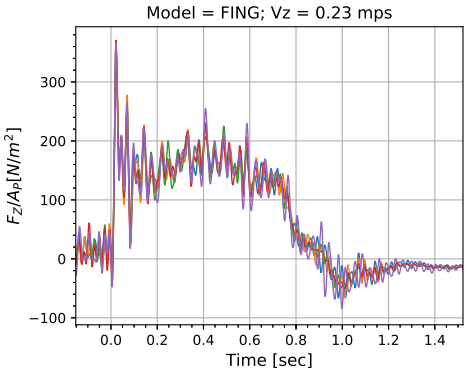
Model = FING; Vz = 0.23 mps
$F_Z/A_P[N/m^2]$
Time [sec]

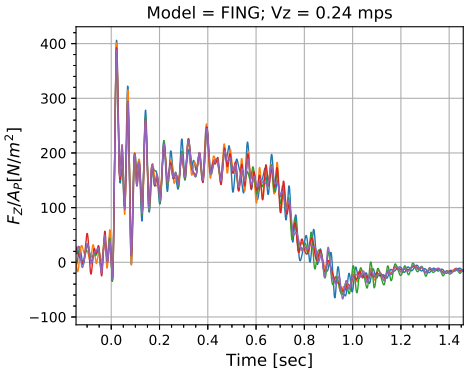
Model = FING; Vz = 0.24 mps
$F_Z/A_P[N/m^2]$
Time [sec]

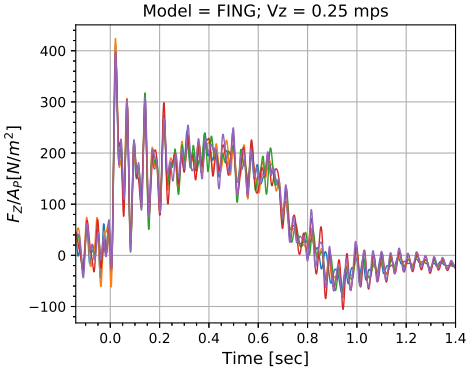
Model = FING; Vz = 0.25 mps
$F_Z/A_P[N/m^2]$
Time [sec]

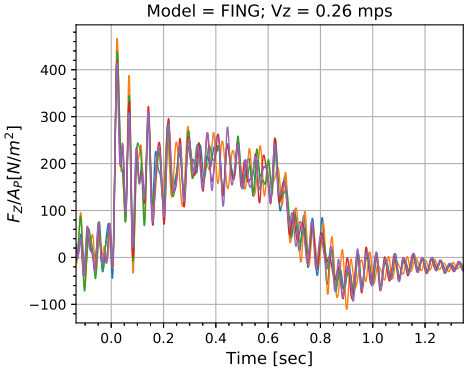
Model = FING; Vz = 0.26 mps
$F_Z/A_P[N/m^2]$
Time [sec]

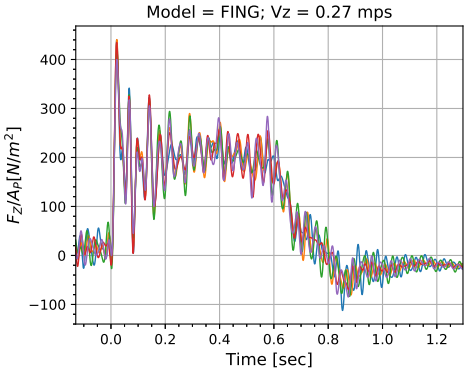
Model = FING; Vz = 0.27 mps
$F_Z/A_P[N/m^2]$
Time [sec]

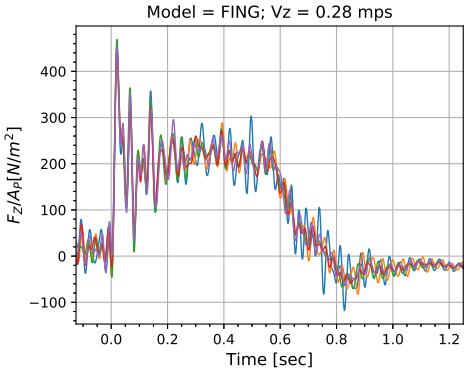
Model = FING; Vz = 0.28 mps
$F_Z/A_P[N/m^2]$
Time [sec]

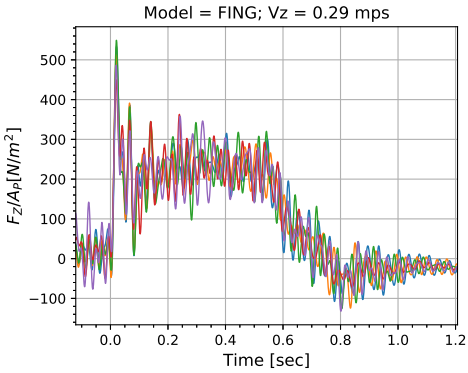
Model = FING; Vz = 0.29 mps
$F_Z/A_P[N/m^2]$
Time [sec]

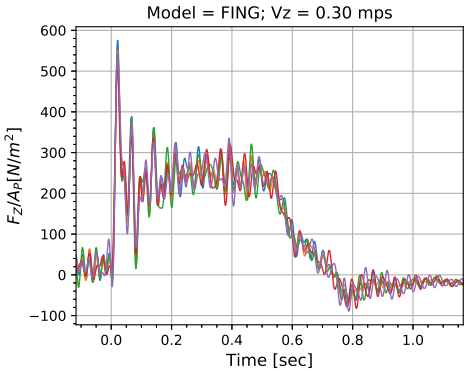
Model = FING; Vz = 0.30 mps
$F_Z/A_P[N/m^2]$
Time [sec]

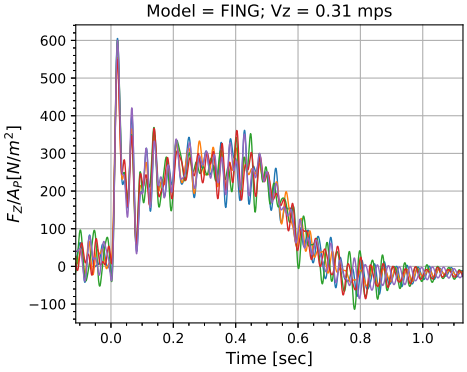
Model = FING; Vz = 0.31 mps
$F_Z/A_P[N/m^2]$
Time [sec]

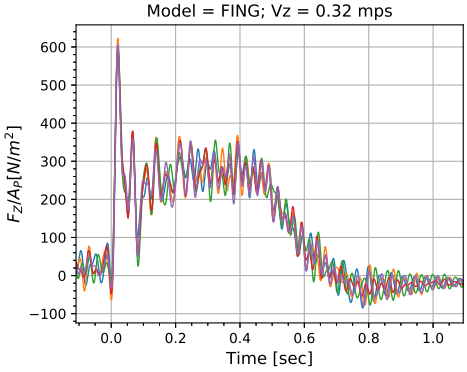
Model = FING; Vz = 0.32 mps
$F_Z/A_P[N/m^2]$
Time [sec]

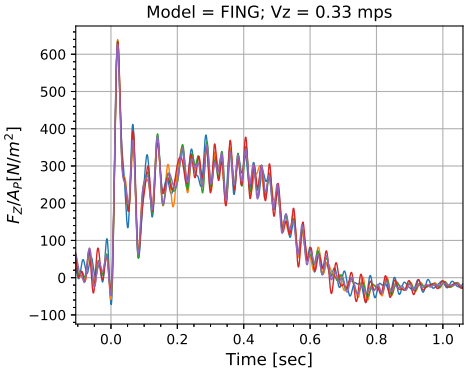
Model = FING; Vz = 0.33 mps
$F_Z/A_P[N/m^2]$
Time [sec]

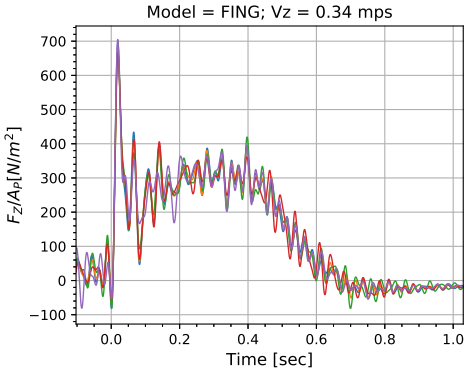
Model = FING; Vz = 0.34 mps
$F_Z/A_P[N/m^2]$
Time [sec]

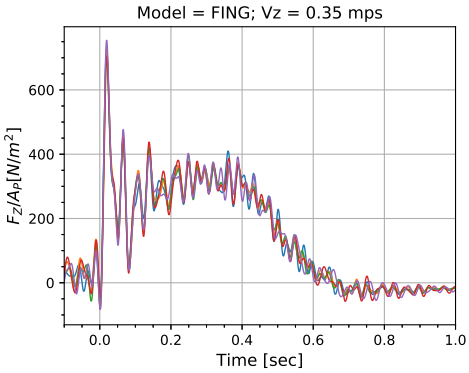
Model = FING; Vz = 0.35 mps
$F_Z/A_P[N/m^2]$
Time [sec]

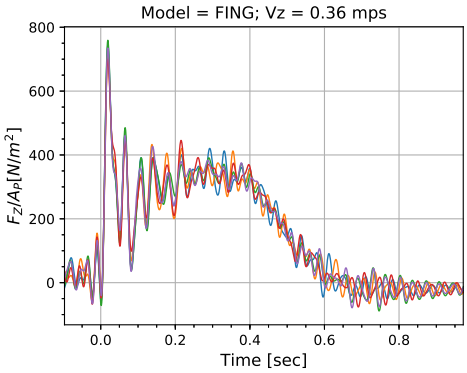
Model = FING; Vz = 0.36 mps
$F_Z/A_P[N/m^2]$
Time [sec]

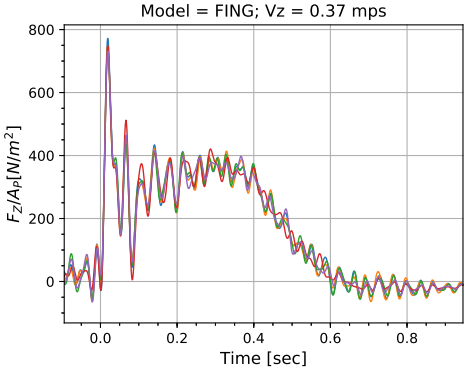
Model = FING; Vz = 0.37 mps
$F_Z/A_P[N/m^2]$
Time [sec]

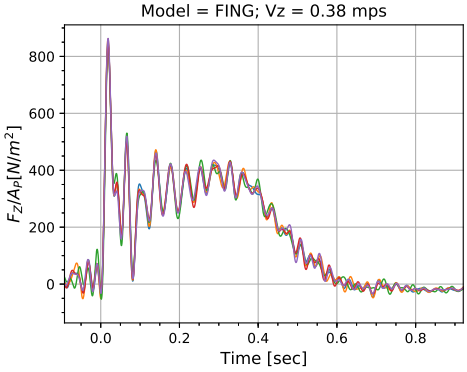
Model = FING; Vz = 0.38 mps
$F_Z/A_P[N/m^2]$
Time [sec]

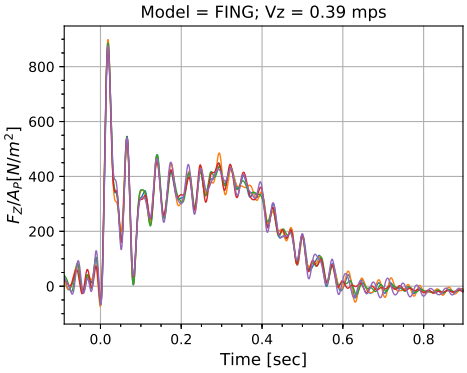
Model = FING; Vz = 0.39 mps
$F_Z/A_P[N/m^2]$
Time [sec]

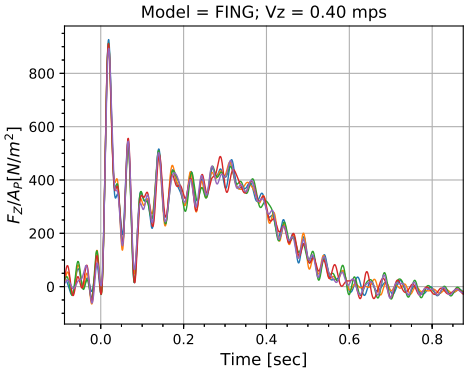
Model = FING; Vz = 0.40 mps
$F_Z/A_P[N/m^2]$
Time [sec]

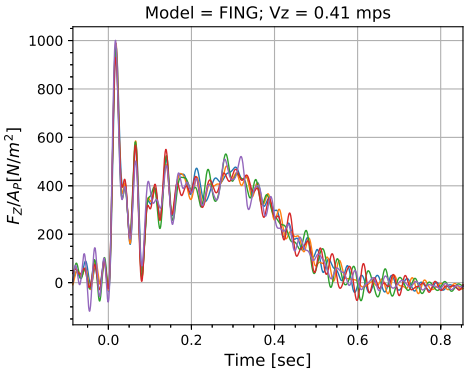
Model = FING; Vz = 0.41 mps
$F_Z/A_P[N/m^2]$
Time [sec]

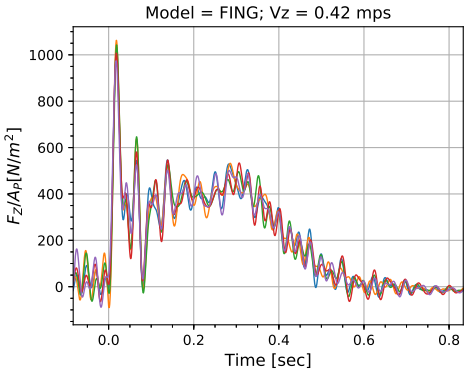
Model = FING; Vz = 0.42 mps
$F_Z/A_P[N/m^2]$
Time [sec]

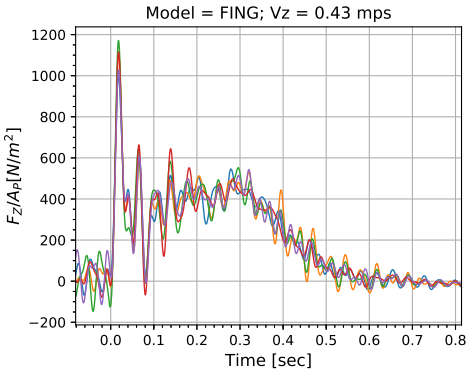
Model = FING; Vz = 0.43 mps
$F_Z/A_P[N/m^2]$
Time [sec]

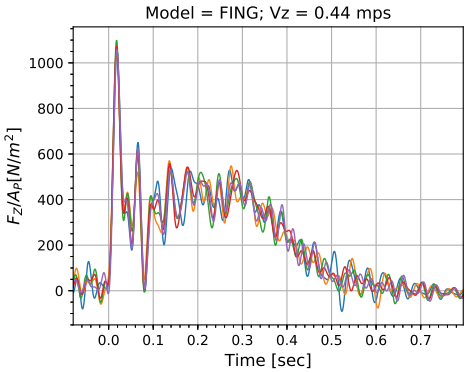
Model = FING; Vz = 0.44 mps
$F_Z/A_P[N/m^2]$
Time [sec]

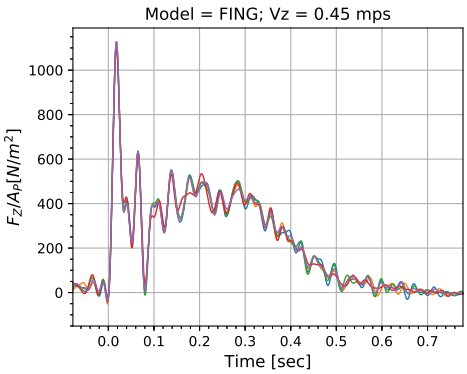
Model = FING; Vz = 0.45 mps
$F_Z/A_P[N/m^2]$
Time [sec]

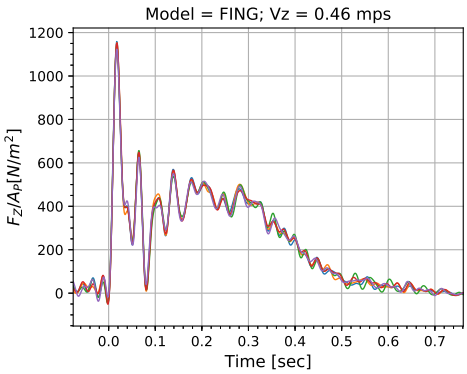
Model = FING; Vz = 0.46 mps
$F_Z/A_P[N/m^2]$
Time [sec]

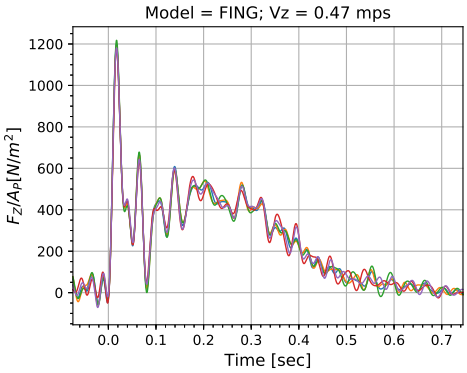
Model = FING; Vz = 0.47 mps
$F_Z/A_P[N/m^2]$
Time [sec]

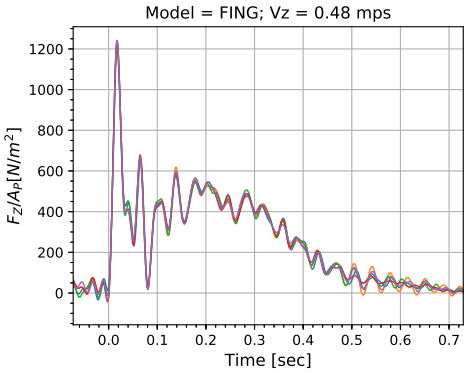
Model = FING; Vz = 0.48 mps
$F_Z/A_P[N/m^2]$
Time [sec]

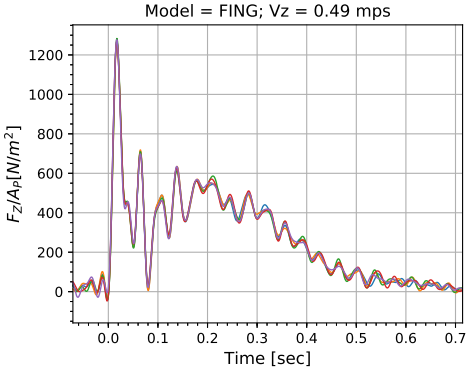
Model = FING; Vz = 0.49 mps
$F_Z/A_P[N/m^2]$
Time [sec]

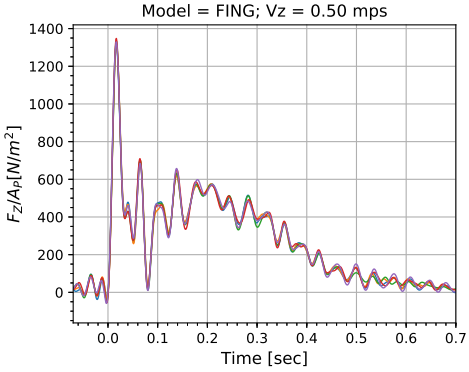
Model = FING; Vz = 0.50 mps
$F_Z/A_P[N/m^2]$
Time [sec]

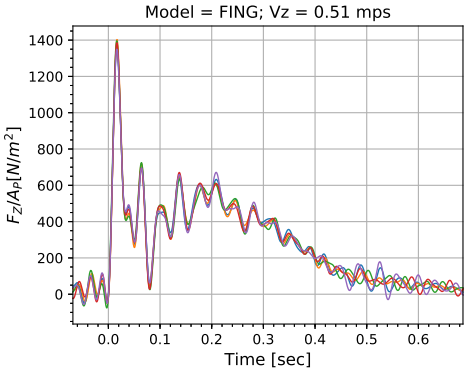
Model = FING; Vz = 0.51 mps
$F_Z/A_P[N/m^2]$
Time [sec]

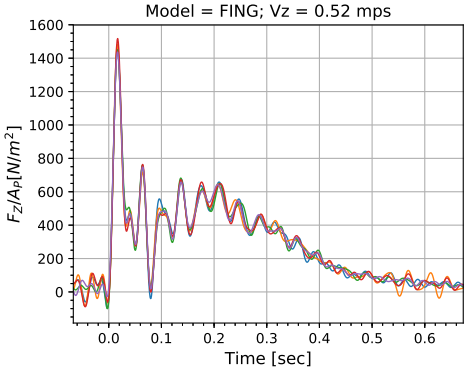
Model = FING; Vz = 0.52 mps
$F_Z/A_P[N/m^2]$
Time [sec]

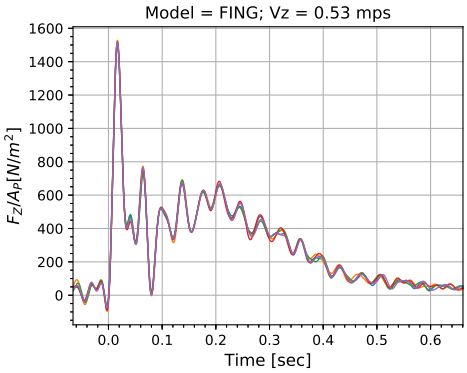
Model = FING; Vz = 0.53 mps
$F_Z/A_P[N/m^2]$
Time [sec]

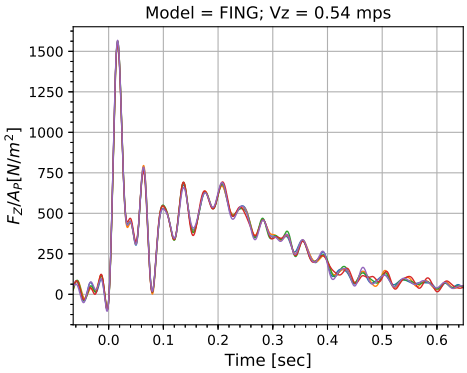
Model = FING; Vz = 0.54 mps
$F_Z/A_P[N/m^2]$
Time [sec]

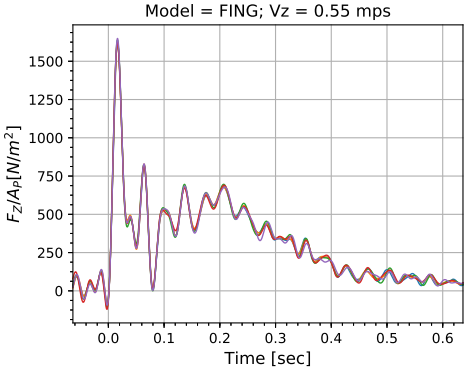
Model = FING; Vz = 0.55 mps
$F_Z/A_P[N/m^2]$
Time [sec]

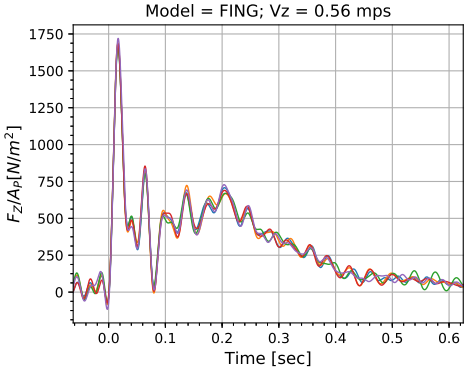
Model = FING; Vz = 0.56 mps
$F_Z/A_P[N/m^2]$
Time [sec]

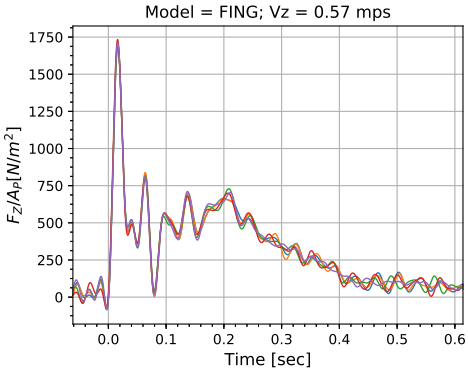
Model = FING; Vz = 0.57 mps
$F_Z/A_P[N/m^2]$
Time [sec]

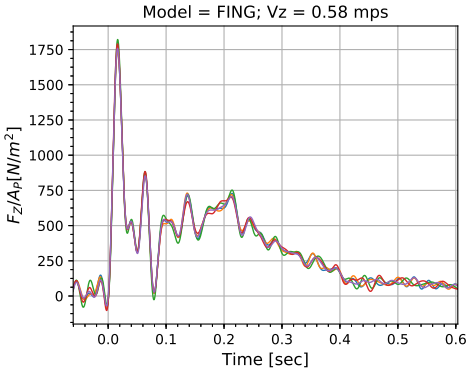
Model = FING; Vz = 0.58 mps
$F_Z/A_P[N/m^2]$
Time [sec]

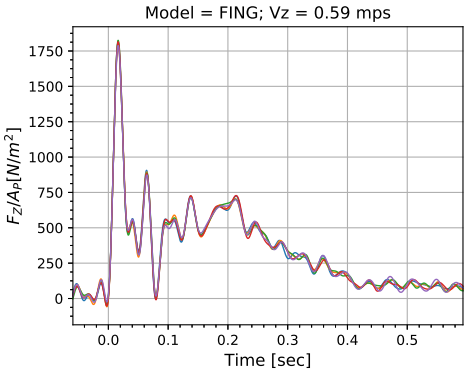
Model = FING; Vz = 0.59 mps
$F_Z/A_P[N/m^2]$
1750
1500
1250
1000
750
500
250
0
0.0
0.1
0.2
0.3
0.4
0.5
Time [sec]

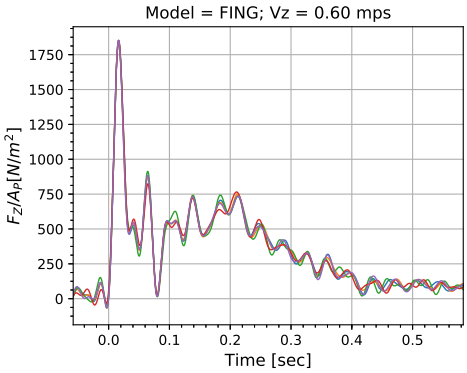
Model = FING; Vz = 0.60 mps
$F_Z/A_P[N/m^2]$
1750
1500
1250
1000
750
500
250
0
0.0
0.1
0.2
0.3
0.4
0.5
Time [sec]

Appendix B: Water-Entry Force (F_z) vs Submergence (V_zT/L)

Model: P19

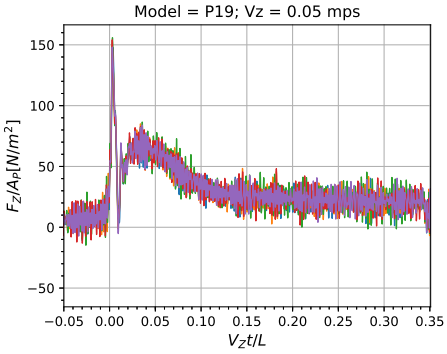

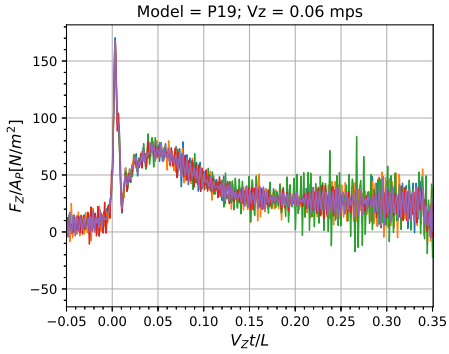

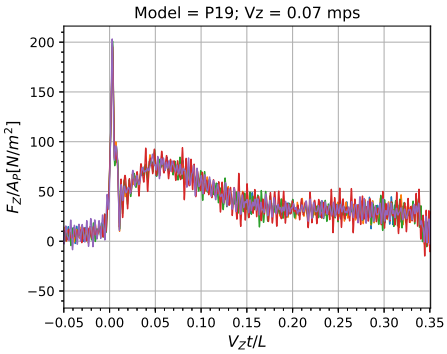

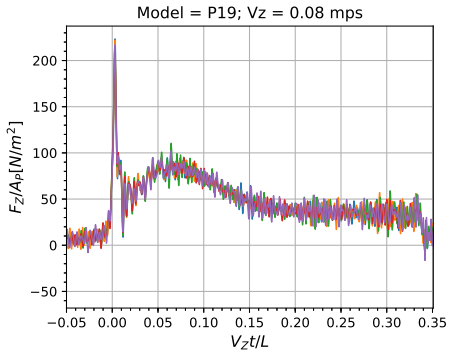

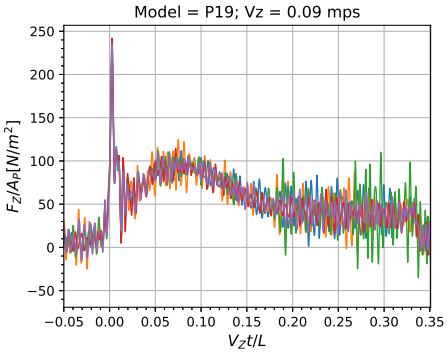

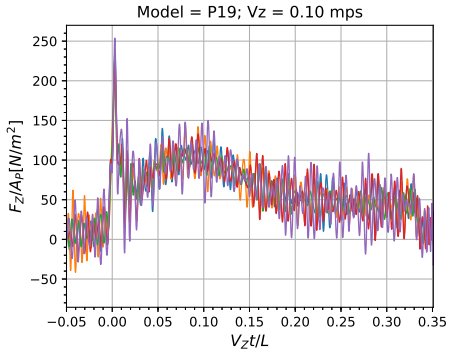

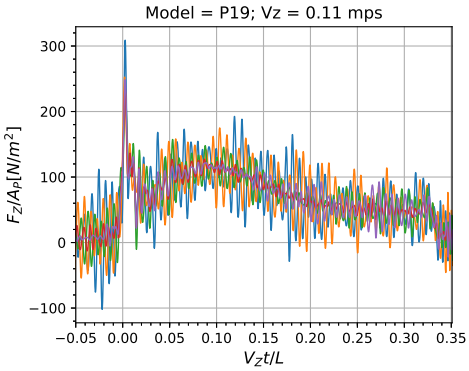
Model = P19; Vz = 0.11 mps
$F_Z/A_P[N/m^2]$
$V_Z t/L$

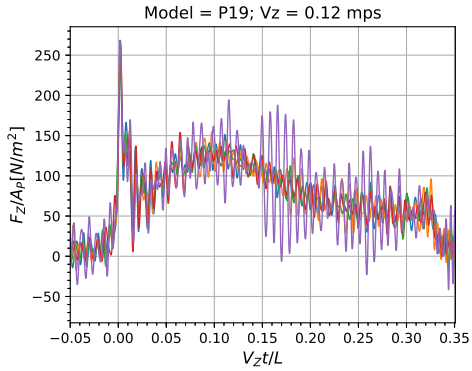
Model = P19; Vz = 0.12 mps
$F_Z/A_P[N/m^2]$
$V_Z t/L$

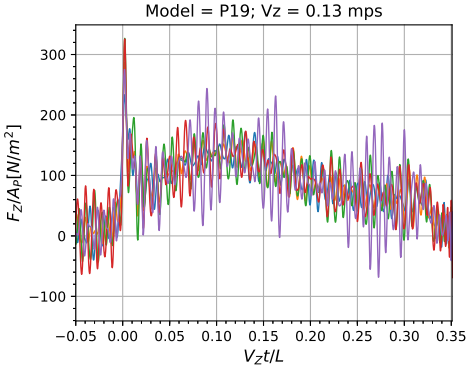
Model = P19; Vz = 0.13 mps
$F_Z/A_P[N/m^2]$
$V_Z t/L$

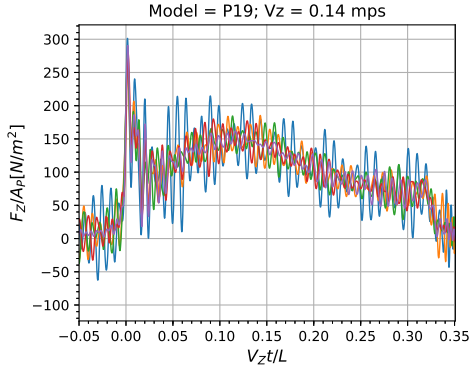
Model = P19; Vz = 0.14 mps
$F_Z/A_P[N/m^2]$
$V_Z t/L$

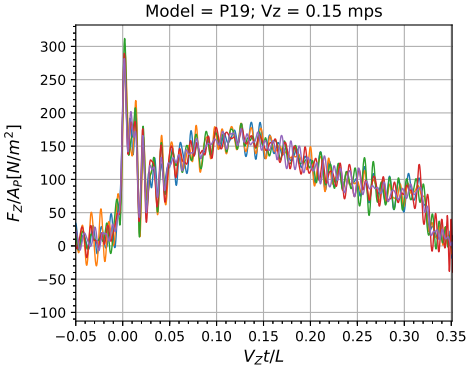
Model = P19; Vz = 0.15 mps
$F_Z/A_P[N/m^2]$
$V_Z t/L$

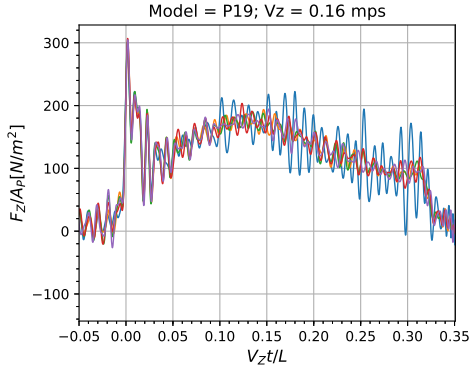
Model = P19; Vz = 0.16 mps
$F_Z/A_P[N/m^2]$
$V_Z t/L$

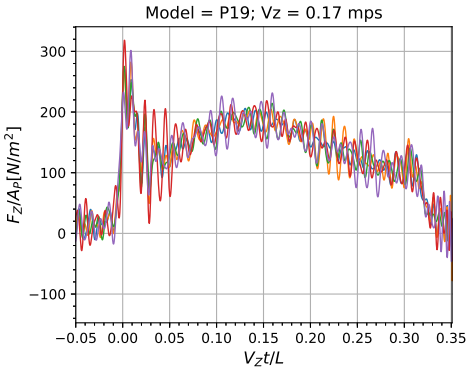
Model = P19; Vz = 0.17 mps
$F_Z/A_P[N/m^2]$
$V_Z t/L$

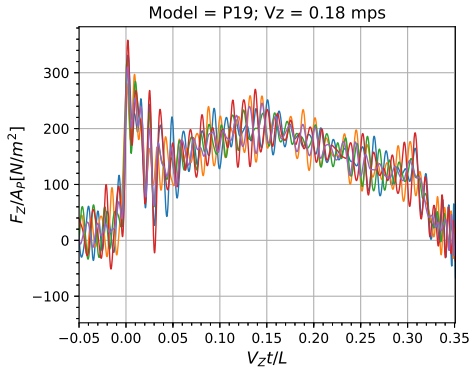
Model = P19; Vz = 0.18 mps
$F_Z/A_P[N/m^2]$
$V_Z t/L$

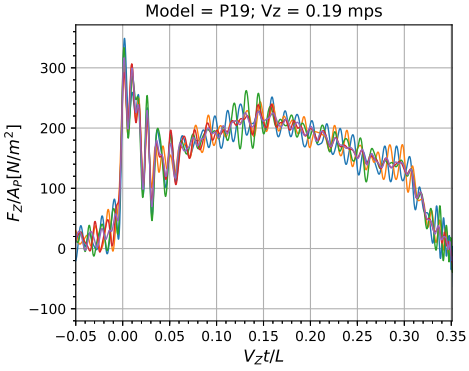
Model = P19; Vz = 0.19 mps
$F_Z/A_P[N/m^2]$
$V_Z t/L$

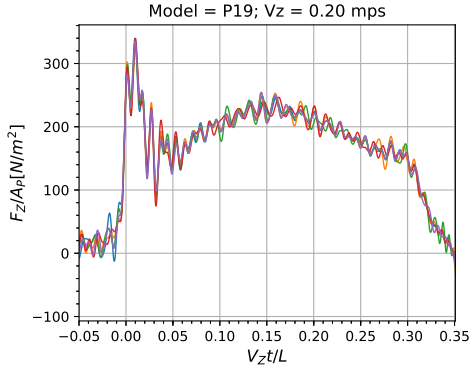
Model = P19; Vz = 0.20 mps
$F_Z/A_P[N/m^2]$
$V_Z t/L$

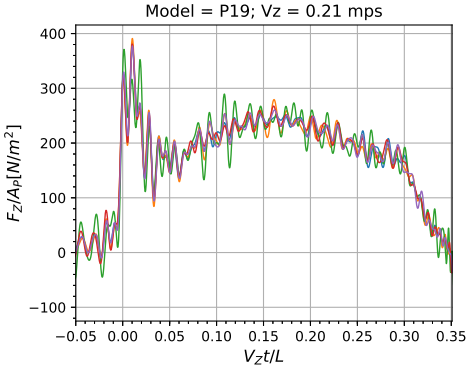
Model = P19; Vz = 0.21 mps
$F_Z/A_P[N/m^2]$
$V_Z t/L$

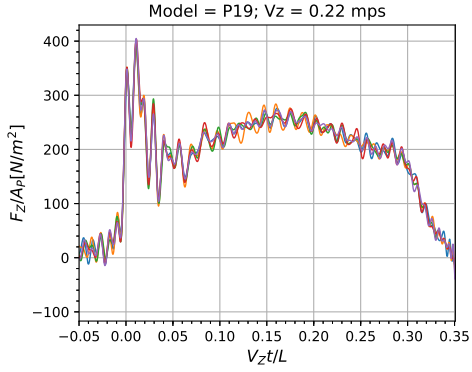
Model = P19; Vz = 0.22 mps
$F_Z/A_P[N/m^2]$
$V_Z t/L$

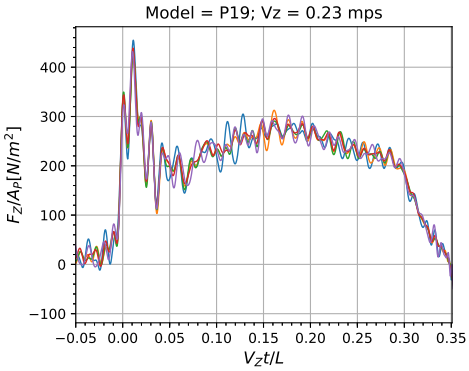
Model = P19; Vz = 0.23 mps
$F_Z/A_P[N/m^2]$
$V_Z t/L$

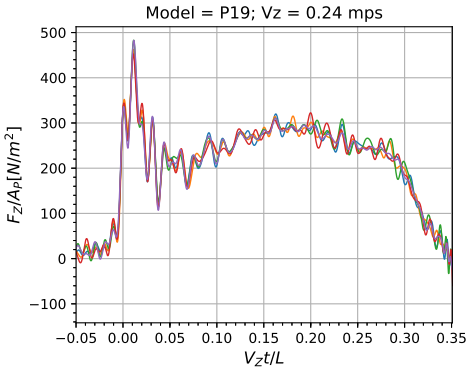
Model = P19; Vz = 0.24 mps
$F_Z/A_P[N/m^2]$
$V_Z t/L$

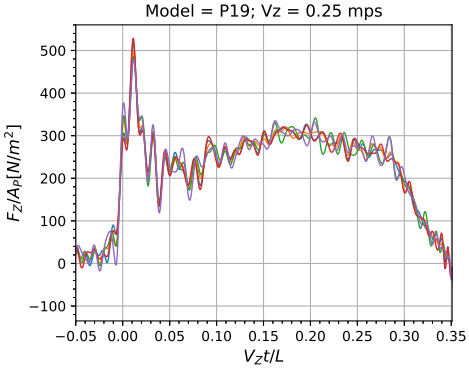
Model = P19; Vz = 0.25 mps
$F_Z/A_P[N/m^2]$
$V_Z t/L$

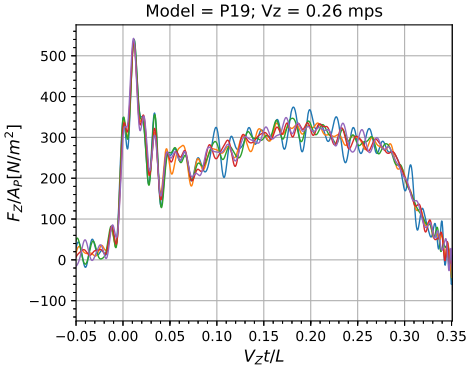
Model = P19; Vz = 0.26 mps
$F_Z/A_P[N/m^2]$
$V_Z t/L$

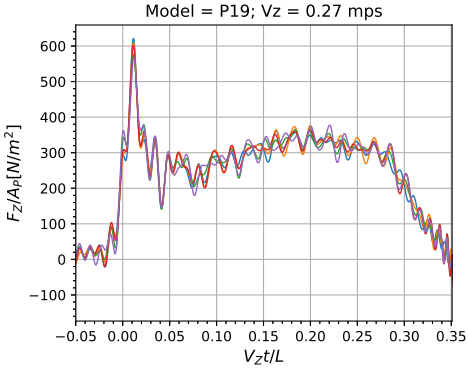
Model = P19; Vz = 0.27 mps
$F_Z/A_P[N/m^2]$
$V_Z t/L$

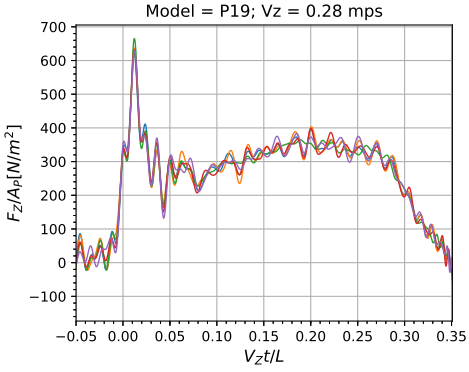
Model = P19; Vz = 0.28 mps
$F_Z/A_P[N/m^2]$
$V_Z t/L$

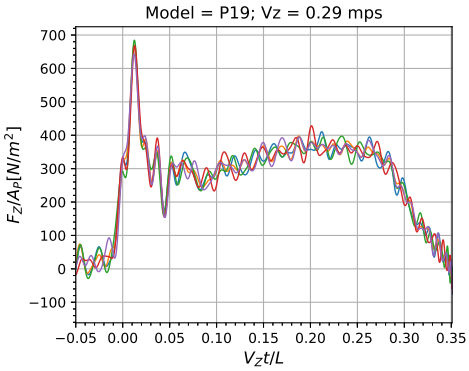
Model = P19; Vz = 0.29 mps
$F_Z/A_P[N/m^2]$
$V_Z t/L$

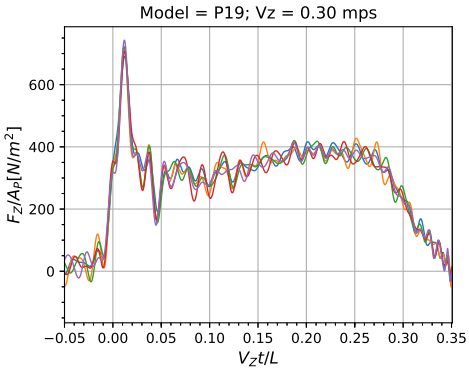
Model = P19; Vz = 0.30 mps
$F_Z/A_P[N/m^2]$
$V_Z t/L$

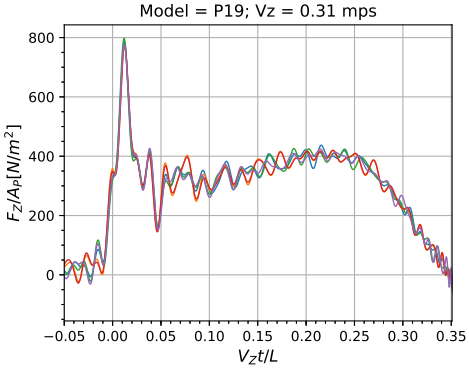
Model = P19; Vz = 0.31 mps
$F_Z/A_P[N/m^2]$
$V_Z t/L$

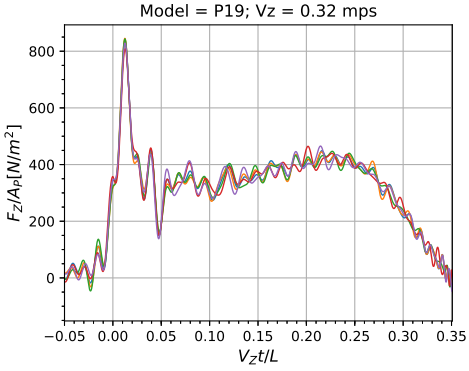
Model = P19; Vz = 0.32 mps
$F_Z/A_P[N/m^2]$
$V_Z t/L$

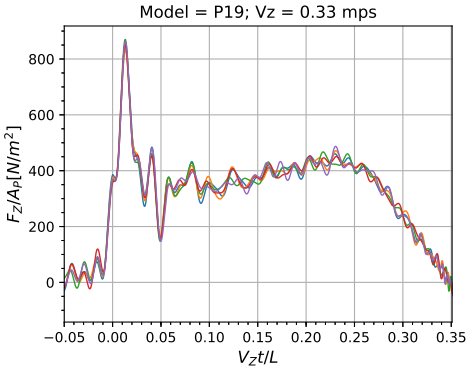
Model = P19; Vz = 0.33 mps
$F_Z/A_P[N/m^2]$
$V_Z t/L$

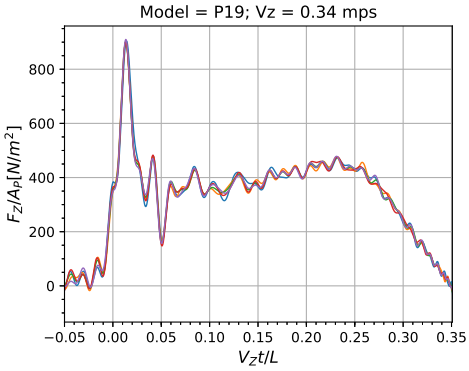
Model = P19; Vz = 0.34 mps
$F_Z/A_P[N/m^2]$
$V_Z t/L$

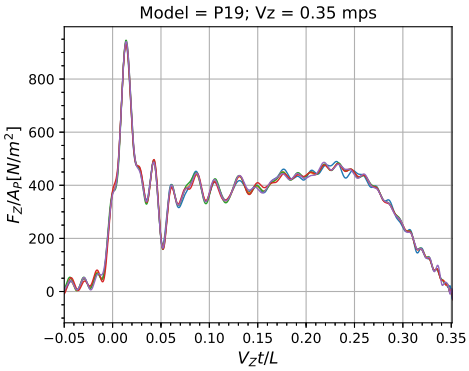
Model = P19; Vz = 0.35 mps
$F_Z/A_P[N/m^2]$
$V_Z t/L$

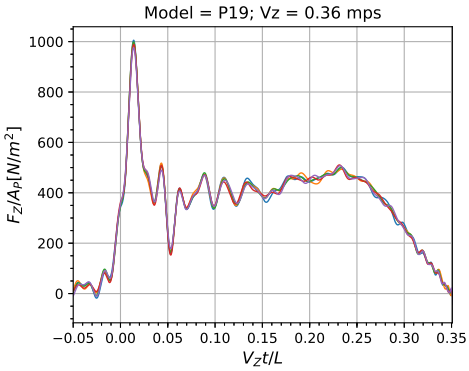
Model = P19; Vz = 0.36 mps
$F_Z/A_P[N/m^2]$
$V_Z t/L$

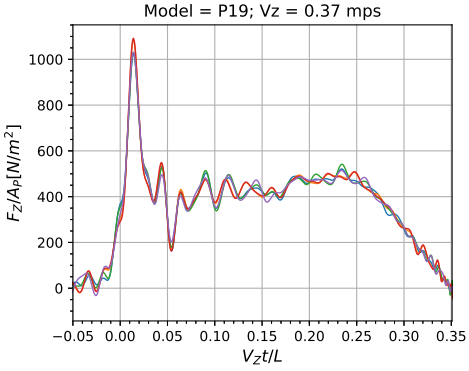
Model = P19; Vz = 0.37 mps
$F_Z/A_P[N/m^2]$
$V_Z t/L$

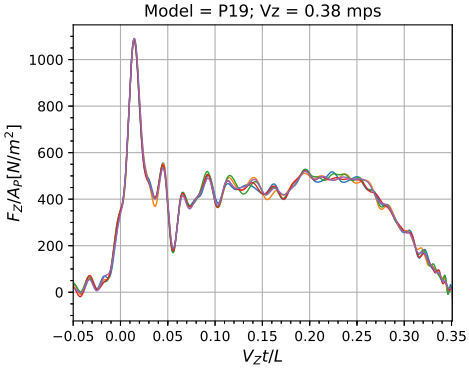
Model = P19; Vz = 0.38 mps
$F_Z/A_P[N/m^2]$
$V_Z t/L$

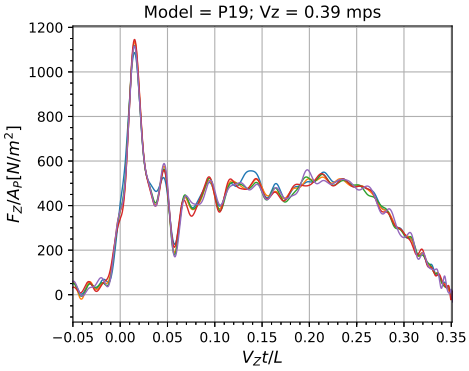
Model = P19; Vz = 0.39 mps
$F_Z/A_P[N/m^2]$
$V_Z t/L$

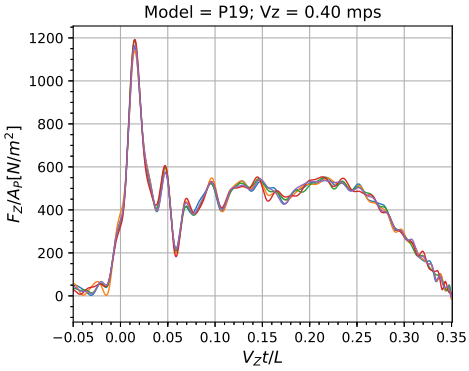
Model = P19; Vz = 0.40 mps
$F_Z/A_P[N/m^2]$
$V_Z t/L$

Model: P28

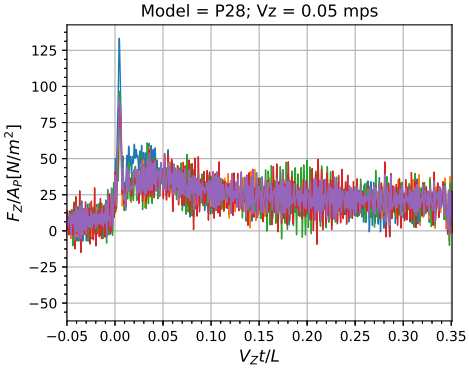
Model = P28; Vz = 0.05 mps
$F_Z/A_P[N/m^2]$
$V_Z t/L$

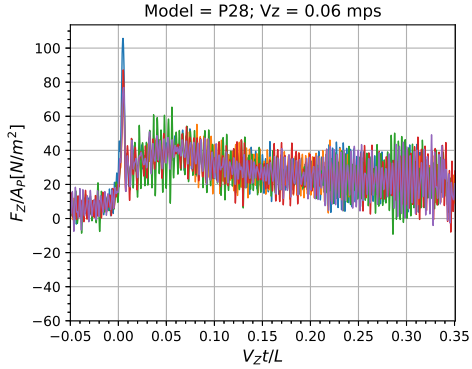
Model = P28; Vz = 0.06 mps
$F_Z/A_P[N/m^2]$
$V_Z t/L$

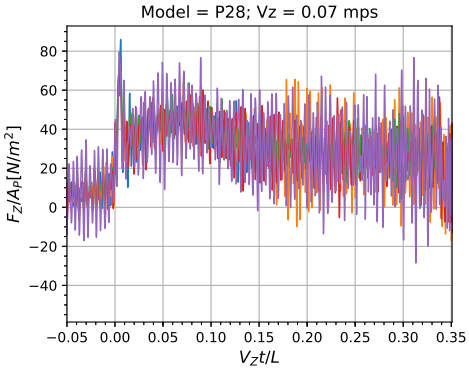
Model = P28; Vz = 0.07 mps
$F_Z/A_P[N/m^2]$
$V_Z t/L$

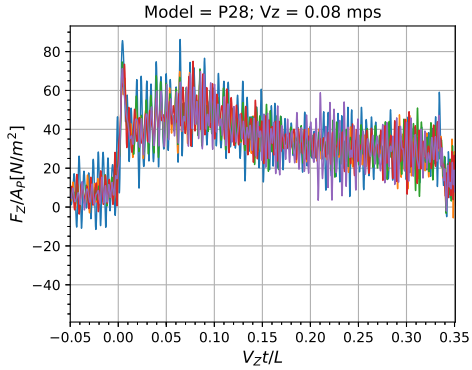
Model = P28; Vz = 0.08 mps
$F_Z/A_P[N/m^2]$
$V_Z t/L$

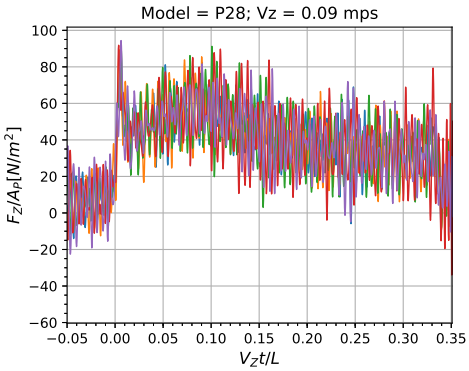
Model = P28; Vz = 0.09 mps
$F_Z/A_P[N/m^2]$
$V_Z t/L$

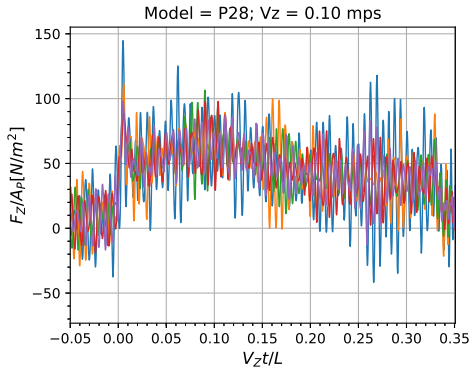
Model = P28; Vz = 0.10 mps
$F_Z/A_P[N/m^2]$
$V_Z t/L$

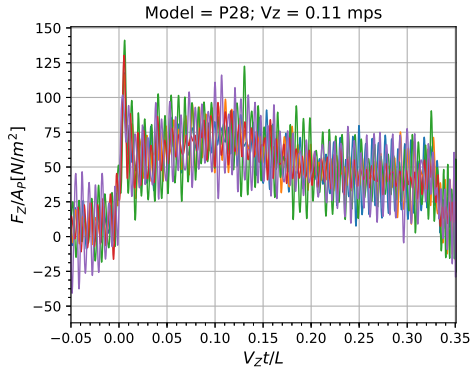
Model = P28; Vz = 0.11 mps
$F_Z/A_P[N/m^2]$
$V_Z t/L$

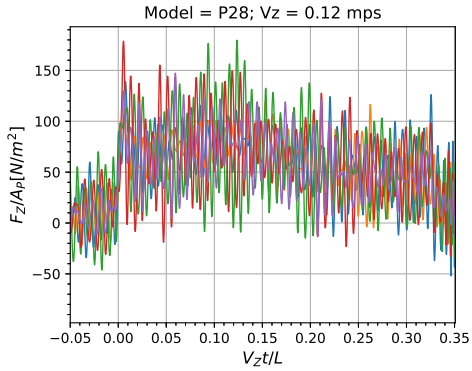
Model = P28; Vz = 0.12 mps
$F_Z/A_P[N/m^2]$
$V_Z t/L$

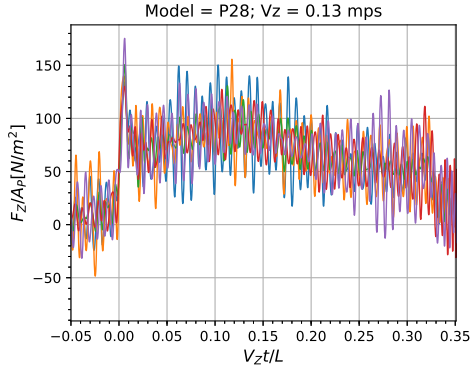
Model = P28; Vz = 0.13 mps
$F_Z/A_P[N/m^2]$
$V_Z t/L$

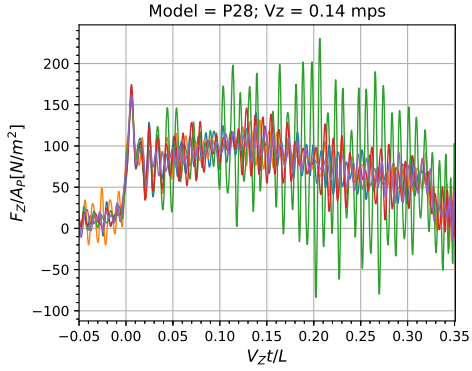
Model = P28; Vz = 0.14 mps
$F_Z/A_P[N/m^2]$
$V_Z t/L$

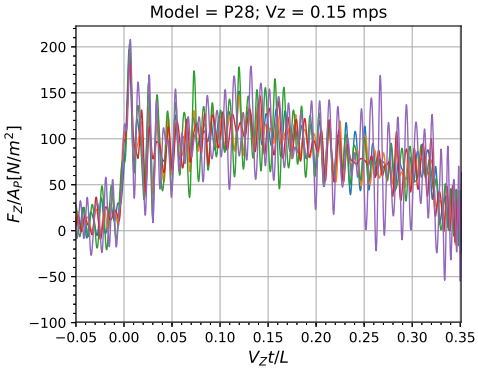
Model = P28; Vz = 0.15 mps
$F_Z/A_P[N/m^2]$
$V_Z t/L$

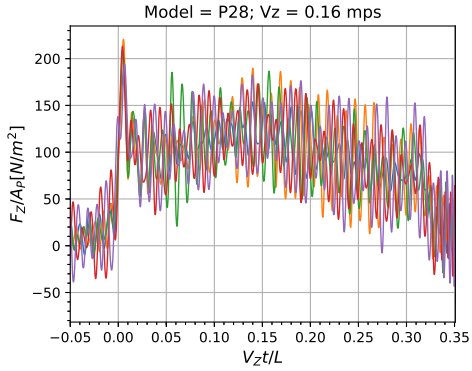
Model = P28; Vz = 0.16 mps
$F_Z/A_P[N/m^2]$
$V_Z t/L$

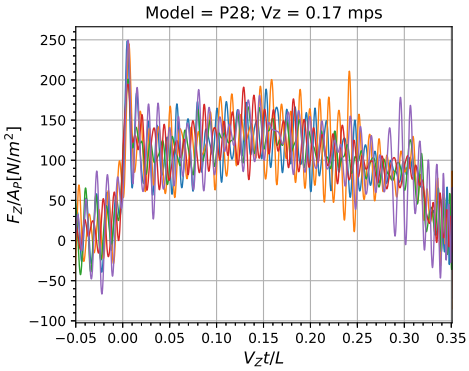
Model = P28; Vz = 0.17 mps
$F_Z/A_P[N/m^2]$
$V_Z t/L$

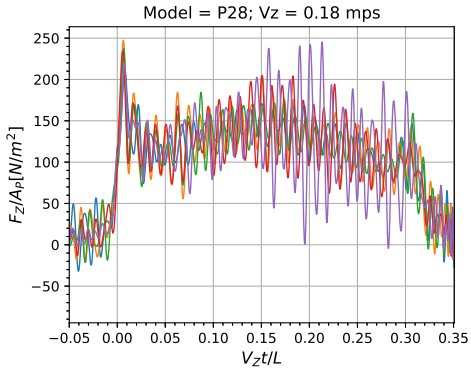
Model = P28; Vz = 0.18 mps
$F_Z/A_P[N/m^2]$
$V_Z t/L$

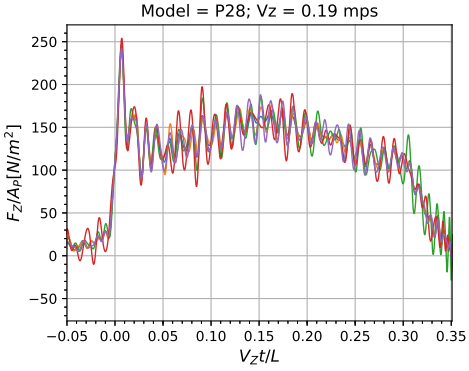
Model = P28; Vz = 0.19 mps
$F_Z/A_P[N/m^2]$
$V_Z t/L$

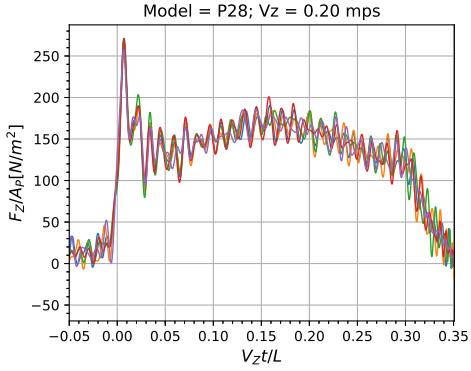
Model = P28; Vz = 0.20 mps
$F_Z/A_P[N/m^2]$
$V_Z t/L$

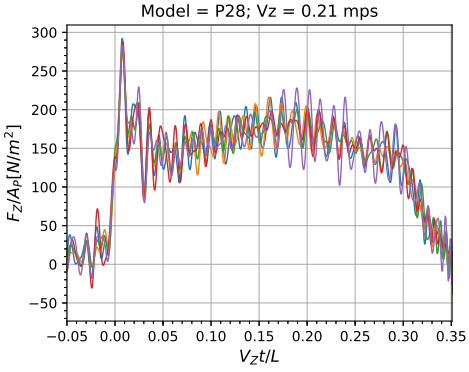
Model = P28; Vz = 0.21 mps
$F_Z/A_P[N/m^2]$
$V_Z t/L$

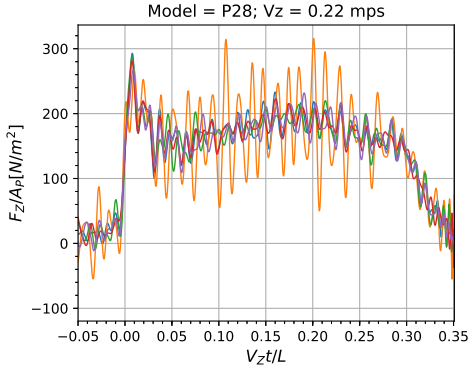
Model = P28; Vz = 0.22 mps
$F_Z/A_P[N/m^2]$
$V_Z t/L$

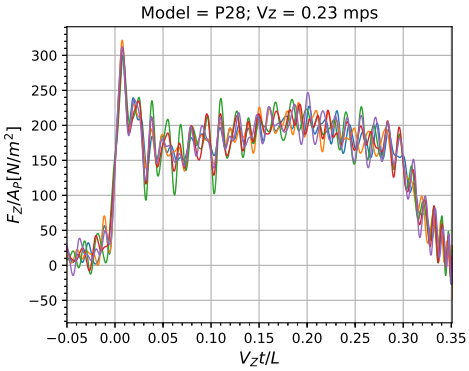
Model = P28; Vz = 0.23 mps
$F_Z/A_P[N/m^2]$
$V_Z t/L$

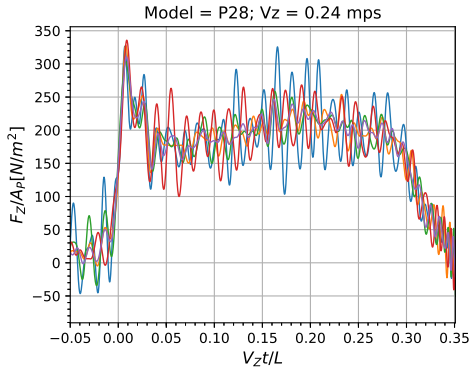
Model = P28; Vz = 0.24 mps
$F_Z/A_P[N/m^2]$
$V_Z t/L$

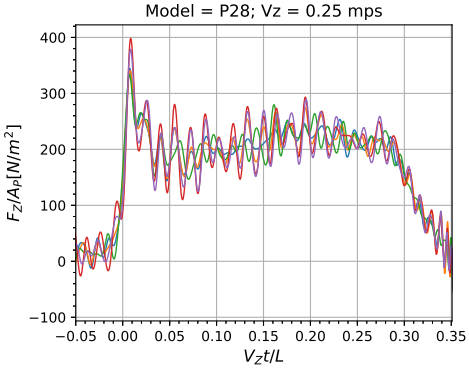
Model = P28; Vz = 0.25 mps
$F_Z/A_P[N/m^2]$
$V_Z t/L$

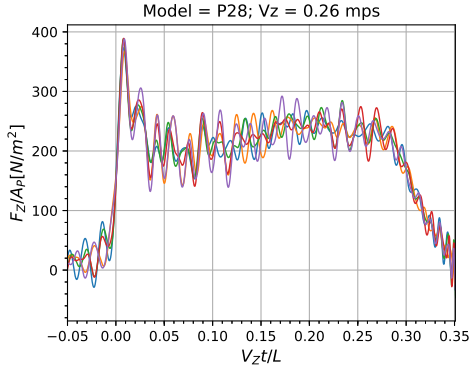
Model = P28; Vz = 0.26 mps
$F_Z/A_P[N/m^2]$
$V_Z t/L$

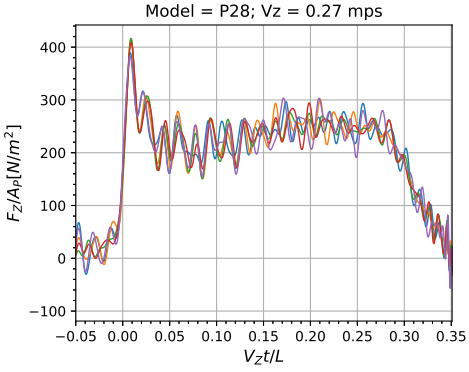
Model = P28; Vz = 0.27 mps
$F_Z/A_P[N/m^2]$
$V_Z t/L$

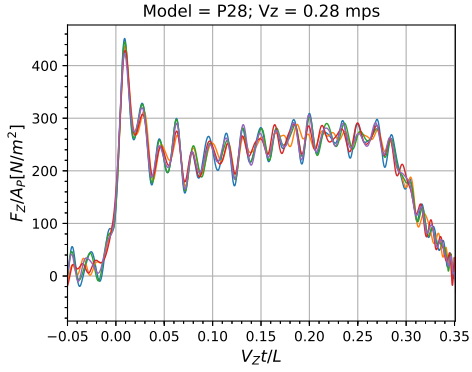
Model = P28; Vz = 0.28 mps
$F_Z/A_P[N/m^2]$
$V_Z t/L$

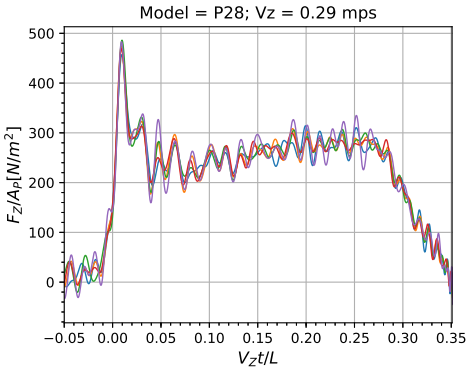
Model = P28; Vz = 0.29 mps
$F_Z/A_P[N/m^2]$
$V_Z t/L$

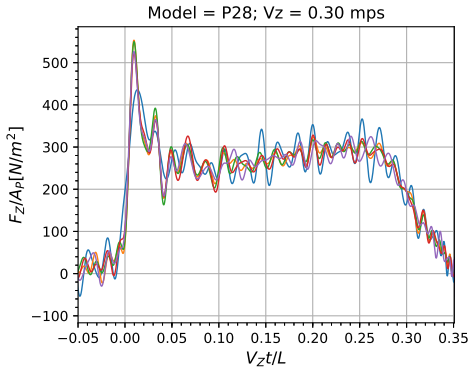
Model = P28; Vz = 0.30 mps
$F_Z/A_P[N/m^2]$
$V_Z t/L$

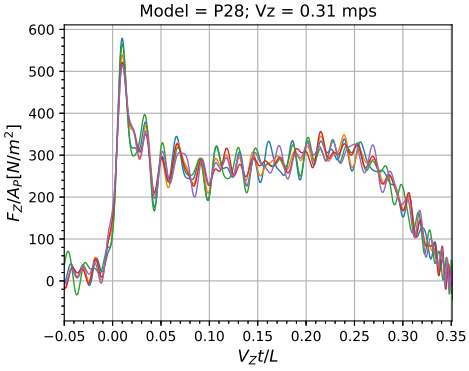
Model = P28; Vz = 0.31 mps
$F_Z/A_P[N/m^2]$
$V_Z t/L$

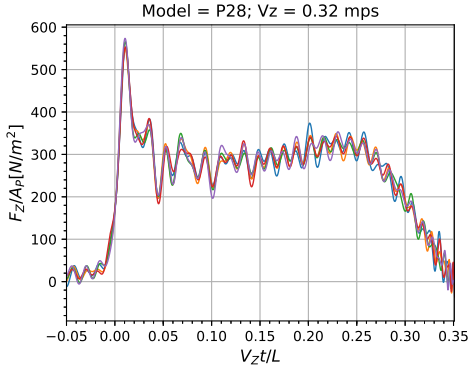
Model = P28; Vz = 0.32 mps
$F_Z/A_P[N/m^2]$
$V_Z t/L$

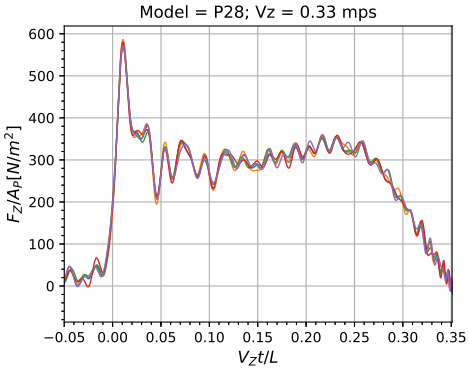
Model = P28; Vz = 0.33 mps
$F_Z/A_P[N/m^2]$
$V_Z t/L$

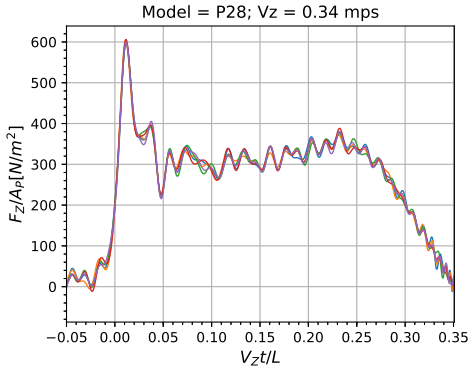
Model = P28; Vz = 0.34 mps
$F_Z/A_P[N/m^2]$
$V_Z t/L$

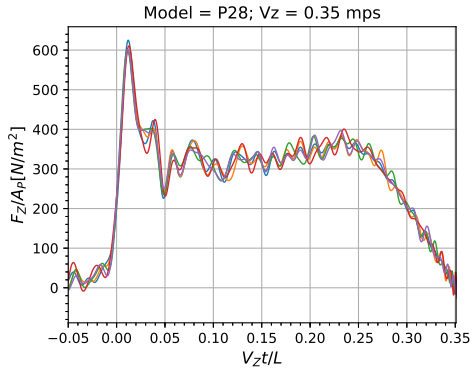
Model = P28; Vz = 0.35 mps
$F_Z/A_P[N/m^2]$
$V_Z t/L$

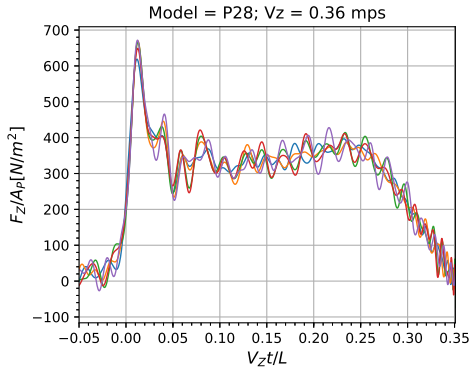
Model = P28; Vz = 0.36 mps
$F_Z/A_P[N/m^2]$
$V_Z t/L$

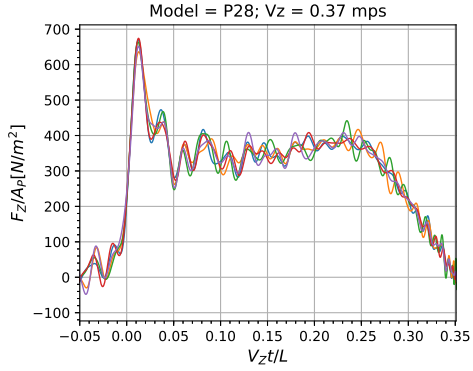
Model = P28; Vz = 0.37 mps
$F_Z/A_P[N/m^2]$
$V_Z t/L$

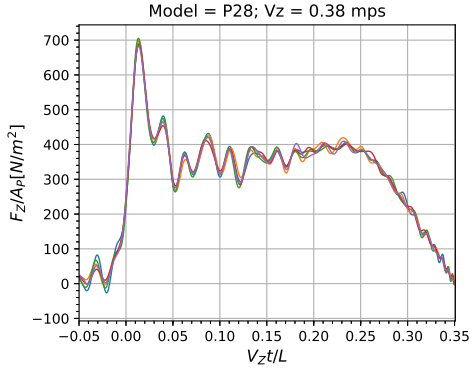
Model = P28; Vz = 0.38 mps
$F_Z/A_P[N/m^2]$
$V_Z t/L$

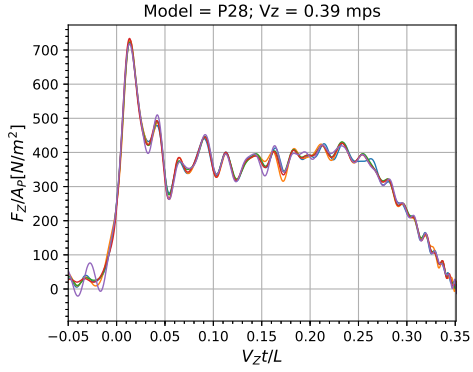
Model = P28; Vz = 0.39 mps
$F_Z/A_P[N/m^2]$
$V_Z t/L$

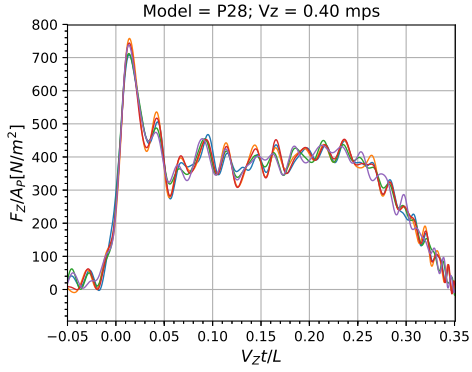
Model = P28; Vz = 0.40 mps
$F_Z/A_P[N/m^2]$
$V_Z t/L$

Model: FING

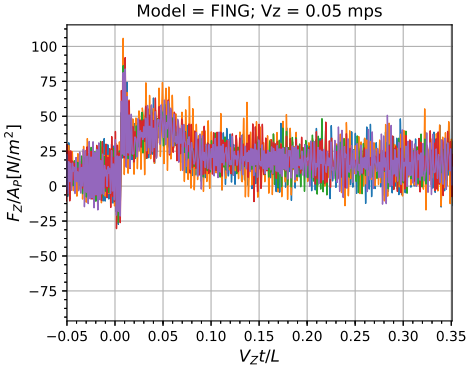
Model = FING; Vz = 0.05 mps
$F_Z/A_P[N/m^2]$
$V_Z t/L$

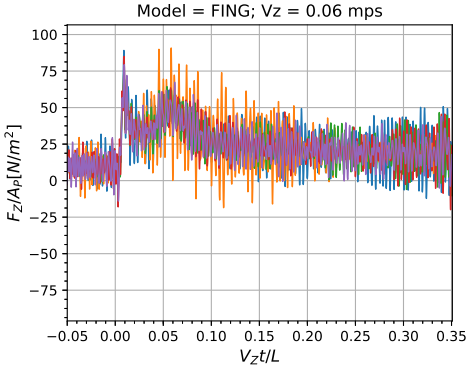
Model = FING; Vz = 0.06 mps
$F_Z/A_P[N/m^2]$
$V_Z t/L$

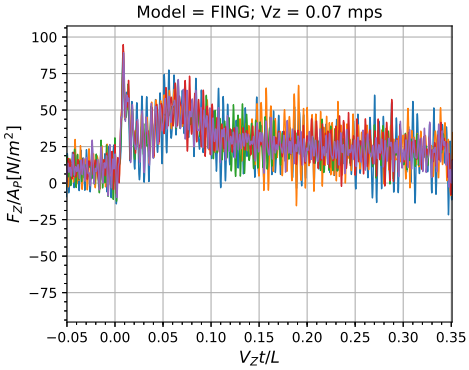
Model = FING; Vz = 0.07 mps
$F_Z/A_P[N/m^2]$
$V_Z t/L$

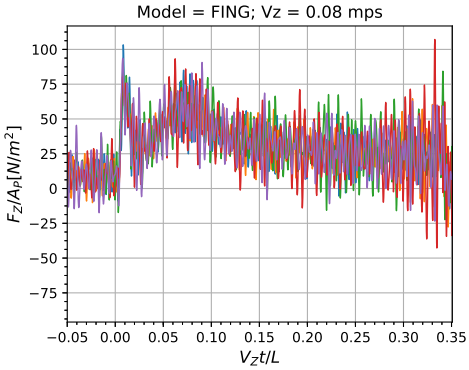
Model = FING; Vz = 0.08 mps
$F_Z/A_P[N/m^2]$
$V_Z t/L$

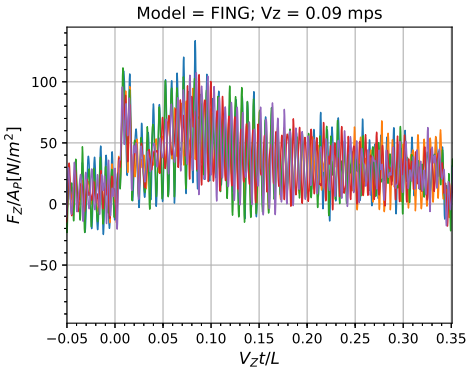
Model = FING; Vz = 0.09 mps
$F_Z/A_P[N/m^2]$
$V_Z t/L$

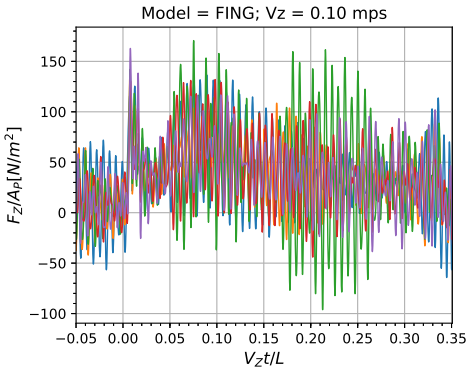
Model = FING; Vz = 0.10 mps
$F_Z/A_P[N/m^2]$
$V_Z t/L$

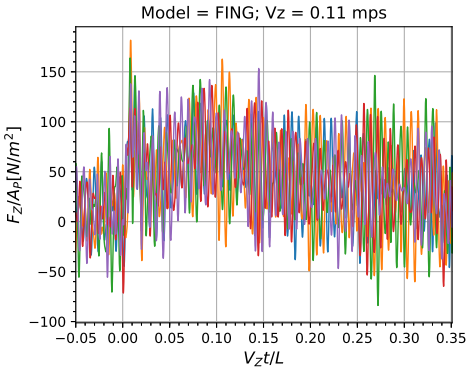
Model = FING; Vz = 0.11 mps
$F_Z/A_P[N/m^2]$
$V_Z t/L$

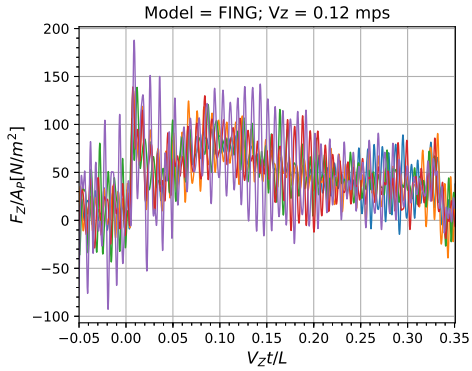
Model = FING; Vz = 0.12 mps
$F_Z/A_P[N/m^2]$
$V_Z t/L$

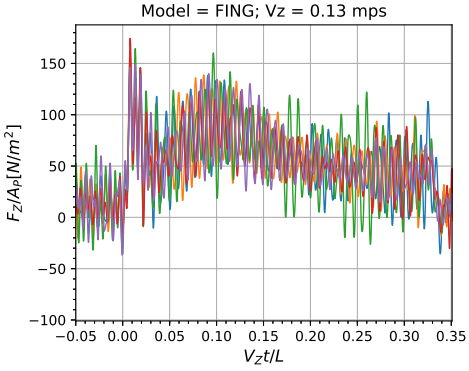
Model = FING; Vz = 0.13 mps
$F_Z/A_P[N/m^2]$
$V_Z t/L$

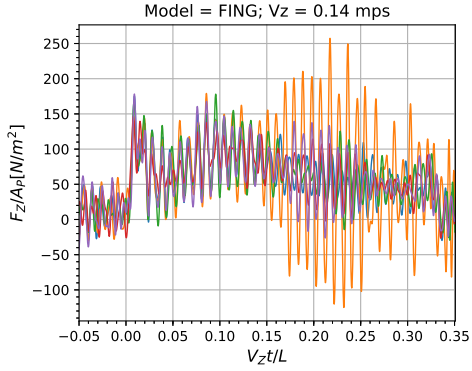
Model = FING; Vz = 0.14 mps
$F_Z/A_P[N/m^2]$
$V_Z t/L$

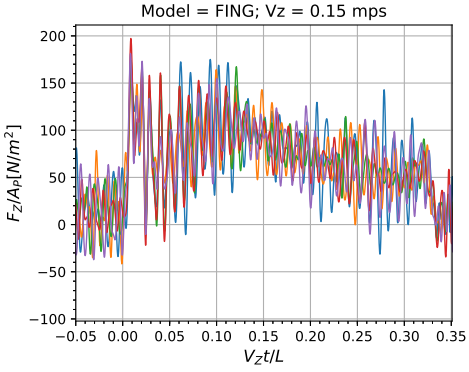
Model = FING; Vz = 0.15 mps
$F_Z/A_P[N/m^2]$
$V_Z t/L$

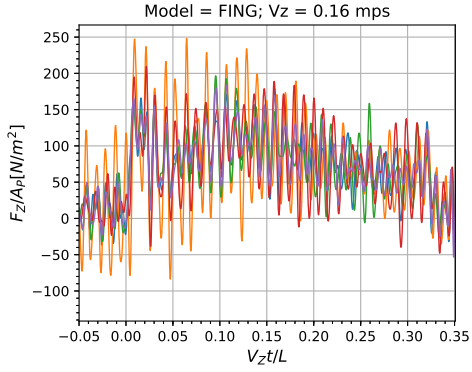
Model = FING; Vz = 0.16 mps
$F_Z/A_P[N/m^2]$
$V_Z t/L$

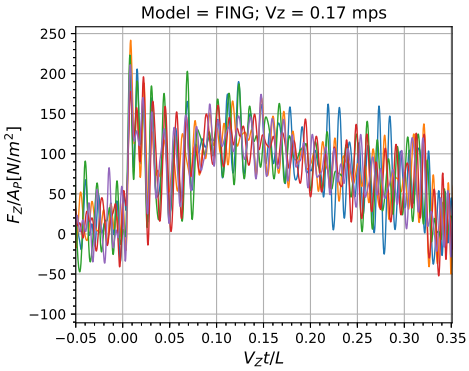
Model = FING; Vz = 0.17 mps
$F_Z/A_P[N/m^2]$
$V_Z t/L$

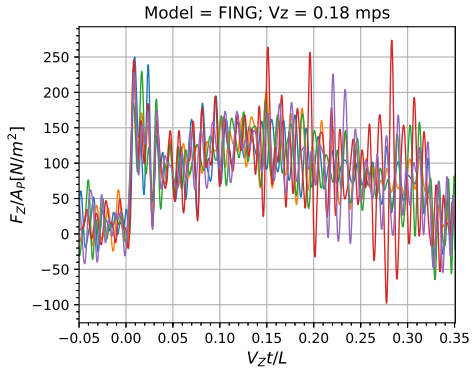
Model = FING; Vz = 0.18 mps
$F_Z/A_P[N/m^2]$
$V_Z t/L$

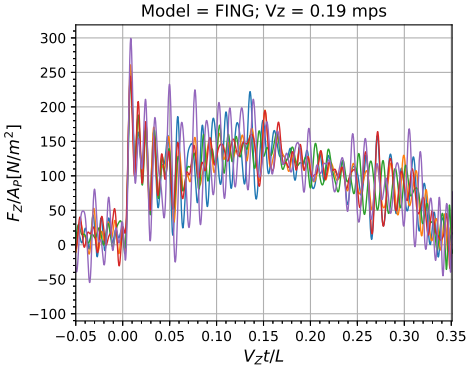
Model = FING; Vz = 0.19 mps
$F_Z/A_P[N/m^2]$
$V_Z t/L$

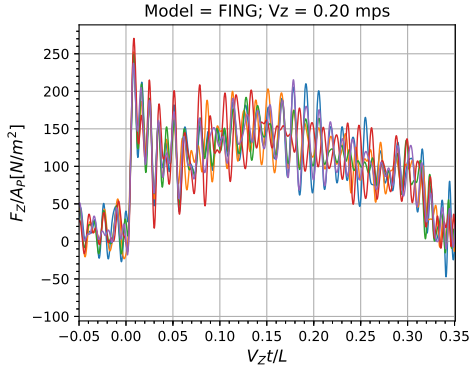
Model = FING; Vz = 0.20 mps
$F_Z/A_P[N/m^2]$
$V_Z t/L$

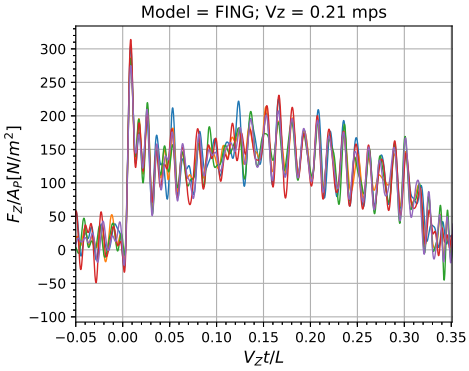
Model = FING; Vz = 0.21 mps
$F_Z/A_P[N/m^2]$
$V_Z t/L$

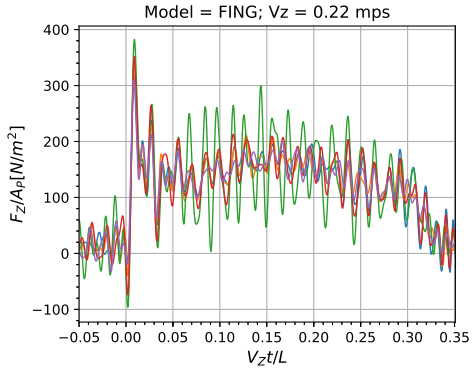
Model = FING; Vz = 0.22 mps
$F_Z/A_P[N/m^2]$
$V_Z t/L$

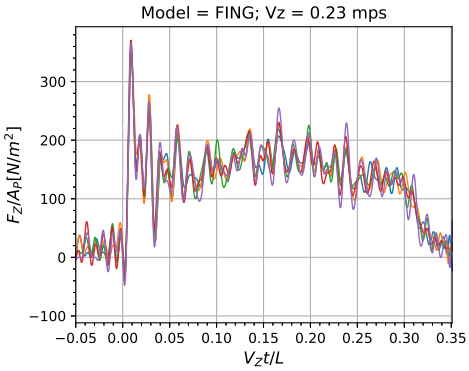
Model = FING; Vz = 0.23 mps
$F_Z/A_P[N/m^2]$
$V_Z t/L$

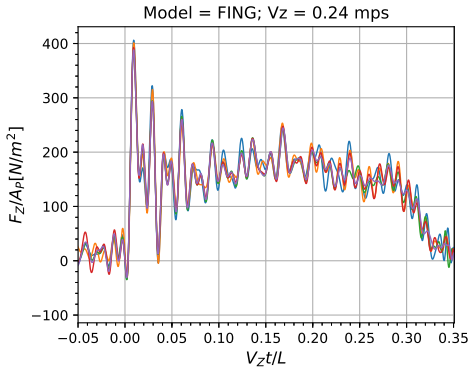
Model = FING; Vz = 0.24 mps
$F_Z/A_P[N/m^2]$
$V_Z t/L$

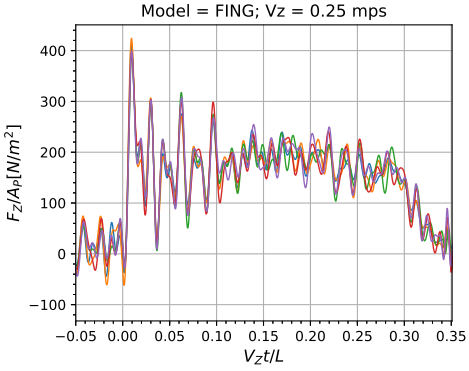
Model = FING; Vz = 0.25 mps
$F_Z/A_P[N/m^2]$
$V_Z t/L$

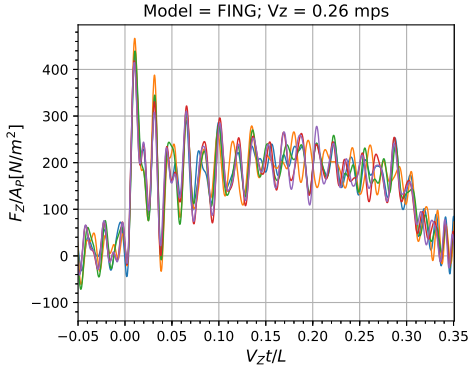
Model = FING; Vz = 0.26 mps
$F_Z/A_P[N/m^2]$
$V_Z t/L$

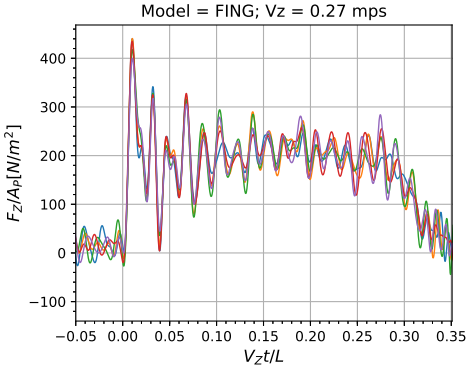
Model = FING; Vz = 0.27 mps
$F_Z/A_P[N/m^2]$
$V_Z t/L$

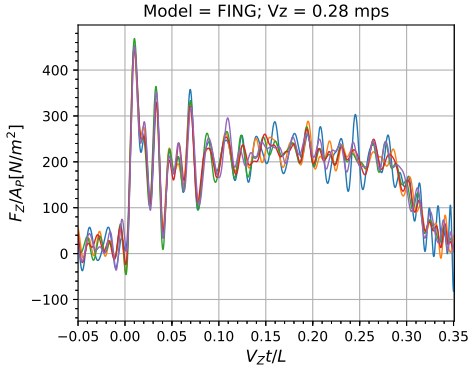
Model = FING; Vz = 0.28 mps
$F_Z/A_P[N/m^2]$
$V_Z t/L$

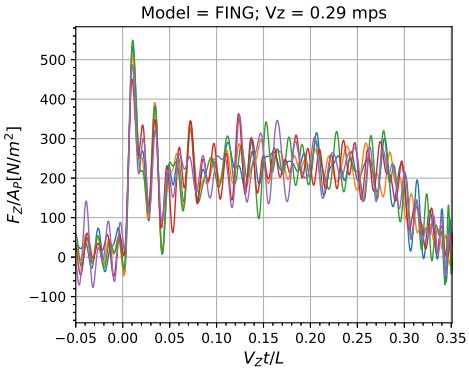
Model = FING; Vz = 0.29 mps
$F_Z/A_P[N/m^2]$
$V_Z t/L$

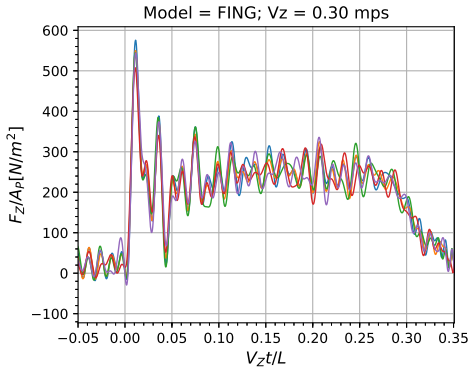
Model = FING; Vz = 0.30 mps
$F_Z/A_P[N/m^2]$
$V_Z t/L$

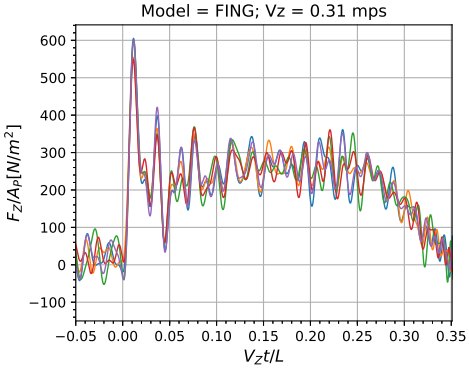
Model = FING; Vz = 0.31 mps
$F_Z/A_P[N/m^2]$
$V_Z t/L$

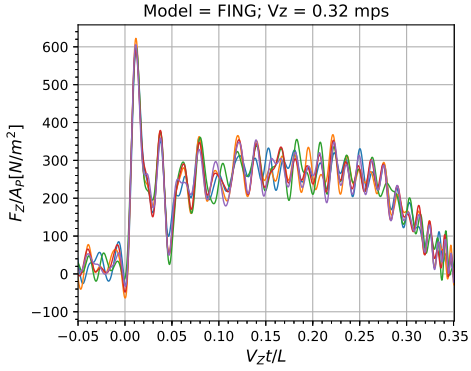
Model = FING; Vz = 0.32 mps
$F_Z/A_P[N/m^2]$
$V_Z t/L$

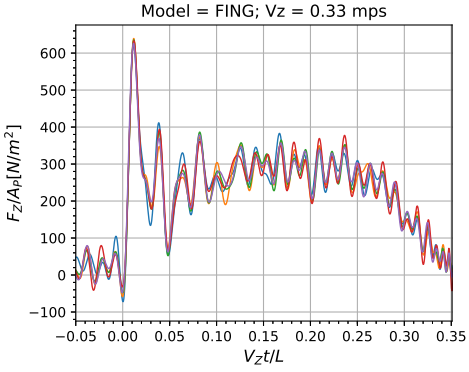
Model = FING; Vz = 0.33 mps
$F_Z/A_P[N/m^2]$
$V_Z t/L$

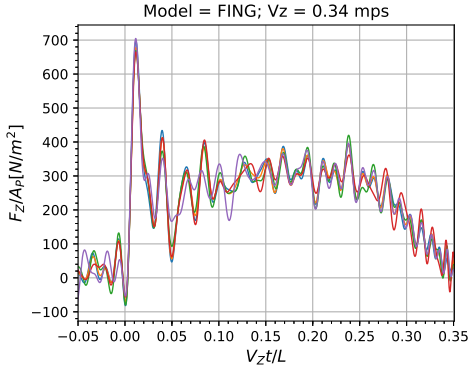
Model = FING; Vz = 0.34 mps
$F_Z/A_P[N/m^2]$
$V_Z t/L$

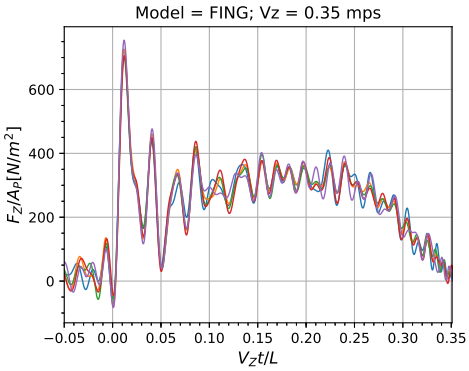
Model = FING; Vz = 0.35 mps
$F_Z/A_P[N/m^2]$
$V_Z t/L$

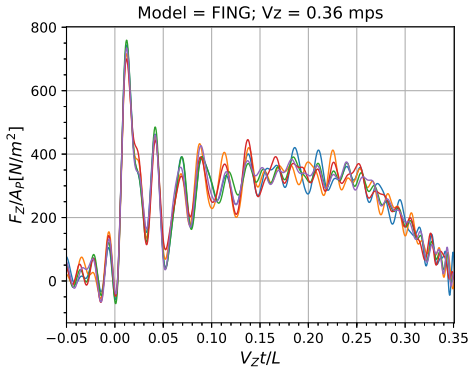
Model = FING; Vz = 0.36 mps
$F_Z/A_P[N/m^2]$
$V_Z t/L$

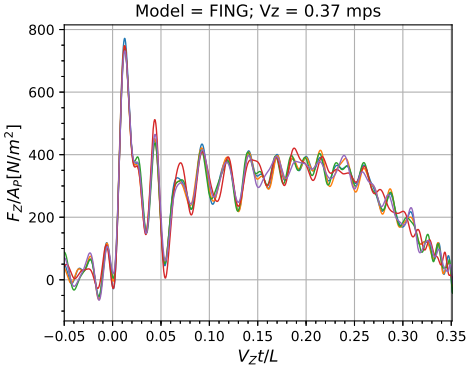
Model = FING; Vz = 0.37 mps
$F_Z/A_P[N/m^2]$
$V_Z t/L$

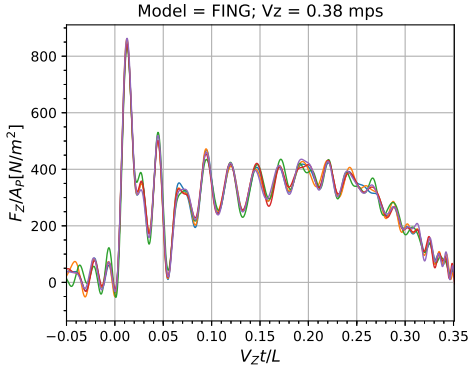
Model = FING; Vz = 0.38 mps
$F_Z/A_P[N/m^2]$
$V_Z t/L$

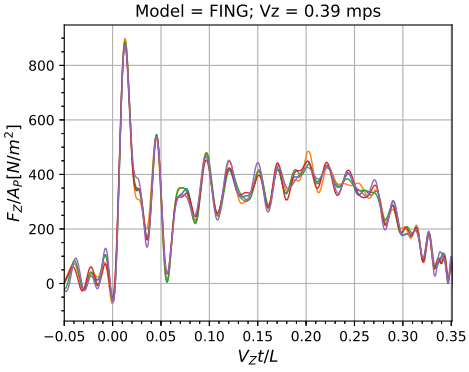
Model = FING; Vz = 0.39 mps
$F_Z/A_P[N/m^2]$
$V_Z t/L$

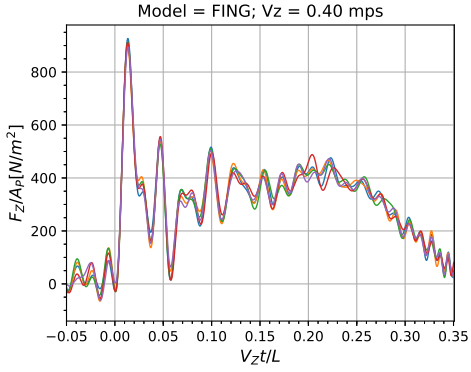
Model = FING; Vz = 0.40 mps
$F_Z/A_P[N/m^2]$
$V_Z t/L$

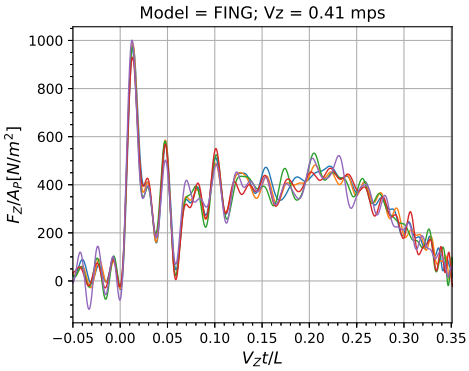
Model = FING; Vz = 0.41 mps
$F_Z/A_P[N/m^2]$
$V_Z t/L$

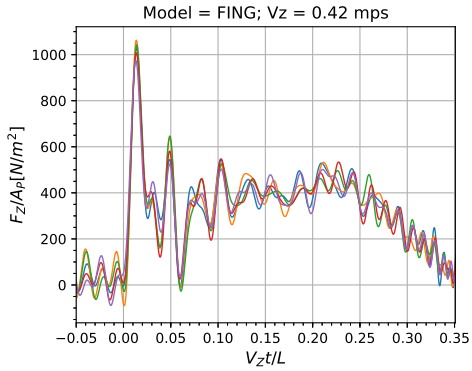
Model = FING; Vz = 0.42 mps
$F_Z/A_P[N/m^2]$
$V_Z t/L$

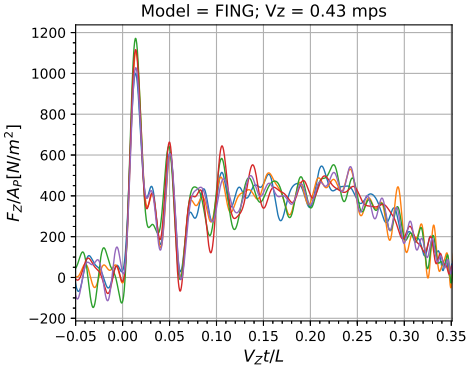
Model = FING; Vz = 0.43 mps
$F_Z/A_P[N/m^2]$
$V_Z t/L$

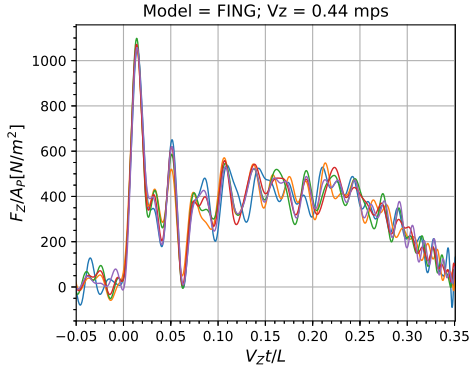
Model = FING; Vz = 0.44 mps
$F_Z/A_P[N/m^2]$
$V_Z t/L$

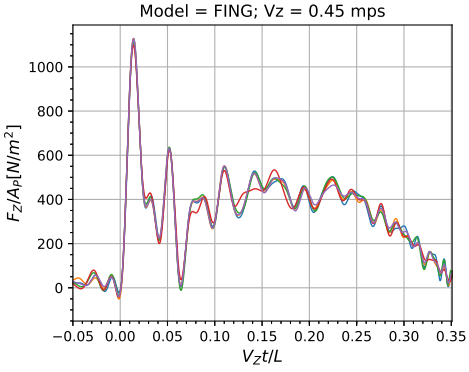
Model = FING; Vz = 0.45 mps
$F_Z/A_P[N/m^2]$
$V_Z t/L$

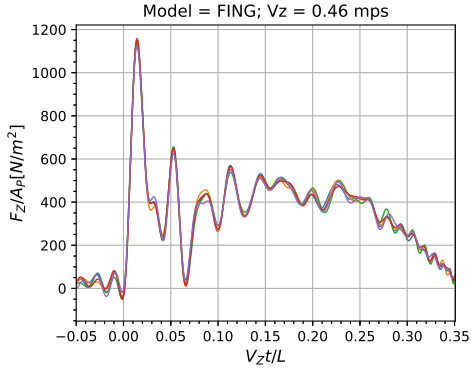
Model = FING; Vz = 0.46 mps
$F_Z/A_P[N/m^2]$
$V_Z t/L$

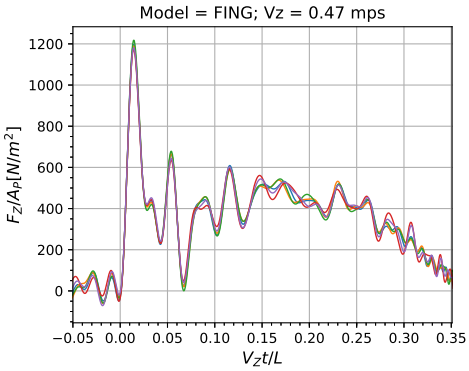
Model = FING; Vz = 0.47 mps
$F_Z/A_P[N/m^2]$
$V_Z t/L$

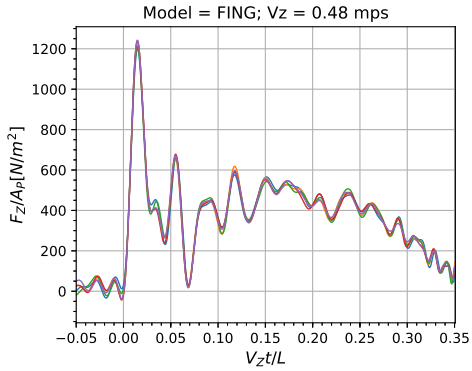
Model = FING; Vz = 0.48 mps
$F_Z/A_P[N/m^2]$
$V_Z t/L$

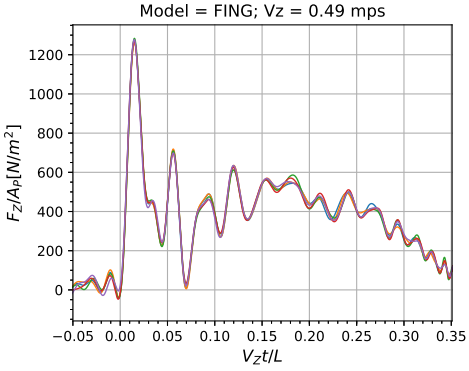
Model = FING; Vz = 0.49 mps
$F_Z/A_P[N/m^2]$
$V_Z t/L$

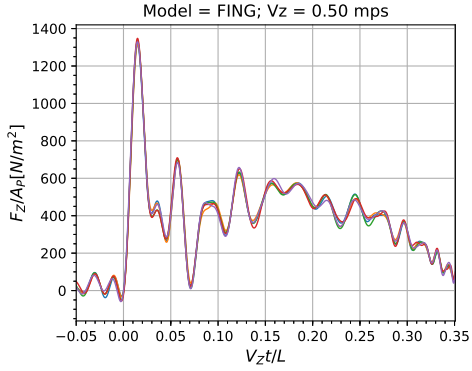
Model = FING; Vz = 0.50 mps
$F_Z/A_P[N/m^2]$
$V_Z t/L$

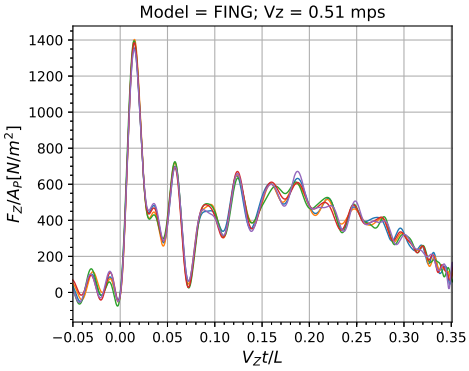
Model = FING; Vz = 0.51 mps
$F_Z/A_P[N/m^2]$
$V_Z t/L$

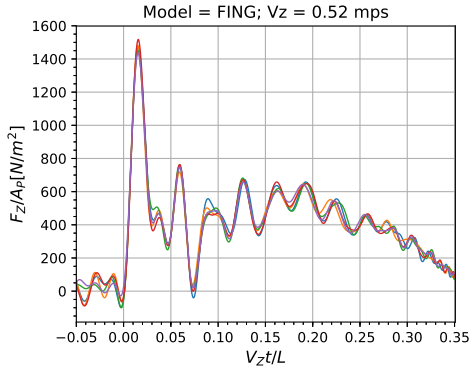
Model = FING; Vz = 0.52 mps
$F_Z/A_P[N/m^2]$
$V_Z t/L$

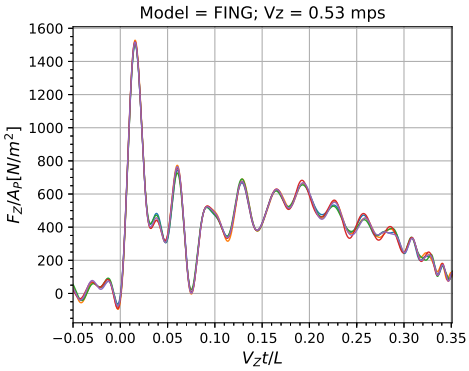
Model = FING; Vz = 0.53 mps
$F_Z/A_P[N/m^2]$
$V_Z t/L$

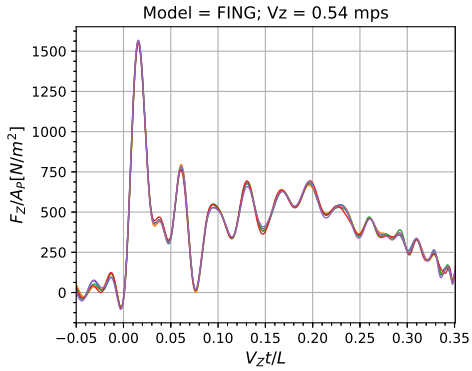
Model = FING; Vz = 0.54 mps
$F_Z/A_P[N/m^2]$
$V_Z t/L$

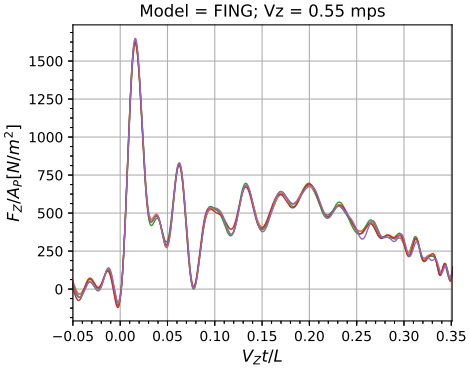
Model = FING; Vz = 0.55 mps
$F_Z/A_P[N/m^2]$
$V_Z t/L$

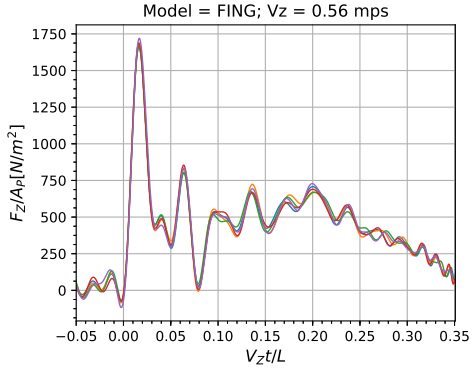
Model = FING; Vz = 0.56 mps
$F_Z/A_P[N/m^2]$
$V_Z t/L$

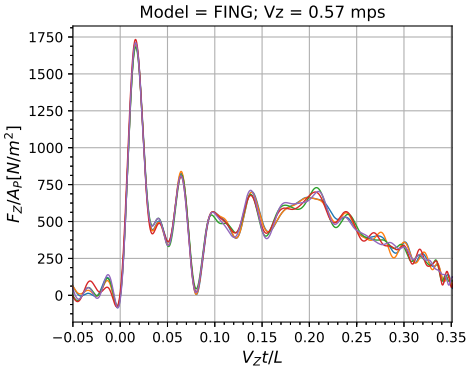
Model = FING; Vz = 0.57 mps
$F_Z/A_P[N/m^2]$
$V_Z t/L$

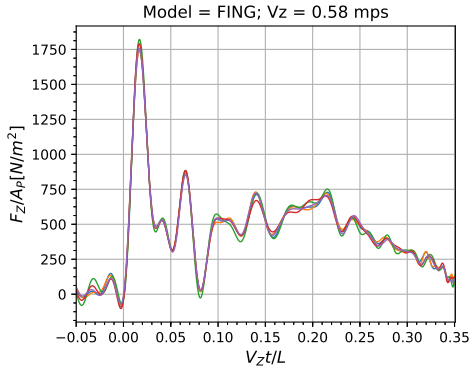
Model = FING; Vz = 0.58 mps
$F_Z/A_P[N/m^2]$
$V_Z t/L$

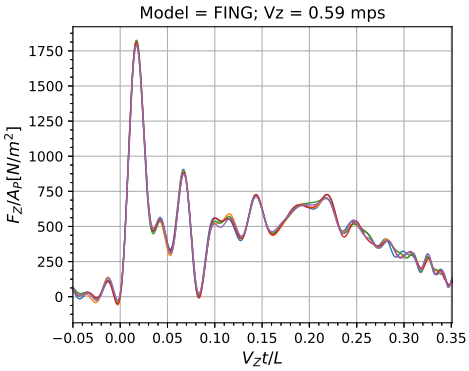
Model = FING; Vz = 0.59 mps
$F_Z/A_P[N/m^2]$
1750
1500
1250
1000
750
500
250
0
−0.05 0.00 0.05 0.10 0.15 0.20 0.25 0.30 0.35
$V_Z t/L$

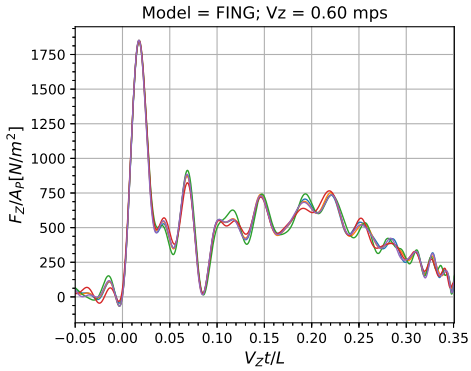
Model = FING; Vz = 0.60 mps
$F_Z/A_P[N/m^2]$
1750
1500
1250
1000
750
500
250
0
−0.05 0.00 0.05 0.10 0.15 0.20 0.25 0.30 0.35
$V_Z t/L$

Appendix C: Wave Tests - Force Time Series

This section presents the force time series for wave tests for FING test model. It should be noted that the first-order force is re-calculated using the Fourier averaged added mass (A) and damping (B) coefficients, and the filtered force also includes 3^{rd} and 5^{th} order force components.

Model: FING

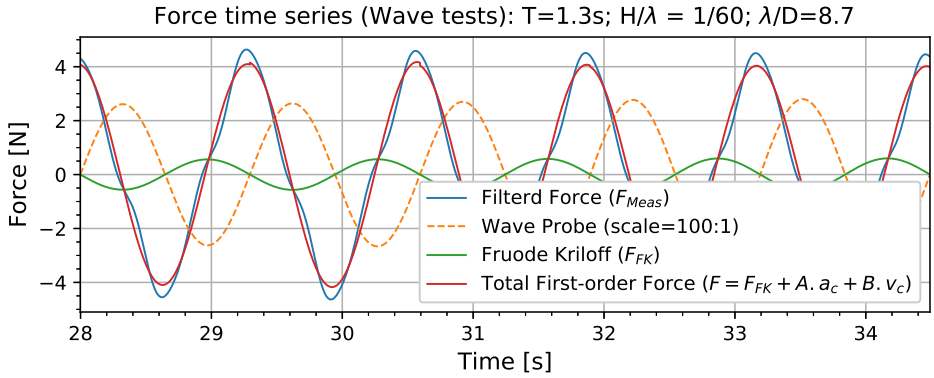

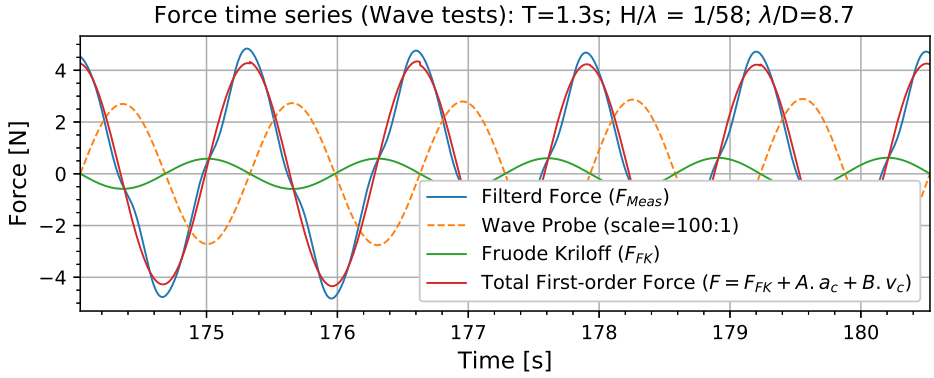

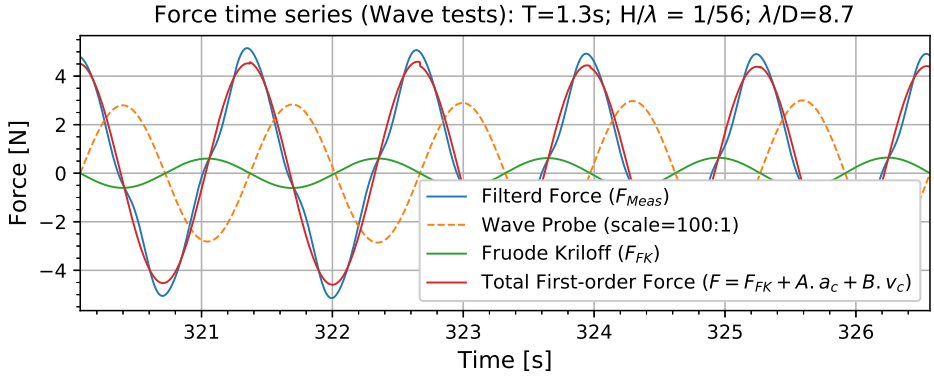
Force time series (Wave tests): T=1.3s; H/λ = 1/56; λ/D=8.7
Force [N]
Time [s]
Filterd Force (F_{Meas})
Wave Probe (scale=100:1)
Fruode Kriloff (F_{FK})
Total First-order Force ($F = F_{FK} + A.a_c + B.v_c$)

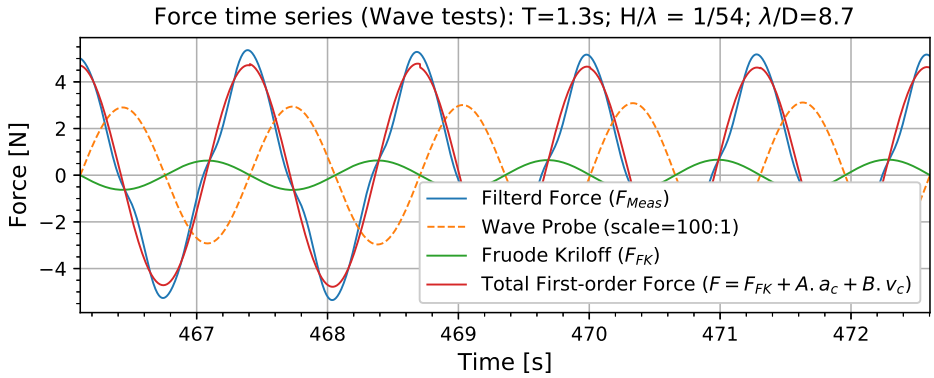
Force time series (Wave tests): T=1.3s; H/λ = 1/54; λ/D=8.7
Force [N]
Time [s]
Filterd Force (F_{Meas})
Wave Probe (scale=100:1)
Fruode Kriloff (F_{FK})
Total First-order Force ($F = F_{FK} + A.\,a_c + B.\,v_c$)

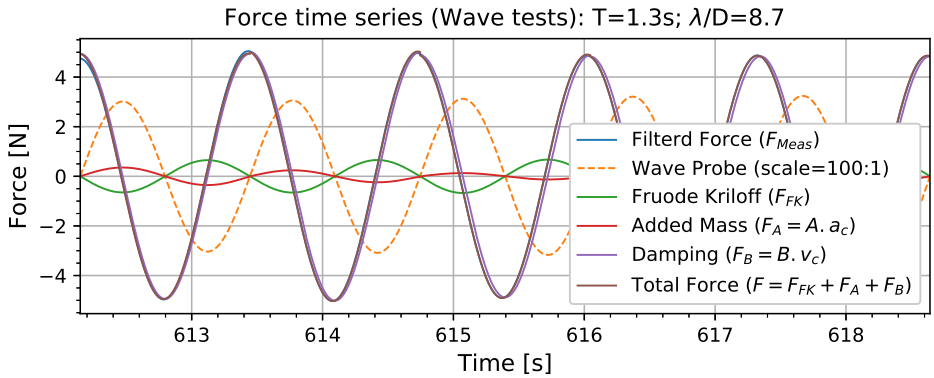
Force time series (Wave tests): T=1.3s; λ/D=8.7
Force [N]
Time [s]
Filterd Force (F_{Meas})
Wave Probe (scale=100:1)
Fruode Kriloff (F_{FK})
Added Mass ($F_A = A.\,a_c$)
Damping ($F_B = B.\,v_c$)
Total Force ($F = F_{FK} + F_A + F_B$)

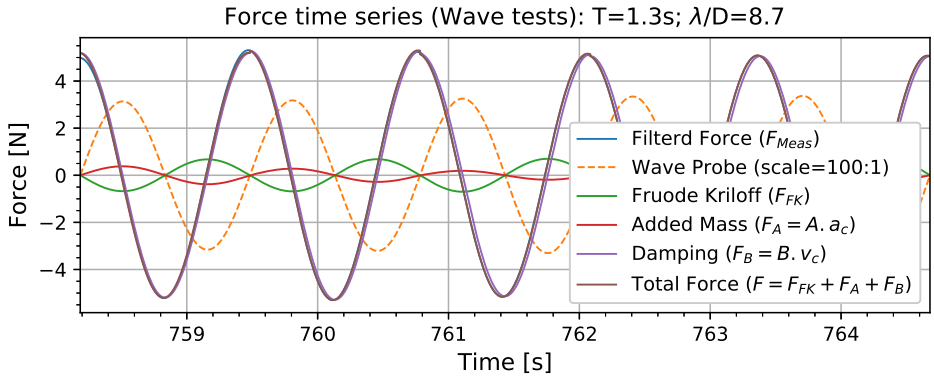
Force time series (Wave tests): T=1.3s; λ/D=8.7
Force [N]
Time [s]
Filterd Force (F_{Meas})
Wave Probe (scale=100:1)
Fruode Kriloff (F_{FK})
Added Mass ($F_A = A.\,a_c$)
Damping ($F_B = B.\,v_c$)
Total Force ($F = F_{FK} + F_A + F_B$)

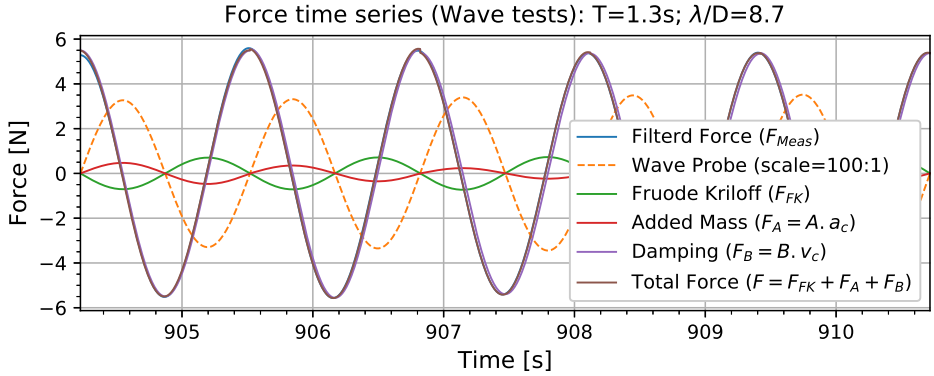
Force time series (Wave tests): T=1.3s; λ/D=8.7
Force [N]
Time [s]
Filterd Force (F_{Meas})
Wave Probe (scale=100:1)
Fruode Kriloff (F_{FK})
Added Mass ($F_A = A.\,a_c$)
Damping ($F_B = B.\,v_c$)
Total Force ($F = F_{FK} + F_A + F_B$)

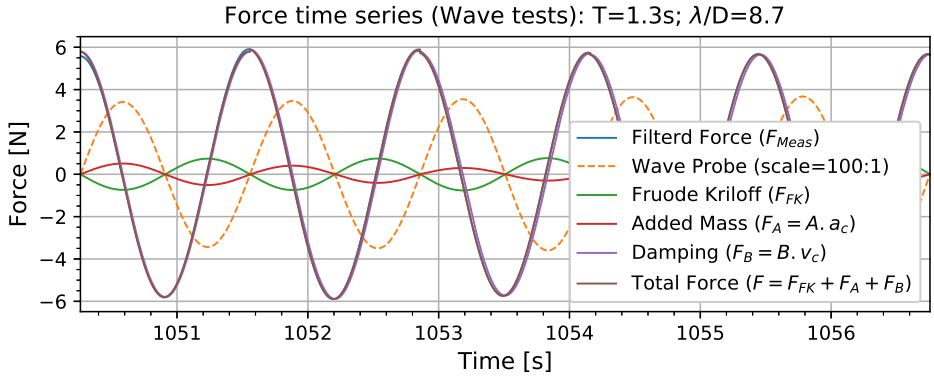
Force time series (Wave tests): T=1.3s; λ/D=8.7
Force [N]
Time [s]
Filterd Force (F_{Meas})
Wave Probe (scale=100:1)
Fruode Kriloff (F_{FK})
Added Mass ($F_A = A.\,a_c$)
Damping ($F_B = B.\,v_c$)
Total Force ($F = F_{FK} + F_A + F_B$)

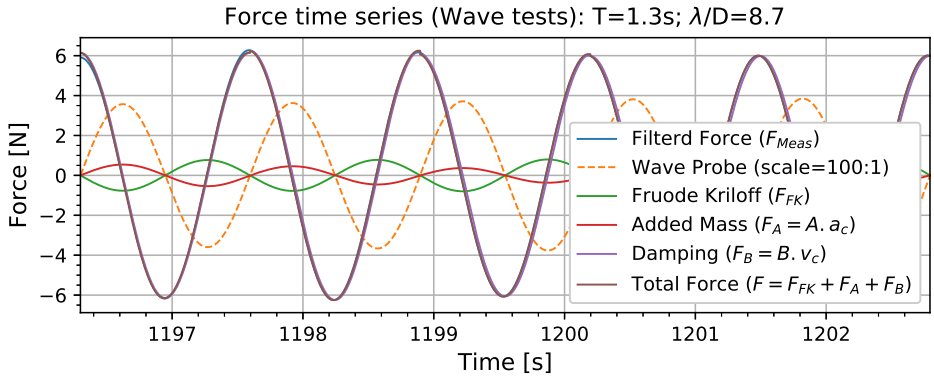
Force time series (Wave tests): T=1.3s; λ/D=8.7
Force [N]
Time [s]
Filterd Force (F_{Meas})
Wave Probe (scale=100:1)
Fruode Kriloff (F_{FK})
Added Mass ($F_A = A.\,a_c$)
Damping ($F_B = B.\,v_c$)
Total Force ($F = F_{FK} + F_A + F_B$)

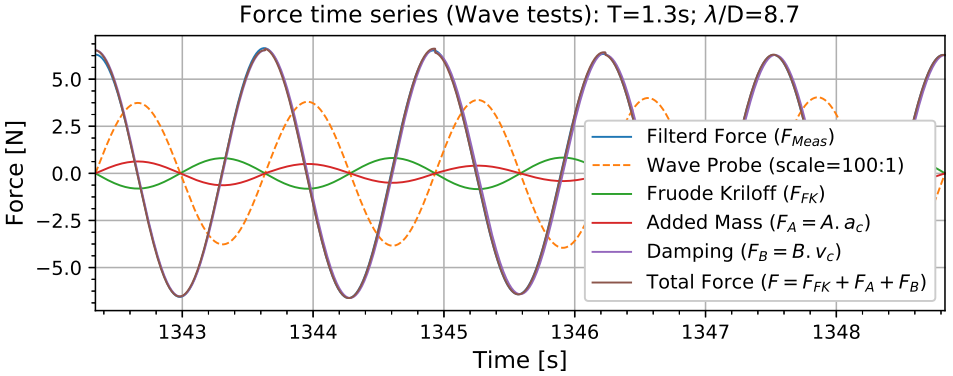
Force time series (Wave tests): T=1.3s; λ/D=8.7
Force [N]
Time [s]
Filterd Force (F_{Meas})
Wave Probe (scale=100:1)
Fruode Kriloff (F_{FK})
Added Mass ($F_A = A.a_c$)
Damping ($F_B = B.v_c$)
Total Force ($F = F_{FK} + F_A + F_B$)

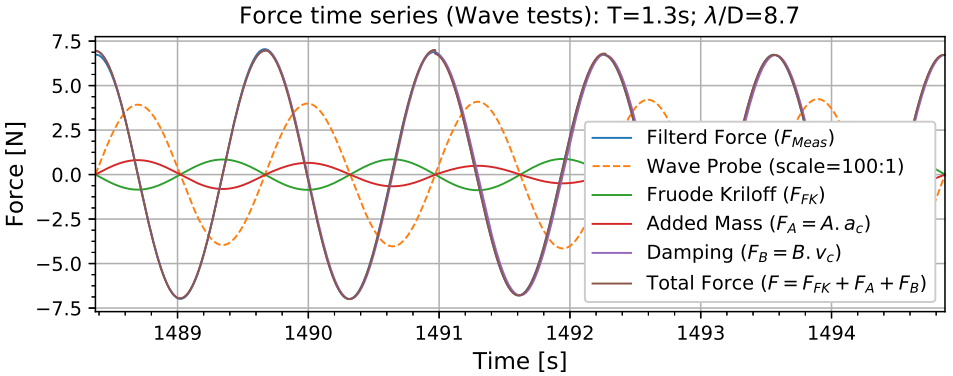
Force time series (Wave tests): T=1.3s; λ/D=8.7
Force [N]
Time [s]
Filterd Force (F_{Meas})
Wave Probe (scale=100:1)
Fruode Kriloff (F_{FK})
Added Mass ($F_A = A.a_c$)
Damping ($F_B = B.v_c$)
Total Force ($F = F_{FK} + F_A + F_B$)

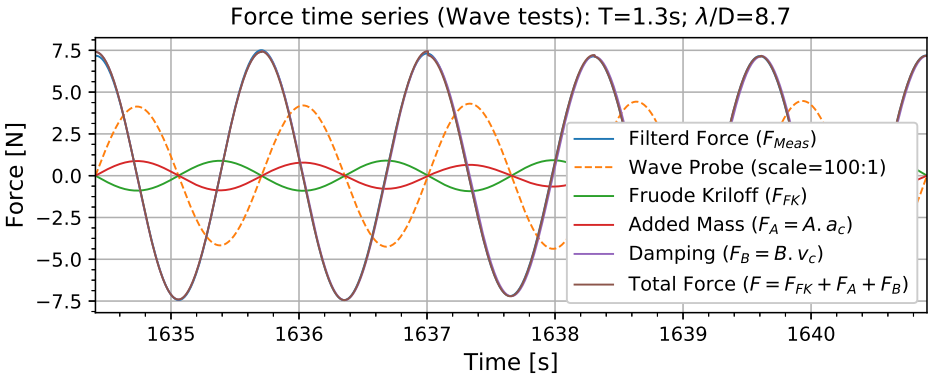
Force time series (Wave tests): T=1.3s; λ/D=8.7
Force [N]
Time [s]
Filterd Force (F_{Meas})
Wave Probe (scale=100:1)
Fruode Kriloff (F_{FK})
Added Mass ($F_A = A.a_c$)
Damping ($F_B = B.v_c$)
Total Force ($F = F_{FK} + F_A + F_B$)

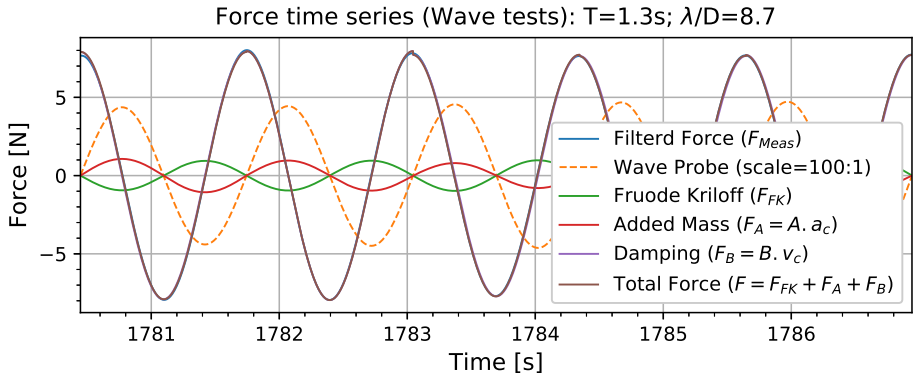
Force time series (Wave tests): T=1.3s; λ/D=8.7
Force [N]
Time [s]
Filterd Force (F_{Meas})
Wave Probe (scale=100:1)
Fruode Kriloff (F_{FK})
Added Mass ($F_A = A.a_c$)
Damping ($F_B = B.v_c$)
Total Force ($F = F_{FK} + F_A + F_B$)

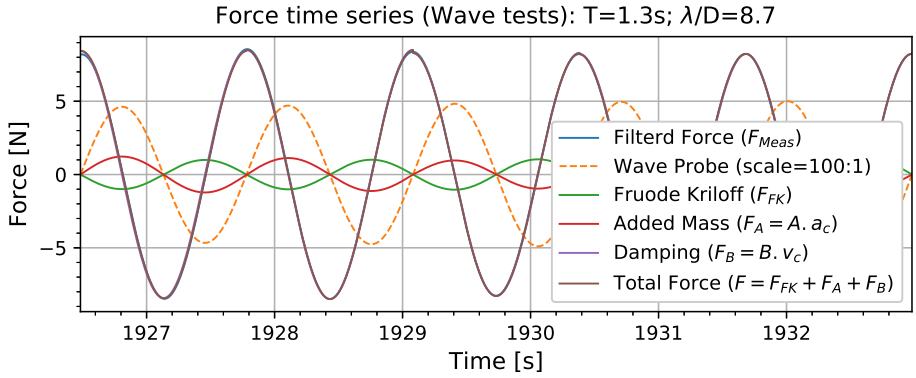
Force time series (Wave tests): T=1.3s; λ/D=8.7
Force [N]
Time [s]
Filterd Force (F_{Meas})
Wave Probe (scale=100:1)
Fruode Kriloff (F_{FK})
Added Mass ($F_A = A.a_c$)
Damping ($F_B = B.v_c$)
Total Force ($F = F_{FK} + F_A + F_B$)

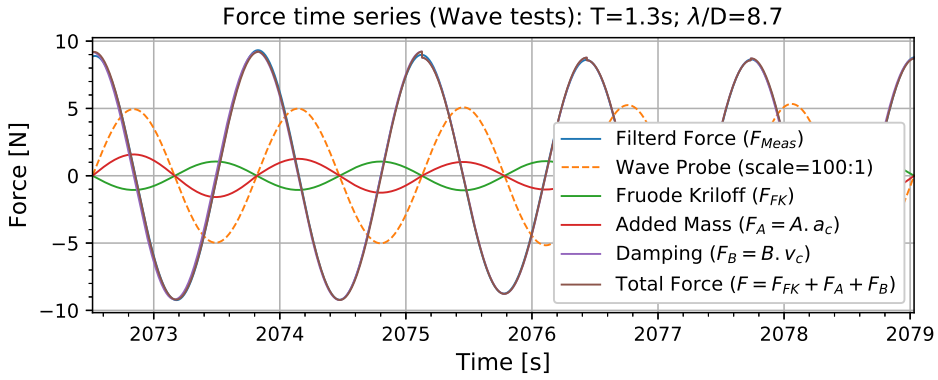
Force time series (Wave tests): T=1.3s; λ/D=8.7
Force [N]
Time [s]
Filterd Force (F_{Meas})
Wave Probe (scale=100:1)
Fruode Kriloff (F_{FK})
Added Mass ($F_A = A.a_c$)
Damping ($F_B = B.v_c$)
Total Force ($F = F_{FK} + F_A + F_B$)

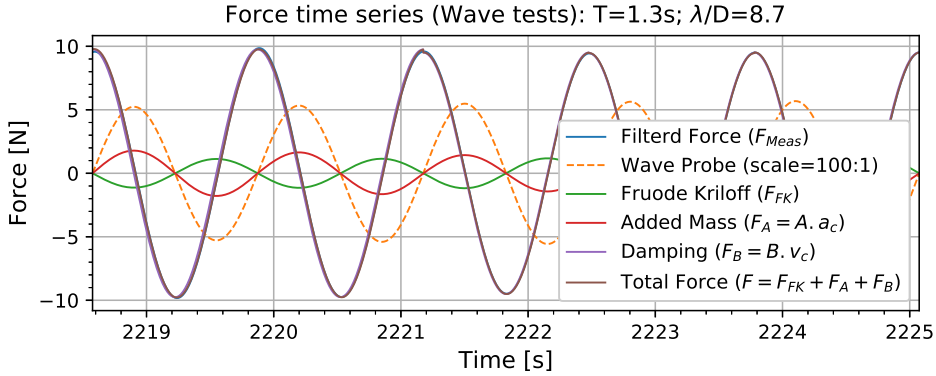
Force time series (Wave tests): T=1.3s; λ/D=8.7
Force [N]
Time [s]
Filterd Force (F_{Meas})
Wave Probe (scale=100:1)
Fruode Kriloff (F_{FK})
Added Mass ($F_A = A.a_c$)
Damping ($F_B = B.v_c$)
Total Force ($F = F_{FK} + F_A + F_B$)

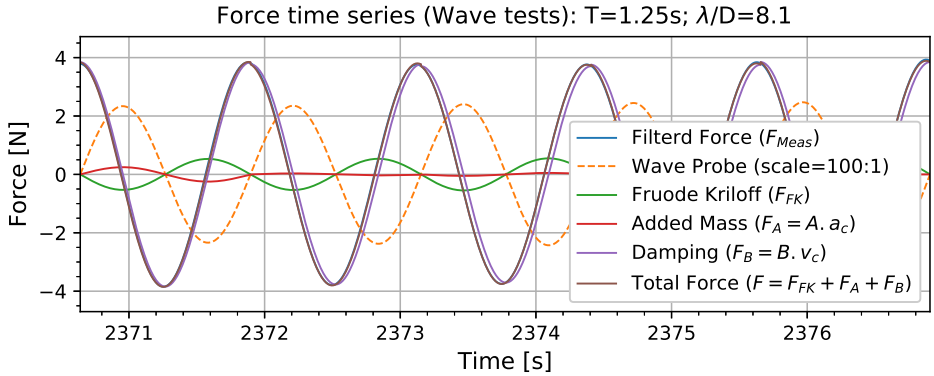
Force time series (Wave tests): T=1.25s; λ/D=8.1
Force [N]
Time [s]
Filterd Force (F_{Meas})
Wave Probe (scale=100:1)
Fruode Kriloff (F_{FK})
Added Mass ($F_A = A.a_c$)
Damping ($F_B = B.v_c$)
Total Force ($F = F_{FK} + F_A + F_B$)

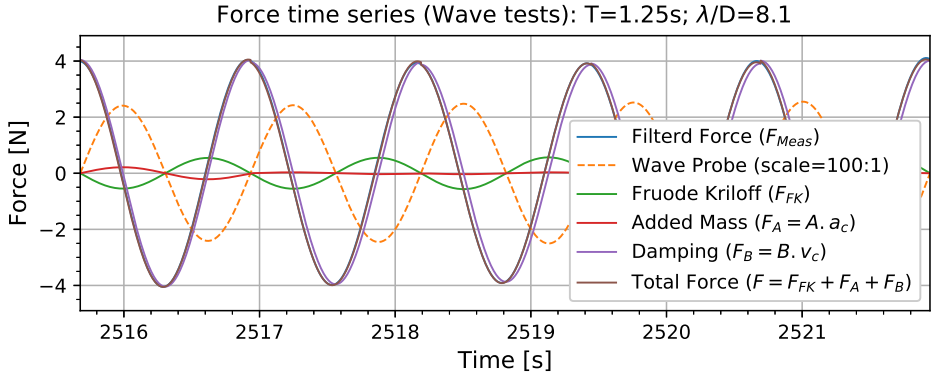
Force time series (Wave tests): T=1.25s; λ/D=8.1
Force [N]
Time [s]
Filterd Force (F_{Meas})
Wave Probe (scale=100:1)
Fruode Kriloff (F_{FK})
Added Mass ($F_A = A.a_c$)
Damping ($F_B = B.v_c$)
Total Force ($F = F_{FK} + F_A + F_B$)

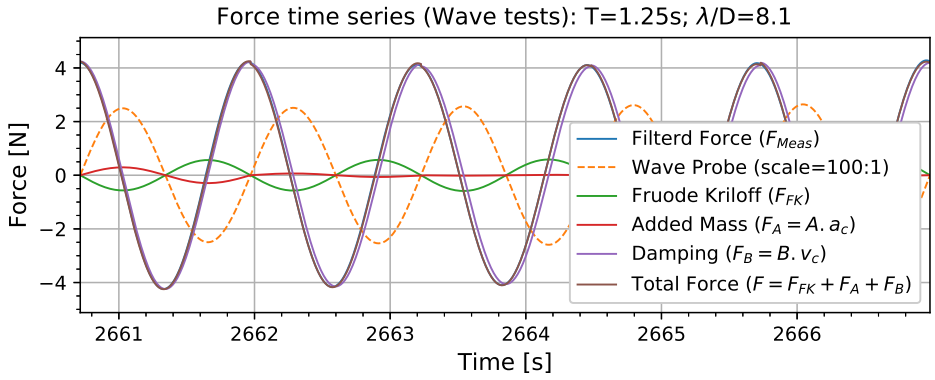
Force time series (Wave tests): T=1.25s; λ/D=8.1
Force [N]
Time [s]
Filterd Force (F_{Meas})
Wave Probe (scale=100:1)
Fruode Kriloff (F_{FK})
Added Mass ($F_A = A.a_c$)
Damping ($F_B = B.v_c$)
Total Force ($F = F_{FK} + F_A + F_B$)

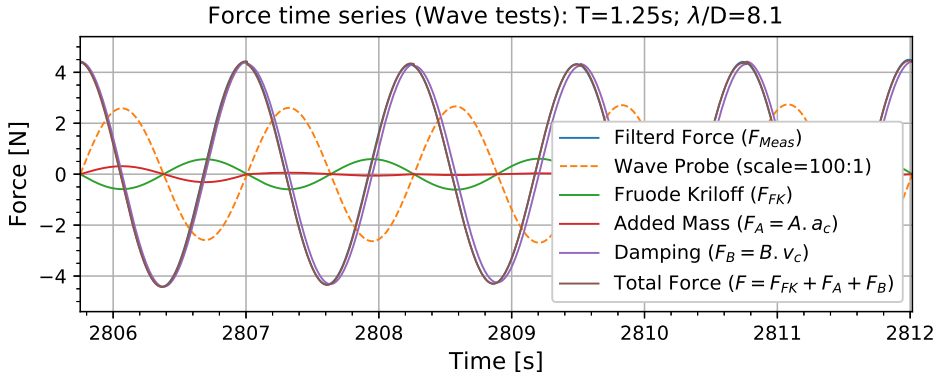
Force time series (Wave tests): T=1.25s; λ/D=8.1
Force [N]
Time [s]
Filterd Force (F_{Meas})
Wave Probe (scale=100:1)
Fruode Kriloff (F_{FK})
Added Mass ($F_A = A.a_c$)
Damping ($F_B = B.v_c$)
Total Force ($F = F_{FK} + F_A + F_B$)

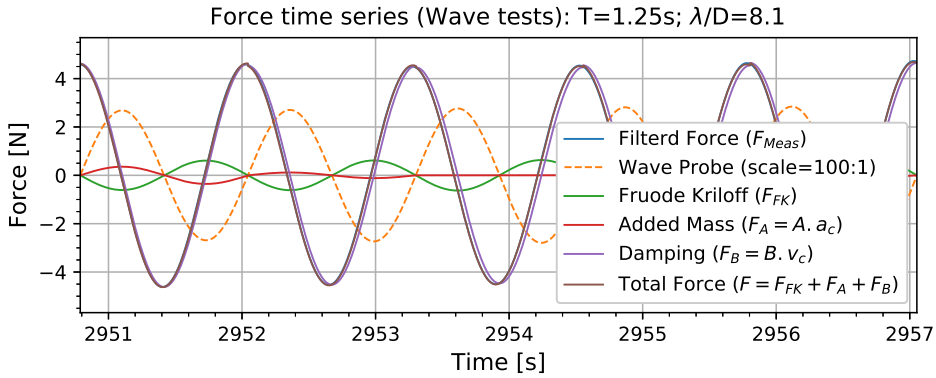
Force time series (Wave tests): T=1.25s; λ/D=8.1
Force [N]
Time [s]
Filterd Force (F_{Meas})
Wave Probe (scale=100:1)
Fruode Kriloff (F_{FK})
Added Mass ($F_A = A.a_c$)
Damping ($F_B = B.v_c$)
Total Force ($F = F_{FK} + F_A + F_B$)

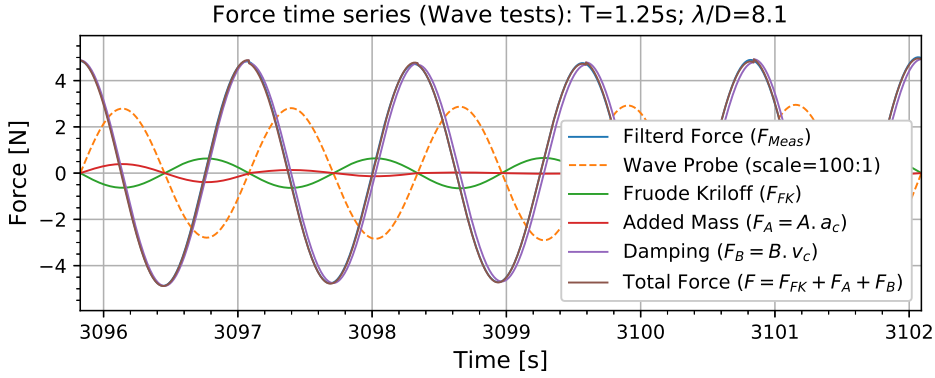
Force time series (Wave tests): T=1.25s; λ/D=8.1
Force [N]
Time [s]
Filterd Force (F_{Meas})
Wave Probe (scale=100:1)
Fruode Kriloff (F_{FK})
Added Mass ($F_A = A.a_c$)
Damping ($F_B = B.v_c$)
Total Force ($F = F_{FK} + F_A + F_B$)

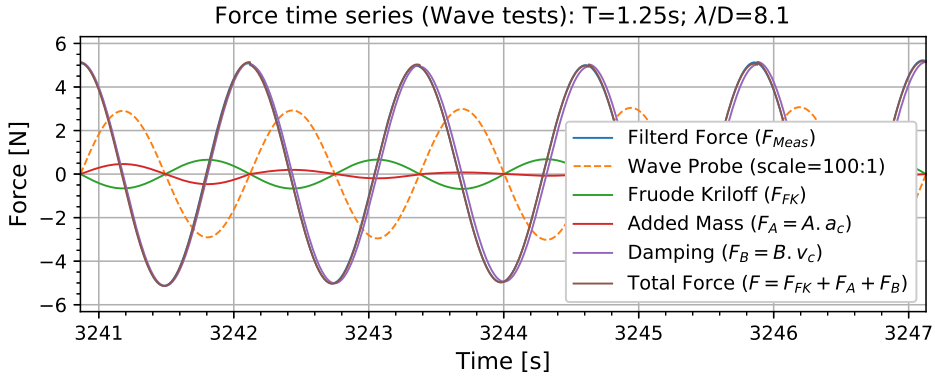
Force time series (Wave tests): T=1.25s; λ/D=8.1
Force [N]
Time [s]
Filterd Force (F_{Meas})
Wave Probe (scale=100:1)
Fruode Kriloff (F_{FK})
Added Mass ($F_A = A.a_c$)
Damping ($F_B = B.v_c$)
Total Force ($F = F_{FK} + F_A + F_B$)

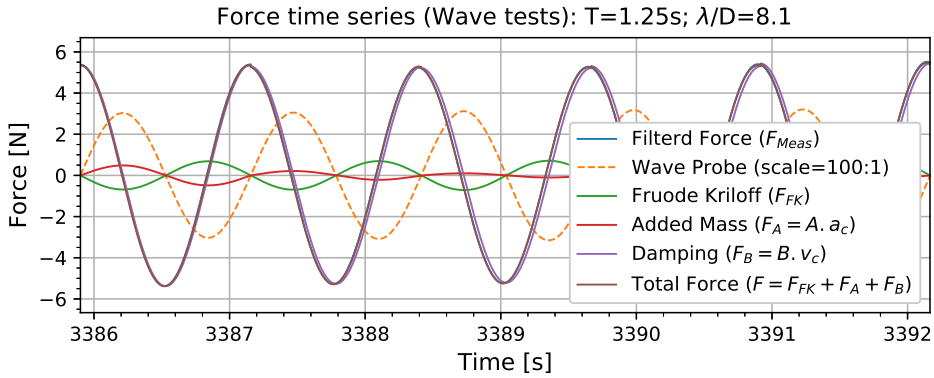
Force time series (Wave tests): T=1.25s; λ/D=8.1
Force [N]
Time [s]
Filterd Force (F_{Meas})
Wave Probe (scale=100:1)
Fruode Kriloff (F_{FK})
Added Mass ($F_A = A.a_c$)
Damping ($F_B = B.v_c$)
Total Force ($F = F_{FK} + F_A + F_B$)

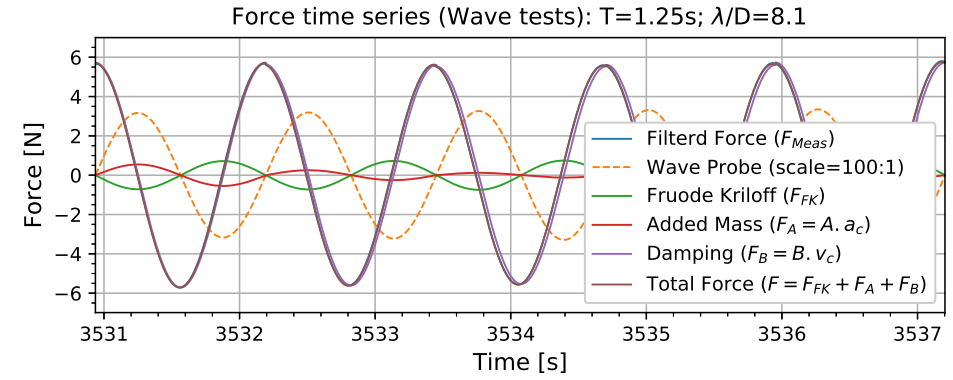
Force time series (Wave tests): T=1.25s; λ/D=8.1
Force [N]
Time [s]
Filterd Force (F_{Meas})
Wave Probe (scale=100:1)
Fruode Kriloff (F_{FK})
Added Mass ($F_A = A.a_c$)
Damping ($F_B = B.v_c$)
Total Force ($F = F_{FK} + F_A + F_B$)

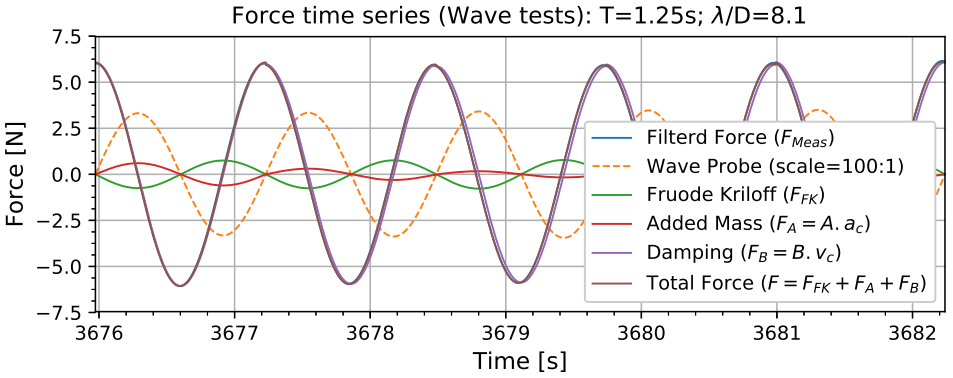
Force time series (Wave tests): T=1.25s; λ/D=8.1
Force [N]
Time [s]
Filterd Force (F_{Meas})
Wave Probe (scale=100:1)
Fruode Kriloff (F_{FK})
Added Mass ($F_A = A.a_c$)
Damping ($F_B = B.v_c$)
Total Force ($F = F_{FK} + F_A + F_B$)

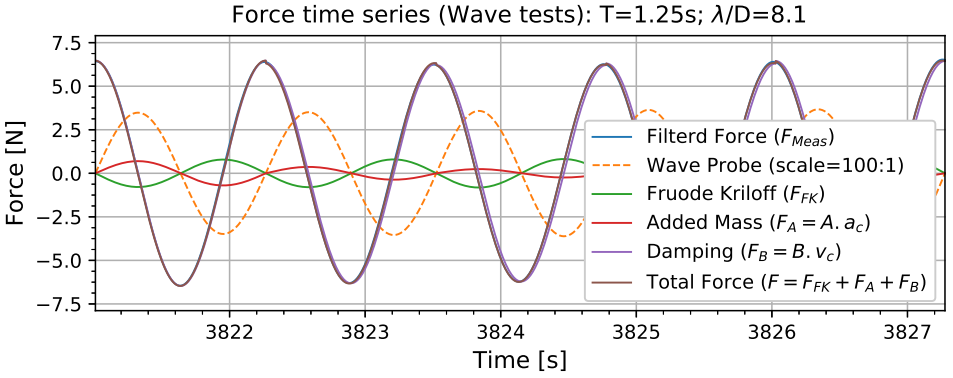
Force time series (Wave tests): T=1.25s; λ/D=8.1
Force [N]
Time [s]
Filterd Force (F_{Meas})
Wave Probe (scale=100:1)
Fruode Kriloff (F_{FK})
Added Mass ($F_A = A.a_c$)
Damping ($F_B = B.v_c$)
Total Force ($F = F_{FK} + F_A + F_B$)

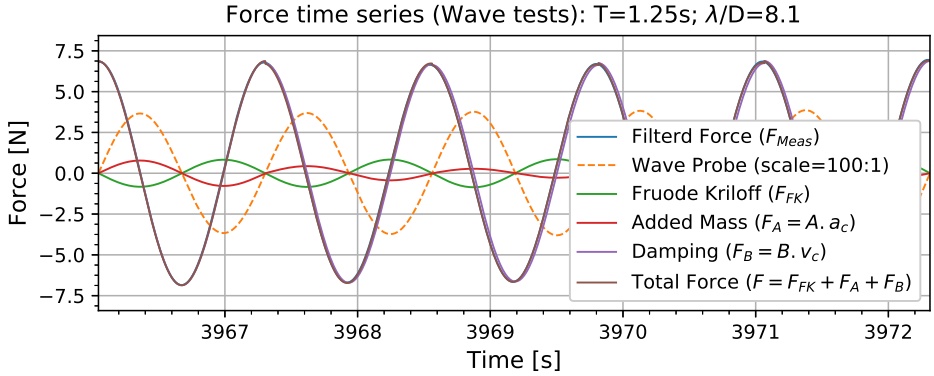
Force time series (Wave tests): T=1.25s; λ/D=8.1
Force [N]
Time [s]
Filterd Force (F_{Meas})
Wave Probe (scale=100:1)
Fruode Kriloff (F_{FK})
Added Mass ($F_A = A.a_c$)
Damping ($F_B = B.v_c$)
Total Force ($F = F_{FK} + F_A + F_B$)

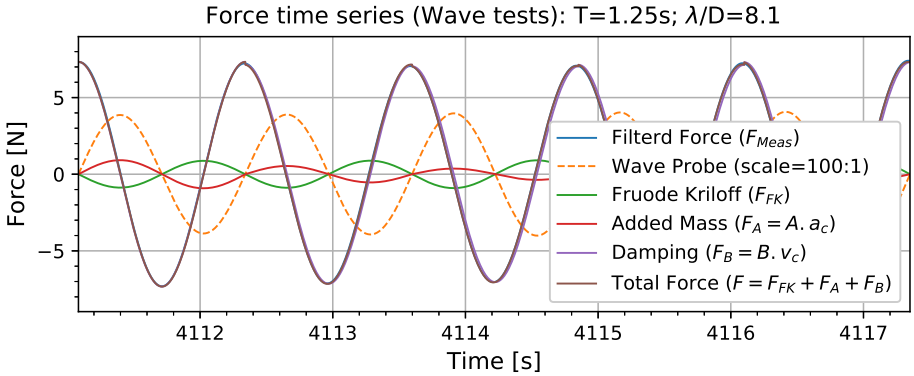
Force time series (Wave tests): T=1.25s; λ/D=8.1
Force [N]
Time [s]
Filterd Force (F_{Meas})
Wave Probe (scale=100:1)
Fruode Kriloff (F_{FK})
Added Mass ($F_A = A.a_c$)
Damping ($F_B = B.v_c$)
Total Force ($F = F_{FK} + F_A + F_B$)

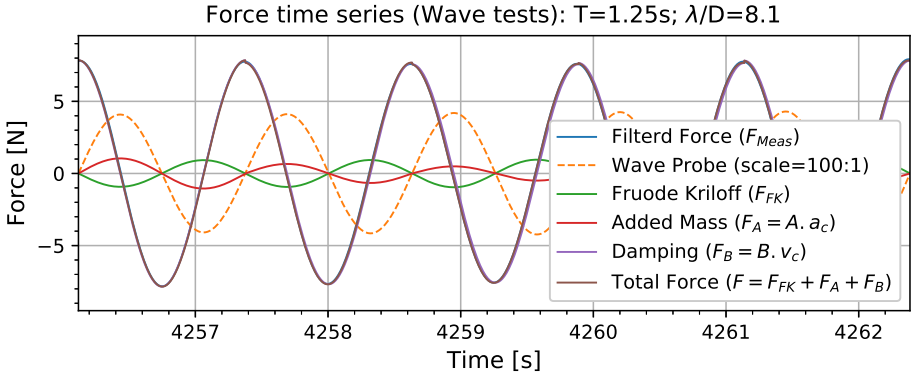
Force time series (Wave tests): T=1.25s; λ/D=8.1
Force [N]
Time [s]
Filterd Force (F_{Meas})
Wave Probe (scale=100:1)
Fruode Kriloff (F_{FK})
Added Mass ($F_A = A.a_c$)
Damping ($F_B = B.v_c$)
Total Force ($F = F_{FK} + F_A + F_B$)

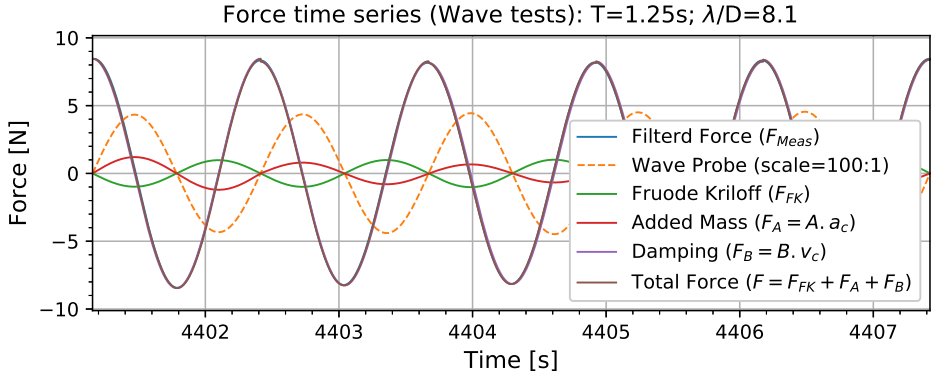
Force time series (Wave tests): T=1.25s; λ/D=8.1
Force [N]
Time [s]
Filterd Force (F_{Meas})
Wave Probe (scale=100:1)
Fruode Kriloff (F_{FK})
Added Mass ($F_A = A.a_c$)
Damping ($F_B = B.v_c$)
Total Force ($F = F_{FK} + F_A + F_B$)

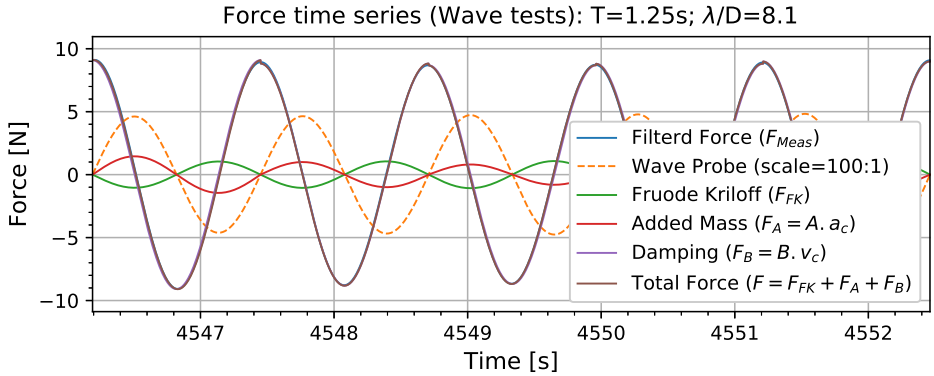
Force time series (Wave tests): T=1.25s; λ/D=8.1
Force [N]
Time [s]
Filterd Force (F_{Meas})
Wave Probe (scale=100:1)
Fruode Kriloff (F_{FK})
Added Mass ($F_A = A.a_c$)
Damping ($F_B = B.v_c$)
Total Force ($F = F_{FK} + F_A + F_B$)

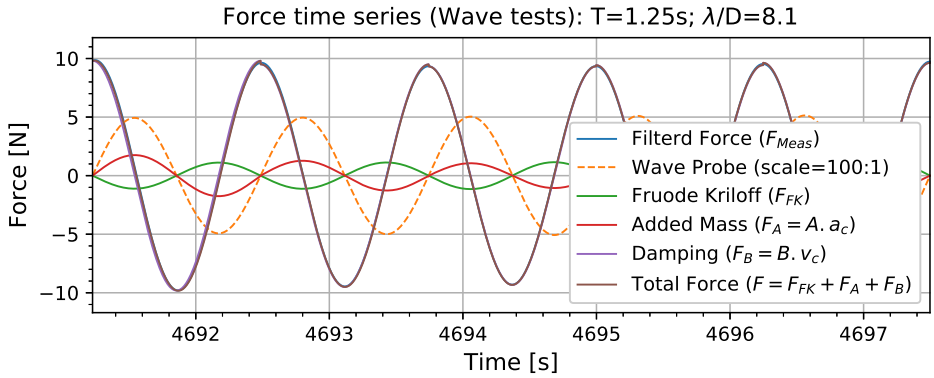
Force time series (Wave tests): T=1.25s; λ/D=8.1
Force [N]
Time [s]
Filterd Force (F_{Meas})
Wave Probe (scale=100:1)
Fruode Kriloff (F_{FK})
Added Mass ($F_A = A.a_c$)
Damping ($F_B = B.v_c$)
Total Force ($F = F_{FK} + F_A + F_B$)

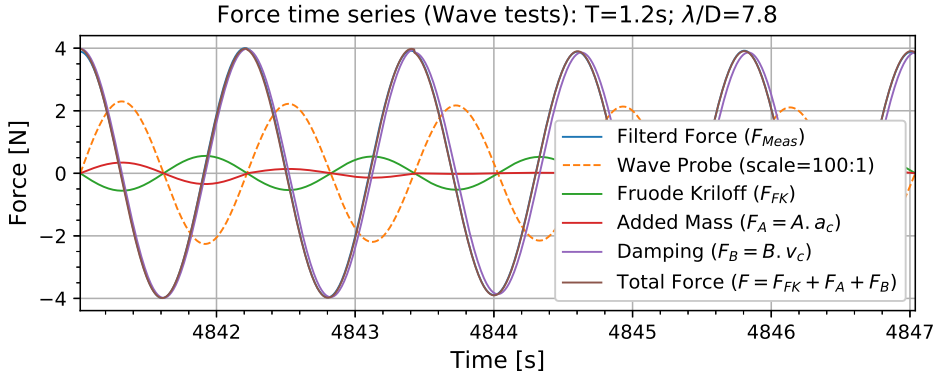
Force time series (Wave tests): T=1.2s; λ/D=7.8
Force [N]
Time [s]
Filterd Force (F_{Meas})
Wave Probe (scale=100:1)
Fruode Kriloff (F_{FK})
Added Mass ($F_A = A.a_c$)
Damping ($F_B = B.v_c$)
Total Force ($F = F_{FK} + F_A + F_B$)

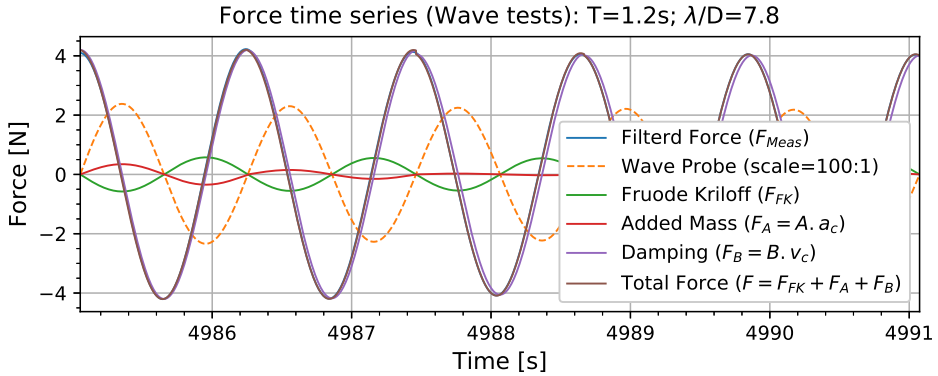
Force time series (Wave tests): T=1.2s; λ/D=7.8
Force [N]
Time [s]
Filterd Force (F_{Meas})
Wave Probe (scale=100:1)
Fruode Kriloff (F_{FK})
Added Mass ($F_A = A.a_c$)
Damping ($F_B = B.v_c$)
Total Force ($F = F_{FK} + F_A + F_B$)

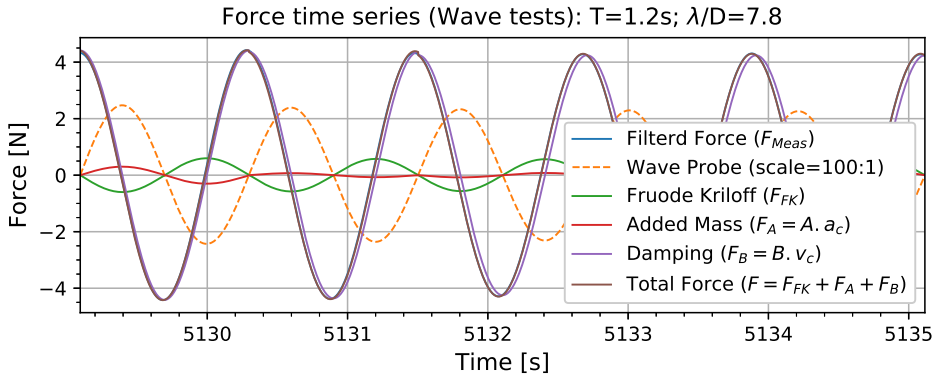
Force time series (Wave tests): T=1.2s; λ/D=7.8
Force [N]
Time [s]
Filterd Force (F_{Meas})
Wave Probe (scale=100:1)
Fruode Kriloff (F_{FK})
Added Mass ($F_A = A.a_c$)
Damping ($F_B = B.v_c$)
Total Force ($F = F_{FK} + F_A + F_B$)

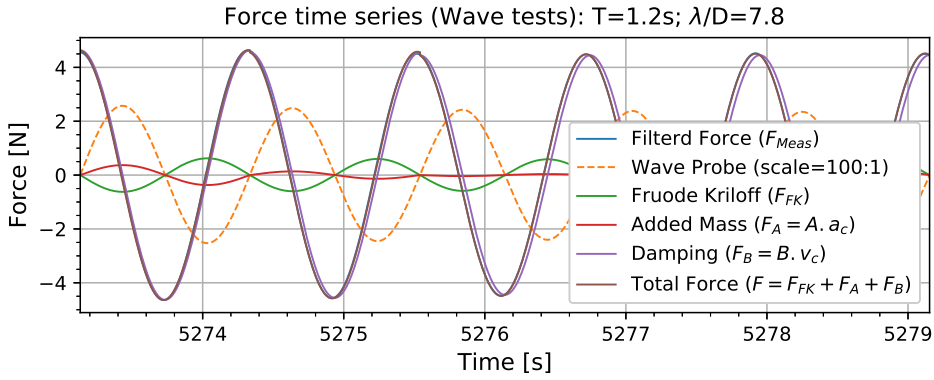
Force time series (Wave tests): T=1.2s; λ/D=7.8
Force [N]
Time [s]
Filterd Force (F_{Meas})
Wave Probe (scale=100:1)
Fruode Kriloff (F_{FK})
Added Mass ($F_A = A.a_c$)
Damping ($F_B = B.v_c$)
Total Force ($F = F_{FK} + F_A + F_B$)

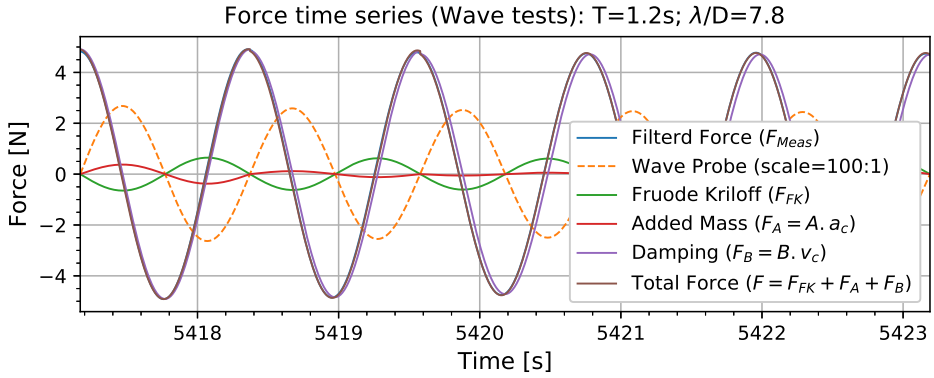
Force time series (Wave tests): T=1.2s; λ/D=7.8
Force [N]
Time [s]
Filterd Force (F_{Meas})
Wave Probe (scale=100:1)
Fruode Kriloff (F_{FK})
Added Mass ($F_A = A.a_c$)
Damping ($F_B = B.v_c$)
Total Force ($F = F_{FK} + F_A + F_B$)

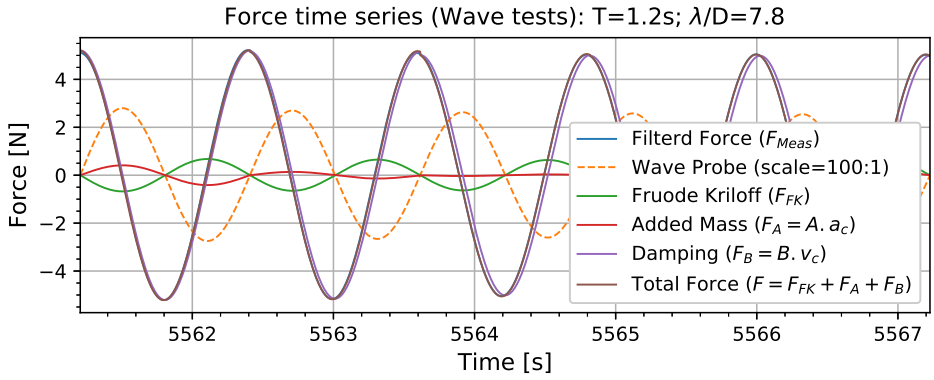
Force time series (Wave tests): T=1.2s; λ/D=7.8
Force [N]
Time [s]
Filterd Force (F_{Meas})
Wave Probe (scale=100:1)
Fruode Kriloff (F_{FK})
Added Mass ($F_A = A.a_c$)
Damping ($F_B = B.v_c$)
Total Force ($F = F_{FK} + F_A + F_B$)

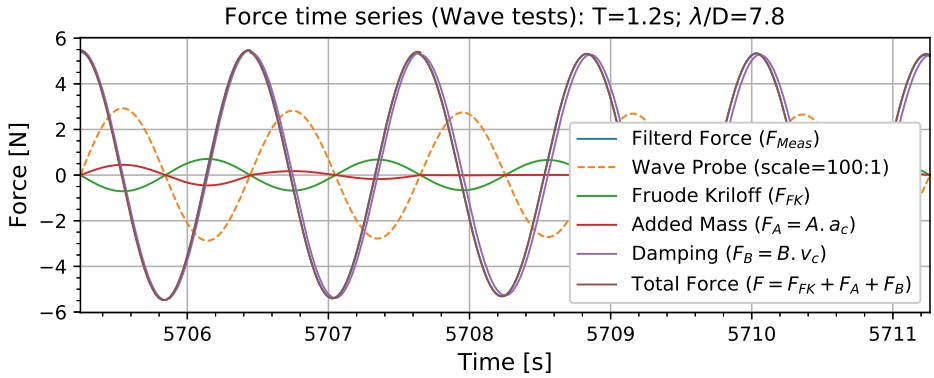
Force time series (Wave tests): T=1.2s; λ/D=7.8
Force [N]
Time [s]
Filterd Force (F_{Meas})
Wave Probe (scale=100:1)
Fruode Kriloff (F_{FK})
Added Mass ($F_A = A.a_c$)
Damping ($F_B = B.v_c$)
Total Force ($F = F_{FK} + F_A + F_B$)

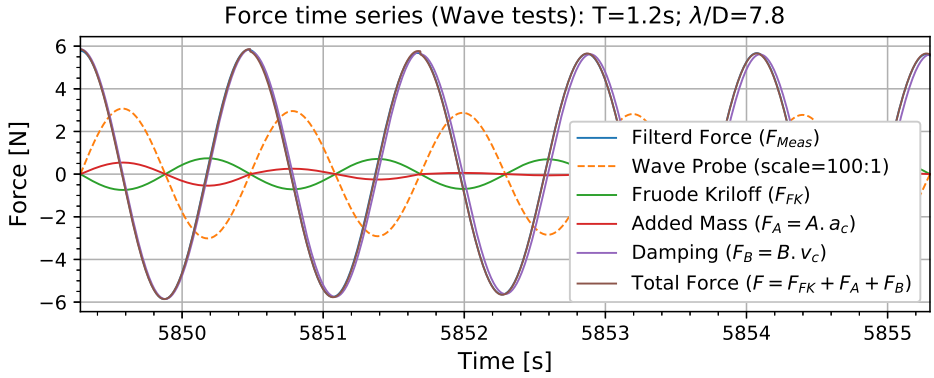
Force time series (Wave tests): T=1.2s; λ/D=7.8
Force [N]
Time [s]
Filterd Force (F_{Meas})
Wave Probe (scale=100:1)
Fruode Kriloff (F_{FK})
Added Mass ($F_A = A.a_c$)
Damping ($F_B = B.v_c$)
Total Force ($F = F_{FK} + F_A + F_B$)

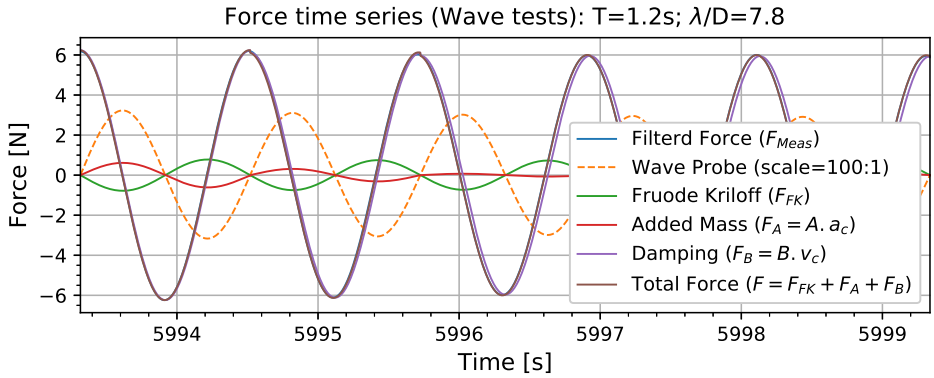
Force time series (Wave tests): T=1.2s; λ/D=7.8
Force [N]
Time [s]
Filterd Force (F_{Meas})
Wave Probe (scale=100:1)
Fruode Kriloff (F_{FK})
Added Mass ($F_A = A.a_c$)
Damping ($F_B = B.v_c$)
Total Force ($F = F_{FK} + F_A + F_B$)

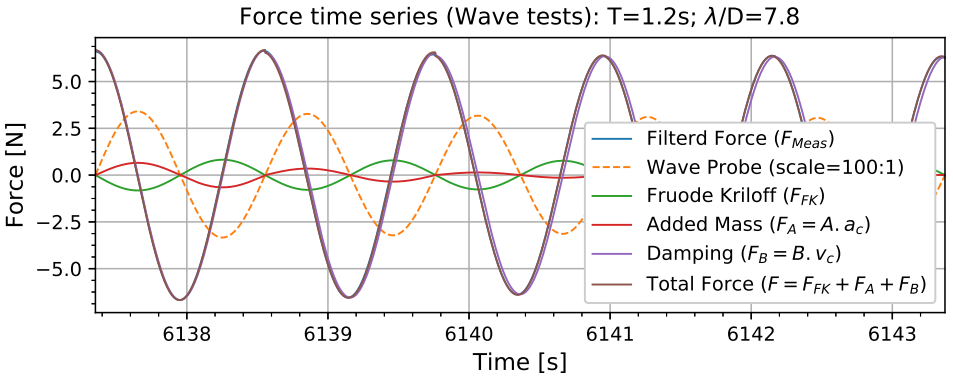
Force time series (Wave tests): T=1.2s; λ/D=7.8
Force [N]
Time [s]
Filterd Force (F_{Meas})
Wave Probe (scale=100:1)
Fruode Kriloff (F_{FK})
Added Mass ($F_A = A.a_c$)
Damping ($F_B = B.v_c$)
Total Force ($F = F_{FK} + F_A + F_B$)

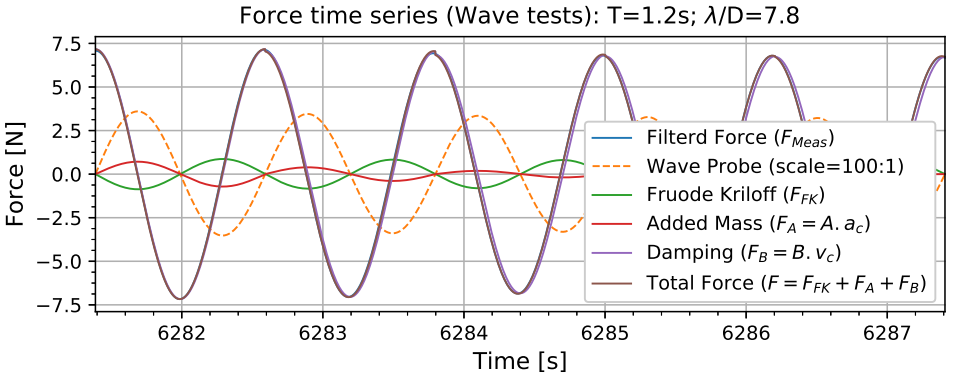
Force time series (Wave tests): T=1.2s; λ/D=7.8
Force [N]
Time [s]
Filterd Force (F_{Meas})
Wave Probe (scale=100:1)
Fruode Kriloff (F_{FK})
Added Mass ($F_A = A.a_c$)
Damping ($F_B = B.v_c$)
Total Force ($F = F_{FK} + F_A + F_B$)

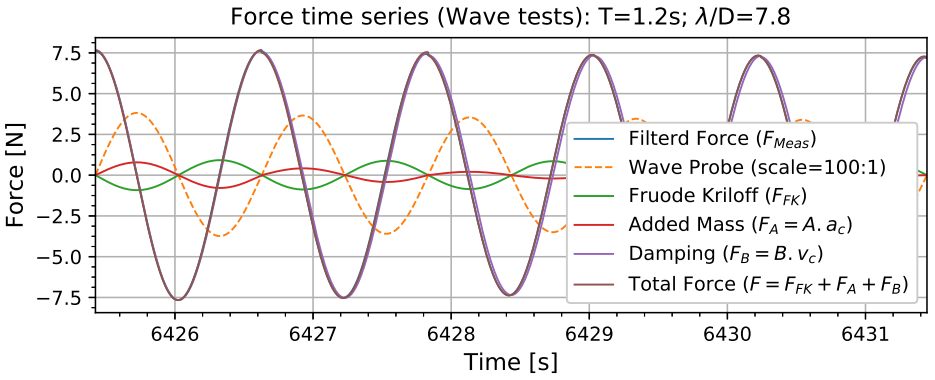
Force time series (Wave tests): T=1.2s; λ/D=7.8
Force [N]
Time [s]
Filterd Force (F_{Meas})
Wave Probe (scale=100:1)
Fruode Kriloff (F_{FK})
Added Mass ($F_A = A.a_c$)
Damping ($F_B = B.v_c$)
Total Force ($F = F_{FK} + F_A + F_B$)

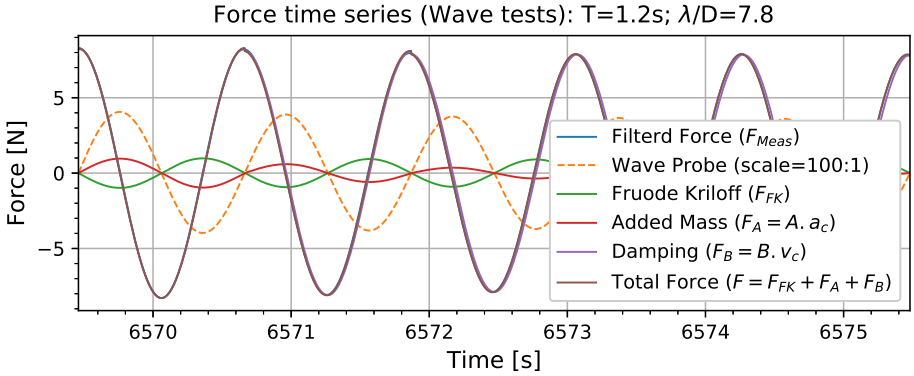
Force time series (Wave tests): T=1.2s; λ/D=7.8
Force [N]
Time [s]
Filterd Force (F_{Meas})
Wave Probe (scale=100:1)
Fruode Kriloff (F_{FK})
Added Mass ($F_A = A.a_c$)
Damping ($F_B = B.v_c$)
Total Force ($F = F_{FK} + F_A + F_B$)

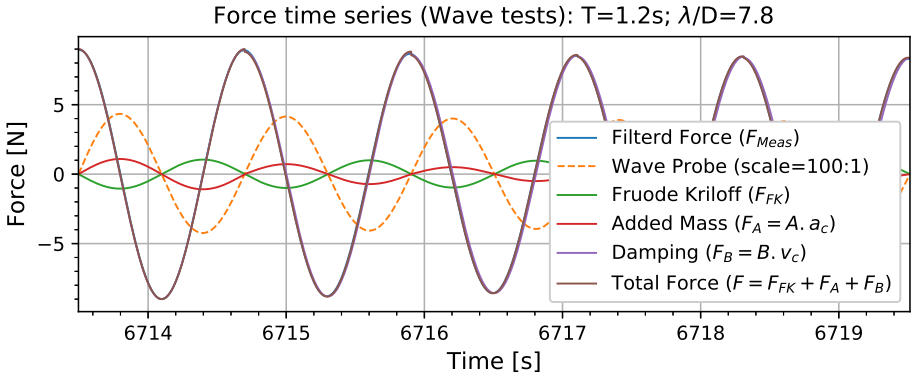
Force time series (Wave tests): T=1.2s; λ/D=7.8
Force [N]
Time [s]
Filterd Force (F_{Meas})
Wave Probe (scale=100:1)
Fruode Kriloff (F_{FK})
Added Mass ($F_A = A.a_c$)
Damping ($F_B = B.v_c$)
Total Force ($F = F_{FK} + F_A + F_B$)

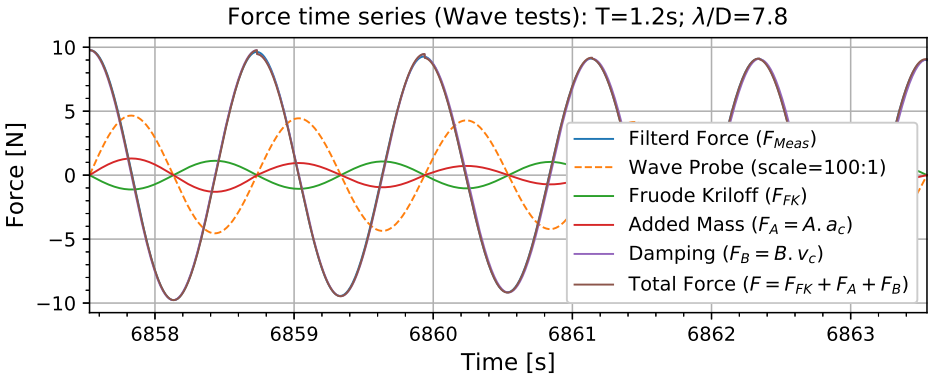
Force time series (Wave tests): T=1.2s; λ/D=7.8
Force [N]
Time [s]
Filterd Force (F_{Meas})
Wave Probe (scale=100:1)
Fruode Kriloff (F_{FK})
Added Mass ($F_A = A.a_c$)
Damping ($F_B = B.v_c$)
Total Force ($F = F_{FK} + F_A + F_B$)

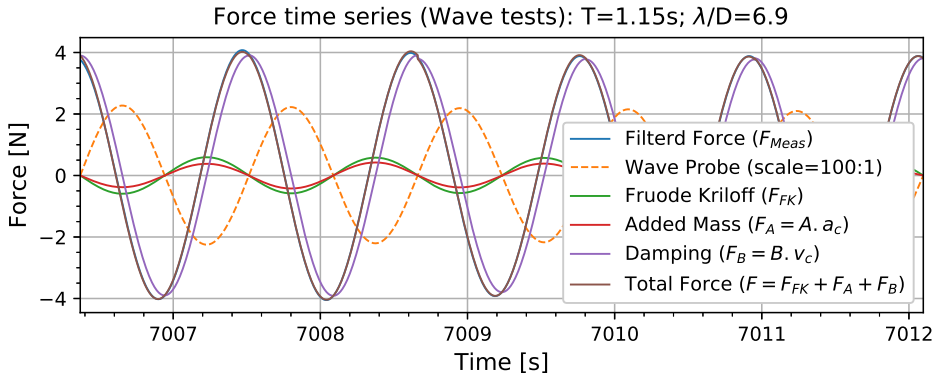
Force time series (Wave tests): T=1.15s; λ/D=6.9
Force [N]
Time [s]
Filterd Force (F_{Meas})
Wave Probe (scale=100:1)
Fruode Kriloff (F_{FK})
Added Mass ($F_A = A.a_c$)
Damping ($F_B = B.v_c$)
Total Force ($F = F_{FK} + F_A + F_B$)

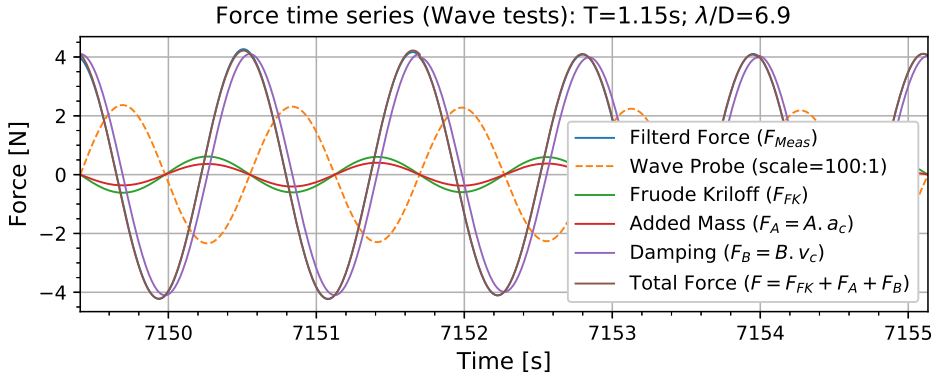
Force time series (Wave tests): T=1.15s; λ/D=6.9
Force [N]
Time [s]
Filterd Force (F_{Meas})
Wave Probe (scale=100:1)
Fruode Kriloff (F_{FK})
Added Mass ($F_A = A.a_c$)
Damping ($F_B = B.v_c$)
Total Force ($F = F_{FK} + F_A + F_B$)

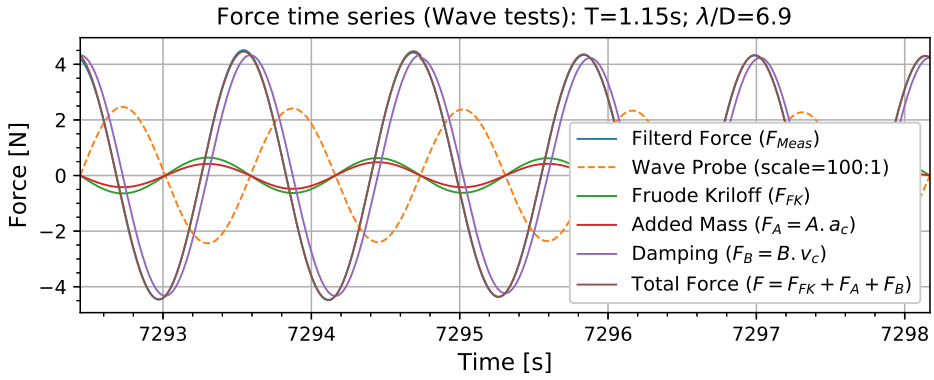
Force time series (Wave tests): T=1.15s; λ/D=6.9
Force [N]
Time [s]
Filterd Force (F_{Meas})
Wave Probe (scale=100:1)
Fruode Kriloff (F_{FK})
Added Mass ($F_A = A.a_c$)
Damping ($F_B = B.v_c$)
Total Force ($F = F_{FK} + F_A + F_B$)

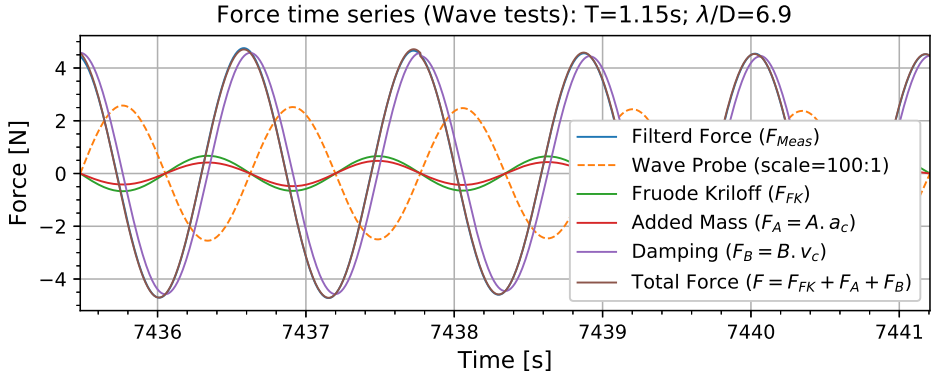
Force time series (Wave tests): T=1.15s; λ/D=6.9
Force [N]
Time [s]
Filterd Force (F_{Meas})
Wave Probe (scale=100:1)
Fruode Kriloff (F_{FK})
Added Mass ($F_A = A.\,a_c$)
Damping ($F_B = B.\,v_c$)
Total Force ($F = F_{FK} + F_A + F_B$)

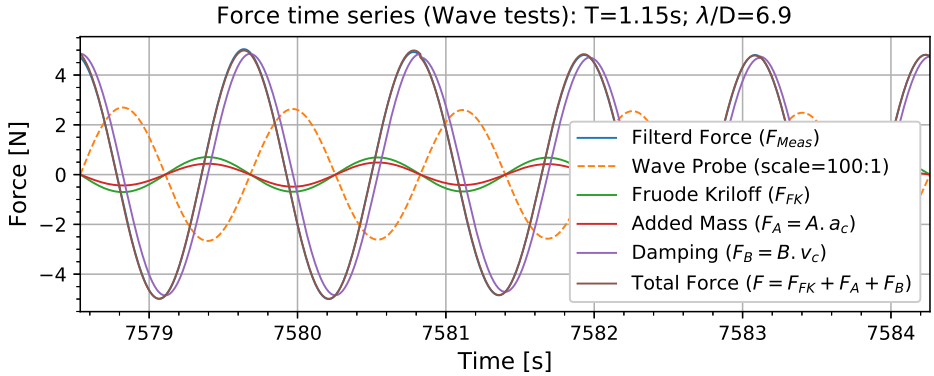
Force time series (Wave tests): T=1.15s; λ/D=6.9
Force [N]
Time [s]
Filterd Force (F_{Meas})
Wave Probe (scale=100:1)
Fruode Kriloff (F_{FK})
Added Mass ($F_A = A.\,a_c$)
Damping ($F_B = B.\,v_c$)
Total Force ($F = F_{FK} + F_A + F_B$)

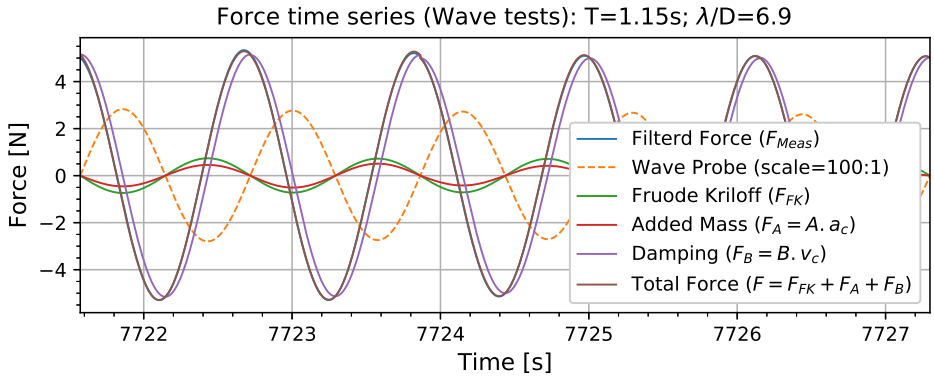
Force time series (Wave tests): T=1.15s; λ/D=6.9
Force [N]
Time [s]
Filterd Force (F_{Meas})
Wave Probe (scale=100:1)
Fruode Kriloff (F_{FK})
Added Mass ($F_A = A.\,a_c$)
Damping ($F_B = B.\,v_c$)
Total Force ($F = F_{FK} + F_A + F_B$)

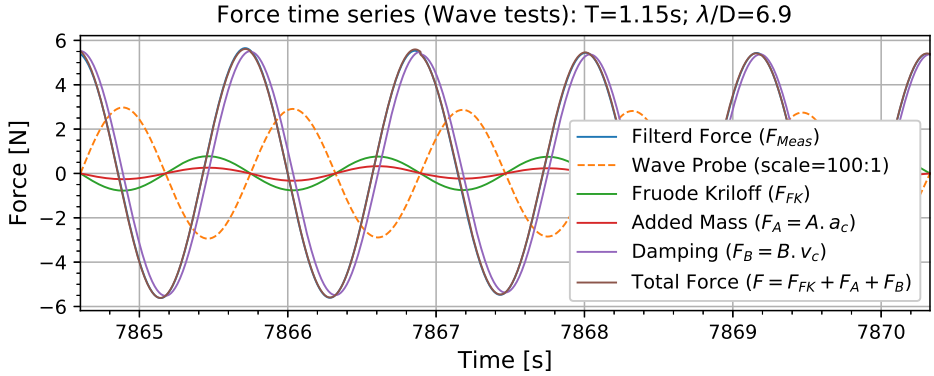
Force time series (Wave tests): T=1.15s; λ/D=6.9
Force [N]
Time [s]
Filterd Force (F_{Meas})
Wave Probe (scale=100:1)
Fruode Kriloff (F_{FK})
Added Mass ($F_A = A.a_c$)
Damping ($F_B = B.v_c$)
Total Force ($F = F_{FK} + F_A + F_B$)

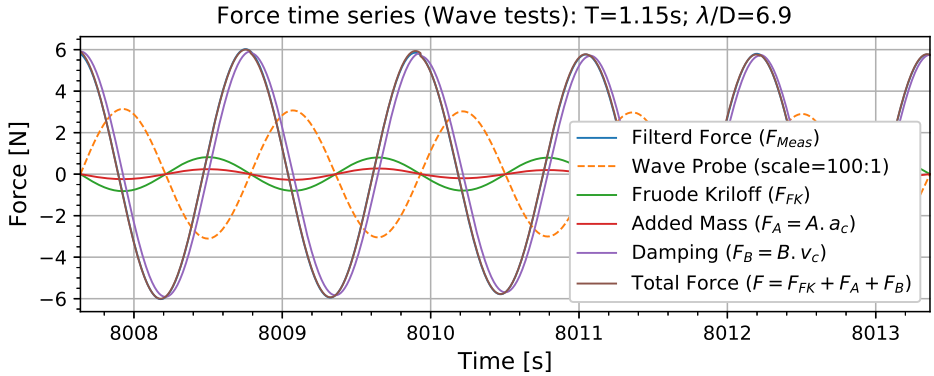
Force time series (Wave tests): T=1.15s; λ/D=6.9
Force [N]
Time [s]
Filterd Force (F_{Meas})
Wave Probe (scale=100:1)
Fruode Kriloff (F_{FK})
Added Mass ($F_A = A.a_c$)
Damping ($F_B = B.v_c$)
Total Force ($F = F_{FK} + F_A + F_B$)

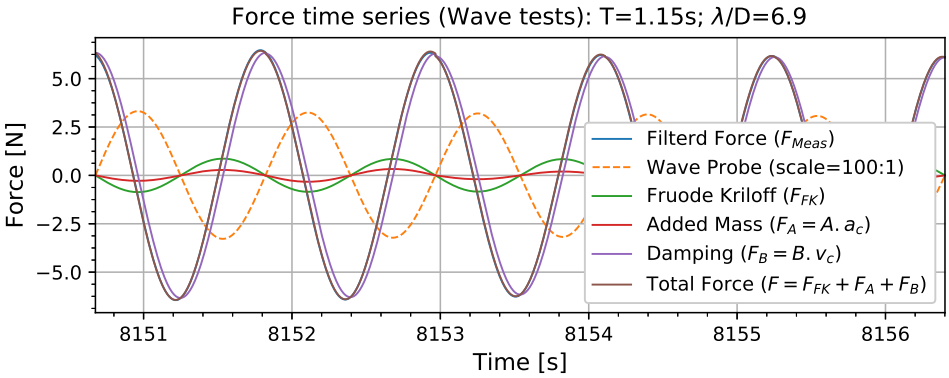
Force time series (Wave tests): T=1.15s; λ/D=6.9
Force [N]
Time [s]
Filterd Force (F_{Meas})
Wave Probe (scale=100:1)
Fruode Kriloff (F_{FK})
Added Mass ($F_A = A.a_c$)
Damping ($F_B = B.v_c$)
Total Force ($F = F_{FK} + F_A + F_B$)

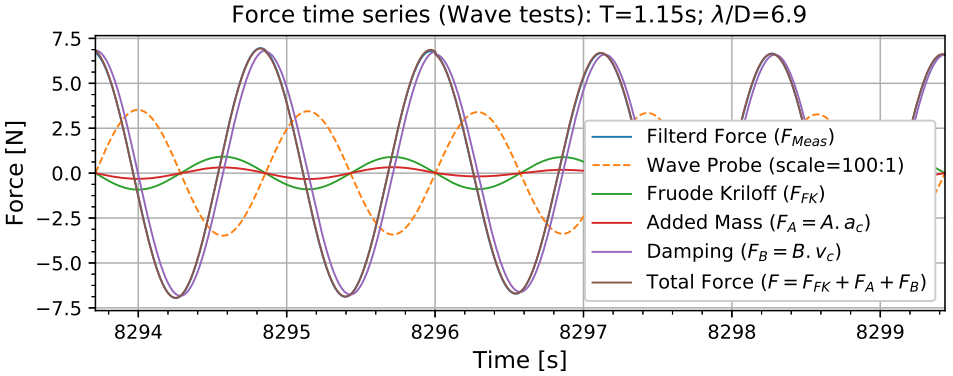
Force time series (Wave tests): T=1.15s; λ/D=6.9
Force [N]
Time [s]
Filterd Force (F_{Meas})
Wave Probe (scale=100:1)
Fruode Kriloff (F_{FK})
Added Mass ($F_A = A.a_c$)
Damping ($F_B = B.v_c$)
Total Force ($F = F_{FK} + F_A + F_B$)

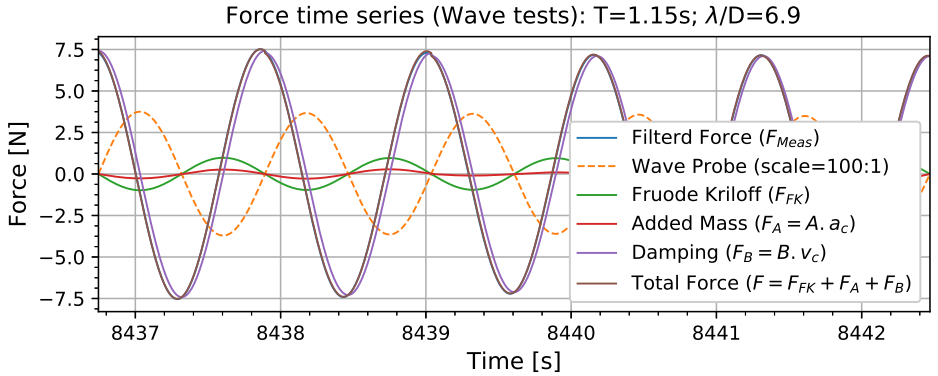
Force time series (Wave tests): T=1.15s; λ/D=6.9
Force [N]
Time [s]
Filterd Force (F_{Meas})
Wave Probe (scale=100:1)
Fruode Kriloff (F_{FK})
Added Mass ($F_A = A.a_c$)
Damping ($F_B = B.v_c$)
Total Force ($F = F_{FK} + F_A + F_B$)

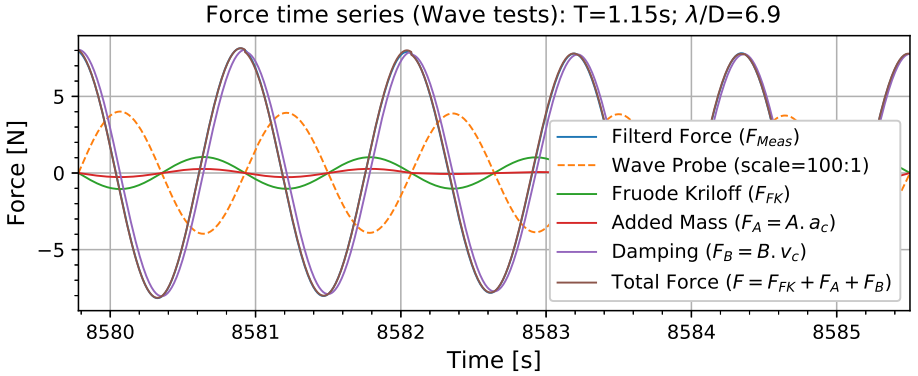
Force time series (Wave tests): T=1.15s; λ/D=6.9
Force [N]
Time [s]
Filterd Force (F_{Meas})
Wave Probe (scale=100:1)
Fruode Kriloff (F_{FK})
Added Mass ($F_A = A.a_c$)
Damping ($F_B = B.v_c$)
Total Force ($F = F_{FK} + F_A + F_B$)

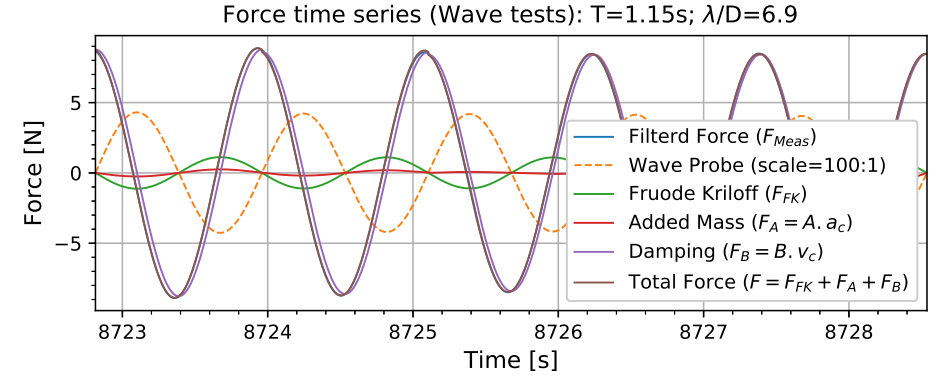
Force time series (Wave tests): T=1.15s; λ/D=6.9
Force [N]
Time [s]
Filterd Force (F_{Meas})
Wave Probe (scale=100:1)
Fruode Kriloff (F_{FK})
Added Mass ($F_A = A.a_c$)
Damping ($F_B = B.v_c$)
Total Force ($F = F_{FK} + F_A + F_B$)

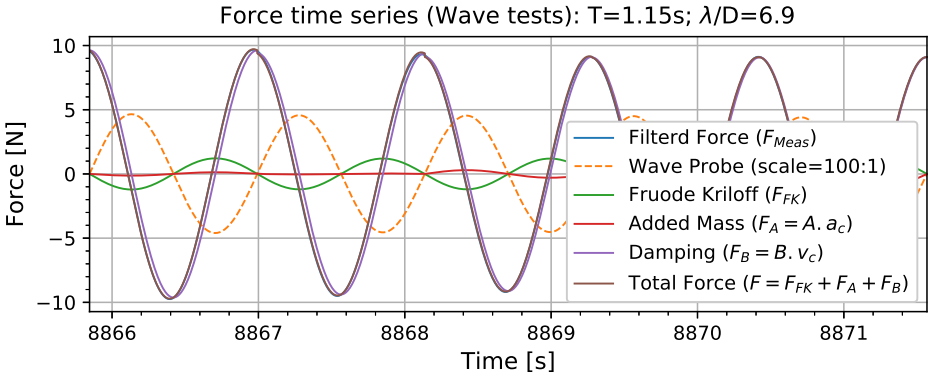
Force time series (Wave tests): T=1.15s; λ/D=6.9
Force [N]
Time [s]
Filterd Force (F_{Meas})
Wave Probe (scale=100:1)
Fruode Kriloff (F_{FK})
Added Mass ($F_A = A.a_c$)
Damping ($F_B = B.v_c$)
Total Force ($F = F_{FK} + F_A + F_B$)

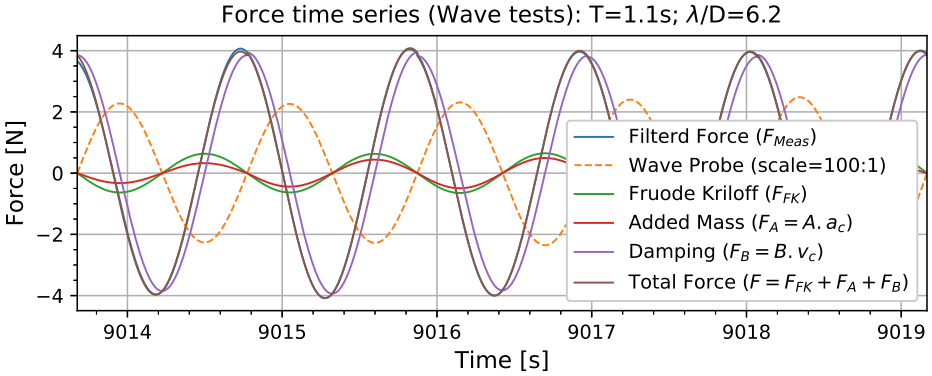
Force time series (Wave tests): T=1.1s; λ/D=6.2
Force [N]
Time [s]
Filterd Force (F_{Meas})
Wave Probe (scale=100:1)
Fruode Kriloff (F_{FK})
Added Mass ($F_A = A.a_c$)
Damping ($F_B = B.v_c$)
Total Force ($F = F_{FK} + F_A + F_B$)

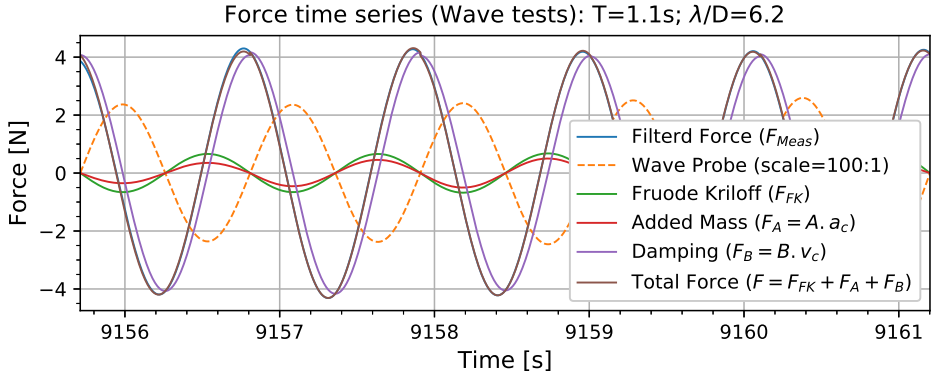
Force time series (Wave tests): T=1.1s; λ/D=6.2
Force [N]
Time [s]
Filterd Force (F_{Meas})
Wave Probe (scale=100:1)
Fruode Kriloff (F_{FK})
Added Mass ($F_A = A.a_c$)
Damping ($F_B = B.v_c$)
Total Force ($F = F_{FK} + F_A + F_B$)

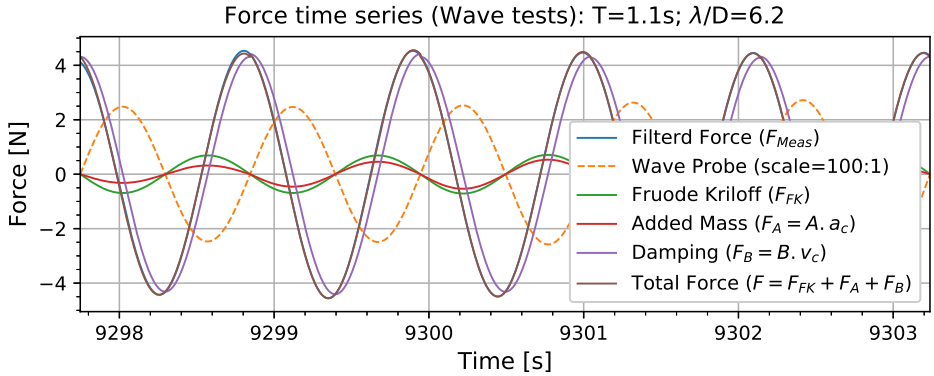
Force time series (Wave tests): T=1.1s; λ/D=6.2
Force [N]
Time [s]
Filterd Force (F_{Meas})
Wave Probe (scale=100:1)
Fruode Kriloff (F_{FK})
Added Mass ($F_A = A.a_c$)
Damping ($F_B = B.v_c$)
Total Force ($F = F_{FK} + F_A + F_B$)

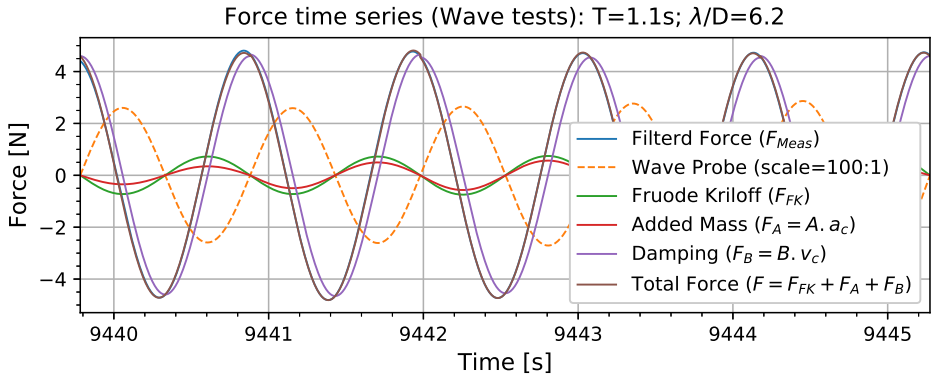
Force time series (Wave tests): T=1.1s; λ/D=6.2
Force [N]
Time [s]
Filterd Force (F_{Meas})
Wave Probe (scale=100:1)
Fruode Kriloff (F_{FK})
Added Mass ($F_A = A.a_c$)
Damping ($F_B = B.v_c$)
Total Force ($F = F_{FK} + F_A + F_B$)

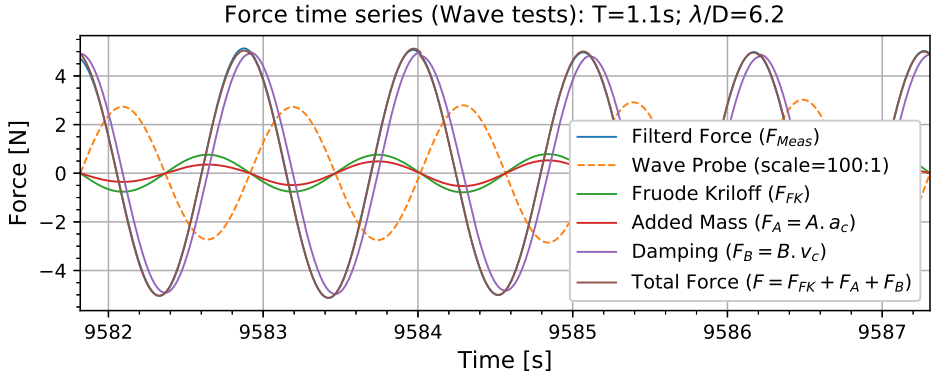
Force time series (Wave tests): T=1.1s; λ/D=6.2
Force [N]
Time [s]
Filterd Force (F_{Meas})
Wave Probe (scale=100:1)
Fruode Kriloff (F_{FK})
Added Mass ($F_A = A.a_c$)
Damping ($F_B = B.v_c$)
Total Force ($F = F_{FK} + F_A + F_B$)

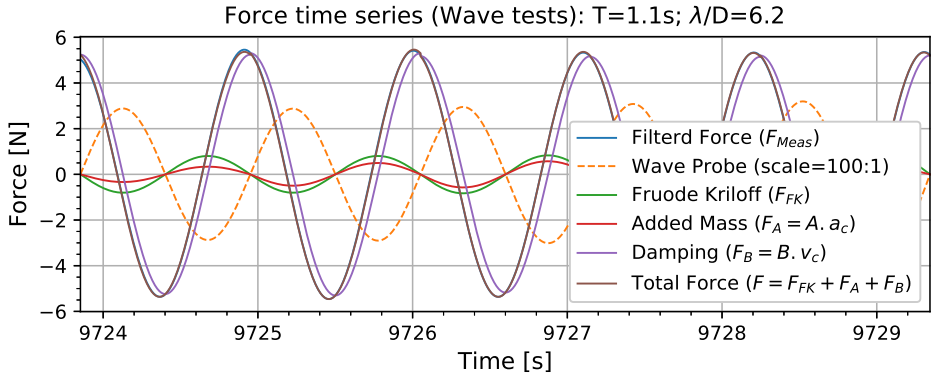
Force time series (Wave tests): T=1.1s; λ/D=6.2
Force [N]
Time [s]
Filterd Force (F_{Meas})
Wave Probe (scale=100:1)
Fruode Kriloff (F_{FK})
Added Mass ($F_A = A.a_c$)
Damping ($F_B = B.v_c$)
Total Force ($F = F_{FK} + F_A + F_B$)

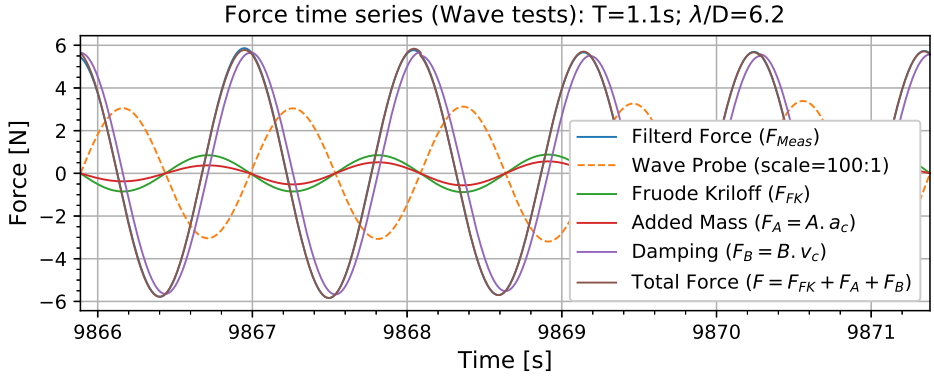
Force time series (Wave tests): T=1.1s; λ/D=6.2
Force [N]
Time [s]
Filterd Force (F_{Meas})
Wave Probe (scale=100:1)
Fruode Kriloff (F_{FK})
Added Mass ($F_A = A.a_c$)
Damping ($F_B = B.v_c$)
Total Force ($F = F_{FK} + F_A + F_B$)

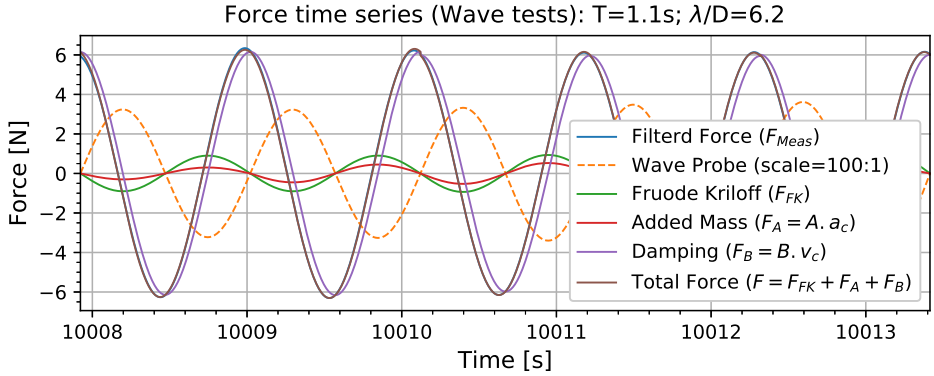
Force time series (Wave tests): T=1.1s; λ/D=6.2
Force [N]
Time [s]
Filterd Force (F_{Meas})
Wave Probe (scale=100:1)
Fruode Kriloff (F_{FK})
Added Mass ($F_A = A.a_c$)
Damping ($F_B = B.v_c$)
Total Force ($F = F_{FK} + F_A + F_B$)

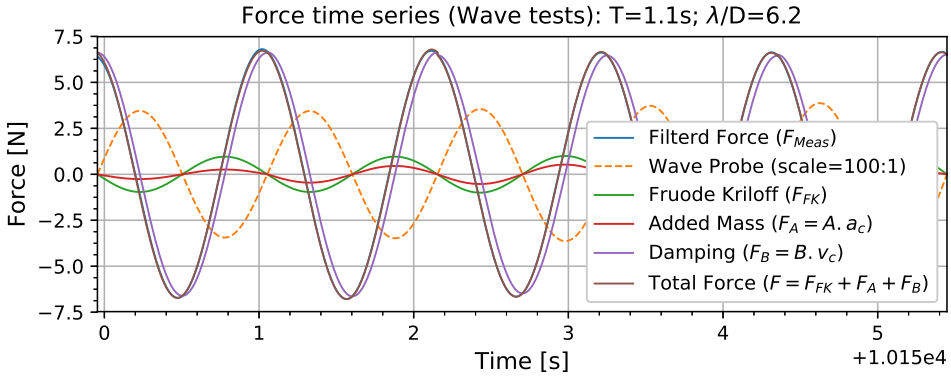
Force time series (Wave tests): T=1.1s; λ/D=6.2
Force [N]
Time [s]
+1.015e4
Filterd Force (F_{Meas})
Wave Probe (scale=100:1)
Fruode Kriloff (F_{FK})
Added Mass ($F_A = A.a_c$)
Damping ($F_B = B.v_c$)
Total Force ($F = F_{FK} + F_A + F_B$)

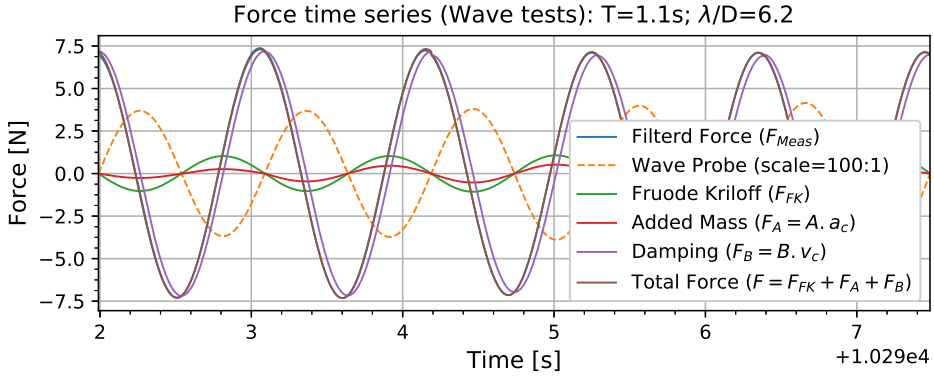
Force time series (Wave tests): T=1.1s; λ/D=6.2
Force [N]
Time [s]
+1.029e4
Filterd Force (F_{Meas})
Wave Probe (scale=100:1)
Fruode Kriloff (F_{FK})
Added Mass ($F_A = A.a_c$)
Damping ($F_B = B.v_c$)
Total Force ($F = F_{FK} + F_A + F_B$)

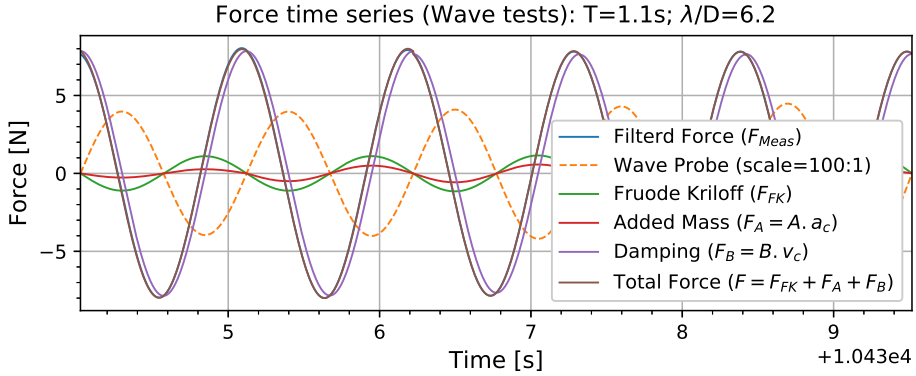
Force time series (Wave tests): T=1.1s; λ/D=6.2
Force [N]
Time [s]
+1.043e4
Filterd Force (F_{Meas})
Wave Probe (scale=100:1)
Fruode Kriloff (F_{FK})
Added Mass ($F_A = A.a_c$)
Damping ($F_B = B.v_c$)
Total Force ($F = F_{FK} + F_A + F_B$)

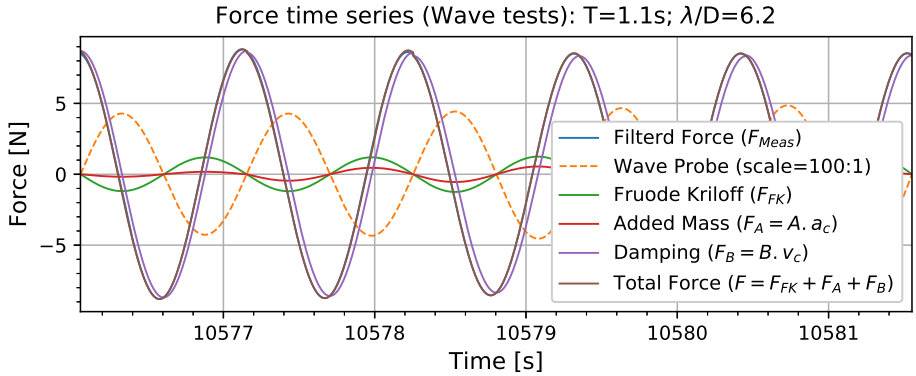
Force time series (Wave tests): T=1.1s; λ/D=6.2
Force [N]
Time [s]
Filterd Force (F_{Meas})
Wave Probe (scale=100:1)
Fruode Kriloff (F_{FK})
Added Mass ($F_A = A.a_c$)
Damping ($F_B = B.v_c$)
Total Force ($F = F_{FK} + F_A + F_B$)

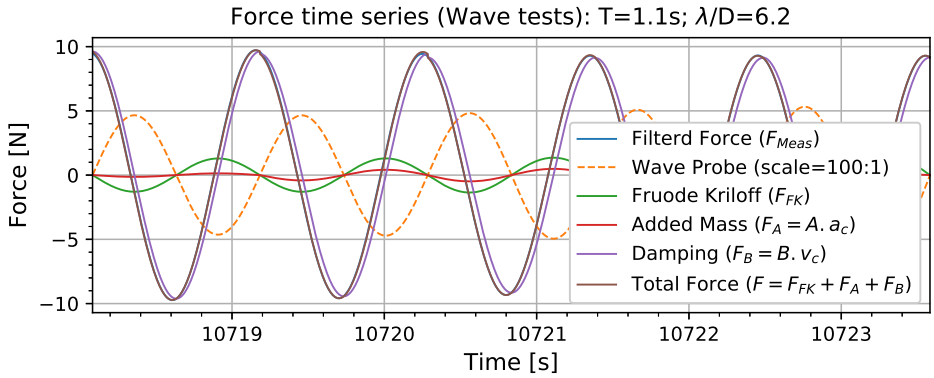
Force time series (Wave tests): T=1.1s; λ/D=6.2
Force [N]
Time [s]
Filterd Force (F_{Meas})
Wave Probe (scale=100:1)
Fruode Kriloff (F_{FK})
Added Mass ($F_A = A.a_c$)
Damping ($F_B = B.v_c$)
Total Force ($F = F_{FK} + F_A + F_B$)

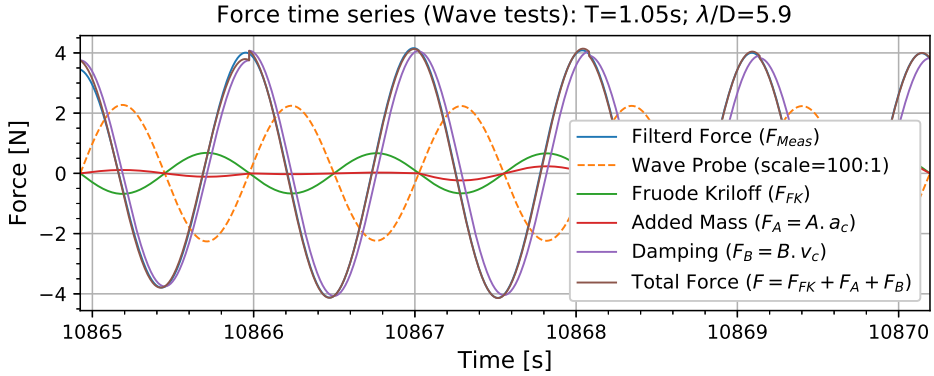
Force time series (Wave tests): T=1.05s; λ/D=5.9
Force [N]
Time [s]
Filterd Force (F_{Meas})
Wave Probe (scale=100:1)
Fruode Kriloff (F_{FK})
Added Mass ($F_A = A.a_c$)
Damping ($F_B = B.v_c$)
Total Force ($F = F_{FK} + F_A + F_B$)

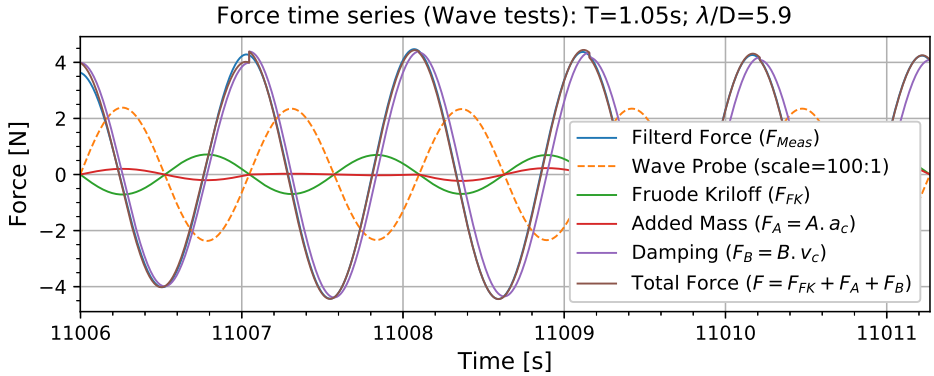
Force time series (Wave tests): T=1.05s; λ/D=5.9
Force [N]
Time [s]
Filterd Force (F_{Meas})
Wave Probe (scale=100:1)
Fruode Kriloff (F_{FK})
Added Mass ($F_A = A.a_c$)
Damping ($F_B = B.v_c$)
Total Force ($F = F_{FK} + F_A + F_B$)

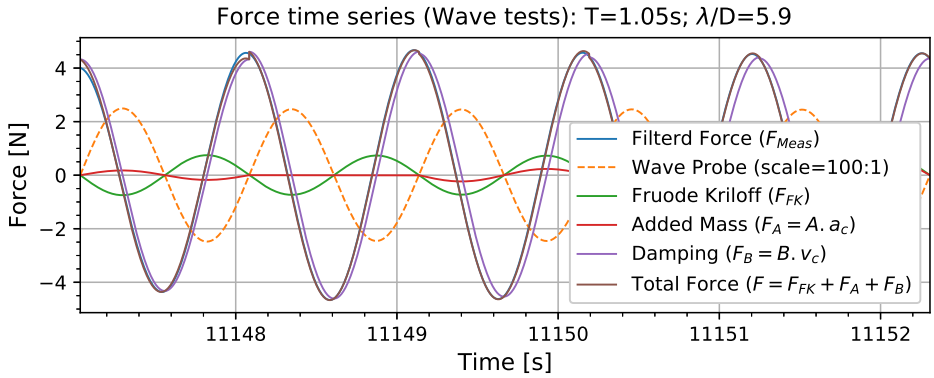
Force time series (Wave tests): T=1.05s; λ/D=5.9
Force [N]
Time [s]
Filterd Force (F_{Meas})
Wave Probe (scale=100:1)
Fruode Kriloff (F_{FK})
Added Mass ($F_A = A.a_c$)
Damping ($F_B = B.v_c$)
Total Force ($F = F_{FK} + F_A + F_B$)

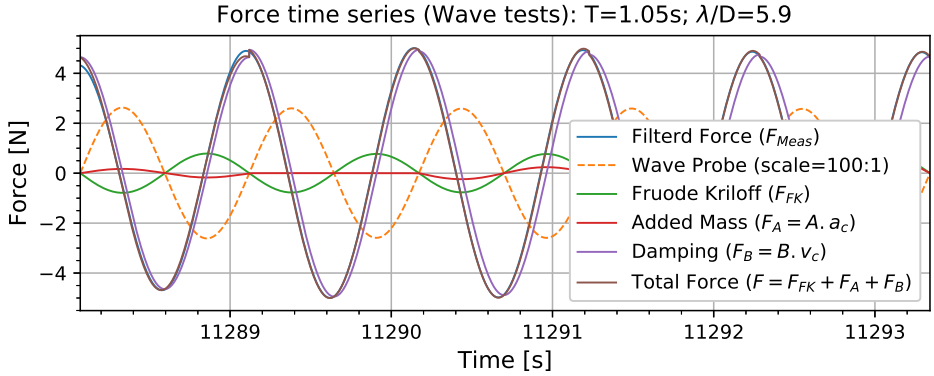
Force time series (Wave tests): T=1.05s; λ/D=5.9
Force [N]
Time [s]
11289
11290
11291
11292
11293
Filterd Force (F_{Meas})
Wave Probe (scale=100:1)
Fruode Kriloff (F_{FK})
Added Mass ($F_A = A.a_c$)
Damping ($F_B = B.v_c$)
Total Force ($F = F_{FK} + F_A + F_B$)

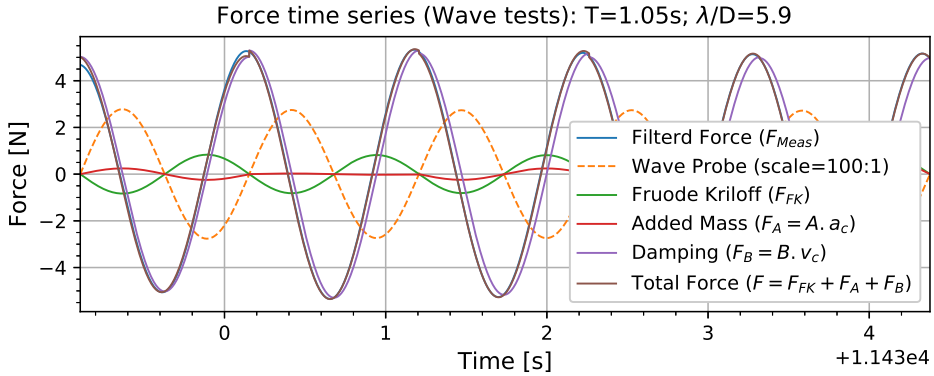
Force time series (Wave tests): T=1.05s; λ/D=5.9
Force [N]
Time [s]
+1.143e4
Filterd Force (F_{Meas})
Wave Probe (scale=100:1)
Fruode Kriloff (F_{FK})
Added Mass ($F_A = A.a_c$)
Damping ($F_B = B.v_c$)
Total Force ($F = F_{FK} + F_A + F_B$)

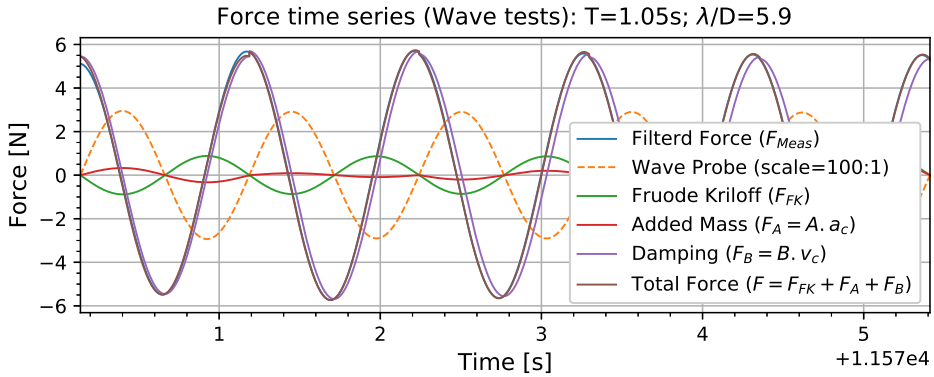
Force time series (Wave tests): T=1.05s; λ/D=5.9
Force [N]
Time [s]
+1.157e4
Filterd Force (F_{Meas})
Wave Probe (scale=100:1)
Fruode Kriloff (F_{FK})
Added Mass ($F_A = A.a_c$)
Damping ($F_B = B.v_c$)
Total Force ($F = F_{FK} + F_A + F_B$)

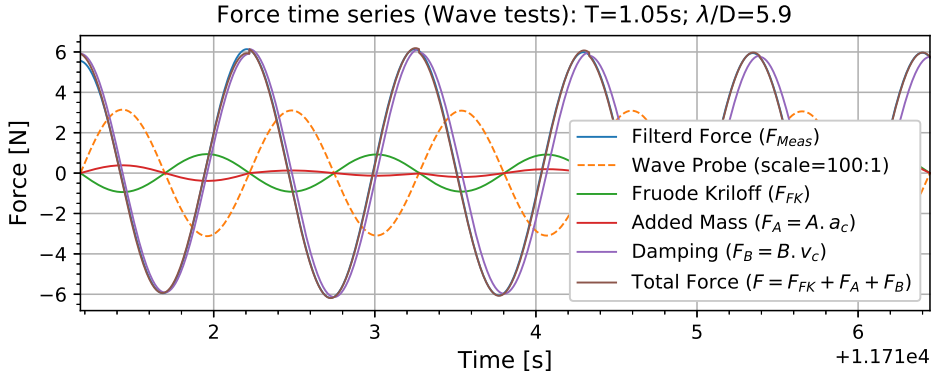
Force time series (Wave tests): T=1.05s; λ/D=5.9
Force [N]
Time [s]
+1.171e4
Filterd Force (F_{Meas})
Wave Probe (scale=100:1)
Fruode Kriloff (F_{FK})
Added Mass ($F_A = A.a_c$)
Damping ($F_B = B.v_c$)
Total Force ($F = F_{FK} + F_A + F_B$)

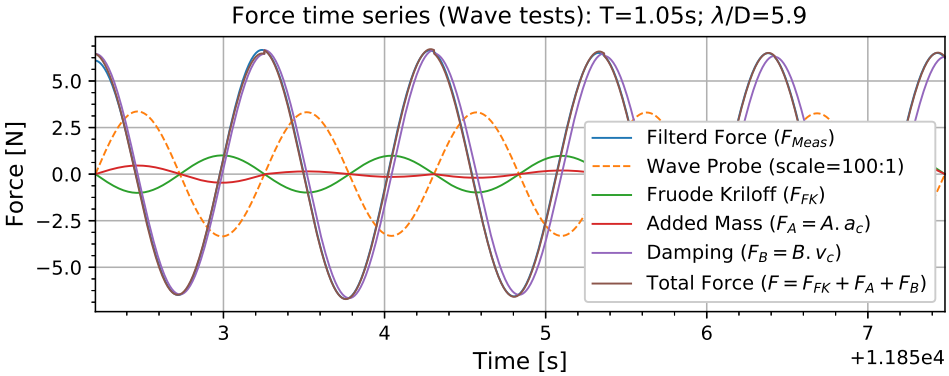
Force time series (Wave tests): T=1.05s; λ/D=5.9
Force [N]
Time [s]
+1.185e4
Filterd Force (F_{Meas})
Wave Probe (scale=100:1)
Fruode Kriloff (F_{FK})
Added Mass ($F_A = A.a_c$)
Damping ($F_B = B.v_c$)
Total Force ($F = F_{FK} + F_A + F_B$)

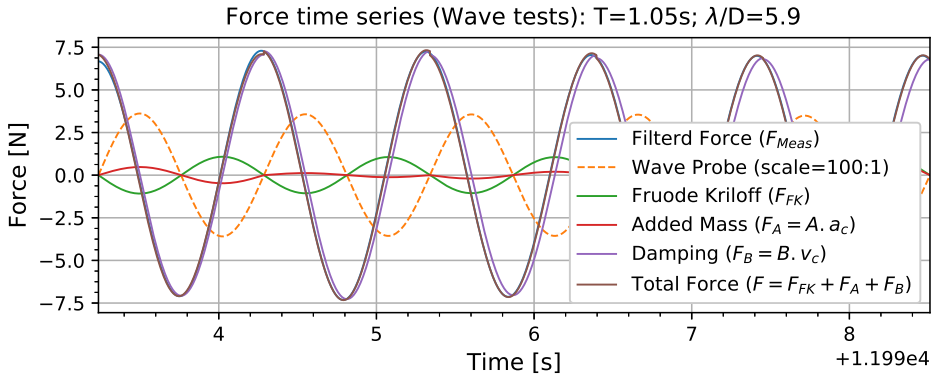
Force time series (Wave tests): T=1.05s; λ/D=5.9
Force [N]
Time [s]
+1.199e4
Filterd Force (F_{Meas})
Wave Probe (scale=100:1)
Fruode Kriloff (F_{FK})
Added Mass ($F_A = A.a_c$)
Damping ($F_B = B.v_c$)
Total Force ($F = F_{FK} + F_A + F_B$)

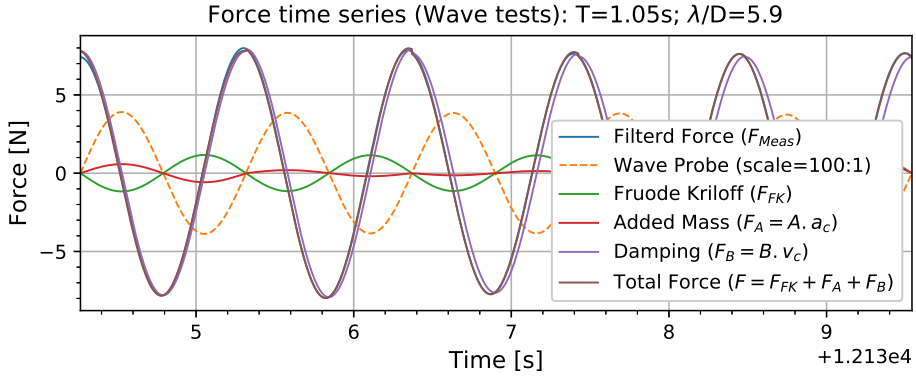
Force time series (Wave tests): T=1.05s; λ/D=5.9
Force [N]
5
0
−5
5
6
7
8
9
+1.213e4
Time [s]
Filterd Force (F_{Meas})
Wave Probe (scale=100:1)
Fruode Kriloff (F_{FK})
Added Mass ($F_A = A.a_c$)
Damping ($F_B = B.v_c$)
Total Force ($F = F_{FK} + F_A + F_B$)

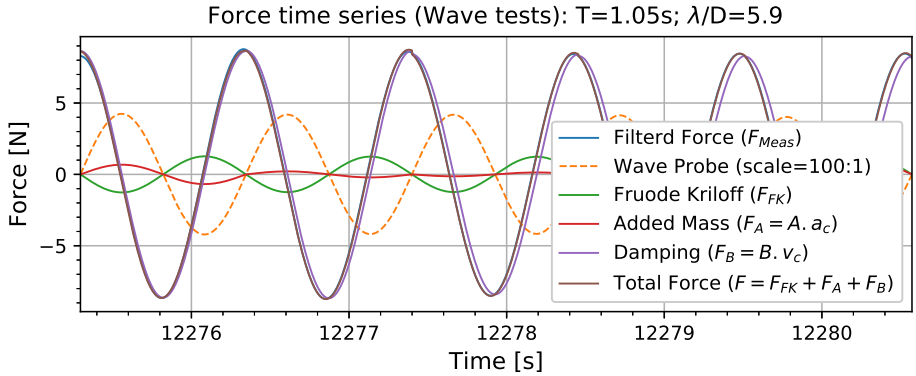
Force time series (Wave tests): T=1.05s; λ/D=5.9
Force [N]
5
0
−5
12276
12277
12278
12279
12280
Time [s]
Filterd Force (F_{Meas})
Wave Probe (scale=100:1)
Fruode Kriloff (F_{FK})
Added Mass ($F_A = A.a_c$)
Damping ($F_B = B.v_c$)
Total Force ($F = F_{FK} + F_A + F_B$)

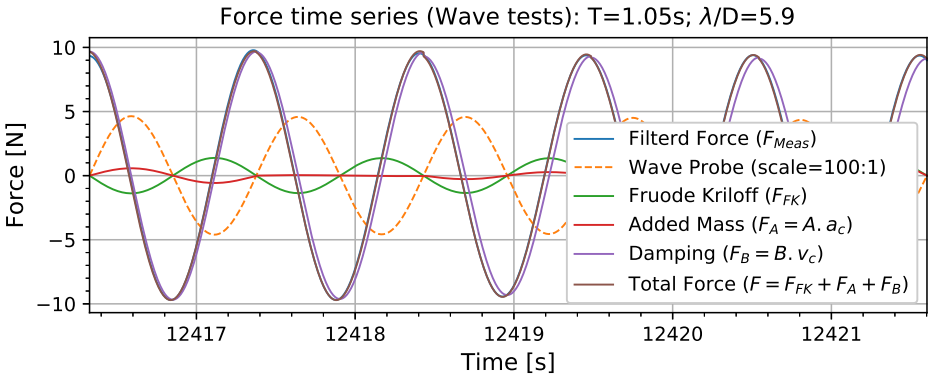
Force time series (Wave tests): T=1.05s; λ/D=5.9
Force [N]
10
5
0
−5
−10
12417
12418
12419
12420
12421
Time [s]
Filterd Force (F_{Meas})
Wave Probe (scale=100:1)
Fruode Kriloff (F_{FK})
Added Mass ($F_A = A.a_c$)
Damping ($F_B = B.v_c$)
Total Force ($F = F_{FK} + F_A + F_B$)

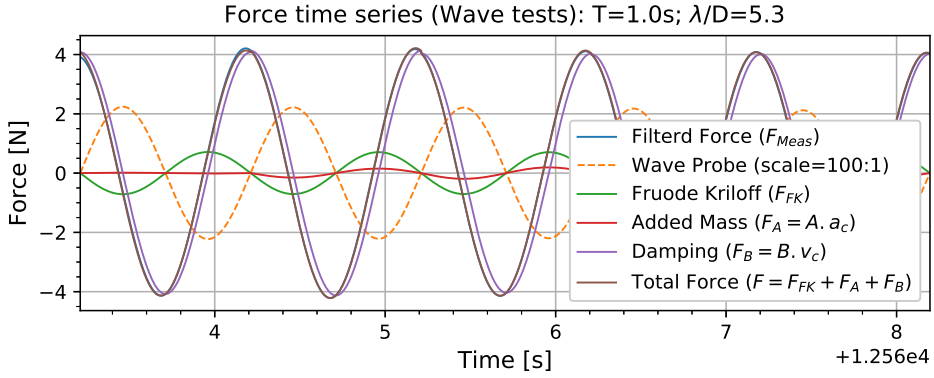
Force time series (Wave tests): T=1.0s; λ/D=5.3
Force [N]
Time [s]
+1.256e4
Filterd Force (F_{Meas})
Wave Probe (scale=100:1)
Fruode Kriloff (F_{FK})
Added Mass ($F_A = A.\,a_c$)
Damping ($F_B = B.\,v_c$)
Total Force ($F = F_{FK} + F_A + F_B$)

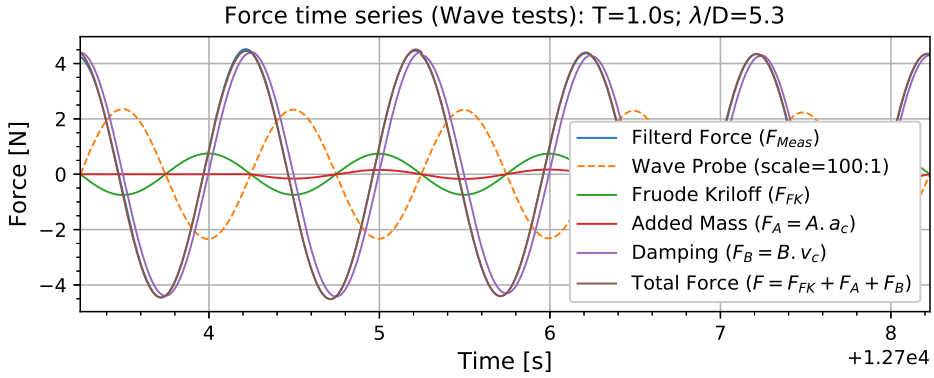
Force time series (Wave tests): T=1.0s; λ/D=5.3
Force [N]
Time [s]
+1.27e4
Filterd Force (F_{Meas})
Wave Probe (scale=100:1)
Fruode Kriloff (F_{FK})
Added Mass ($F_A = A.\,a_c$)
Damping ($F_B = B.\,v_c$)
Total Force ($F = F_{FK} + F_A + F_B$)

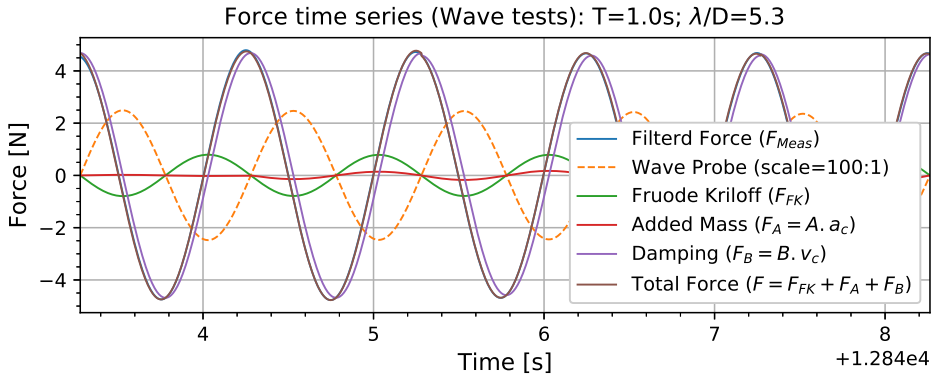
Force time series (Wave tests): T=1.0s; λ/D=5.3
Force [N]
Time [s]
+1.284e4
Filterd Force (F_{Meas})
Wave Probe (scale=100:1)
Fruode Kriloff (F_{FK})
Added Mass ($F_A = A.\,a_c$)
Damping ($F_B = B.\,v_c$)
Total Force ($F = F_{FK} + F_A + F_B$)

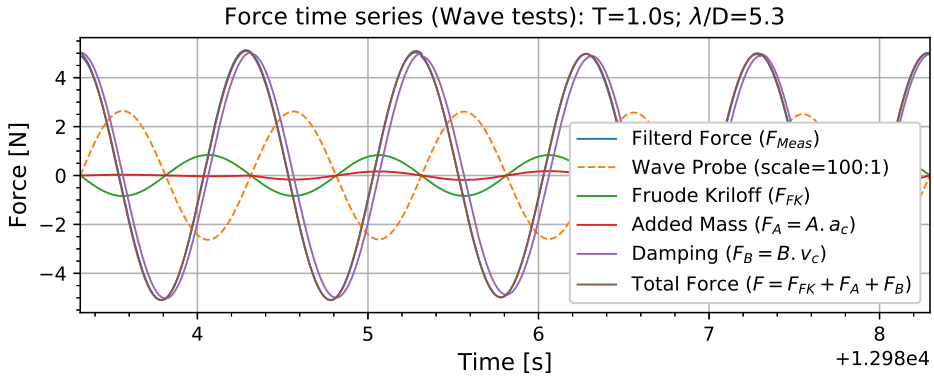
Force time series (Wave tests): T=1.0s; λ/D=5.3
Force [N]
Time [s]
+1.298e4
Filterd Force (F_{Meas})
Wave Probe (scale=100:1)
Fruode Kriloff (F_{FK})
Added Mass ($F_A = A.a_c$)
Damping ($F_B = B.v_c$)
Total Force ($F = F_{FK} + F_A + F_B$)

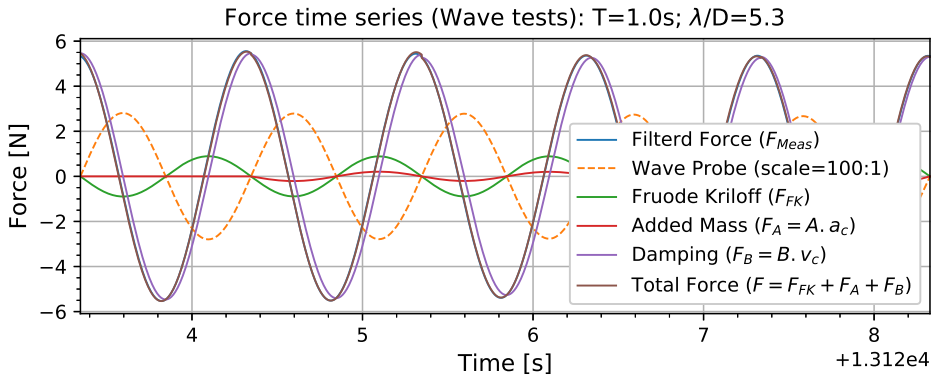
Force time series (Wave tests): T=1.0s; λ/D=5.3
Force [N]
Time [s]
+1.312e4
Filterd Force (F_{Meas})
Wave Probe (scale=100:1)
Fruode Kriloff (F_{FK})
Added Mass ($F_A = A.a_c$)
Damping ($F_B = B.v_c$)
Total Force ($F = F_{FK} + F_A + F_B$)

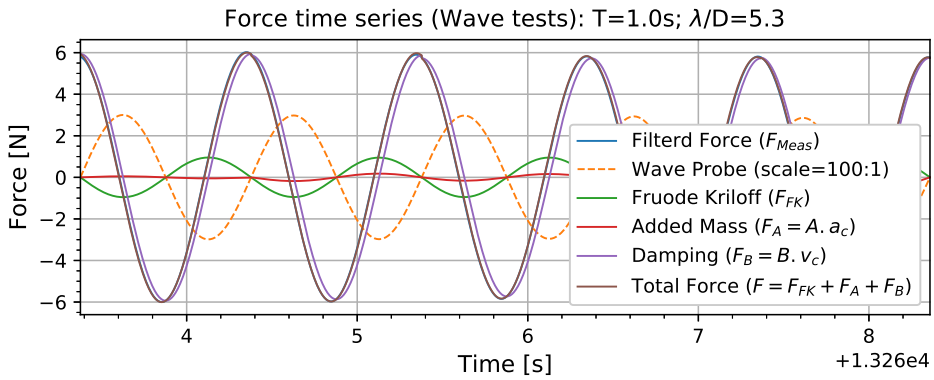
Force time series (Wave tests): T=1.0s; λ/D=5.3
Force [N]
Time [s]
+1.326e4
Filterd Force (F_{Meas})
Wave Probe (scale=100:1)
Fruode Kriloff (F_{FK})
Added Mass ($F_A = A.a_c$)
Damping ($F_B = B.v_c$)
Total Force ($F = F_{FK} + F_A + F_B$)

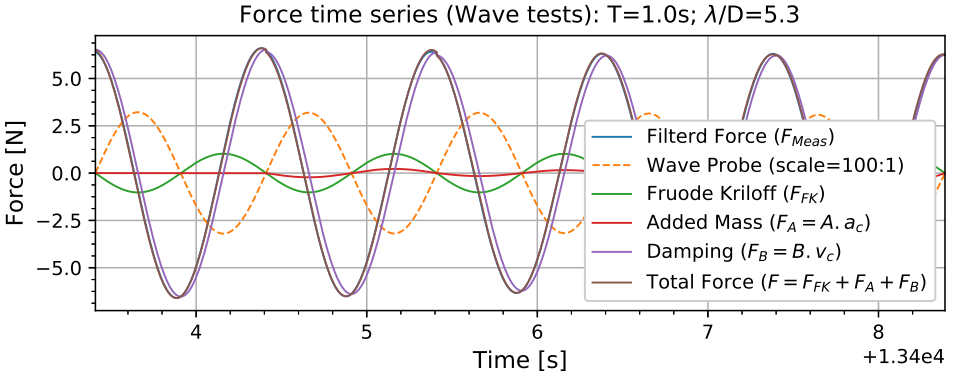
Force time series (Wave tests): T=1.0s; λ/D=5.3
Force [N]
5.0
2.5
0.0
−2.5
−5.0
4
5
6
7
8
Time [s]
+1.34e4
Filterd Force (F_{Meas})
Wave Probe (scale=100:1)
Fruode Kriloff (F_{FK})
Added Mass ($F_A = A.a_c$)
Damping ($F_B = B.v_c$)
Total Force ($F = F_{FK} + F_A + F_B$)

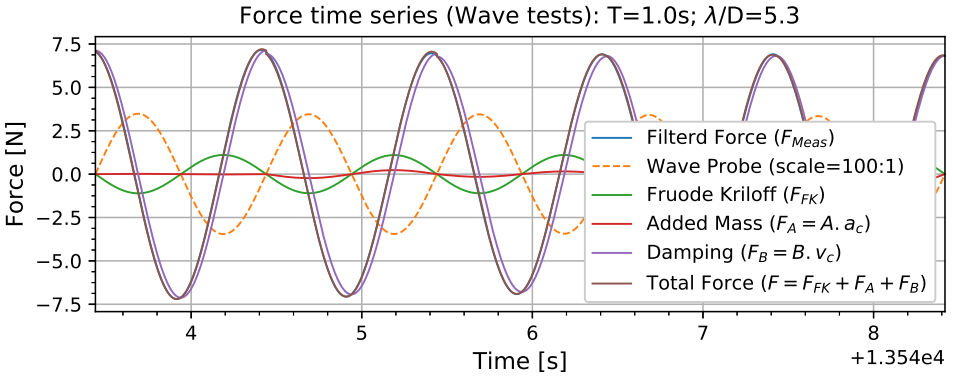
Force time series (Wave tests): T=1.0s; λ/D=5.3
Force [N]
7.5
5.0
2.5
0.0
−2.5
−5.0
−7.5
4
5
6
7
8
Time [s]
+1.354e4
Filterd Force (F_{Meas})
Wave Probe (scale=100:1)
Fruode Kriloff (F_{FK})
Added Mass ($F_A = A.a_c$)
Damping ($F_B = B.v_c$)
Total Force ($F = F_{FK} + F_A + F_B$)

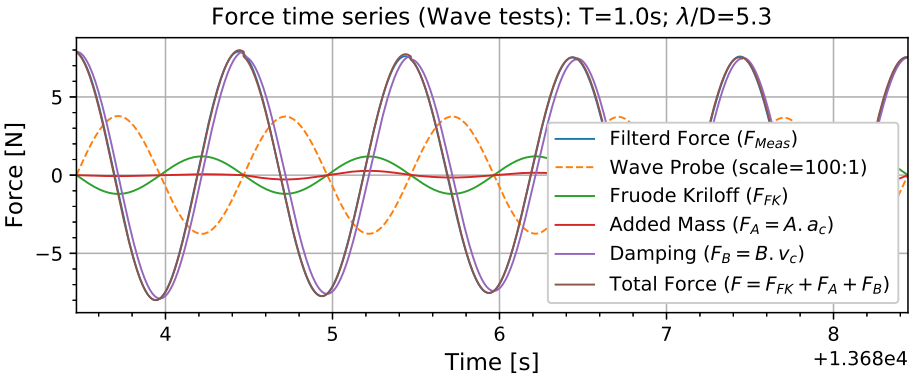
Force time series (Wave tests): T=1.0s; λ/D=5.3
Force [N]
5
0
−5
4
5
6
7
8
Time [s]
+1.368e4
Filterd Force (F_{Meas})
Wave Probe (scale=100:1)
Fruode Kriloff (F_{FK})
Added Mass ($F_A = A.a_c$)
Damping ($F_B = B.v_c$)
Total Force ($F = F_{FK} + F_A + F_B$)

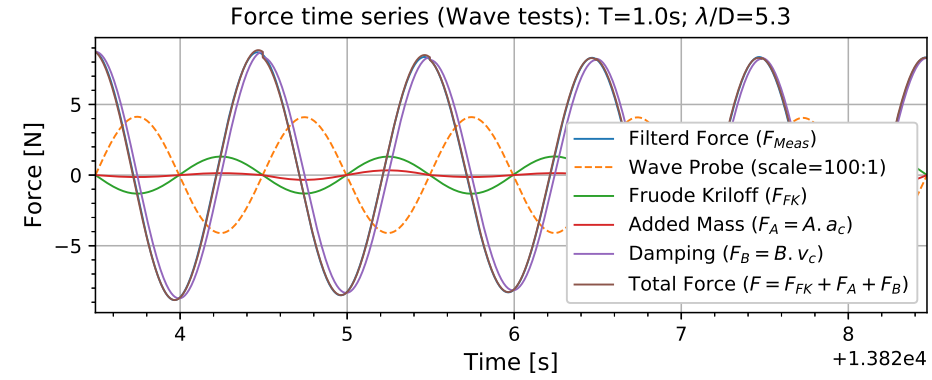
Force time series (Wave tests): T=1.0s; λ/D=5.3
Force [N]
Time [s]
+1.382e4
Filterd Force (F_{Meas})
Wave Probe (scale=100:1)
Fruode Kriloff (F_{FK})
Added Mass ($F_A = A.a_c$)
Damping ($F_B = B.v_c$)
Total Force ($F = F_{FK} + F_A + F_B$)

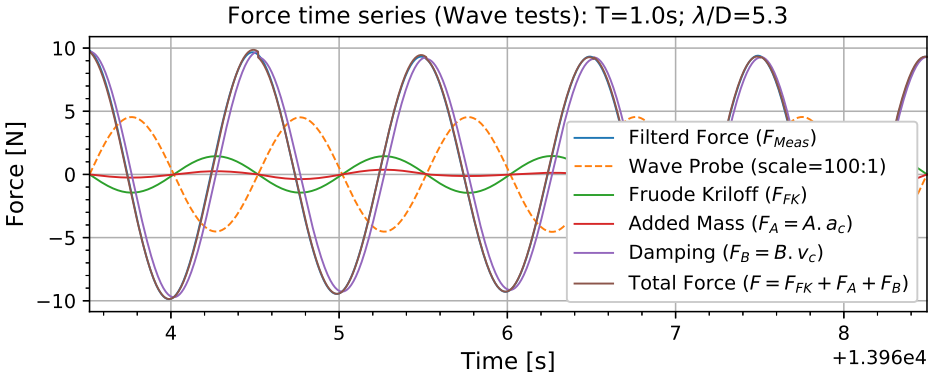
Force time series (Wave tests): T=1.0s; λ/D=5.3
Force [N]
Time [s]
+1.396e4
Filterd Force (F_{Meas})
Wave Probe (scale=100:1)
Fruode Kriloff (F_{FK})
Added Mass ($F_A = A.a_c$)
Damping ($F_B = B.v_c$)
Total Force ($F = F_{FK} + F_A + F_B$)

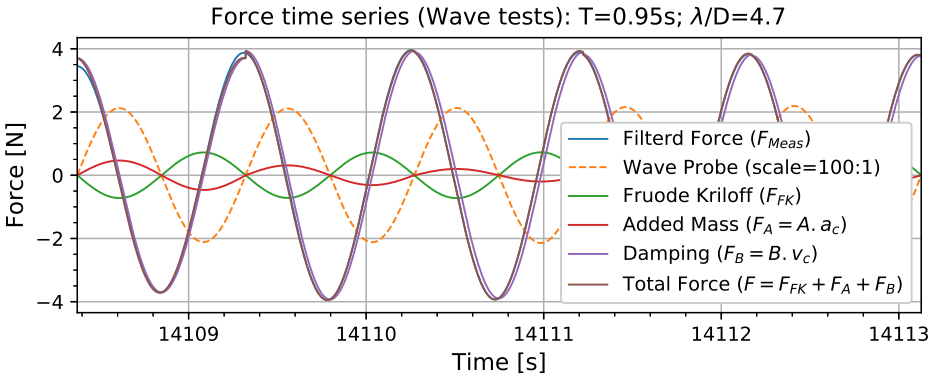
Force time series (Wave tests): T=0.95s; λ/D=4.7
Force [N]
Time [s]
Filterd Force (F_{Meas})
Wave Probe (scale=100:1)
Fruode Kriloff (F_{FK})
Added Mass ($F_A = A.a_c$)
Damping ($F_B = B.v_c$)
Total Force ($F = F_{FK} + F_A + F_B$)

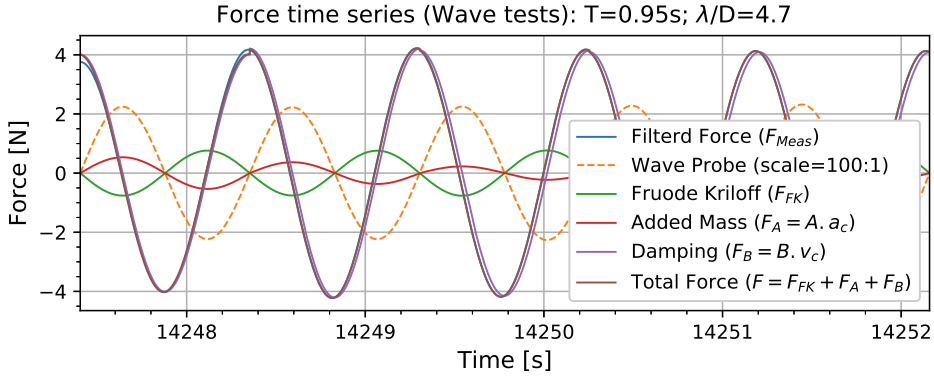
Force time series (Wave tests): T=0.95s; λ/D=4.7
Force [N]
Time [s]
Filterd Force (F_{Meas})
Wave Probe (scale=100:1)
Fruode Kriloff (F_{FK})
Added Mass ($F_A = A.a_c$)
Damping ($F_B = B.v_c$)
Total Force ($F = F_{FK} + F_A + F_B$)

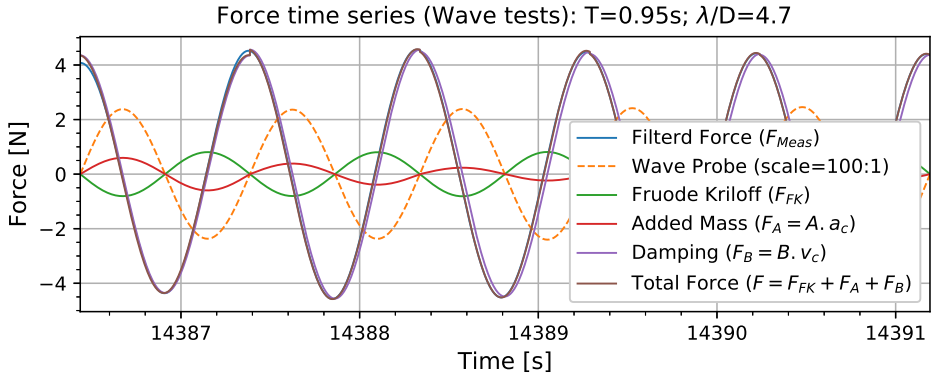
Force time series (Wave tests): T=0.95s; λ/D=4.7
Force [N]
Time [s]
Filterd Force (F_{Meas})
Wave Probe (scale=100:1)
Fruode Kriloff (F_{FK})
Added Mass ($F_A = A.a_c$)
Damping ($F_B = B.v_c$)
Total Force ($F = F_{FK} + F_A + F_B$)

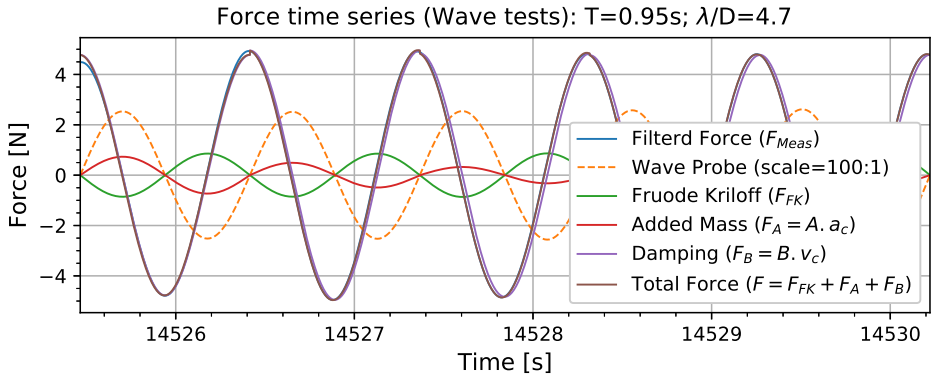
Force time series (Wave tests): T=0.95s; λ/D=4.7
Force [N]
Time [s]
Filterd Force (F_{Meas})
Wave Probe (scale=100:1)
Fruode Kriloff (F_{FK})
Added Mass ($F_A = A.a_c$)
Damping ($F_B = B.v_c$)
Total Force ($F = F_{FK} + F_A + F_B$)

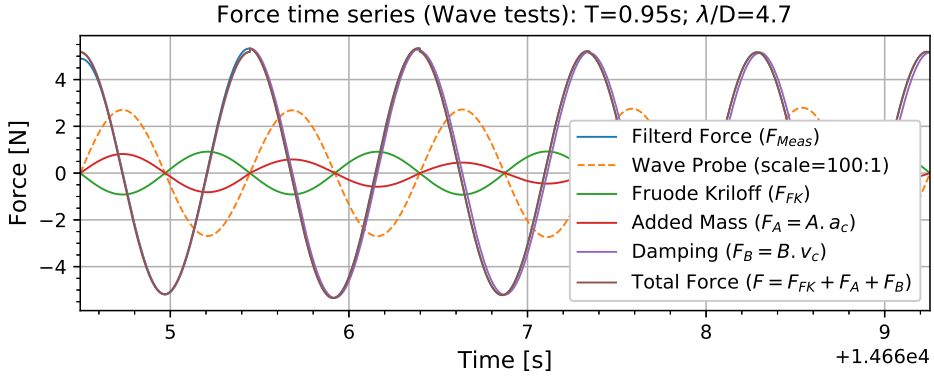
Force time series (Wave tests): T=0.95s; λ/D=4.7
Force [N]
Time [s]
+1.466e4
Filterd Force (F_{Meas})
Wave Probe (scale=100:1)
Fruode Kriloff (F_{FK})
Added Mass ($F_A = A.a_c$)
Damping ($F_B = B.v_c$)
Total Force ($F = F_{FK} + F_A + F_B$)

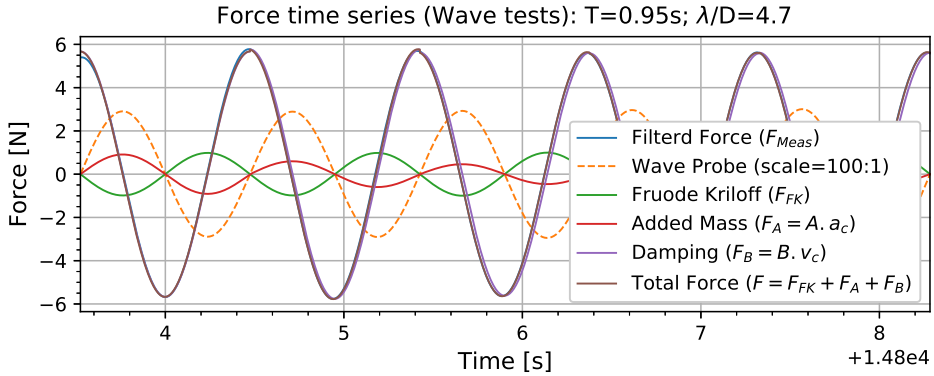
Force time series (Wave tests): T=0.95s; λ/D=4.7
Force [N]
Time [s]
+1.48e4
Filterd Force (F_{Meas})
Wave Probe (scale=100:1)
Fruode Kriloff (F_{FK})
Added Mass ($F_A = A.a_c$)
Damping ($F_B = B.v_c$)
Total Force ($F = F_{FK} + F_A + F_B$)

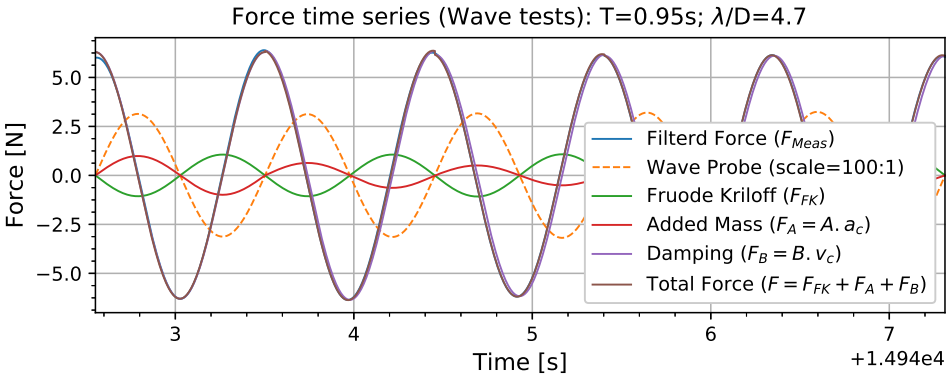
Force time series (Wave tests): T=0.95s; λ/D=4.7
Force [N]
Time [s]
+1.494e4
Filterd Force (F_{Meas})
Wave Probe (scale=100:1)
Fruode Kriloff (F_{FK})
Added Mass ($F_A = A.a_c$)
Damping ($F_B = B.v_c$)
Total Force ($F = F_{FK} + F_A + F_B$)

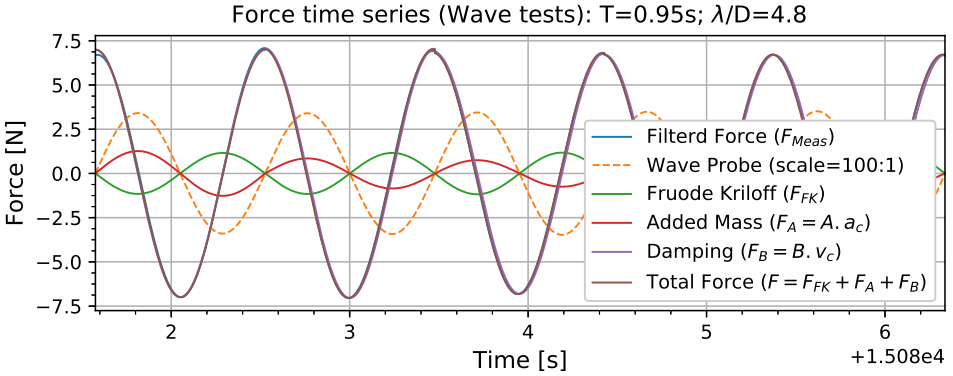
Force time series (Wave tests): T=0.95s; λ/D=4.8
Force [N]
Time [s]
+1.508e4
Filterd Force (F_{Meas})
Wave Probe (scale=100:1)
Fruode Kriloff (F_{FK})
Added Mass ($F_A = A.a_c$)
Damping ($F_B = B.v_c$)
Total Force ($F = F_{FK} + F_A + F_B$)

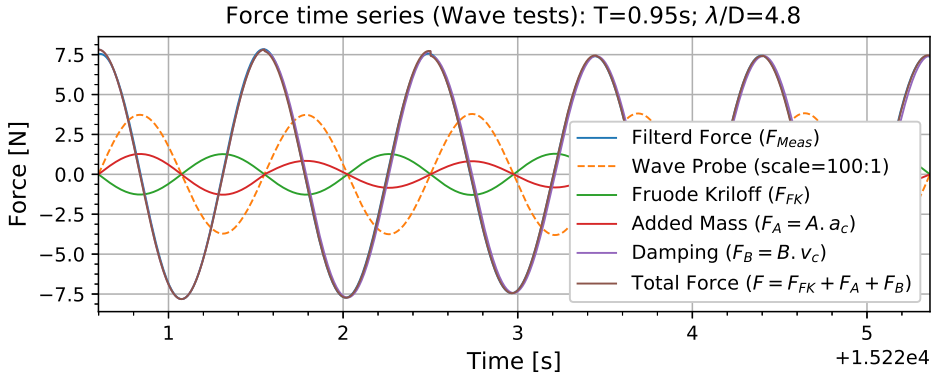
Force time series (Wave tests): T=0.95s; λ/D=4.8
Force [N]
Time [s]
+1.522e4
Filterd Force (F_{Meas})
Wave Probe (scale=100:1)
Fruode Kriloff (F_{FK})
Added Mass ($F_A = A.a_c$)
Damping ($F_B = B.v_c$)
Total Force ($F = F_{FK} + F_A + F_B$)

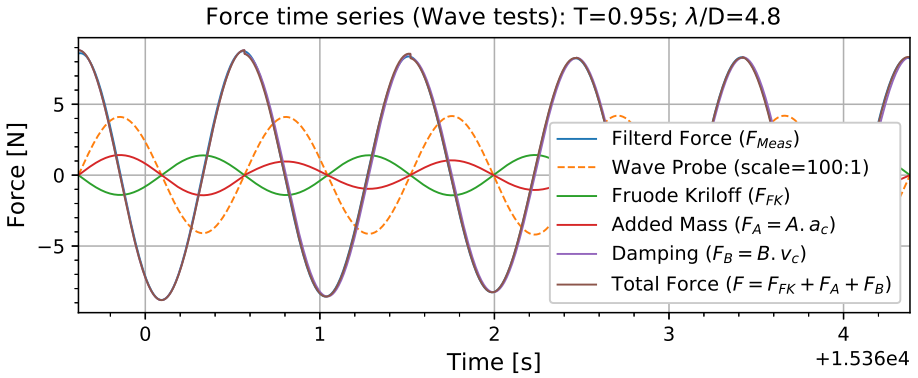
Force time series (Wave tests): T=0.95s; λ/D=4.8
Force [N]
Time [s]
+1.536e4
Filterd Force (F_{Meas})
Wave Probe (scale=100:1)
Fruode Kriloff (F_{FK})
Added Mass ($F_A = A.a_c$)
Damping ($F_B = B.v_c$)
Total Force ($F = F_{FK} + F_A + F_B$)

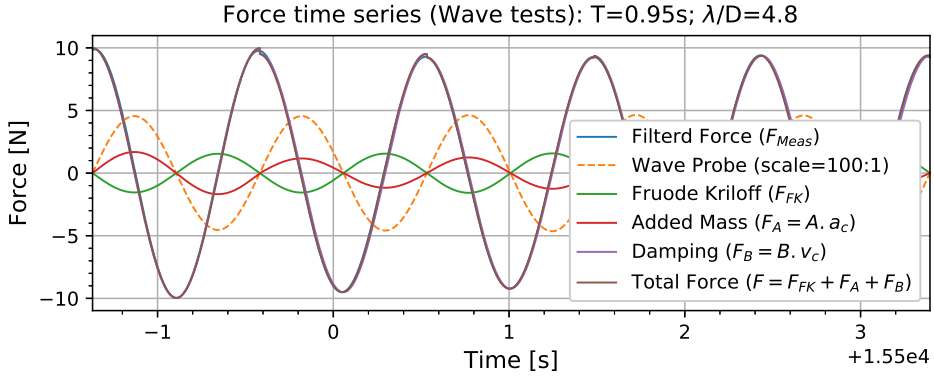
Force time series (Wave tests): T=0.95s; λ/D=4.8
Force [N]
Time [s]
+1.55e4
Filterd Force (F_{Meas})
Wave Probe (scale=100:1)
Fruode Kriloff (F_{FK})
Added Mass ($F_A = A.a_c$)
Damping ($F_B = B.v_c$)
Total Force ($F = F_{FK} + F_A + F_B$)

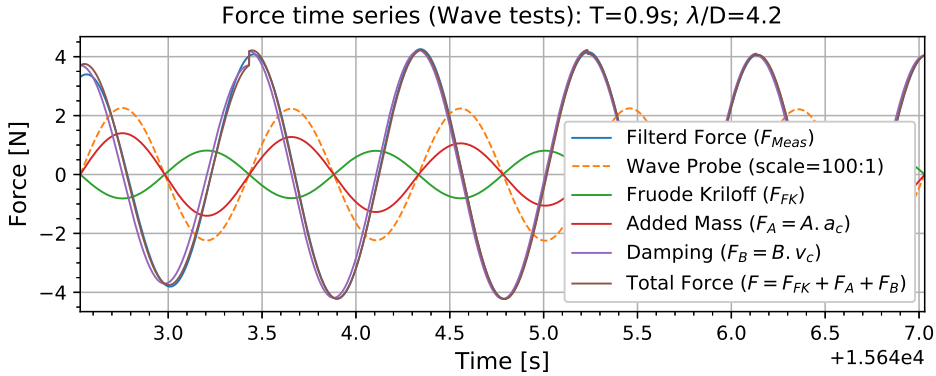
Force time series (Wave tests): T=0.9s; λ/D=4.2
Force [N]
Time [s]
+1.564e4
Filterd Force (F_{Meas})
Wave Probe (scale=100:1)
Fruode Kriloff (F_{FK})
Added Mass ($F_A = A.a_c$)
Damping ($F_B = B.v_c$)
Total Force ($F = F_{FK} + F_A + F_B$)

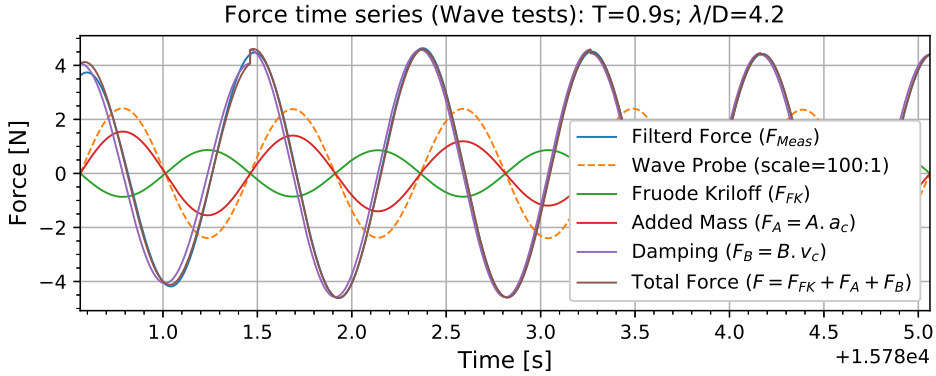
Force time series (Wave tests): T=0.9s; λ/D=4.2
Force [N]
Time [s]
+1.578e4
Filterd Force (F_{Meas})
Wave Probe (scale=100:1)
Fruode Kriloff (F_{FK})
Added Mass ($F_A = A.a_c$)
Damping ($F_B = B.v_c$)
Total Force ($F = F_{FK} + F_A + F_B$)

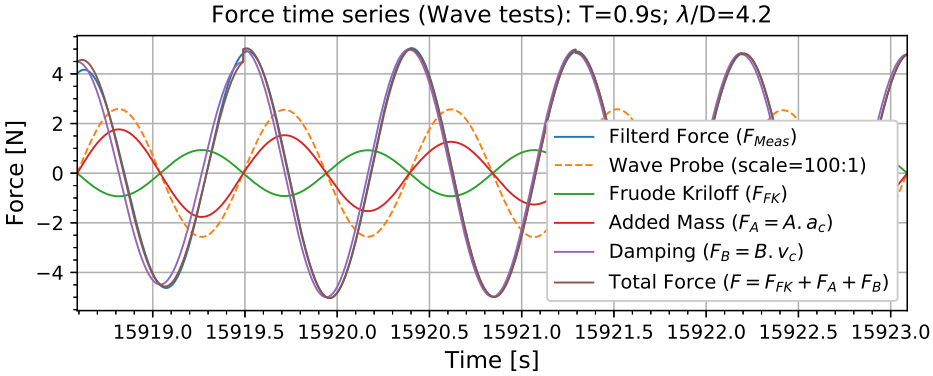
Force time series (Wave tests): T=0.9s; λ/D=4.2
Force [N]
Time [s]
4
2
0
−2
−4
15919.0
15919.5
15920.0
15920.5
15921.0
15921.5
15922.0
15922.5
15923.0
Filterd Force (F_{Meas})
Wave Probe (scale=100:1)
Fruode Kriloff (F_{FK})
Added Mass ($F_A = A.\,a_c$)
Damping ($F_B = B.\,v_c$)
Total Force ($F = F_{FK} + F_A + F_B$)

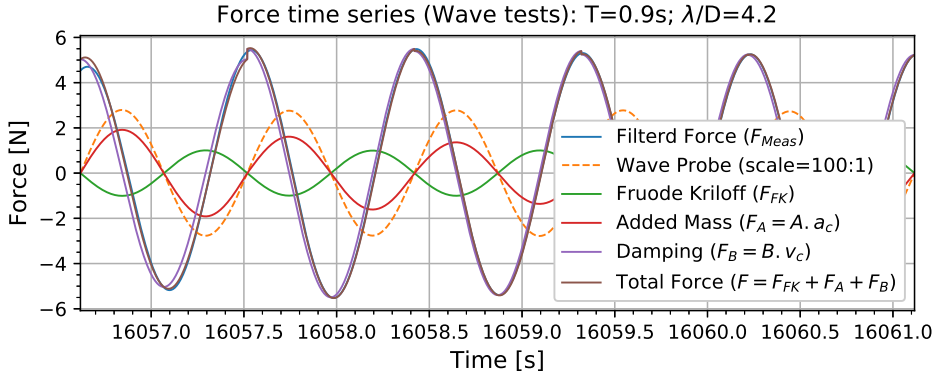
Force time series (Wave tests): T=0.9s; λ/D=4.2
Force [N]
Time [s]
Filterd Force (F_{Meas})
Wave Probe (scale=100:1)
Fruode Kriloff (F_{FK})
Added Mass ($F_A = A.a_c$)
Damping ($F_B = B.v_c$)
Total Force ($F = F_{FK} + F_A + F_B$)

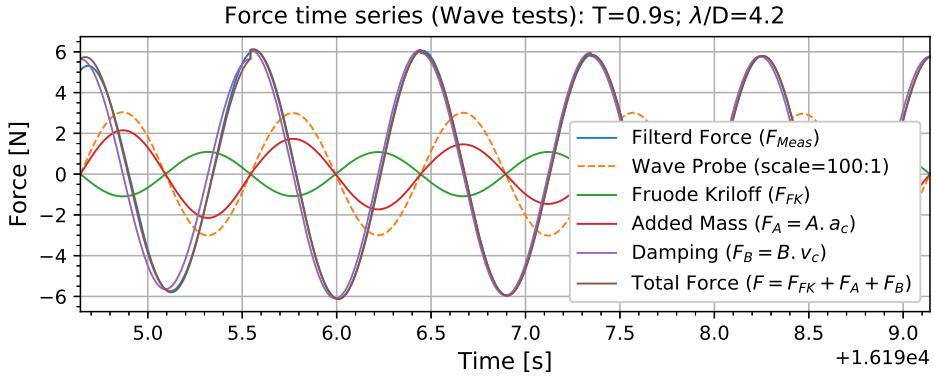
Force time series (Wave tests): T=0.9s; λ/D=4.2
Force [N]
Time [s]
+1.619e4
Filterd Force (F_{Meas})
Wave Probe (scale=100:1)
Fruode Kriloff (F_{FK})
Added Mass ($F_A = A.a_c$)
Damping ($F_B = B.v_c$)
Total Force ($F = F_{FK} + F_A + F_B$)

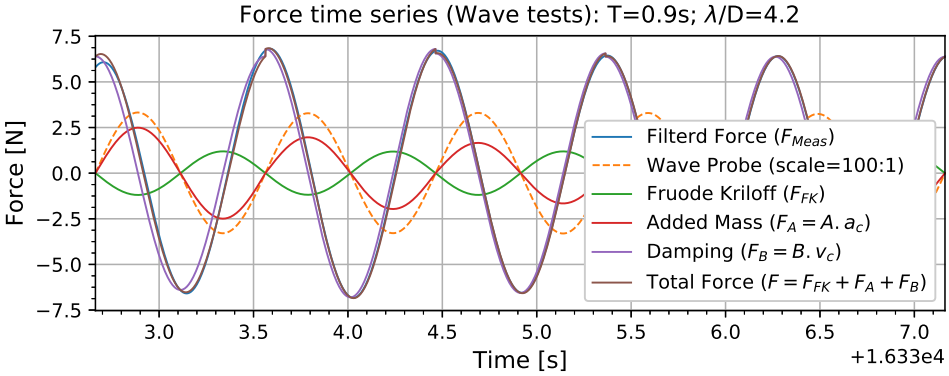
Force time series (Wave tests): T=0.9s; λ/D=4.2
Force [N]
Time [s]
+1.633e4
Filterd Force (F_{Meas})
Wave Probe (scale=100:1)
Fruode Kriloff (F_{FK})
Added Mass ($F_A = A.a_c$)
Damping ($F_B = B.v_c$)
Total Force ($F = F_{FK} + F_A + F_B$)

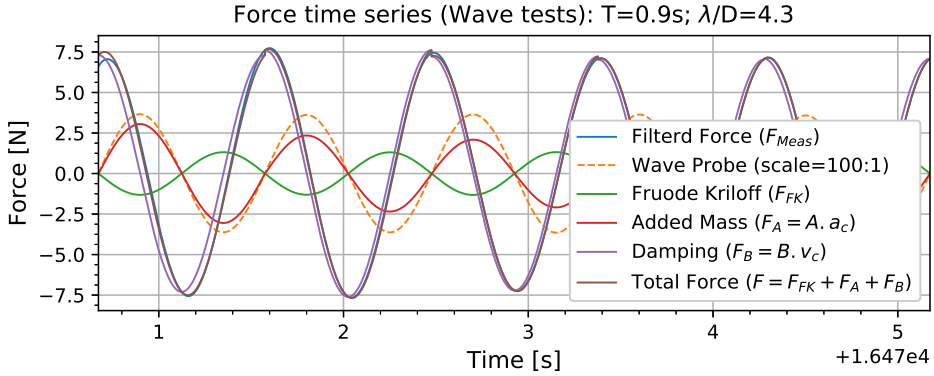
Force time series (Wave tests): T=0.9s; λ/D=4.3
Force [N]
7.5
5.0
2.5
0.0
−2.5
−5.0
−7.5
1
2
3
4
5
Time [s]
+1.647e4
Filterd Force (F_{Meas})
Wave Probe (scale=100:1)
Fruode Kriloff (F_{FK})
Added Mass ($F_A = A.a_c$)
Damping ($F_B = B.v_c$)
Total Force ($F = F_{FK} + F_A + F_B$)

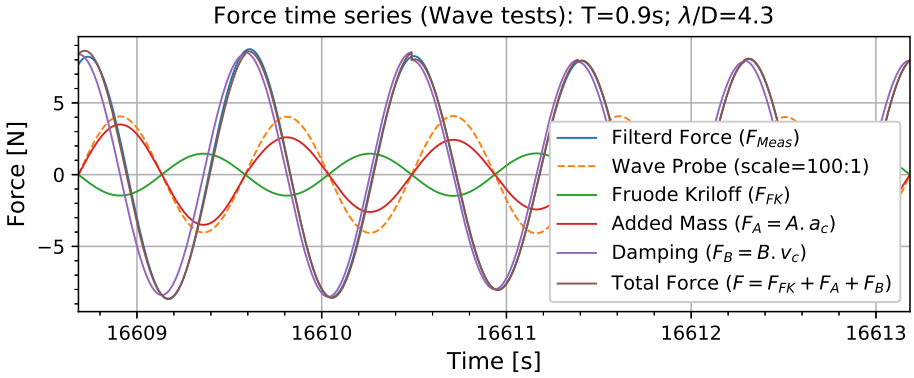
Force time series (Wave tests): T=0.9s; λ/D=4.3
Force [N]
5
0
−5
16609
16610
16611
16612
16613
Time [s]
Filterd Force (F_{Meas})
Wave Probe (scale=100:1)
Fruode Kriloff (F_{FK})
Added Mass ($F_A = A.a_c$)
Damping ($F_B = B.v_c$)
Total Force ($F = F_{FK} + F_A + F_B$)

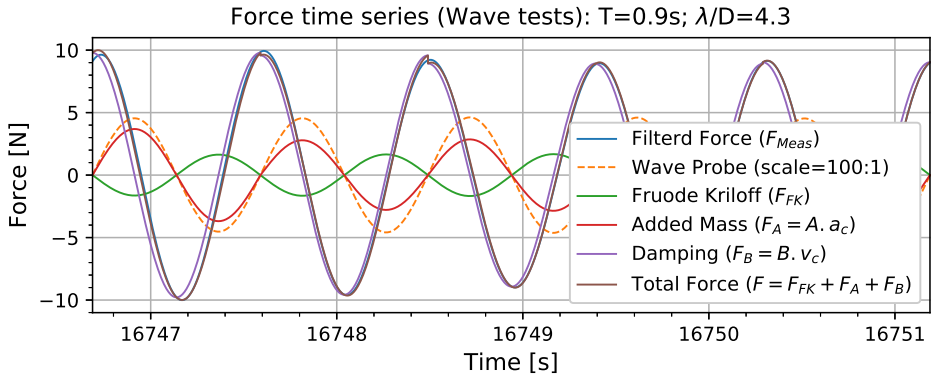
Force time series (Wave tests): T=0.9s; λ/D=4.3
Force [N]
10
5
0
−5
−10
16747
16748
16749
16750
16751
Time [s]
Filterd Force (F_{Meas})
Wave Probe (scale=100:1)
Fruode Kriloff (F_{FK})
Added Mass ($F_A = A.a_c$)
Damping ($F_B = B.v_c$)
Total Force ($F = F_{FK} + F_A + F_B$)

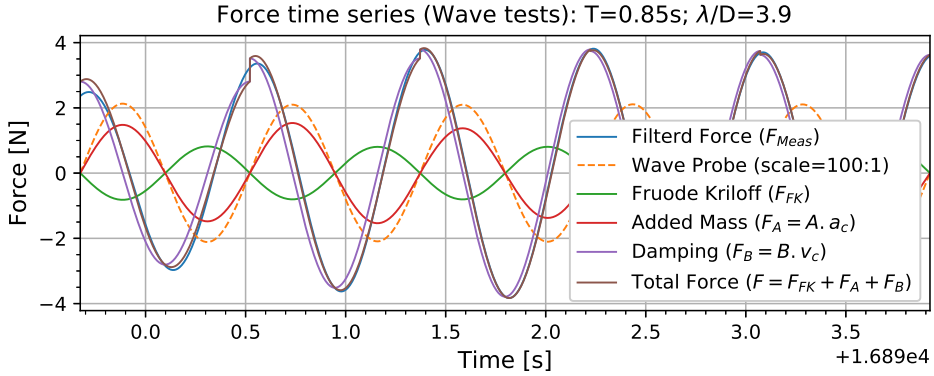
Force time series (Wave tests): T=0.85s; λ/D=3.9
Force [N]
Time [s]
+1.689e4
Filterd Force (F_{Meas})
Wave Probe (scale=100:1)
Fruode Kriloff (F_{FK})
Added Mass ($F_A = A.a_c$)
Damping ($F_B = B.v_c$)
Total Force ($F = F_{FK} + F_A + F_B$)

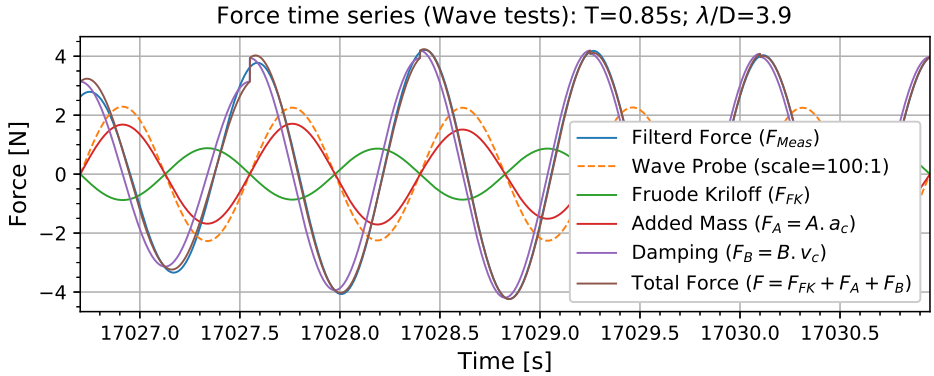
Force time series (Wave tests): T=0.85s; λ/D=3.9
Force [N]
Time [s]
Filterd Force (F_{Meas})
Wave Probe (scale=100:1)
Fruode Kriloff (F_{FK})
Added Mass ($F_A = A.a_c$)
Damping ($F_B = B.v_c$)
Total Force ($F = F_{FK} + F_A + F_B$)

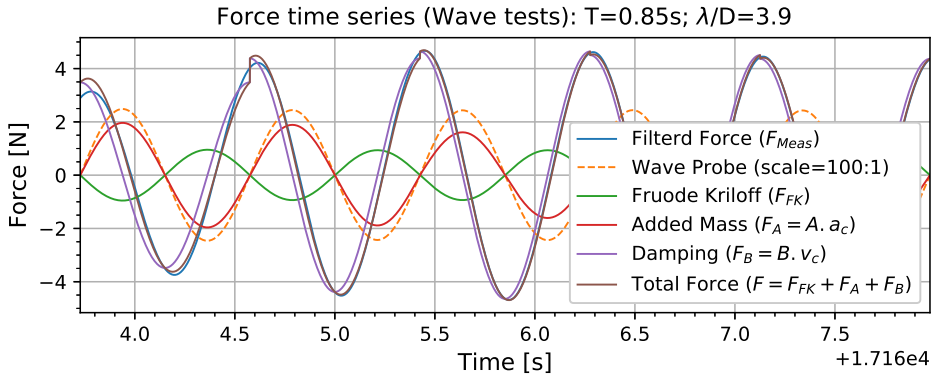
Force time series (Wave tests): T=0.85s; λ/D=3.9
Force [N]
Time [s]
+1.716e4
Filterd Force (F_{Meas})
Wave Probe (scale=100:1)
Fruode Kriloff (F_{FK})
Added Mass ($F_A = A.a_c$)
Damping ($F_B = B.v_c$)
Total Force ($F = F_{FK} + F_A + F_B$)

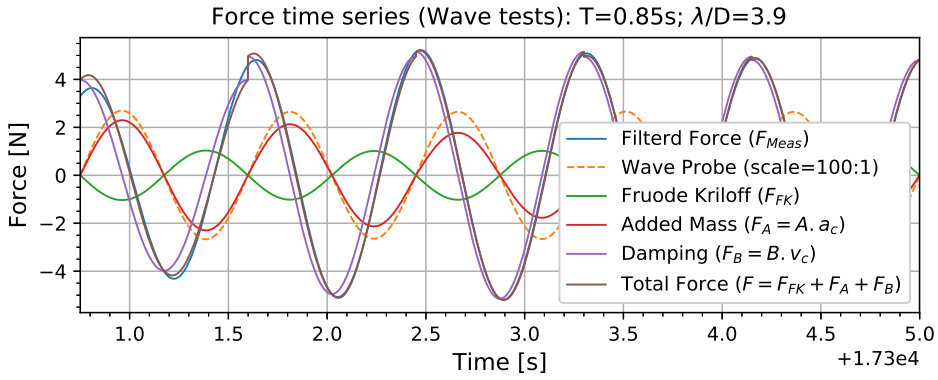
Force time series (Wave tests): T=0.85s; λ/D=3.9
Force [N]
Time [s]
+1.73e4
Filterd Force (F_{Meas})
Wave Probe (scale=100:1)
Fruode Kriloff (F_{FK})
Added Mass ($F_A = A.a_c$)
Damping ($F_B = B.v_c$)
Total Force ($F = F_{FK} + F_A + F_B$)

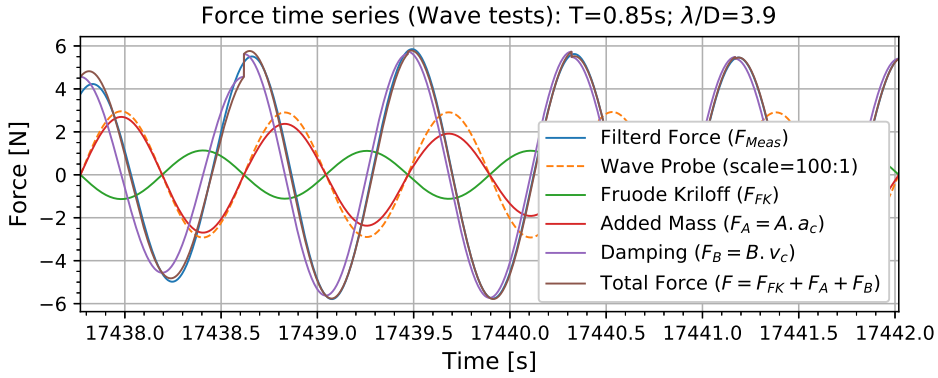
Force time series (Wave tests): T=0.85s; λ/D=3.9
Force [N]
Time [s]
Filterd Force (F_{Meas})
Wave Probe (scale=100:1)
Fruode Kriloff (F_{FK})
Added Mass ($F_A = A.a_c$)
Damping ($F_B = B.v_c$)
Total Force ($F = F_{FK} + F_A + F_B$)

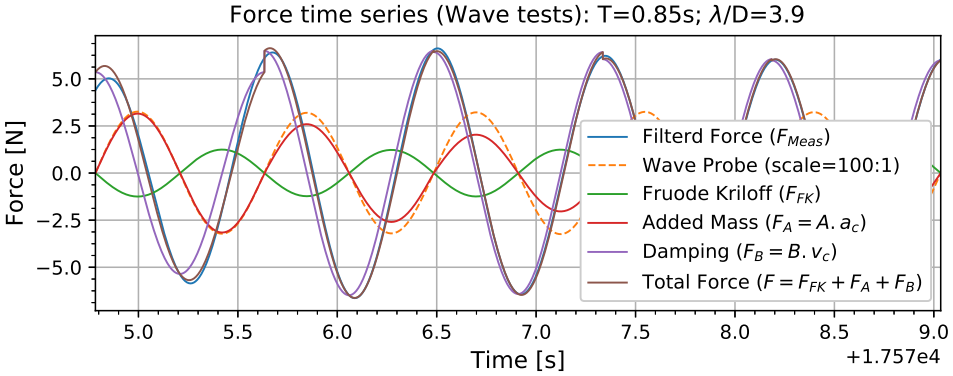
Force time series (Wave tests): T=0.85s; λ/D=3.9
Force [N]
Time [s]
+1.757e4
Filterd Force (F_{Meas})
Wave Probe (scale=100:1)
Fruode Kriloff (F_{FK})
Added Mass ($F_A = A.a_c$)
Damping ($F_B = B.v_c$)
Total Force ($F = F_{FK} + F_A + F_B$)

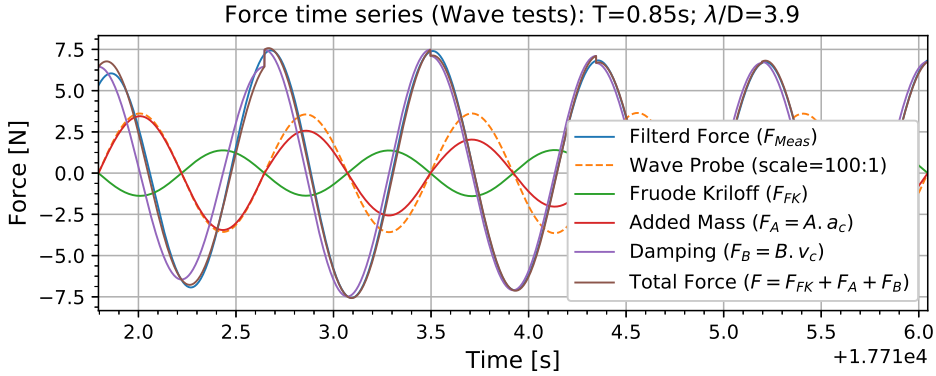
Force time series (Wave tests): T=0.85s; λ/D=3.9
Force [N]
Time [s]
+1.771e4
Filterd Force (F_{Meas})
Wave Probe (scale=100:1)
Fruode Kriloff (F_{FK})
Added Mass ($F_A = A.a_c$)
Damping ($F_B = B.v_c$)
Total Force ($F = F_{FK} + F_A + F_B$)

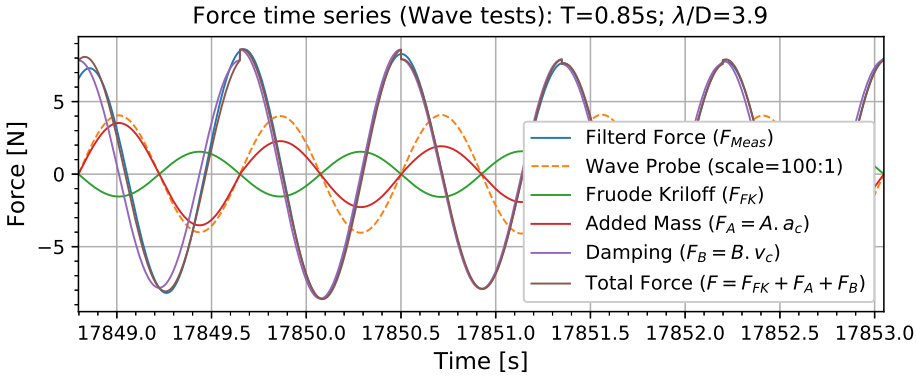
Force time series (Wave tests): T=0.85s; λ/D=3.9
Force [N]
Time [s]
Filterd Force (F_{Meas})
Wave Probe (scale=100:1)
Fruode Kriloff (F_{FK})
Added Mass ($F_A = A.a_c$)
Damping ($F_B = B.v_c$)
Total Force ($F = F_{FK} + F_A + F_B$)

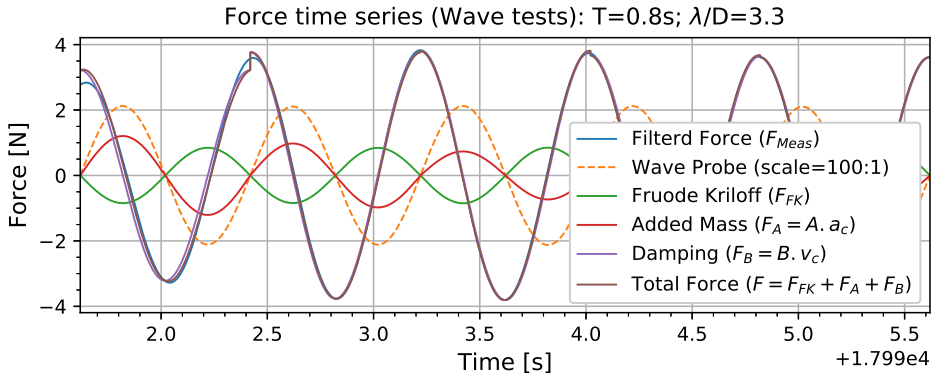
Force time series (Wave tests): T=0.8s; λ/D=3.3
Force [N]
Time [s]
+1.799e4
Filterd Force (F_{Meas})
Wave Probe (scale=100:1)
Fruode Kriloff (F_{FK})
Added Mass ($F_A = A.a_c$)
Damping ($F_B = B.v_c$)
Total Force ($F = F_{FK} + F_A + F_B$)

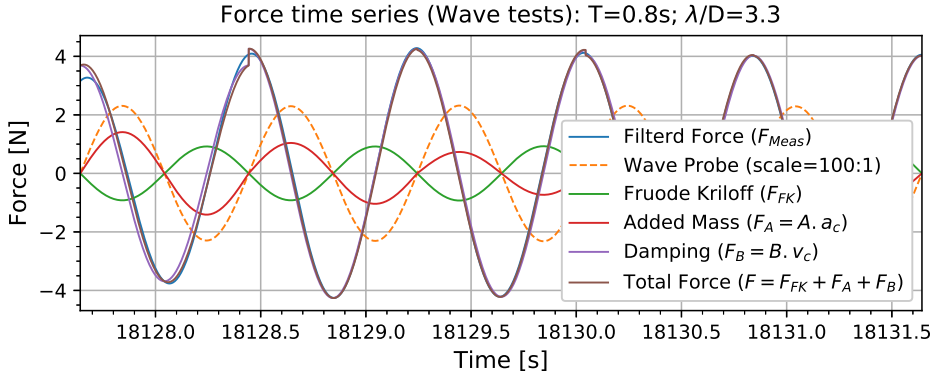
Force time series (Wave tests): T=0.8s; λ/D=3.3
Force [N]
Time [s]
Filterd Force (F_{Meas})
Wave Probe (scale=100:1)
Fruode Kriloff (F_{FK})
Added Mass ($F_A = A.a_c$)
Damping ($F_B = B.v_c$)
Total Force ($F = F_{FK} + F_A + F_B$)

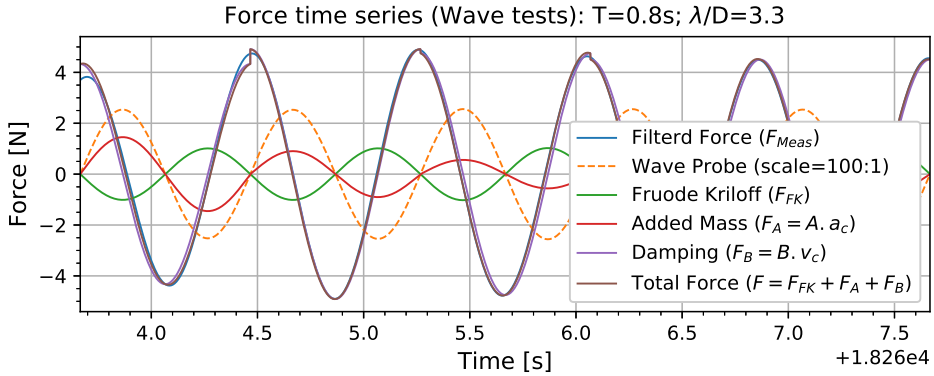
Force time series (Wave tests): T=0.8s; λ/D=3.3
Force [N]
Time [s]
+1.826e4
Filterd Force (F_{Meas})
Wave Probe (scale=100:1)
Fruode Kriloff (F_{FK})
Added Mass ($F_A = A.a_c$)
Damping ($F_B = B.v_c$)
Total Force ($F = F_{FK} + F_A + F_B$)

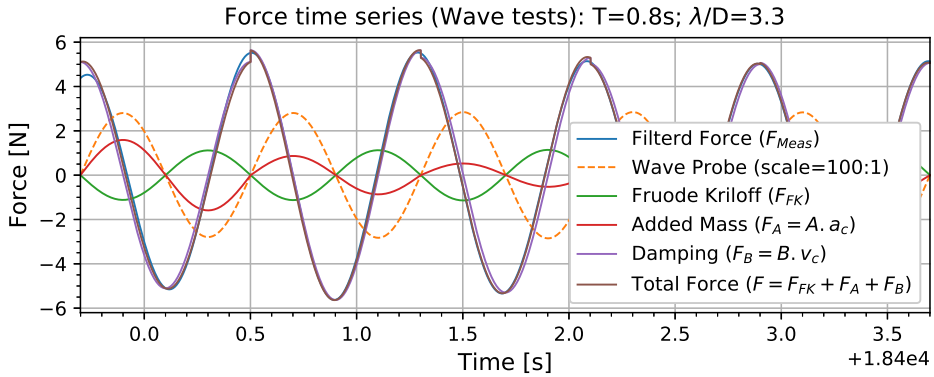
Force time series (Wave tests): T=0.8s; λ/D=3.3
Force [N]
Time [s]
+1.84e4
Filterd Force (F_{Meas})
Wave Probe (scale=100:1)
Fruode Kriloff (F_{FK})
Added Mass ($F_A = A.a_c$)
Damping ($F_B = B.v_c$)
Total Force ($F = F_{FK} + F_A + F_B$)

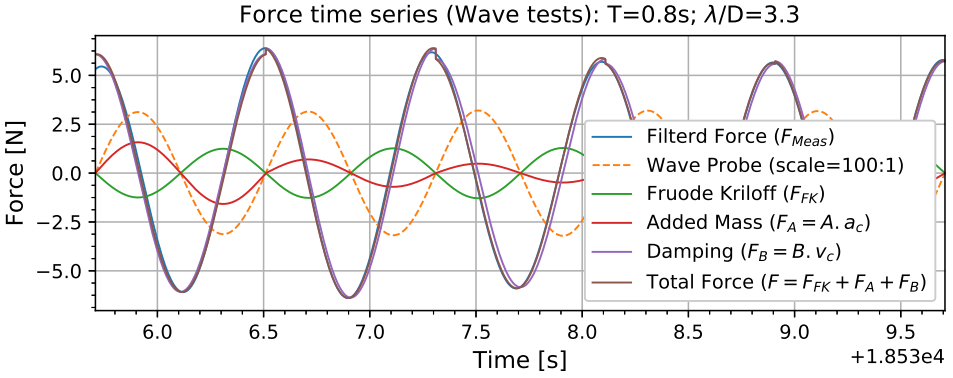
Force time series (Wave tests): T=0.8s; λ/D=3.3
Force [N]
Time [s]
+1.853e4
Filterd Force (F_{Meas})
Wave Probe (scale=100:1)
Fruode Kriloff (F_{FK})
Added Mass ($F_A = A.a_c$)
Damping ($F_B = B.v_c$)
Total Force ($F = F_{FK} + F_A + F_B$)

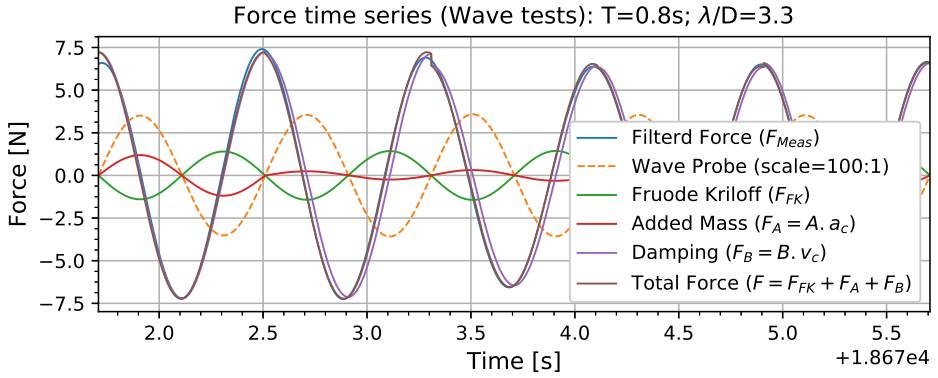
Force time series (Wave tests): T=0.8s; λ/D=3.3
Force [N]
Time [s]
+1.867e4
Filterd Force (F_{Meas})
Wave Probe (scale=100:1)
Fruode Kriloff (F_{FK})
Added Mass ($F_A = A.a_c$)
Damping ($F_B = B.v_c$)
Total Force ($F = F_{FK} + F_A + F_B$)

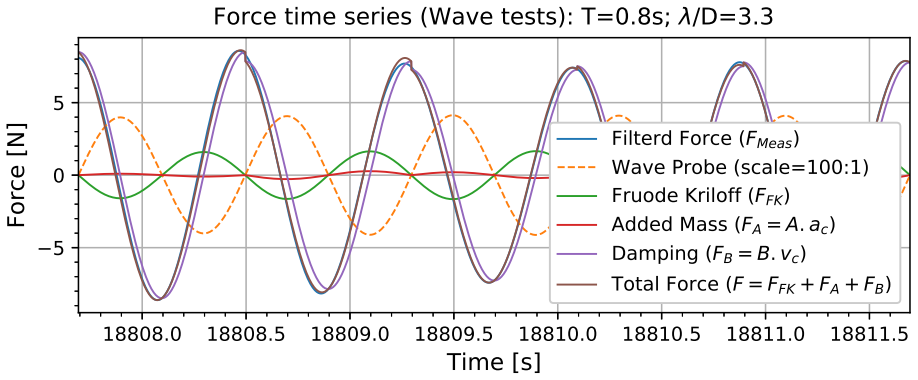
Force time series (Wave tests): T=0.8s; λ/D=3.3
Force [N]
Time [s]
Filterd Force (F_{Meas})
Wave Probe (scale=100:1)
Fruode Kriloff (F_{FK})
Added Mass ($F_A = A.a_c$)
Damping ($F_B = B.v_c$)
Total Force ($F = F_{FK} + F_A + F_B$)

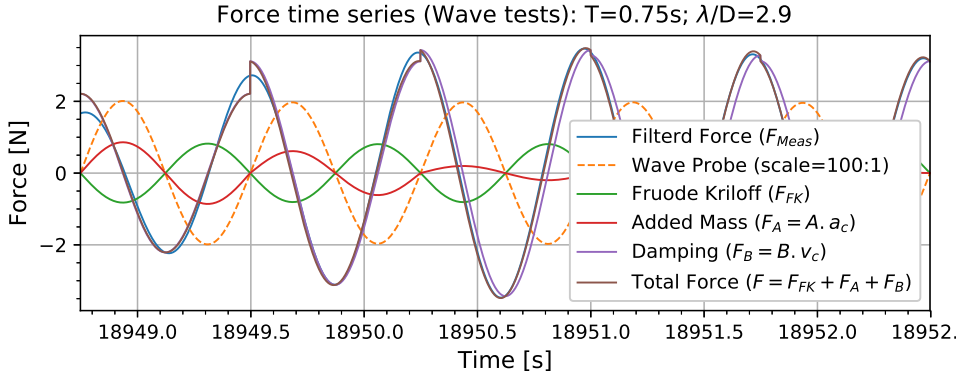
Force time series (Wave tests): T=0.75s; λ/D=2.9
Force [N]
Time [s]
Filterd Force (F_{Meas})
Wave Probe (scale=100:1)
Fruode Kriloff (F_{FK})
Added Mass ($F_A = A.\,a_c$)
Damping ($F_B = B.\,v_c$)
Total Force ($F = F_{FK} + F_A + F_B$)

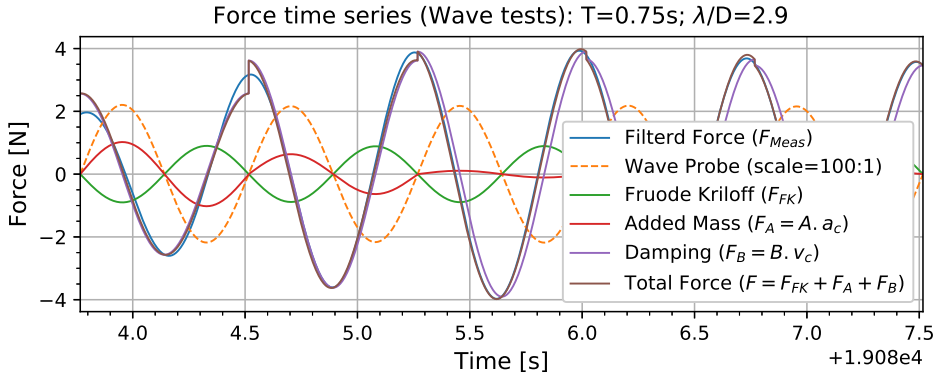
Force time series (Wave tests): T=0.75s; λ/D=2.9
Force [N]
Time [s]
+1.908e4
Filterd Force (F_{Meas})
Wave Probe (scale=100:1)
Fruode Kriloff (F_{FK})
Added Mass ($F_A = A.\,a_c$)
Damping ($F_B = B.\,v_c$)
Total Force ($F = F_{FK} + F_A + F_B$)

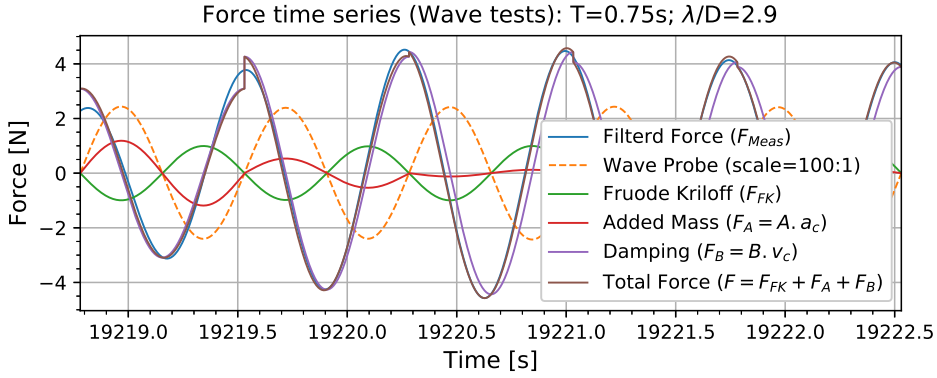
Force time series (Wave tests): T=0.75s; λ/D=2.9
Force [N]
Time [s]
Filterd Force (F_{Meas})
Wave Probe (scale=100:1)
Fruode Kriloff (F_{FK})
Added Mass ($F_A = A.\,a_c$)
Damping ($F_B = B.\,v_c$)
Total Force ($F = F_{FK} + F_A + F_B$)

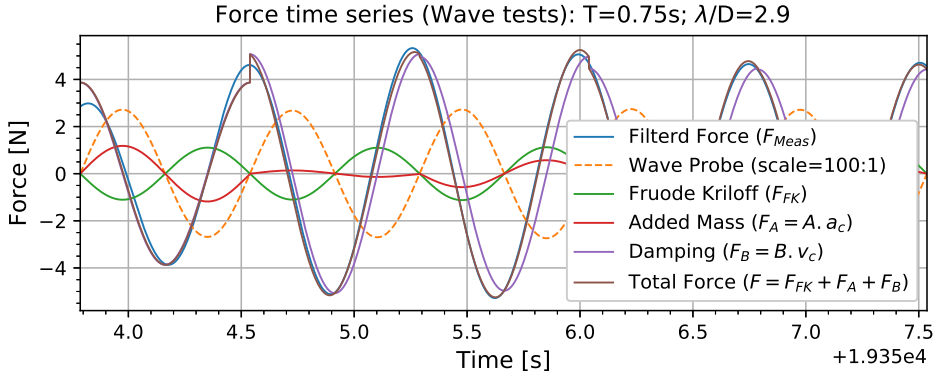
Force time series (Wave tests): T=0.75s; λ/D=2.9
Force [N]
Time [s]
+1.935e4
Filterd Force (F_{Meas})
Wave Probe (scale=100:1)
Fruode Kriloff (F_{FK})
Added Mass ($F_A = A.\,a_c$)
Damping ($F_B = B.\,v_c$)
Total Force ($F = F_{FK} + F_A + F_B$)

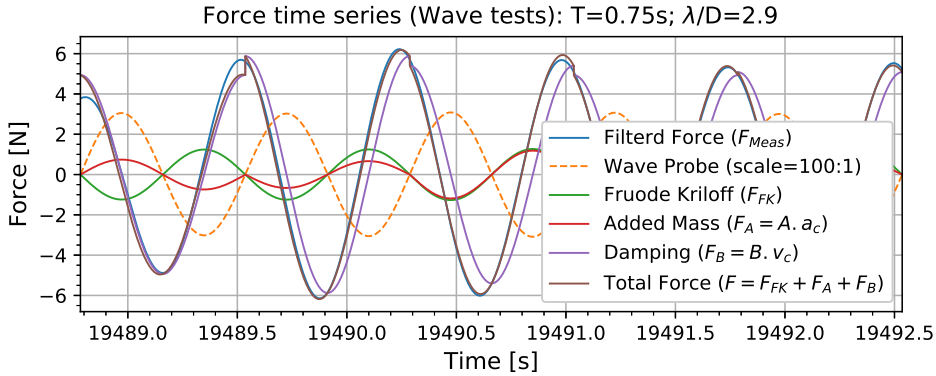
Force time series (Wave tests): T=0.75s; λ/D=2.9
Force [N]
Time [s]
Filterd Force (F_{Meas})
Wave Probe (scale=100:1)
Fruode Kriloff (F_{FK})
Added Mass ($F_A = A.\,a_c$)
Damping ($F_B = B.\,v_c$)
Total Force ($F = F_{FK} + F_A + F_B$)

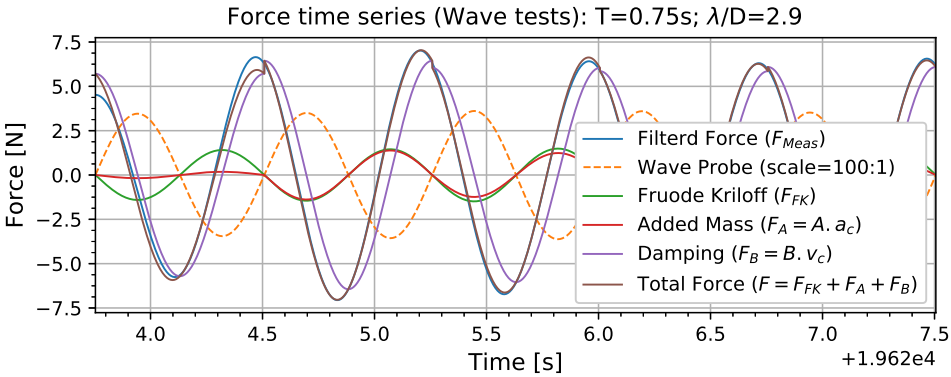
Force time series (Wave tests): T=0.75s; λ/D=2.9
Force [N]
Time [s]
+1.962e4
Filterd Force (F_{Meas})
Wave Probe (scale=100:1)
Fruode Kriloff (F_{FK})
Added Mass ($F_A = A.\,a_c$)
Damping ($F_B = B.\,v_c$)
Total Force ($F = F_{FK} + F_A + F_B$)

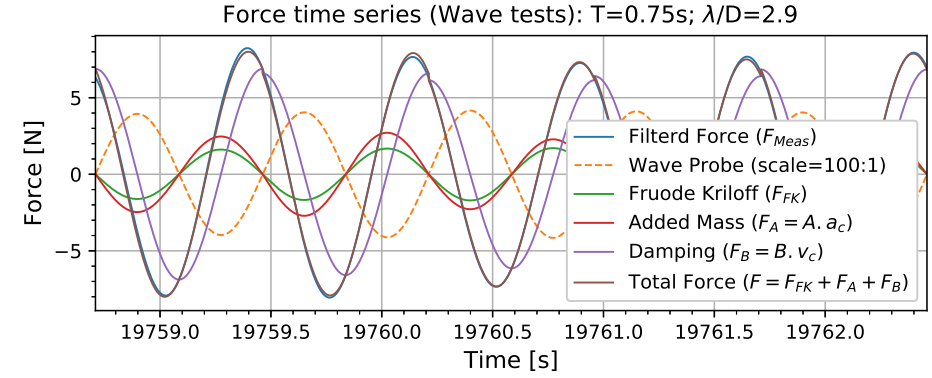
Force time series (Wave tests): T=0.75s; λ/D=2.9
Force [N]
Time [s]
Filterd Force (F_{Meas})
Wave Probe (scale=100:1)
Fruode Kriloff (F_{FK})
Added Mass ($F_A = A.a_c$)
Damping ($F_B = B.v_c$)
Total Force ($F = F_{FK} + F_A + F_B$)

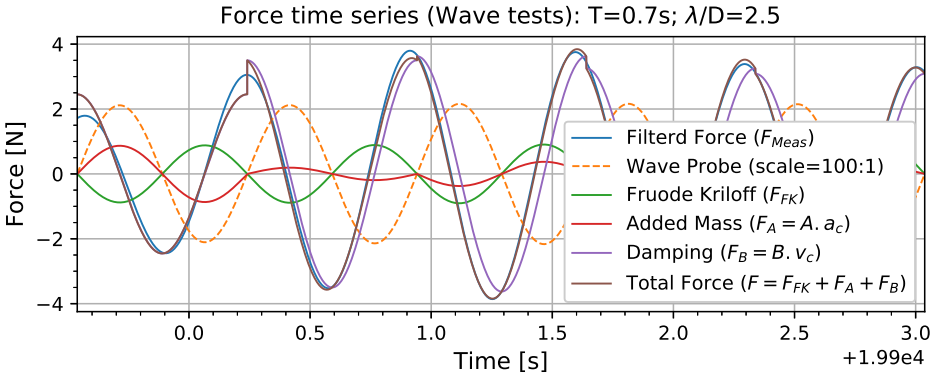
Force time series (Wave tests): T=0.7s; λ/D=2.5
Force [N]
Time [s]
+1.99e4
Filterd Force (F_{Meas})
Wave Probe (scale=100:1)
Fruode Kriloff (F_{FK})
Added Mass ($F_A = A.a_c$)
Damping ($F_B = B.v_c$)
Total Force ($F = F_{FK} + F_A + F_B$)

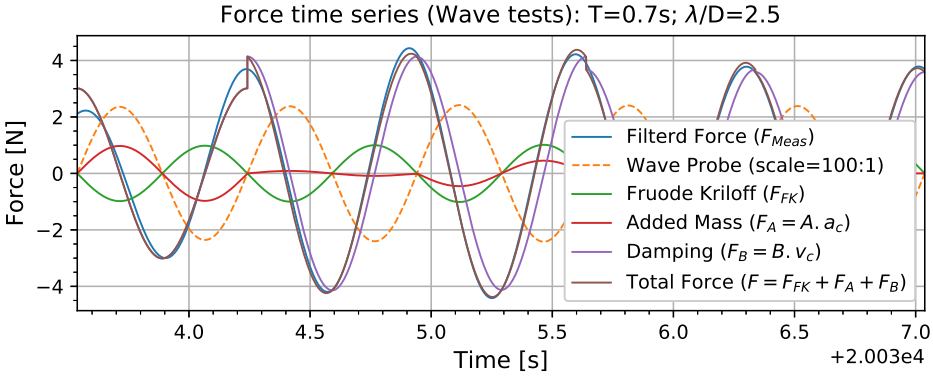
Force time series (Wave tests): T=0.7s; λ/D=2.5
Force [N]
Time [s]
+2.003e4
Filterd Force (F_{Meas})
Wave Probe (scale=100:1)
Fruode Kriloff (F_{FK})
Added Mass ($F_A = A.a_c$)
Damping ($F_B = B.v_c$)
Total Force ($F = F_{FK} + F_A + F_B$)

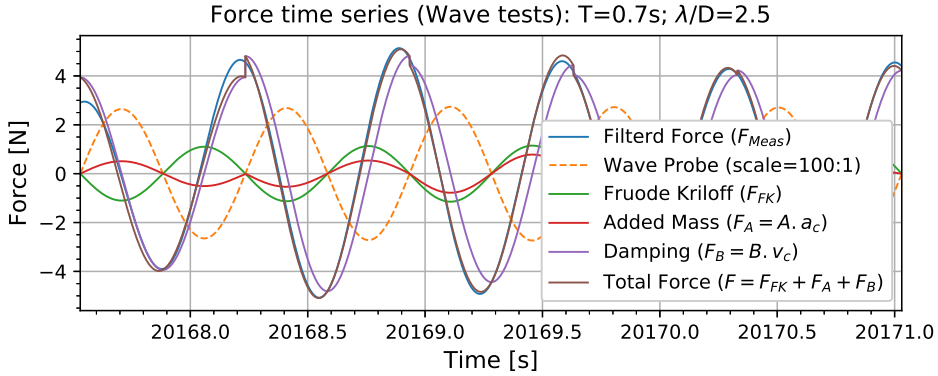
Force time series (Wave tests): T=0.7s; λ/D=2.5
Force [N]
Time [s]
Filterd Force (F_{Meas})
Wave Probe (scale=100:1)
Fruode Kriloff (F_{FK})
Added Mass ($F_A = A.a_c$)
Damping ($F_B = B.v_c$)
Total Force ($F = F_{FK} + F_A + F_B$)

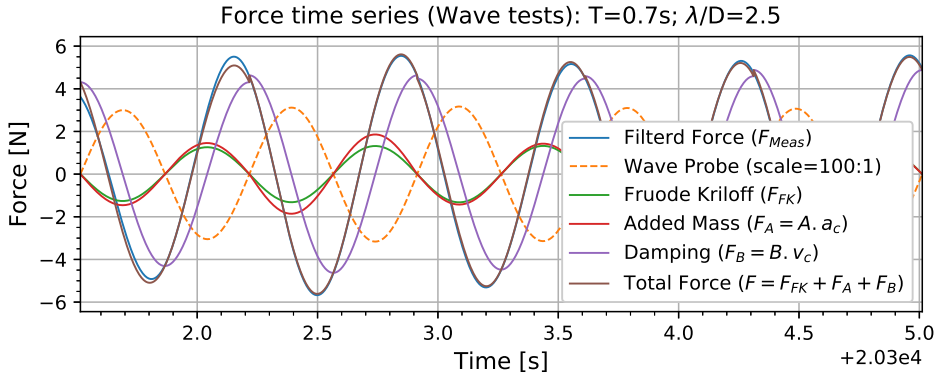
Force time series (Wave tests): T=0.7s; λ/D=2.5
Force [N]
Time [s]
+2.03e4
Filterd Force (F_{Meas})
Wave Probe (scale=100:1)
Fruode Kriloff (F_{FK})
Added Mass ($F_A = A.a_c$)
Damping ($F_B = B.v_c$)
Total Force ($F = F_{FK} + F_A + F_B$)

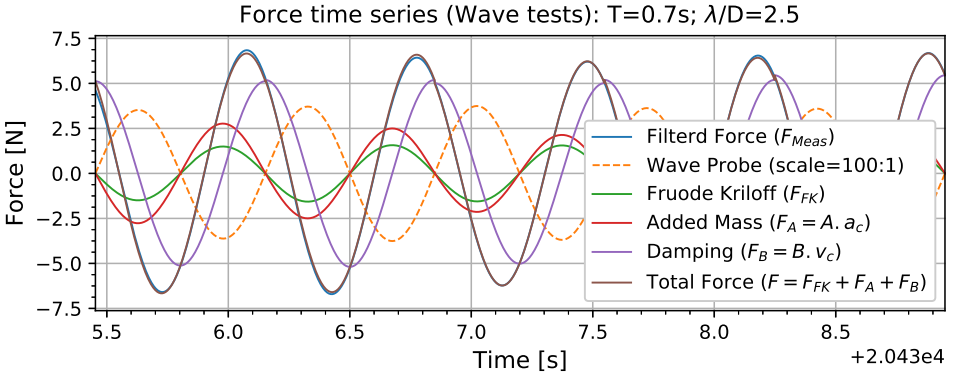
Force time series (Wave tests): T=0.7s; λ/D=2.5
Force [N]
Time [s]
+2.043e4
Filterd Force (F_{Meas})
Wave Probe (scale=100:1)
Fruode Kriloff (F_{FK})
Added Mass ($F_A = A.a_c$)
Damping ($F_B = B.v_c$)
Total Force ($F = F_{FK} + F_A + F_B$)

Appendix D: Deep Water Oscillations - Force Time Series

This section presents the force time series for deep water forced oscillations tests only for FING test model. It should be noted that the first-order force is re-calculated using the Fourier averaged added mass (A) and damping (B) coefficients, and the filtered force also includes 3^{rd} and 5^{th} order force components.

Model: FING

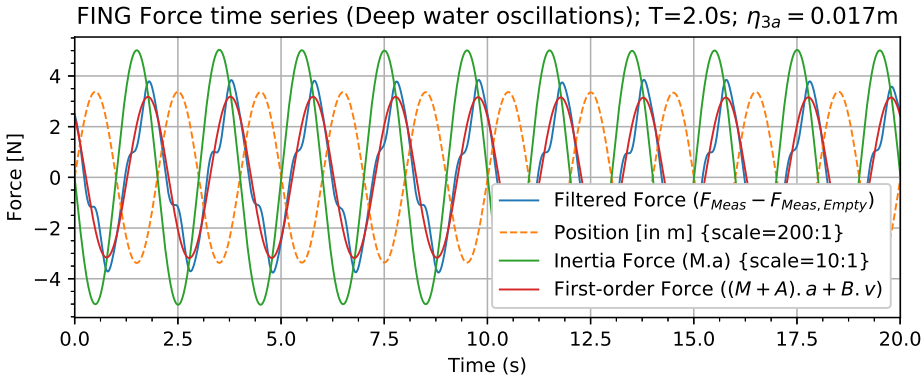

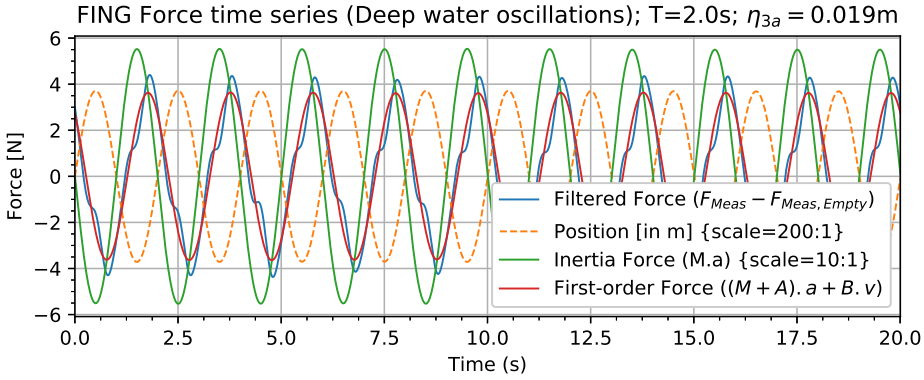

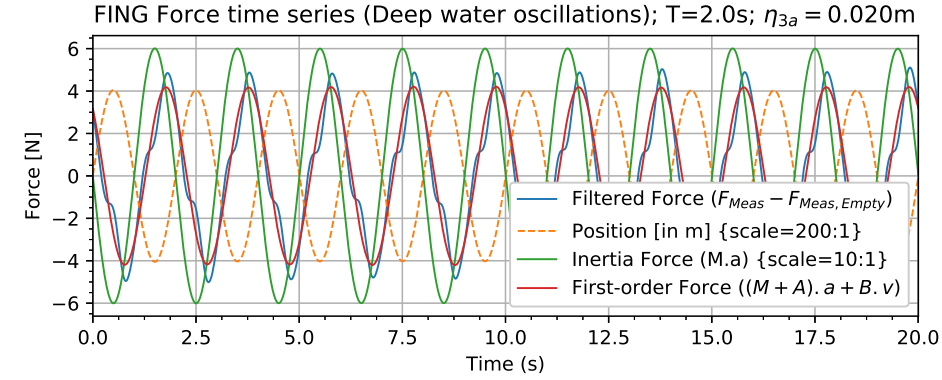
FING Force time series (Deep water oscillations); T=2.0s; $\eta_{3a} = 0.020$m
Force [N]
Time (s)
Filtered Force ($F_{Meas} - F_{Meas,Empty}$)
Position [in m] {scale=200:1}
Inertia Force (M.a) {scale=10:1}
First-order Force ($(M+A).a + B.v$)

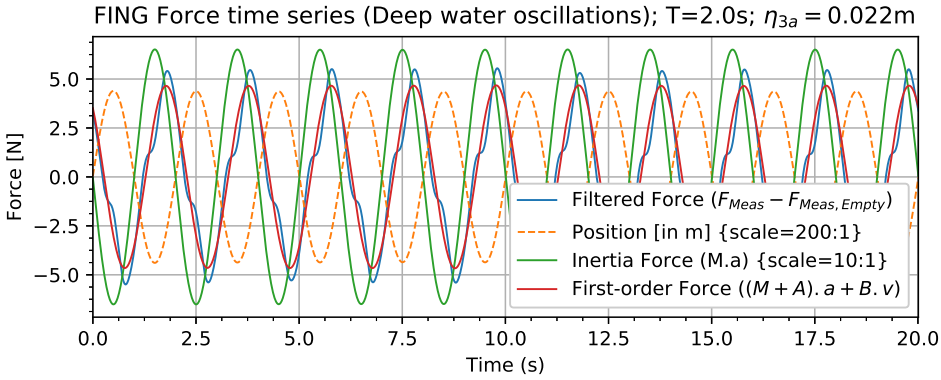
FING Force time series (Deep water oscillations); T=2.0s; $\eta_{3a} = 0.022$m
Force [N]
Time (s)
Filtered Force ($F_{Meas} - F_{Meas,Empty}$)
Position [in m] {scale=200:1}
Inertia Force (M.a) {scale=10:1}
First-order Force ($(M+A).a + B.v$)

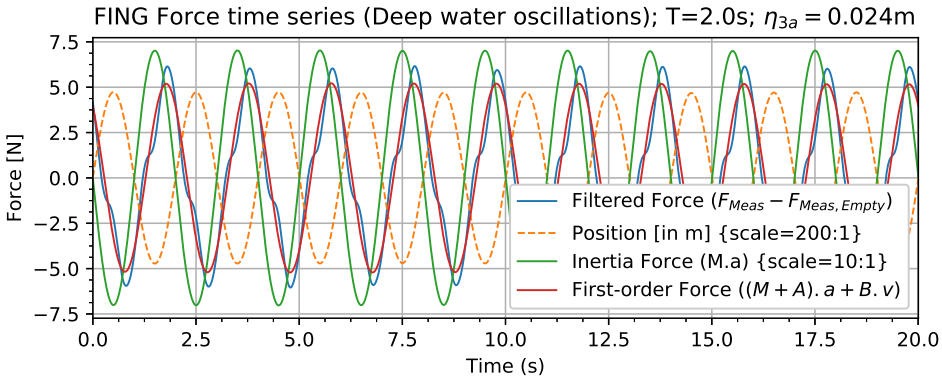
FING Force time series (Deep water oscillations); T=2.0s; $\eta_{3a} = 0.024$m
Force [N]
Time (s)
Filtered Force ($F_{Meas} - F_{Meas,Empty}$)
Position [in m] {scale=200:1}
Inertia Force (M.a) {scale=10:1}
First-order Force ($(M+A).a + B.v$)

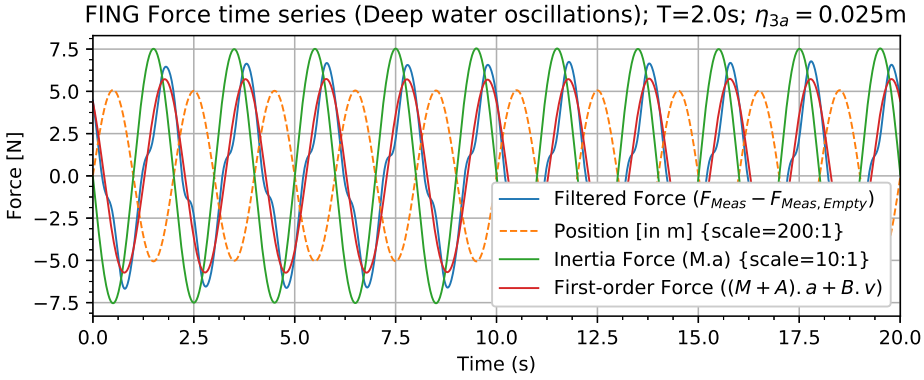
FING Force time series (Deep water oscillations); T=2.0s; $\eta_{3a} = 0.025$m
Force [N]
Time (s)
Filtered Force ($F_{Meas} - F_{Meas,Empty}$)
Position [in m] {scale=200:1}
Inertia Force (M.a) {scale=10:1}
First-order Force ($(M+A).a + B.v$)

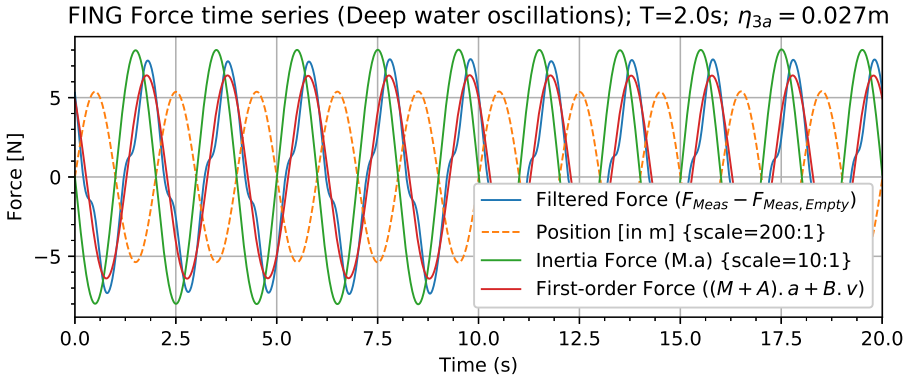
FING Force time series (Deep water oscillations); T=2.0s; $\eta_{3a} = 0.027$m
Force [N]
Time (s)
Filtered Force ($F_{Meas} - F_{Meas,Empty}$)
Position [in m] {scale=200:1}
Inertia Force (M.a) {scale=10:1}
First-order Force ($(M+A).a + B.v$)

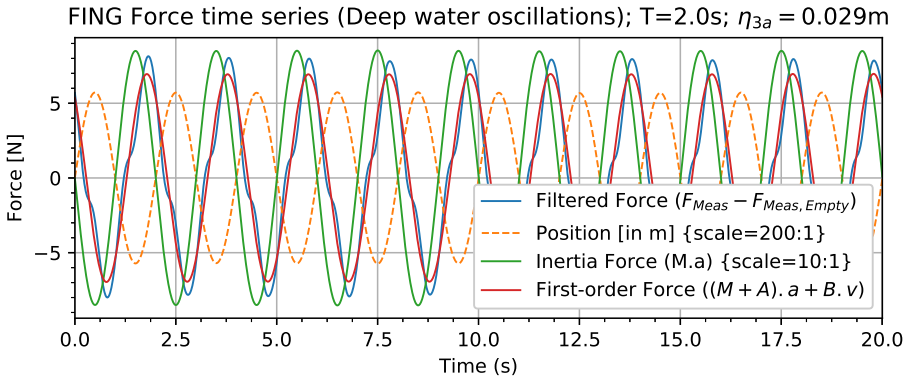
FING Force time series (Deep water oscillations); T=2.0s; $\eta_{3a} = 0.029$m
Force [N]
Time (s)
Filtered Force ($F_{Meas} - F_{Meas,Empty}$)
Position [in m] {scale=200:1}
Inertia Force (M.a) {scale=10:1}
First-order Force ($(M+A).a + B.v$)

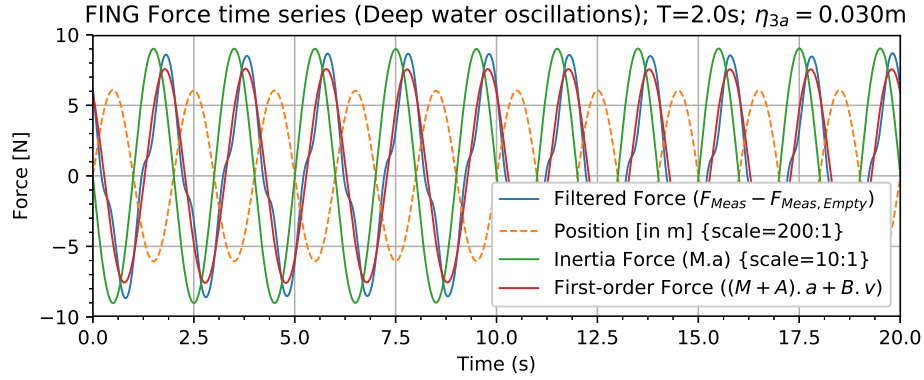
FING Force time series (Deep water oscillations); T=2.0s; $\eta_{3a} = 0.030$m
Force [N]
Time (s)
Filtered Force ($F_{Meas} - F_{Meas,Empty}$)
Position [in m] {scale=200:1}
Inertia Force (M.a) {scale=10:1}
First-order Force ($(M+A).a + B.v$)

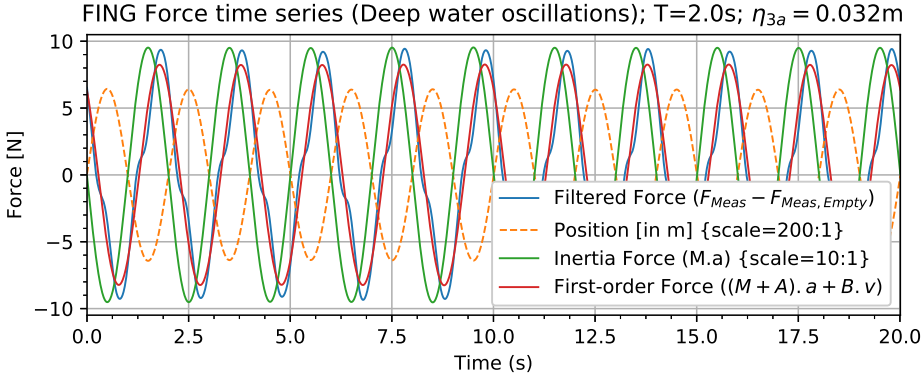
FING Force time series (Deep water oscillations); T=2.0s; $\eta_{3a} = 0.032$m
Force [N]
Time (s)
Filtered Force ($F_{Meas} - F_{Meas,Empty}$)
Position [in m] {scale=200:1}
Inertia Force (M.a) {scale=10:1}
First-order Force ($(M+A).a + B.v$)

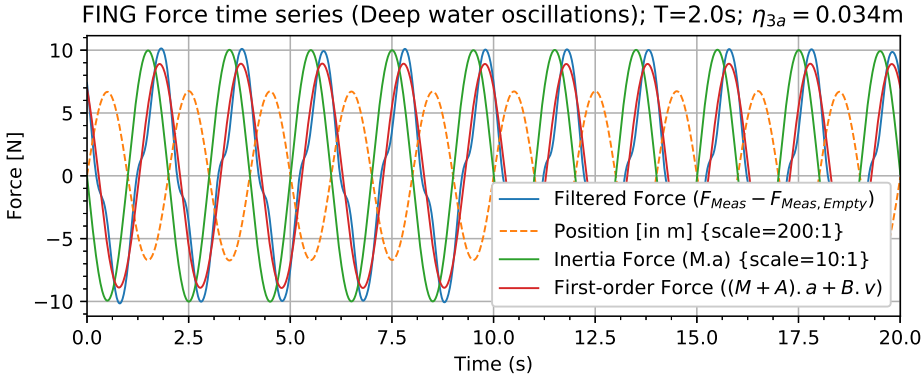
FING Force time series (Deep water oscillations); T=2.0s; $\eta_{3a} = 0.034$m
Force [N]
Time (s)
Filtered Force ($F_{Meas} - F_{Meas,Empty}$)
Position [in m] {scale=200:1}
Inertia Force (M.a) {scale=10:1}
First-order Force ($(M+A).a + B.v$)

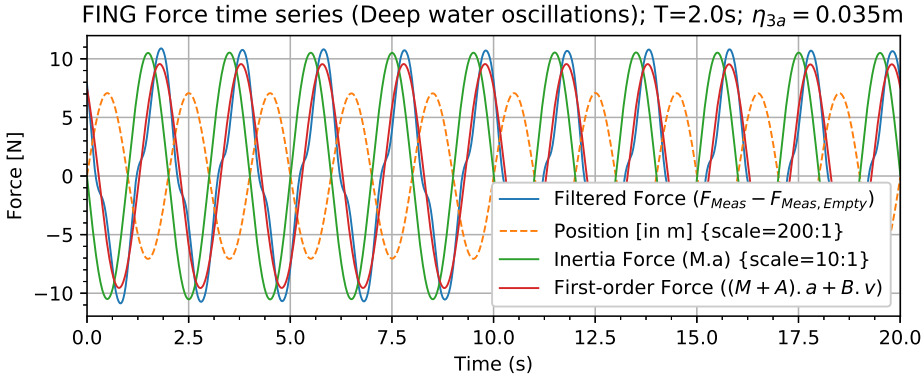
FING Force time series (Deep water oscillations); T=2.0s; $\eta_{3a} = 0.035$m
Force [N]
Time (s)
Filtered Force ($F_{Meas} - F_{Meas,Empty}$)
Position [in m] {scale=200:1}
Inertia Force (M.a) {scale=10:1}
First-order Force ($(M+A).a + B.v$)

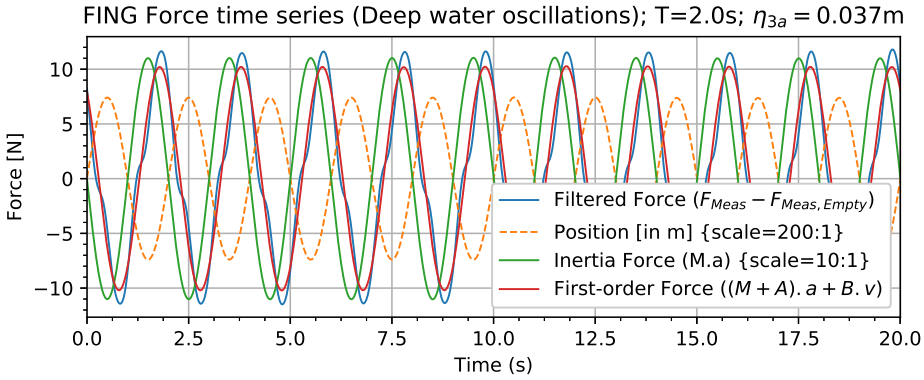
FING Force time series (Deep water oscillations); T=2.0s; $\eta_{3a} = 0.037$m
Force [N]
Time (s)
Filtered Force ($F_{Meas} - F_{Meas,Empty}$)
Position [in m] {scale=200:1}
Inertia Force (M.a) {scale=10:1}
First-order Force ($(M+A).a + B.v$)

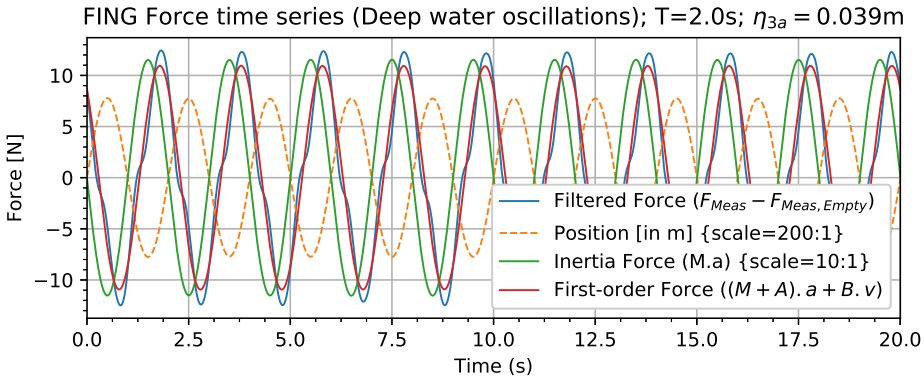
FING Force time series (Deep water oscillations); T=2.0s; $\eta_{3a} = 0.039$m
Force [N]
Time (s)
Filtered Force ($F_{Meas} - F_{Meas,Empty}$)
Position [in m] {scale=200:1}
Inertia Force (M.a) {scale=10:1}
First-order Force ($(M+A).a + B.v$)

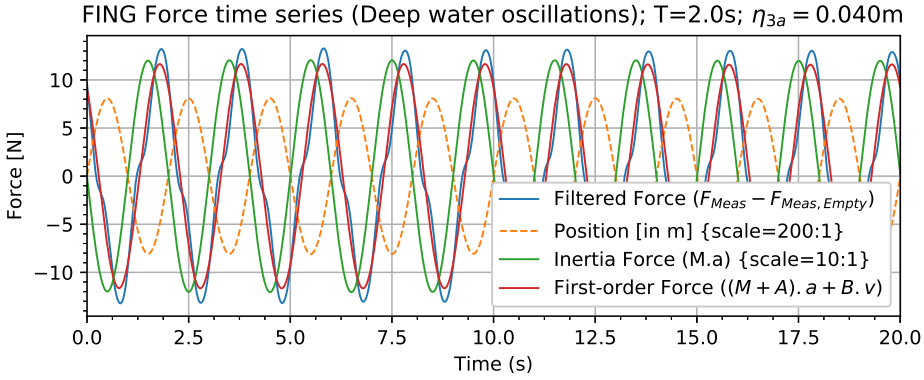
FING Force time series (Deep water oscillations); T=2.0s; $\eta_{3a} = 0.040$m
Force [N]
Time (s)
Filtered Force ($F_{Meas} - F_{Meas,Empty}$)
Position [in m] {scale=200:1}
Inertia Force (M.a) {scale=10:1}
First-order Force ($(M+A).a + B.v$)

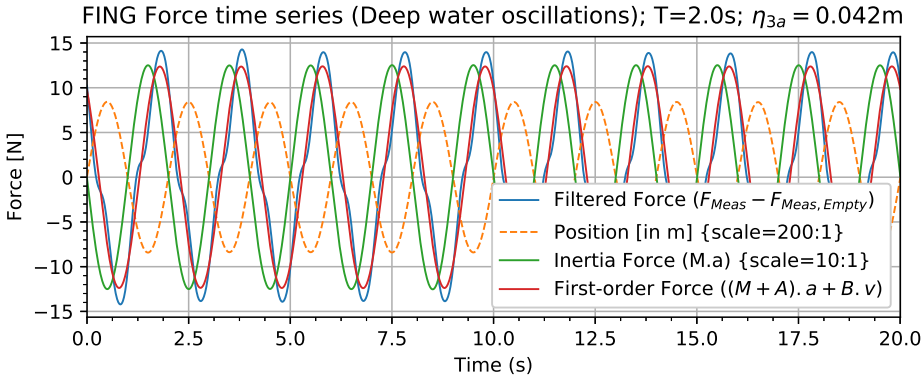
FING Force time series (Deep water oscillations); T=2.0s; $\eta_{3a} = 0.042$m
Force [N]
Time (s)
Filtered Force ($F_{Meas} - F_{Meas,Empty}$)
Position [in m] {scale=200:1}
Inertia Force (M.a) {scale=10:1}
First-order Force ($(M+A).a + B.v$)

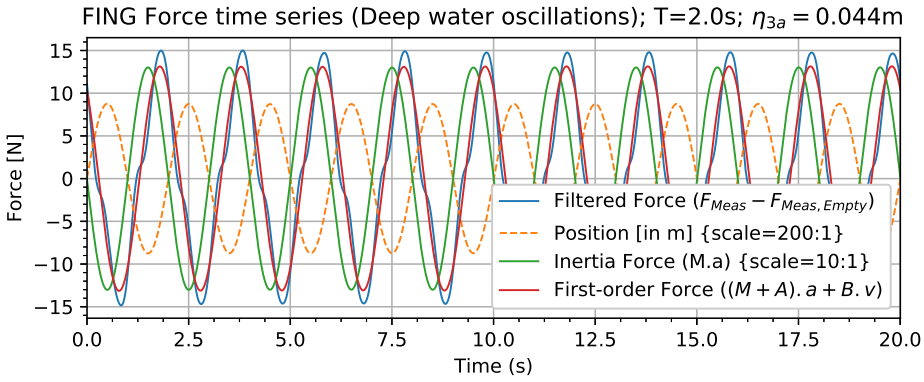
FING Force time series (Deep water oscillations); T=2.0s; $\eta_{3a} = 0.044$m
Force [N]
Time (s)
Filtered Force ($F_{Meas} - F_{Meas,Empty}$)
Position [in m] {scale=200:1}
Inertia Force (M.a) {scale=10:1}
First-order Force ($(M+A).a + B.v$)

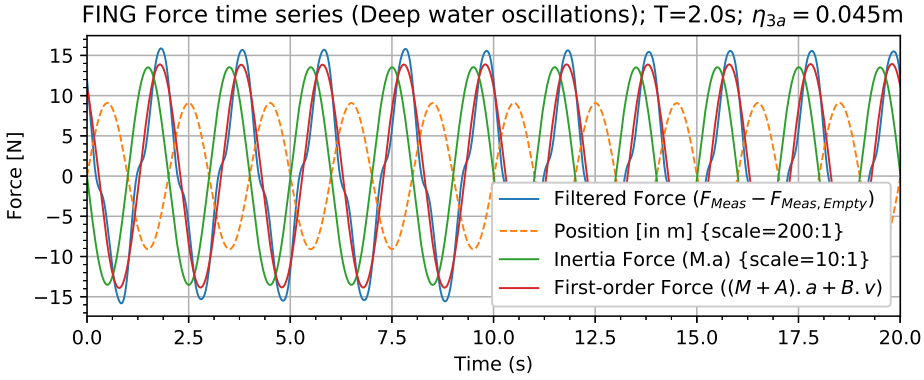
FING Force time series (Deep water oscillations); T=2.0s; $\eta_{3a} = 0.045$m
Force [N]
Time (s)
Filtered Force ($F_{Meas} - F_{Meas,Empty}$)
Position [in m] {scale=200:1}
Inertia Force (M.a) {scale=10:1}
First-order Force ($(M+A).a + B.v$)

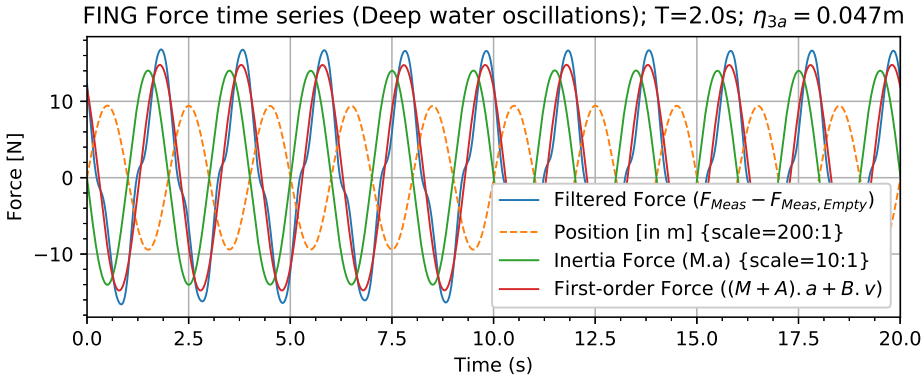
FING Force time series (Deep water oscillations); T=2.0s; $\eta_{3a} = 0.047$m
Force [N]
Time (s)
Filtered Force ($F_{Meas} - F_{Meas,Empty}$)
Position [in m] {scale=200:1}
Inertia Force (M.a) {scale=10:1}
First-order Force ($(M+A).a + B.v$)

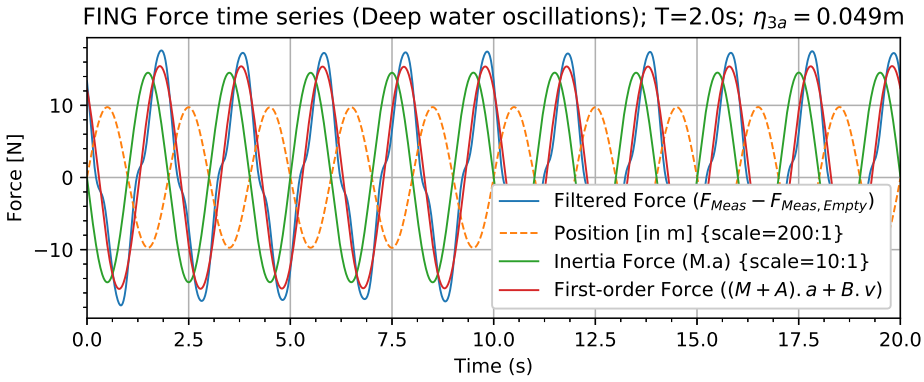
FING Force time series (Deep water oscillations); T=2.0s; $\eta_{3a} = 0.049$m
Force [N]
Time (s)
Filtered Force ($F_{Meas} - F_{Meas,Empty}$)
Position [in m] {scale=200:1}
Inertia Force (M.a) {scale=10:1}
First-order Force ($(M+A).a + B.v$)

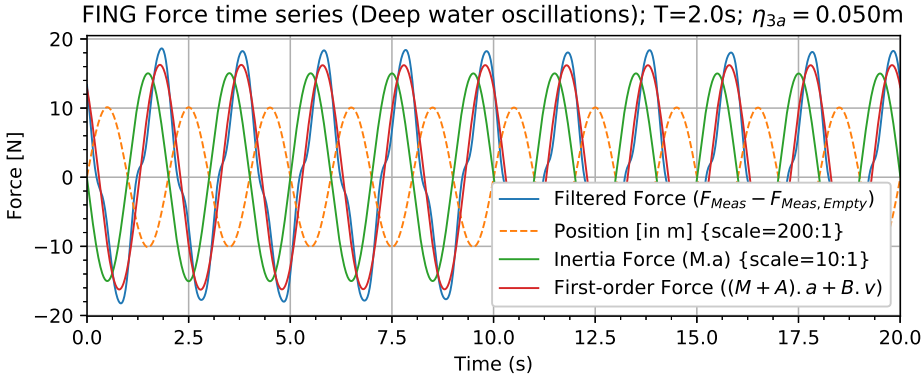
FING Force time series (Deep water oscillations); T=2.0s; $\eta_{3a} = 0.050$m
Force [N]
Time (s)
Filtered Force ($F_{Meas} - F_{Meas,Empty}$)
Position [in m] {scale=200:1}
Inertia Force (M.a) {scale=10:1}
First-order Force ($(M+A).a + B.v$)

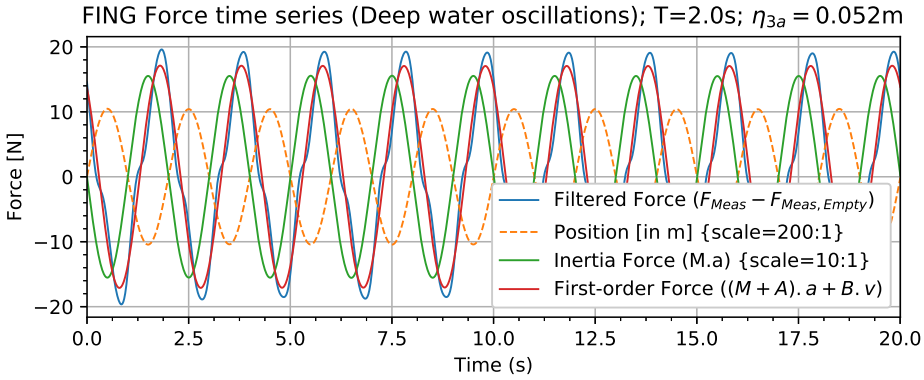
FING Force time series (Deep water oscillations); T=2.0s; $\eta_{3a} = 0.052$m
Force [N]
Time (s)
Filtered Force ($F_{Meas} - F_{Meas,Empty}$)
Position [in m] {scale=200:1}
Inertia Force (M.a) {scale=10:1}
First-order Force ($(M+A).a + B.v$)

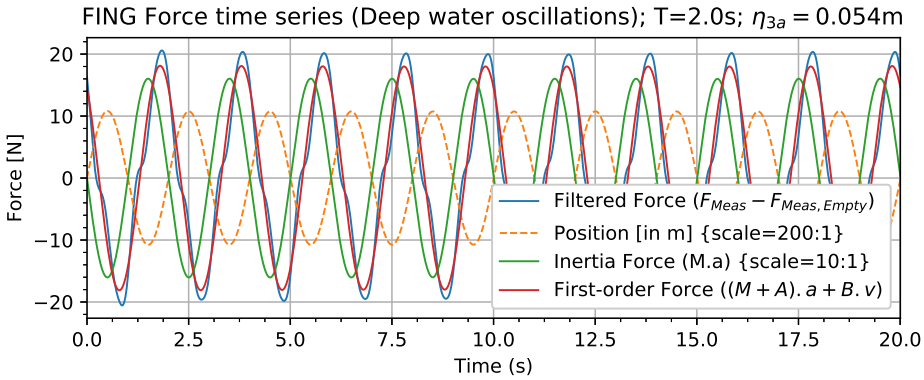
FING Force time series (Deep water oscillations); T=2.0s; $\eta_{3a} = 0.054$m
Force [N]
Time (s)
Filtered Force ($F_{Meas} - F_{Meas,Empty}$)
Position [in m] {scale=200:1}
Inertia Force (M.a) {scale=10:1}
First-order Force ($(M+A).a + B.v$)

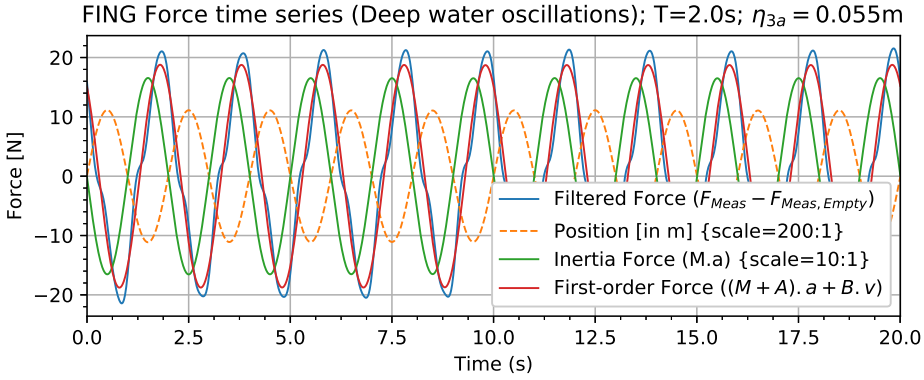
FING Force time series (Deep water oscillations); T=2.0s; $\eta_{3a} = 0.055$m
Force [N]
Time (s)
Filtered Force ($F_{Meas} - F_{Meas,Empty}$)
Position [in m] {scale=200:1}
Inertia Force (M.a) {scale=10:1}
First-order Force ($(M+A).a + B.v$)

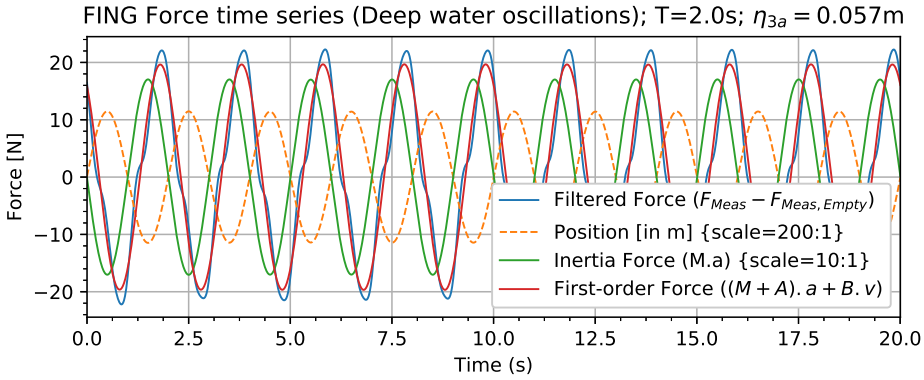
FING Force time series (Deep water oscillations); T=2.0s; $\eta_{3a} = 0.057$m
Force [N]
Time (s)
Filtered Force ($F_{Meas} - F_{Meas,Empty}$)
Position [in m] {scale=200:1}
Inertia Force (M.a) {scale=10:1}
First-order Force ($(M+A).a + B.v$)

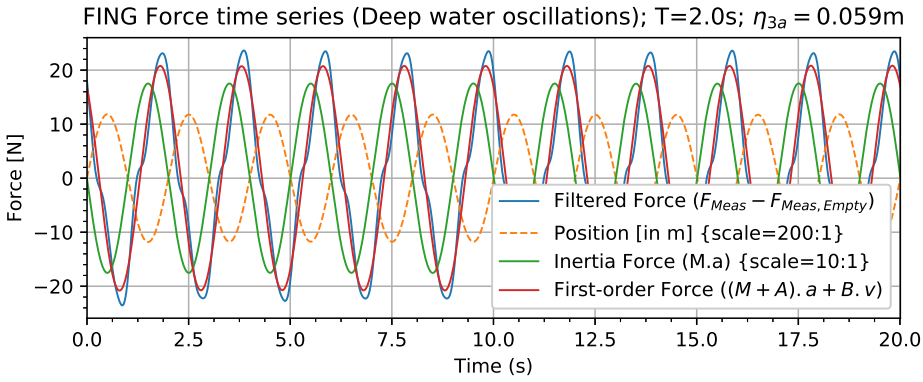
FING Force time series (Deep water oscillations); T=2.0s; $\eta_{3a} = 0.059$m
Force [N]
Time (s)
Filtered Force ($F_{Meas} - F_{Meas,Empty}$)
Position [in m] {scale=200:1}
Inertia Force (M.a) {scale=10:1}
First-order Force ($(M+A).a + B.v$)

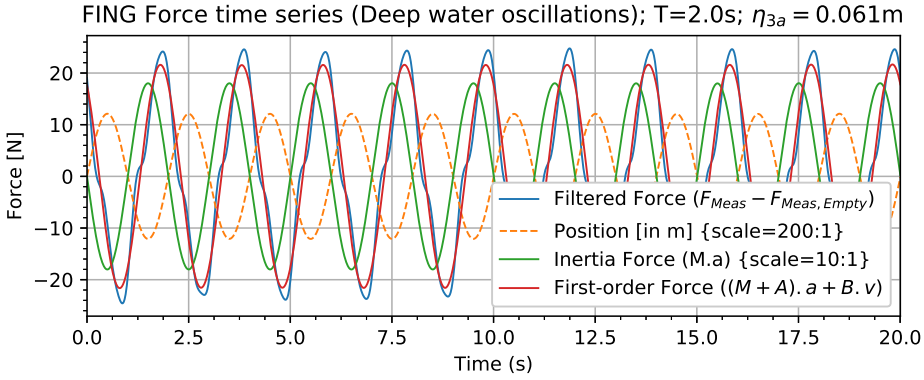
FING Force time series (Deep water oscillations); T=2.0s; $\eta_{3a} = 0.061$m
Force [N]
Time (s)
Filtered Force ($F_{Meas} - F_{Meas,Empty}$)
Position [in m] {scale=200:1}
Inertia Force (M.a) {scale=10:1}
First-order Force ($(M+A).a + B.v$)

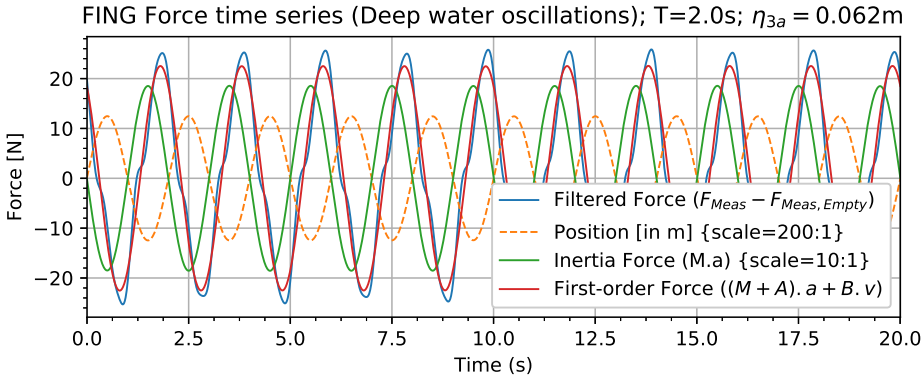
FING Force time series (Deep water oscillations); T=2.0s; $\eta_{3a} = 0.062$m
Force [N]
Time (s)
Filtered Force ($F_{Meas} - F_{Meas,Empty}$)
Position [in m] {scale=200:1}
Inertia Force (M.a) {scale=10:1}
First-order Force ($(M+A).a + B.v$)

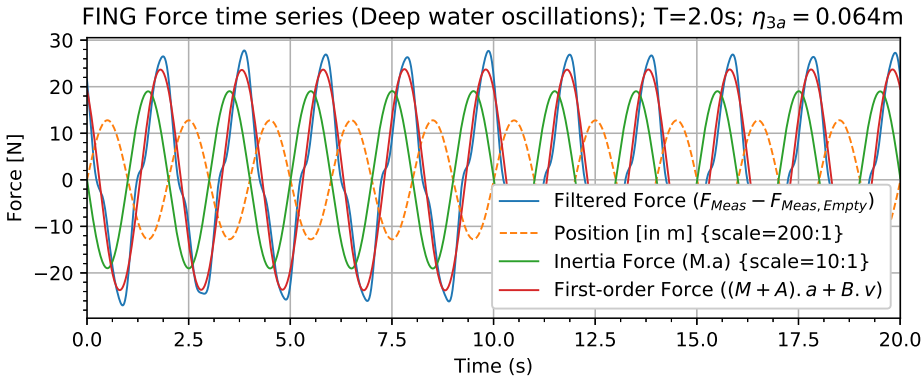
FING Force time series (Deep water oscillations); T=2.0s; $\eta_{3a} = 0.064$m
Force [N]
Time (s)
Filtered Force ($F_{Meas} - F_{Meas,Empty}$)
Position [in m] {scale=200:1}
Inertia Force (M.a) {scale=10:1}
First-order Force ($(M+A).a + B.v$)

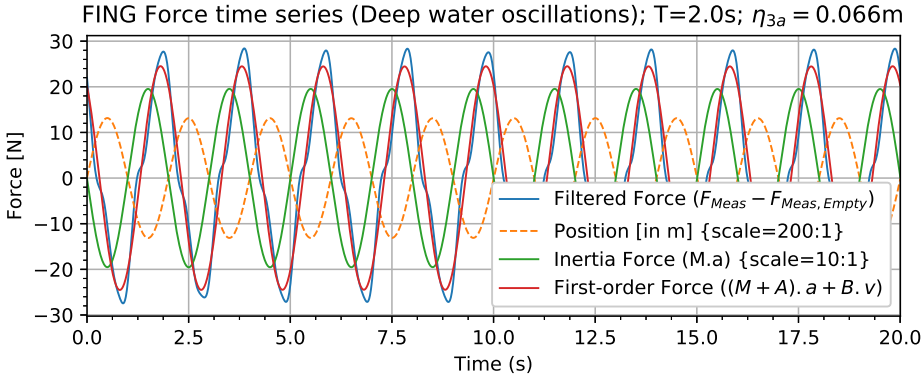
FING Force time series (Deep water oscillations); T=2.0s; $\eta_{3a} = 0.066$m
Force [N]
Time (s)
Filtered Force ($F_{Meas} - F_{Meas,Empty}$)
Position [in m] {scale=200:1}
Inertia Force (M.a) {scale=10:1}
First-order Force ($(M+A).a + B.v$)

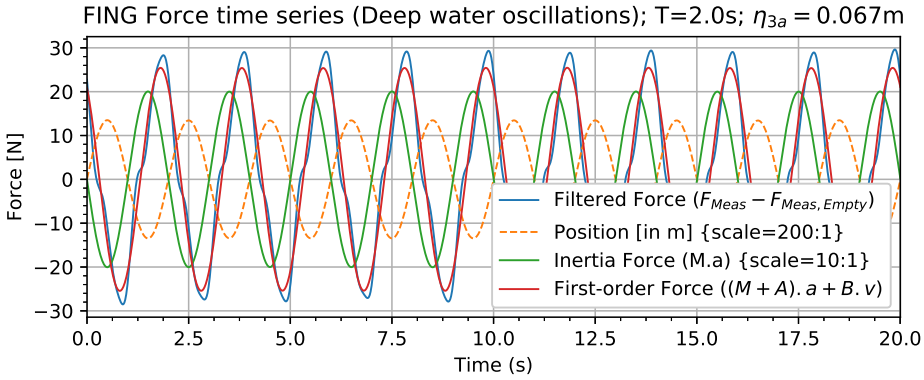
FING Force time series (Deep water oscillations); T=2.0s; $\eta_{3a} = 0.067$m
Force [N]
Time (s)
Filtered Force ($F_{Meas} - F_{Meas,Empty}$)
Position [in m] {scale=200:1}
Inertia Force (M.a) {scale=10:1}
First-order Force ($(M+A).a + B.v$)

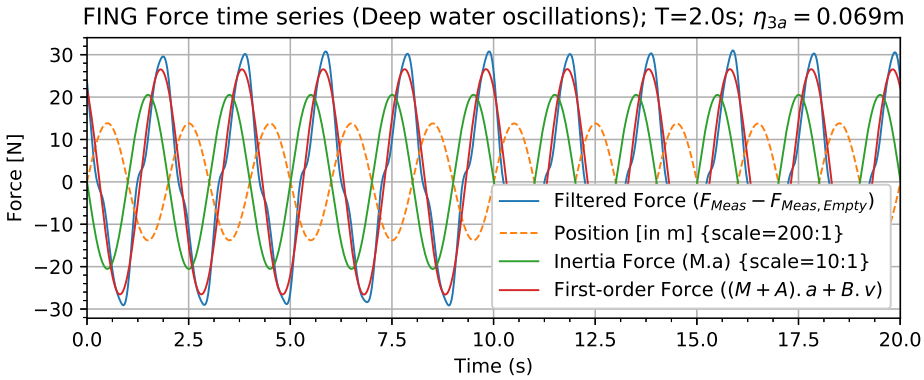
FING Force time series (Deep water oscillations); T=2.0s; $\eta_{3a} = 0.069$m
Force [N]
Time (s)
Filtered Force ($F_{Meas} - F_{Meas,Empty}$)
Position [in m] {scale=200:1}
Inertia Force (M.a) {scale=10:1}
First-order Force ($(M+A).a + B.v$)

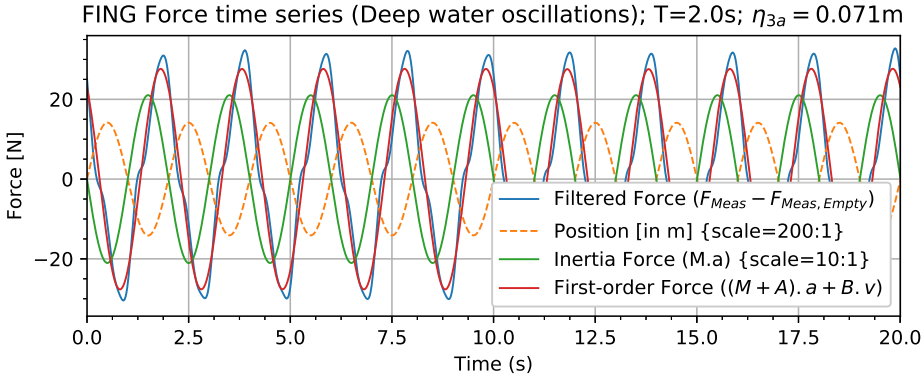
FING Force time series (Deep water oscillations); T=2.0s; $\eta_{3a} = 0.071$m
Force [N]
Time (s)
Filtered Force ($F_{Meas} - F_{Meas,Empty}$)
Position [in m] {scale=200:1}
Inertia Force (M.a) {scale=10:1}
First-order Force ($(M+A).a + B.v$)

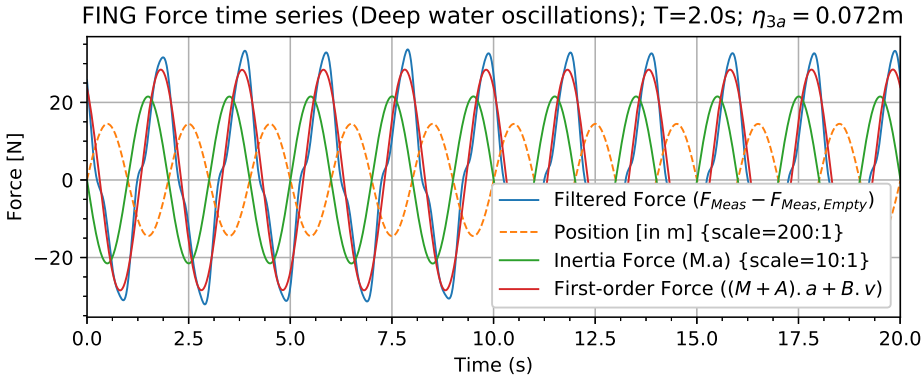
FING Force time series (Deep water oscillations); T=2.0s; $\eta_{3a} = 0.072$m
Force [N]
Time (s)
Filtered Force ($F_{Meas} - F_{Meas,Empty}$)
Position [in m] {scale=200:1}
Inertia Force (M.a) {scale=10:1}
First-order Force ($(M+A).a + B.v$)

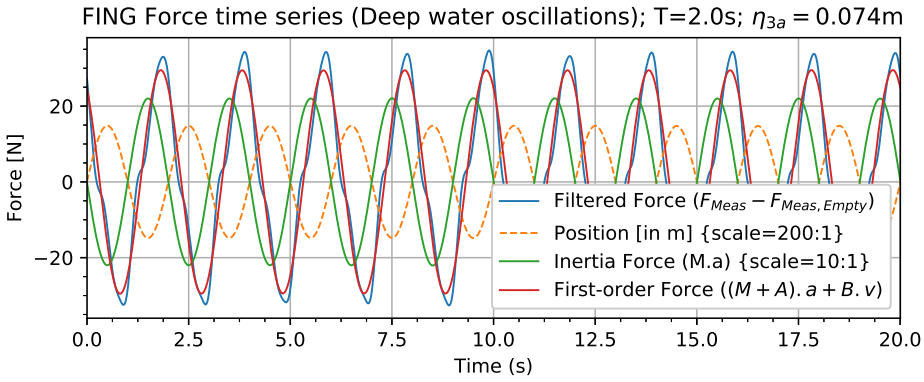
FING Force time series (Deep water oscillations); T=2.0s; $\eta_{3a} = 0.074$m
Force [N]
Time (s)
Filtered Force ($F_{Meas} - F_{Meas,Empty}$)
Position [in m] {scale=200:1}
Inertia Force (M.a) {scale=10:1}
First-order Force ($(M+A).a + B.v$)

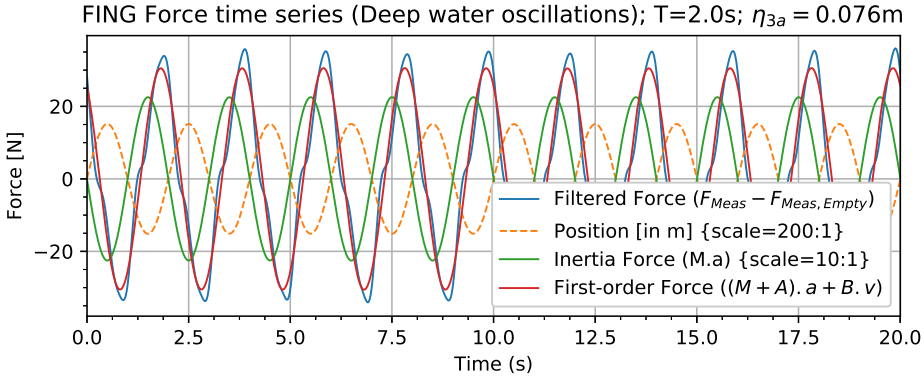
FING Force time series (Deep water oscillations); T=2.0s; $\eta_{3a} = 0.076$m
Force [N]
Time (s)
Filtered Force ($F_{Meas} - F_{Meas,Empty}$)
Position [in m] {scale=200:1}
Inertia Force (M.a) {scale=10:1}
First-order Force ($(M+A).a + B.v$)

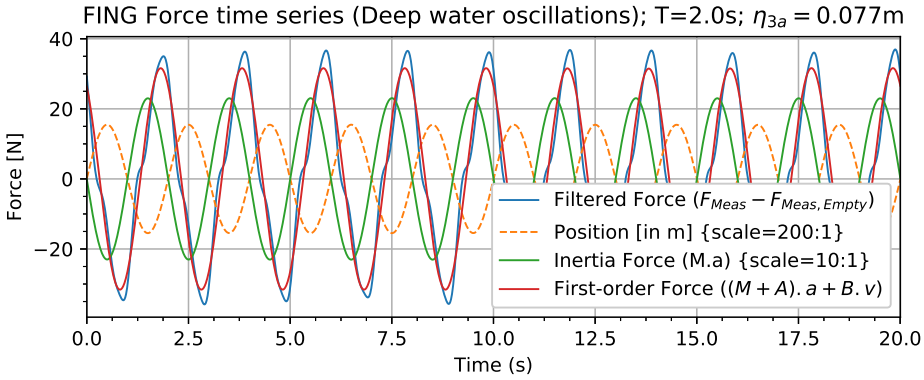
FING Force time series (Deep water oscillations); T=2.0s; $\eta_{3a} = 0.077$m
Force [N]
Time (s)
Filtered Force ($F_{Meas} - F_{Meas,Empty}$)
Position [in m] {scale=200:1}
Inertia Force (M.a) {scale=10:1}
First-order Force ($(M+A).a + B.v$)

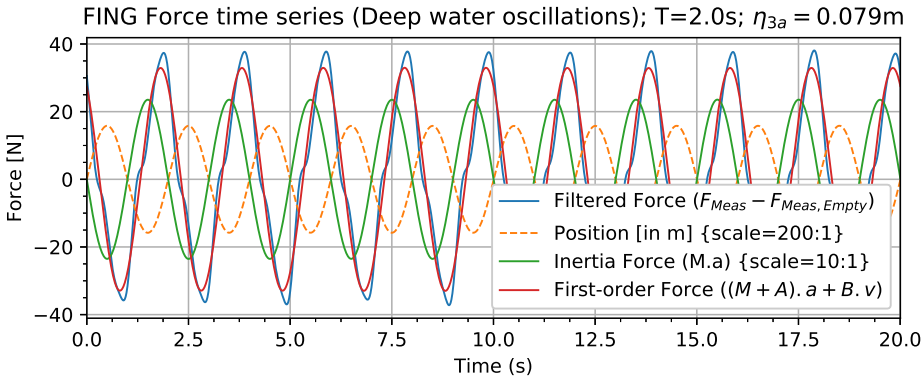
FING Force time series (Deep water oscillations); T=2.0s; $\eta_{3a} = 0.079$m
Force [N]
Time (s)
Filtered Force ($F_{Meas} - F_{Meas,Empty}$)
Position [in m] {scale=200:1}
Inertia Force (M.a) {scale=10:1}
First-order Force ($(M+A).a + B.v$)

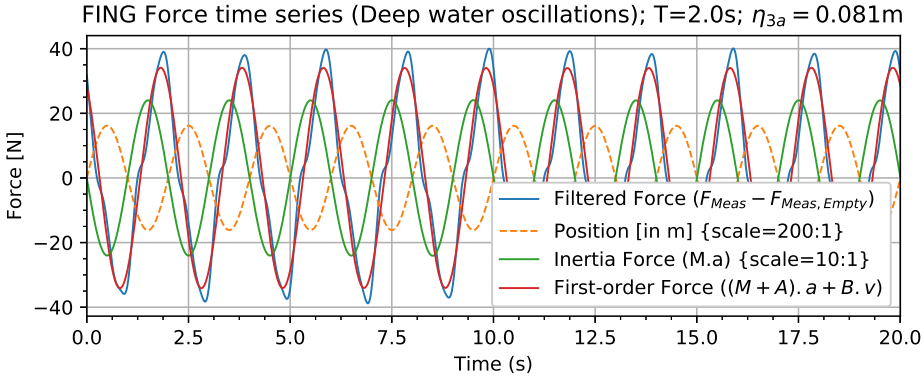
FING Force time series (Deep water oscillations); T=2.0s; $\eta_{3a} = 0.081$m
Force [N]
Time (s)
Filtered Force ($F_{Meas} - F_{Meas,Empty}$)
Position [in m] {scale=200:1}
Inertia Force (M.a) {scale=10:1}
First-order Force ($(M+A).a + B.v$)

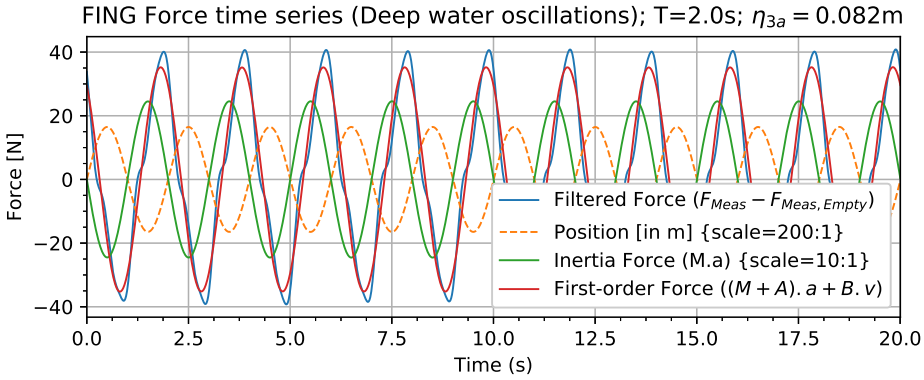
FING Force time series (Deep water oscillations); T=2.0s; $\eta_{3a} = 0.082$m
Force [N]
Time (s)
Filtered Force ($F_{Meas} - F_{Meas,Empty}$)
Position [in m] {scale=200:1}
Inertia Force (M.a) {scale=10:1}
First-order Force ($(M+A).a + B.v$)

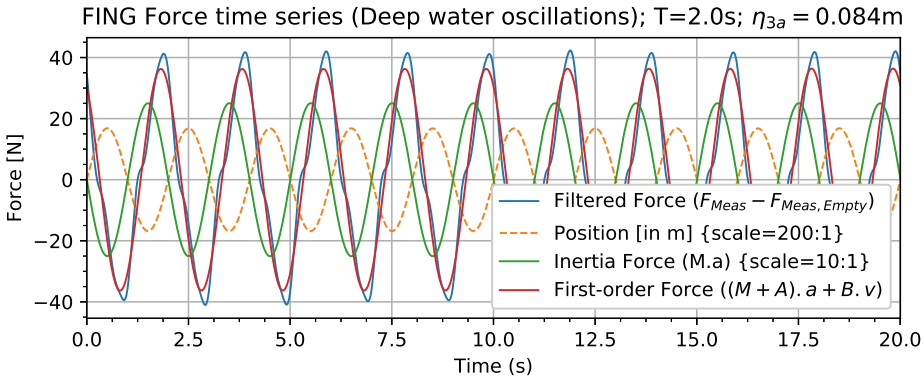
FING Force time series (Deep water oscillations); T=2.0s; $\eta_{3a} = 0.084$m
Force [N]
Time (s)
Filtered Force ($F_{Meas} - F_{Meas,Empty}$)
Position [in m] {scale=200:1}
Inertia Force (M.a) {scale=10:1}
First-order Force ($(M+A).a + B.v$)

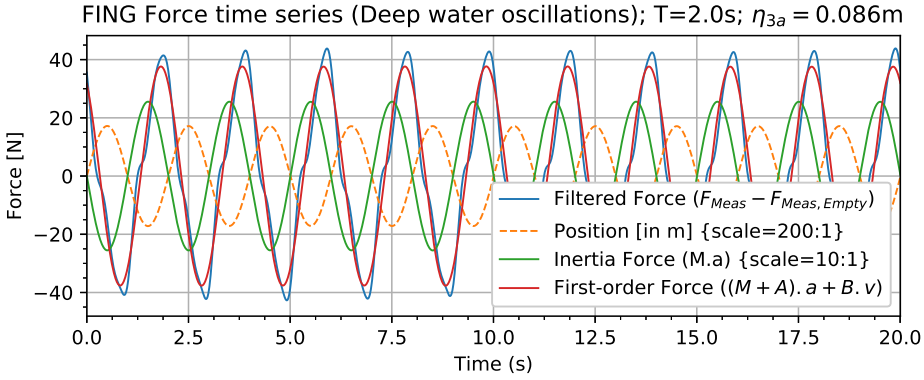
FING Force time series (Deep water oscillations); T=2.0s; $\eta_{3a} = 0.086$m
Force [N]
Time (s)
Filtered Force ($F_{Meas} - F_{Meas,Empty}$)
Position [in m] {scale=200:1}
Inertia Force (M.a) {scale=10:1}
First-order Force ($(M+A).a + B.v$)

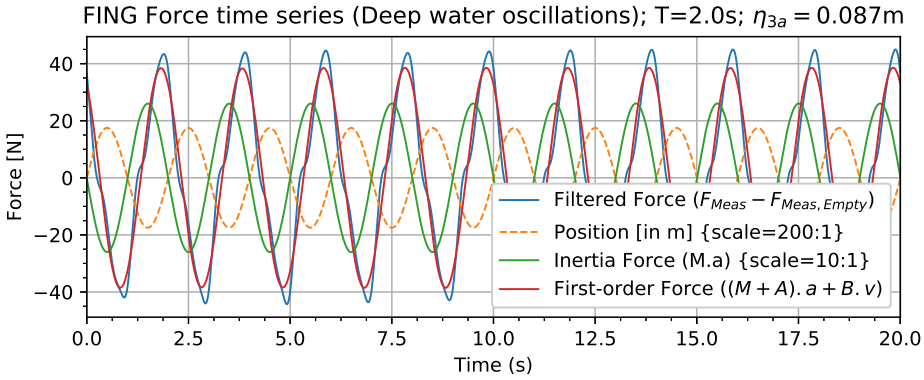
FING Force time series (Deep water oscillations); T=2.0s; $\eta_{3a} = 0.087$m
Force [N]
Time (s)
Filtered Force ($F_{Meas} - F_{Meas,Empty}$)
Position [in m] {scale=200:1}
Inertia Force (M.a) {scale=10:1}
First-order Force ($(M+A).a + B.v$)

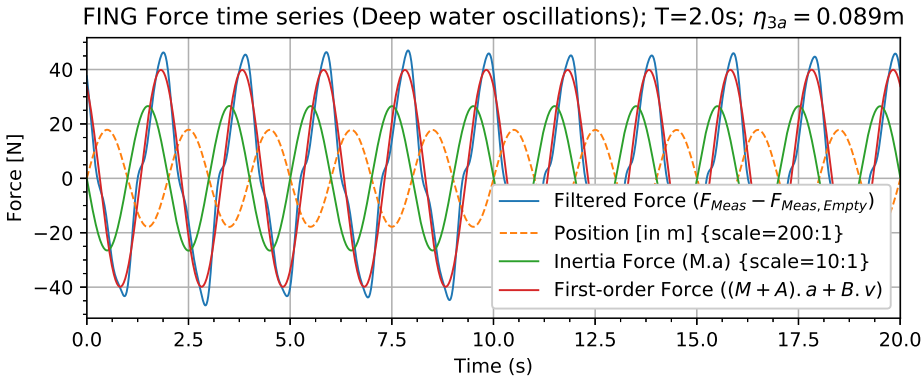
FING Force time series (Deep water oscillations); T=2.0s; $\eta_{3a} = 0.089$m
Force [N]
Time (s)
Filtered Force ($F_{Meas} - F_{Meas,Empty}$)
Position [in m] {scale=200:1}
Inertia Force (M.a) {scale=10:1}
First-order Force ($(M+A).a + B.v$)

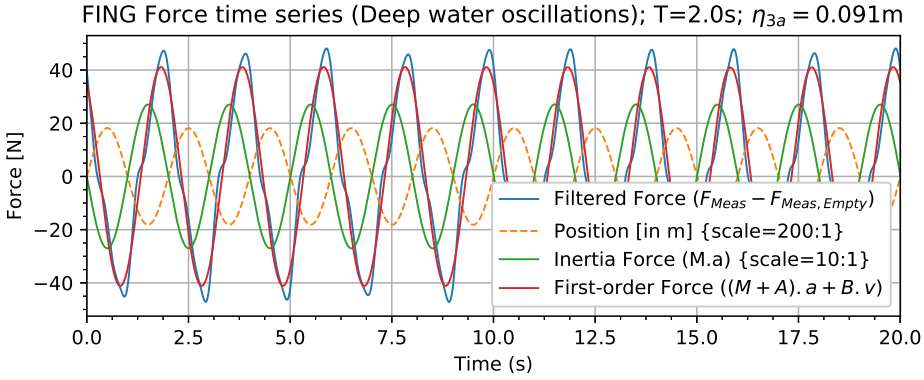
FING Force time series (Deep water oscillations); T=2.0s; $\eta_{3a} = 0.091$m
Force [N]
Time (s)
Filtered Force ($F_{Meas} - F_{Meas,Empty}$)
Position [in m] {scale=200:1}
Inertia Force (M.a) {scale=10:1}
First-order Force ($(M+A).a + B.v$)

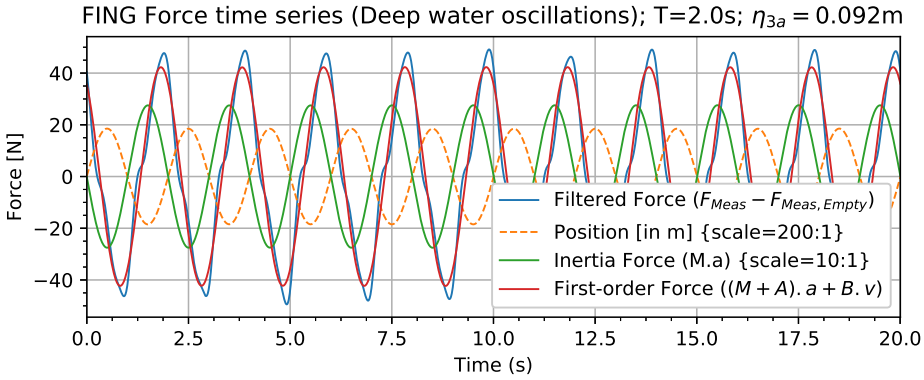
FING Force time series (Deep water oscillations); T=2.0s; $\eta_{3a} = 0.092$m
Force [N]
Time (s)
Filtered Force ($F_{Meas} - F_{Meas,Empty}$)
Position [in m] {scale=200:1}
Inertia Force (M.a) {scale=10:1}
First-order Force ($(M+A).a + B.v$)

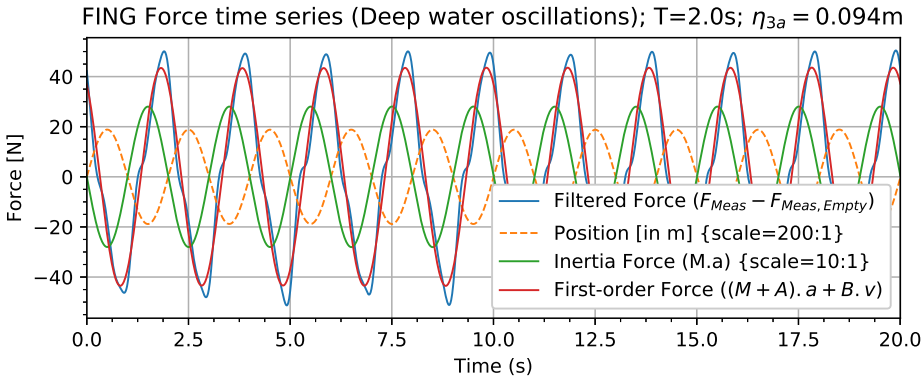
FING Force time series (Deep water oscillations); T=2.0s; $\eta_{3a} = 0.094$m
Force [N]
Time (s)
Filtered Force ($F_{Meas} - F_{Meas,Empty}$)
Position [in m] {scale=200:1}
Inertia Force (M.a) {scale=10:1}
First-order Force ($(M+A).a + B.v$)

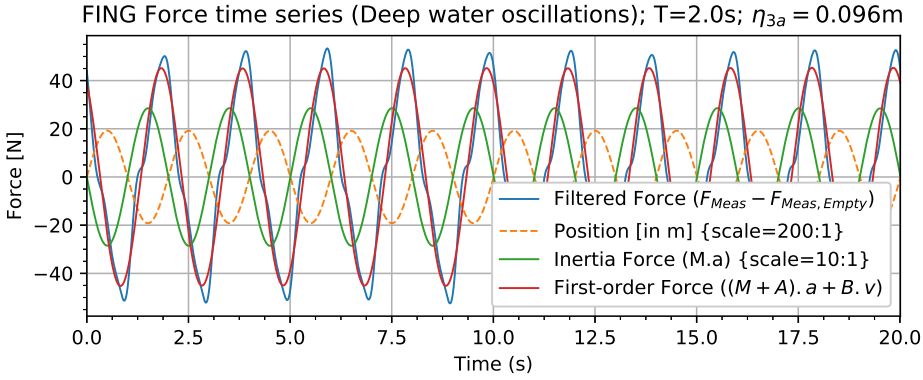
FING Force time series (Deep water oscillations); T=2.0s; $\eta_{3a} = 0.096$m
Force [N]
Time (s)
Filtered Force ($F_{Meas} - F_{Meas,Empty}$)
Position [in m] {scale=200:1}
Inertia Force (M.a) {scale=10:1}
First-order Force ($(M+A).a + B.v$)

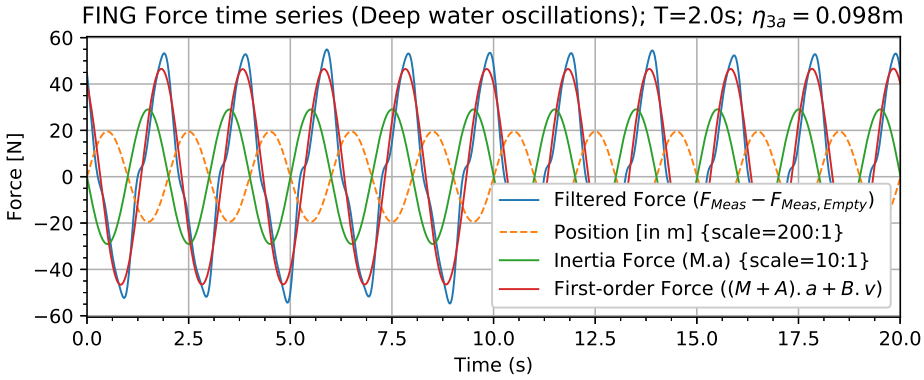
FING Force time series (Deep water oscillations); T=2.0s; $\eta_{3a} = 0.098$m
Force [N]
Time (s)
Filtered Force ($F_{Meas} - F_{Meas,Empty}$)
Position [in m] {scale=200:1}
Inertia Force (M.a) {scale=10:1}
First-order Force ($(M+A).a + B.v$)

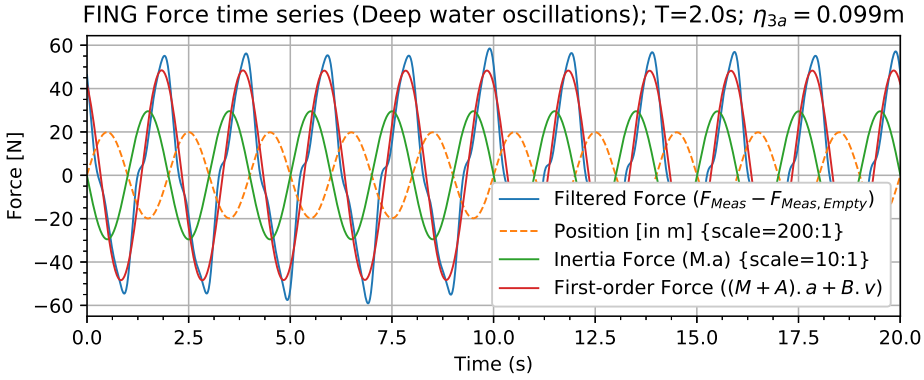
FING Force time series (Deep water oscillations); T=2.0s; $\eta_{3a} = 0.099$m
Force [N]
Time (s)
Filtered Force ($F_{Meas} - F_{Meas,Empty}$)
Position [in m] {scale=200:1}
Inertia Force (M.a) {scale=10:1}
First-order Force ($(M+A).a + B.v$)

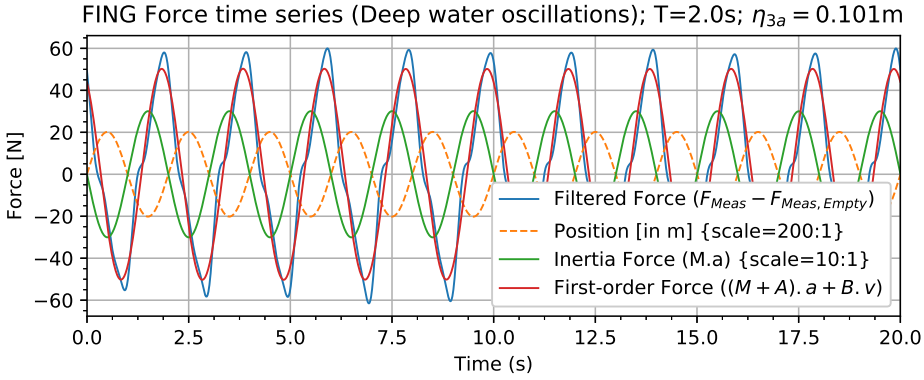
FING Force time series (Deep water oscillations); T=2.0s; $\eta_{3a} = 0.101$m
Force [N]
Time (s)
Filtered Force ($F_{Meas} - F_{Meas,Empty}$)
Position [in m] {scale=200:1}
Inertia Force (M.a) {scale=10:1}
First-order Force ($(M+A).a + B.v$)

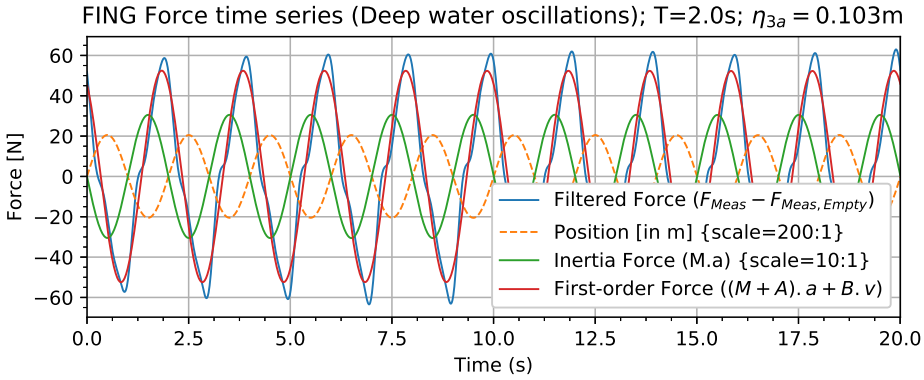
FING Force time series (Deep water oscillations); T=2.0s; $\eta_{3a} = 0.103$m
Force [N]
Time (s)
Filtered Force ($F_{Meas} - F_{Meas,Empty}$)
Position [in m] {scale=200:1}
Inertia Force (M.a) {scale=10:1}
First-order Force ($(M+A).a + B.v$)

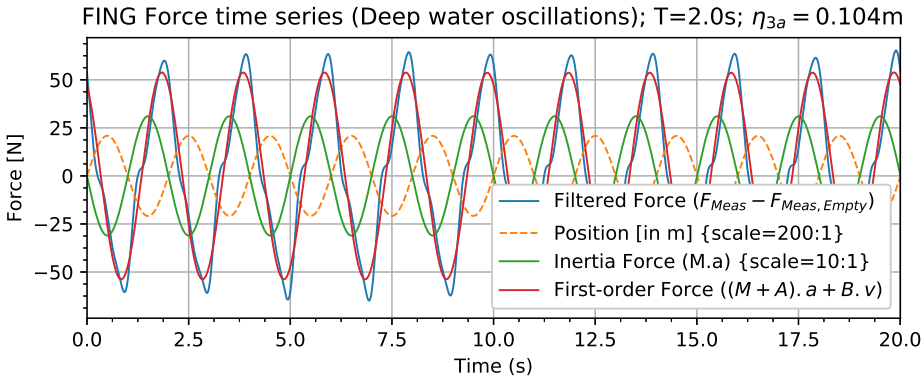
FING Force time series (Deep water oscillations); T=2.0s; $\eta_{3a} = 0.104$m
Force [N]
Time (s)
Filtered Force ($F_{Meas} - F_{Meas,Empty}$)
Position [in m] {scale=200:1}
Inertia Force (M.a) {scale=10:1}
First-order Force ($(M+A).a + B.v$)

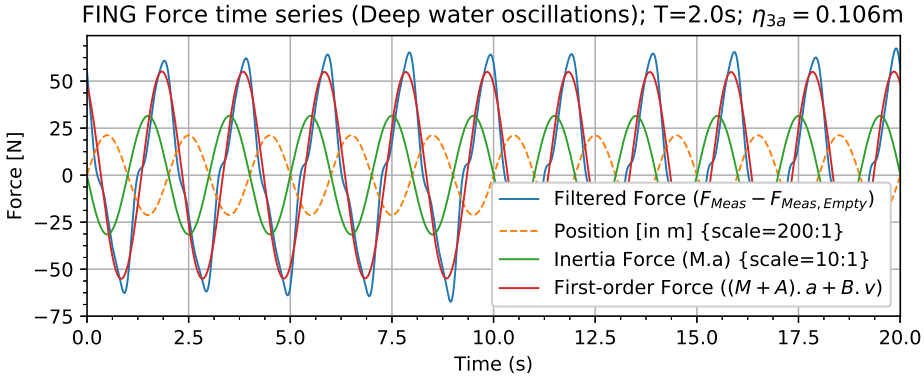
FING Force time series (Deep water oscillations); T=2.0s; $\eta_{3a} = 0.106$m
Force [N]
Time (s)
Filtered Force ($F_{Meas} - F_{Meas,Empty}$)
Position [in m] {scale=200:1}
Inertia Force (M.a) {scale=10:1}
First-order Force ($(M+A).a + B.v$)

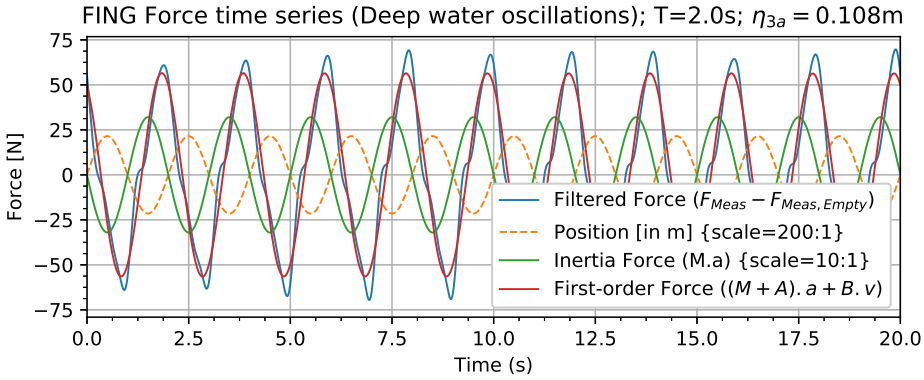
FING Force time series (Deep water oscillations); T=2.0s; $\eta_{3a} = 0.108$m
Force [N]
Time (s)
Filtered Force ($F_{Meas} - F_{Meas,Empty}$)
Position [in m] {scale=200:1}
Inertia Force (M.a) {scale=10:1}
First-order Force ($(M+A).a + B.v$)

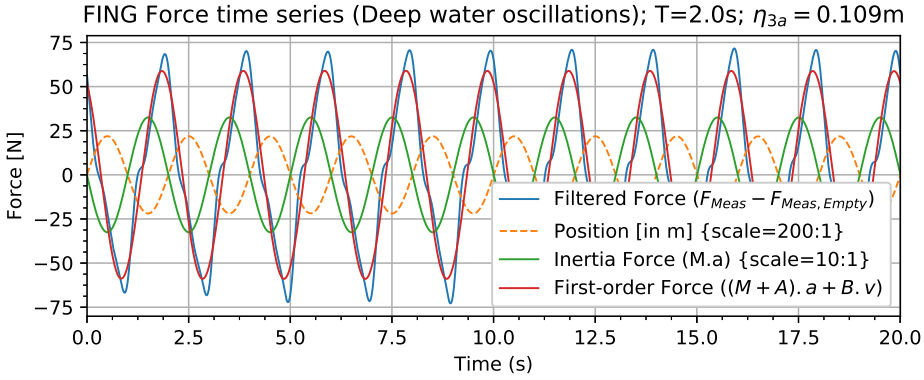
FING Force time series (Deep water oscillations); T=2.0s; $\eta_{3a} = 0.109$m
Force [N]
Time (s)
Filtered Force ($F_{Meas} - F_{Meas,Empty}$)
Position [in m] {scale=200:1}
Inertia Force (M.a) {scale=10:1}
First-order Force ($(M+A).a + B.v$)

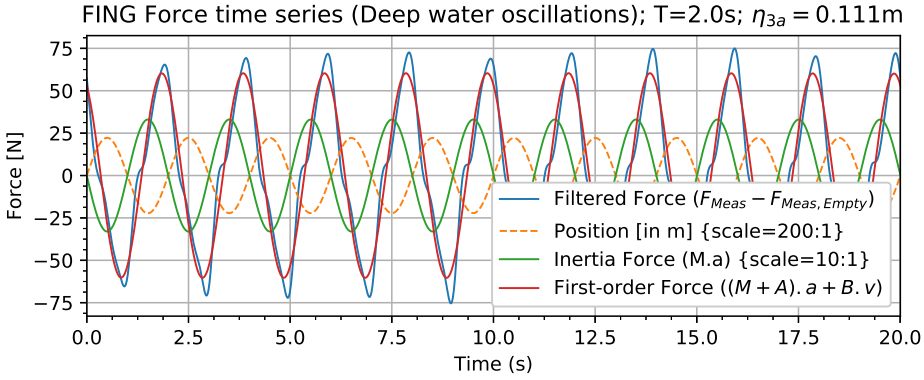
FING Force time series (Deep water oscillations); T=2.0s; $\eta_{3a} = 0.111$m
Force [N]
Time (s)
Filtered Force ($F_{Meas} - F_{Meas,Empty}$)
Position [in m] {scale=200:1}
Inertia Force (M.a) {scale=10:1}
First-order Force ($(M+A).a + B.v$)

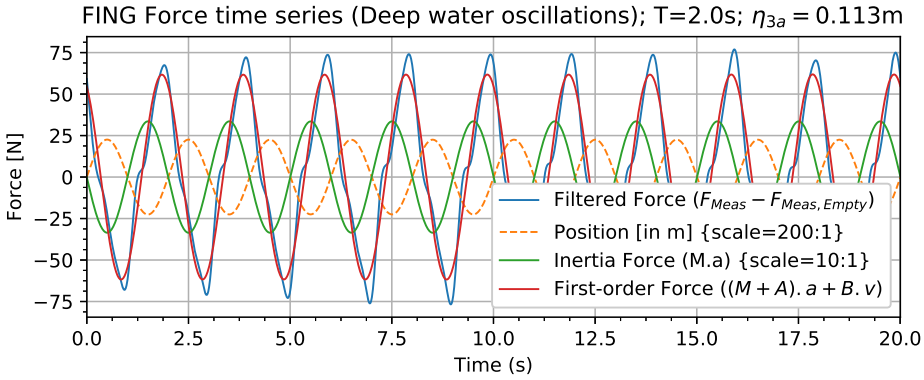
FING Force time series (Deep water oscillations); T=2.0s; $\eta_{3a} = 0.113$m
Force [N]
Time (s)
Filtered Force ($F_{Meas} - F_{Meas,Empty}$)
Position [in m] {scale=200:1}
Inertia Force (M.a) {scale=10:1}
First-order Force ($(M+A).a + B.v$)

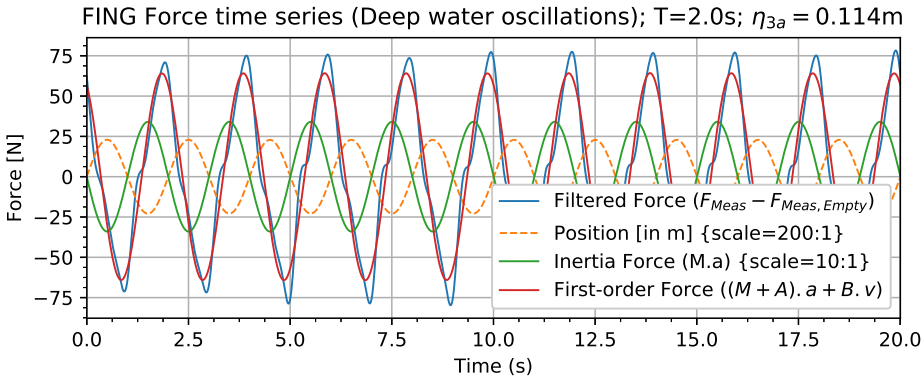
FING Force time series (Deep water oscillations); T=2.0s; $\eta_{3a} = 0.114$m
Force [N]
Time (s)
Filtered Force ($F_{Meas} - F_{Meas,Empty}$)
Position [in m] {scale=200:1}
Inertia Force (M.a) {scale=10:1}
First-order Force ($(M+A).a + B.v$)

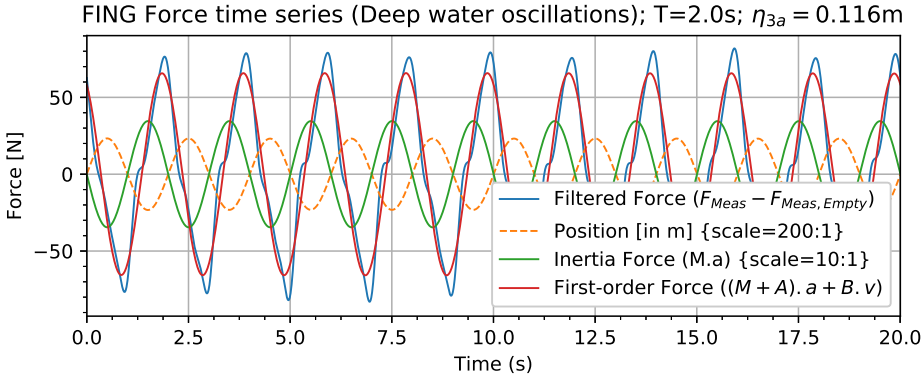
FING Force time series (Deep water oscillations); T=2.0s; $\eta_{3a} = 0.116$m
Force [N]
Time (s)
Filtered Force ($F_{Meas} - F_{Meas,Empty}$)
Position [in m] {scale=200:1}
Inertia Force (M.a) {scale=10:1}
First-order Force ($(M+A).a + B.v$)

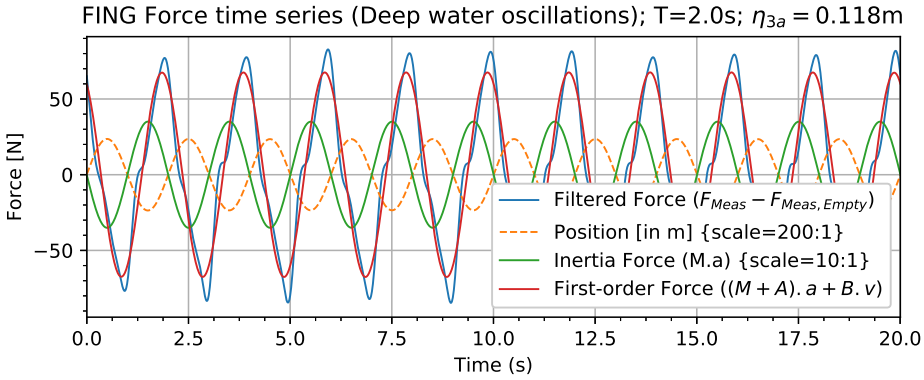
FING Force time series (Deep water oscillations); T=2.0s; $\eta_{3a} = 0.118$m
Force [N]
Time (s)
Filtered Force ($F_{Meas} - F_{Meas,Empty}$)
Position [in m] {scale=200:1}
Inertia Force (M.a) {scale=10:1}
First-order Force ($(M+A).a + B.v$)

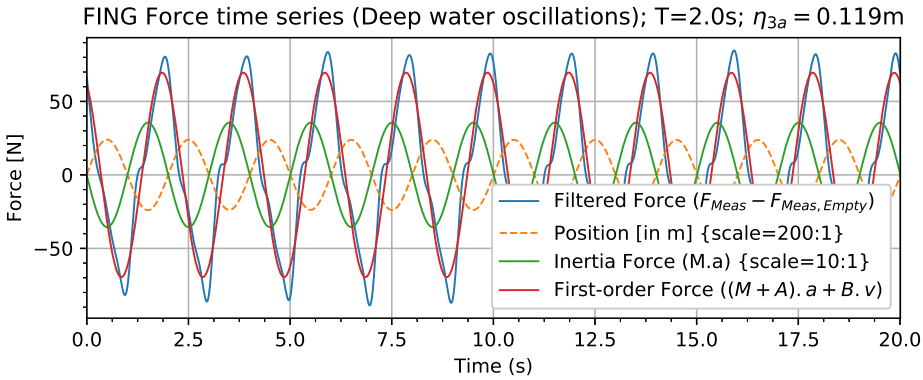
FING Force time series (Deep water oscillations); T=2.0s; $\eta_{3a} = 0.119$m
Force [N]
Time (s)
Filtered Force ($F_{Meas} - F_{Meas,Empty}$)
Position [in m] {scale=200:1}
Inertia Force (M.a) {scale=10:1}
First-order Force ($(M+A).a + B.v$)

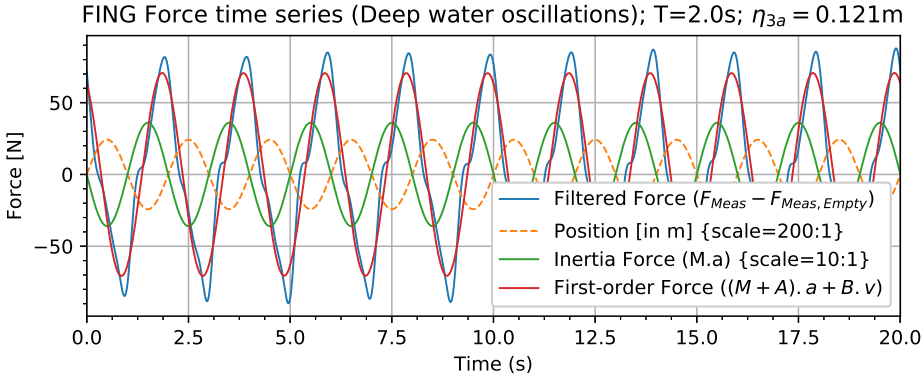
FING Force time series (Deep water oscillations); T=2.0s; $\eta_{3a} = 0.121$m
Force [N]
Time (s)
Filtered Force ($F_{Meas} - F_{Meas,Empty}$)
Position [in m] {scale=200:1}
Inertia Force (M.a) {scale=10:1}
First-order Force ($(M+A).a + B.v$)

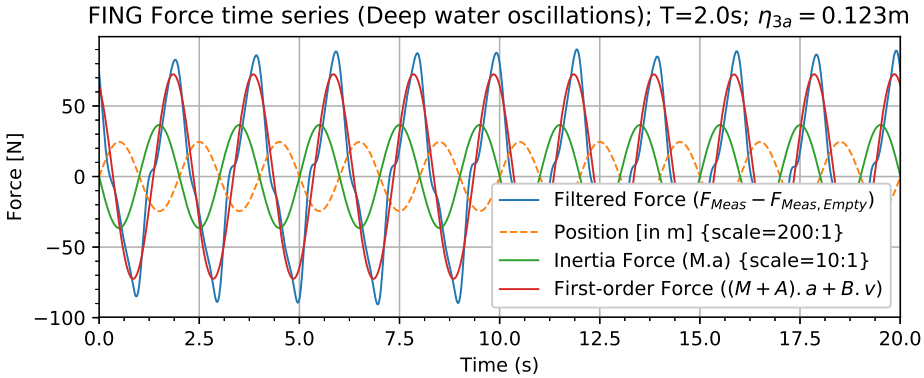
FING Force time series (Deep water oscillations); T=2.0s; $\eta_{3a} = 0.123$m
Force [N]
Time (s)
Filtered Force ($F_{Meas} - F_{Meas,Empty}$)
Position [in m] {scale=200:1}
Inertia Force (M.a) {scale=10:1}
First-order Force ($(M+A).a + B.v$)

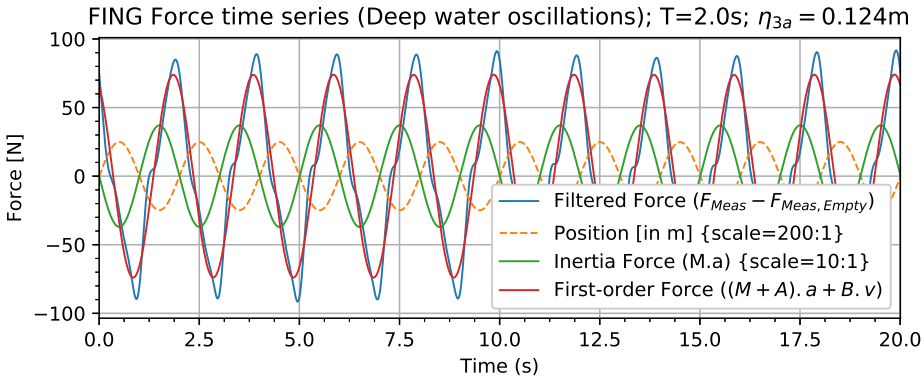
FING Force time series (Deep water oscillations); T=2.0s; $\eta_{3a} = 0.124$m
Force [N]
Time (s)
Filtered Force ($F_{Meas} - F_{Meas,Empty}$)
Position [in m] {scale=200:1}
Inertia Force (M.a) {scale=10:1}
First-order Force ($(M+A).a + B.v$)

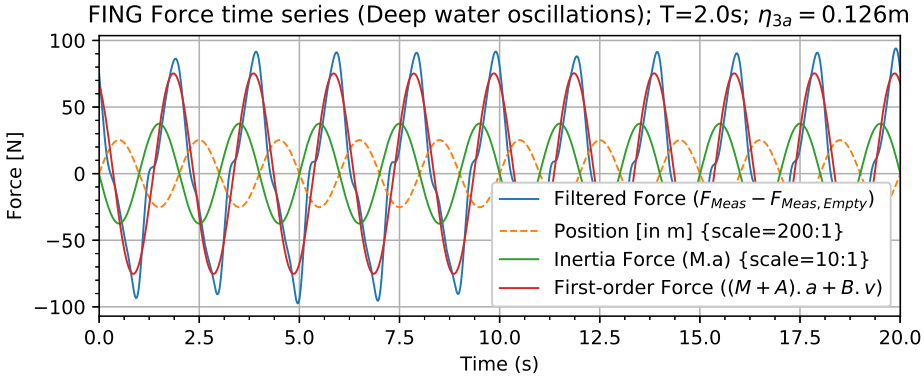
FING Force time series (Deep water oscillations); T=2.0s; $\eta_{3a} = 0.126$m
Force [N]
Time (s)
Filtered Force ($F_{Meas} - F_{Meas,Empty}$)
Position [in m] {scale=200:1}
Inertia Force (M.a) {scale=10:1}
First-order Force ($(M+A).a + B.v$)

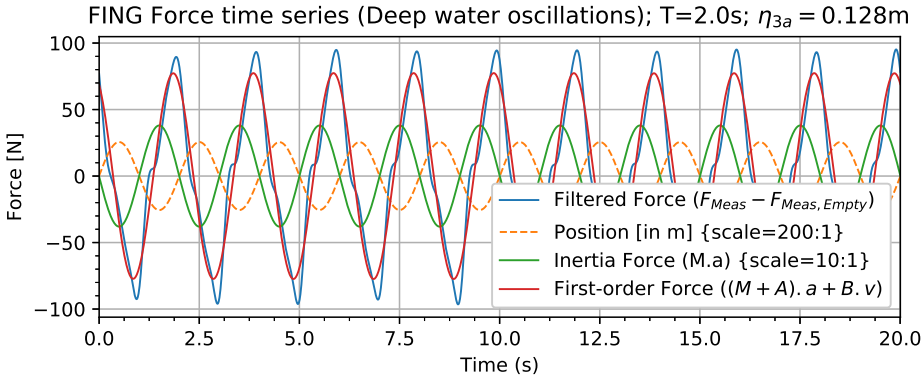
FING Force time series (Deep water oscillations); T=2.0s; $\eta_{3a} = 0.128$m
Force [N]
Time (s)
Filtered Force ($F_{Meas} - F_{Meas,Empty}$)
Position [in m] {scale=200:1}
Inertia Force (M.a) {scale=10:1}
First-order Force ($(M+A).a + B.v$)

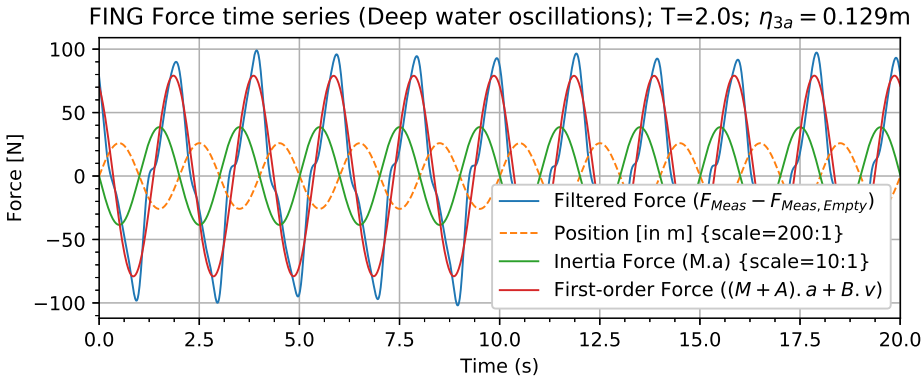
FING Force time series (Deep water oscillations); T=2.0s; $\eta_{3a} = 0.129$m
Force [N]
Time (s)
Filtered Force ($F_{Meas} - F_{Meas,Empty}$)
Position [in m] {scale=200:1}
Inertia Force (M.a) {scale=10:1}
First-order Force ($(M+A).a + B.v$)

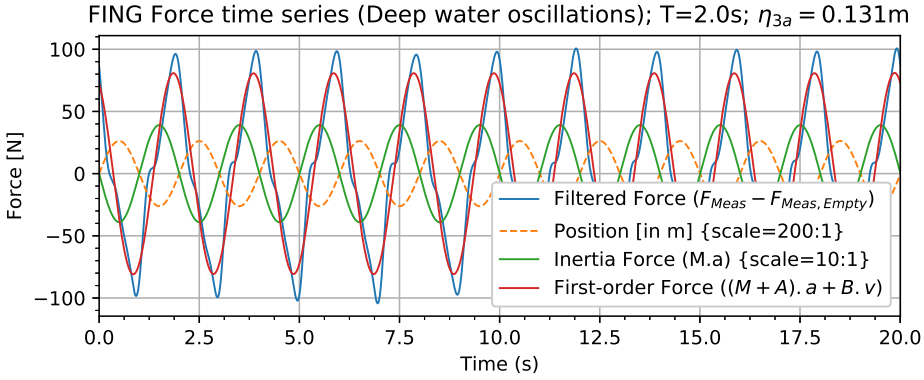
FING Force time series (Deep water oscillations); T=2.0s; $\eta_{3a} = 0.131$m
Force [N]
Time (s)
Filtered Force ($F_{Meas} - F_{Meas,Empty}$)
Position [in m] {scale=200:1}
Inertia Force (M.a) {scale=10:1}
First-order Force ($(M+A).a + B.v$)

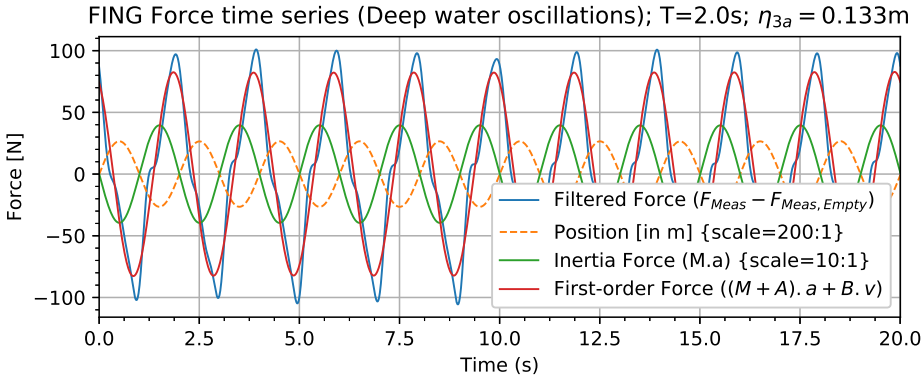
FING Force time series (Deep water oscillations); T=2.0s; $\eta_{3a} = 0.133$m
Force [N]
Time (s)
Filtered Force ($F_{Meas} - F_{Meas,Empty}$)
Position [in m] {scale=200:1}
Inertia Force (M.a) {scale=10:1}
First-order Force ($(M+A).a + B.v$)

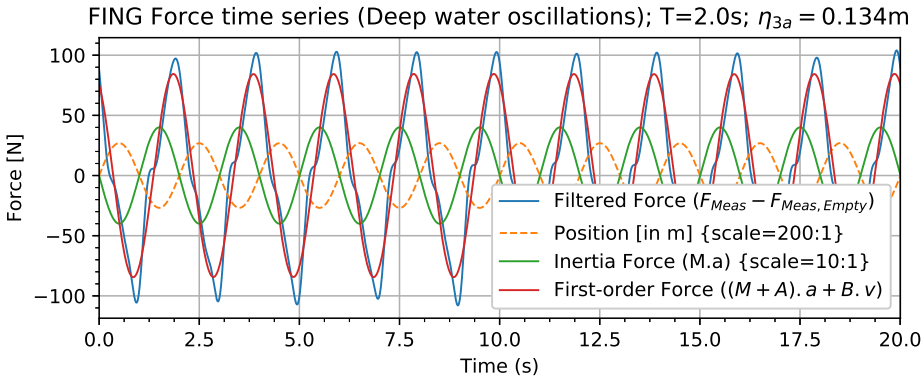
FING Force time series (Deep water oscillations); T=2.0s; $\eta_{3a} = 0.134$m
Force [N]
Time (s)
Filtered Force ($F_{Meas} - F_{Meas,Empty}$)
Position [in m] {scale=200:1}
Inertia Force (M.a) {scale=10:1}
First-order Force ($(M+A).a + B.v$)

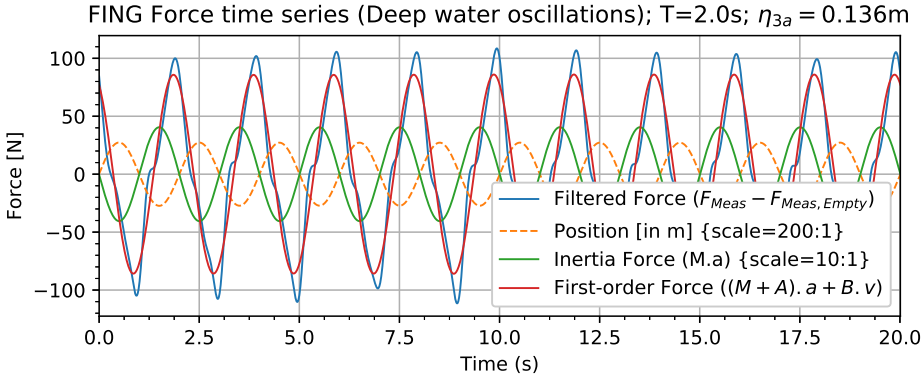
FING Force time series (Deep water oscillations); T=2.0s; $\eta_{3a} = 0.136$m
Force [N]
Time (s)
Filtered Force ($F_{Meas} - F_{Meas,Empty}$)
Position [in m] {scale=200:1}
Inertia Force (M.a) {scale=10:1}
First-order Force ($(M+A).a + B.v$)

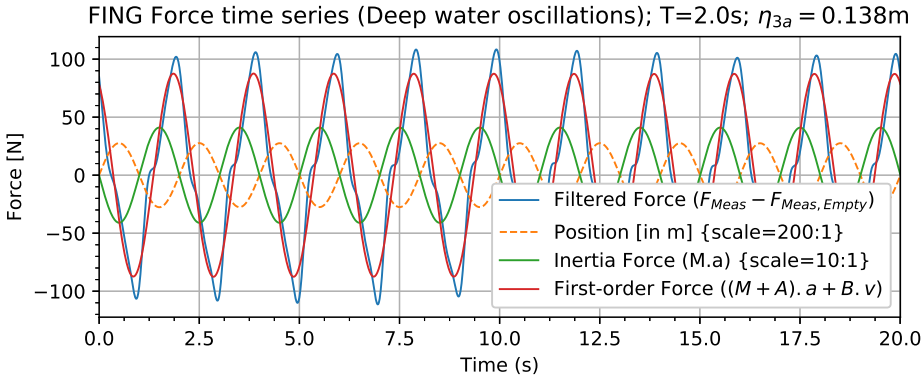
FING Force time series (Deep water oscillations); T=2.0s; $\eta_{3a} = 0.138$m
Force [N]
Time (s)
Filtered Force ($F_{Meas} - F_{Meas,Empty}$)
Position [in m] {scale=200:1}
Inertia Force (M.a) {scale=10:1}
First-order Force ($(M+A).a + B.v$)

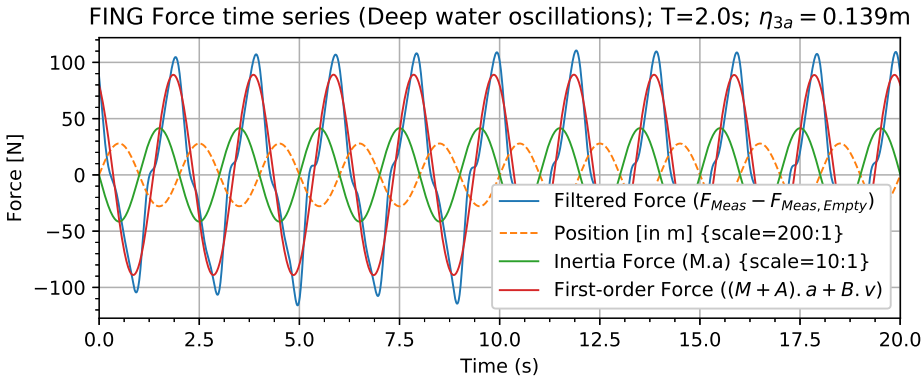
FING Force time series (Deep water oscillations); T=2.0s; $\eta_{3a} = 0.139$m
Force [N]
Time (s)
Filtered Force ($F_{Meas} - F_{Meas,Empty}$)
Position [in m] {scale=200:1}
Inertia Force (M.a) {scale=10:1}
First-order Force ($(M+A).a + B.v$)

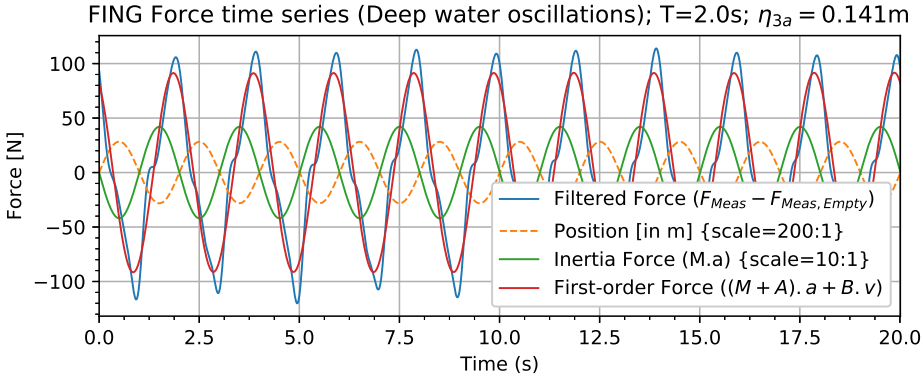
FING Force time series (Deep water oscillations); T=2.0s; $\eta_{3a} = 0.141$m
Force [N]
Time (s)
Filtered Force ($F_{Meas} - F_{Meas,Empty}$)
Position [in m] {scale=200:1}
Inertia Force (M.a) {scale=10:1}
First-order Force ($(M+A).a + B.v$)

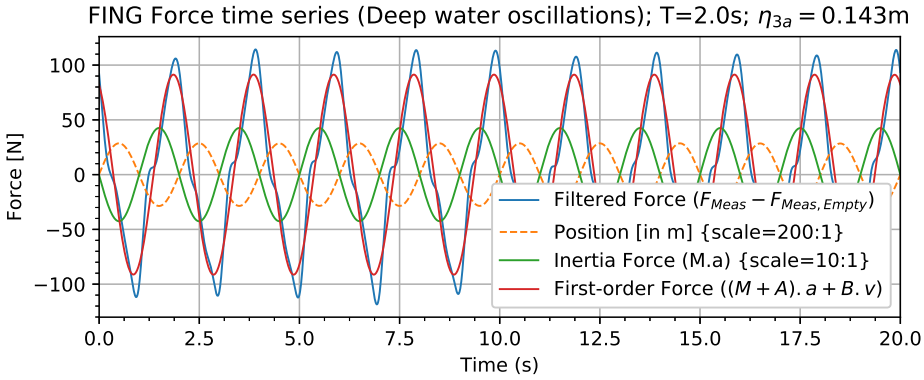
FING Force time series (Deep water oscillations); T=2.0s; $\eta_{3a} = 0.143$m
Force [N]
Time (s)
Filtered Force ($F_{Meas} - F_{Meas,Empty}$)
Position [in m] {scale=200:1}
Inertia Force (M.a) {scale=10:1}
First-order Force ($(M+A).a + B.v$)

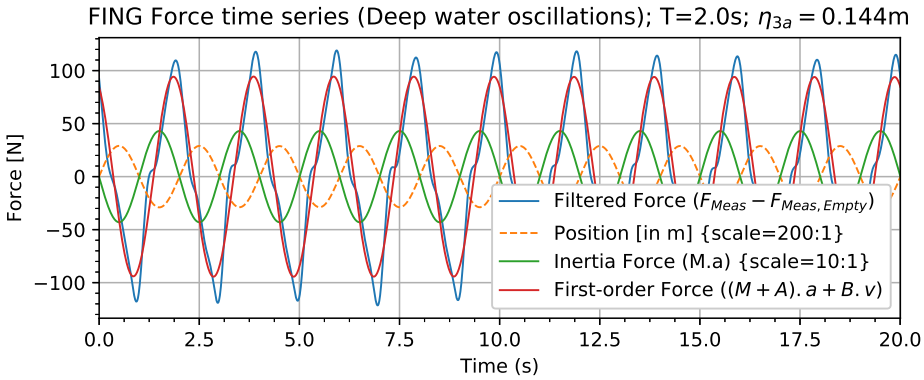
FING Force time series (Deep water oscillations); T=2.0s; $\eta_{3a} = 0.144$m
Force [N]
Time (s)
Filtered Force ($F_{Meas} - F_{Meas,Empty}$)
Position [in m] {scale=200:1}
Inertia Force (M.a) {scale=10:1}
First-order Force ($(M+A).a + B.v$)

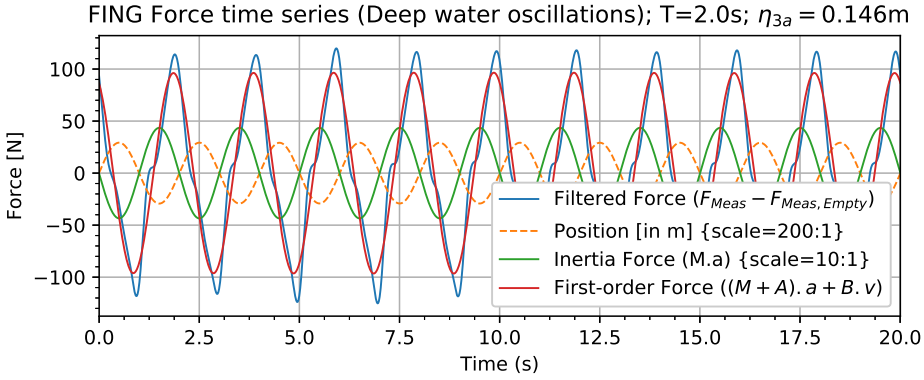
FING Force time series (Deep water oscillations); T=2.0s; $\eta_{3a} = 0.146$m
Force [N]
Time (s)
Filtered Force ($F_{Meas} - F_{Meas,Empty}$)
Position [in m] {scale=200:1}
Inertia Force (M.a) {scale=10:1}
First-order Force ($(M+A).a + B.v$)

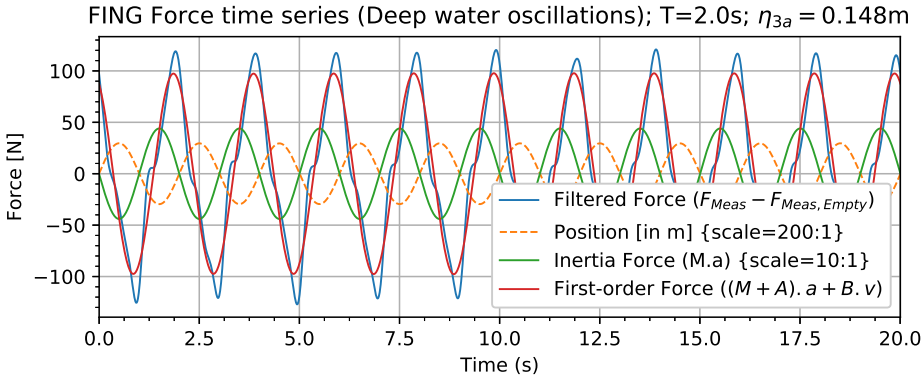
FING Force time series (Deep water oscillations); T=2.0s; $\eta_{3a} = 0.148$m
Force [N]
Time (s)
Filtered Force ($F_{Meas} - F_{Meas,Empty}$)
Position [in m] {scale=200:1}
Inertia Force (M.a) {scale=10:1}
First-order Force ($(M+A).a + B.v$)

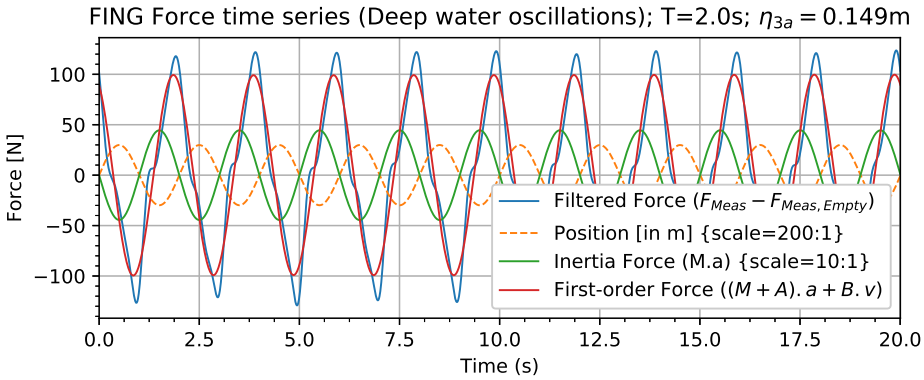
FING Force time series (Deep water oscillations); T=2.0s; $\eta_{3a} = 0.149$m
Force [N]
Time (s)
Filtered Force ($F_{Meas} - F_{Meas,Empty}$)
Position [in m] {scale=200:1}
Inertia Force (M.a) {scale=10:1}
First-order Force ($(M+A).a + B.v$)

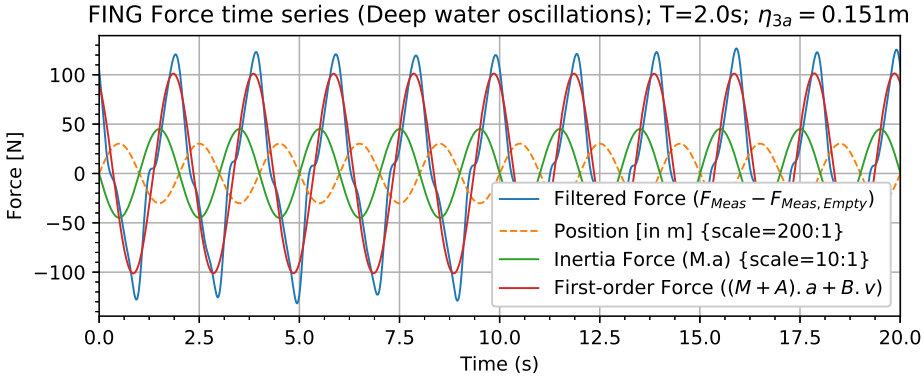
FING Force time series (Deep water oscillations); T=2.0s; $\eta_{3a} = 0.151$m
Force [N]
Time (s)
Filtered Force ($F_{Meas} - F_{Meas,Empty}$)
Position [in m] {scale=200:1}
Inertia Force (M.a) {scale=10:1}
First-order Force ($(M+A).a + B.v$)

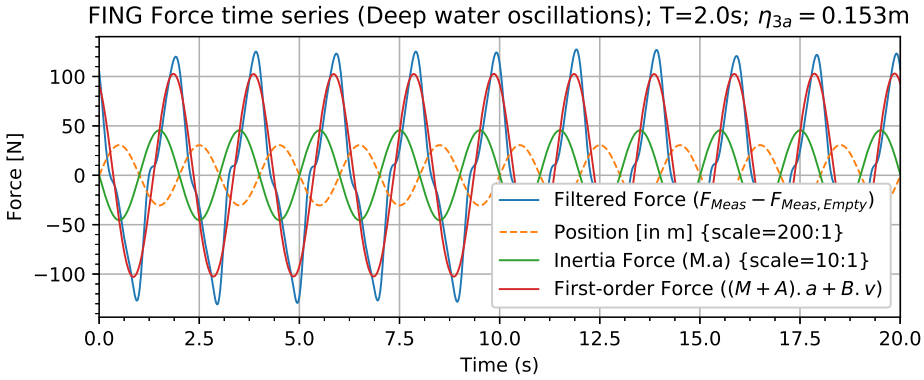
FING Force time series (Deep water oscillations); T=2.0s; $\eta_{3a} = 0.153$m
Force [N]
Time (s)
Filtered Force ($F_{Meas} - F_{Meas,Empty}$)
Position [in m] {scale=200:1}
Inertia Force (M.a) {scale=10:1}
First-order Force ($(M+A).a + B.v$)

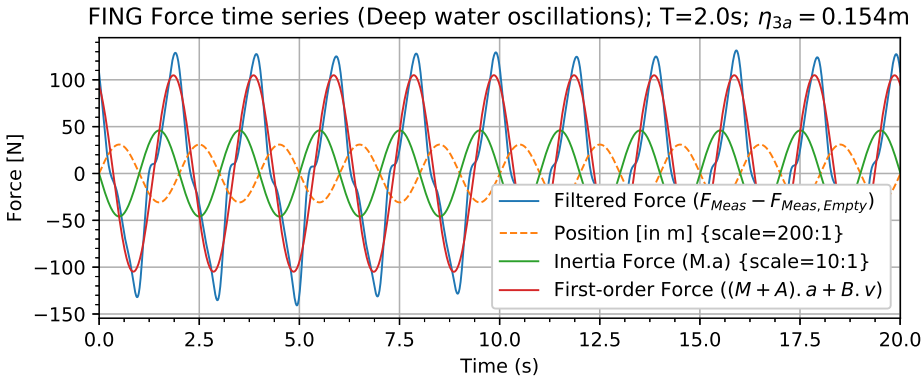
FING Force time series (Deep water oscillations); T=2.0s; $\eta_{3a} = 0.154$m
Force [N]
Time (s)
Filtered Force ($F_{Meas} - F_{Meas,Empty}$)
Position [in m] {scale=200:1}
Inertia Force (M.a) {scale=10:1}
First-order Force ($(M+A).a + B.v$)

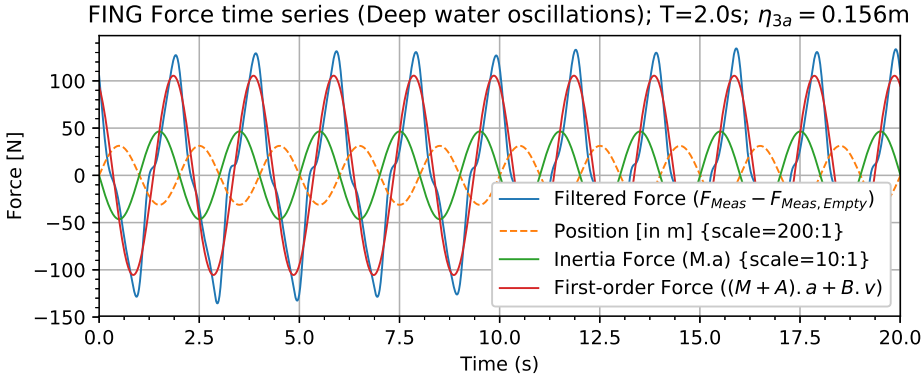
FING Force time series (Deep water oscillations); T=2.0s; $\eta_{3a} = 0.156$m
Force [N]
Time (s)
Filtered Force ($F_{Meas} - F_{Meas,Empty}$)
Position [in m] {scale=200:1}
Inertia Force (M.a) {scale=10:1}
First-order Force ($(M+A).a + B.v$)

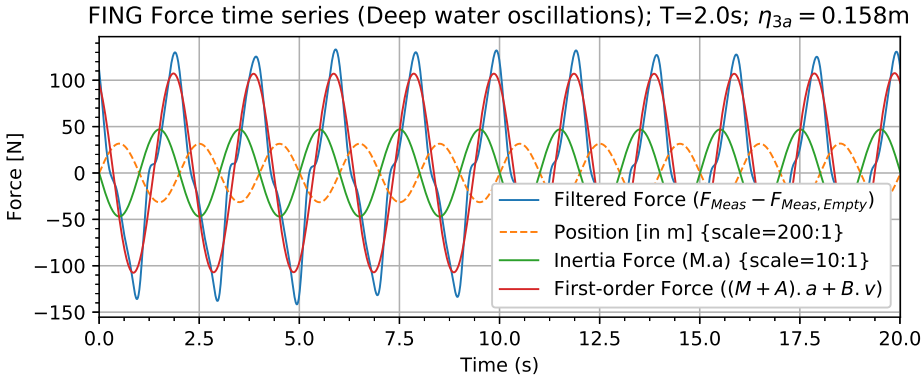
FING Force time series (Deep water oscillations); T=2.0s; $\eta_{3a} = 0.158$m
Force [N]
Time (s)
Filtered Force ($F_{Meas} - F_{Meas,Empty}$)
Position [in m] {scale=200:1}
Inertia Force (M.a) {scale=10:1}
First-order Force ($(M+A).a + B.v$)

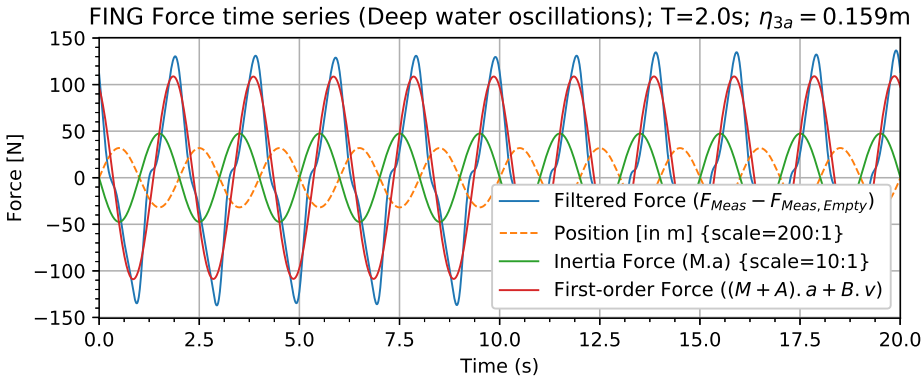
FING Force time series (Deep water oscillations); T=2.0s; $\eta_{3a} = 0.159$m
Force [N]
Time (s)
Filtered Force ($F_{Meas} - F_{Meas,Empty}$)
Position [in m] {scale=200:1}
Inertia Force (M.a) {scale=10:1}
First-order Force ($(M+A).a + B.v$)

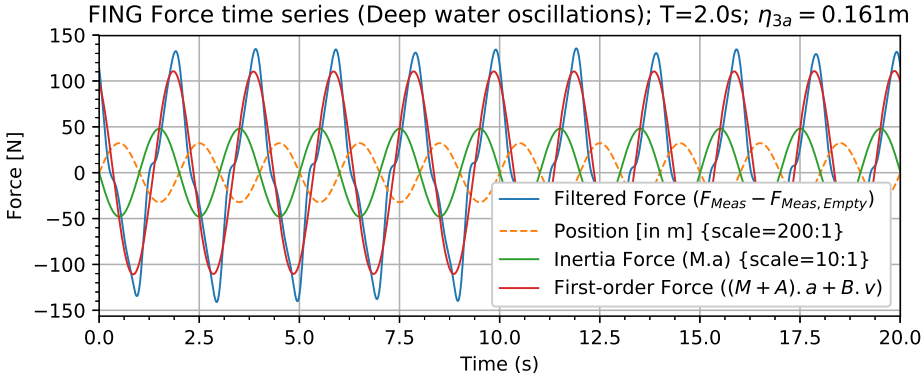
FING Force time series (Deep water oscillations); T=2.0s; $\eta_{3a} = 0.161$m
Force [N]
Time (s)
Filtered Force ($F_{Meas} - F_{Meas,Empty}$)
Position [in m] {scale=200:1}
Inertia Force (M.a) {scale=10:1}
First-order Force ($(M+A).a + B.v$)

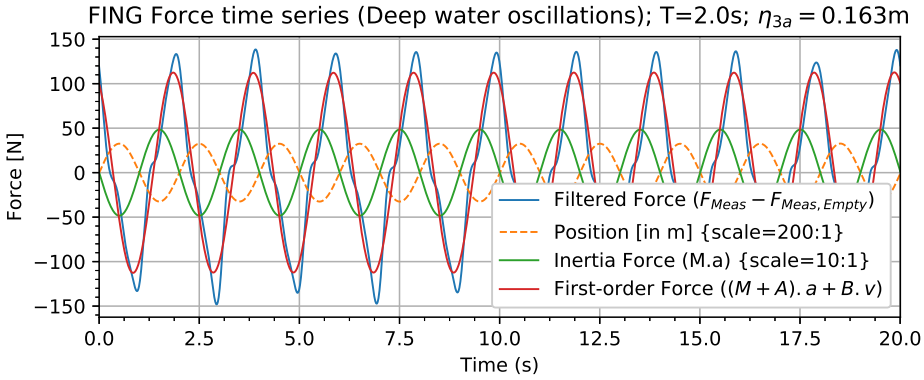
FING Force time series (Deep water oscillations); T=2.0s; $\eta_{3a} = 0.163$m
Force [N]
Time (s)
Filtered Force ($F_{Meas} - F_{Meas,Empty}$)
Position [in m] {scale=200:1}
Inertia Force (M.a) {scale=10:1}
First-order Force ($(M+A).a + B.v$)

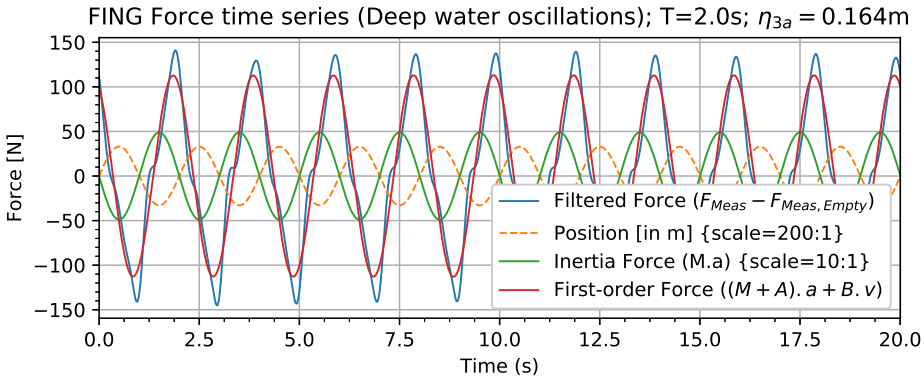
FING Force time series (Deep water oscillations); T=2.0s; $\eta_{3a} = 0.164$m
Force [N]
Time (s)
Filtered Force ($F_{Meas} - F_{Meas,Empty}$)
Position [in m] {scale=200:1}
Inertia Force (M.a) {scale=10:1}
First-order Force ($(M+A).a + B.v$)

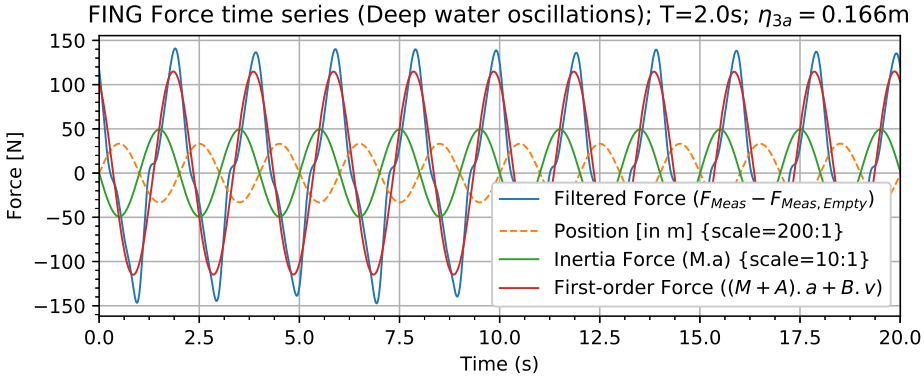
FING Force time series (Deep water oscillations); T=2.0s; $\eta_{3a} = 0.166$m
Force [N]
Time (s)
Filtered Force ($F_{Meas} - F_{Meas,Empty}$)
Position [in m] {scale=200:1}
Inertia Force (M.a) {scale=10:1}
First-order Force ($(M+A).a + B.v$)

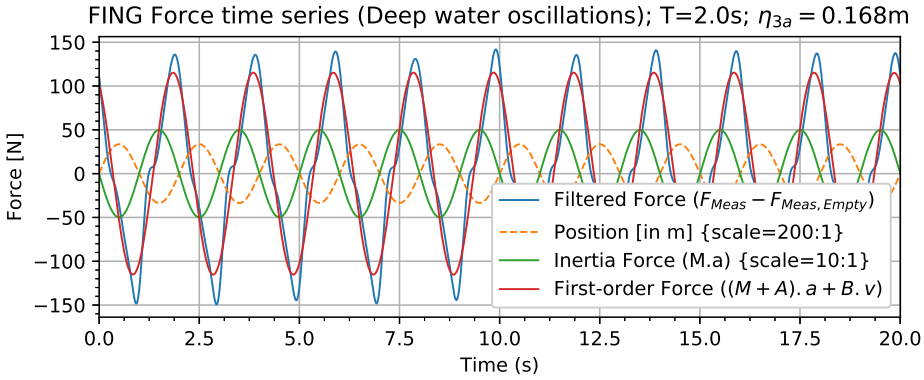
FING Force time series (Deep water oscillations); T=2.0s; $\eta_{3a} = 0.168$m
Force [N]
Time (s)
Filtered Force ($F_{Meas} - F_{Meas,Empty}$)
Position [in m] {scale=200:1}
Inertia Force (M.a) {scale=10:1}
First-order Force ($(M+A).a + B.v$)

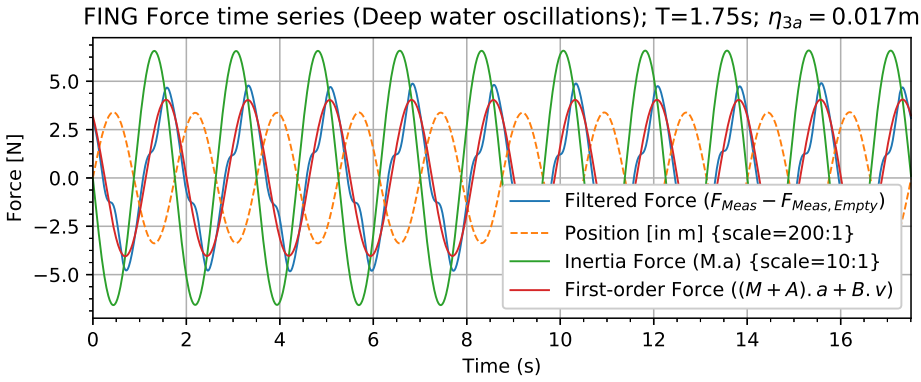
FING Force time series (Deep water oscillations); T=1.75s; $\eta_{3a} = 0.017$m
Force [N]
Time (s)
Filtered Force ($F_{Meas} - F_{Meas,Empty}$)
Position [in m] {scale=200:1}
Inertia Force (M.a) {scale=10:1}
First-order Force ($(M+A).a + B.v$)

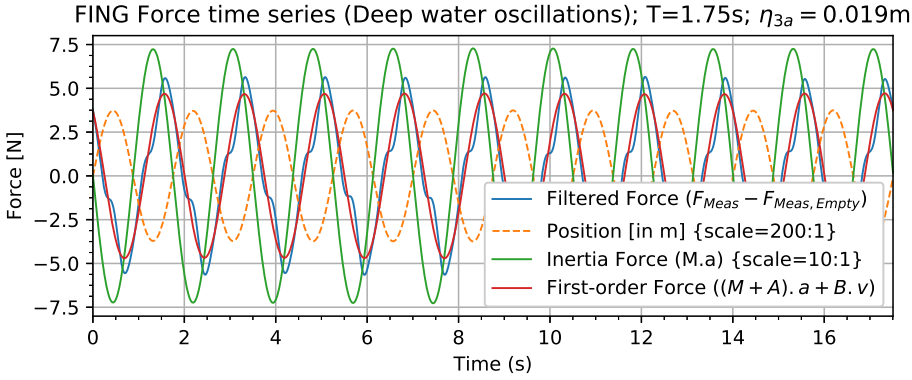
FING Force time series (Deep water oscillations); T=1.75s; $\eta_{3a} = 0.019$m
Force [N]
Time (s)
Filtered Force ($F_{Meas} - F_{Meas,Empty}$)
Position [in m] {scale=200:1}
Inertia Force (M.a) {scale=10:1}
First-order Force ($(M+A).a + B.v$)

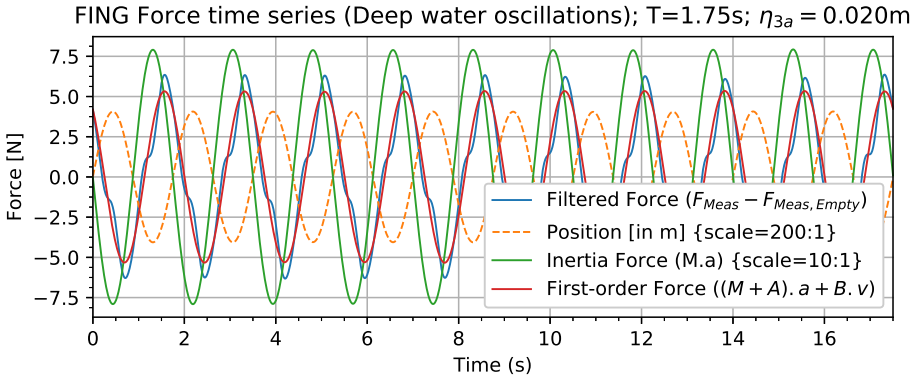
FING Force time series (Deep water oscillations); T=1.75s; $\eta_{3a} = 0.020$m
Force [N]
Time (s)
Filtered Force ($F_{Meas} - F_{Meas,Empty}$)
Position [in m] {scale=200:1}
Inertia Force (M.a) {scale=10:1}
First-order Force ($(M+A).a + B.v$)

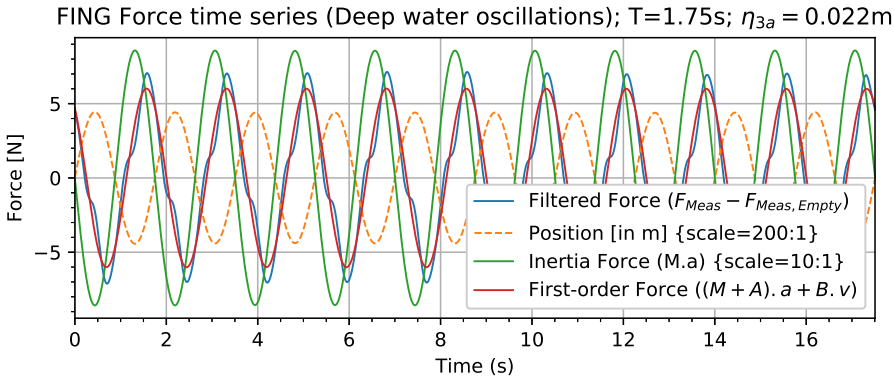
FING Force time series (Deep water oscillations); T=1.75s; $\eta_{3a} = 0.022$m
Force [N]
Time (s)
Filtered Force ($F_{Meas} - F_{Meas,Empty}$)
Position [in m] {scale=200:1}
Inertia Force (M.a) {scale=10:1}
First-order Force ($(M+A).a + B.v$)

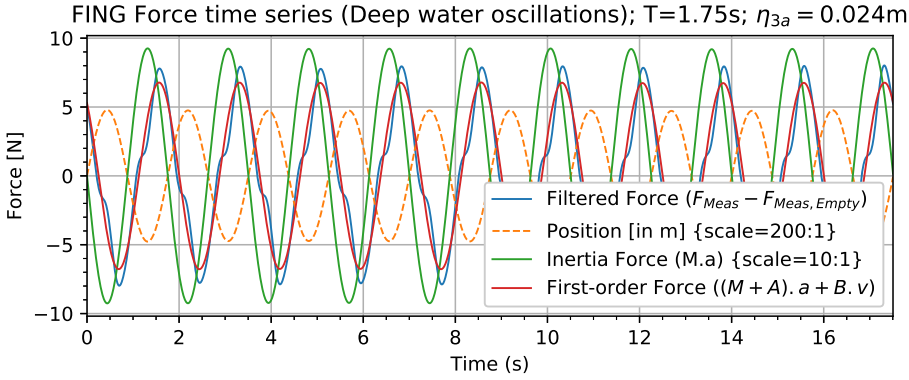
FING Force time series (Deep water oscillations); T=1.75s; $\eta_{3a} = 0.024$m
Force [N]
Time (s)
Filtered Force ($F_{Meas} - F_{Meas,Empty}$)
Position [in m] {scale=200:1}
Inertia Force (M.a) {scale=10:1}
First-order Force ($(M+A).a + B.v$)

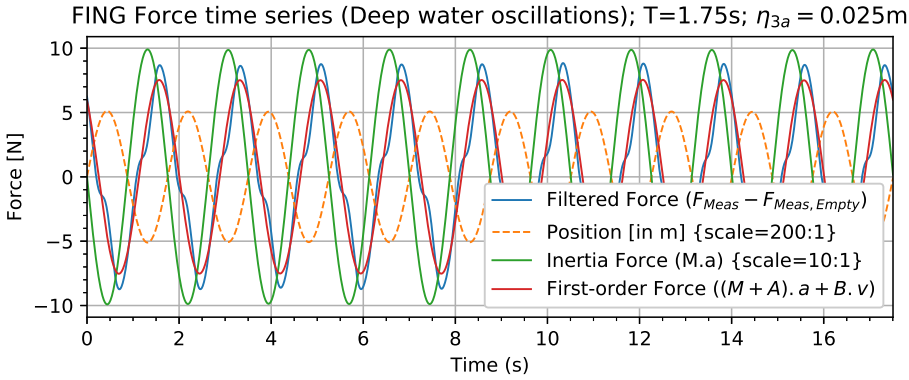
FING Force time series (Deep water oscillations); T=1.75s; $\eta_{3a} = 0.025$m
Force [N]
Time (s)
Filtered Force ($F_{Meas} - F_{Meas,Empty}$)
Position [in m] {scale=200:1}
Inertia Force (M.a) {scale=10:1}
First-order Force ($(M+A).a + B.v$)

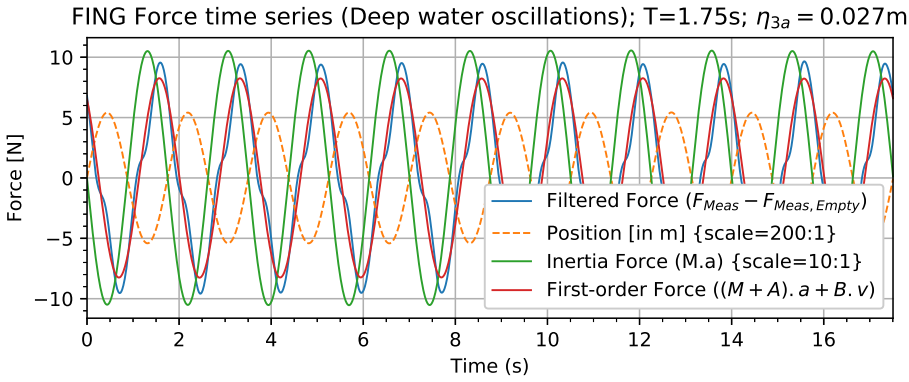
FING Force time series (Deep water oscillations); T=1.75s; $\eta_{3a} = 0.027$m
Force [N]
Time (s)
Filtered Force ($F_{Meas} - F_{Meas,Empty}$)
Position [in m] {scale=200:1}
Inertia Force (M.a) {scale=10:1}
First-order Force ($(M+A).a + B.v$)

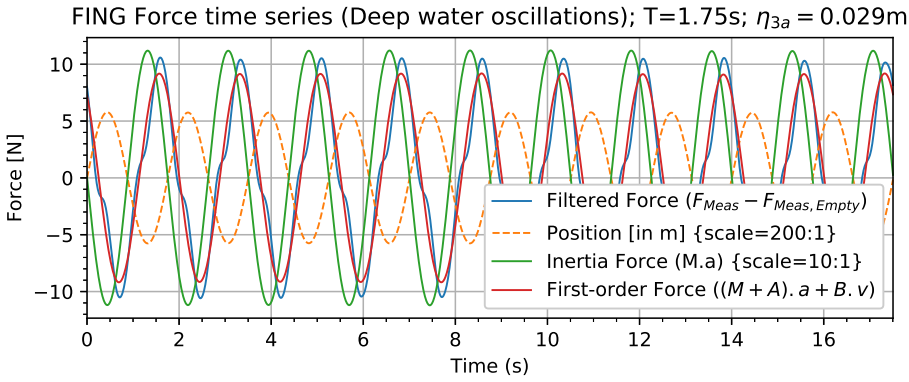
FING Force time series (Deep water oscillations); T=1.75s; $\eta_{3a} = 0.029$m
Force [N]
Time (s)
Filtered Force ($F_{Meas} - F_{Meas,Empty}$)
Position [in m] {scale=200:1}
Inertia Force (M.a) {scale=10:1}
First-order Force ($(M+A).a + B.v$)

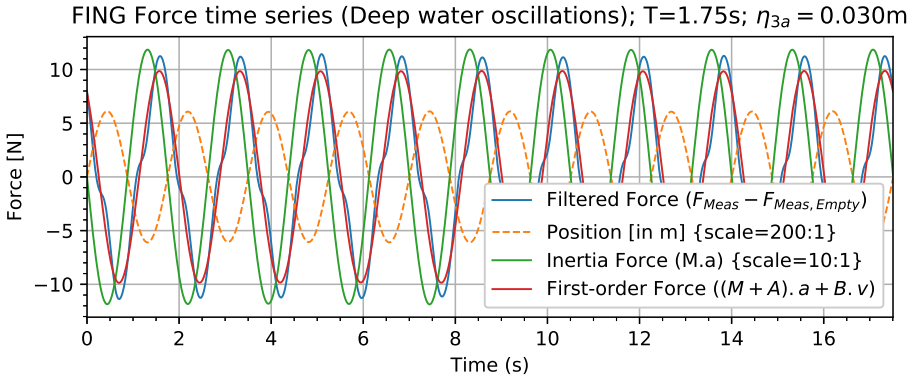
FING Force time series (Deep water oscillations); T=1.75s; $\eta_{3a} = 0.030$m
Force [N]
Time (s)
Filtered Force ($F_{Meas} - F_{Meas,Empty}$)
Position [in m] {scale=200:1}
Inertia Force (M.a) {scale=10:1}
First-order Force ($(M+A).a + B.v$)

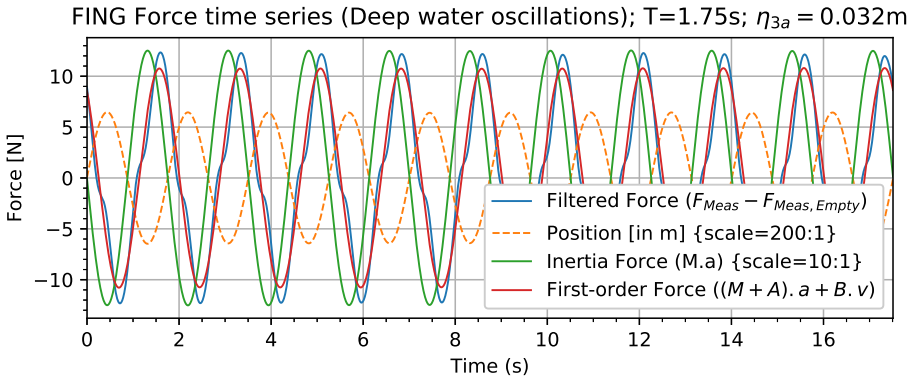
FING Force time series (Deep water oscillations); T=1.75s; $\eta_{3a} = 0.032$m
Force [N]
Time (s)
Filtered Force ($F_{Meas} - F_{Meas,Empty}$)
Position [in m] {scale=200:1}
Inertia Force (M.a) {scale=10:1}
First-order Force ($(M+A).a + B.v$)

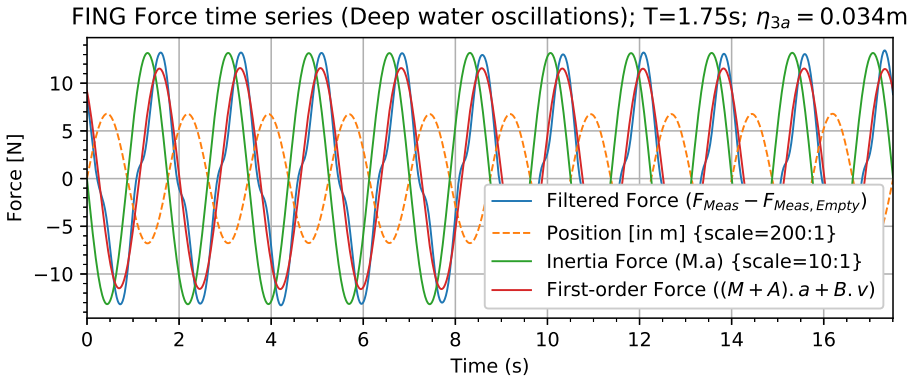
FING Force time series (Deep water oscillations); T=1.75s; $\eta_{3a} = 0.034$m
Force [N]
Time (s)
Filtered Force ($F_{Meas} - F_{Meas,Empty}$)
Position [in m] {scale=200:1}
Inertia Force (M.a) {scale=10:1}
First-order Force ($(M+A).a + B.v$)

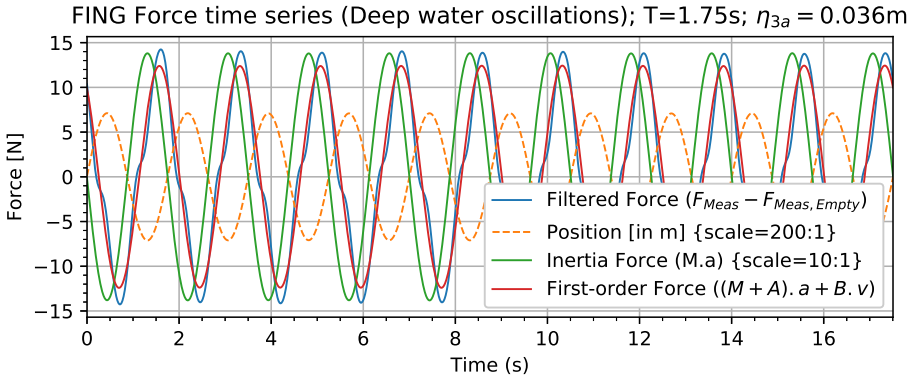
FING Force time series (Deep water oscillations); T=1.75s; $\eta_{3a} = 0.036$m
Force [N]
Time (s)
Filtered Force ($F_{Meas} - F_{Meas,Empty}$)
Position [in m] {scale=200:1}
Inertia Force (M.a) {scale=10:1}
First-order Force ($(M+A).a + B.v$)

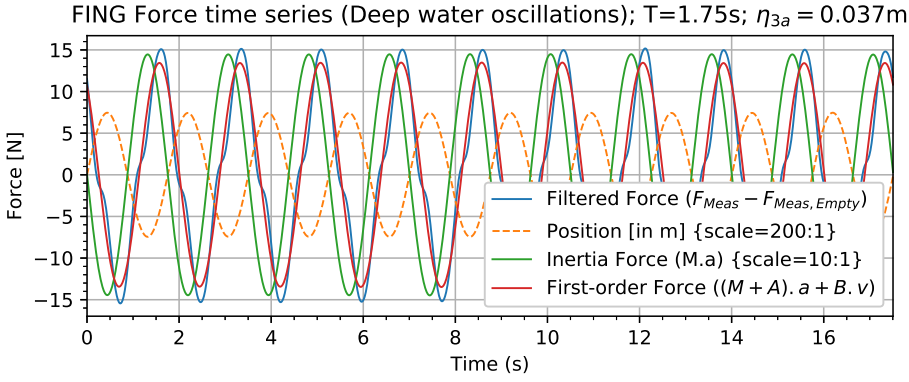
FING Force time series (Deep water oscillations); T=1.75s; $\eta_{3a} = 0.037$m
Force [N]
Time (s)
Filtered Force ($F_{Meas} - F_{Meas,Empty}$)
Position [in m] {scale=200:1}
Inertia Force (M.a) {scale=10:1}
First-order Force ($(M+A).a + B.v$)

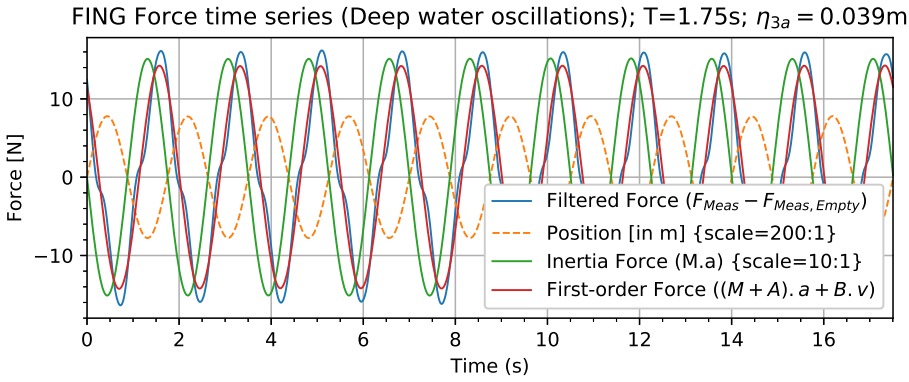
FING Force time series (Deep water oscillations); T=1.75s; $\eta_{3a} = 0.039$m
Force [N]
Time (s)
Filtered Force ($F_{Meas} - F_{Meas,Empty}$)
Position [in m] {scale=200:1}
Inertia Force (M.a) {scale=10:1}
First-order Force ($(M+A).a + B.v$)

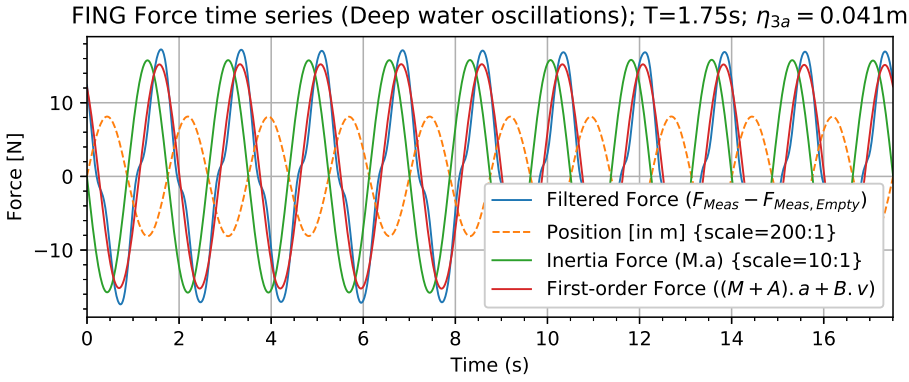
FING Force time series (Deep water oscillations); T=1.75s; $\eta_{3a} = 0.041$m
Force [N]
Time (s)
Filtered Force ($F_{Meas} - F_{Meas,Empty}$)
Position [in m] {scale=200:1}
Inertia Force (M.a) {scale=10:1}
First-order Force ($(M+A).a + B.v$)

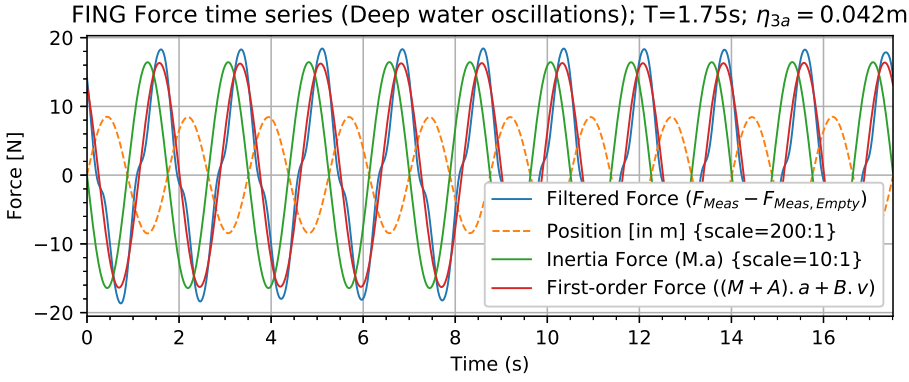
FING Force time series (Deep water oscillations); T=1.75s; $\eta_{3a} = 0.042$m
Force [N]
Time (s)
Filtered Force ($F_{Meas} - F_{Meas,Empty}$)
Position [in m] {scale=200:1}
Inertia Force (M.a) {scale=10:1}
First-order Force ($(M+A).a + B.v$)

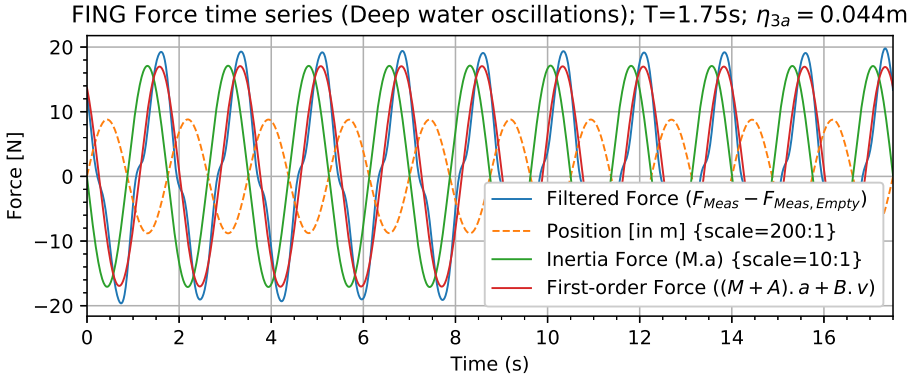
FING Force time series (Deep water oscillations); T=1.75s; $\eta_{3a} = 0.044$m
Force [N]
Time (s)
Filtered Force ($F_{Meas} - F_{Meas,Empty}$)
Position [in m] {scale=200:1}
Inertia Force (M.a) {scale=10:1}
First-order Force ($(M+A).a + B.v$)

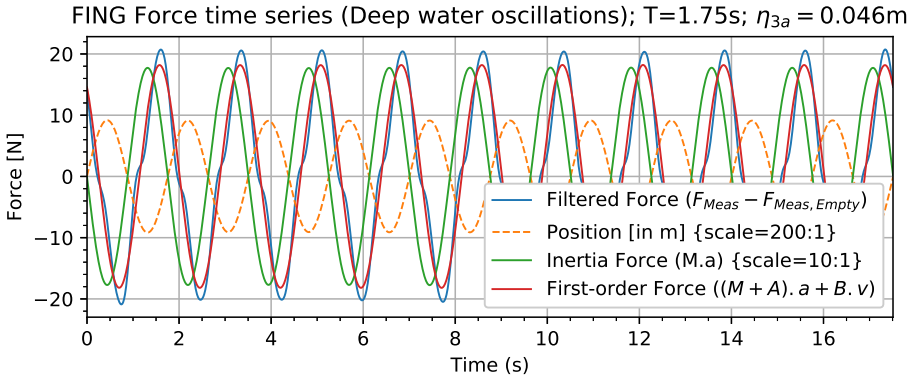
FING Force time series (Deep water oscillations); T=1.75s; $\eta_{3a} = 0.046$m
Force [N]
Time (s)
Filtered Force ($F_{Meas} - F_{Meas,Empty}$)
Position [in m] {scale=200:1}
Inertia Force (M.a) {scale=10:1}
First-order Force ($(M+A).a + B.v$)

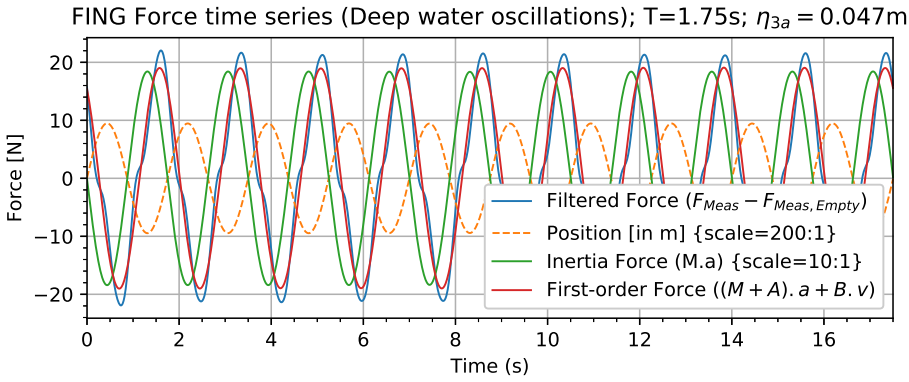
FING Force time series (Deep water oscillations); T=1.75s; $\eta_{3a} = 0.047$m
Force [N]
Time (s)
Filtered Force ($F_{Meas} - F_{Meas,Empty}$)
Position [in m] {scale=200:1}
Inertia Force (M.a) {scale=10:1}
First-order Force ($(M+A).a + B.v$)

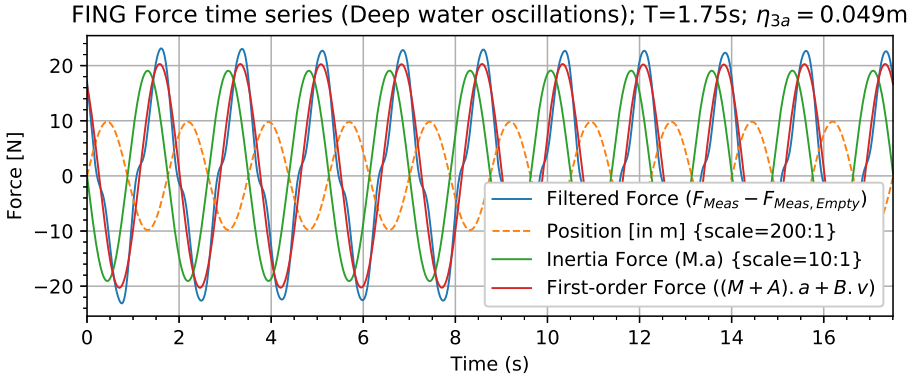
FING Force time series (Deep water oscillations); T=1.75s; $\eta_{3a} = 0.049$m
Force [N]
Time (s)
Filtered Force ($F_{Meas} - F_{Meas,Empty}$)
Position [in m] {scale=200:1}
Inertia Force (M.a) {scale=10:1}
First-order Force ($(M + A).a + B.v$)

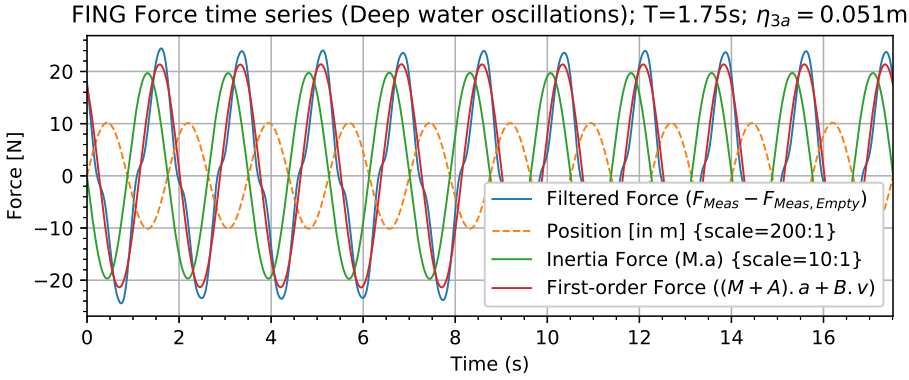
FING Force time series (Deep water oscillations); T=1.75s; $\eta_{3a} = 0.051$m
Force [N]
Time (s)
Filtered Force ($F_{Meas} - F_{Meas,Empty}$)
Position [in m] {scale=200:1}
Inertia Force (M.a) {scale=10:1}
First-order Force ($(M + A).a + B.v$)

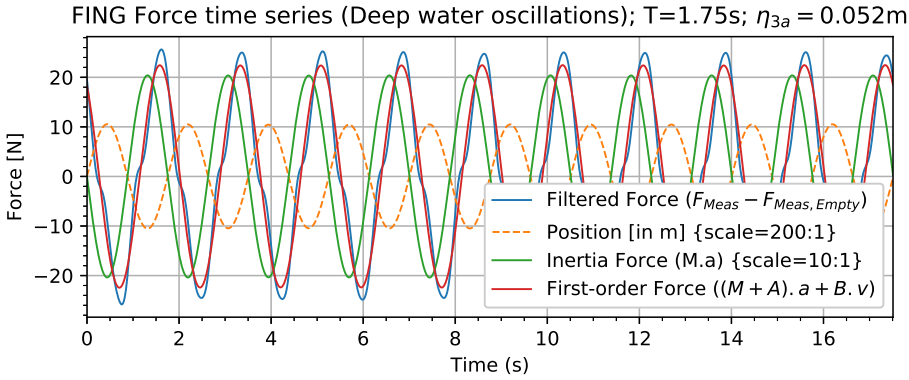
FING Force time series (Deep water oscillations); T=1.75s; $\eta_{3a} = 0.052$m
Force [N]
Time (s)
Filtered Force ($F_{Meas} - F_{Meas,Empty}$)
Position [in m] {scale=200:1}
Inertia Force (M.a) {scale=10:1}
First-order Force ($(M + A).a + B.v$)

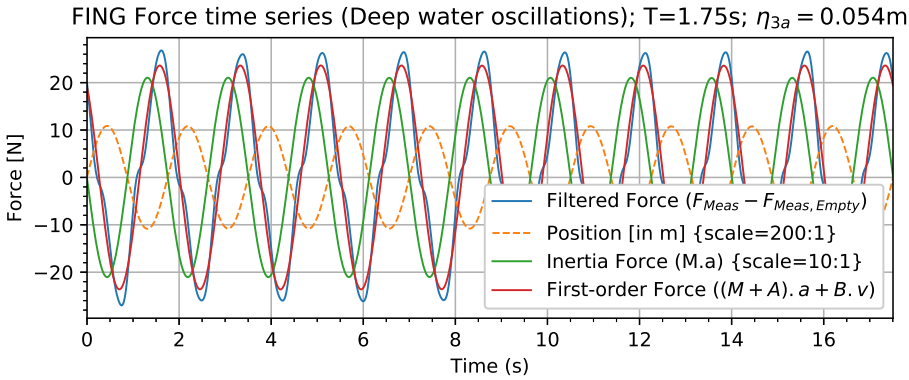
FING Force time series (Deep water oscillations); T=1.75s; $\eta_{3a} = 0.054$m
Force [N]
Time (s)
Filtered Force ($F_{Meas} - F_{Meas,Empty}$)
Position [in m] {scale=200:1}
Inertia Force (M.a) {scale=10:1}
First-order Force ($(M + A).a + B.v$)

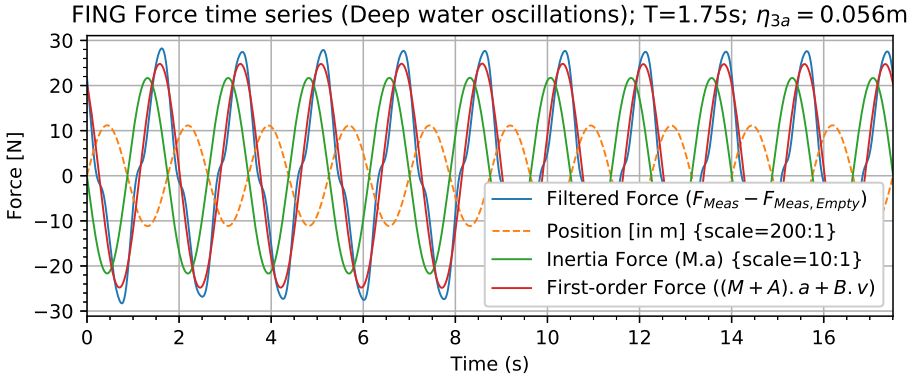
FING Force time series (Deep water oscillations); T=1.75s; $\eta_{3a} = 0.056$m
Force [N]
Time (s)
Filtered Force ($F_{Meas} - F_{Meas,Empty}$)
Position [in m] {scale=200:1}
Inertia Force (M.a) {scale=10:1}
First-order Force ($(M+A).a + B.v$)

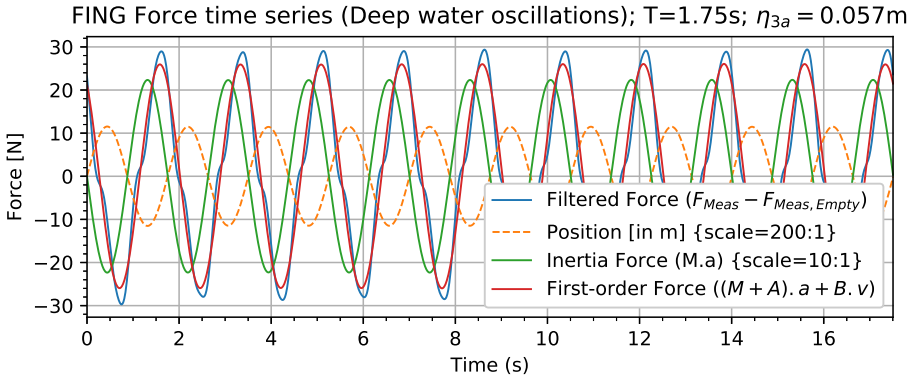
FING Force time series (Deep water oscillations); T=1.75s; $\eta_{3a} = 0.057$m
Force [N]
Time (s)
Filtered Force ($F_{Meas} - F_{Meas,Empty}$)
Position [in m] {scale=200:1}
Inertia Force (M.a) {scale=10:1}
First-order Force ($(M+A).a + B.v$)

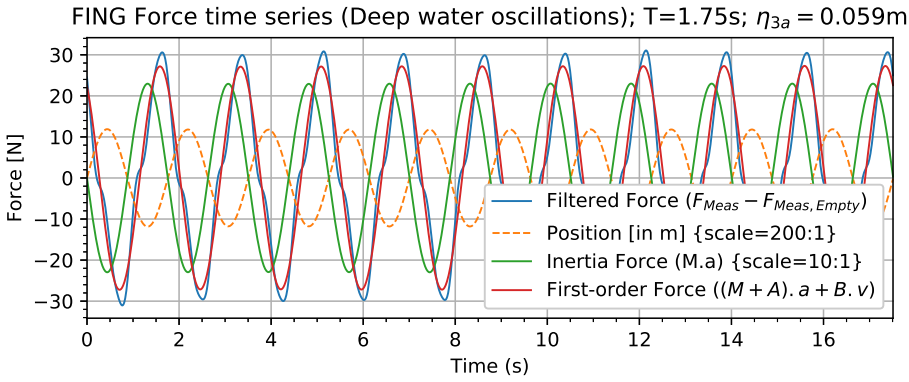
FING Force time series (Deep water oscillations); T=1.75s; $\eta_{3a} = 0.059$m
Force [N]
Time (s)
Filtered Force ($F_{Meas} - F_{Meas,Empty}$)
Position [in m] {scale=200:1}
Inertia Force (M.a) {scale=10:1}
First-order Force ($(M+A).a + B.v$)

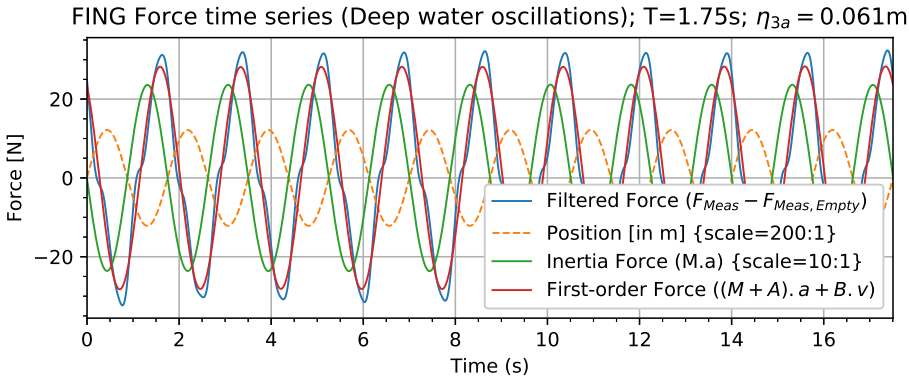
FING Force time series (Deep water oscillations); T=1.75s; $\eta_{3a} = 0.061$m
Force [N]
Time (s)
Filtered Force ($F_{Meas} - F_{Meas,Empty}$)
Position [in m] {scale=200:1}
Inertia Force (M.a) {scale=10:1}
First-order Force ($(M+A).a + B.v$)

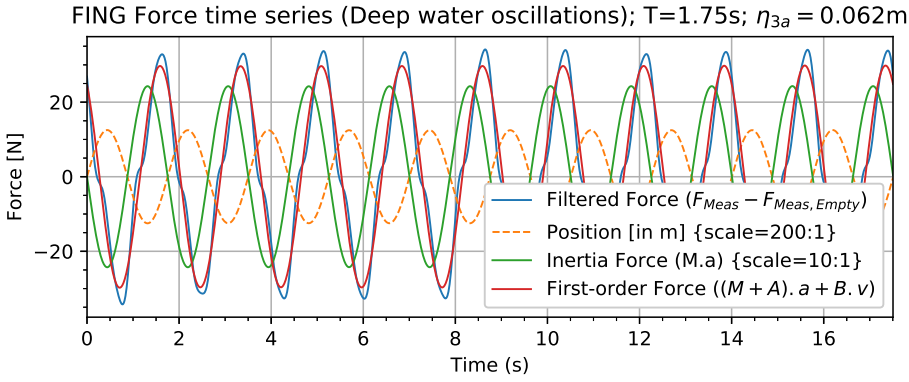
FING Force time series (Deep water oscillations); T=1.75s; $\eta_{3a} = 0.062$m
Force [N]
Time (s)
Filtered Force ($F_{Meas} - F_{Meas,Empty}$)
Position [in m] {scale=200:1}
Inertia Force (M.a) {scale=10:1}
First-order Force ($(M+A).a + B.v$)

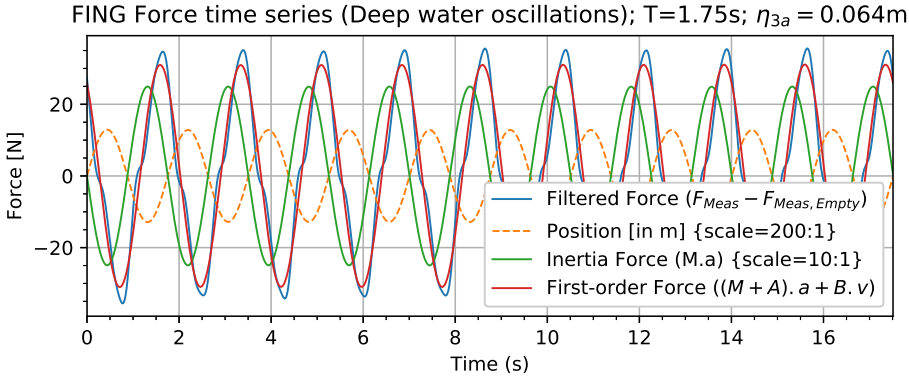
FING Force time series (Deep water oscillations); T=1.75s; $\eta_{3a} = 0.064$m
Force [N]
Time (s)
Filtered Force ($F_{Meas} - F_{Meas,Empty}$)
Position [in m] {scale=200:1}
Inertia Force (M.a) {scale=10:1}
First-order Force ($(M+A).a + B.v$)

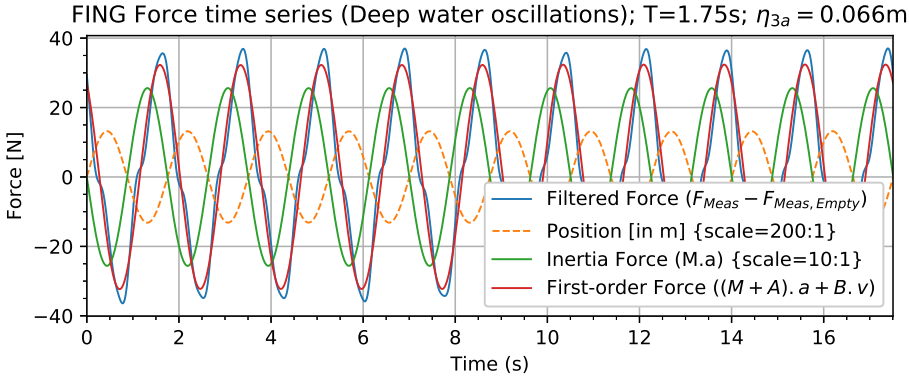
FING Force time series (Deep water oscillations); T=1.75s; $\eta_{3a} = 0.066$m
Force [N]
Time (s)
Filtered Force ($F_{Meas} - F_{Meas,Empty}$)
Position [in m] {scale=200:1}
Inertia Force (M.a) {scale=10:1}
First-order Force ($(M+A).a + B.v$)

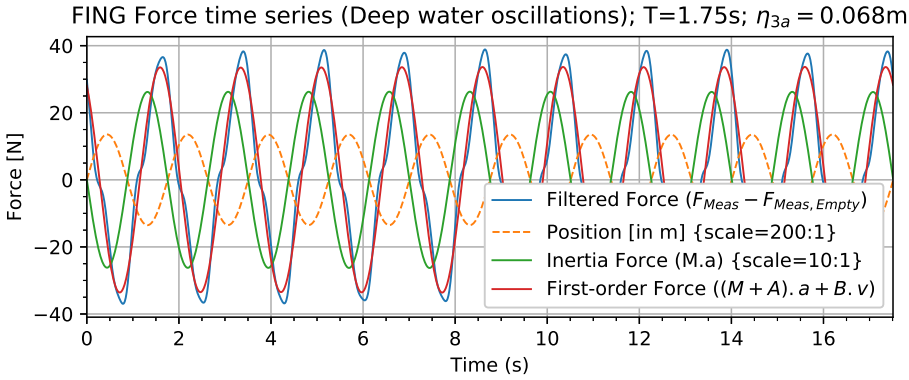
FING Force time series (Deep water oscillations); T=1.75s; $\eta_{3a} = 0.068$m
Force [N]
Time (s)
Filtered Force ($F_{Meas} - F_{Meas,Empty}$)
Position [in m] {scale=200:1}
Inertia Force (M.a) {scale=10:1}
First-order Force ($(M+A).a + B.v$)

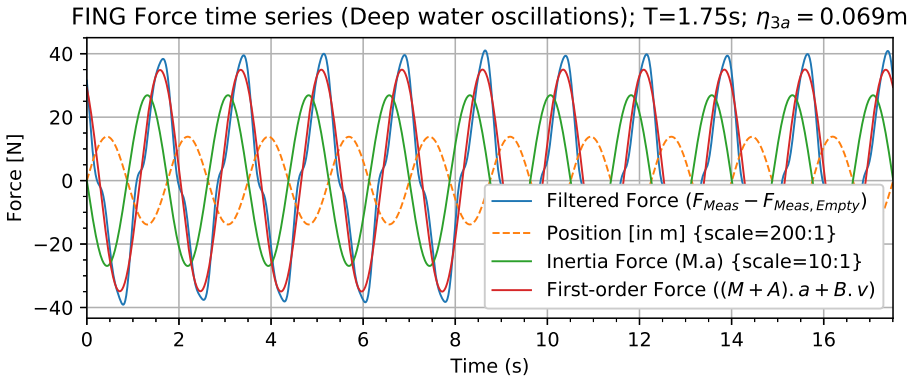
FING Force time series (Deep water oscillations); T=1.75s; $\eta_{3a} = 0.069$m
Force [N]
Time (s)
Filtered Force ($F_{Meas} - F_{Meas,Empty}$)
Position [in m] {scale=200:1}
Inertia Force (M.a) {scale=10:1}
First-order Force ($(M+A).a + B.v$)

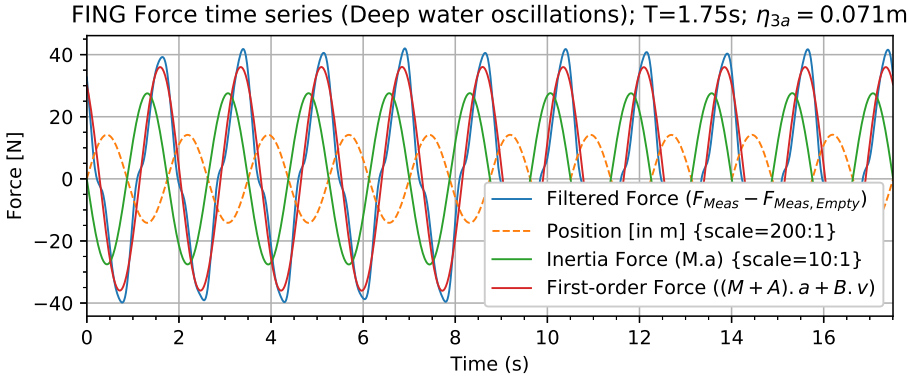
FING Force time series (Deep water oscillations); T=1.75s; $\eta_{3a} = 0.071$m
Force [N]
Time (s)
Filtered Force ($F_{Meas} - F_{Meas,Empty}$)
Position [in m] {scale=200:1}
Inertia Force (M.a) {scale=10:1}
First-order Force ($(M+A).a + B.v$)

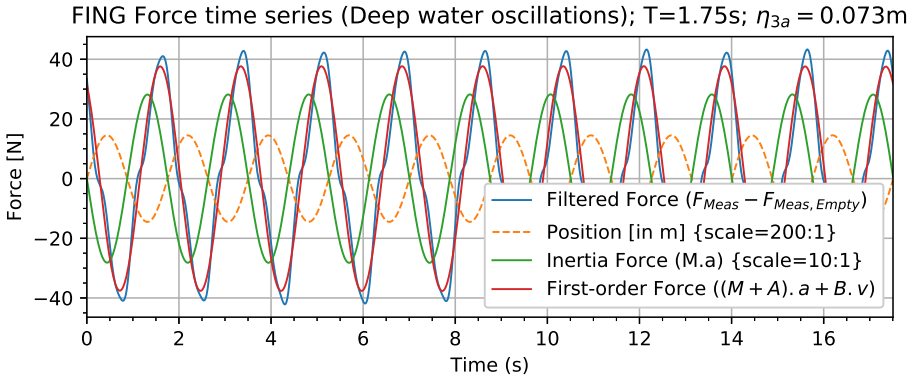
FING Force time series (Deep water oscillations); T=1.75s; $\eta_{3a} = 0.073$m
Force [N]
Time (s)
Filtered Force ($F_{Meas} - F_{Meas,Empty}$)
Position [in m] {scale=200:1}
Inertia Force (M.a) {scale=10:1}
First-order Force ($(M+A).a + B.v$)

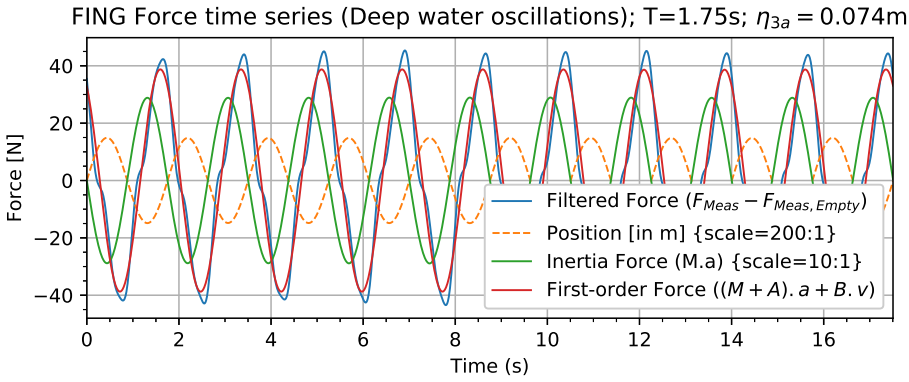
FING Force time series (Deep water oscillations); T=1.75s; $\eta_{3a} = 0.074$m
Force [N]
Time (s)
Filtered Force ($F_{Meas} - F_{Meas,Empty}$)
Position [in m] {scale=200:1}
Inertia Force (M.a) {scale=10:1}
First-order Force ($(M+A).a + B.v$)

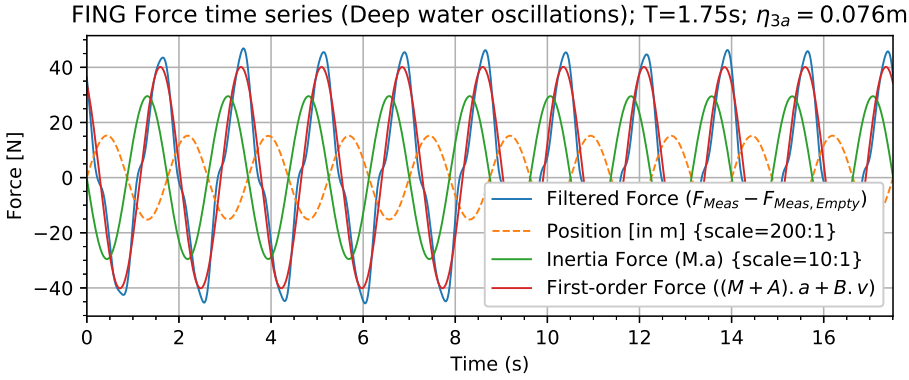
FING Force time series (Deep water oscillations); T=1.75s; $\eta_{3a} = 0.076$m
Force [N]
Time (s)
Filtered Force ($F_{Meas} - F_{Meas,Empty}$)
Position [in m] {scale=200:1}
Inertia Force (M.a) {scale=10:1}
First-order Force ($(M+A).a + B.v$)

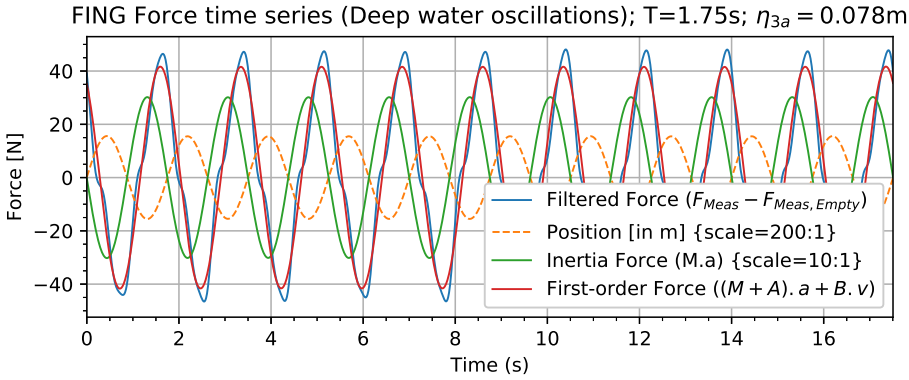
FING Force time series (Deep water oscillations); T=1.75s; $\eta_{3a} = 0.078$m
Force [N]
Time (s)
Filtered Force ($F_{Meas} - F_{Meas,Empty}$)
Position [in m] {scale=200:1}
Inertia Force (M.a) {scale=10:1}
First-order Force ($(M+A).a + B.v$)

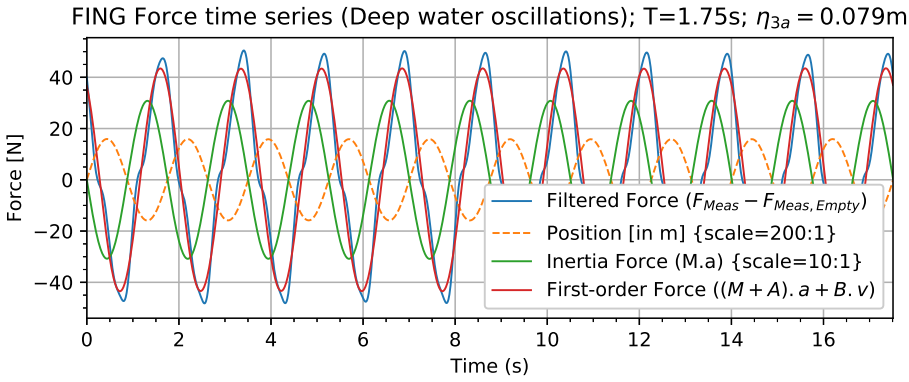
FING Force time series (Deep water oscillations); T=1.75s; $\eta_{3a} = 0.079$m
Force [N]
Time (s)
Filtered Force ($F_{Meas} - F_{Meas,Empty}$)
Position [in m] {scale=200:1}
Inertia Force (M.a) {scale=10:1}
First-order Force ($(M+A).a + B.v$)

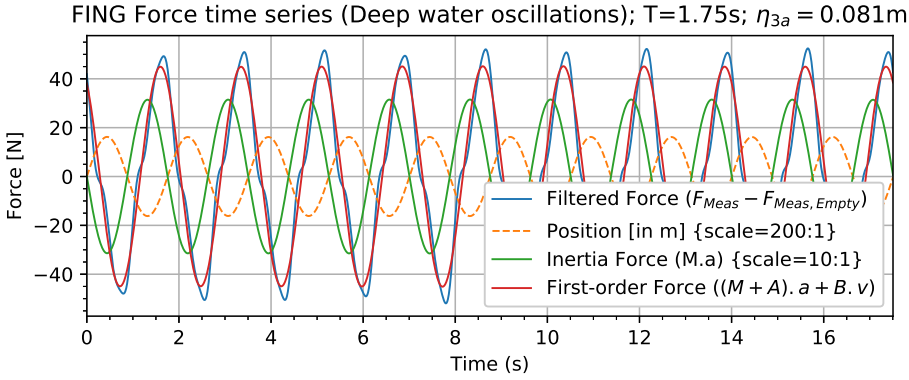
FING Force time series (Deep water oscillations); T=1.75s; $\eta_{3a} = 0.081$m
Force [N]
Time (s)
Filtered Force ($F_{Meas} - F_{Meas,Empty}$)
Position [in m] {scale=200:1}
Inertia Force (M.a) {scale=10:1}
First-order Force ($(M+A).a + B.v$)

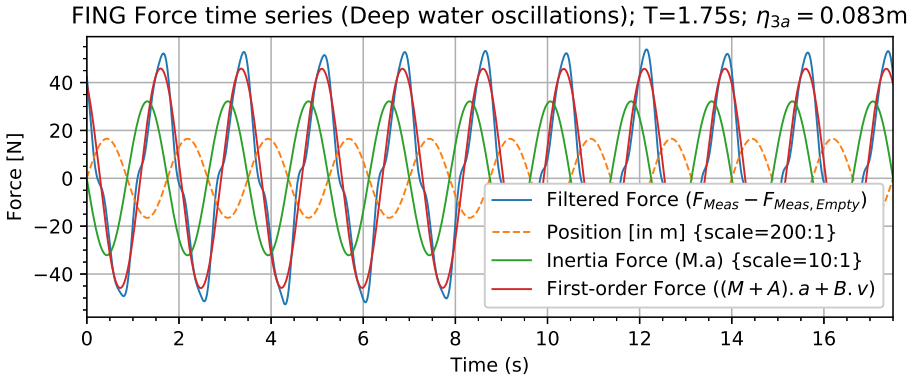
FING Force time series (Deep water oscillations); T=1.75s; $\eta_{3a} = 0.083$m
Force [N]
Time (s)
Filtered Force ($F_{Meas} - F_{Meas,Empty}$)
Position [in m] {scale=200:1}
Inertia Force (M.a) {scale=10:1}
First-order Force ($(M+A).a + B.v$)

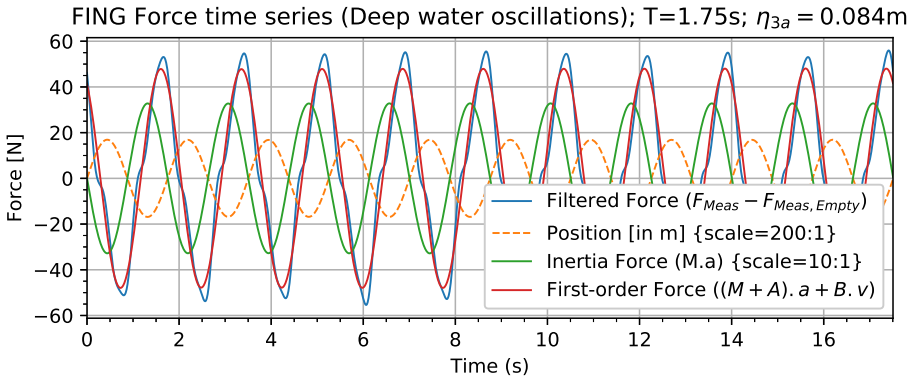
FING Force time series (Deep water oscillations); T=1.75s; $\eta_{3a} = 0.084$m
Force [N]
Time (s)
Filtered Force ($F_{Meas} - F_{Meas,Empty}$)
Position [in m] {scale=200:1}
Inertia Force (M.a) {scale=10:1}
First-order Force ($(M+A).a + B.v$)

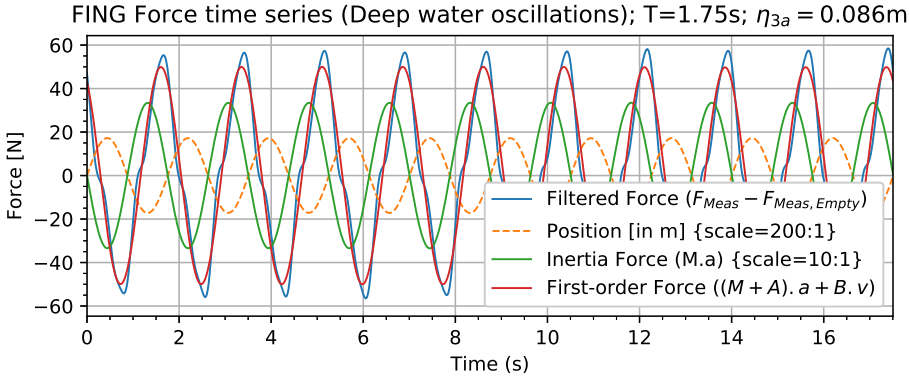
FING Force time series (Deep water oscillations); T=1.75s; $\eta_{3a} = 0.086$m
Force [N]
Time (s)
Filtered Force ($F_{Meas} - F_{Meas,Empty}$)
Position [in m] {scale=200:1}
Inertia Force (M.a) {scale=10:1}
First-order Force ($(M+A).a + B.v$)

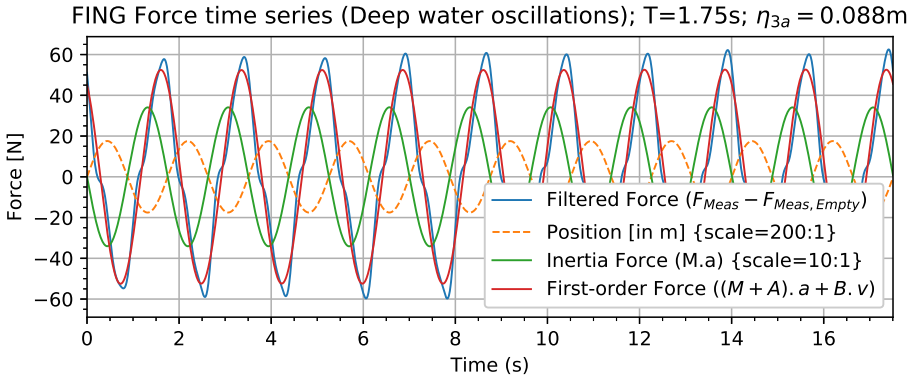
FING Force time series (Deep water oscillations); T=1.75s; $\eta_{3a} = 0.088$m
Force [N]
Time (s)
Filtered Force ($F_{Meas} - F_{Meas,Empty}$)
Position [in m] {scale=200:1}
Inertia Force (M.a) {scale=10:1}
First-order Force ($(M+A).a + B.v$)

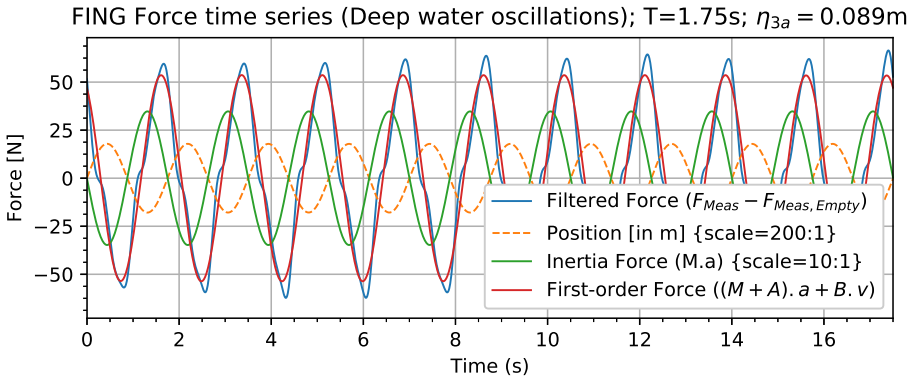
FING Force time series (Deep water oscillations); T=1.75s; $\eta_{3a} = 0.089$m
Force [N]
Time (s)
Filtered Force ($F_{Meas} - F_{Meas,Empty}$)
Position [in m] {scale=200:1}
Inertia Force (M.a) {scale=10:1}
First-order Force ($(M+A).a + B.v$)

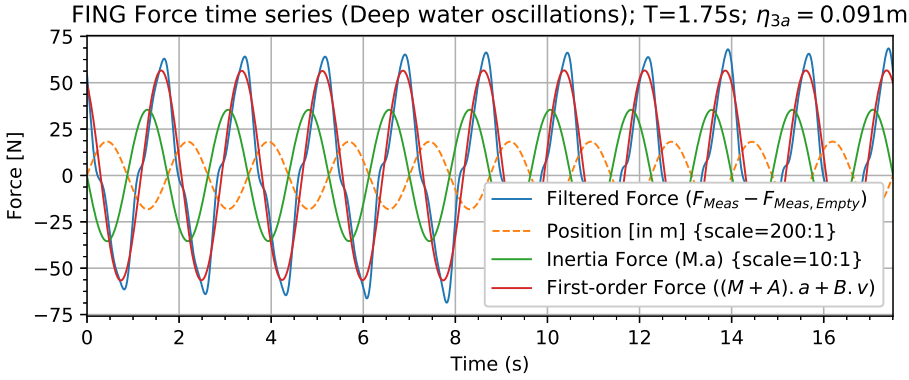
FING Force time series (Deep water oscillations); T=1.75s; $\eta_{3a} = 0.091$m
Force [N]
Time (s)
Filtered Force ($F_{Meas} - F_{Meas,Empty}$)
Position [in m] {scale=200:1}
Inertia Force (M.a) {scale=10:1}
First-order Force ($(M+A).a + B.v$)

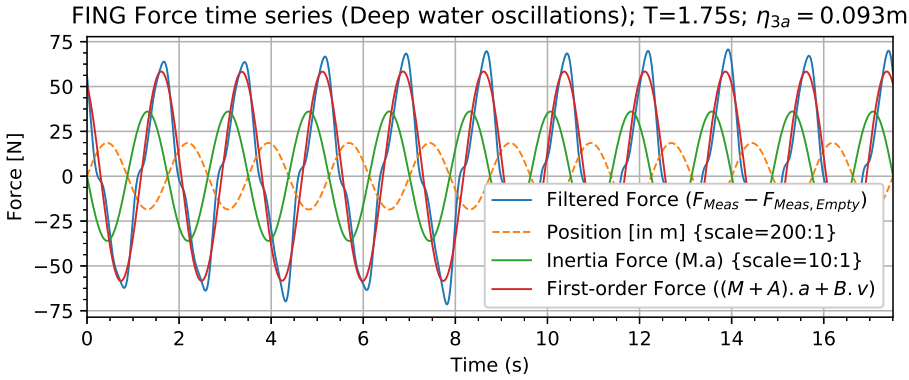
FING Force time series (Deep water oscillations); T=1.75s; $\eta_{3a} = 0.093$m
Force [N]
Time (s)
Filtered Force ($F_{Meas} - F_{Meas,Empty}$)
Position [in m] {scale=200:1}
Inertia Force (M.a) {scale=10:1}
First-order Force ($(M+A).a + B.v$)

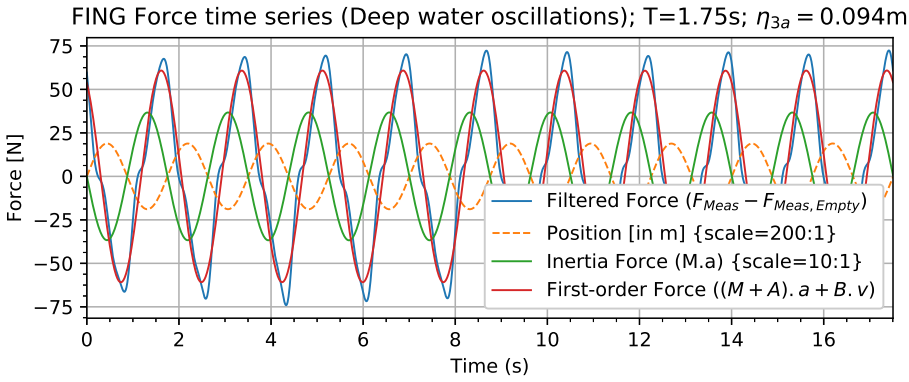
FING Force time series (Deep water oscillations); T=1.75s; $\eta_{3a} = 0.094$m
Force [N]
Time (s)
Filtered Force ($F_{Meas} - F_{Meas,Empty}$)
Position [in m] {scale=200:1}
Inertia Force (M.a) {scale=10:1}
First-order Force ($(M+A).a + B.v$)

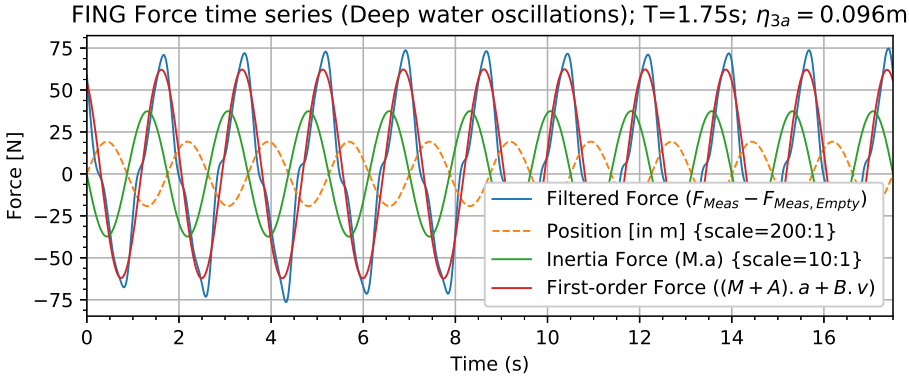
FING Force time series (Deep water oscillations); T=1.75s; $\eta_{3a} = 0.096$m
Force [N]
Time (s)
Filtered Force ($F_{Meas} - F_{Meas,Empty}$)
Position [in m] {scale=200:1}
Inertia Force (M.a) {scale=10:1}
First-order Force ($(M+A).a + B.v$)

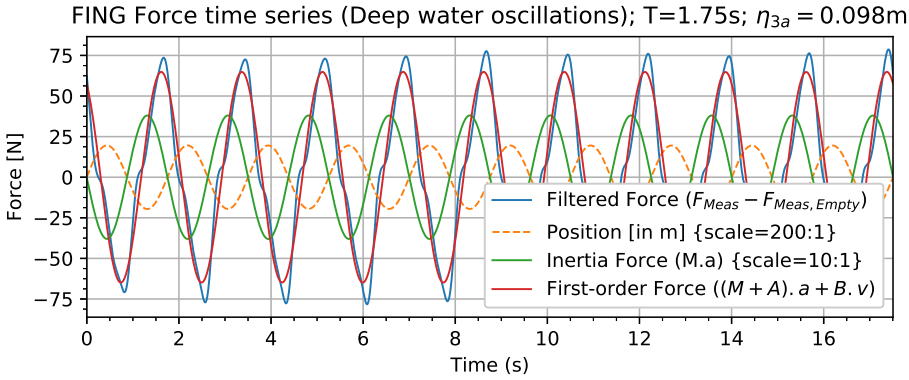
FING Force time series (Deep water oscillations); T=1.75s; $\eta_{3a} = 0.098$m
Force [N]
Time (s)
Filtered Force ($F_{Meas} - F_{Meas,Empty}$)
Position [in m] {scale=200:1}
Inertia Force (M.a) {scale=10:1}
First-order Force ($(M+A).a + B.v$)

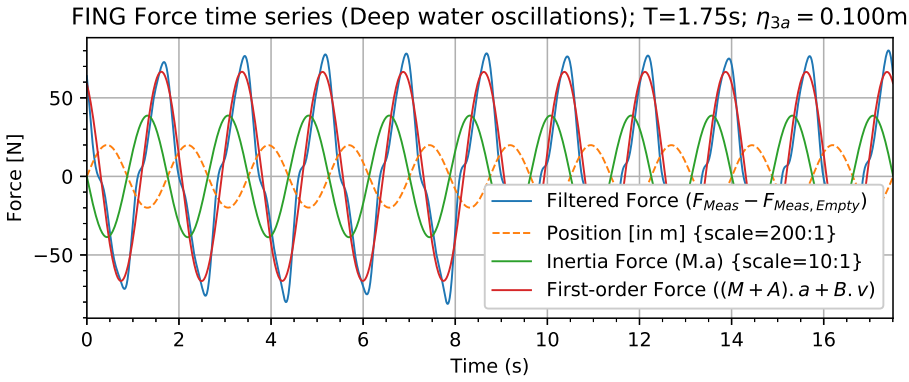
FING Force time series (Deep water oscillations); T=1.75s; $\eta_{3a} = 0.100$m
Force [N]
Time (s)
Filtered Force ($F_{Meas} - F_{Meas,Empty}$)
Position [in m] {scale=200:1}
Inertia Force (M.a) {scale=10:1}
First-order Force ($(M+A).a + B.v$)

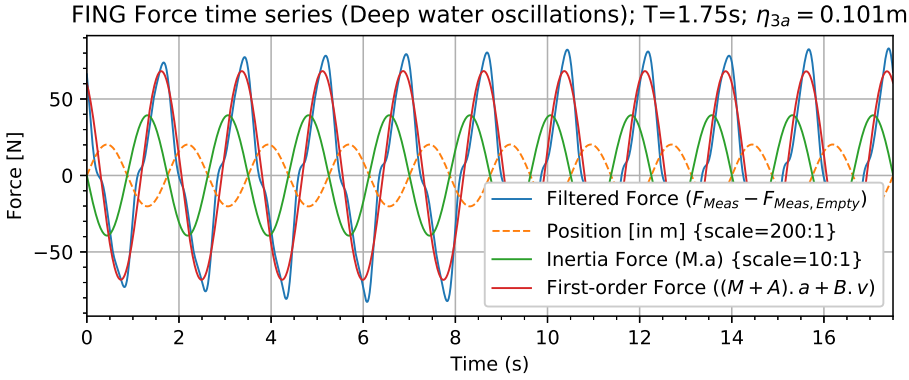
FING Force time series (Deep water oscillations); T=1.75s; $\eta_{3a} = 0.101$m
Force [N]
Time (s)
Filtered Force ($F_{Meas} - F_{Meas,Empty}$)
Position [in m] {scale=200:1}
Inertia Force (M.a) {scale=10:1}
First-order Force ($(M+A).a + B.v$)

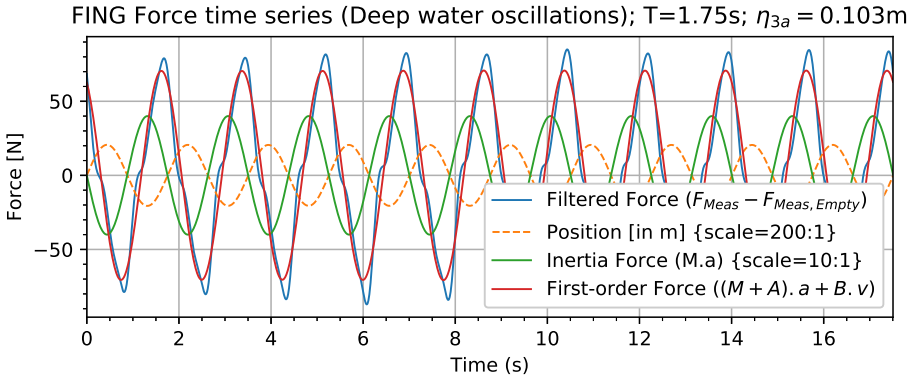
FING Force time series (Deep water oscillations); T=1.75s; $\eta_{3a} = 0.103$m
Force [N]
Time (s)
Filtered Force ($F_{Meas} - F_{Meas,Empty}$)
Position [in m] {scale=200:1}
Inertia Force (M.a) {scale=10:1}
First-order Force ($(M+A).a + B.v$)

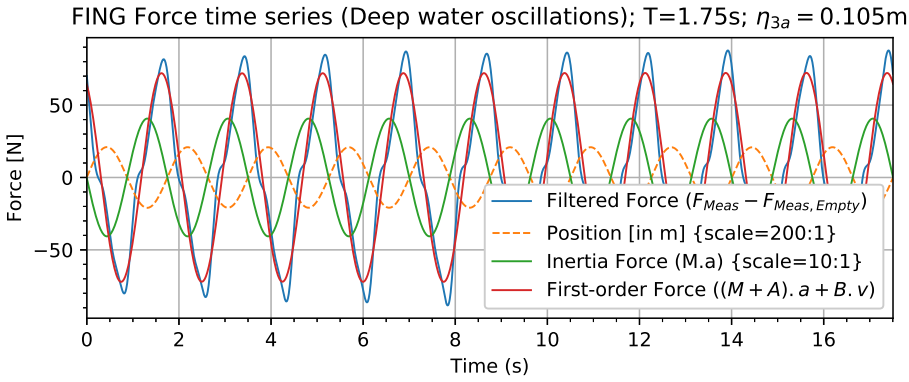
FING Force time series (Deep water oscillations); T=1.75s; $\eta_{3a} = 0.105$m
Force [N]
Time (s)
Filtered Force ($F_{Meas} - F_{Meas,Empty}$)
Position [in m] {scale=200:1}
Inertia Force (M.a) {scale=10:1}
First-order Force ($(M+A).a + B.v$)

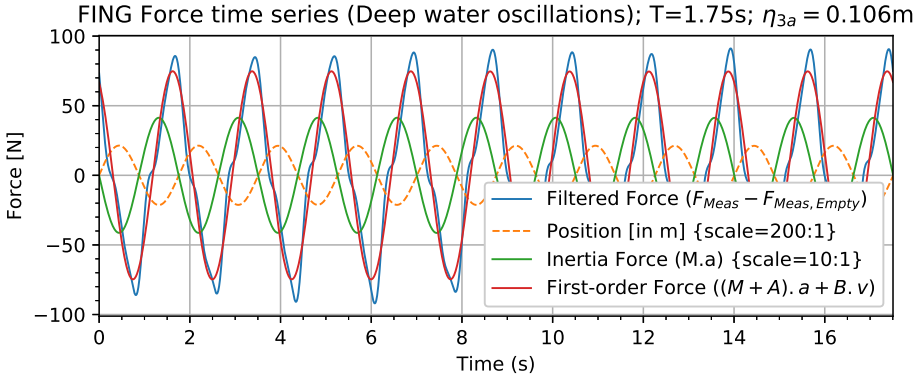
FING Force time series (Deep water oscillations); T=1.75s; $\eta_{3a} = 0.106$m
Force [N]
Time (s)
Filtered Force ($F_{Meas} - F_{Meas,Empty}$)
Position [in m] {scale=200:1}
Inertia Force (M.a) {scale=10:1}
First-order Force ($(M+A).a + B.v$)

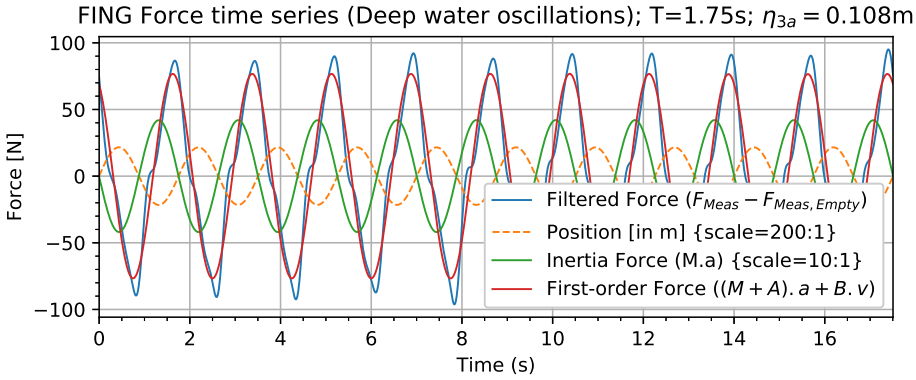
FING Force time series (Deep water oscillations); T=1.75s; $\eta_{3a} = 0.108$m
Force [N]
Time (s)
Filtered Force ($F_{Meas} - F_{Meas,Empty}$)
Position [in m] {scale=200:1}
Inertia Force (M.a) {scale=10:1}
First-order Force ($(M+A).a + B.v$)

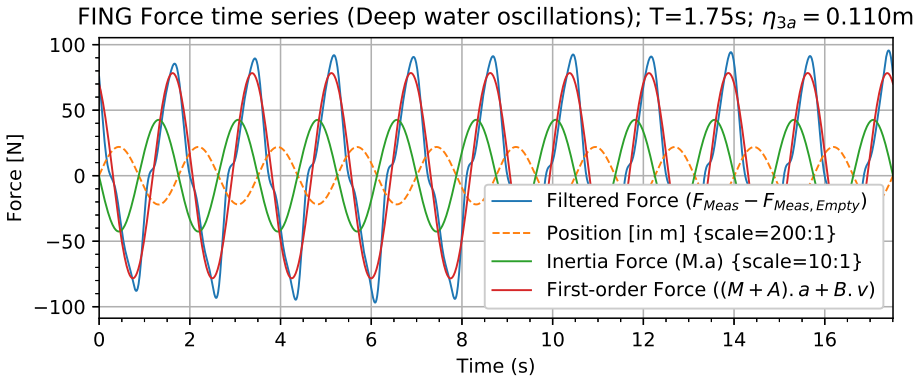
FING Force time series (Deep water oscillations); T=1.75s; $\eta_{3a} = 0.110$m
Force [N]
Time (s)
Filtered Force ($F_{Meas} - F_{Meas,Empty}$)
Position [in m] {scale=200:1}
Inertia Force (M.a) {scale=10:1}
First-order Force ($(M+A).a + B.v$)

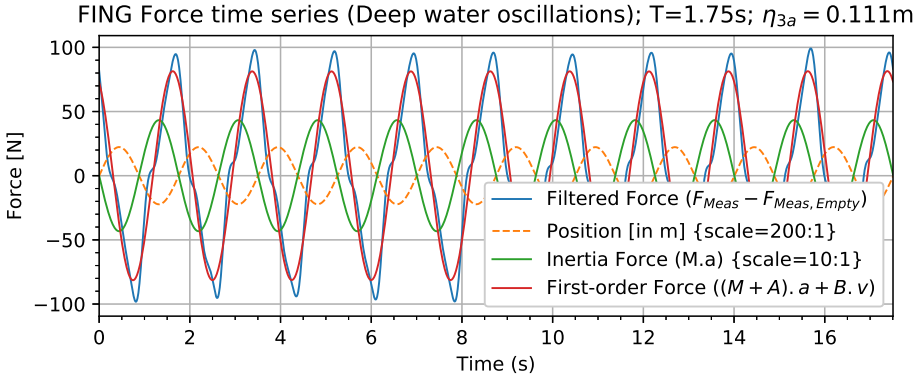
FING Force time series (Deep water oscillations); T=1.75s; $\eta_{3a} = 0.111$m
Force [N]
Time (s)
Filtered Force ($F_{Meas} - F_{Meas,Empty}$)
Position [in m] {scale=200:1}
Inertia Force (M.a) {scale=10:1}
First-order Force ($(M+A).a + B.v$)

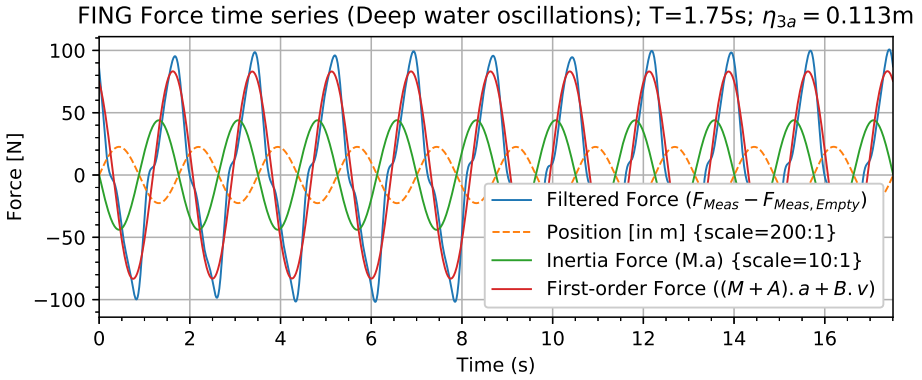
FING Force time series (Deep water oscillations); T=1.75s; $\eta_{3a} = 0.113$m
Force [N]
Time (s)
Filtered Force ($F_{Meas} - F_{Meas,Empty}$)
Position [in m] {scale=200:1}
Inertia Force (M.a) {scale=10:1}
First-order Force ($(M+A).a + B.v$)

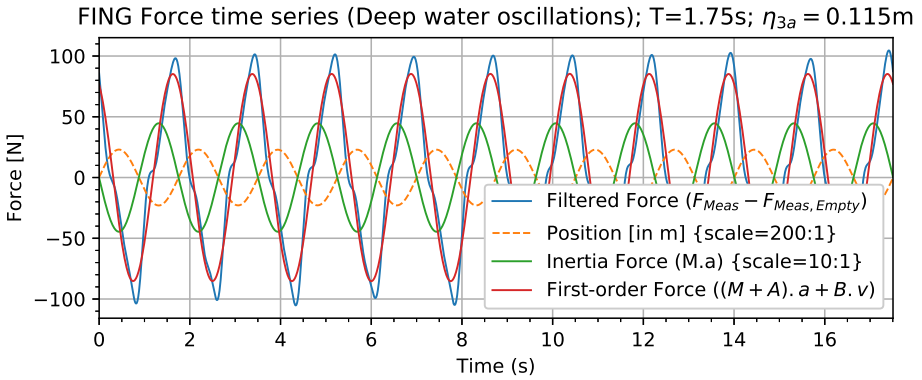
FING Force time series (Deep water oscillations); T=1.75s; $\eta_{3a} = 0.115$m
Force [N]
Time (s)
Filtered Force ($F_{Meas} - F_{Meas,Empty}$)
Position [in m] {scale=200:1}
Inertia Force (M.a) {scale=10:1}
First-order Force ($(M+A).a + B.v$)

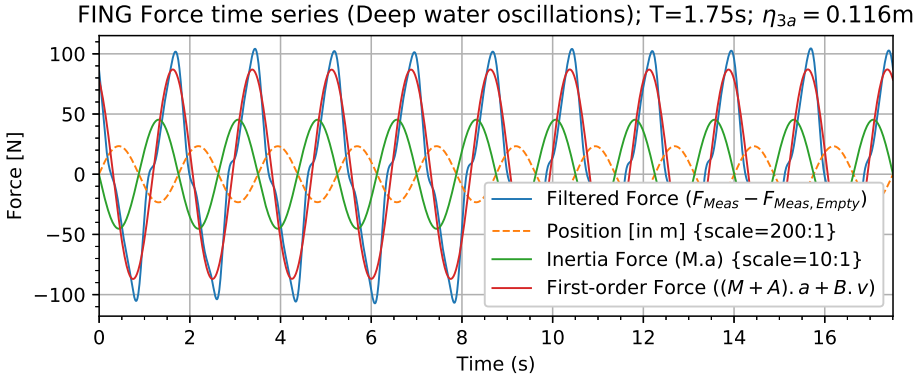
FING Force time series (Deep water oscillations); T=1.75s; $\eta_{3a} = 0.116$m
Force [N]
Time (s)
Filtered Force ($F_{Meas} - F_{Meas,Empty}$)
Position [in m] {scale=200:1}
Inertia Force (M.a) {scale=10:1}
First-order Force ($(M+A).a + B.v$)

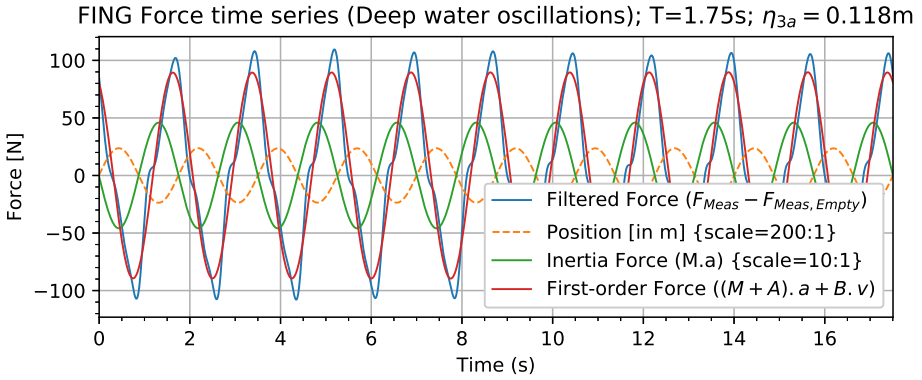
FING Force time series (Deep water oscillations); T=1.75s; $\eta_{3a} = 0.118$m
Force [N]
Time (s)
Filtered Force ($F_{Meas} - F_{Meas,Empty}$)
Position [in m] {scale=200:1}
Inertia Force (M.a) {scale=10:1}
First-order Force ($(M+A).a + B.v$)

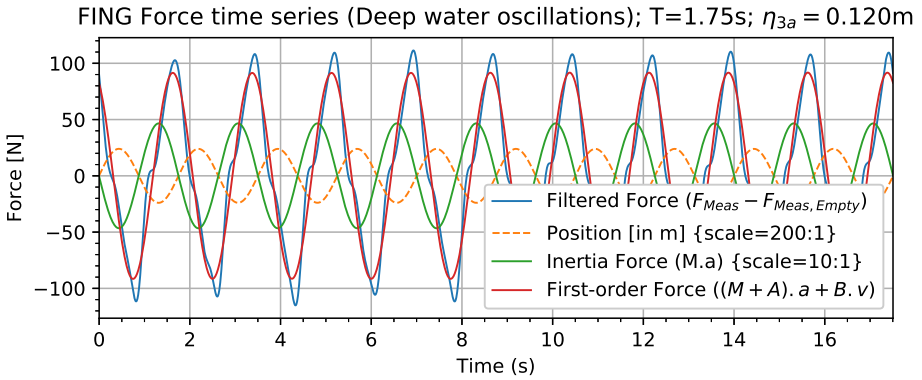
FING Force time series (Deep water oscillations); T=1.75s; $\eta_{3a} = 0.120$m
Force [N]
Time (s)
Filtered Force ($F_{Meas} - F_{Meas,Empty}$)
Position [in m] {scale=200:1}
Inertia Force (M.a) {scale=10:1}
First-order Force ($(M+A).a + B.v$)

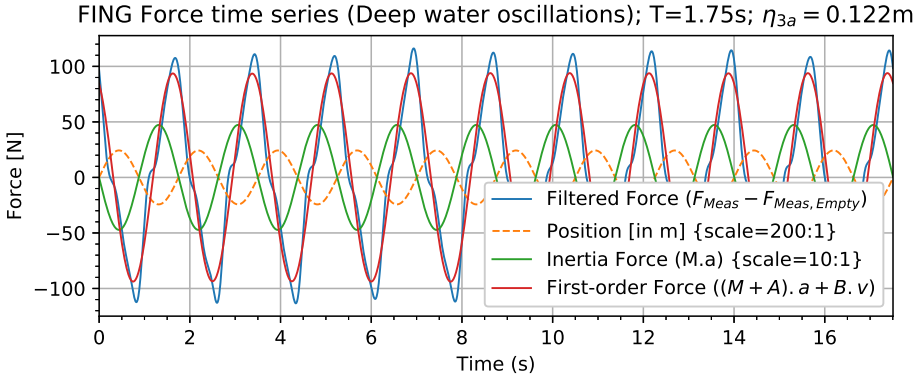
FING Force time series (Deep water oscillations); T=1.75s; $\eta_{3a} = 0.122$m
Force [N]
Time (s)
Filtered Force ($F_{Meas} - F_{Meas,Empty}$)
Position [in m] {scale=200:1}
Inertia Force (M.a) {scale=10:1}
First-order Force ($(M+A).a + B.v$)

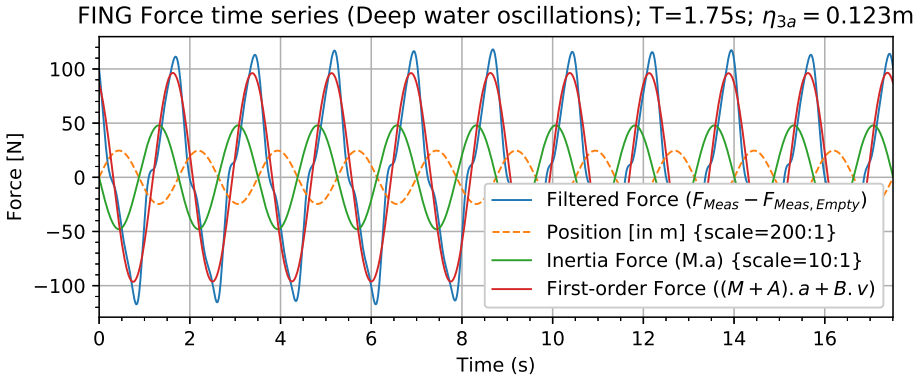
FING Force time series (Deep water oscillations); T=1.75s; $\eta_{3a} = 0.123$m
Force [N]
Time (s)
Filtered Force ($F_{Meas} - F_{Meas,Empty}$)
Position [in m] {scale=200:1}
Inertia Force (M.a) {scale=10:1}
First-order Force ($(M+A).a + B.v$)

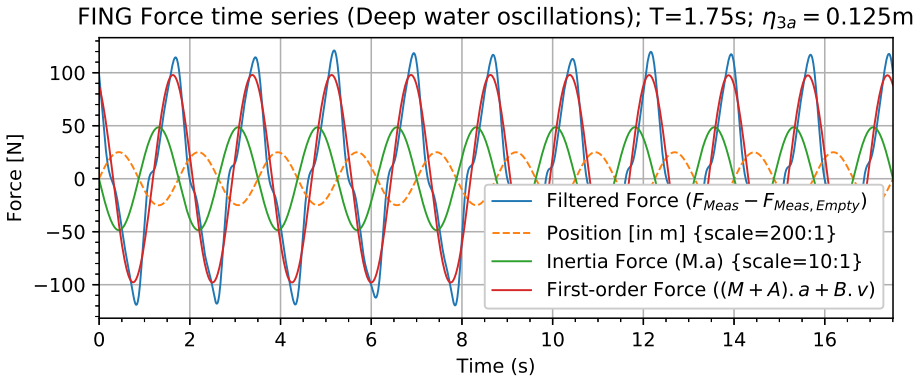
FING Force time series (Deep water oscillations); T=1.75s; $\eta_{3a} = 0.125$m
Force [N]
Time (s)
Filtered Force ($F_{Meas} - F_{Meas,Empty}$)
Position [in m] {scale=200:1}
Inertia Force (M.a) {scale=10:1}
First-order Force ($(M+A).a + B.v$)

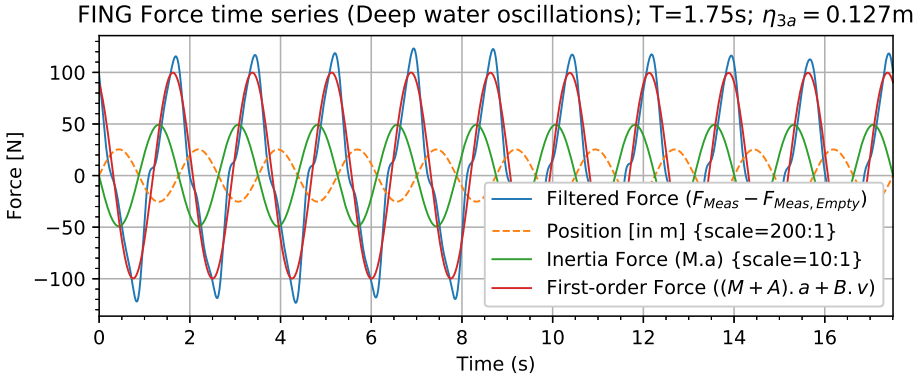
FING Force time series (Deep water oscillations); T=1.75s; $\eta_{3a} = 0.127$m
Force [N]
Time (s)
Filtered Force ($F_{Meas} - F_{Meas,Empty}$)
Position [in m] {scale=200:1}
Inertia Force (M.a) {scale=10:1}
First-order Force ($(M+A).a + B.v$)

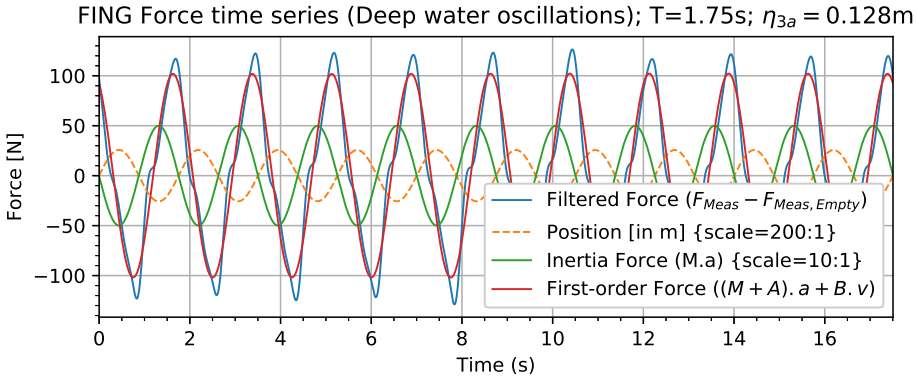
FING Force time series (Deep water oscillations); T=1.75s; $\eta_{3a} = 0.128$m
Force [N]
Time (s)
Filtered Force ($F_{Meas} - F_{Meas,Empty}$)
Position [in m] {scale=200:1}
Inertia Force (M.a) {scale=10:1}
First-order Force ($(M+A).a + B.v$)

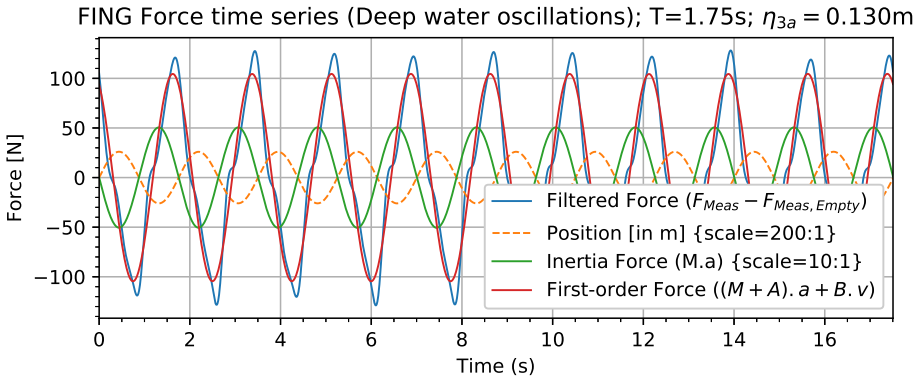
FING Force time series (Deep water oscillations); T=1.75s; $\eta_{3a} = 0.130$m
Force [N]
Time (s)
Filtered Force ($F_{Meas} - F_{Meas,Empty}$)
Position [in m] {scale=200:1}
Inertia Force (M.a) {scale=10:1}
First-order Force ($(M+A).a + B.v$)

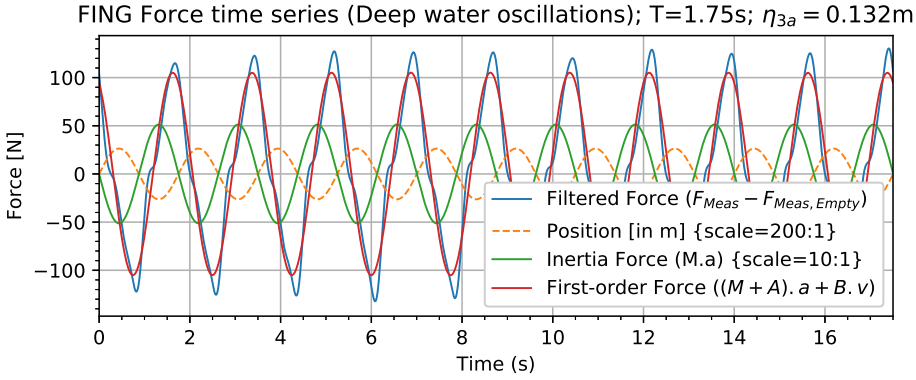
FING Force time series (Deep water oscillations); T=1.75s; $\eta_{3a} = 0.132$m
Force [N]
Time (s)
Filtered Force ($F_{Meas} - F_{Meas,Empty}$)
Position [in m] {scale=200:1}
Inertia Force (M.a) {scale=10:1}
First-order Force ($(M+A).a + B.v$)

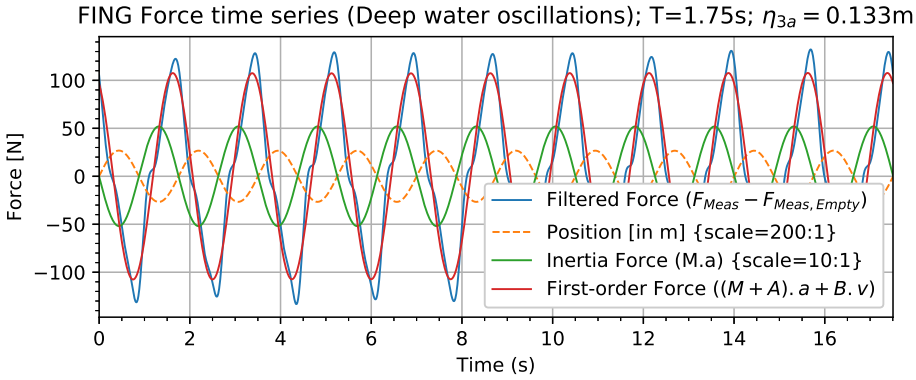
FING Force time series (Deep water oscillations); T=1.75s; $\eta_{3a} = 0.133$m
Force [N]
Time (s)
Filtered Force ($F_{Meas} - F_{Meas,Empty}$)
Position [in m] {scale=200:1}
Inertia Force (M.a) {scale=10:1}
First-order Force ($(M+A).a + B.v$)

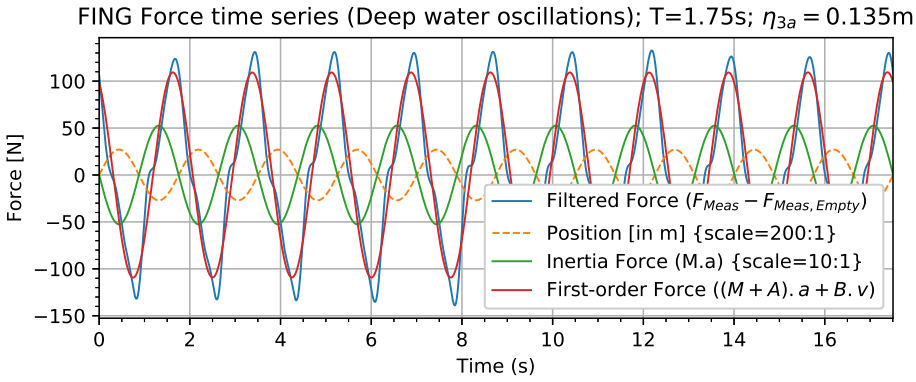
FING Force time series (Deep water oscillations); T=1.75s; $\eta_{3a} = 0.135$m
Force [N]
Time (s)
Filtered Force ($F_{Meas} - F_{Meas,Empty}$)
Position [in m] {scale=200:1}
Inertia Force (M.a) {scale=10:1}
First-order Force ($(M+A).a + B.v$)

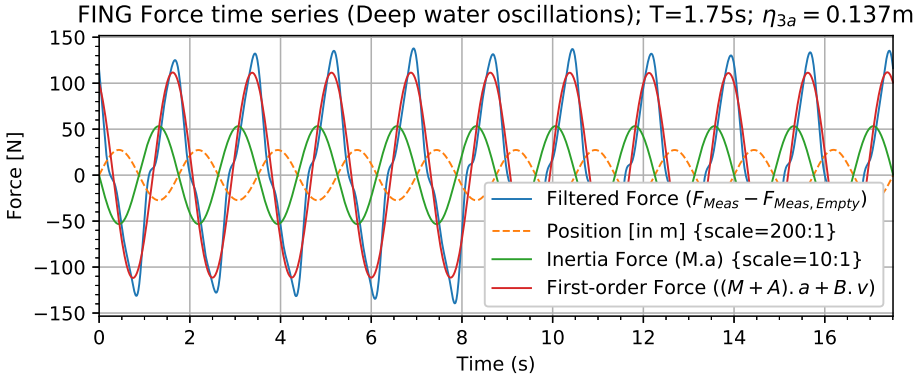
FING Force time series (Deep water oscillations); T=1.75s; $\eta_{3a} = 0.137$m
Force [N]
Time (s)
Filtered Force ($F_{Meas} - F_{Meas,Empty}$)
Position [in m] {scale=200:1}
Inertia Force (M.a) {scale=10:1}
First-order Force ($(M+A).a + B.v$)

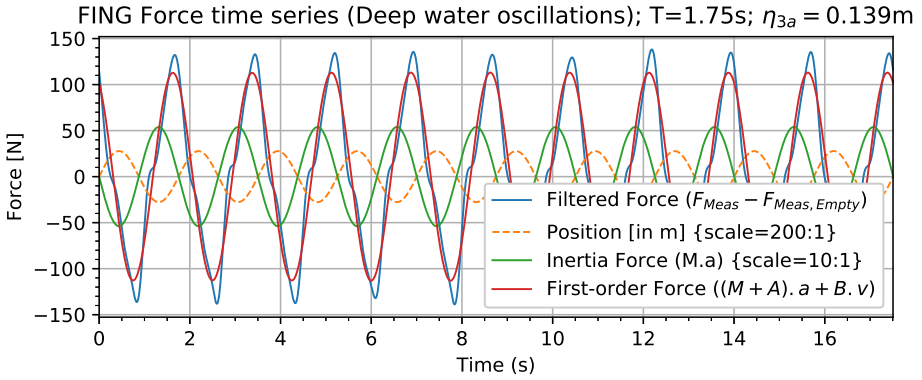
FING Force time series (Deep water oscillations); T=1.75s; $\eta_{3a} = 0.139$m
Force [N]
Time (s)
Filtered Force ($F_{Meas} - F_{Meas,Empty}$)
Position [in m] {scale=200:1}
Inertia Force (M.a) {scale=10:1}
First-order Force ($(M+A).a + B.v$)

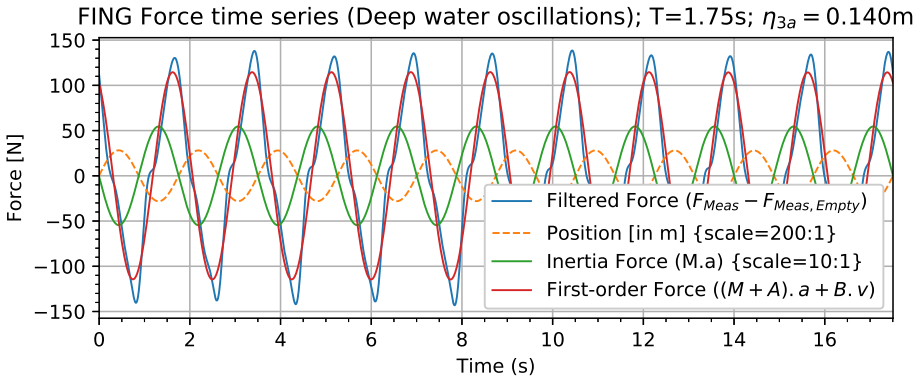
FING Force time series (Deep water oscillations); T=1.75s; $\eta_{3a} = 0.140$m
Force [N]
Time (s)
Filtered Force ($F_{Meas} - F_{Meas,Empty}$)
Position [in m] {scale=200:1}
Inertia Force (M.a) {scale=10:1}
First-order Force ($(M+A).a + B.v$)

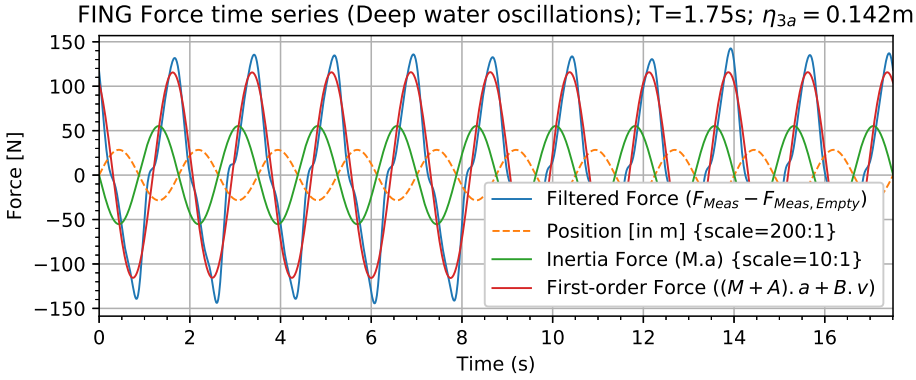
FING Force time series (Deep water oscillations); T=1.75s; $\eta_{3a} = 0.142$m
Force [N]
Time (s)
Filtered Force ($F_{Meas} - F_{Meas,Empty}$)
Position [in m] {scale=200:1}
Inertia Force (M.a) {scale=10:1}
First-order Force ($(M+A).a + B.v$)

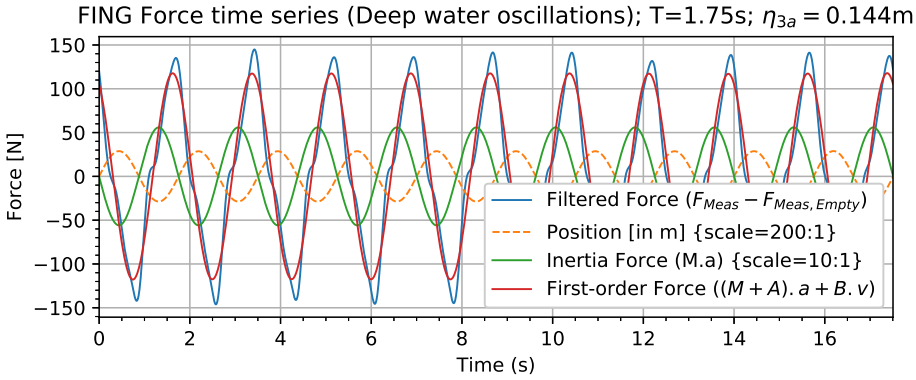
FING Force time series (Deep water oscillations); T=1.75s; $\eta_{3a} = 0.144$m
Force [N]
Time (s)
Filtered Force ($F_{Meas} - F_{Meas,Empty}$)
Position [in m] {scale=200:1}
Inertia Force (M.a) {scale=10:1}
First-order Force ($(M+A).a + B.v$)

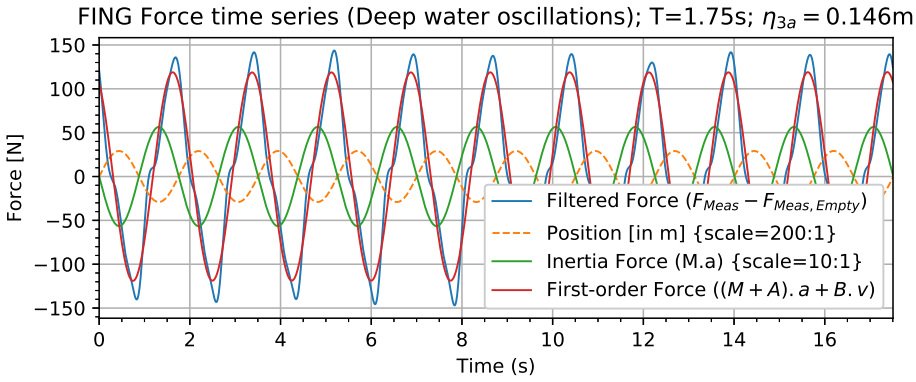
FING Force time series (Deep water oscillations); T=1.75s; $\eta_{3a} = 0.146$m
Force [N]
Time (s)
Filtered Force ($F_{Meas} - F_{Meas,Empty}$)
Position [in m] {scale=200:1}
Inertia Force (M.a) {scale=10:1}
First-order Force ($(M+A).a + B.v$)

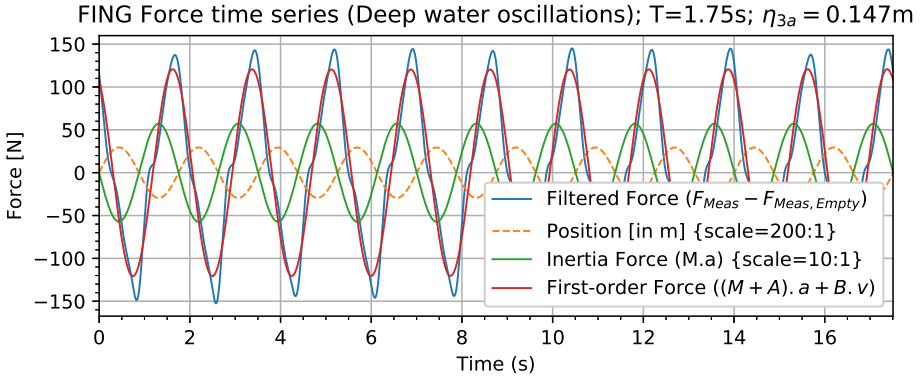
FING Force time series (Deep water oscillations); T=1.75s; $\eta_{3a} = 0.147$m
Force [N]
Time (s)
Filtered Force ($F_{Meas} - F_{Meas,Empty}$)
Position [in m] {scale=200:1}
Inertia Force (M.a) {scale=10:1}
First-order Force ($(M+A).a + B.v$)

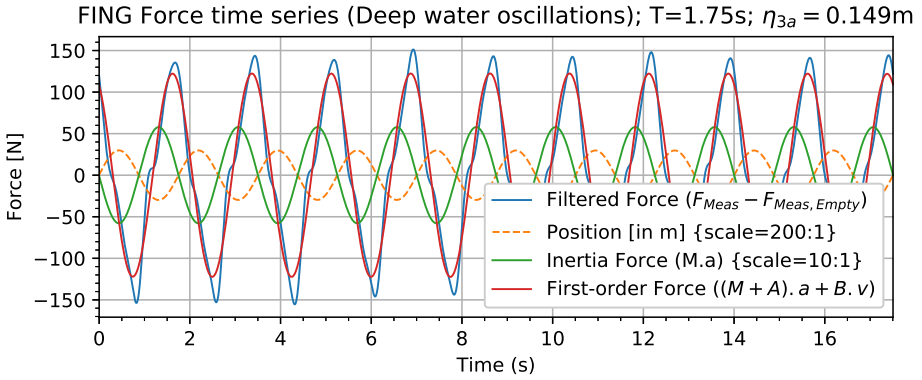
FING Force time series (Deep water oscillations); T=1.75s; $\eta_{3a} = 0.149$m
Force [N]
Time (s)
Filtered Force ($F_{Meas} - F_{Meas,Empty}$)
Position [in m] {scale=200:1}
Inertia Force (M.a) {scale=10:1}
First-order Force ($(M+A).a + B.v$)

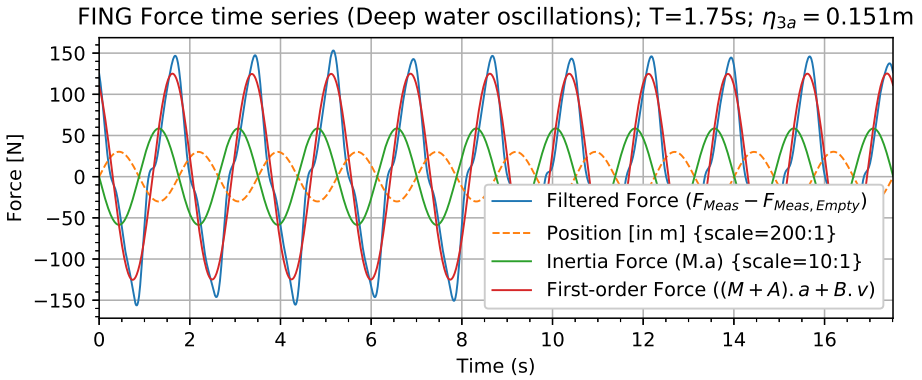
FING Force time series (Deep water oscillations); T=1.75s; $\eta_{3a} = 0.151$m
Force [N]
Time (s)
Filtered Force ($F_{Meas} - F_{Meas,Empty}$)
Position [in m] {scale=200:1}
Inertia Force (M.a) {scale=10:1}
First-order Force ($(M+A).a + B.v$)

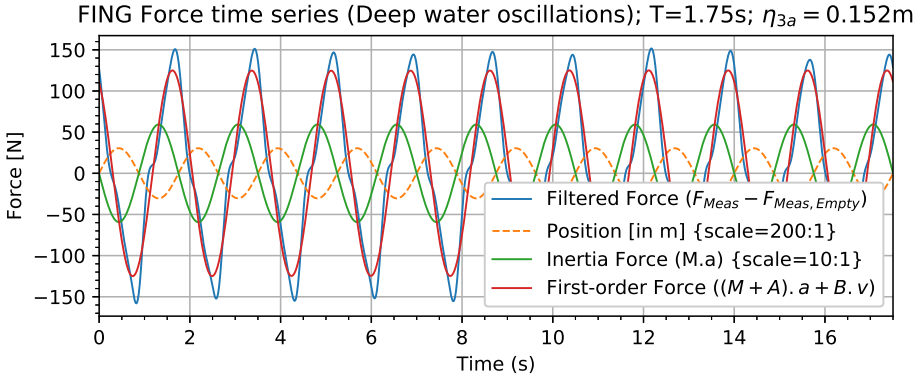
FING Force time series (Deep water oscillations); T=1.75s; $\eta_{3a} = 0.152$m
Force [N]
Time (s)
Filtered Force ($F_{Meas} - F_{Meas,Empty}$)
Position [in m] {scale=200:1}
Inertia Force (M.a) {scale=10:1}
First-order Force ($(M + A).a + B.v$)

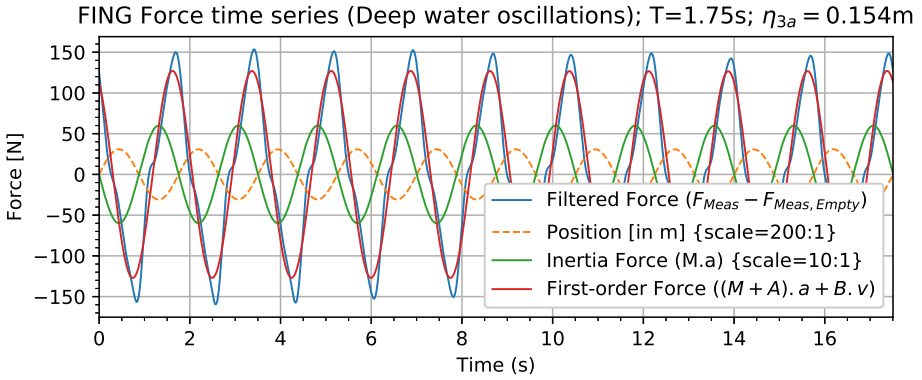
FING Force time series (Deep water oscillations); T=1.75s; $\eta_{3a} = 0.154$m
Force [N]
Time (s)
Filtered Force ($F_{Meas} - F_{Meas,Empty}$)
Position [in m] {scale=200:1}
Inertia Force (M.a) {scale=10:1}
First-order Force ($(M + A).a + B.v$)

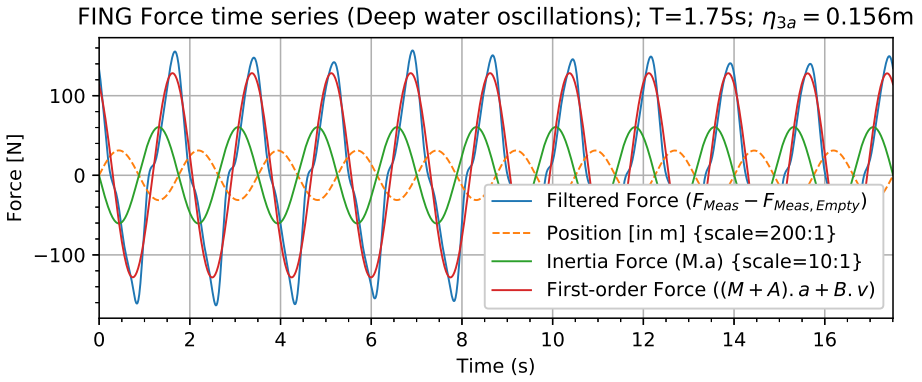
FING Force time series (Deep water oscillations); T=1.75s; $\eta_{3a} = 0.156$m
Force [N]
Time (s)
Filtered Force ($F_{Meas} - F_{Meas,Empty}$)
Position [in m] {scale=200:1}
Inertia Force (M.a) {scale=10:1}
First-order Force ($(M + A).a + B.v$)

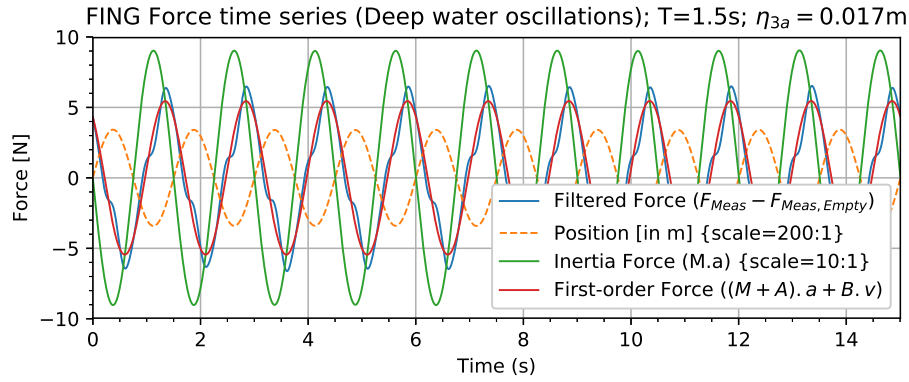
FING Force time series (Deep water oscillations); T=1.5s; $\eta_{3a} = 0.017$m
Force [N]
Time (s)
Filtered Force ($F_{Meas} - F_{Meas,Empty}$)
Position [in m] {scale=200:1}
Inertia Force (M.a) {scale=10:1}
First-order Force ($(M+A).a + B.v$)

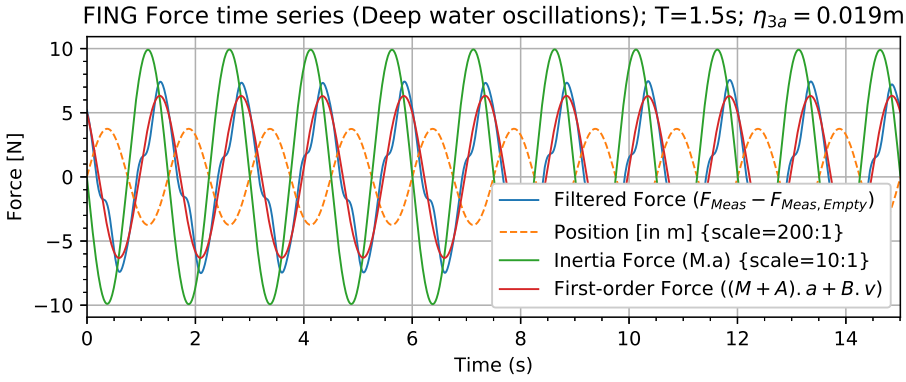
FING Force time series (Deep water oscillations); T=1.5s; $\eta_{3a} = 0.019$m
Force [N]
Time (s)
Filtered Force ($F_{Meas} - F_{Meas,Empty}$)
Position [in m] {scale=200:1}
Inertia Force (M.a) {scale=10:1}
First-order Force ($(M+A).a + B.v$)

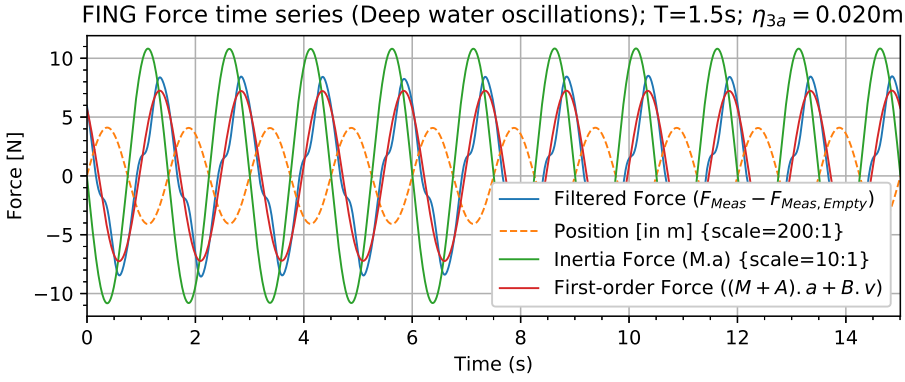
FING Force time series (Deep water oscillations); T=1.5s; $\eta_{3a} = 0.020$m
Force [N]
Time (s)
Filtered Force ($F_{Meas} - F_{Meas,Empty}$)
Position [in m] {scale=200:1}
Inertia Force (M.a) {scale=10:1}
First-order Force ($(M+A).a + B.v$)

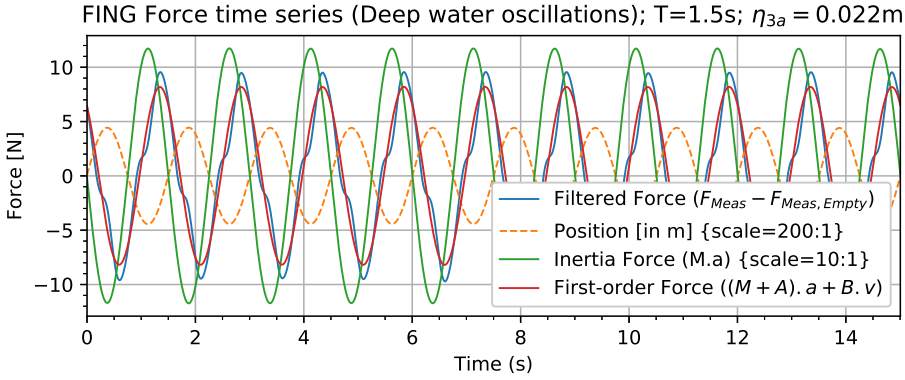
FING Force time series (Deep water oscillations); T=1.5s; $\eta_{3a} = 0.022$m
Force [N]
Time (s)
Filtered Force ($F_{Meas} - F_{Meas,Empty}$)
Position [in m] {scale=200:1}
Inertia Force (M.a) {scale=10:1}
First-order Force ($(M+A).a + B.v$)

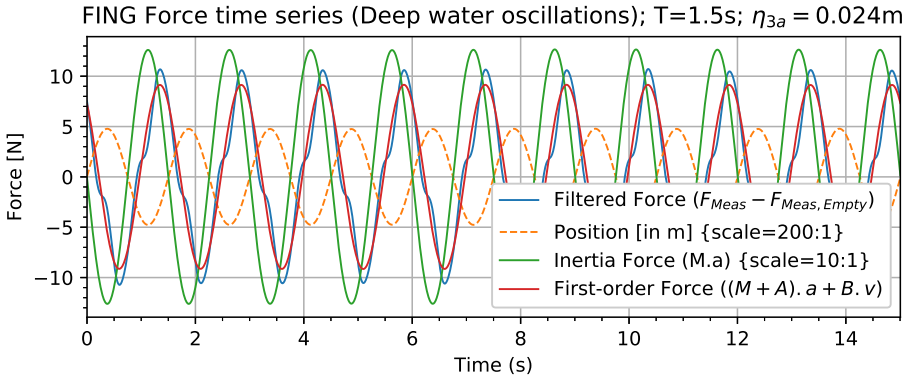
FING Force time series (Deep water oscillations); T=1.5s; $\eta_{3a} = 0.024$m
Force [N]
Time (s)
Filtered Force ($F_{Meas} - F_{Meas,Empty}$)
Position [in m] {scale=200:1}
Inertia Force (M.a) {scale=10:1}
First-order Force ($(M+A).a + B.v$)

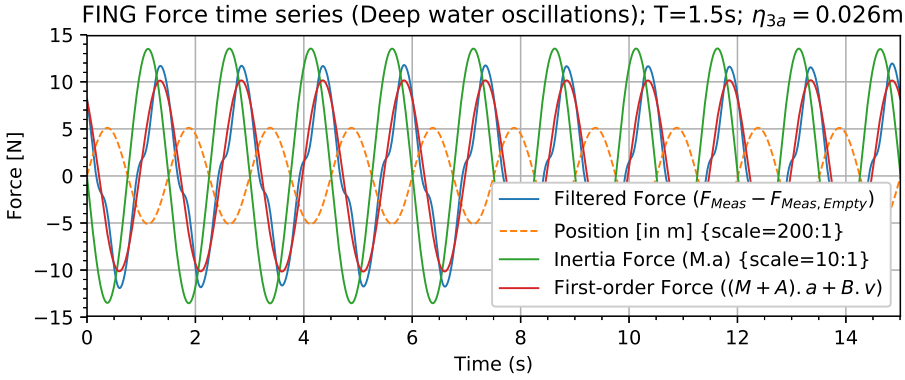
FING Force time series (Deep water oscillations); T=1.5s; $\eta_{3a} = 0.026$m
Force [N]
Time (s)
Filtered Force ($F_{Meas} - F_{Meas,Empty}$)
Position [in m] {scale=200:1}
Inertia Force (M.a) {scale=10:1}
First-order Force ($(M+A).a + B.v$)

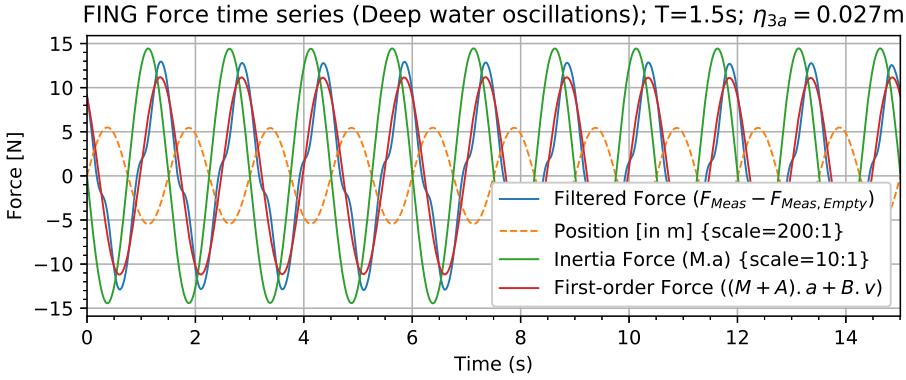
FING Force time series (Deep water oscillations); T=1.5s; $\eta_{3a} = 0.027$m
Force [N]
Time (s)
Filtered Force ($F_{Meas} - F_{Meas,Empty}$)
Position [in m] {scale=200:1}
Inertia Force (M.a) {scale=10:1}
First-order Force ($(M+A).a + B.v$)

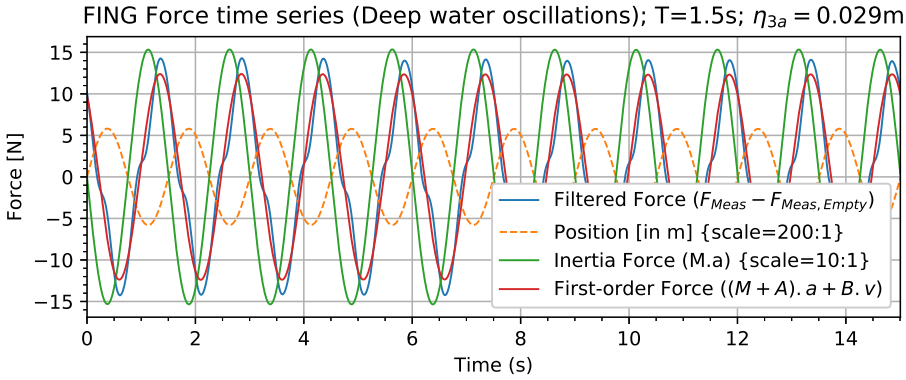
FING Force time series (Deep water oscillations); T=1.5s; $\eta_{3a} = 0.029$m
Force [N]
Time (s)
Filtered Force ($F_{Meas} - F_{Meas,Empty}$)
Position [in m] {scale=200:1}
Inertia Force (M.a) {scale=10:1}
First-order Force ($(M+A).a + B.v$)

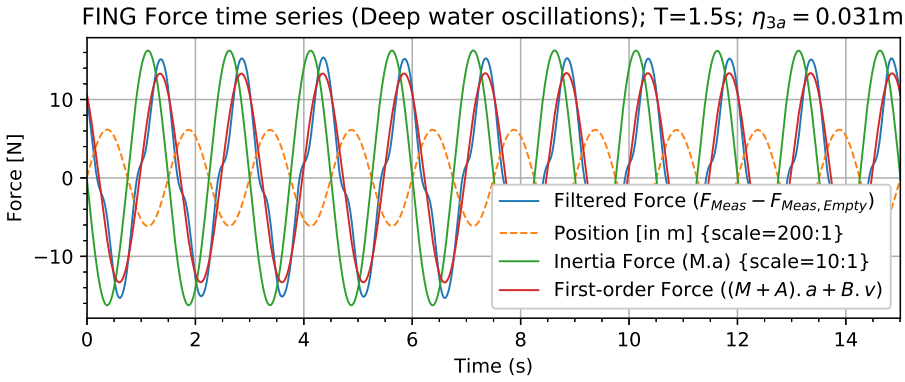
FING Force time series (Deep water oscillations); T=1.5s; $\eta_{3a} = 0.031$m
Force [N]
Time (s)
Filtered Force ($F_{Meas} - F_{Meas,Empty}$)
Position [in m] {scale=200:1}
Inertia Force (M.a) {scale=10:1}
First-order Force ($(M+A).a + B.v$)

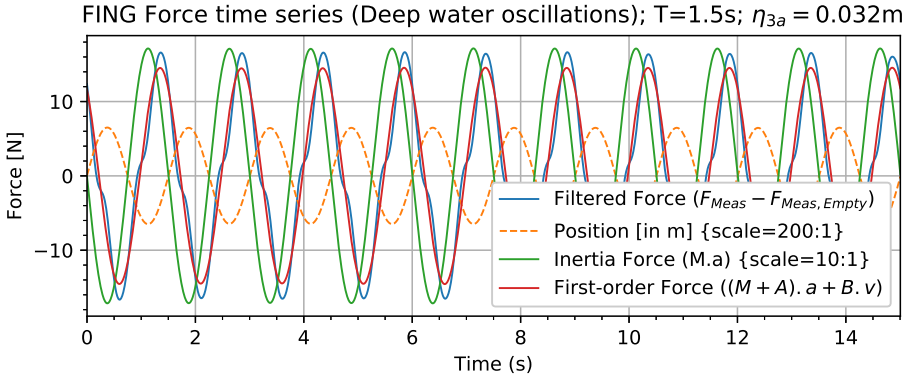
FING Force time series (Deep water oscillations); T=1.5s; $\eta_{3a} = 0.032$m
Force [N]
Time (s)
Filtered Force ($F_{Meas} - F_{Meas,Empty}$)
Position [in m] {scale=200:1}
Inertia Force (M.a) {scale=10:1}
First-order Force ($(M+A).a + B.v$)

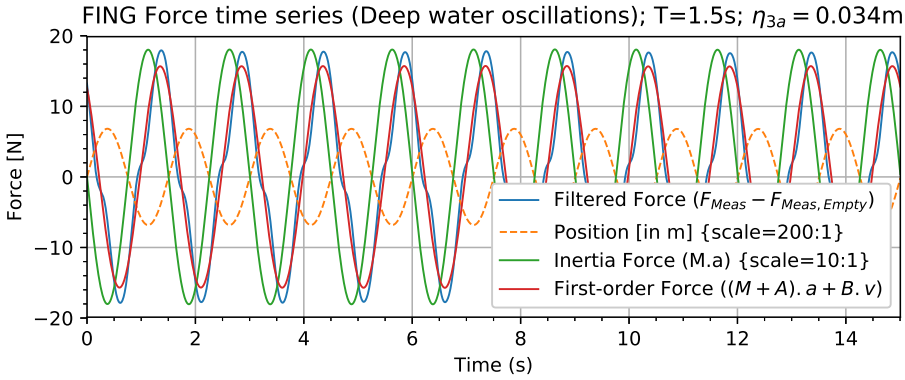
FING Force time series (Deep water oscillations); T=1.5s; $\eta_{3a} = 0.034$m
Force [N]
Time (s)
Filtered Force ($F_{Meas} - F_{Meas,Empty}$)
Position [in m] {scale=200:1}
Inertia Force (M.a) {scale=10:1}
First-order Force ($(M+A).a + B.v$)

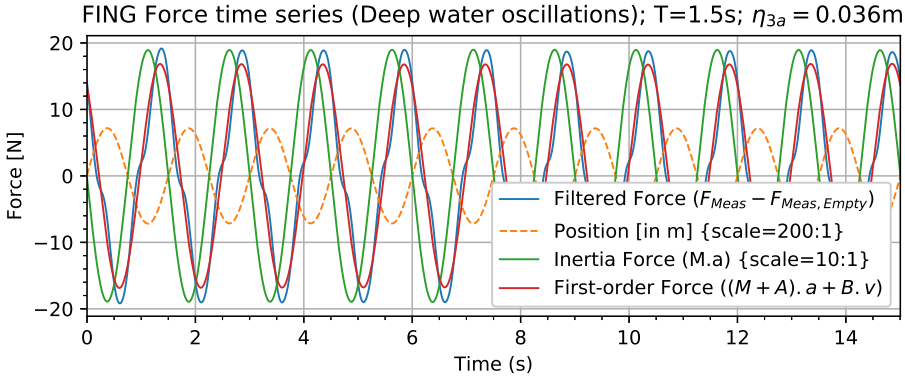
FING Force time series (Deep water oscillations); T=1.5s; $\eta_{3a} = 0.036$m
Force [N]
Time (s)
Filtered Force ($F_{Meas} - F_{Meas,Empty}$)
Position [in m] {scale=200:1}
Inertia Force (M.a) {scale=10:1}
First-order Force ($(M+A).a + B.v$)

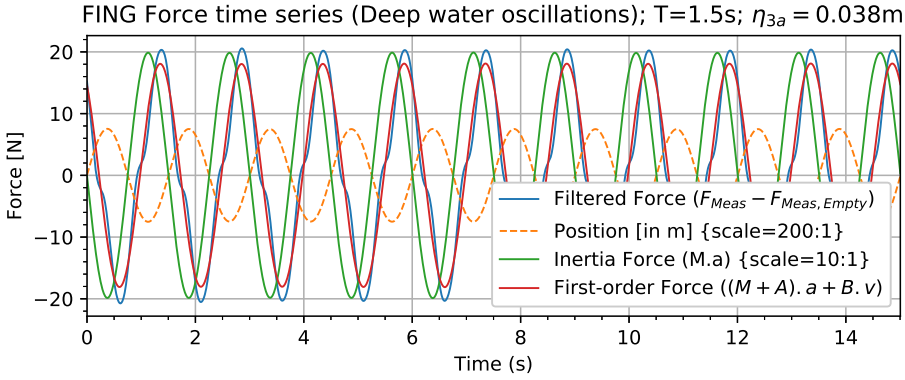
FING Force time series (Deep water oscillations); T=1.5s; $\eta_{3a} = 0.038$m
Force [N]
Time (s)
Filtered Force ($F_{Meas} - F_{Meas,Empty}$)
Position [in m] {scale=200:1}
Inertia Force (M.a) {scale=10:1}
First-order Force ($(M+A).a + B.v$)

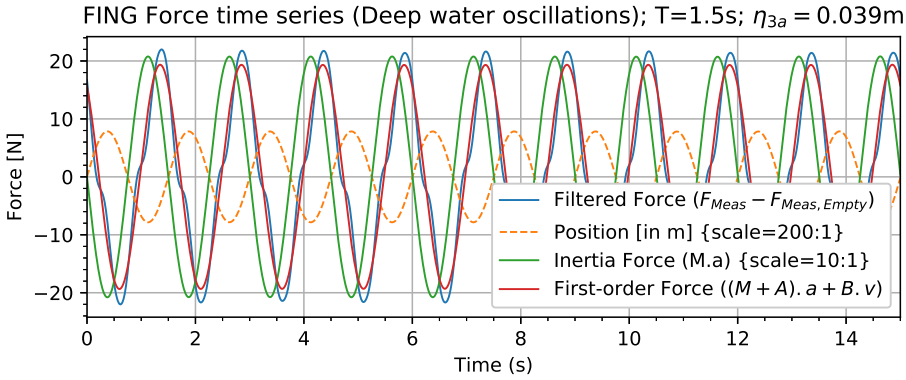
FING Force time series (Deep water oscillations); T=1.5s; $\eta_{3a} = 0.039$m
Force [N]
Time (s)
Filtered Force ($F_{Meas} - F_{Meas,Empty}$)
Position [in m] {scale=200:1}
Inertia Force (M.a) {scale=10:1}
First-order Force ($(M+A).a + B.v$)

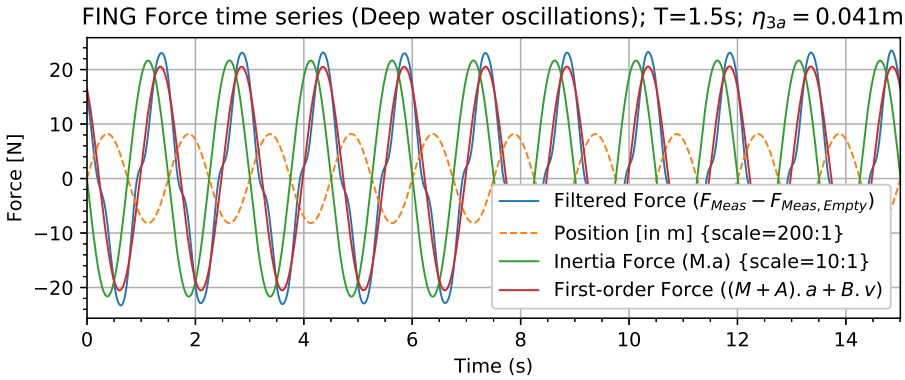
FING Force time series (Deep water oscillations); T=1.5s; $\eta_{3a} = 0.041$m
Force [N]
Time (s)
Filtered Force ($F_{Meas} - F_{Meas,Empty}$)
Position [in m] {scale=200:1}
Inertia Force (M.a) {scale=10:1}
First-order Force ($(M+A).a + B.v$)

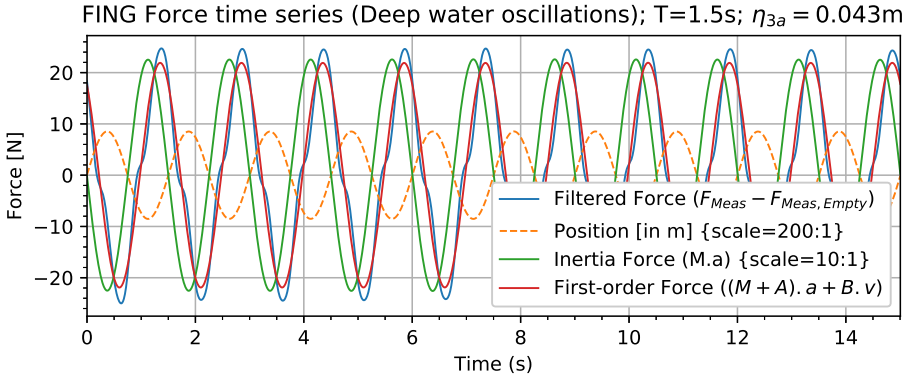
FING Force time series (Deep water oscillations); T=1.5s; $\eta_{3a} = 0.043$m
Force [N]
Time (s)
Filtered Force ($F_{Meas} - F_{Meas,Empty}$)
Position [in m] {scale=200:1}
Inertia Force (M.a) {scale=10:1}
First-order Force ($(M+A).a + B.v$)

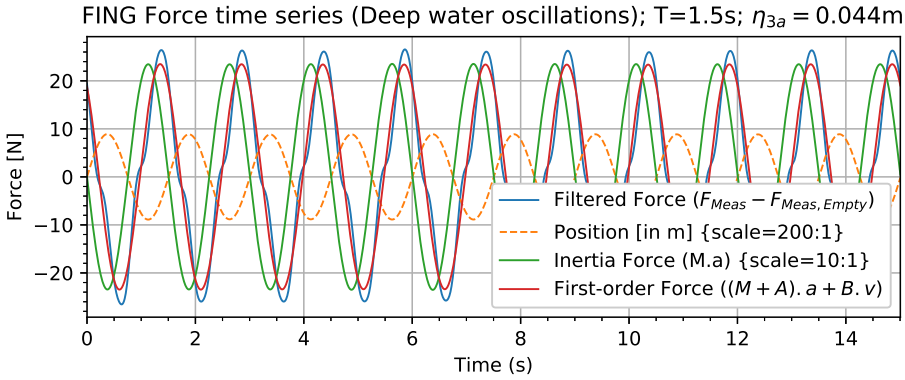
FING Force time series (Deep water oscillations); T=1.5s; $\eta_{3a} = 0.044$m
Force [N]
Time (s)
Filtered Force ($F_{Meas} - F_{Meas,Empty}$)
Position [in m] {scale=200:1}
Inertia Force (M.a) {scale=10:1}
First-order Force ($(M+A).a + B.v$)

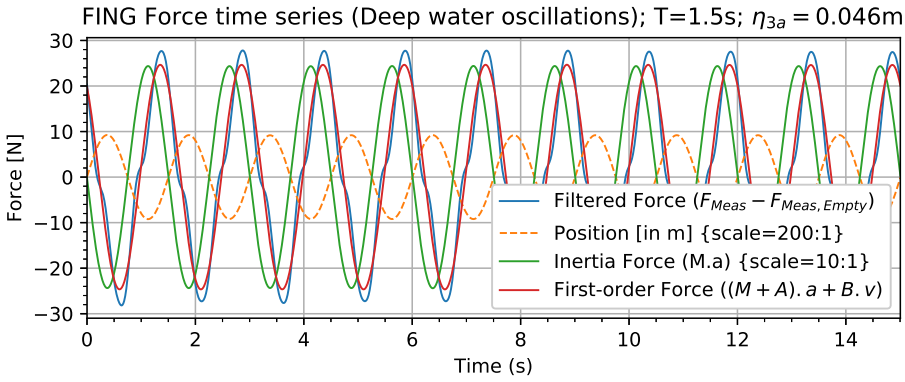
FING Force time series (Deep water oscillations); T=1.5s; $\eta_{3a} = 0.046$m
Force [N]
Time (s)
Filtered Force ($F_{Meas} - F_{Meas,Empty}$)
Position [in m] {scale=200:1}
Inertia Force (M.a) {scale=10:1}
First-order Force ($(M+A).a + B.v$)

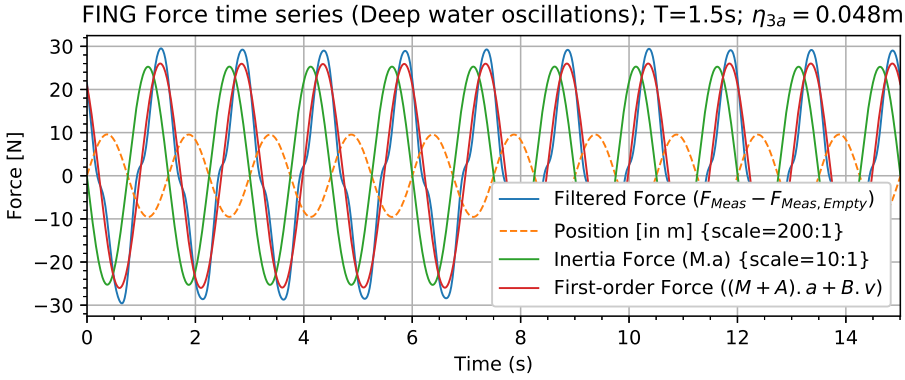
FING Force time series (Deep water oscillations); T=1.5s; $\eta_{3a} = 0.048$m
Force [N]
Time (s)
Filtered Force ($F_{Meas} - F_{Meas,Empty}$)
Position [in m] {scale=200:1}
Inertia Force (M.a) {scale=10:1}
First-order Force ($(M+A).a + B.v$)

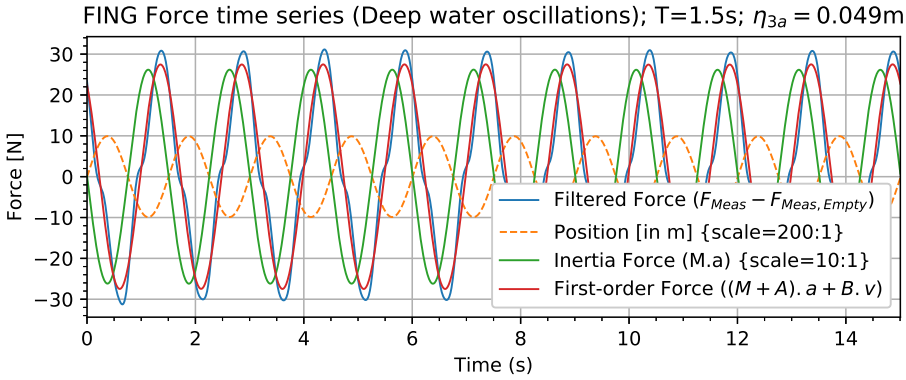
FING Force time series (Deep water oscillations); T=1.5s; $\eta_{3a} = 0.049$m
Force [N]
Time (s)
Filtered Force ($F_{Meas} - F_{Meas,Empty}$)
Position [in m] {scale=200:1}
Inertia Force (M.a) {scale=10:1}
First-order Force ($(M+A).a + B.v$)

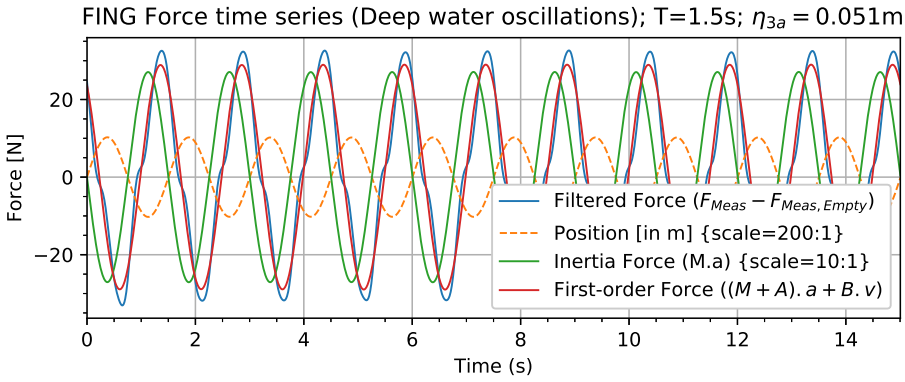
FING Force time series (Deep water oscillations); T=1.5s; $\eta_{3a} = 0.051$m
Force [N]
Time (s)
Filtered Force ($F_{Meas} - F_{Meas,Empty}$)
Position [in m] {scale=200:1}
Inertia Force (M.a) {scale=10:1}
First-order Force ($(M+A).a + B.v$)

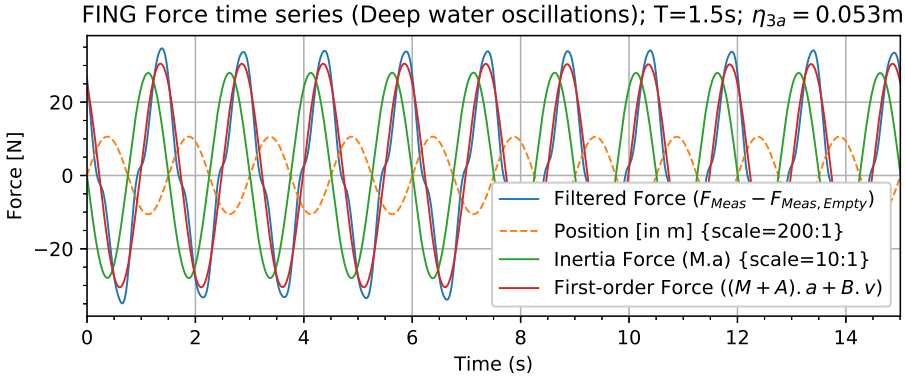
FING Force time series (Deep water oscillations); T=1.5s; $\eta_{3a} = 0.053$m
Force [N]
Time (s)
Filtered Force ($F_{Meas} - F_{Meas,Empty}$)
Position [in m] {scale=200:1}
Inertia Force (M.a) {scale=10:1}
First-order Force ($(M+A).a + B.v$)

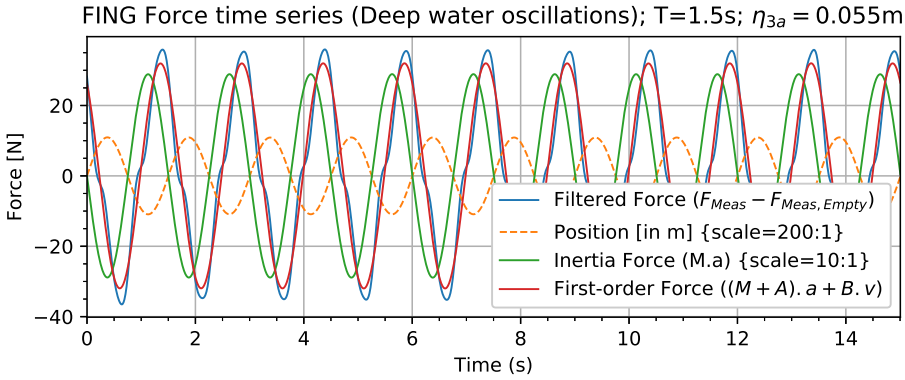
FING Force time series (Deep water oscillations); T=1.5s; $\eta_{3a} = 0.055$m
Force [N]
Time (s)
Filtered Force ($F_{Meas} - F_{Meas,Empty}$)
Position [in m] {scale=200:1}
Inertia Force (M.a) {scale=10:1}
First-order Force ($(M+A).a + B.v$)

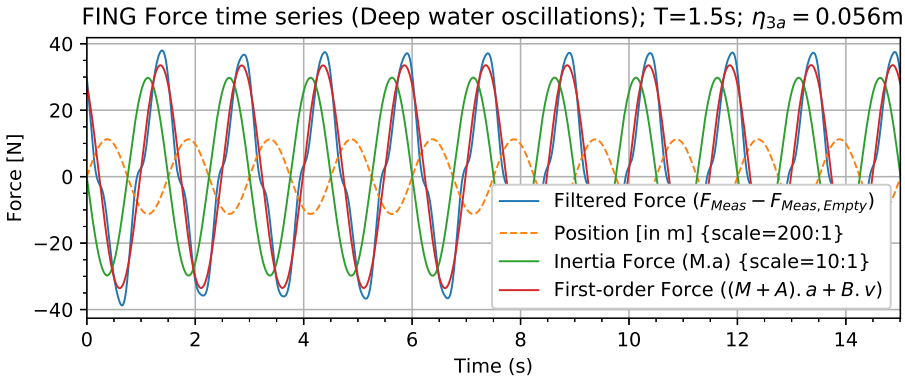
FING Force time series (Deep water oscillations); T=1.5s; $\eta_{3a} = 0.056$m
Force [N]
Time (s)
Filtered Force ($F_{Meas} - F_{Meas,Empty}$)
Position [in m] {scale=200:1}
Inertia Force (M.a) {scale=10:1}
First-order Force ($(M+A).a + B.v$)

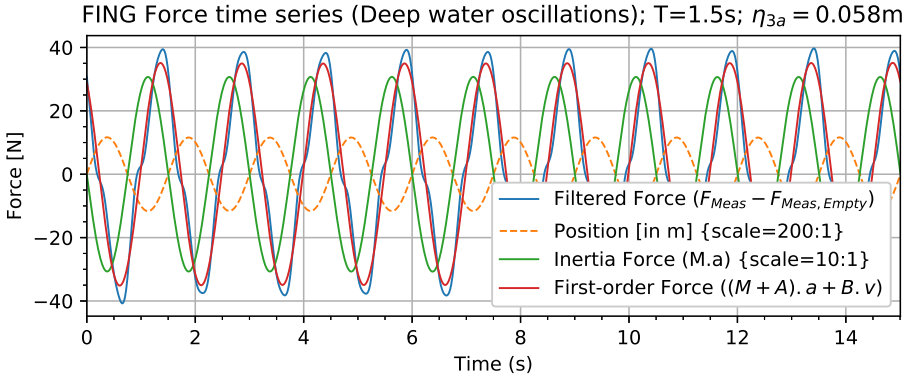
FING Force time series (Deep water oscillations); T=1.5s; $\eta_{3a} = 0.058$m
Force [N]
Time (s)
Filtered Force ($F_{Meas} - F_{Meas,Empty}$)
Position [in m] {scale=200:1}
Inertia Force (M.a) {scale=10:1}
First-order Force ($(M+A).a + B.v$)

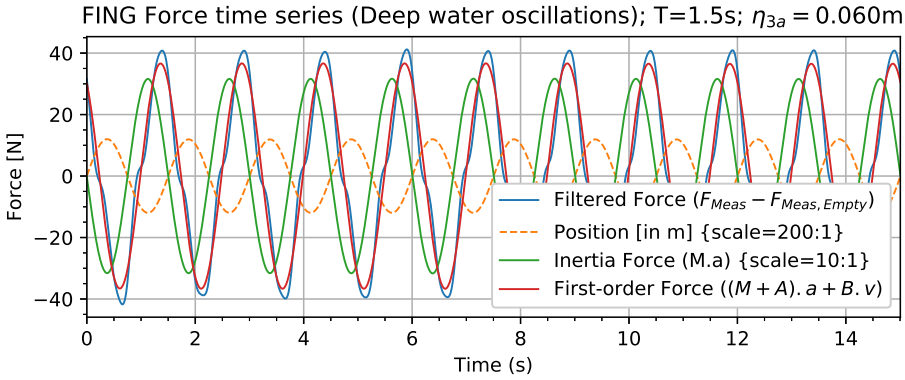
FING Force time series (Deep water oscillations); T=1.5s; $\eta_{3a} = 0.060$m
Force [N]
Time (s)
Filtered Force ($F_{Meas} - F_{Meas,Empty}$)
Position [in m] {scale=200:1}
Inertia Force (M.a) {scale=10:1}
First-order Force ($(M+A).a + B.v$)

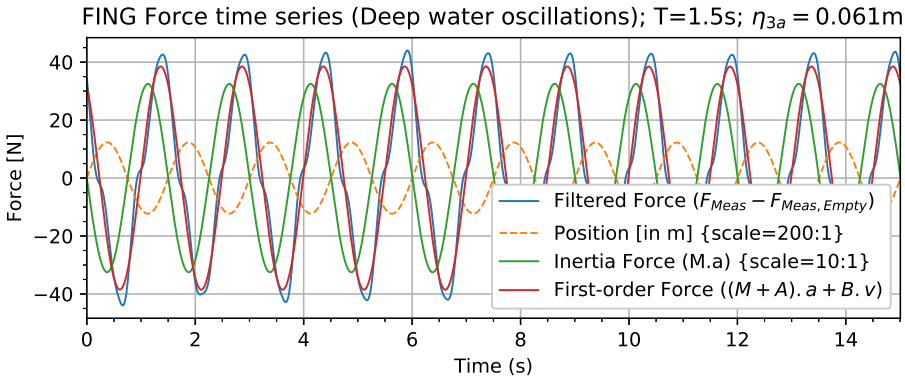
FING Force time series (Deep water oscillations); T=1.5s; $\eta_{3a} = 0.061$m
Force [N]
Time (s)
Filtered Force ($F_{Meas} - F_{Meas,Empty}$)
Position [in m] {scale=200:1}
Inertia Force (M.a) {scale=10:1}
First-order Force ($(M+A).a + B.v$)

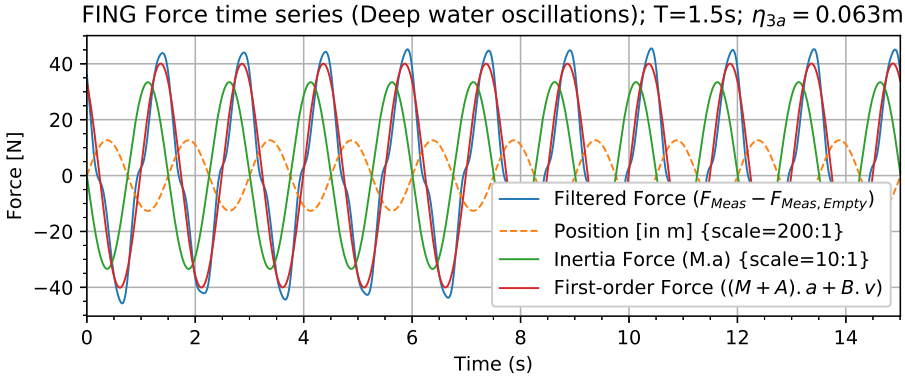
FING Force time series (Deep water oscillations); T=1.5s; $\eta_{3a} = 0.063$m
Force [N]
Time (s)
Filtered Force ($F_{Meas} - F_{Meas,Empty}$)
Position [in m] {scale=200:1}
Inertia Force (M.a) {scale=10:1}
First-order Force ($(M+A).a + B.v$)

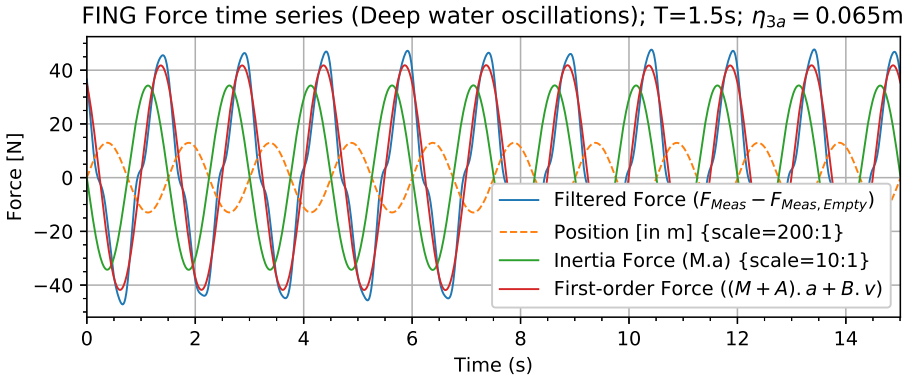
FING Force time series (Deep water oscillations); T=1.5s; $\eta_{3a} = 0.065$m
Force [N]
Time (s)
Filtered Force ($F_{Meas} - F_{Meas,Empty}$)
Position [in m] {scale=200:1}
Inertia Force (M.a) {scale=10:1}
First-order Force ($(M+A).a + B.v$)

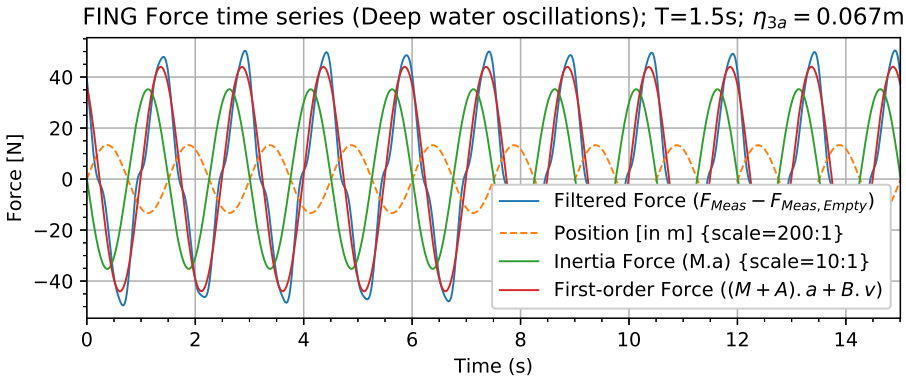
FING Force time series (Deep water oscillations); T=1.5s; $\eta_{3a} = 0.067$m
Force [N]
Time (s)
Filtered Force ($F_{Meas} - F_{Meas,Empty}$)
Position [in m] {scale=200:1}
Inertia Force (M.a) {scale=10:1}
First-order Force ($(M+A).a + B.v$)

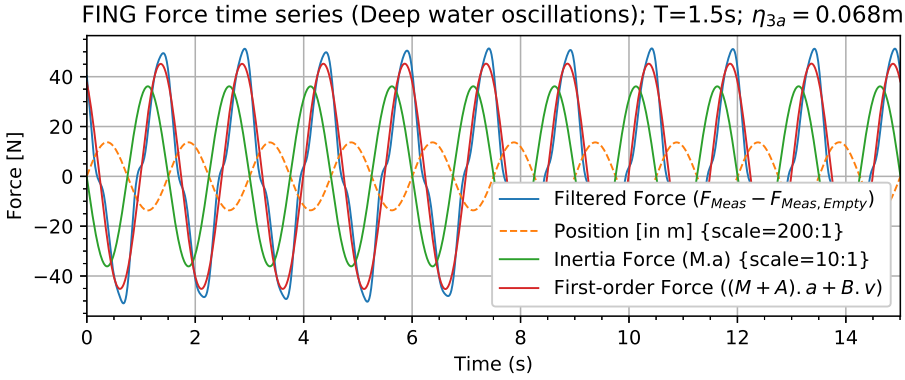
FING Force time series (Deep water oscillations); T=1.5s; $\eta_{3a} = 0.068$m
Force [N]
Time (s)
Filtered Force ($F_{Meas} - F_{Meas,Empty}$)
Position [in m] {scale=200:1}
Inertia Force (M.a) {scale=10:1}
First-order Force ($(M+A).a + B.v$)

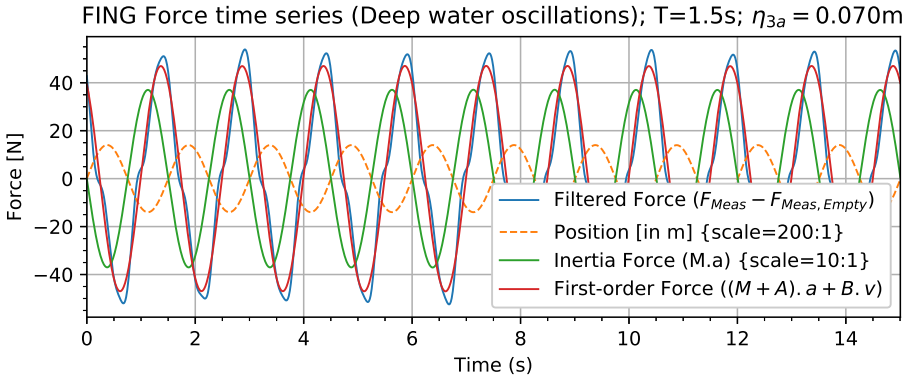
FING Force time series (Deep water oscillations); T=1.5s; $\eta_{3a} = 0.070$m
Force [N]
Time (s)
Filtered Force ($F_{Meas} - F_{Meas,Empty}$)
Position [in m] {scale=200:1}
Inertia Force (M.a) {scale=10:1}
First-order Force ($(M+A).a + B.v$)

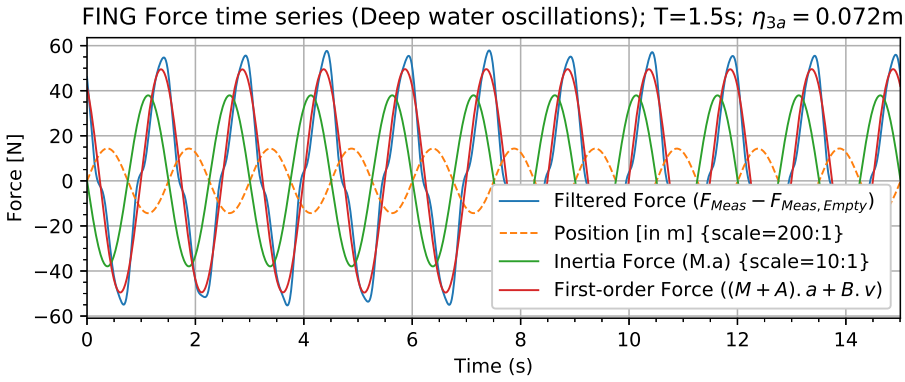
FING Force time series (Deep water oscillations); T=1.5s; $\eta_{3a} = 0.072$m
Force [N]
Time (s)
Filtered Force ($F_{Meas} - F_{Meas,Empty}$)
Position [in m] {scale=200:1}
Inertia Force (M.a) {scale=10:1}
First-order Force ($(M+A).a + B.v$)

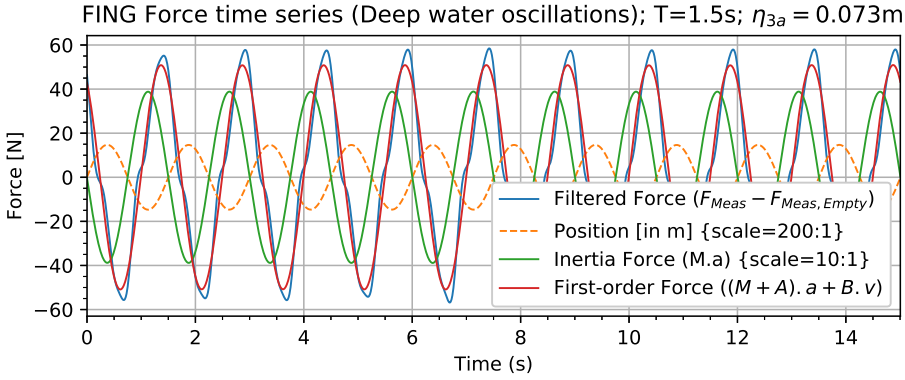
FING Force time series (Deep water oscillations); T=1.5s; $\eta_{3a} = 0.073$m
Force [N]
Time (s)
Filtered Force ($F_{Meas} - F_{Meas,Empty}$)
Position [in m] {scale=200:1}
Inertia Force (M.a) {scale=10:1}
First-order Force ($(M+A).a + B.v$)

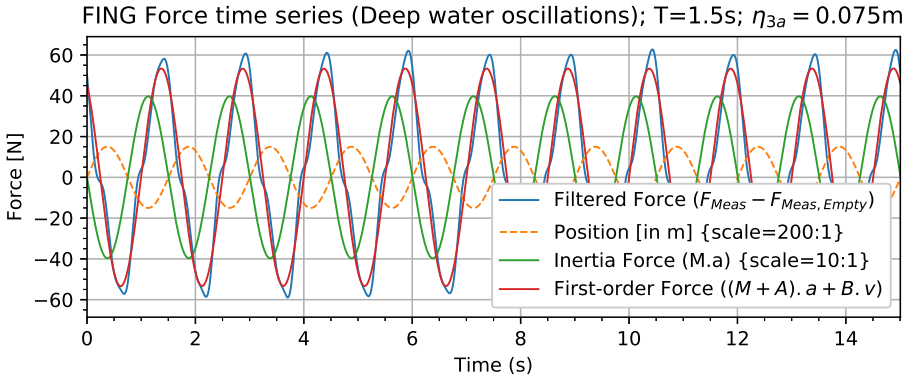
FING Force time series (Deep water oscillations); T=1.5s; $\eta_{3a} = 0.075$m
Force [N]
Time (s)
Filtered Force ($F_{Meas} - F_{Meas,Empty}$)
Position [in m] {scale=200:1}
Inertia Force (M.a) {scale=10:1}
First-order Force ($(M+A).a + B.v$)

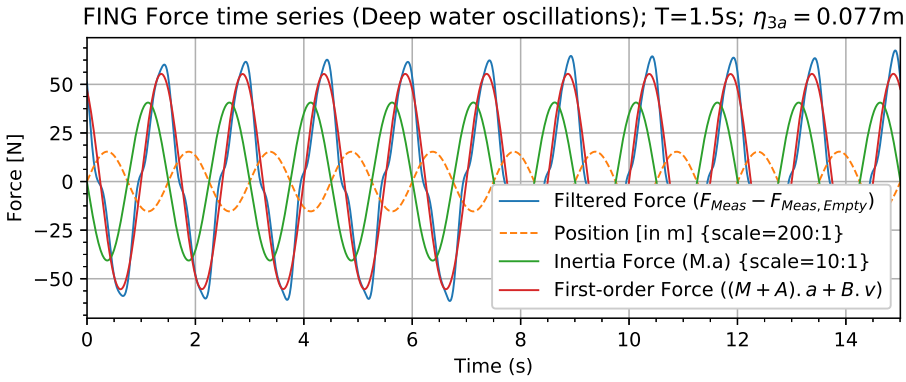
FING Force time series (Deep water oscillations); T=1.5s; $\eta_{3a} = 0.077$m
Force [N]
Time (s)
Filtered Force ($F_{Meas} - F_{Meas,Empty}$)
Position [in m] {scale=200:1}
Inertia Force (M.a) {scale=10:1}
First-order Force ($(M+A).a + B.v$)

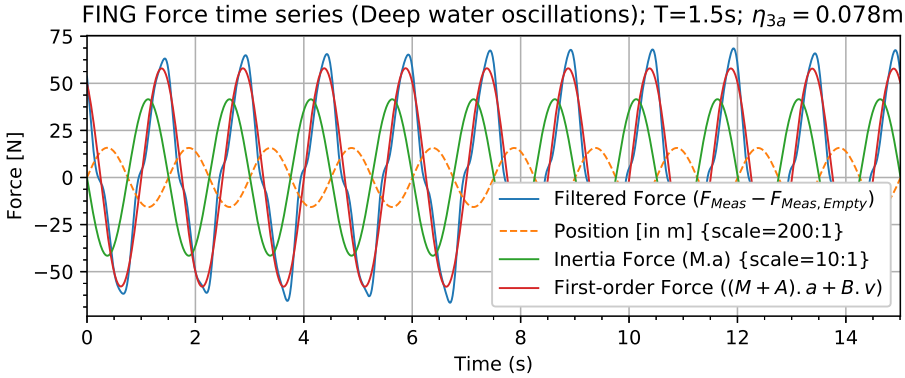
FING Force time series (Deep water oscillations); T=1.5s; $\eta_{3a} = 0.078$m
Force [N]
Time (s)
Filtered Force ($F_{Meas} - F_{Meas,Empty}$)
Position [in m] {scale=200:1}
Inertia Force (M.a) {scale=10:1}
First-order Force ($(M+A).a + B.v$)

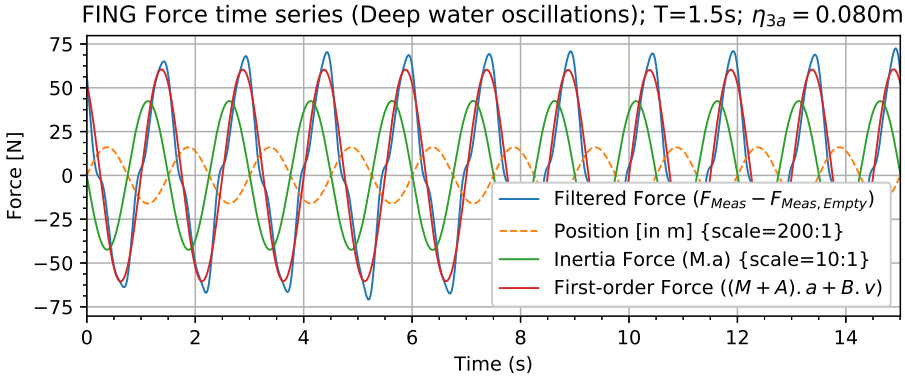
FING Force time series (Deep water oscillations); T=1.5s; $\eta_{3a} = 0.080$m
Force [N]
Time (s)
Filtered Force ($F_{Meas} - F_{Meas,Empty}$)
Position [in m] {scale=200:1}
Inertia Force (M.a) {scale=10:1}
First-order Force ($(M+A).a + B.v$)

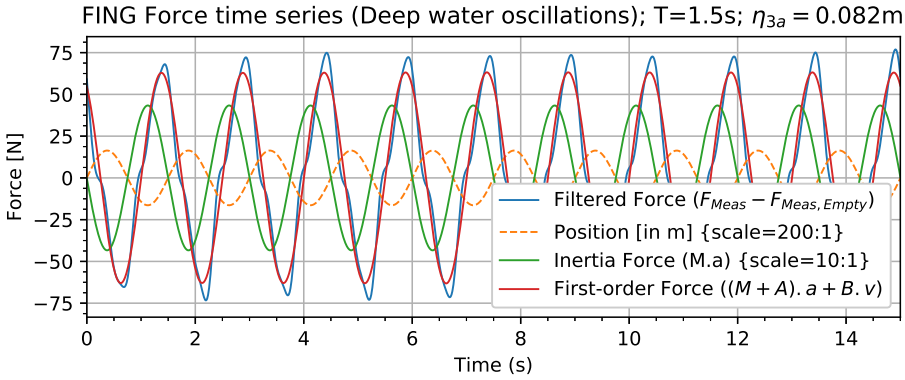
FING Force time series (Deep water oscillations); T=1.5s; $\eta_{3a} = 0.082$m
Force [N]
Time (s)
Filtered Force ($F_{Meas} - F_{Meas,Empty}$)
Position [in m] {scale=200:1}
Inertia Force (M.a) {scale=10:1}
First-order Force ($(M+A).a + B.v$)

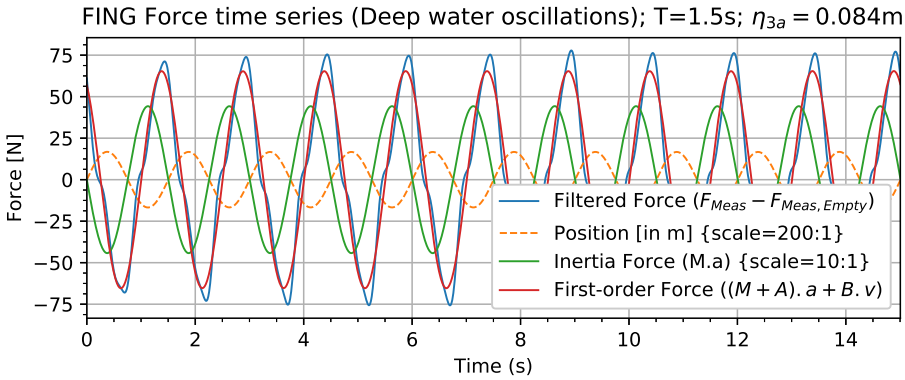
FING Force time series (Deep water oscillations); T=1.5s; $\eta_{3a} = 0.084$m
Force [N]
Time (s)
Filtered Force ($F_{Meas} - F_{Meas,Empty}$)
Position [in m] {scale=200:1}
Inertia Force (M.a) {scale=10:1}
First-order Force ($(M+A).a + B.v$)

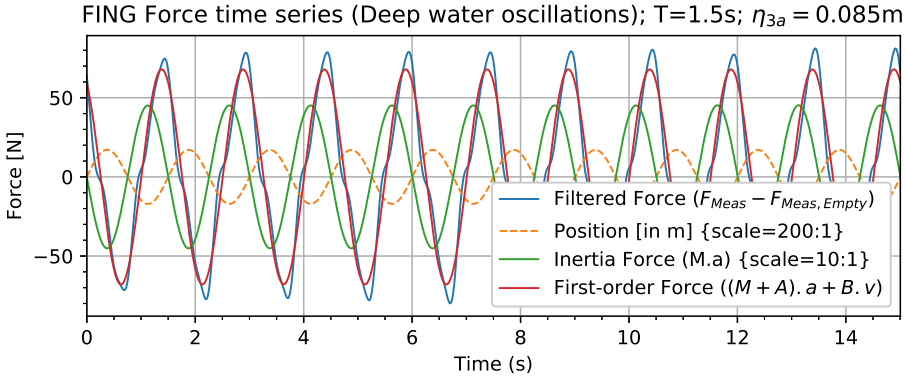
FING Force time series (Deep water oscillations); T=1.5s; $\eta_{3a} = 0.085$m
Force [N]
Time (s)
Filtered Force ($F_{Meas} - F_{Meas,Empty}$)
Position [in m] {scale=200:1}
Inertia Force (M.a) {scale=10:1}
First-order Force ($(M+A).a + B.v$)

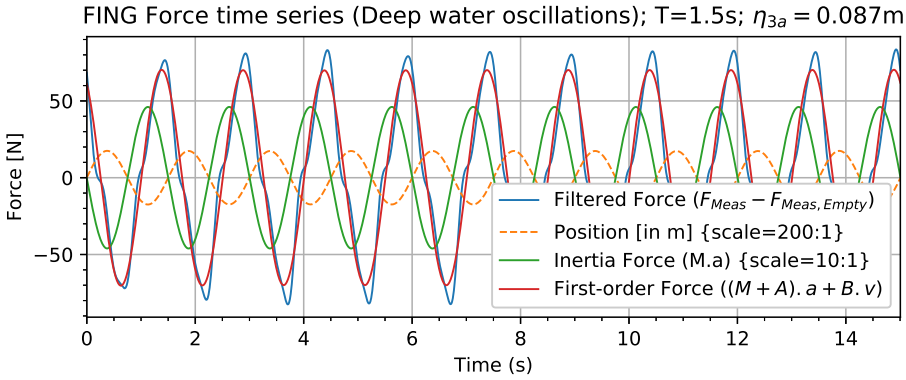
FING Force time series (Deep water oscillations); T=1.5s; $\eta_{3a} = 0.087$m
Force [N]
Time (s)
Filtered Force ($F_{Meas} - F_{Meas,Empty}$)
Position [in m] {scale=200:1}
Inertia Force (M.a) {scale=10:1}
First-order Force ($(M+A).a + B.v$)

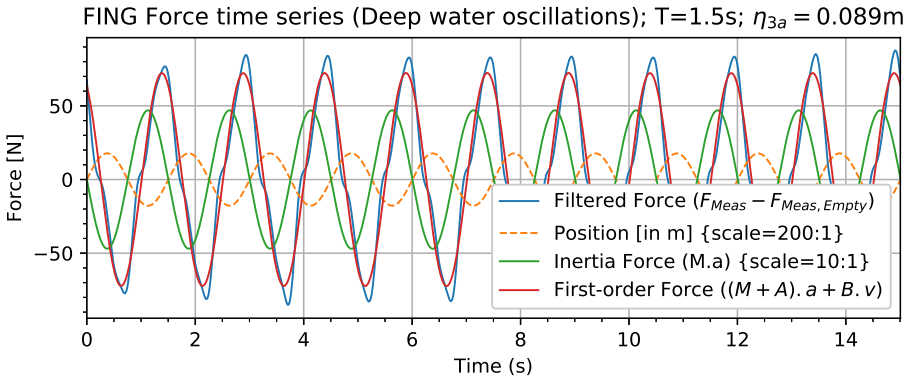
FING Force time series (Deep water oscillations); T=1.5s; $\eta_{3a} = 0.089$m
Force [N]
Time (s)
Filtered Force ($F_{Meas} - F_{Meas,Empty}$)
Position [in m] {scale=200:1}
Inertia Force (M.a) {scale=10:1}
First-order Force ($(M+A).a + B.v$)

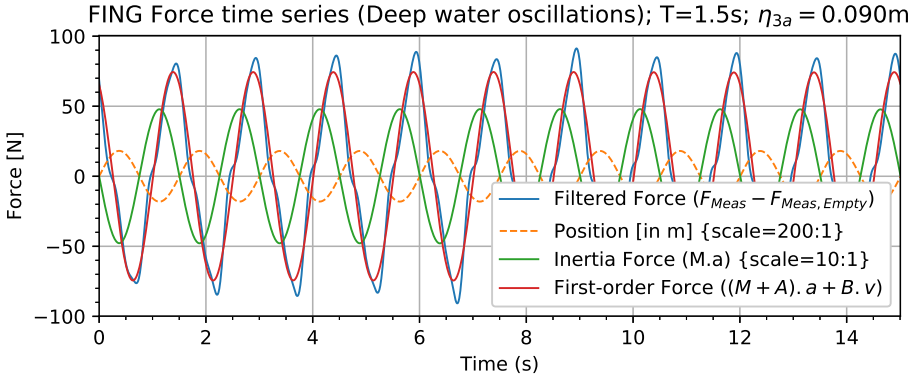
FING Force time series (Deep water oscillations); T=1.5s; $\eta_{3a} = 0.090$m
Force [N]
Time (s)
Filtered Force ($F_{Meas} - F_{Meas,Empty}$)
Position [in m] {scale=200:1}
Inertia Force (M.a) {scale=10:1}
First-order Force ($(M+A).a + B.v$)

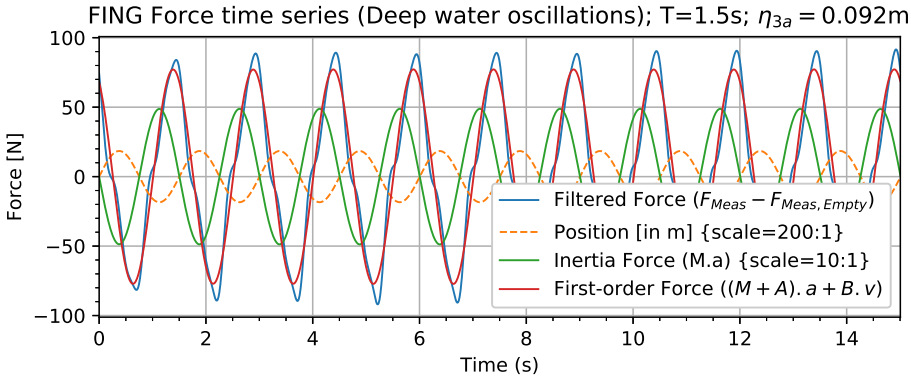
FING Force time series (Deep water oscillations); T=1.5s; $\eta_{3a} = 0.092$m
Force [N]
Time (s)
Filtered Force ($F_{Meas} - F_{Meas,Empty}$)
Position [in m] {scale=200:1}
Inertia Force (M.a) {scale=10:1}
First-order Force ($(M+A).a + B.v$)

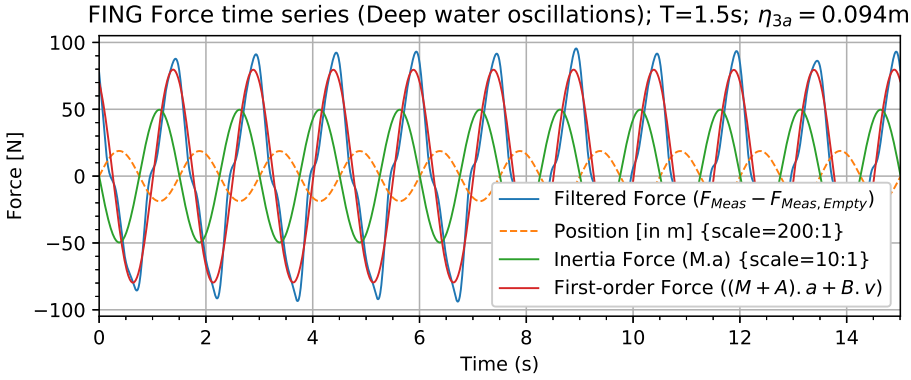
FING Force time series (Deep water oscillations); T=1.5s; $\eta_{3a} = 0.094$m
Force [N]
Time (s)
Filtered Force ($F_{Meas} - F_{Meas,Empty}$)
Position [in m] {scale=200:1}
Inertia Force (M.a) {scale=10:1}
First-order Force ($(M+A).a + B.v$)

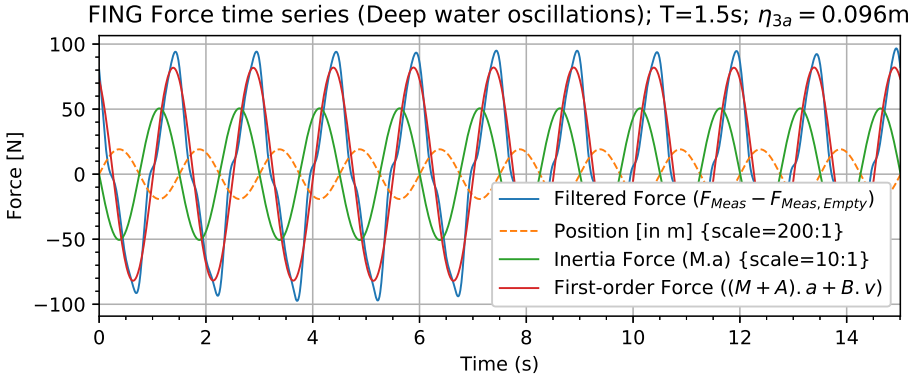
FING Force time series (Deep water oscillations); T=1.5s; $\eta_{3a} = 0.096$m
Force [N]
Time (s)
Filtered Force ($F_{Meas} - F_{Meas,Empty}$)
Position [in m] {scale=200:1}
Inertia Force (M.a) {scale=10:1}
First-order Force ($(M+A).a + B.v$)

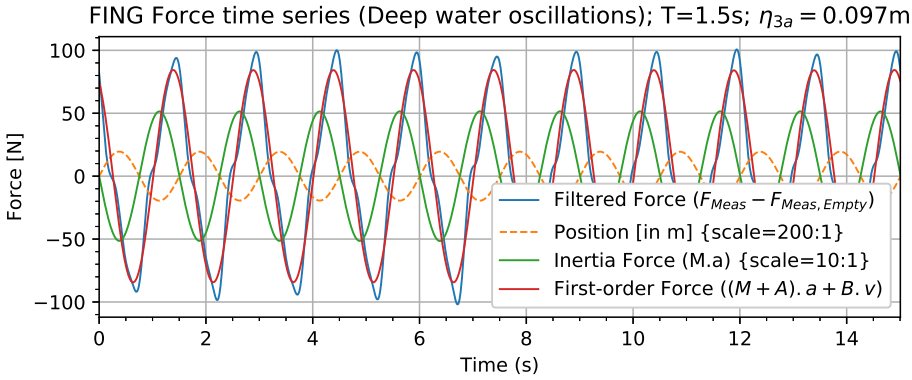
FING Force time series (Deep water oscillations); T=1.5s; $\eta_{3a} = 0.097$m
Force [N]
Time (s)
Filtered Force ($F_{Meas} - F_{Meas,Empty}$)
Position [in m] {scale=200:1}
Inertia Force (M.a) {scale=10:1}
First-order Force ($(M+A).a + B.v$)

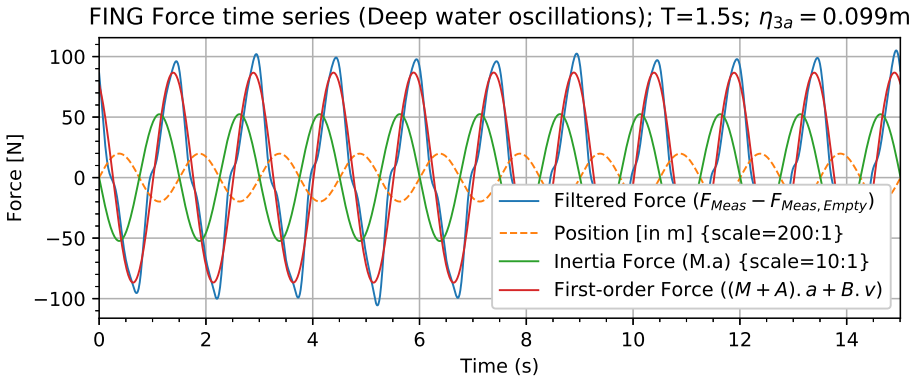
FING Force time series (Deep water oscillations); T=1.5s; $\eta_{3a} = 0.099$m
Force [N]
Time (s)
Filtered Force ($F_{Meas} - F_{Meas,Empty}$)
Position [in m] {scale=200:1}
Inertia Force (M.a) {scale=10:1}
First-order Force ($(M+A).a + B.v$)

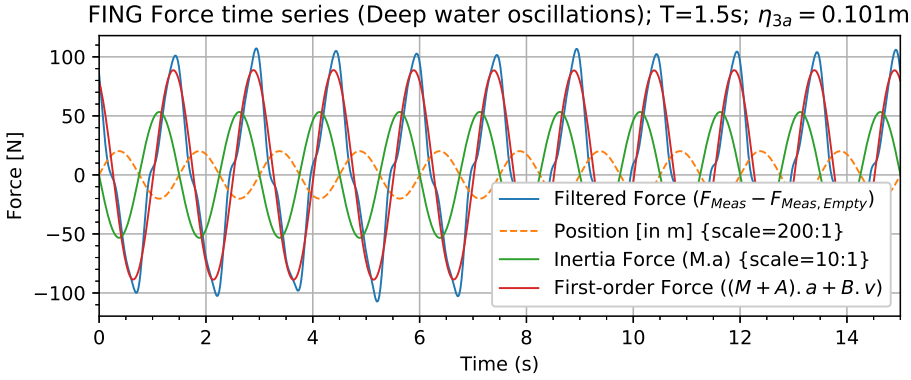
FING Force time series (Deep water oscillations); T=1.5s; $\eta_{3a} = 0.101$m
Force [N]
Time (s)
Filtered Force ($F_{Meas} - F_{Meas,Empty}$)
Position [in m] {scale=200:1}
Inertia Force (M.a) {scale=10:1}
First-order Force ($(M+A).a + B.v$)

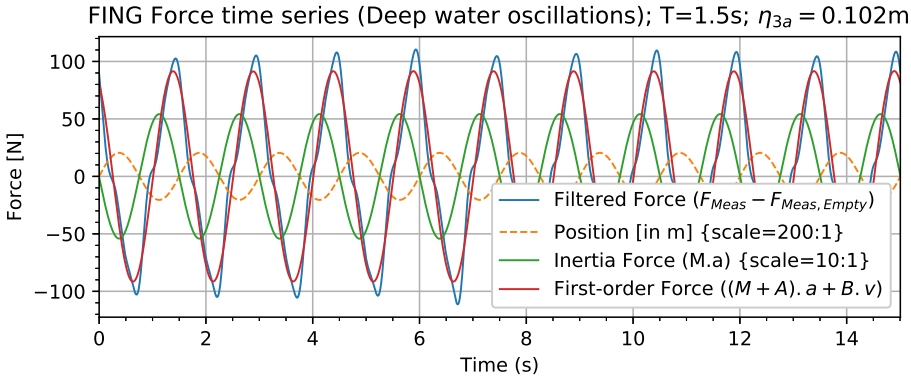
FING Force time series (Deep water oscillations); T=1.5s; $\eta_{3a} = 0.102$m
Force [N]
Time (s)
Filtered Force ($F_{Meas} - F_{Meas,Empty}$)
Position [in m] {scale=200:1}
Inertia Force (M.a) {scale=10:1}
First-order Force ($(M+A).a + B.v$)

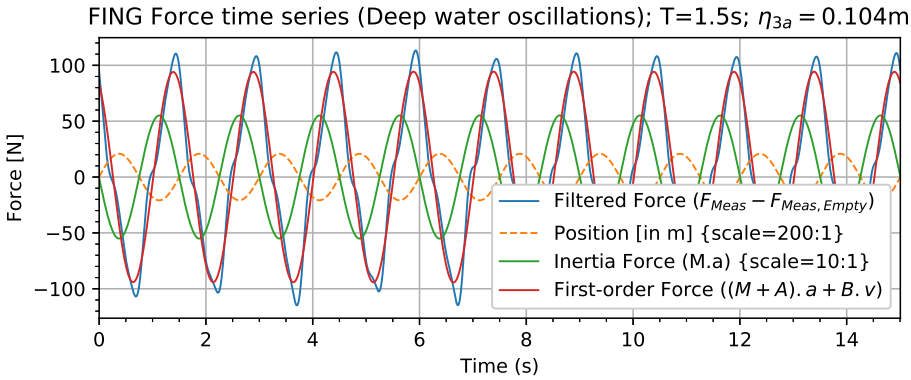
FING Force time series (Deep water oscillations); T=1.5s; $\eta_{3a} = 0.104$m
Force [N]
Time (s)
Filtered Force ($F_{Meas} - F_{Meas,Empty}$)
Position [in m] {scale=200:1}
Inertia Force (M.a) {scale=10:1}
First-order Force ($(M+A).a + B.v$)

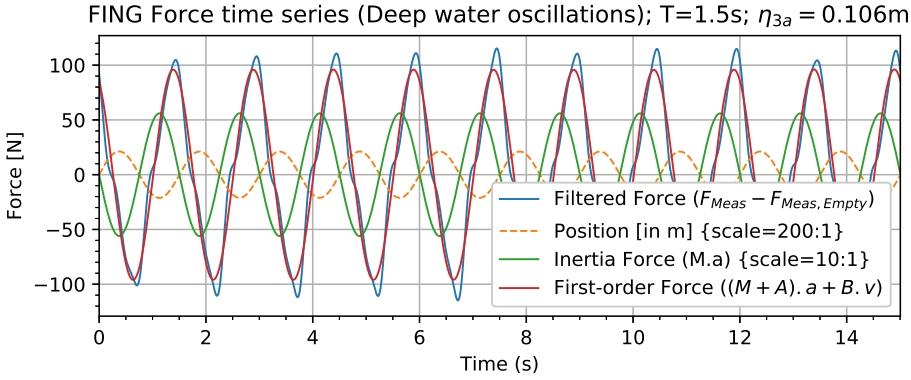
FING Force time series (Deep water oscillations); T=1.5s; $\eta_{3a} = 0.106$m
Force [N]
Time (s)
Filtered Force ($F_{Meas} - F_{Meas,Empty}$)
Position [in m] {scale=200:1}
Inertia Force (M.a) {scale=10:1}
First-order Force ($(M+A).a + B.v$)

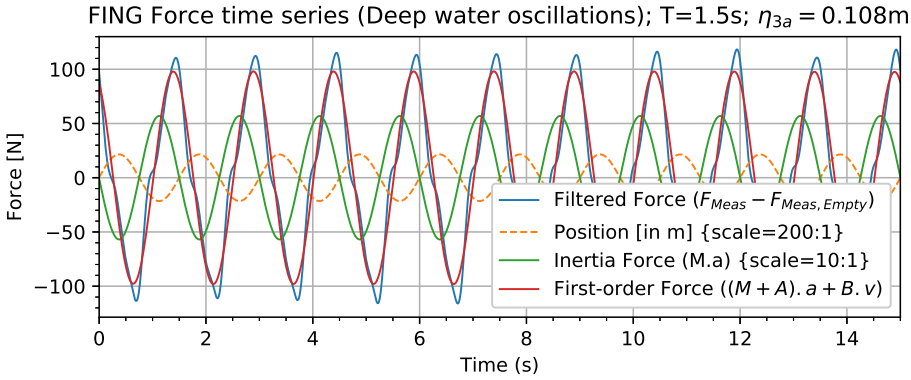
FING Force time series (Deep water oscillations); T=1.5s; $\eta_{3a} = 0.108$m
Force [N]
Time (s)
Filtered Force ($F_{Meas} - F_{Meas,Empty}$)
Position [in m] {scale=200:1}
Inertia Force (M.a) {scale=10:1}
First-order Force ($(M+A).a + B.v$)

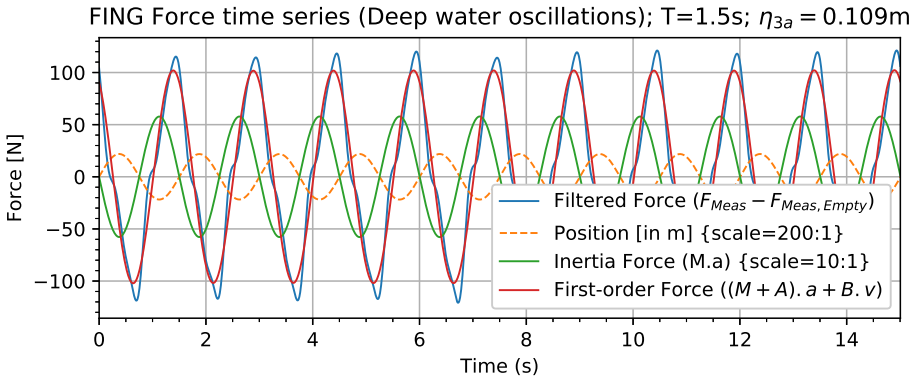
FING Force time series (Deep water oscillations); T=1.5s; $\eta_{3a} = 0.109$m
Force [N]
Time (s)
Filtered Force ($F_{Meas} - F_{Meas,Empty}$)
Position [in m] {scale=200:1}
Inertia Force (M.a) {scale=10:1}
First-order Force ($(M+A).a + B.v$)

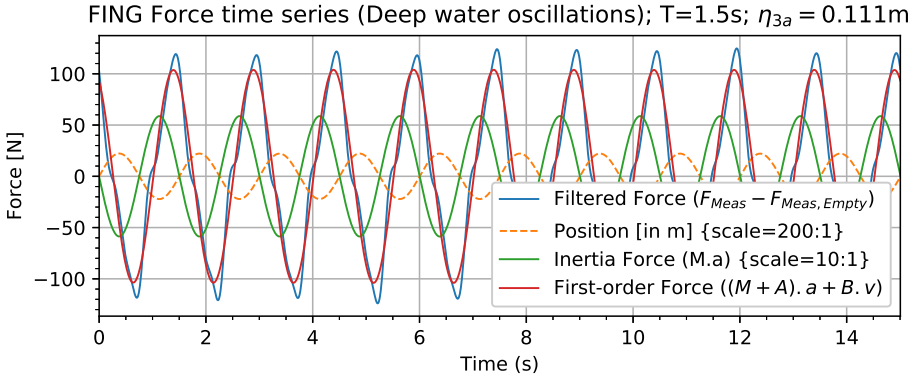
FING Force time series (Deep water oscillations); T=1.5s; $\eta_{3a} = 0.111$m
Force [N]
Time (s)
Filtered Force ($F_{Meas} - F_{Meas,Empty}$)
Position [in m] {scale=200:1}
Inertia Force (M.a) {scale=10:1}
First-order Force ($(M+A).a + B.v$)

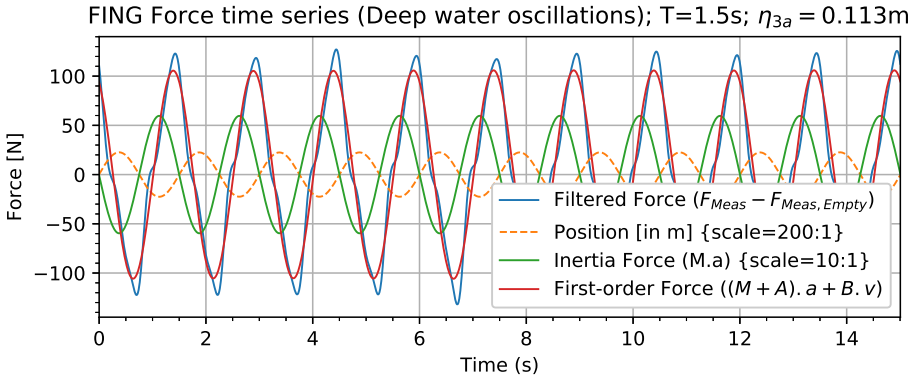
FING Force time series (Deep water oscillations); T=1.5s; $\eta_{3a} = 0.113$m
Force [N]
Time (s)
Filtered Force ($F_{Meas} - F_{Meas,Empty}$)
Position [in m] {scale=200:1}
Inertia Force (M.a) {scale=10:1}
First-order Force ($(M+A).a + B.v$)

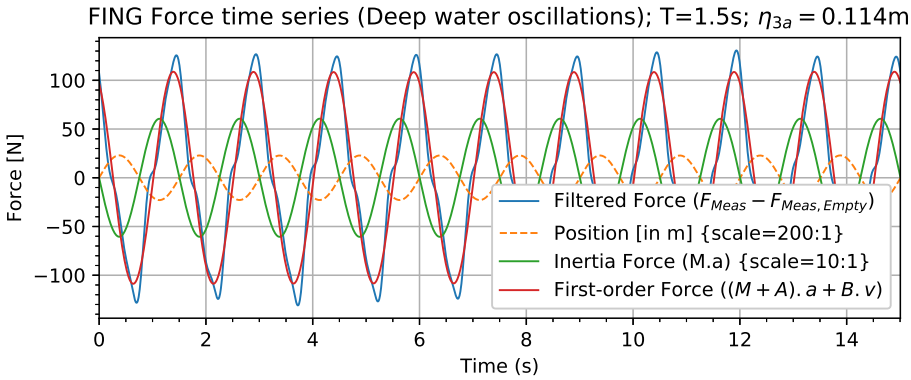
FING Force time series (Deep water oscillations); T=1.5s; $\eta_{3a} = 0.114$m
Force [N]
Time (s)
Filtered Force ($F_{Meas} - F_{Meas,Empty}$)
Position [in m] {scale=200:1}
Inertia Force (M.a) {scale=10:1}
First-order Force ($(M+A).a + B.v$)

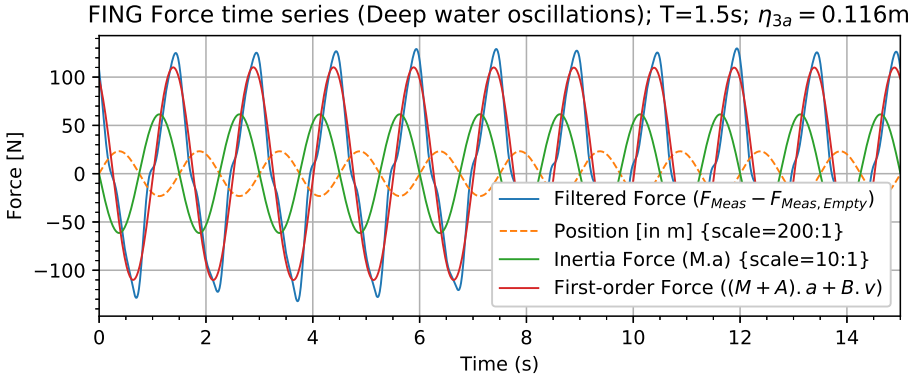
FING Force time series (Deep water oscillations); T=1.5s; $\eta_{3a} = 0.116$m
Force [N]
Time (s)
Filtered Force ($F_{Meas} - F_{Meas,Empty}$)
Position [in m] {scale=200:1}
Inertia Force (M.a) {scale=10:1}
First-order Force ($(M+A).a + B.v$)

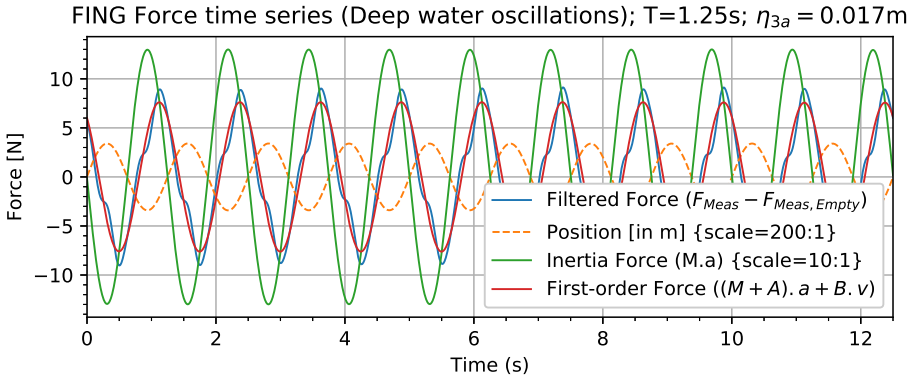
FING Force time series (Deep water oscillations); T=1.25s; $\eta_{3a} = 0.017$m
Force [N]
Time (s)
Filtered Force ($F_{Meas} - F_{Meas,Empty}$)
Position [in m] {scale=200:1}
Inertia Force (M.a) {scale=10:1}
First-order Force ($(M+A).a + B.v$)

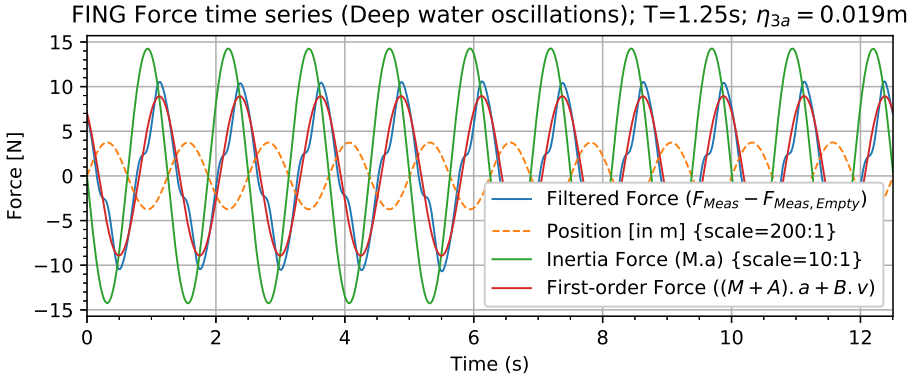
FING Force time series (Deep water oscillations); T=1.25s; $\eta_{3a} = 0.019$m
Force [N]
Time (s)
Filtered Force ($F_{Meas} - F_{Meas,Empty}$)
Position [in m] {scale=200:1}
Inertia Force (M.a) {scale=10:1}
First-order Force ($(M+A).a + B.v$)

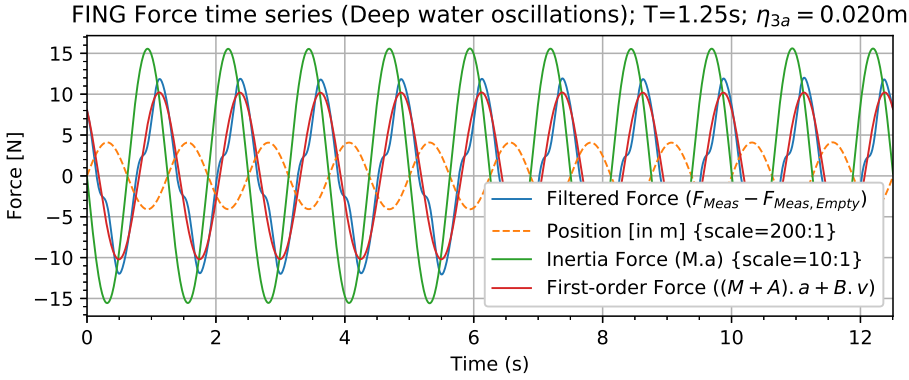
FING Force time series (Deep water oscillations); T=1.25s; $\eta_{3a} = 0.020$m
Force [N]
Time (s)
Filtered Force ($F_{Meas} - F_{Meas,Empty}$)
Position [in m] {scale=200:1}
Inertia Force (M.a) {scale=10:1}
First-order Force ($(M+A).a + B.v$)

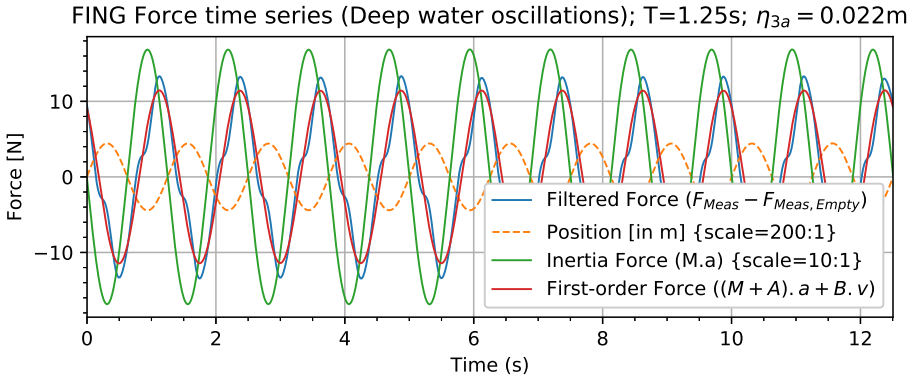
FING Force time series (Deep water oscillations); T=1.25s; $\eta_{3a} = 0.022$m
Force [N]
Time (s)
Filtered Force ($F_{Meas} - F_{Meas,Empty}$)
Position [in m] {scale=200:1}
Inertia Force (M.a) {scale=10:1}
First-order Force ($(M+A).a + B.v$)

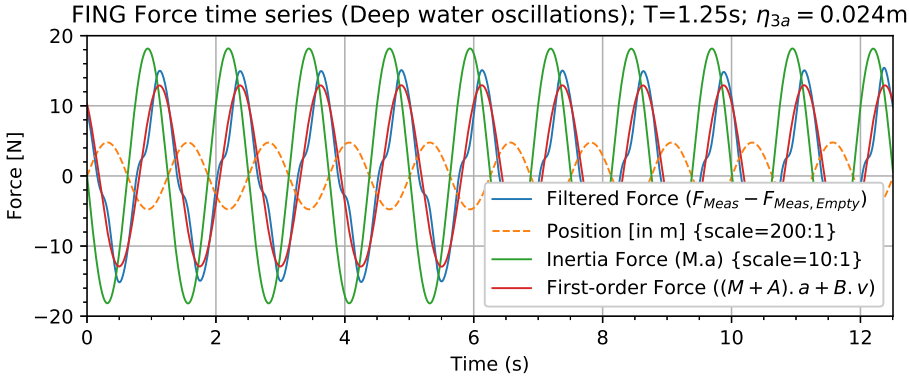
FING Force time series (Deep water oscillations); T=1.25s; $\eta_{3a} = 0.024$m
Force [N]
Time (s)
Filtered Force ($F_{Meas} - F_{Meas,Empty}$)
Position [in m] {scale=200:1}
Inertia Force (M.a) {scale=10:1}
First-order Force ($(M+A).a + B.v$)

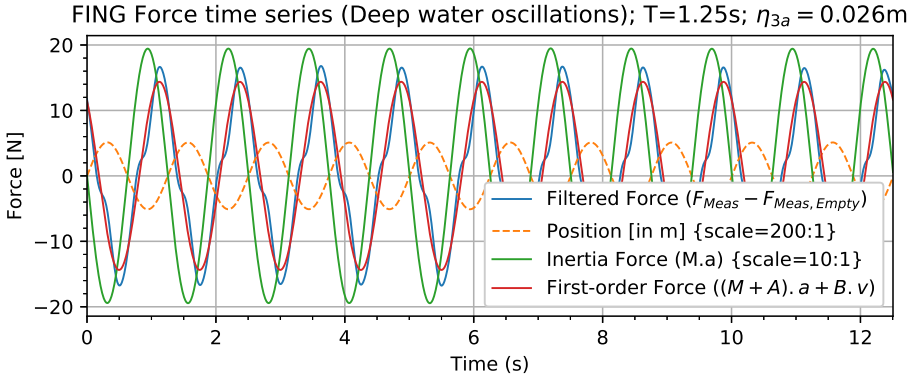
FING Force time series (Deep water oscillations); T=1.25s; $\eta_{3a} = 0.026$m
Force [N]
Time (s)
Filtered Force ($F_{Meas} - F_{Meas,Empty}$)
Position [in m] {scale=200:1}
Inertia Force (M.a) {scale=10:1}
First-order Force ($(M+A).a + B.v$)

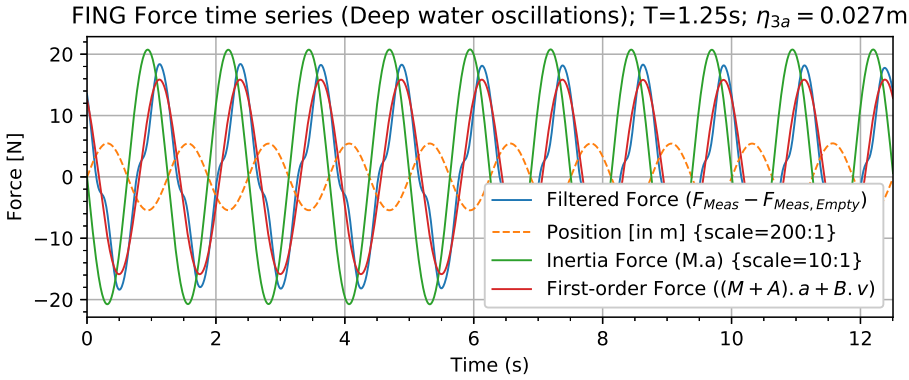
FING Force time series (Deep water oscillations); T=1.25s; $\eta_{3a} = 0.027$m
Force [N]
Time (s)
Filtered Force ($F_{Meas} - F_{Meas,Empty}$)
Position [in m] {scale=200:1}
Inertia Force (M.a) {scale=10:1}
First-order Force ($(M+A).a + B.v$)

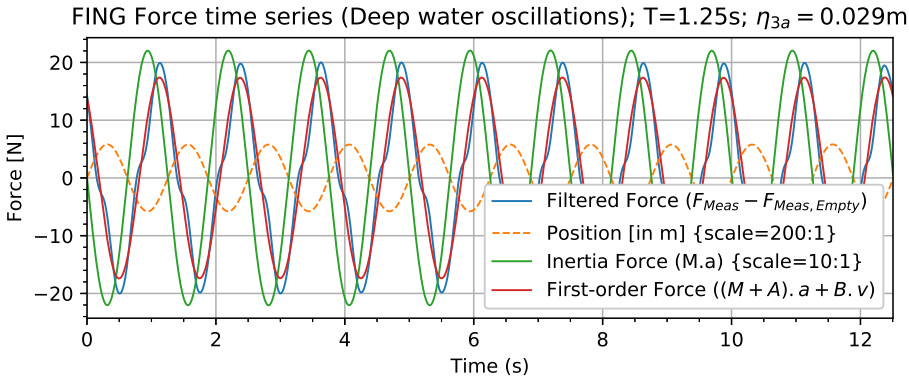
FING Force time series (Deep water oscillations); T=1.25s; $\eta_{3a} = 0.029$m
Force [N]
Time (s)
Filtered Force ($F_{Meas} - F_{Meas,Empty}$)
Position [in m] {scale=200:1}
Inertia Force (M.a) {scale=10:1}
First-order Force ($(M+A).a + B.v$)

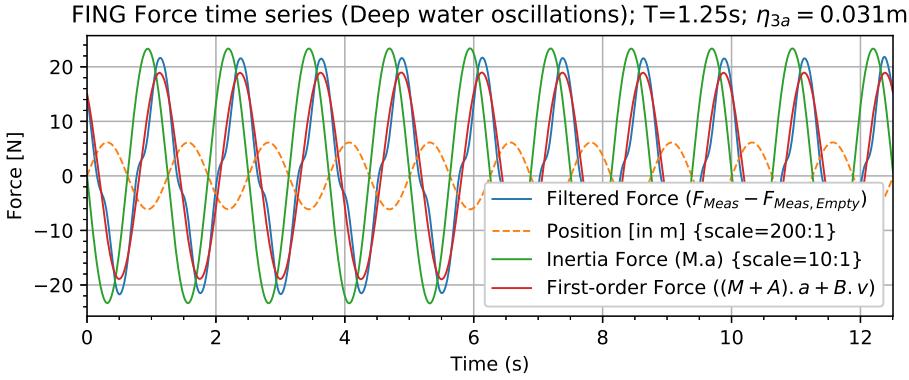
FING Force time series (Deep water oscillations); T=1.25s; $\eta_{3a} = 0.031$m
Force [N]
Time (s)
Filtered Force ($F_{Meas} - F_{Meas,Empty}$)
Position [in m] {scale=200:1}
Inertia Force (M.a) {scale=10:1}
First-order Force ($(M + A).a + B.v$)

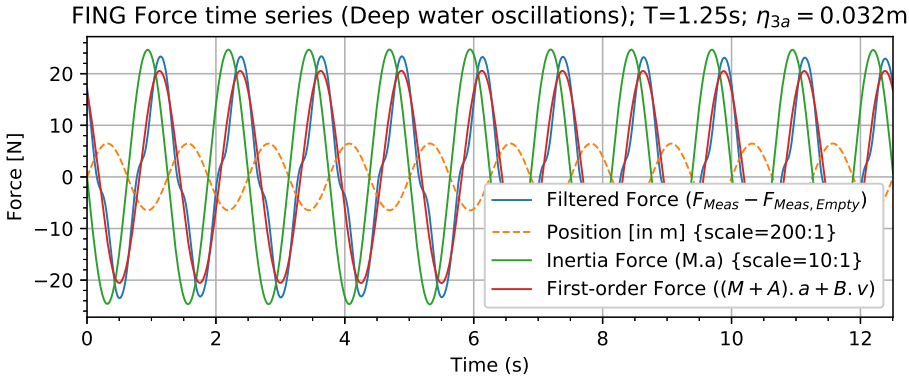
FING Force time series (Deep water oscillations); T=1.25s; $\eta_{3a} = 0.032$m
Force [N]
Time (s)
Filtered Force ($F_{Meas} - F_{Meas,Empty}$)
Position [in m] {scale=200:1}
Inertia Force (M.a) {scale=10:1}
First-order Force ($(M + A).a + B.v$)

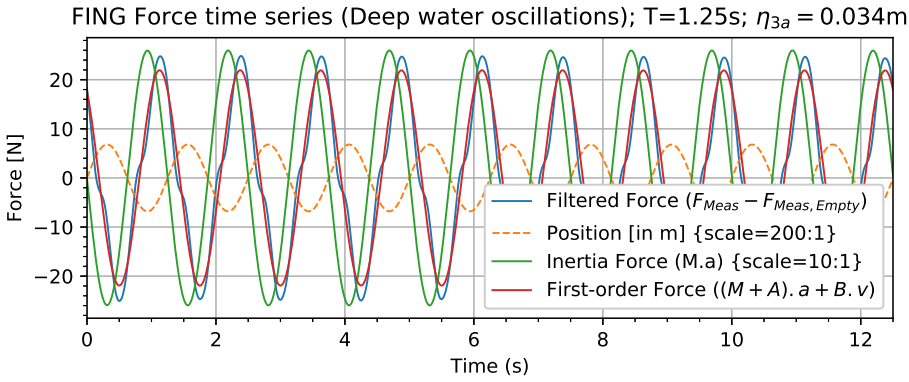
FING Force time series (Deep water oscillations); T=1.25s; $\eta_{3a} = 0.034$m
Force [N]
Time (s)
Filtered Force ($F_{Meas} - F_{Meas,Empty}$)
Position [in m] {scale=200:1}
Inertia Force (M.a) {scale=10:1}
First-order Force ($(M + A).a + B.v$)

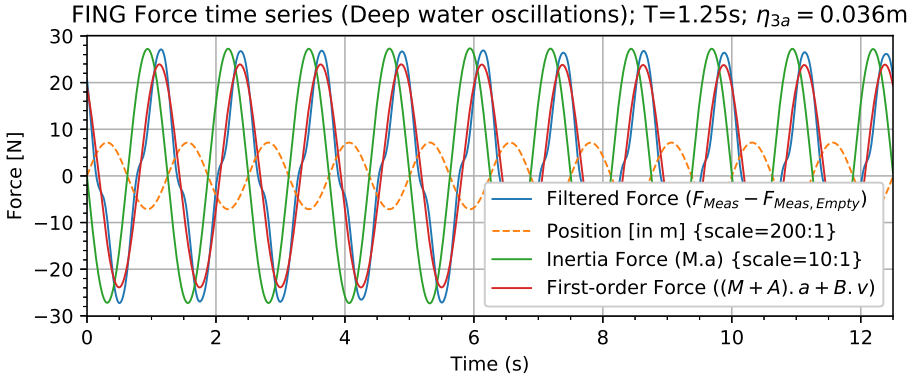
FING Force time series (Deep water oscillations); T=1.25s; $\eta_{3a} = 0.036$m
Force [N]
Time (s)
Filtered Force ($F_{Meas} - F_{Meas,Empty}$)
Position [in m] {scale=200:1}
Inertia Force (M.a) {scale=10:1}
First-order Force ($(M+A).a + B.v$)

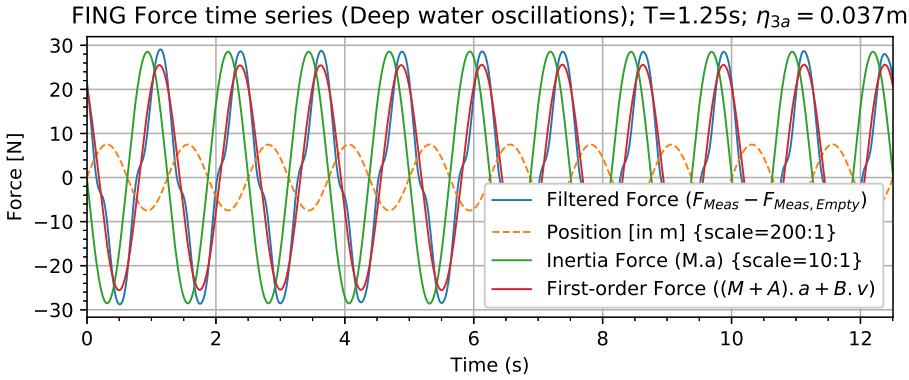
FING Force time series (Deep water oscillations); T=1.25s; $\eta_{3a} = 0.037$m
Force [N]
Time (s)
Filtered Force ($F_{Meas} - F_{Meas,Empty}$)
Position [in m] {scale=200:1}
Inertia Force (M.a) {scale=10:1}
First-order Force ($(M+A).a + B.v$)

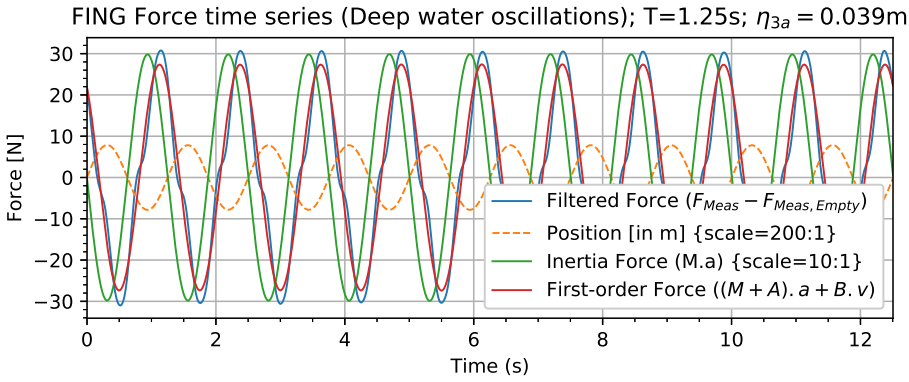
FING Force time series (Deep water oscillations); T=1.25s; $\eta_{3a} = 0.039$m
Force [N]
Time (s)
Filtered Force ($F_{Meas} - F_{Meas,Empty}$)
Position [in m] {scale=200:1}
Inertia Force (M.a) {scale=10:1}
First-order Force ($(M+A).a + B.v$)

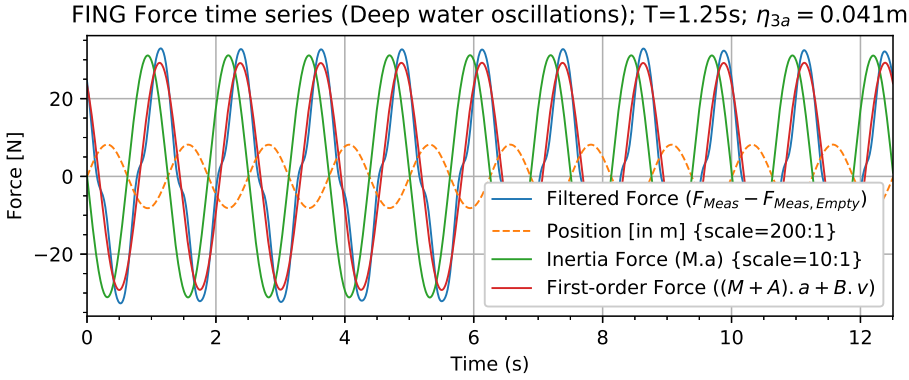
FING Force time series (Deep water oscillations); T=1.25s; $\eta_{3a} = 0.041$m
Force [N]
Time (s)
Filtered Force ($F_{Meas} - F_{Meas,Empty}$)
Position [in m] {scale=200:1}
Inertia Force (M.a) {scale=10:1}
First-order Force ($(M+A).a + B.v$)

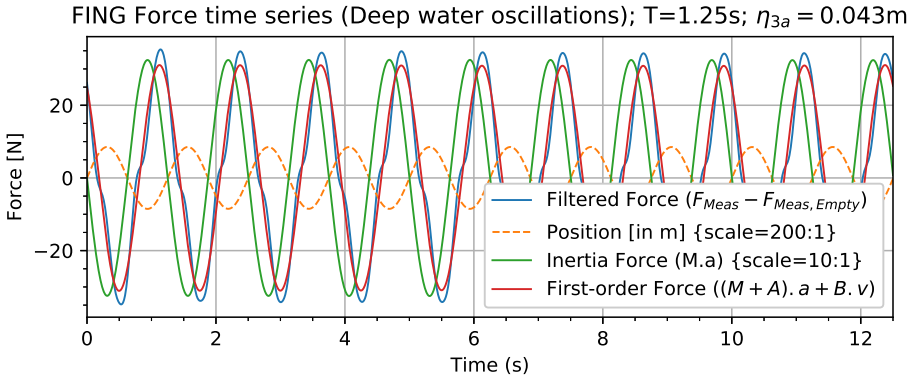
FING Force time series (Deep water oscillations); T=1.25s; $\eta_{3a} = 0.043$m
Force [N]
Time (s)
Filtered Force ($F_{Meas} - F_{Meas,Empty}$)
Position [in m] {scale=200:1}
Inertia Force (M.a) {scale=10:1}
First-order Force ($(M+A).a + B.v$)

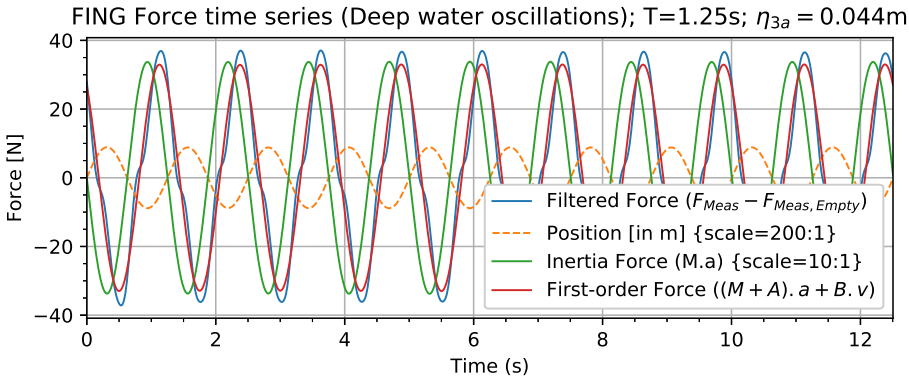
FING Force time series (Deep water oscillations); T=1.25s; $\eta_{3a} = 0.044$m
Force [N]
Time (s)
Filtered Force ($F_{Meas} - F_{Meas,Empty}$)
Position [in m] {scale=200:1}
Inertia Force (M.a) {scale=10:1}
First-order Force ($(M+A).a + B.v$)

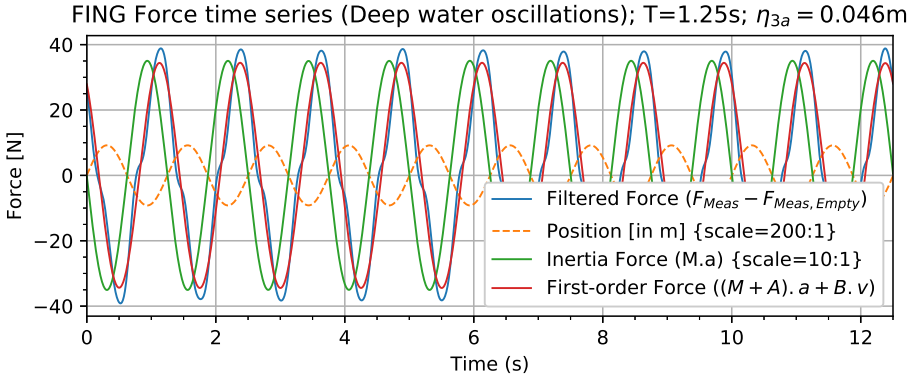
FING Force time series (Deep water oscillations); T=1.25s; $\eta_{3a} = 0.046$m
Force [N]
Time (s)
Filtered Force ($F_{Meas} - F_{Meas,Empty}$)
Position [in m] {scale=200:1}
Inertia Force (M.a) {scale=10:1}
First-order Force ($(M+A).a + B.v$)

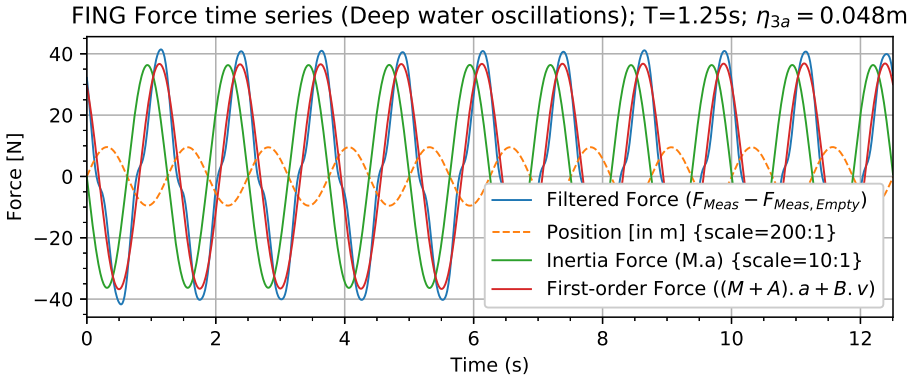
FING Force time series (Deep water oscillations); T=1.25s; $\eta_{3a} = 0.048$m
Force [N]
Time (s)
Filtered Force ($F_{Meas} - F_{Meas,Empty}$)
Position [in m] {scale=200:1}
Inertia Force (M.a) {scale=10:1}
First-order Force ($(M+A).a + B.v$)

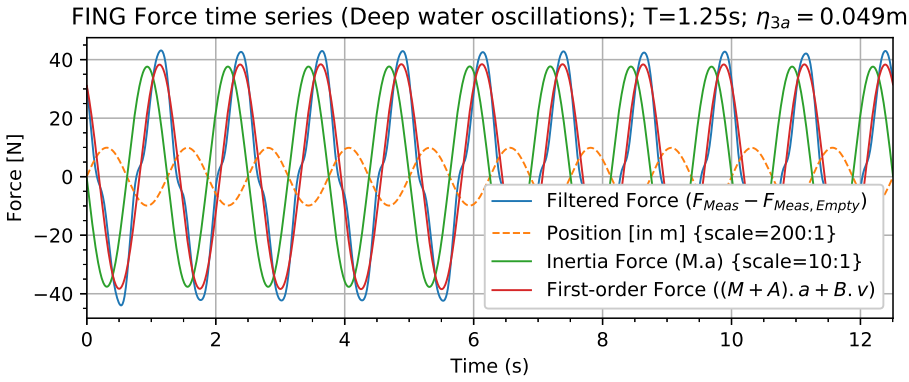
FING Force time series (Deep water oscillations); T=1.25s; $\eta_{3a} = 0.049$m
Force [N]
Time (s)
Filtered Force ($F_{Meas} - F_{Meas,Empty}$)
Position [in m] {scale=200:1}
Inertia Force (M.a) {scale=10:1}
First-order Force ($(M+A).a + B.v$)

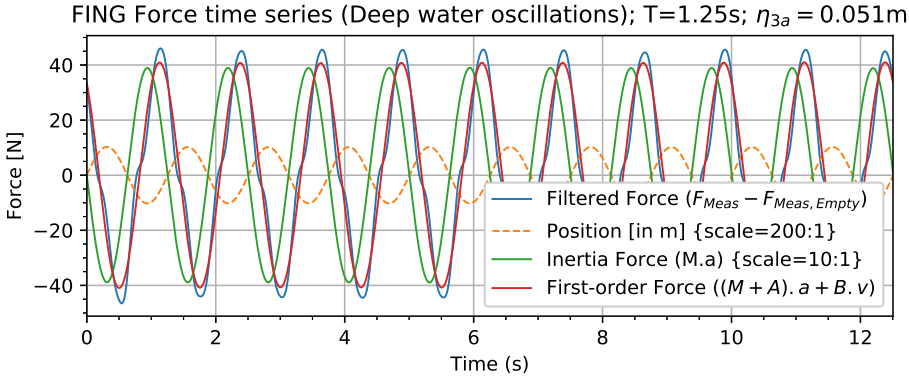
FING Force time series (Deep water oscillations); T=1.25s; $\eta_{3a} = 0.051$m
Force [N]
Time (s)
Filtered Force ($F_{Meas} - F_{Meas,Empty}$)
Position [in m] {scale=200:1}
Inertia Force (M.a) {scale=10:1}
First-order Force ($(M+A).a + B.v$)

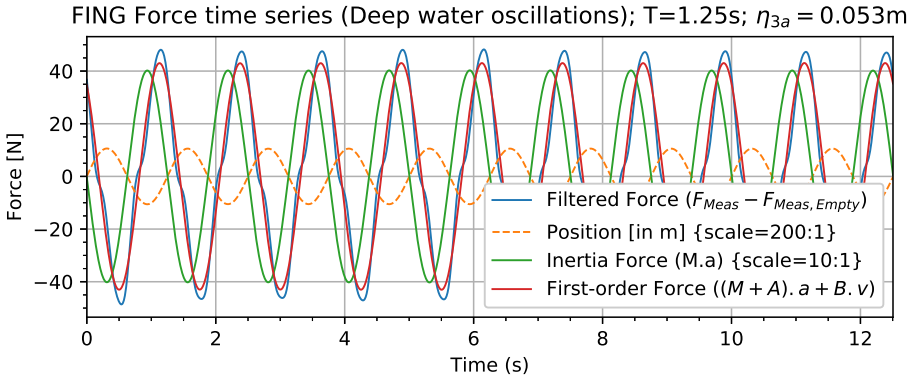
FING Force time series (Deep water oscillations); T=1.25s; $\eta_{3a} = 0.053$m
Force [N]
Time (s)
Filtered Force ($F_{Meas} - F_{Meas,Empty}$)
Position [in m] {scale=200:1}
Inertia Force (M.a) {scale=10:1}
First-order Force ($(M+A).a + B.v$)

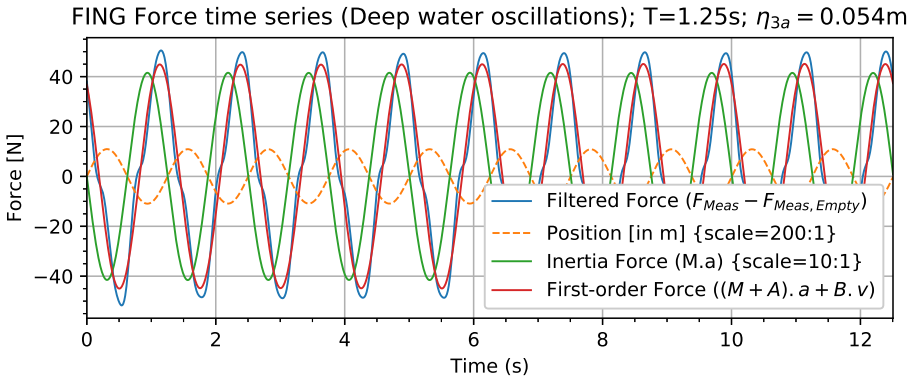
FING Force time series (Deep water oscillations); T=1.25s; $\eta_{3a} = 0.054$m
Force [N]
Time (s)
Filtered Force ($F_{Meas} - F_{Meas,Empty}$)
Position [in m] {scale=200:1}
Inertia Force (M.a) {scale=10:1}
First-order Force ($(M+A).a + B.v$)

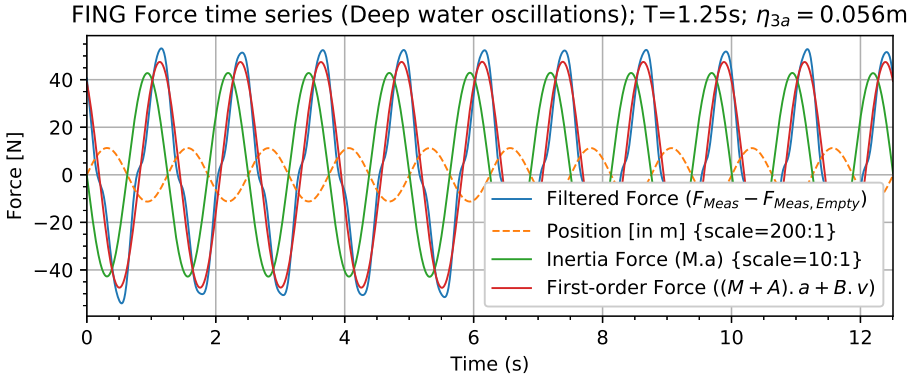
FING Force time series (Deep water oscillations); T=1.25s; $\eta_{3a} = 0.056$m
Force [N]
Time (s)
Filtered Force ($F_{Meas} - F_{Meas,Empty}$)
Position [in m] {scale=200:1}
Inertia Force (M.a) {scale=10:1}
First-order Force ($(M+A).a + B.v$)

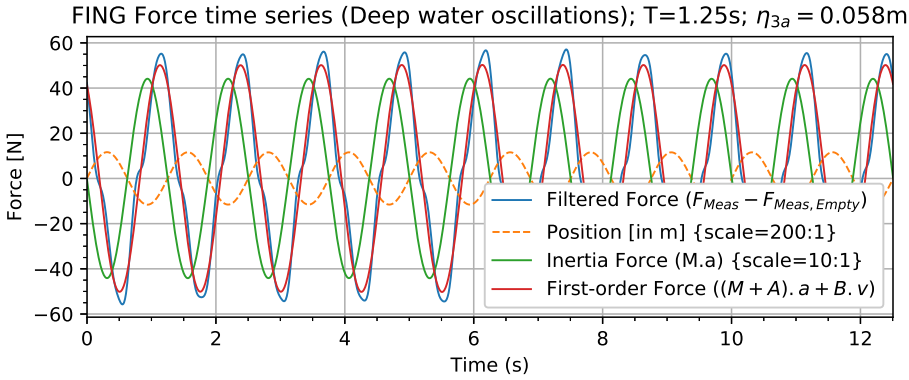
FING Force time series (Deep water oscillations); T=1.25s; $\eta_{3a} = 0.058$m
Force [N]
Time (s)
Filtered Force ($F_{Meas} - F_{Meas,Empty}$)
Position [in m] {scale=200:1}
Inertia Force (M.a) {scale=10:1}
First-order Force ($(M+A).a + B.v$)

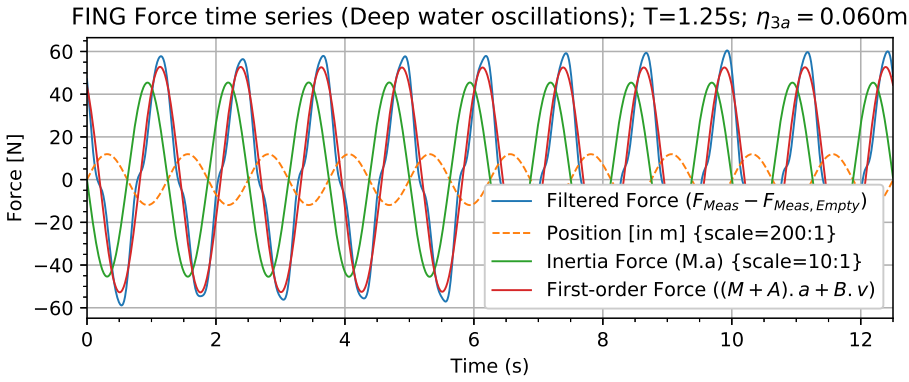
FING Force time series (Deep water oscillations); T=1.25s; $\eta_{3a} = 0.060$m
Force [N]
Time (s)
Filtered Force ($F_{Meas} - F_{Meas,Empty}$)
Position [in m] {scale=200:1}
Inertia Force (M.a) {scale=10:1}
First-order Force ($(M+A).a + B.v$)

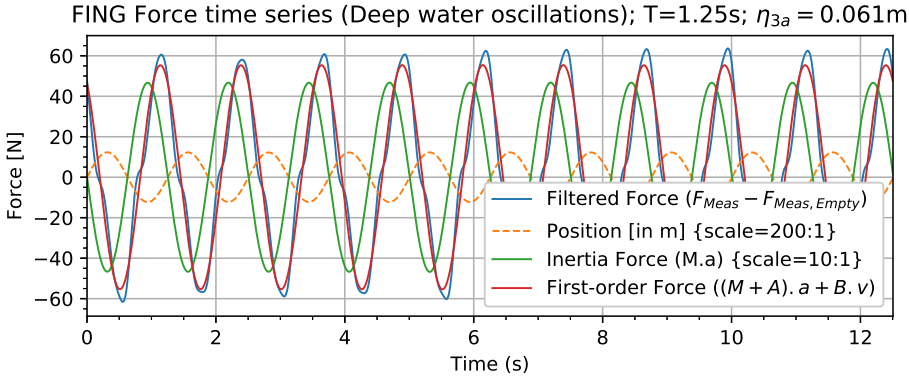
FING Force time series (Deep water oscillations); T=1.25s; $\eta_{3a} = 0.061$m
Force [N]
Time (s)
Filtered Force ($F_{Meas} - F_{Meas,Empty}$)
Position [in m] {scale=200:1}
Inertia Force (M.a) {scale=10:1}
First-order Force ($(M+A).a + B.v$)

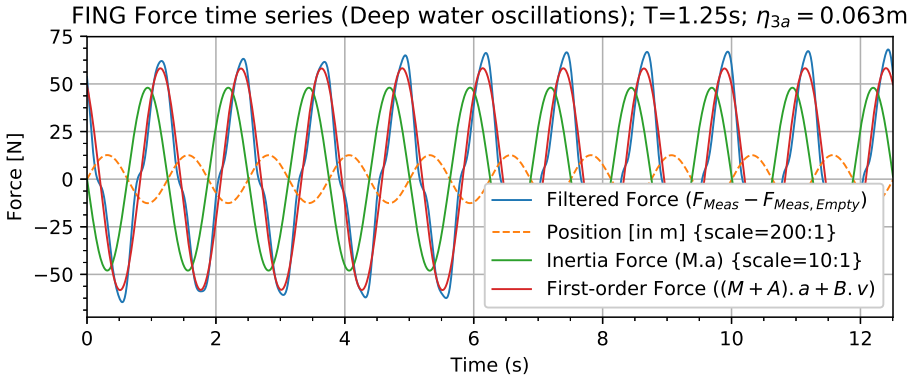
FING Force time series (Deep water oscillations); T=1.25s; $\eta_{3a} = 0.063$m
Force [N]
Time (s)
Filtered Force ($F_{Meas} - F_{Meas,Empty}$)
Position [in m] {scale=200:1}
Inertia Force (M.a) {scale=10:1}
First-order Force ($(M+A).a + B.v$)

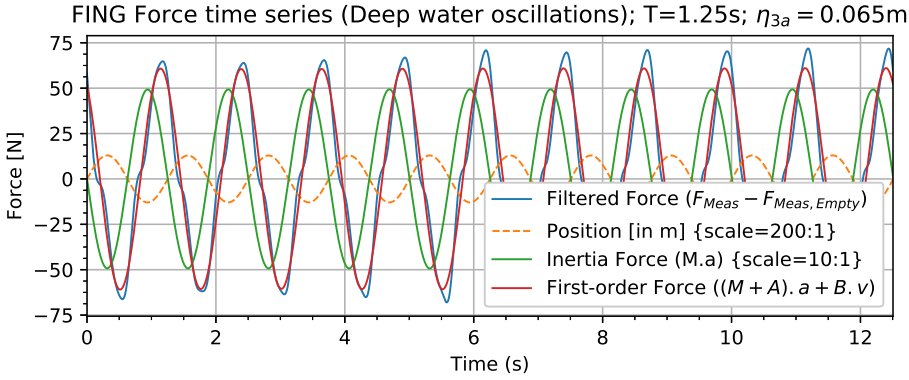
FING Force time series (Deep water oscillations); T=1.25s; $\eta_{3a} = 0.065$m
Force [N]
Time (s)
Filtered Force ($F_{Meas} - F_{Meas,Empty}$)
Position [in m] {scale=200:1}
Inertia Force (M.a) {scale=10:1}
First-order Force ($(M+A).a + B.v$)

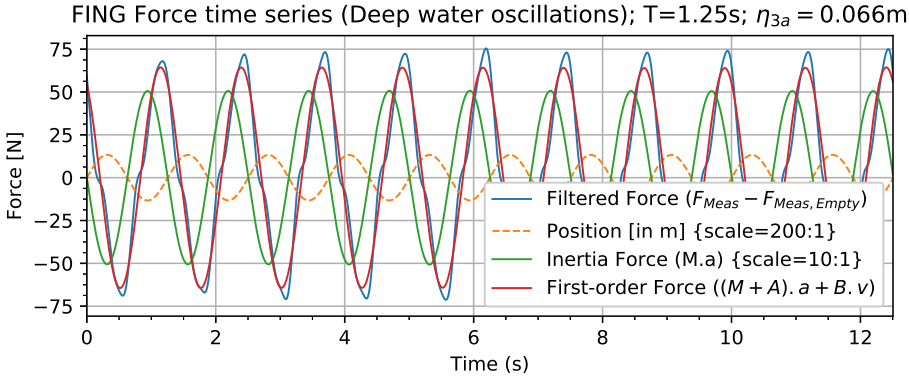
FING Force time series (Deep water oscillations); T=1.25s; $\eta_{3a} = 0.066$m
Force [N]
Time (s)
Filtered Force ($F_{Meas} - F_{Meas,Empty}$)
Position [in m] {scale=200:1}
Inertia Force (M.a) {scale=10:1}
First-order Force ($(M+A).a + B.v$)

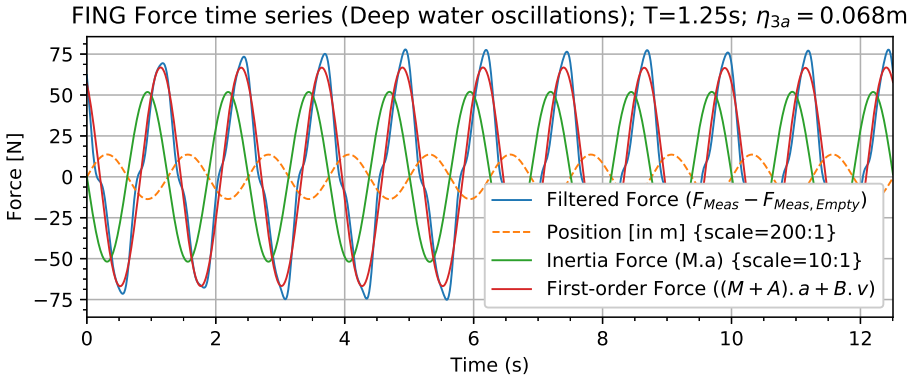
FING Force time series (Deep water oscillations); T=1.25s; $\eta_{3a} = 0.068$m
Force [N]
Time (s)
Filtered Force ($F_{Meas} - F_{Meas,Empty}$)
Position [in m] {scale=200:1}
Inertia Force (M.a) {scale=10:1}
First-order Force ($(M+A).a + B.v$)

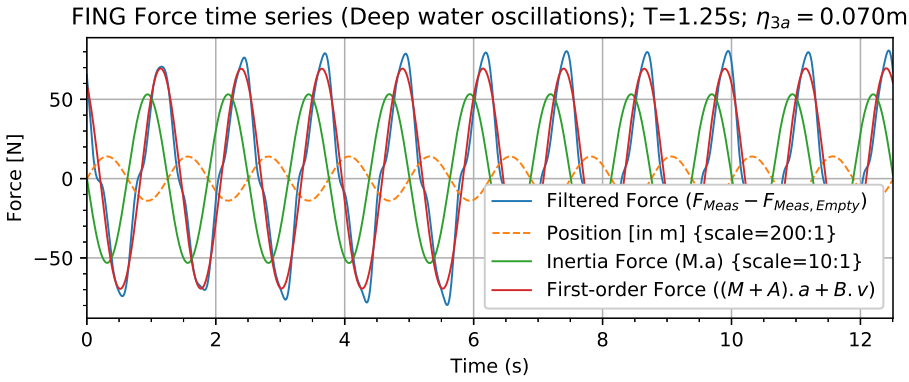
FING Force time series (Deep water oscillations); T=1.25s; $\eta_{3a} = 0.070$m
Force [N]
Time (s)
Filtered Force ($F_{Meas} - F_{Meas,Empty}$)
Position [in m] {scale=200:1}
Inertia Force (M.a) {scale=10:1}
First-order Force ($(M+A).a + B.v$)

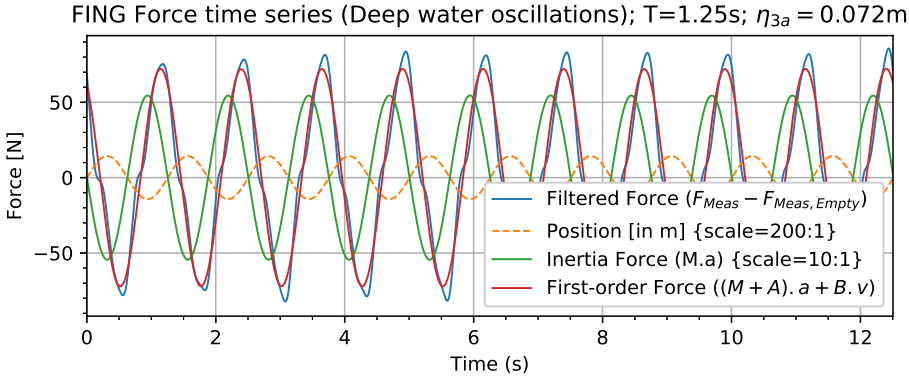
FING Force time series (Deep water oscillations); T=1.25s; $\eta_{3a} = 0.072$m
Force [N]
Time (s)
Filtered Force ($F_{Meas} - F_{Meas,Empty}$)
Position [in m] {scale=200:1}
Inertia Force (M.a) {scale=10:1}
First-order Force ($(M+A).a + B.v$)

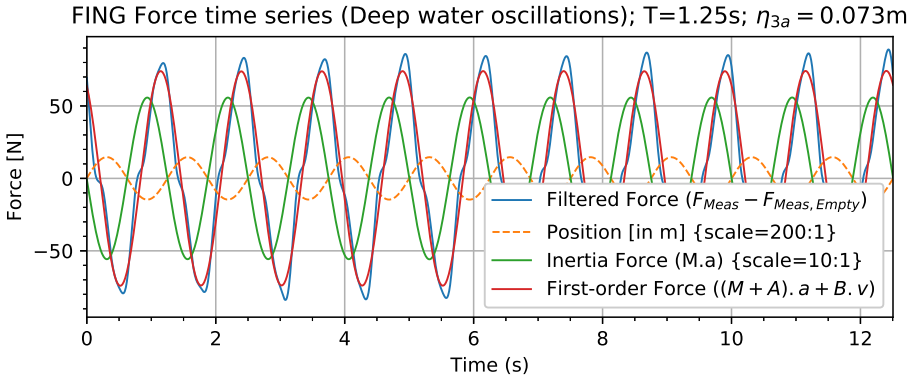
FING Force time series (Deep water oscillations); T=1.25s; $\eta_{3a} = 0.073$m
Force [N]
Time (s)
Filtered Force ($F_{Meas} - F_{Meas,Empty}$)
Position [in m] {scale=200:1}
Inertia Force (M.a) {scale=10:1}
First-order Force ($(M+A).a + B.v$)

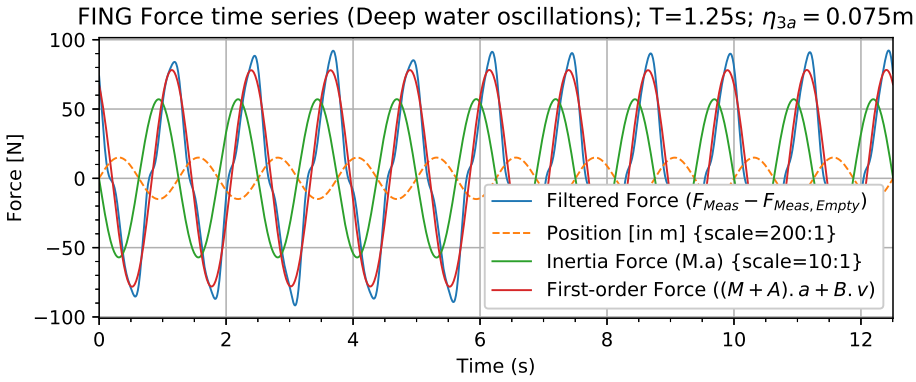
FING Force time series (Deep water oscillations); T=1.25s; $\eta_{3a} = 0.075$m
Force [N]
Time (s)
Filtered Force ($F_{Meas} - F_{Meas,Empty}$)
Position [in m] {scale=200:1}
Inertia Force (M.a) {scale=10:1}
First-order Force ($(M+A).a + B.v$)

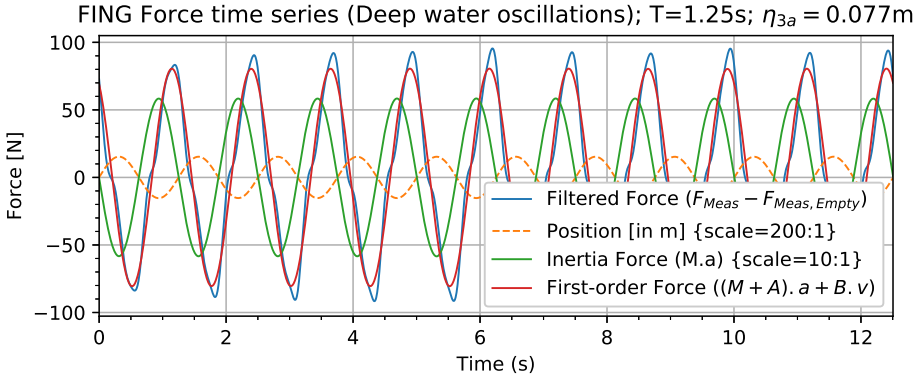
FING Force time series (Deep water oscillations); T=1.25s; $\eta_{3a} = 0.077$m
Force [N]
Time (s)
Filtered Force ($F_{Meas} - F_{Meas,Empty}$)
Position [in m] {scale=200:1}
Inertia Force (M.a) {scale=10:1}
First-order Force ($(M+A).a + B.v$)

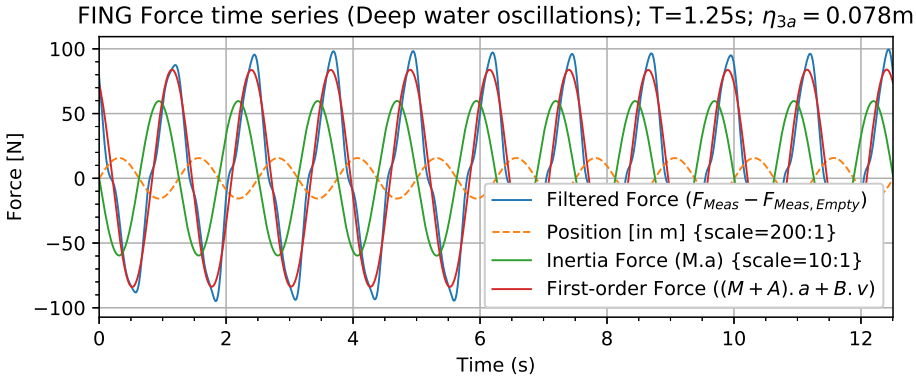
FING Force time series (Deep water oscillations); T=1.25s; $\eta_{3a} = 0.078$m
Force [N]
Time (s)
Filtered Force ($F_{Meas} - F_{Meas,Empty}$)
Position [in m] {scale=200:1}
Inertia Force (M.a) {scale=10:1}
First-order Force ($(M+A).a + B.v$)

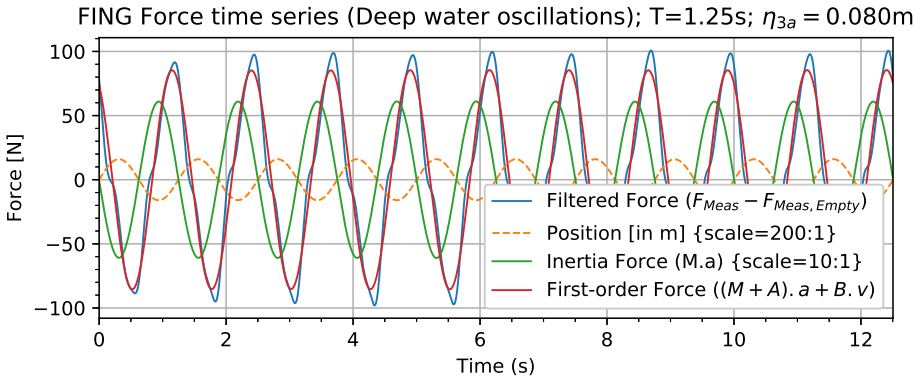
FING Force time series (Deep water oscillations); T=1.25s; $\eta_{3a} = 0.080$m
Force [N]
Time (s)
Filtered Force ($F_{Meas} - F_{Meas,Empty}$)
Position [in m] {scale=200:1}
Inertia Force (M.a) {scale=10:1}
First-order Force ($(M+A).a + B.v$)

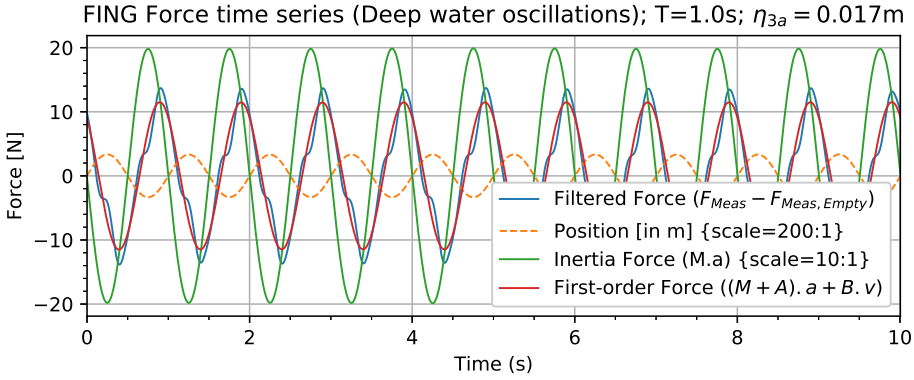
FING Force time series (Deep water oscillations); T=1.0s; $\eta_{3a} = 0.017$m
Force [N]
Time (s)
Filtered Force ($F_{Meas} - F_{Meas,Empty}$)
Position [in m] {scale=200:1}
Inertia Force (M.a) {scale=10:1}
First-order Force ($(M+A).a + B.v$)

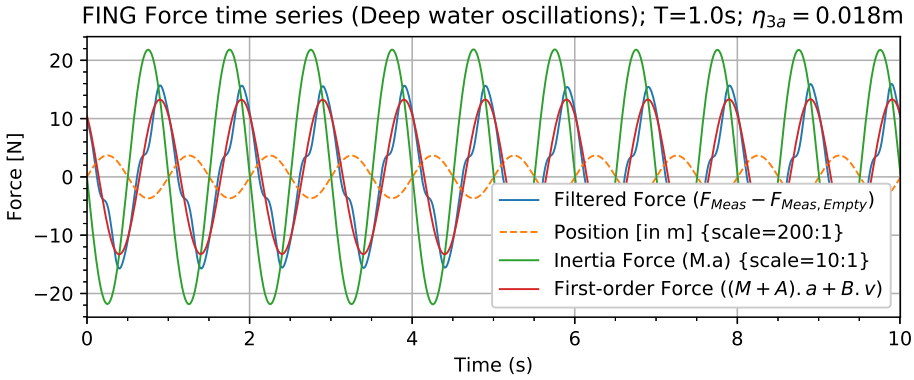
FING Force time series (Deep water oscillations); T=1.0s; $\eta_{3a} = 0.018$m
Force [N]
Time (s)
Filtered Force ($F_{Meas} - F_{Meas,Empty}$)
Position [in m] {scale=200:1}
Inertia Force (M.a) {scale=10:1}
First-order Force ($(M+A).a + B.v$)

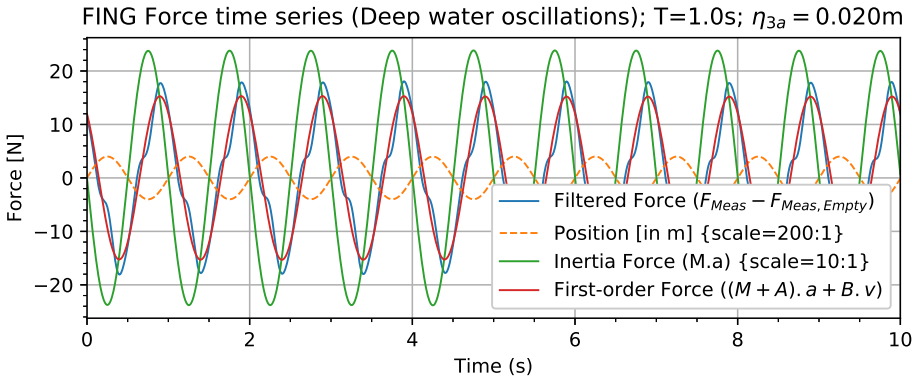
FING Force time series (Deep water oscillations); T=1.0s; $\eta_{3a} = 0.020$m
Force [N]
Time (s)
Filtered Force ($F_{Meas} - F_{Meas,Empty}$)
Position [in m] {scale=200:1}
Inertia Force (M.a) {scale=10:1}
First-order Force ($(M+A).a + B.v$)

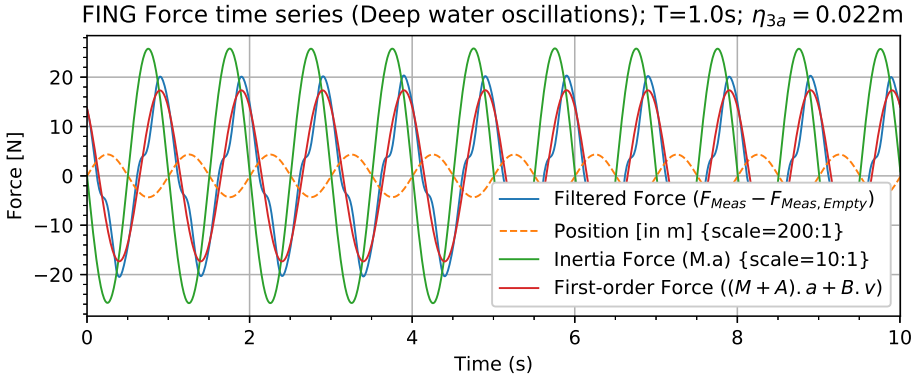
FING Force time series (Deep water oscillations); T=1.0s; $\eta_{3a} = 0.022$m
Force [N]
Time (s)
Filtered Force ($F_{Meas} - F_{Meas,Empty}$)
Position [in m] {scale=200:1}
Inertia Force (M.a) {scale=10:1}
First-order Force ($(M+A).a + B.v$)

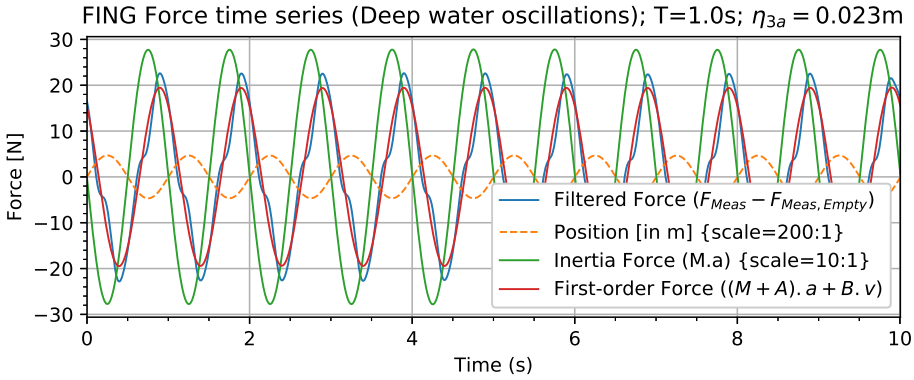
FING Force time series (Deep water oscillations); T=1.0s; $\eta_{3a} = 0.023$m
Force [N]
Time (s)
Filtered Force ($F_{Meas} - F_{Meas,Empty}$)
Position [in m] {scale=200:1}
Inertia Force (M.a) {scale=10:1}
First-order Force ($(M+A).a + B.v$)

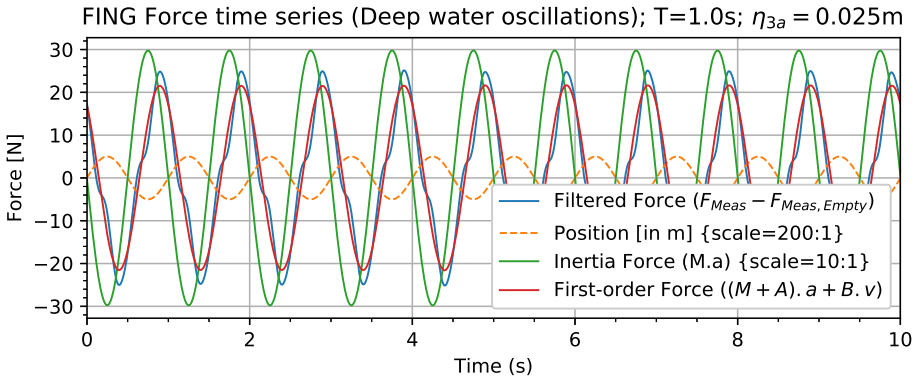
FING Force time series (Deep water oscillations); T=1.0s; $\eta_{3a} = 0.025$m
Force [N]
Time (s)
Filtered Force ($F_{Meas} - F_{Meas,Empty}$)
Position [in m] {scale=200:1}
Inertia Force (M.a) {scale=10:1}
First-order Force ($(M+A).a + B.v$)

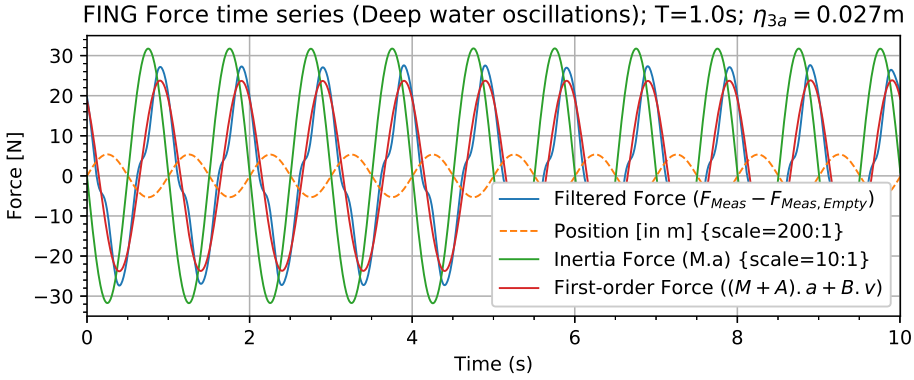
FING Force time series (Deep water oscillations); T=1.0s; $\eta_{3a} = 0.027$m
Force [N]
Time (s)
Filtered Force ($F_{Meas} - F_{Meas,Empty}$)
Position [in m] {scale=200:1}
Inertia Force (M.a) {scale=10:1}
First-order Force ($(M+A).a + B.v$)

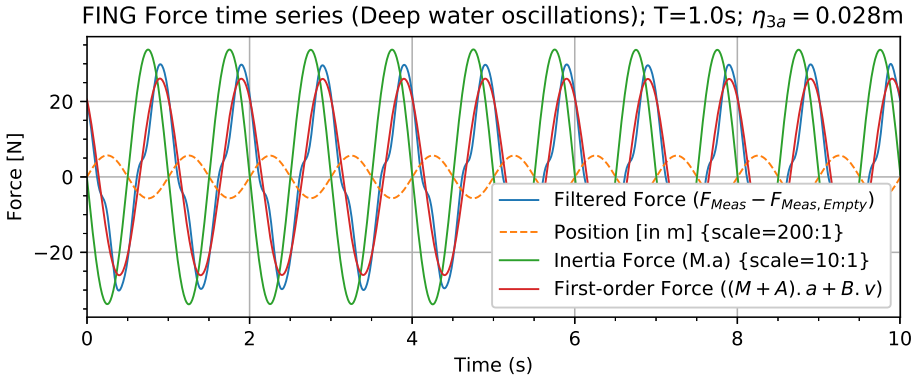
FING Force time series (Deep water oscillations); T=1.0s; $\eta_{3a} = 0.028$m
Force [N]
Time (s)
Filtered Force ($F_{Meas} - F_{Meas,Empty}$)
Position [in m] {scale=200:1}
Inertia Force (M.a) {scale=10:1}
First-order Force ($(M+A).a + B.v$)

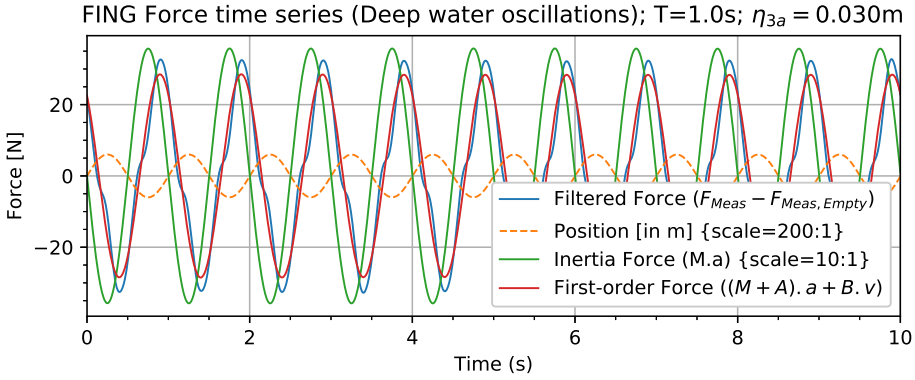
FING Force time series (Deep water oscillations); T=1.0s; $\eta_{3a} = 0.030$m
Force [N]
Time (s)
Filtered Force ($F_{Meas} - F_{Meas,Empty}$)
Position [in m] {scale=200:1}
Inertia Force (M.a) {scale=10:1}
First-order Force ($(M+A).a + B.v$)

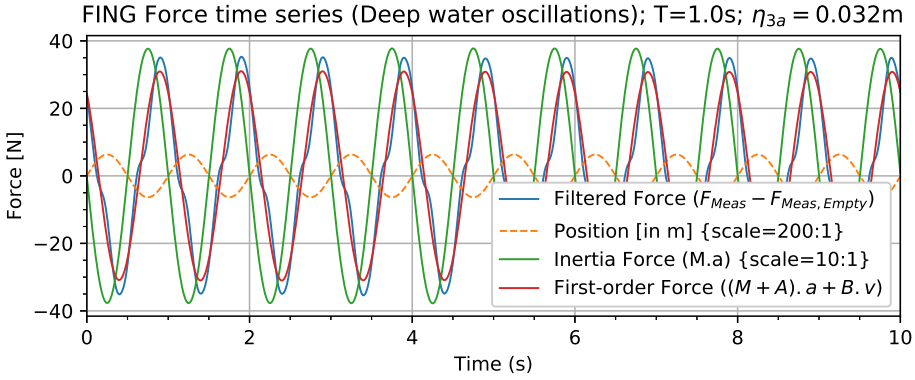
FING Force time series (Deep water oscillations); T=1.0s; $\eta_{3a} = 0.032$m
Force [N]
Time (s)
Filtered Force ($F_{Meas} - F_{Meas,Empty}$)
Position [in m] {scale=200:1}
Inertia Force (M.a) {scale=10:1}
First-order Force ($(M+A).a + B.v$)

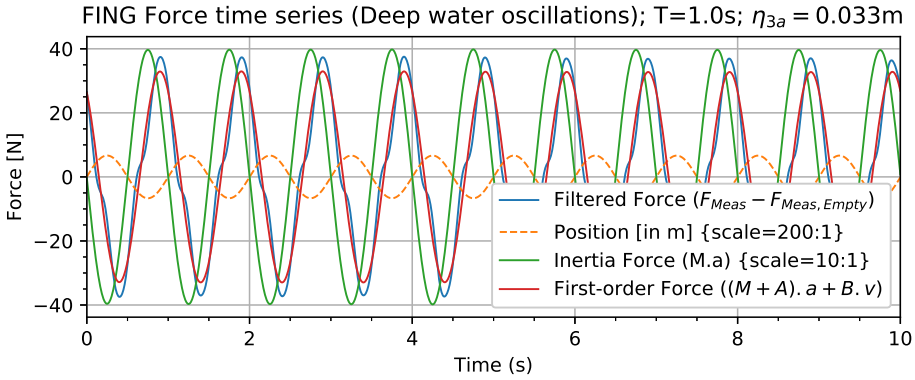
FING Force time series (Deep water oscillations); T=1.0s; $\eta_{3a} = 0.033$m
Force [N]
Time (s)
Filtered Force ($F_{Meas} - F_{Meas,Empty}$)
Position [in m] {scale=200:1}
Inertia Force (M.a) {scale=10:1}
First-order Force ($(M+A).a + B.v$)

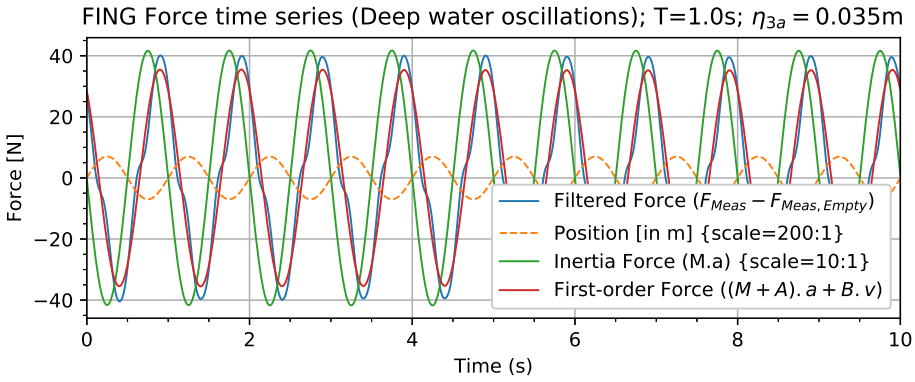
FING Force time series (Deep water oscillations); T=1.0s; $\eta_{3a} = 0.035$m
Force [N]
Time (s)
Filtered Force ($F_{Meas} - F_{Meas,Empty}$)
Position [in m] {scale=200:1}
Inertia Force (M.a) {scale=10:1}
First-order Force ($(M+A).a + B.v$)

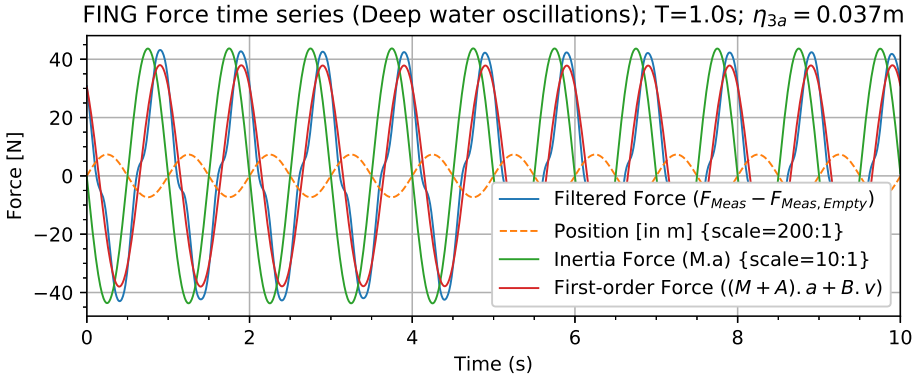
FING Force time series (Deep water oscillations); T=1.0s; $\eta_{3a} = 0.037$m
Force [N]
Time (s)
Filtered Force ($F_{Meas} - F_{Meas,Empty}$)
Position [in m] {scale=200:1}
Inertia Force (M.a) {scale=10:1}
First-order Force ($(M+A).a + B.v$)

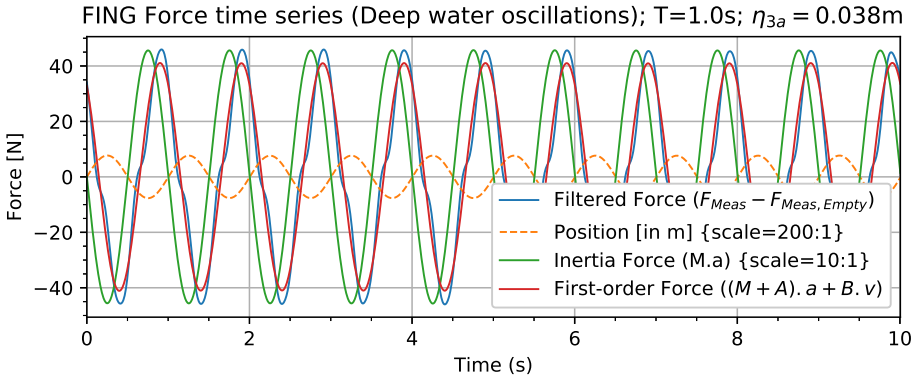
FING Force time series (Deep water oscillations); T=1.0s; $\eta_{3a} = 0.038$m
Force [N]
Time (s)
Filtered Force ($F_{Meas} - F_{Meas,Empty}$)
Position [in m] {scale=200:1}
Inertia Force (M.a) {scale=10:1}
First-order Force ($(M+A).a + B.v$)

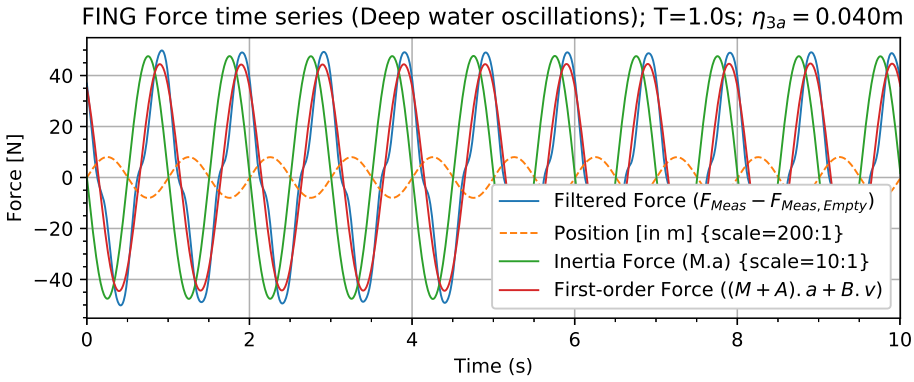
FING Force time series (Deep water oscillations); T=1.0s; $\eta_{3a} = 0.040$m
Force [N]
Time (s)
Filtered Force ($F_{Meas} - F_{Meas,Empty}$)
Position [in m] {scale=200:1}
Inertia Force (M.a) {scale=10:1}
First-order Force ($(M+A).a + B.v$)

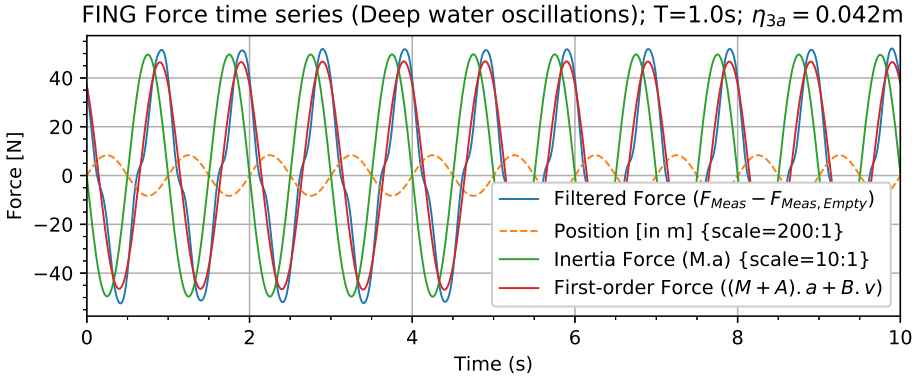
FING Force time series (Deep water oscillations); T=1.0s; $\eta_{3a} = 0.042$m
Force [N]
Time (s)
Filtered Force ($F_{Meas} - F_{Meas,Empty}$)
Position [in m] {scale=200:1}
Inertia Force (M.a) {scale=10:1}
First-order Force ($(M+A).a + B.v$)

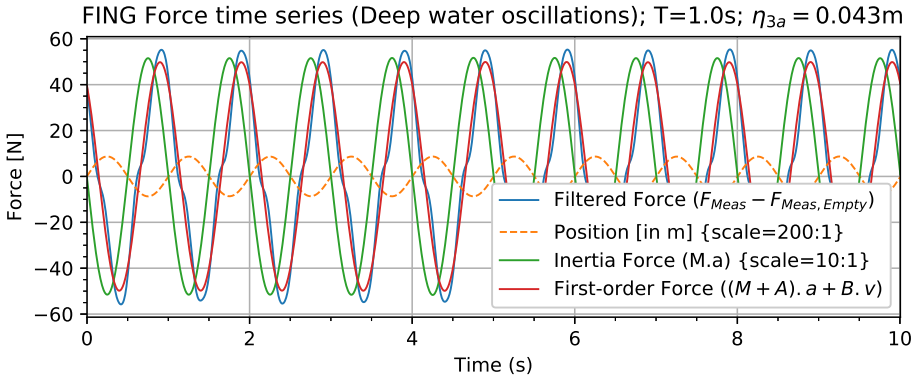
FING Force time series (Deep water oscillations); T=1.0s; $\eta_{3a} = 0.043$m
Force [N]
Time (s)
Filtered Force ($F_{Meas} - F_{Meas,Empty}$)
Position [in m] {scale=200:1}
Inertia Force (M.a) {scale=10:1}
First-order Force ($(M+A).a + B.v$)

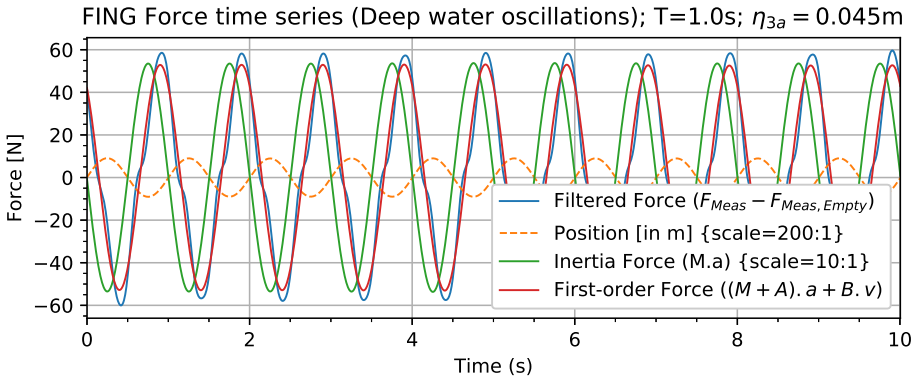
FING Force time series (Deep water oscillations); T=1.0s; $\eta_{3a} = 0.045$m
Force [N]
Time (s)
Filtered Force ($F_{Meas} - F_{Meas,Empty}$)
Position [in m] {scale=200:1}
Inertia Force (M.a) {scale=10:1}
First-order Force ($(M+A).a + B.v$)

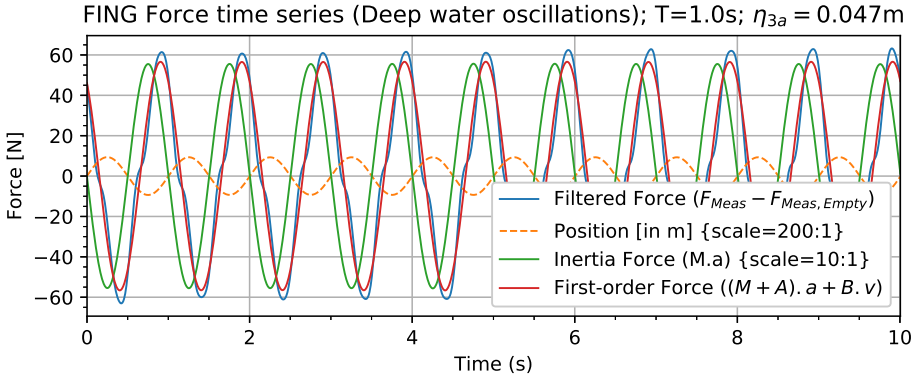
FING Force time series (Deep water oscillations); T=1.0s; $\eta_{3a} = 0.047$m
Force [N]
Time (s)
Filtered Force ($F_{Meas} - F_{Meas,Empty}$)
Position [in m] {scale=200:1}
Inertia Force (M.a) {scale=10:1}
First-order Force ($(M+A).a + B.v$)

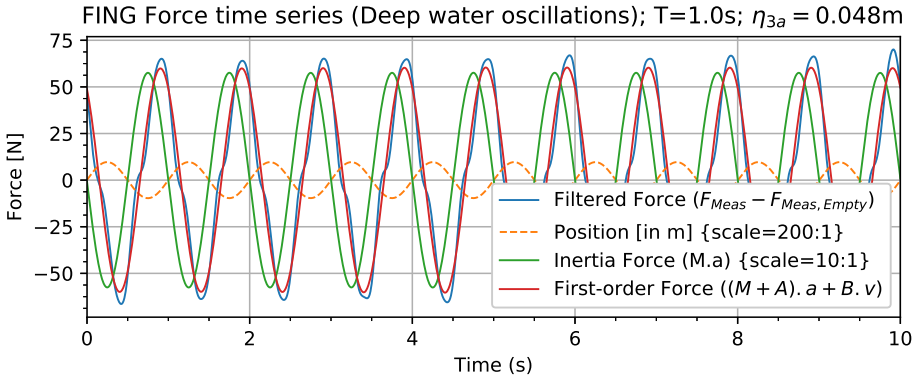
FING Force time series (Deep water oscillations); T=1.0s; $\eta_{3a} = 0.048$m
Force [N]
Time (s)
Filtered Force ($F_{Meas} - F_{Meas,Empty}$)
Position [in m] {scale=200:1}
Inertia Force (M.a) {scale=10:1}
First-order Force ($(M+A).a + B.v$)